THE UNIVERSITY OF ALBERTA

FROST HEAVE MECHANICS

by

Jean-Marie KONRAD

A THESIS

SUBMITTED TO THE FACULTY OF GRADUATE STUDIES AND RESEARCH

IN PARTIAL FULFILMENT OF THE REQUIREMENTS FOR THE DEGREE

OF DOCTOR OF PHILOSOPHY

DEPARTMENT OF CIVIL ENGINEERING

EDMONTON, ALBERTA

FALL 1980

THE UNIVERSITY OF ALBERTA

RELEASE FORM

NAME OF AUTHOR   Jean-Marie KONRAD

TITLE OF THESIS   FROST HEAVE MECHANICS

DEGREE FOR WHICH THESIS WAS PRESENTED   DOCTOR OF PHILOSOPHY

YEAR THIS DEGREE GRANTED   FALL 1980

Permission is hereby granted to THE UNIVERSITY OF ALBERTA LIBRARY to reproduce single copies of this thesis and to lend or sell such copies for private, scholarly or scientific research purposes only.

The author reserves other publication rights, and neither the thesis nor extensive extracts from it may be printed or otherwise reproduced without the author's written permission.

(SIGNED) *JM Konrad*

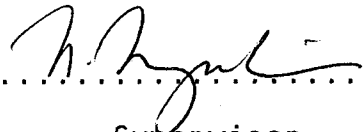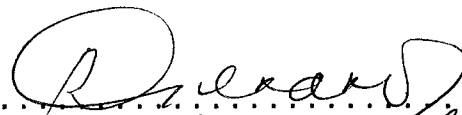PERMANENT ADDRESS:

800 Est Maisonneuve

S.E.B.J. Service de l'ingénierie

MONTREAL   P.Q.

DATED ...2nd october...1980

THE UNIVERSITY OF ALBERTA
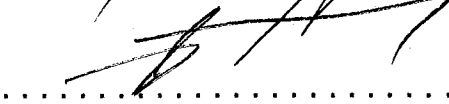
FACULTY OF GRADUATE STUDIES AND RESEARCH

The undersigned certify that they have read, and recommend to the Faculty of Graduate Studies and Research, for acceptance, a thesis entitled FROST HEAVE MECHANICS submitted by Jean-Marie KONRAD in partial fulfilment of the requirements for the degree of DOCTOR OF PHILOSOPHY.

Dr. N. Morgenstern ....

Supervisor
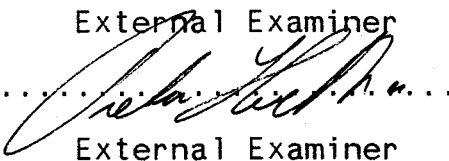
Dr. R. Gerard ....

Dr. D. Sego ....

Dr. R. Gilpin ....

Dr. E. Penner ....

External Examiner

Dr. P. Hoekstra ....

External Examiner

Date. October. 2nd,. 1980 ....

Il n'y a de repos

que pour celui qui cherche

Il n'y a de repos

que pour celui qui trouve

Tout est toujours à recommencer....

Raoul Duguay

à   Bout'Chou

REMERCIEMENTS - ACKNOWLEDMENTS

ABSTRACT

Frost action in soils is associated with two very destructive phenomena: the expansion or lifting of the soil in winter, known as frost heaving, and the loss of soil-bearing strength by thaw weakening in the spring.

This thesis is concerned with the first of the forementioned phenomena and is aimed at a quantitative understanding of frost heave mechanics and the development of a comprehensive engineering theory of frost heave.

This study confirms that an ice lens in a freezing soil grows somewhere in the frozen zone, slightly behind the frost front, i.e. the 0 C isotherm. The frozen soil that lies between the ice lens and the unfrozen soil is referred to as the frozen fringe.

At the formation of the final ice lens, frost heave can be treated as a problem of impeded drainage to the warmest ice lens through the frozen fringe and the unfrozen soil. Furthermore, the frost heave characteristics at these conditions are defined either by the segregation-freezing temperature and the overall permeability of the frozen fringe or by the segregation potential, which is the ratio of water intake flux and temperature gradient in the fringe.

These parameters are dependent upon applied surcharge, average suction in the fringe, and degree of thermal imbalance. This latter has been introduced by means of the rate of cooling of the frozen fringe which is the rate of

change of the average temperature in the frozen fringe. This study establishes that, at a given surcharge, a unique relationship between the segregation potential, the suction at the frost front, and the rate of cooling of the fringe exits in any freezing soil. This characteristic freezing surface is independent of thermal and geometrical boundary conditions.

Water expulsion during an advancing frost front is a function of applied load and rate of cooling of the fringe. There is a unique relation for a given soil between these two parameters for which water is attracted to the freezing front. Evidence of a shut-off pressure, for which no water flow to the freezing soil occurs, is given.

A frost heave model is developed to simulate laboratory freezing tests for one dimensional heat flow and with zero surcharge. The input to mass transfer is the characteristic freezing surface which can be determined from controlled laboratory freezing tests. This model is able to predict closely any freezing test performed in the present study.

The growth of the final ice lens is solely governed by the net heat extraction rate at the freezing front. This growth stops when the pore water pressure at the base of the ice lens becomes atmospheric, which is a function of its temperature, applied load, and solute concentration.

The frost heave characteristics in field situations are identical to those obtained in laboratory freezing tests at the formation of the final ice lens and for a suction at the

frost front close to atmospheric pressure.

A frost heave model with one dimensional radial heat flow using the forementioned freezing characteristics as input to mass transfer simulates successfully the behavior of four chilled pipelines over several years of freezing.

A simple frost heave calculation using the segregation potential predicts in a straight forward manner subgrade behavior during seasonal freezing.

Two new frost susceptibility criteria have been proposed. The first one is valid during an advancing frost front and is based upon the segregation potential. The second one indicates the growth potential of the final ice lens during a retreating frost front and is based upon the segregation-freezing temperature.

RESUME

Le gel dans les sols produit deux phénomènes très destructifs: l'expansion ou le soulèvement du sol en hiver et la perte de résistance lors du dégel printanier.

Les observations experimentales effectuées dans le cadre de cette recherche ont permis de définir les paramètres fondamentaux affectant le soulèvement dans un sol qui gèle et d'établir une méthode de calcul pratique pour l'ingénieur confronté à ce phénomène.

Cette étude confirme que lorsque qu'un sol est soumis au gel, la lentille de glace se forme dans la zone gelée, légèrement à l'arrière du front de gel, c.à.d. l'isotherme 0° C. Cette partie de sol gelé, situé entre le sol non gelé et la lentille de glace, constitue la frange gelée.

A la formation de la dernière lentille de glace, la migration d'eau vers la base de cette lentille peut être traitée comme un problème d'écoulement à travers deux zones: la frange gelée et le sol non gelé. Dans ce cas, les caractéristiques de gonflement peuvent être définies soit par la température de ségrégation à la base de la lentille et par la perméabilité moyenne de la frange gelée, soit par le potentiel de ségrégation défini par le rapport de la vitesse d'écoulement et du gradient de température.

Ces paramètres dépendent de la pression appliquée au front de segrégation, de la succion moyenne dans la frange gelée et du degré de déséquilibre thermique. Ce dernier

paramètre est représenté par le taux de refroidissement de la frange gelée qui est égal au taux de changement de la température moyenne de la frange gelée.

Cette étude révèle que, pour une pression donnée, une relation unique existe dans tout sol entre le potentiel de ségrégation, la succion au front de gel et le taux de refroidissement de la frange gelée. Cette surface caractéristique d'un sol soumis au gel est indépendante des conditions aux limites.

L'expulsion d'eau observée lorsque le front de gel pénètre est fonction de la pression appliquée sur le front de gel et du taux de refroidissement de la frange gelée. Il existe une relation unique entre ces deux paramètres définissant le domaine dans lequel l'eau sera attirée vers le front de ségrégation. Ce travail fournit également une preuve d'existence d'une pression d'arrêt qui rend tout écoulement dans la frange gelée impossible.

Un modèle calculant le soulèvement est développé pour simuler les essais de gel unidirectionnel sans pression externe. La surface caractéristique du sol soumis au gel est la donnée permettant d'évaluer le transfert de masse. Les résultats obtenus par ce modèle sont très satisfaisants.

La croissance de la dernière lentille de glace est uniquement gouvernée par le déficit de chaleur au front de ségrégation. L'arrêt de cette croissance a lieu lorsque la pression dans le film d'eau adjacent à la lentille est atmosphérique. Ceci est une fonction de la pression dans la

lentille, de la température a sa base et de la concentration ionique du fluide.

Les caractéristiques d'un sol qui gèle dans la nature sont identiques à celles obtenues au laboratoire à la formation de la dernière lentille de glace et pour une succion au front de gel voisine de la pression atmosphérique.

Un modèle mathématique utilisant les paramètres décrits ci-dessus permet le calcul du gonflement pour un écoulement radial de la chaleur. Ce modèle a été utilisé pour simuler avec succès le comportement de quatre pipelines dont la température est en dessous du point de congélation de l'eau sur une période de plusieurs années.

Une méthode simple utilisant le potentiel de segrégation permet le calcul rapide du soulèvement des structures soumises au gel saisonnier.

On a proposé deux nouveaux critères de susceptibilité au gel.L'un ,fondé sur le potentiel de segrégation,est applicable pendant l'avancement du front de gel, tandis que l'autre, fondé sur la température de ségrégation, indique le potentiel de croissance de la dernière lentille de glace, lorsque le front de ségrégation est stationnaire.

GLOSSARY

Segregation Freezing Temperature, T_s,: Temperature at which the intake water freezes and creates the segregational heaving process.

In-Situ Freezing Temperature, T_i,: The warmest temperature at which ice exists in the soil.

Frozen Fringe: The frozen soil that is confined between T_s and T_i.

Active System: The freezing soil composed of the frozen fringe and the unfrozen soil.

Passive System: The frozen soil confined between T_s and the cold - side freezing temperature.

Frost Front: The T_i isotherm.

Freezing Front: The T_s isotherm.

Rate of Cooling of the Frozen Fringe: The change in average temperature of the current fringe per unit time.

Segregation Potential, SP,: The ratio of the water intake rate and the temperature gradient in the frozen fringe.

Characteristic Freezing Surface of a Soil: The relationship between the segregation potential, the suction at the frost front, and the rate of cooling of the current fringe.

LIST OF IMPORTANT SYMBOLS

h : Total Heave

hs : Heave by Water Intake

hi : Heave from In-Situ Freezing

hu : Water Pressure in cm of Water

Hw : Suction Potential in cm of Water

ku , kf : Thermal Conductivities of Unfrozen and Frozen Soil

Ku : Permeability of Unfrozen Soil

Kf : Overall Permeability of Frozen Fringe

Kfo : Kf at the Formation of the Final Ice Lens

Pw : Suction Potential at the Ice Lens

Pu : Water Pressure at the Frost Front

Pi : Ice Pressure

Pe : External Applied Pressure

Pb : Applied Back Pressure

SP : Segregation Potential

SPo : SP at the Formation of the Final Ice Lens

Vw : Specific Volume of Water

Vi : Specific Volume of Ice

V : Water Intake Rate

Vo : V at the Formation of the Final Ice Lens

Ts : Segregation Freezing Temperature

Tso : Ts at the Formation f the Final Ice Lens

Ti : In Situ Freezing Temperature

Tc : Cold-Side Step Temperature

Tw : Warm-Side Temperature

X : Thickness of Frozen Soil

lu : Thickness of Unfrozen Soil

Table of Contents

LIST OF TABLES

Obtained for Both Laboratory and Field

LIST OF PLATES

1. FROZEN AND FREEZING SOILS

1.1 FROST HEAVE: AN AREA OF CONSIDERABLE RESEARCH INTEREST

Recent petroleum discoveries and development in the Canadian north have brought about a need to develop transportation facilities to southern and foreign markets. The trans-Alaska oil pipeline is already built and a gas pipeline is being considered at this time. Each of these routes crosses a great variety of terrains, through continuous permafrost, the warmer discontinuous permafrost zone, and the nonpermafrost northern boreal forest.

Although the design and construction of the oil pipeline has widened our understanding of the mechanics of cold region geotechnics, particularly in problems associated with thawing, certain features of the chilled gas pipeline offer a number of new problems. In the permafrost zone, the gas pipline will be maintained below freezing to prevent undue thermal degradation of the permafrost material. In relatively warm permafrost regions, the pipeline may easily pass from thick permafrost to a total absence. It will be more difficult in these areas to maintain the pipe near the ambient ground temperature and, as a result, certain normally unfrozen regions will freeze and remain frozen for many years.

The effects of freezing a frost susceptible soil are most clearly exhibited by a heaving of the ground surface as a result of the formation of discrete ice lenses from water supplied from the unfrozen soil or an external source (Taber, 1929). The propensity for heave of a soil under freezing conditions is affected by grain size distribution, availibility of water, rate of heat extraction, and applied loads. For a given soil an engineering theory of frost heave would lead to the prediction of the magnitude and rate of frost heave as a function of certain characteristics of the freezing system and boundary conditions. Prior to freezing, the temperature profile and boundary conditions controlling the availability of water can be established by measurement. A knowledge of the soil profile can be translated into the moisture content distribution, the thermal conductivity and the permeability of the soil. A change in heat flux or temperature at a boundary must be specified in order to account for the onset of freezing. As a frost front advances into the soil, moisture is drawn to it and it is the coupling of the heat and mass flow that constitutes the complex element in the theory of frost heave. Notwithstanding the very considerable research devoted in the past to the frost heave process, agreement on an engineering theory of frost heave remains an elusive goal. This constitutes a serious impediment to the rational design of buried chilled gas pipelines in discontinuous permafrost and the solution of other problems requiring heave

predictions.

Most studies into the frost heave of soils have fallen into one of the following classes:

1. index tests to establish the degree of frost susceptibility of various soils;

2. fundamental thermodynamic analyses;

3. empirical studies attempting to relate quantitatively laboratory investigations to field performance.

More recently, there have been several attempts to embrace heat and mass flux in a coupled theory but predictive results from these studies are not convincing.

Finally, frost action in soils is not restricted to ground heaving but may also result in other critical phenomena. If the ice lens growth is restrained during freezing, severe heaving pressures may arise which could cause damage to engineering structures. Furthermore, in problems involving seasonal freezing severe stability and settlement problems might be anticipated on thawing of fine-grained soils containing segregated ice created during the freezing phase.

1.2 PHYSICAL PROPERTIES OF FROZEN AND FREEZING SOILS

This section will draw attention to some commonly accepted phenomena related to frozen and freezing soils. The physical properties of frozen and freezing soils will be

explored both from the theoretical (thermodynamics) and experimental point of view.

1.2.1 Thermodynamic Equilibrium Between Ice and Water in Porous Media

1.2.1.1. The Clausius-Clapeyron Equation

Thermodynamic equilibrium between ice and water in a frozen soil requires that the free energy of the ice equals that of the water. A fundamental equation of thermodynamics gives the differential of the Gibbs free energy of a monocomponent system as:

$$dG = V.dP - S.dT* \dotfill 1.1$$

where   S is the entropy of the system

T* is the absolute temperature

V is the volume

P is the pressure

The equality of the free energies of an ice/water system can be expressed as:

$$Vi.dPi - Si.dT* = Vw.dPw - Sw.dT* \dotfill 1.2$$

where   the subscripts i and w refer respectively to ice and water

Vi, Vw: specific volume

If the phase transition is considered to take place reversibly at T*, the latent heat of phase change, L, for one mole is equal to:

$$L = (Sw - Si)T* \dotfill 1.3$$

where   L > 0 for freezing

L < 0 for thawing

Equation 1.1 can then be recast as follows:

$$V_w.dP_w - V_i.dP_w = L \, dT*/T* \quad \dots\dots\dots\dots\dots\dots 1.4$$

Equation 1.4 represents the differential form of the generalized Clausius-Clapeyron equation. The general relation between the water pressure and the ice pressure at T* can be obtained by integration of Equation 1.4 from the standard state (Pw = Pi = 0; T* = To* = 273.15°K) to the final state (Pw, Pi, T*) (Kay and Groenevelt, 1974):

$$P_w = \int_{T_o*}^{T} (L/V_w) \, dT*/T* + \int_{0}^{P_i} (V_i/V_w)dP_i \dots\dots\dots\dots 1.5$$

$$P_w = L/V_w \ln(T*/T_o*) + (V_i/V_w)P_i \dots\dots\dots\dots 1.6$$

Equation 1.6 can be simplified for the case of atmospheric pressure in the ice and if T* is very close to To*. In these conditions, ln T*/To* can be approximated by (T* - To*)/To* and Equation 1.6 reduces to

$$P_w = L(T*-T_o*)/(V_w.T_o*) \dots\dots\dots\dots\dots\dots 1.7$$

(T* - To*) is the temperature in degree Celsius at which ice and water are considered to be in equilibrium. For the sake of convenience, it was decided to adopt the following notation:

$$T = T*-T_o* \dots\dots\dots\dots\dots\dots\dots\dots\dots\dots 1.8$$

where   T is the temperature expressed in °C

T* is the same temperature expressed in °K

It must be emphasized that the previous derivations are valid for the case of pure water only. The effect of solutes can be included in the formulation of the Gibbs free energy

as shown by Loch (1979). The pressure in the water phase is then affected by an additional osmotic pressure term. However, this study takes the view that salt effects can be neglected as a first approximation in well controlled laboratory freezing tests.

1.2.1.2. Validity of the Clausius-Clapeyron Equation

at an Ice Lens.

If the ice is under atmospheric pressure, i.e. Pi=0, the Clausius-Clapeyron equation predicts that as the temperature decreases below To*, the water pressure is negative and decreases too. Moreover, for negative temperature close to 0°C, there is a linear relationship between the suction in the water films and the temperature.

Some verification of the Clausius-Clapeyron equation is afforded by recent experimental data.

a) Vignes and Dijkema (1974) measured water migration rates using an experimental set-up shown schematically in Figure 1.1. Two reservoirs, one containing liquid water either above 0°C or super-cooled, the other containing liquid water and ice, were separated by a narrow slit, 50 nm by 2 mm in cross section, 50 mm long. As predicted by the Clausius-Clapeyron equation, water flowed towards the ice regardless of the temperature in reservoir B. Since ice was not present in reservoir B, the Clausius-Clapeyron equation cannot be applied and the water is atmospheric. The flow rate was constant for a given temperature of reservoir A. Moreover, Equation 1.7 reveals that Pw/T is constant. Since

the hydraulic conductivity of the slit is constant, the flow rate to the ice is proportional to the suction potential Pw. Therefore, the Clausius-Clapeyron equation predicts that the flow rate should be proportional to the temperature of the ice-water interface. Table 1.1 summarizes the results obtained by Vignes and Dijkema (op. cit.) and confirms the validity of the Clausius-Clapeyron Equation in their experiments, since V/T(A) was fairly constant.

Vignes and Dijkema also establish that there is a thin unfrozen water layer situated between the ice and the solid substrate. This water is in equilibrium with the ice.

b) Using glass filters in order to increase the flow, Biermans et al (1978) also proved the validity of classical reversible thermodynamics when applied to the ice lens-liquid layer system. This was achieved by measuring the suction Pw one had to apply to the water in the reservoir B in order to stop the flow to the ice lens and comparing it with theoretical prediction. The Clausius-Clapeyron equation, simplified for atmospheric pressure in the ice, was supported to a high degree of accuracy as shown in Figure 1.2.

c) Hoekstra (1969) and Radd and Oertle (1973) measured the pressure necessary to prevent heave as a function of temperature in freezing soils. If one assumes that Pw = 0 at the ice lens and that the ice pressure is equal to the heaving pressure, Ph, the generalized Clausius-Clapeyron can be recast as:
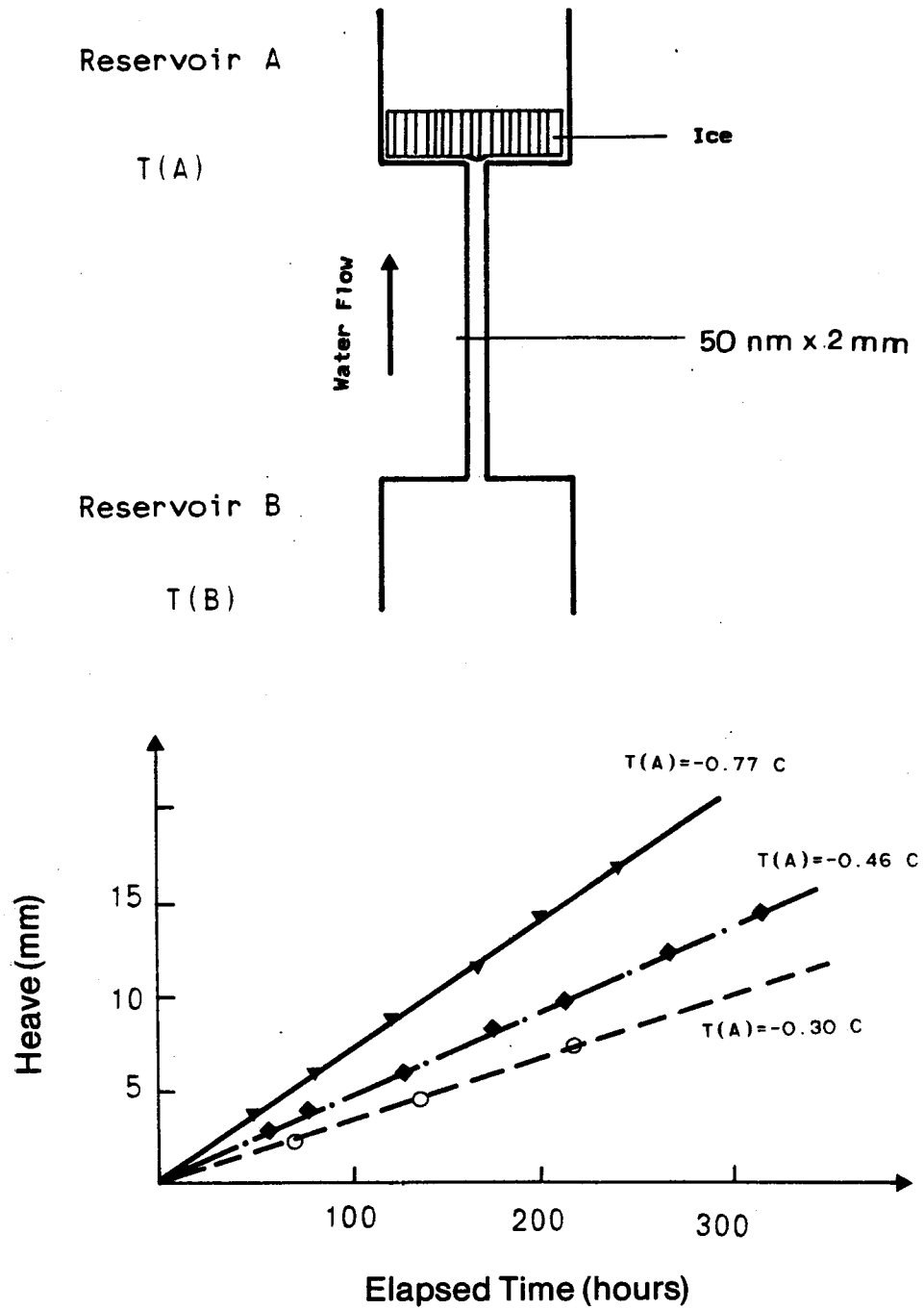
Figure 1.1   Experimental Results obtained by Vignes and
Dijkema (1974)
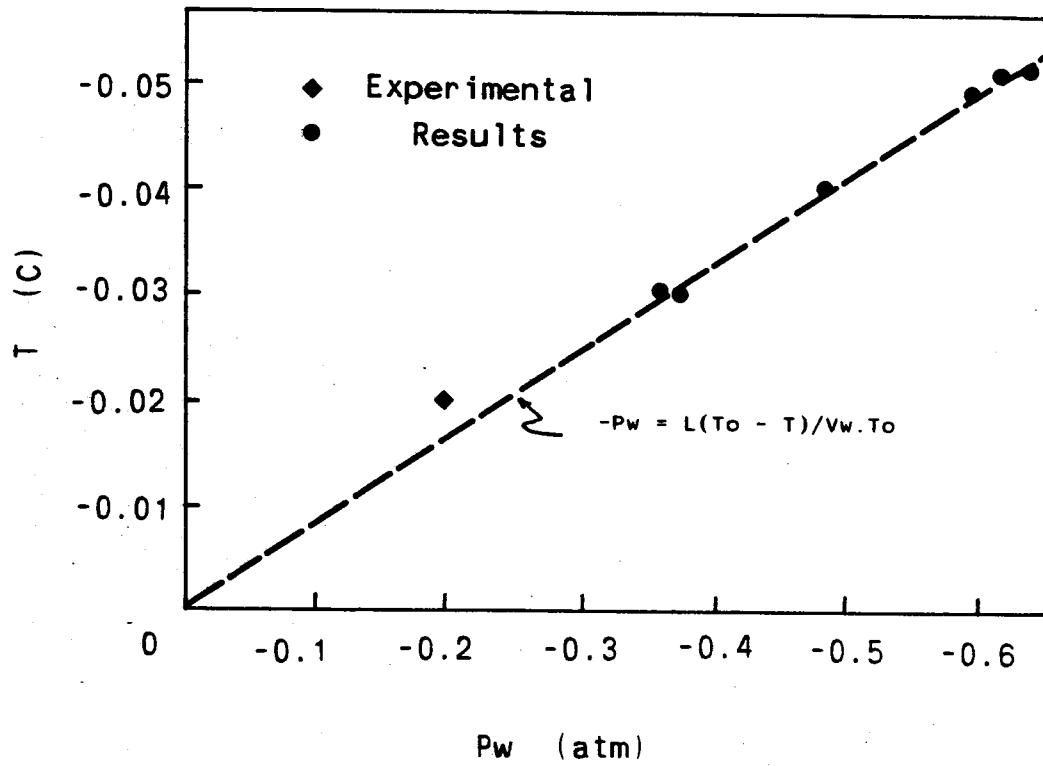
Figure 1.2 Experimental Results obtained by Biermans et al
(1978)

Table 1.1   Water flow to an Ice Lens after
            Vignes and Dijkema (1974)

Temperature C		Water Flow V m/s	V/T(A)
A	B		
-0.3	-0.6	2.65	1.10
-0.3	-0.1	2.65	
-0.46	-0.5	3.55	0.96
-0.77	-0.3	5.70	
-0.77	+0.1	5.70	0.92

$$Ph = -(L/Vi) \ln(T*/To*) \quad \ldots\ldots\ldots\ldots\ldots\ldots 1.9$$

The data obtained by the previous researchers show good
agreement with Equation 1.9 as illustrated in Figure 1.3.

It transpires from the previous results that the
Clausius-Clapeyron equation does apply at an ice lens-liquid
water layer interface, at least at temperatures several
degrees below freezing.

1.2.2 Unfrozen Water in Freezing Soils

When a fine-grained soil is frozen not all the water
within the soil pores freezes at 0°C (Bouyocous, 1916;
Lovell, 1957). In some clay soils, up to 50% of the moisture
may exist as a liquid at temperatures of -2°C (Nersesova and
Tsytovich, 1963).

The unfrozen water content is the amount of liquid
water in a soil at a given sub-zero temperature. It is
usually expressed as a percentage of the dry weight of the
soil. This definition is the most used since experimental
evidence which showed that Wu is a function of temperature
only and virtually independent of the total water content
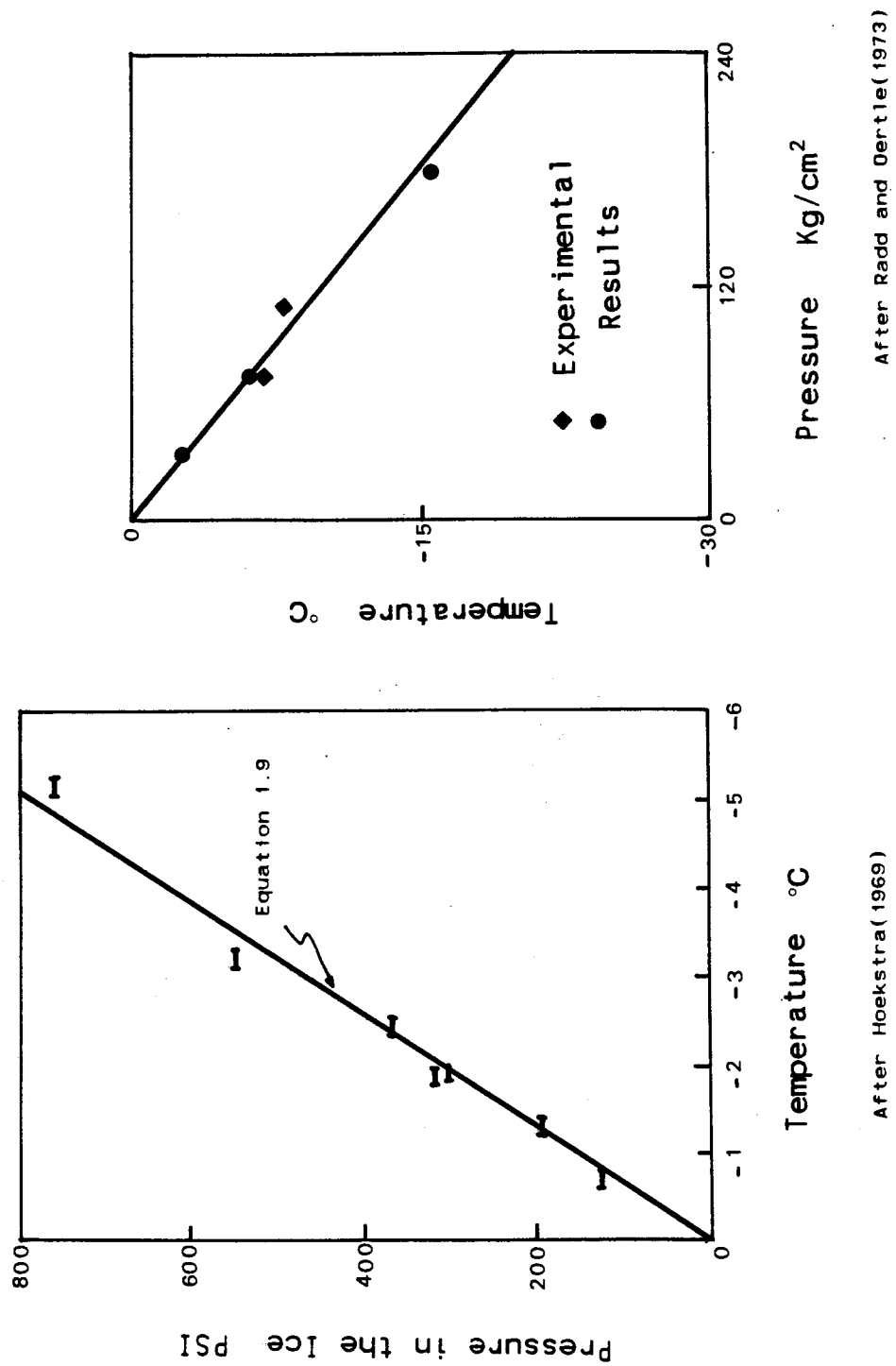
Figure 1.3   Relationship between Maximum Heaving Pressure and Temperature

for closed system freezing was given by Nersesova and Tsytovich (1963) and Jame and Norum (1972).

Measurements of unfrozen water contents in soils of varying water contents and physical properties have been made by dilatometry, adiabatic calorimetry, X-ray diffraction, heat capacity, nuclear magnetic resonance, differential thermal analysis, and several indirect techniques (Anderson and Morgenstern, 1973). Although each involves its own set of assumption and approximations, the results obtained on the same soils by each method are remarkably consistent. In each of the previous laboratory tests, the sample is frozen to its final temperature in a closed system, i.e. no water supply during freezing. In these conditions, experimental results show that the unfrozen water content may be expressed as a function of temperature only.

The relationship between unfrozen water content and temperature for soils of different texture is found to depend upon many factors, the most important of which are listed below:

a)   specific surface of the soil (Anderson et al, 1973)

b)   configuration of individual soil particles

c)   quantity and type of exchangeable cations (Nersesova and Tsytovich, 1963)

d)   pressure in ice and water phase

e)   solute concentration

f)   freezing history. (hysteresis) (Williams, 1963)

In general, the unfrozen water content in a frozen soil decreases with decreasing temperature. This has an important bearing on predicting the behavior of freezing soil since the unfrozen water content can be viewed as a water film of a given thickness that separates pore ice from the mineral grains in frozen soil. Therefore, if one assumes, as discussed in the next section, that transport of liquid water through unfrozen water films along particle surfaces is occurring in freezing soils, the hydraulic conductivity of the frozen soil decreases with decreasing temperature in response to decreasing thickness of the unfrozen water films.

1.2.3 Transport of Water in Freezing Soils

1.2.3.1 Moisture Movement through Unfrozen Water Films

From the previous discussion on unfrozen water and suction potential at an ice lens, it seems reasonable to postulate that the unfrozen water is mobile and can migrate through the frozen zone under the action of a temperature induced suction gradient.

Hoekstra and Chamberlain (1964) found that water is transported in frozen silt under electrical gradients, at a temperature of -1.5°C. The test results revealed that a considerable quantity of water moved in frozen soil towards the cathode. The authors noted that in the final state all the ice from the anode region was removed and large bodies of ice were formed in the vicinity of the cathode.

Kudryavcev et al. (1973) did measurements of moisture transfer in frozen soil under temperature gradients. From thermodynamic theory they derived a linear relation between flux density of water and temperature gradient.

Dirksen (1964) found clear evidence of mass transport through a frozen zone underneath an ice lens in an unsaturated sample of New Hampshire silt, under the influence of a temperature gradient. Similar observations were made on Fairbanks silt by Hoekstra (1966). Although vapor transport was possible, Hoekstra concluded from the magnitude of his flux densities that flow was mainly by movement in the liquid water films. He derived a linear relation between flux density and temperature gradient similar to that of Kudryavcev et al. He recognized that film thickness, and so the coefficient of the previous relation, decreases rapidly with temperature below zero.

1.2.3.2 The Frozen Fringe in Freezing Soils

Freden (1965) assumes water transport to the lens to take place through liquid films between ice and mineral matter. In fact he assumes a zone of frozen soil to be present in between the ice lens and the unfrozen soil. Moreover he states that the flow is laminar in that frozen zone.

Freden's (op. cit.) work and the conclusion of Hoekstra (1966) and Dirksen (1964), together with reported discrepancies between measured maximum heaving pressures and those derived from capillary theory (Everett, 1961), led

Miller (1972) to propose that an ice lens in a freezing soil grows somewhere in the frozen zone, slightly behind the frost front (i.e. 0°C isotherm). The temperature at the coldest part of the frozen fringe, i.e. at the base of the ice lens, is referred to here as the segregation-freezing temperature, Ts, because the segregational heaving process takes place at that temperature. The temperature of the warmest part of the frozen fringe corresponds to that at which ice can grow in the soil pores. The Kelvin equation has been applied to give the temperature Ti at which ice, under atmospheric pressure, will propagate through a pore restriction of radius r:

$$Ti = 2To*.5 \text{ iw}/(L.r.pi)\dots\dots\dots\dots\dots\dots\dots\dots\dots\dots\dots 1.10$$

where   pi is the density of ice

   6iw is the ice-water interfacial energy.

In silty soils, the average pore size is relatively large and Ti is close to 0°C. The temperature of the warmest end of the frozen fringe is termed here as the *in-situ* freezing temperature. It is obvious that Ti is affected by other factors such as solute concentration and pressure in both ice and water. If one assumes that solute effects can be neglected and if the pressure in the pore ice is atmospheric, which in the case if no external load is applied and if the self weight of the soil can be neglected, Equation 1.10 is then adequate. Throughout this thesis, the Ts isotherm is referred to as the freezing front and the Ti isotherm is referred to as the frost front in a freezing

soil.

Recently direct experimental evidence for the existence of a frozen fringe beneath an ice lens in a freezing system was obtained by Loch and Kay (1978) and Loch (1979). A dual energy gamma scanning system was employed to locate the position of the growing ice lens relative to the frost front. For New Hampshire silt, Loch and Kay inferred values of the segregation freezing temperature around - 0.3°C ± 0.1°C. For silty clay soils, Loch (1979) inferred from visual observation that the ice lens was growing at approximately -0.4 to -0.6°C. From the previous experimental results, one can readily conclude that Ts is probably soil type dependent.

Finally, Penner and Goodrich(1980) used X-ray photography to locate the position of the growing ice lens in soil under laboratory conditions. For Calgary silt, they measured a negative temperature at the base of the final ice lens of approximately -0.39°C. This is further evidence of the existence of a frozen fringe beneath an ice lens.

1.2.3.3 Moisture Movement to the Freezing Front under a Temperature Gradient

It appears that moisture migration occurs solely in the frozen fringe. Moisture movement in the frozen zone above the ice lens should be significantly reduced due to extremely low unfrozen water contents. Mageau (1978) conducted frost heave tests on uniformly frozen Devon silt to study moisture migration characteristics of frozen soil.

From his tests it was found that moisture can be transported through the unfrozen films under the influence of a temperature gradient. Test results also indicated that the frozen soil above the warmest ice lens has little to no effect on the rate of water intake to that ice lens. The author suggested that the dominant suction pressure develops in the frozen fringe. This statement was deduced from the fact that significant changes in water content were observed in the open system tests with no premade ice lens while very little migration of water appeared to have occurred behind the pre-made ice lens. This is clearly illustrated in Figure 1.4. Furthermore, although regelation probably occurs in the frozen zone behind the ice lens, the process, which is very slow, would only contribute to redistribution of existing water and therefore would not lead to an increase in heave of the sample. Mageau (Op. Cit) concluded that regelation was a secondary phenomenon since the increase in water content behind the pre-made ice lens was almost nil over 20 days of sustained freezing as shown in Figure 1.4. Hoekstra (1969) concluded also that an ice lens acts like a cutoff with regard to water migration.

Recent large scale freezing tests suggest that this proposition, i.e. very little or no flow behind the warmest ice lens, can be extended to field conditions, at least over a period of several years. The results from a test pipeline designed to study *in-situ* frost heave showed that all the heave occurred near the frost front (Slusarchuk et al.,
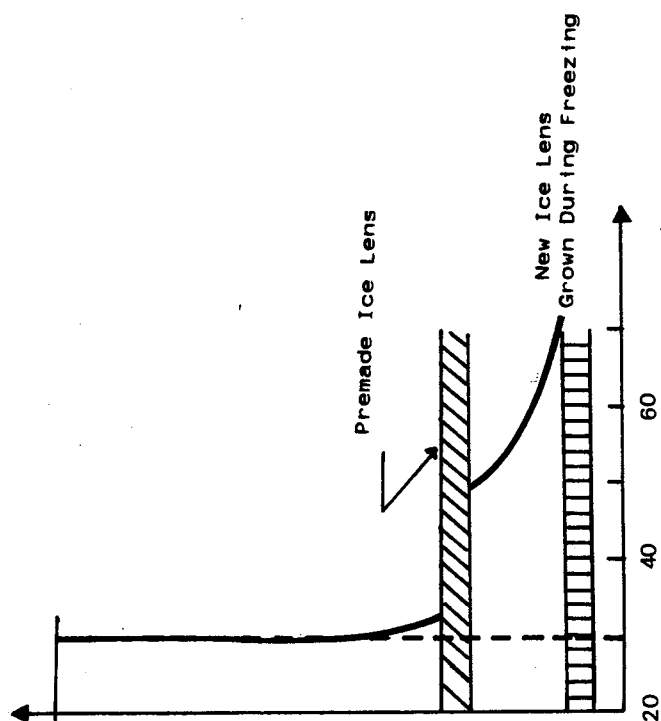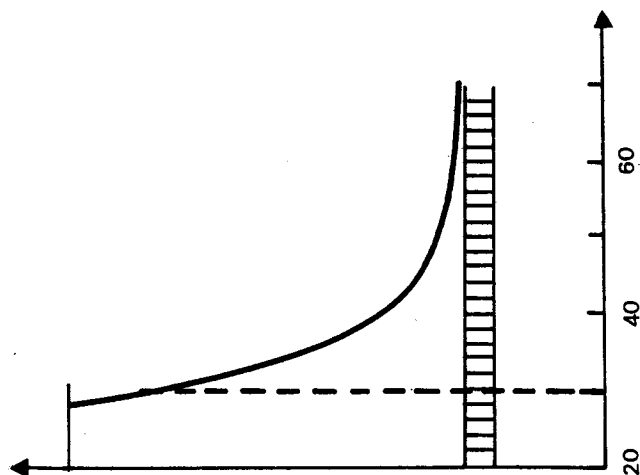
Figure 1.4   Ice Lens as a Cutoff to Water Migration

1978). This was inferred from the fact that heaving probes installed throughout the soil profile did not exhibit any further movement once the frost front had penetrated beyond them.

1.2.4 Permeability of Frozen Soils

In the light of the previous results, it appears that the hydraulic conductivity - water content relationship is the most significant property for predicting the heave behavior of a freezing soil.

Williams and Burt (1974) used a special permeameter for measuring the hydraulic conductivity of frozen soil at various temperatures. In their experiments, frozen soil was positioned between two compartments filled with an aqueous solution of lactose. Lactose concentration was adjusted in order to equalize soil temperature and freezing point of the solution, at least until flow across the sample was induced by pressure differentials between end chambers. Permeabilities based on Darcy's law could then be calculated. The authors found that permeability generally increases as the temperature rises towards $0°C$; commonly observed values being in the range 10^{-6} to 10^{-10} cm/s. A major drawback to their tests was that the membrane pores were too large to prevent lactose molecules from passing through. Thus, one side of the soil became saturated with lactose causing melting of ice in this region. Furthermore, some consolidation could have occurred as a consequence of

this partial thawing. It is believed that the permeabilities given by Williams and Burt are strongly affected by these factors and are most likely too high.

More recently, Horiguchi and Miller (1980) studied moisture transfer in frozen soil with an "ice sandwich" permeameter. The central chamber contains the frozen soil and the end chambers contain pure supercooled water held in that state by porous phase barriers interposed between them and the frozen soil. Measured water flux at a given hydraulic gradient allows one to calculate the permeability using Darcy's law. It must be stressed that the permeability inferred from these tests corresponds to a given temperature and an average pressure in the pore water. Hydraulic conductivity data (shown in Figure 1.5) from two freezing sequences and an intervening thawing sequence showed strong hysteresis effects. The permeability of a 4-8 μm silt fraction frozen soil is found to vary between 10^{-6} and 10^{-10} cm/s at temperatures of $0°C$ to $-0.15°C$. It must be stressed that in the previous testing procedure, equal pressure is applied to both water and ice phases in the frozen soil. This may not necessarily be the case in freezing soils under zero external surcharge.

1.3 SCOPE OF THE THESIS

The development of frost heave during sustained freezing is one of the major impediments to burying a
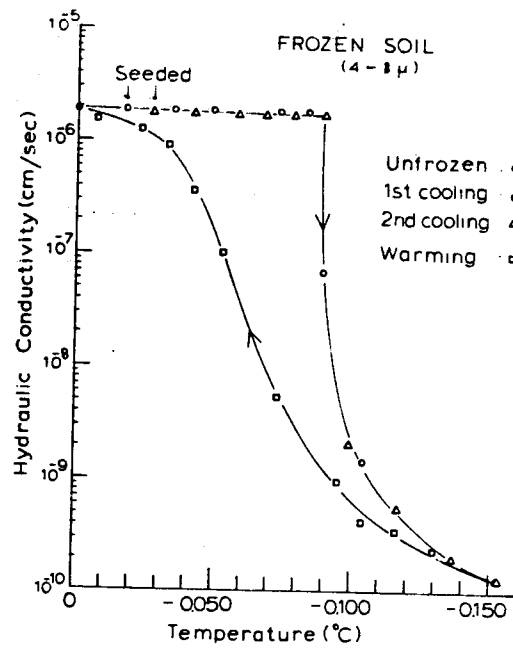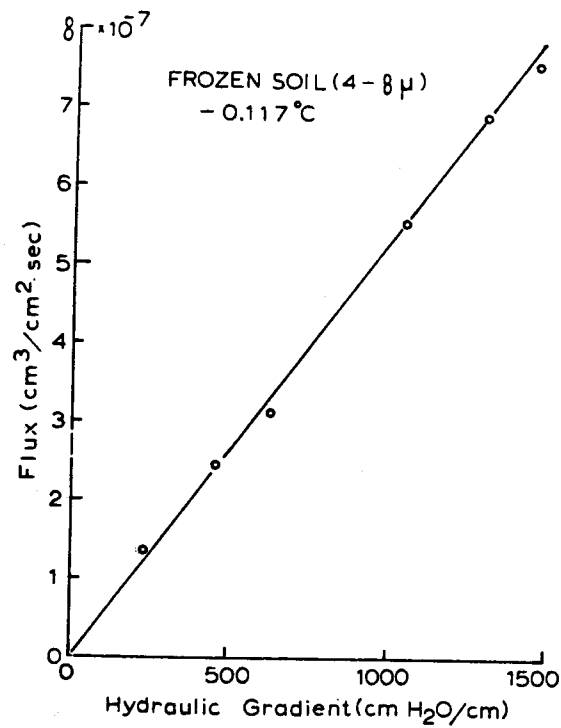
Figure 1.5   Permeability of Frozen Soil.(after Horiguchi and Miller (1980)

chilled gas pipeline in discontinuous permafrost. A comprehensive theory of frost heave should predict rates of heave, cummulative heave, cummulative ice-water contents, rise of heaving pressure, and maximum heaving pressures from a set of equations that incorporate the heat and soil water fluxes induced by prevailing thermal and water content gradients. In addition, the equations should contain one or more parameters to characterize both the freezing soil and the unfrozen soil. Notwithstanding the extensive research carried out on this problem, such a theory is not yet at hand.

The research program of this thesis is aimed at the development of a comprehensive engineering theory of frost heave that will be of value in artic pipeline design. Furthermore, the position is adopted that any theory requiring local measurements of high accuracy such as temperature, unfrozen water content, and permeability of frozen soil cannot result in a theory that will yield practical results. Therefore, this study is directed towards demonstrating that unique frost heave characteristics for soils are deducible from controlled laboratory freezing tests and that these frost heave characteristics constitute input parameters to a general theoretical formulation of simultaneous heat and mass transfer.

Due to the inherent complexity of frost heave physics in freezing soils, distinctions will be made between the processes at work when a frost front is advancing and when

it is held stationary by a continuous ice lens respectively under zero applied load and with different surcharges.

This thesis also extends the results of laboratory freezing tests to some field problems confronting geotechnical engineers at the present, and indicates the manner in which problems involving seasonal freezing might be solved.

Finally, results obtained in the present investigation lead to the development of a new classification system for frost susceptibility of freezing soils.

2. LABORATORY TESTS FOR THE STUDY OF FREEZING SOILS

2.1 DESCRIPTION OF EQUIPMENT

The experimental apparatus utilized in this study is basically a modified oedometer designed for controlled temperature conditions. A schematic diagram of the equipment for a standard freezing test is given in Figure 2.1.

At the beginning of this investigation, one freezing cell was available at the University of Alberta. Details of this cell are given by Mageau (1978). This freezing cell was used to run the first series of tests, i.e. Series S. All the other series were conducted on modified freezing cells described here.

The new experimental set-up has been designed for one dimensional freezing of a soil sample. The freezing cell is therefore placed in a controlled temperature room maintained at a constant temperature of approximately +1°C. However, defrosting cycles, which are necessary to prevent ice build-up on the refrigeration pipes cause slight temperature fluctuations of ±1°C. The use of a cold room helps to minimize radial heat flow into the soil specimen. The freezing cell is a 10 cm I.D. teflon lined cylinder. The outer jacket is machined P.V.C. pipe and provides lateral restraint during application of load. Insulation with a

styrofoam cylinder around the P.V.C. pipe reduces significantly radial heat flow. One freezing cell has a 4 cm thick urethane foam layer around the outer wall of the P.V.C. pipe. The advantage of this type of insulation is that almost no preferential heat flow surfaces are created since the foam is sprayed onto the P.V.C. wall.

The top piston can be used either as a heat sink through which anti-freeze from the cold temperature bath is pumped or as a heat source maintained at a constant temperature above 0°C by forced fluid circulation. Moreover, it can also be used to transmit a pressure to the freezing soil. The applied pressure is obtained by means of a hanger-weight assembly. The piston also allows the measurement of either the amount of heave or the heaving pressure that develops in a constant volume test. It slides freely in the cell since the I.D. is 9.8 cm. To measure the amount of heave, the rod from a displacement transducer (LVDT) mounted on the piston rests on the top of the P.V.C. jacket, so that any movement of the piston is measured by the displacement transducer. This device is accurate to ±0.025 cm. The output (in volts) is recorded on a data acquisition system.

To measure the heaving pressure, a load cell is installed between a rigid frame and the piston.

The bottom plate can be used either as a heat sink or as a heat source depending on the use of the top piston.

The temperatures at the top and bottom plate are

Figure 2.1   Schematic Diagram of Experimental Apparatus

controlled by continuous circulation of an anti-freeze/water mixture. The fluid temperature is maintained by separate Hotpack constant temperature baths. A high rate of pumping, 80 ml/s, minimizes temperature fluctuations at each plate.

During open system freezing tests, i.e. free access of water, the amount of water that goes into or out of the specimen is measured either by a sensitive differential pressure transducer or a volume change device when a back pressure is applied during freezing. In this latter case, the volume change is the only datum that cannot be monitored as an electric signal.

In an open system freezing test with no applied back pressure, the volume change in the burette is calculated from the change in water height monitored continuously by a very sensitive pore pressure transducer. This device was introduced by Mageau (1978) and proved to be reliable. Checks can be made periodically which improves significantly its reliability. The volume change in the burette can be obtained within ±0.1 ml.

A freezing cell was designed to permit the application of a back pressure to the soil sample. Freezing with an applied back pressure to the pore fluid was conducted from the top downwards because the base plate provided good support for the pore pressure transducer as illustrated in Figure 2.2. The bottom seal was an o-ring and groove construction, effective to pressures above 400 kPa.

Thermistors are used for monitoring soil, top and
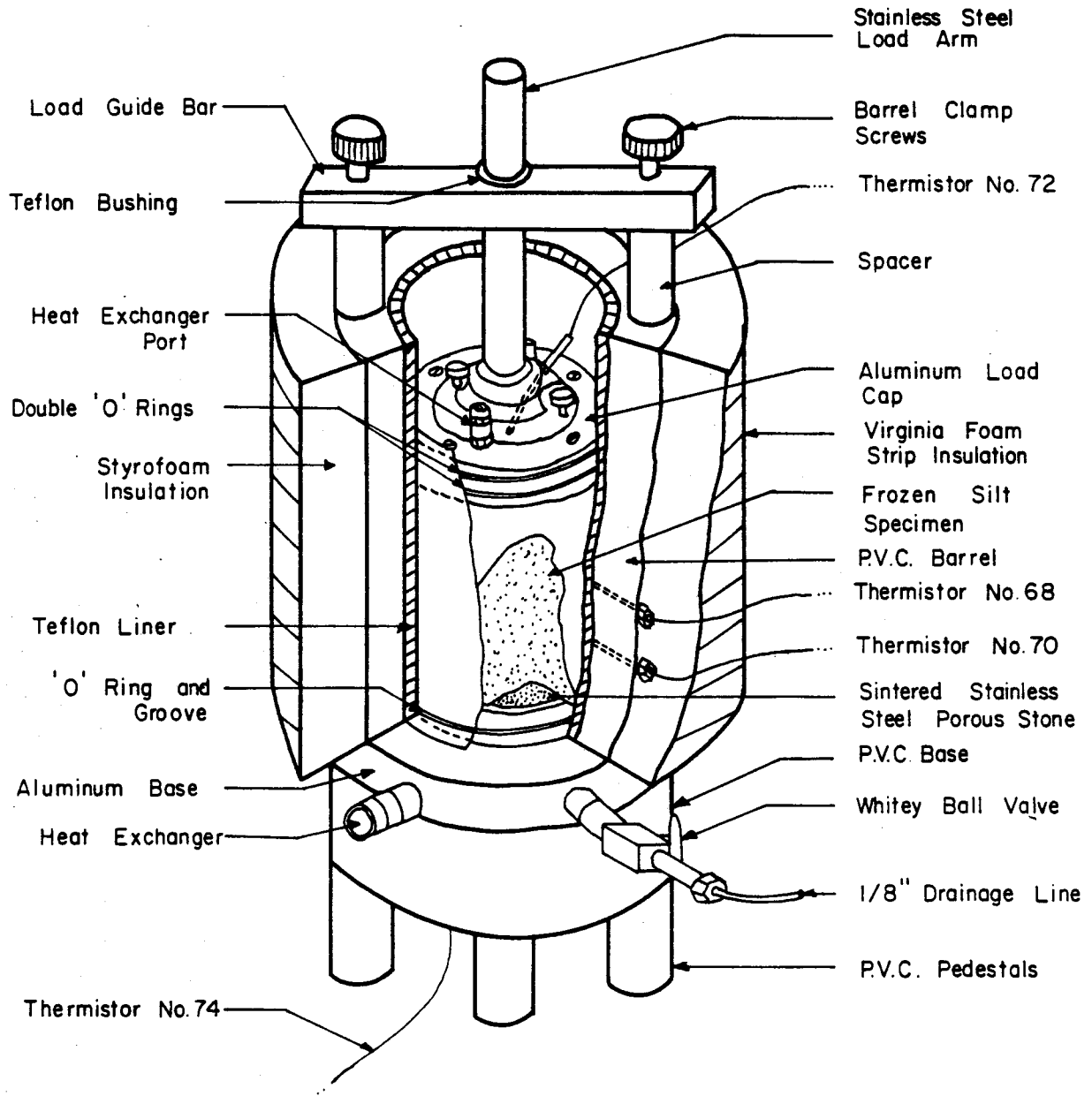
Figure 2.2   Cutaway View of a Freezing Cell

Load Guide Bar

Teflon Bushing

Heat Exchanger Port

Double 'O' Rings

Styrofoam Insulation

Teflon Liner

'O' Ring and Groove

Aluminum Base

Heat Exchanger

Thermistor No. 74

Stainless Steel Load Arm

Barrel Clamp Screws

Thermistor No. 72

Spacer

Aluminum Load Cap

Virginia Foam Strip Insulation

Frozen Silt Specimen

P.V.C. Barrel

Thermistor No. 68

Thermistor No. 70

Sintered Stainless Steel Porous Stone

P.V.C. Base

Whitey Ball Valve

1/8" Drainage Line

P.V.C. Pedestals

University of Alberta

bottom plate temperatures in the four freezing cells. The thermistors were calibrated with a Hewlett-Packard quartz thermometer accurate to 0.001°C. However, due to the inherent difficulties in calibration, it is expected that the temperature measuring system is accurate to only ±0.05°C. In general, four to six thermistors were sealed in the side wall of the cylinders to measure the temperature distribution in the soil specimen.

During the present research a fourth cell with sprayed urethane foam insulation, was equipped with a different type of temperature sensor. Five flat shaped platinium resistance detectors were installed in the side of the freezing cell and one at each heat exchanger plate. The advantages of the platinium resistance temperature detectors (R.T.D.) are a small sensing tip, rapid response time of the thermocouple, and fair precision. The dimensions of the R.T.D's used in this cell are 2.3 x 2.0 x 1.0 mm. The same calibration procedure as for thermistors has been adopted.

Experimental data are collected by means of a Fluke data acquisition system employing a digital voltmeter. The variables (temperature, heave, pore water pressure, heaving pressure, volume change) can be monitored at any selected time interval. The information, in volts, is stored on a cassette tape and is easily processed by computer.

2.2 SAMPLE PREPARATION

Tests were carried out on Devon silt. This material was obtained from two different borrow pits. Series S was conducted using Devon silt from the first location (1976) and all the other tests were performed using the silt from the second borrow pit (1977).

The properties were slightly different and are summarized in Appendix A. This material was chosen for its high frost susceptibility, availability and its similarity to silty materials found in northern regions.

The samples were prepared as a slurry at a moisture content of about 50% to 60% (1.5 times its liquid limit). The slurry, which is a mixture of air-dried silt and deaired-distilled water, is allowed to stand overnight to permit saturation. The mixture is then poured into a vacuum dessicator. A vacuum of approximately 68 cm Hg is applied while vigorously vibrating on a shaking table for about one hour. This procedure removes nearly all entrapped air (Hill, 1977).

Consolidation of the slurry to 210 kPa is performed in three stages in a slightly undersized (9.7 cm I.D) consolidometer. The water content after consolidation averaged between 27 and 30% and was relatively uniform throughout the specimen. Different heights of samples can be obtained depending on the amount of slurry poured in the consolidometer.

After primary consolidation is complete, the height and weight of the sample is determined. The specimen is then placed on the bottom plate of the freezing cell and a cylindrical rubber membrane is put over it. Both, the teflon liner of the two hemispherical parts of the cell and the rubber membrane, are coated with molybdenum powder, a lubricant, in order to reduce skin friction.

The permeability of some unfrozen samples, prior to freezing, was determined with a constant head permeameter at a temperature of about +0.5°C. This temperature corresponds to the average temperature in the unfrozen soil in freezing tests where one end is kept at about +1°C.

2.3 FREEZING TESTS USED IN THE PRESENT STUDY

In general, three types of freezing tests were conducted:

1. Open system freezing tests with constant temperature boundary conditions.

2. Closed system freezing tests with applied back pressure, constant temperature boundary conditions and measurement of the pore pressure change.

3. Open system freezing tests followed by a closed system both with applied back pressure and under fixed temperature boundary conditions and measurement of the pore pressure change in the second phase.

Only one freezing test at constant soil volume during which the heaving pressure was monitored was performed.

Prior to freezing, the temperature in the sample is allowed to equilibrate at a uniform temperature above 0°C. Usually this temperature was approximately +1°C and a uniform distribution was achieved by keeping both boundary plates at +1°C.

Nucleation of ice crystals at one end of the sample is accomplished by imposing a negative step temperature on the soil surface. This is achieved by the circulation of a precooled liquid through the heat exchange maze. While the step temperature is maintained constant during freezing, the other extremity of the specimen is also maintained at a constant temperature above 0°C. These thermal conditions result in a penetrating frost front phase followed by the formation of a final ice lens with a quasi stationary frost front. Thus, these freezing tests create a period of decelerating frost penetration followed by a period of stationary frost front during which a major ice lens can grow somewhere within the sample.

Some specimens were frozen in several stages by varying the temperatures at both plates at the end of each phase. This procedure results then in the formation of several major ice lenses, separated by an appreciable thickness of frozen soil.

Two closed system freezing tests with applied back pressure under different vertical loadings were conducted in

a modified triaxial cell (Appendix A).

2.4 COLLECTION OF DATA AT THE END OF A FREEZING TEST

Upon completion of a freezing test, the sample is again weighed and its final height is measured. This allows a check on the amount of water drawn into the sample measured from the burette and of the amount of total heave obtained from the LVDT readings.

The thickness of the different zones in the specimen are also measured on the periphery. In the frozen part, it was decided to distinguish between a frozen zone with no visible ice, a zone of active lensing, and the final ice lens. The remainder of the sample is essentially unfrozen soil. Photographs were taken to record the structure of the frozen sample.

The specimen was then cut in two parts along a longitudinal axis. The position of the final ice lens is carefully determined from one part. Another important measurement is the accurate determination of the thickness of the final ice lens. This allows one to back calculate exactly the time of it's formation using the measured total heave - time relationship. One can also verify if all the water entering into the soil flows to the base of the ice lens.

The longitudinal section of the sample also provides useful information on the amount of radial heat flow that

occurred during the freezing test. If radial heat flow is negligible, the ice structure should be parallel to horizontal planes since the 0°C isotherm penetrates horizontally downwards in one dimensional freezing. Radial heat flow, on the other hand, will produce slightly curved ice lenses, since the temperature along the sides of the sample will be warmer than that within the specimen in a given horizontal plane. Photographs were also taken of this longitudinal section.

The second half of the sample is cut into slices with a band saw kept in a cold room at -5°C. The thickness of the slices varied dependent on the ice structure. In the zone of active lensing, slices of about 4 mm thick could be cut. The position of each slice is determined and then the small soil portion is weighed and ovendried (105°C) to determine its water content.

2.5 SPECIAL FREEZING TEST TO EVALUATE THE SEGREGATION FREEZING TEMPERATURE

2.5.1 Theoretical Analysis

The aim of the third category of freezing tests is to assess as close as possible the value of the segregation freezing temperature at the formation of the final ice lens in a freezing soil with zero overburden. This can be done by measuring the drop of the pore water pressure and by relating the magnitude of the water pressure change to

temperature through the Clausius-Clapeyron equation. The next paragraph establishes, firstly, that a conventional freezing test can be simulated by a freezing test with an applied back pressure provided that the temperature boundary conditions are identical. Then the analysis of such tests in order to ascertain the value of Ts at the formation of the final ice lens is given.

As demonstrated by the Clausius-Clapeyron equation, high suctions are generated at the base of an ice lens. For example, if the temperature at the base of an ice lens is -0.10°C, a suction of -125 kPa is created. Unfortunately such high suctions cannot, at present, be measured directly. However, Equation 1.2 reveals that an equal change in the free energy in both ice and water will not alter thermodynamic equilibrium at the ice lens. Therefore, the conditions at an ice lens obtained during an open-system test with zero overburden will be similar to those obtained in a freezing test with an applied back pressure, provided that the applied vertical pressure on the sample produces an equal change in the free energy in the ice phase. For isothermal conditions, i.e. dT = 0, the change in free energy of the water is D(Pw.Vw) whereas the change in free energy in the bulk ice is D(Pe.Vi). The equality in the free energy changes requires then a change in external pressure of (Vw/Vi)DPw, which is approximately 92% of the applied back pressure. Equation 1.6 can be rewritten as

$$Pb + Pw = (L/Vw) \ln Ts*/To* + (Vi/Vw)(Pi + Vw.Pb/Vi).2.1$$

where   Pb is the applied back pressure

For the case of zero applied surcharge, Pi = 0 Equation 2.1 reduces to:

$$Pb + Pw = (L/Vw) \ln Ts*/To* + Pb\dots\dots\dots\dots 2.2$$

where   Pb+Pw is the measured drop in pore pressure

2.5.2 Experimental Evidence

In order to verify the previous statement, two identical samples were frozen under the same thermal boundary conditions respectively with zero surcharge and free access of water and with an applied back pressure and vertical load. The samples were preconsolidated to 210 kPa and were 7 cm high. The cold plate and the warm plate in each freezing cell were connected to the same temperature bath. This procedure ensured identical temperature conditions during freezing of both samples. Specimen G1 was frozen from the bottom upwards with free water supply at its top. No external pressure was applied. Sample G2 was stressed to 110 kPa by means of a dead load and a back pressure of 120 kPa was applied to the water reservoir.

Unfortunately, the cold temperature bath warmed up and had to be replaced after 500 minutes of testing. This influenced significantly the temperature gradient in the frozen zone as well as the rate of frost penetration. However, the temperature change was identical in both samples and their response to these most unusual freezing conditions was very similar as shown in Figure 2.3. Because

freezing was initiated in sample G2 15 minutes after it began in specimen G1, the total heave curves are different by a constant amount equal to the total heave that occurred in sample G1 during the first 15 minutes. Both curves show clearly that the total heave rate is fairly identical for the same period of freezing.

After 700 minutes, the water intake line of test G2 froze due to its proximity to the refrigeration system in the cold room.

Despite those unfortunate events, the tests demonstrate clearly that a conventional freezing test with zero overburden can be simulated by a freezing test with an applied back pressure provided that an external pressure equal to 92% of the back pressure, is applied to the sample.

2.5.3 Determination of the Segregation Freezing Temperature

When a back pressure is applied, the waterline is closed as the final ice lens is initiated. The change in pore water pressure is then monitored. The pore pressure transducer is situated at the base of the unfrozen soil and measures therefore the change in the pore water pressure of the unfrozen soil. Initially the pore pressure is equal to the existing back pressure. However, since a suction potential exists at the ice lens, and because the system is closed, equalization of pore pressures will occur with time. This phenomenon can be visualized by the steady drop in the pore pressure recorded by the transducer with time. This
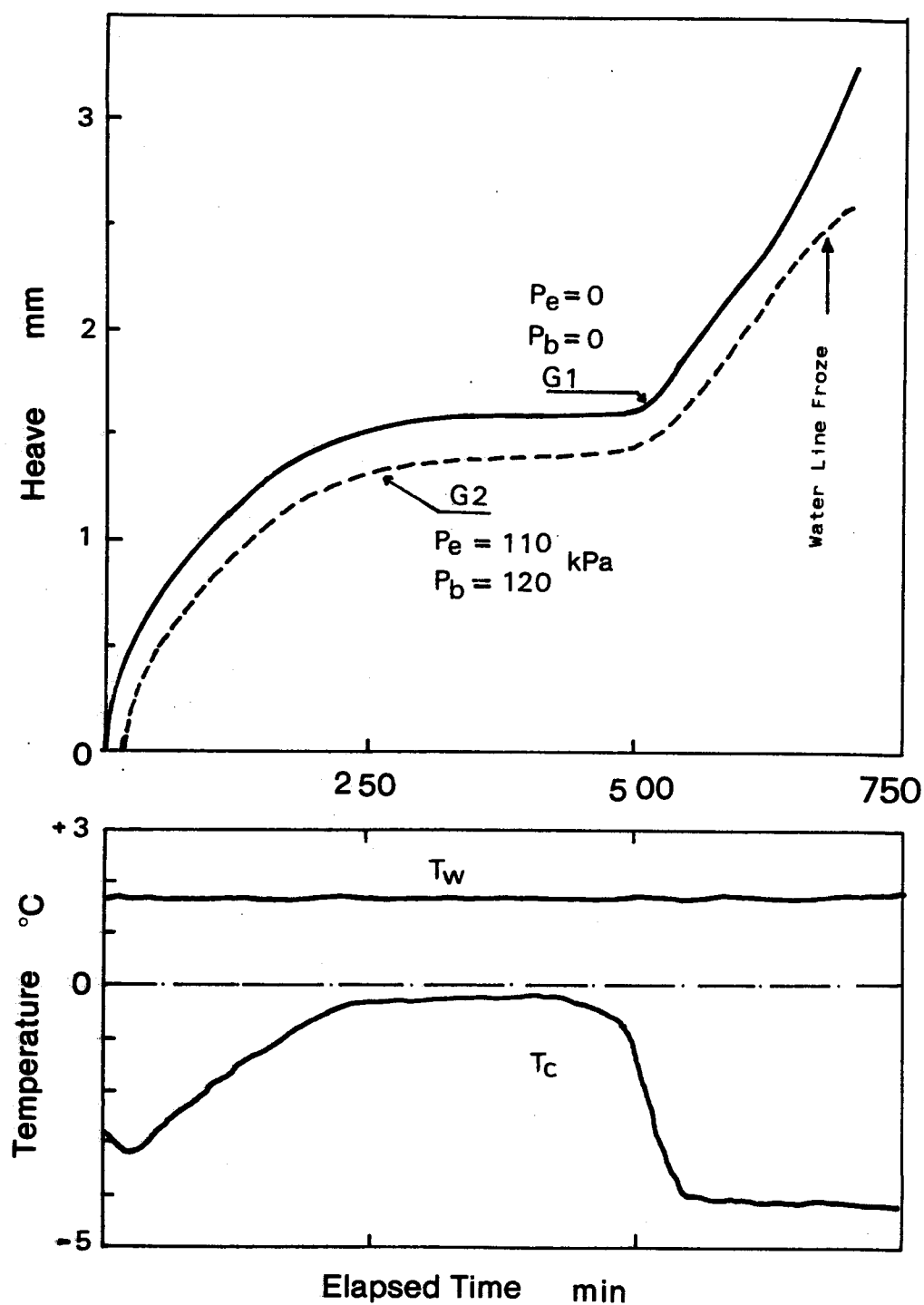
Figure 2.3 Comparison Between Freezing with Zero Applied
Load and with an Applied Back Pressure

change in pore pressure is accompanied by a consolidation process in the unfrozen soil. The excess water migrates to the ice lens where it freezes. Equilibrium is reached when the pore pressure in the unfrozen soil is equal to that existing beneath the ice lens. This is illustrated in Figure 2.4.

The maximum drop in pore pressure is then equal to the suction that is generated beneath an ice lens in conventional test with the same thermal conditions. As seen previously, one can relate the maximum drop in pore pressure to the temperature at the ice lens by virtue of the Clausius-Clapeyron equation. However, it is clear that the temperature deduced by this procedure corresponds solely to the final state of the closed system phase of the freezing test with applied back pressure. In order to evaluate the temperature existing at the onset of the formation of the final ice lens, the following approach can be considered.

Figure 2.5 illustrates the conditions prevailing in the specimen at the beginning and the end of the closed system freezing phase. When the water line is closed, penetration of the frost front results due to the loss of heat generation at the ice lens, e.g. (Vo.L). This further advance of the 0°C isotherm chills the ice lens as shown in Figure 2.5. When the system reaches equilibrium the temperature conditions in the sample can be approximated by two straight lines whose slopes are a function of temperature and geometrical boundary conditions as well as

of the thermal properties of the frozen and unfrozen soil.

At the end of a freezing test, lo and Xo may be measured directly. Thermistor readings provide the temperatures at both ends, i.e. Tw and Tc. Finally, Tm is inferred from the measured drop in pore water pressure. The water intake flux, before the waterline is closed, is also easily obtained during testing.

Thermal balance before the system is closed is given by:

$$kf.grad\ Tf = ku.grad\ Tu + Vo.L \dots\dots\dots\dots\dots 2.3$$

Equation 2.3 can be recast as:

$$kf.grad\ Tf = (ku + A)\ grad\ Tu \dots\dots\dots\dots 2.4$$

where $A = Vo.L/grad\ Tu$

The ratio of the temperature gradients is then easily obtained as:

$$grad\ Tf/grad\ Tu = ku/kf + A/kf = B \dots\dots\dots 2.5$$

Thermal balance at the end of the closed system phase is expressed by:

$$ku/kf = (Tw/|Tc|)(Xo+d)/(lo-d) \dots\dots\dots\dots 2.6$$

where $d = Xo.Tm/|Tc-Tm|$

Substitution of the value of ku/kf and of kf, calculated from equation 2.6 assuming a known value of ku, in Equation 2.5 results in the value of B, which is the ratio of the temperature gradients. This latter can also be obtained from the following equation, deducible from the temperature profile in the sample before closed system freezing:

Figure 2.4   Pore Pressure Profile in Conventional Freezing and Freezing with Applied Back Pressure

Figure 2.5 Conditions Existing in the Sample at Different Stades in a Freezing Test with Applied Back Pressure

$$\text{grad } Tf/\text{grad } Tu = (|Tc-Ts|/Xo)/((|Ts|+Tw)/lo)....2.7$$

Substitution of the first term of Equation 2.7 by B results in

$$Ts = (lo.|Tc| - B.Xo.Tw)/(lo+B.Xo)................2.8$$

It should be emphasized that, due to the inherent high sensitivity of suction to small temperature change at the ice lens, these tests provide a range of possible temperatures at the ice lens. Nevertheless, it is thought to be a valuable method of indirect measurement of the segregation freezing temperature for quasi-steady state conditions. This temperature is warmer than the temperature inferred from the maximum drop in pore pressure at the end of the previous type of freezing test.

2.6 QUALITATIVE INVESTIGATION OF A FREEZING SOIL

The general aim of the first test series was to assess, from a qualitative point of view, the behavior of a freezing soil, in order to determine the parameters that affect significantly frost heave, to verify some fundamental assumptions found in the literature, and to test if the freezing procedures used yield adequate information.

As discussed in Chapter 1, one of the most important contibutions to a comprehensive understanding of frost heave in soils has been made by Miller (1972) who suggested that water is able to accumulate and freeze somewhere within the frozen soil, behind the 0°C isotherm. The frozen zone

between that accumulation zone and the unfrozen soil has been referred to as the frozen fringe.

Another very important contribution was made by Vignes and Dijkema (1974). They established that the temperature at the base of the ice lens is a fundamental parameter in a freezing system. In their experiments, the rate of heaving is directly proportional to this temperature.

2.6.1 Effect of Ice Lens Temperature

These new developments in frost heave research suggest that the temperature at the base of the warmest ice lens in a freezing soil should also be a basic parameter in frost heave. In order to verify this statement the following test was conducted. A 5.6 cm high Devon silt sample was frozen with a back pressure of 200 kPa. The temperature conditions were such that the final ice lens grew somewhere in the middle of the specimen. When the final ice lens was initiated after approximately 5 hours, the water line was closed for about 8 minutes. It was closed two more times during the growth of the final ice lens for about 20 minutes after 18 hours and 65 hours. As illustrated on Figure 2.6, the temperatures at both ends were fairly constant during that freezing phase. However, it was noticed that the heaving rate decreased steadily with time during the growth of the final ice lens. After 65 hours of freezing, the heaving rate was very small.

Since the heave rate is thought to be related to the

suction at the ice lens, the author took the view that the suction at the ice lens also decreased with time. This is realistic since the temperature boundary conditions are constant while the sample continues to heave due to the thickening of the final ice lens. This, in turn, produces a change in the temperature profile across the specimen and it can readily be shown that an open system freezing test in which the length of the sample increases continually with time is associated with a warming of the base of the final ice lens, which position remains constant. According to the Clausius-Clapeyron equation a concomittant decrease in suction then results.

The same line of thought will predict dramatic increases in heave rate if the temperature at the base of the ice lens becomes colder. This can be achieved by slightly lowering the warm plate temperature. The temperature profile changes and the temperature of the existing ice lens cools as illustrated in Figure 2.7. As expected, the heave rate changes substantially as shown in Figure 2.6. Moreover, since the temperature at the ice lens decreased, a higher suction induces a much higher heave rate.

This operation was repeated after 96 hours and the same phenomenon was observed.

2.6.2 Existence of a Frozen Fringe

The drop in pore pressure recorded during the previous
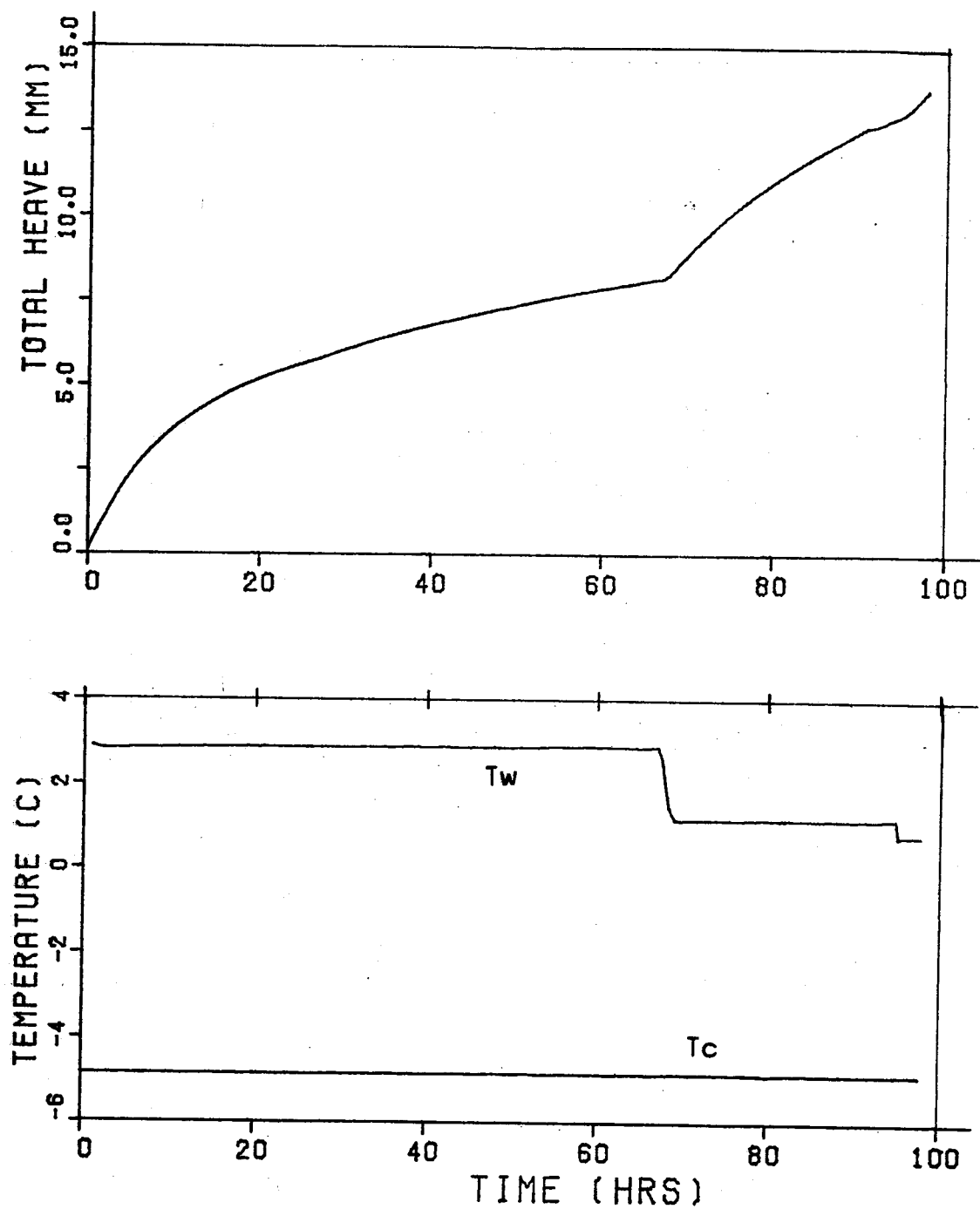
Figure 2.6   Influence of Ice Lens Temperature
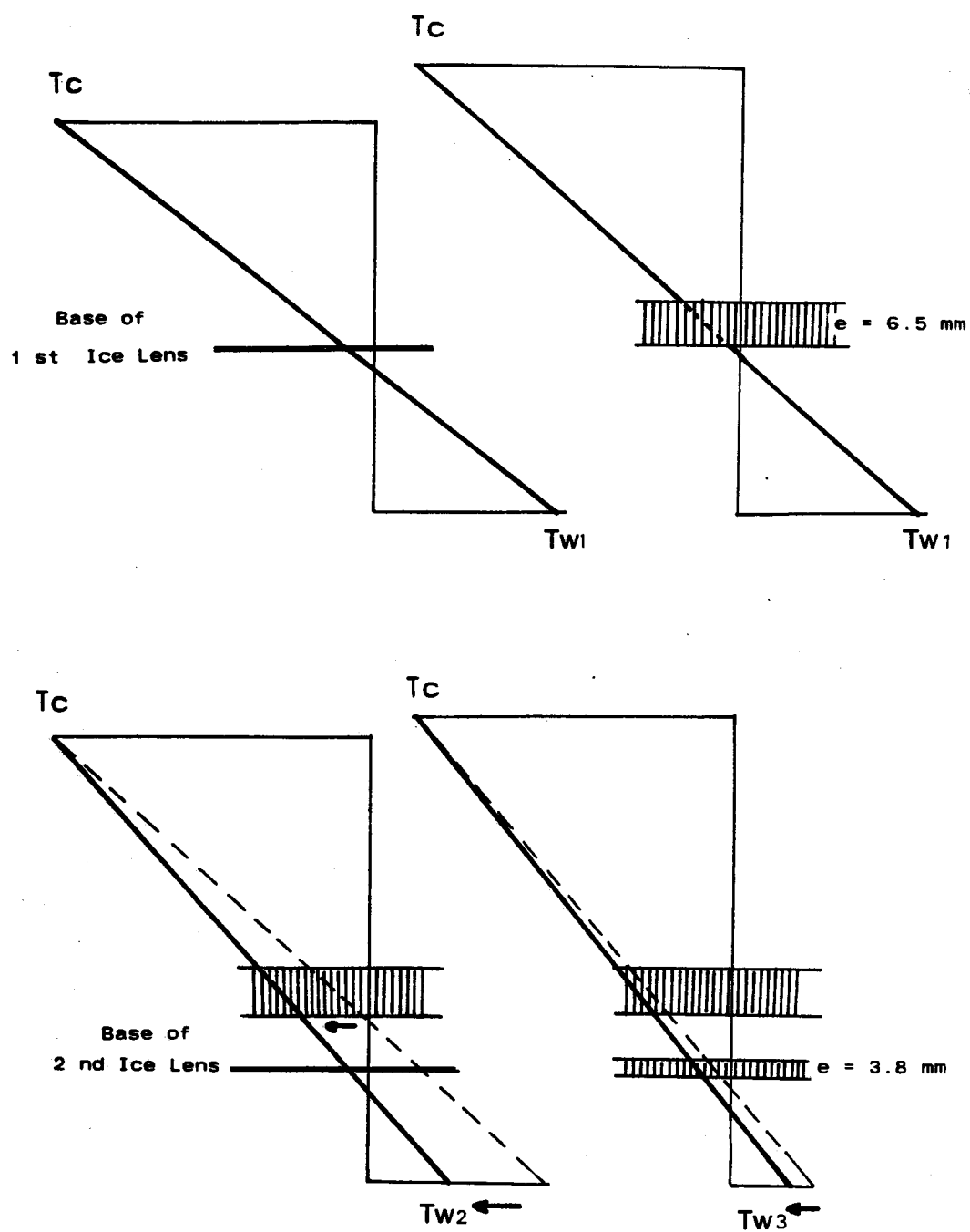
Figure 2.7   Temperature Conditions Existing in Sample S1 at
Different Stades

test as the water line was closed suggests that the suction at the ice lens is relatively high, approximately -50 to -100 kPa. These results were extrapolated since the system did not reach equilibrium during the short closed system freezing period. The results are given in detail in Chapter 5. Nevertheless, the magnitude of these suctions establish that the temperature at which the ice lens is created is lower than that at which the ice penetrates into a pore, i.e. Ti. For a temperature equal to Ti, one should expect suctions of the order of -10 kPa for Devon silt, which is approximately one order of magnitude smaller than the measured suctions. The previous results, therefore, confirm the plausibility of the existence of a frozen fringe beneath the final ice lens.

2.6.3 Rate of Heaving During the Growth of the Final Ice Lens

Test S1 revealed that the rate of heaving decreases continually with time during the growth of the final ice lens. In order to gain more insight, test S4 was run for a long period, of about 200 hours. Sample S4 was frozen with free access of water and fixed temperature boundary conditions. The results are presented in Figure 2.8 and confirm that the heave rate decreases with time and that the total heave reaches an ultimate value in these type of freezing tests.

2.6.4 Influence of Temperature Gradient

Test S5 indicates that there is no simple relation between the heave rate and the temperature gradient. This can be inferred from the results of a multistage freezing test. As illustrated in Figure 2.9, when the temperature gradient is changed from 1.4°C/cm to 0.5°C/cm, after 48 hours of freezing, no significant change in the heaving rate is noticed. However, a second change in the temperature gradient to 1.35°C/cm after 96 hours of freezing produces a dramatic change in the heaving rate.

2.6.5 Ice Structure in Freezing Soils

Test S7 was conducted on a 7 cm high sample with a relatively high cold plate temperature of about -2.8°C. The warm plate temperature was around +0.4°C. This resulted in a small heat extraction rate and the characteristic ice structure of freezing soils could develop fully as illustrated in Figure 2.10. This enables one to identify clearly the different zones in the frozen sample as described earlier, in section 2.5.

2.7 CONCLUSIONS FROM THE PRELIMINARY TESTING PROGRAM

From the previous data it appears realistic to assume the existence of a frozen fringe through which water is able to flow. Also, the results established by Vignes and Dijkema (1974) and Biermans et al (1978) for an ice lens created either on a quartz substrate or a glass substrate can be
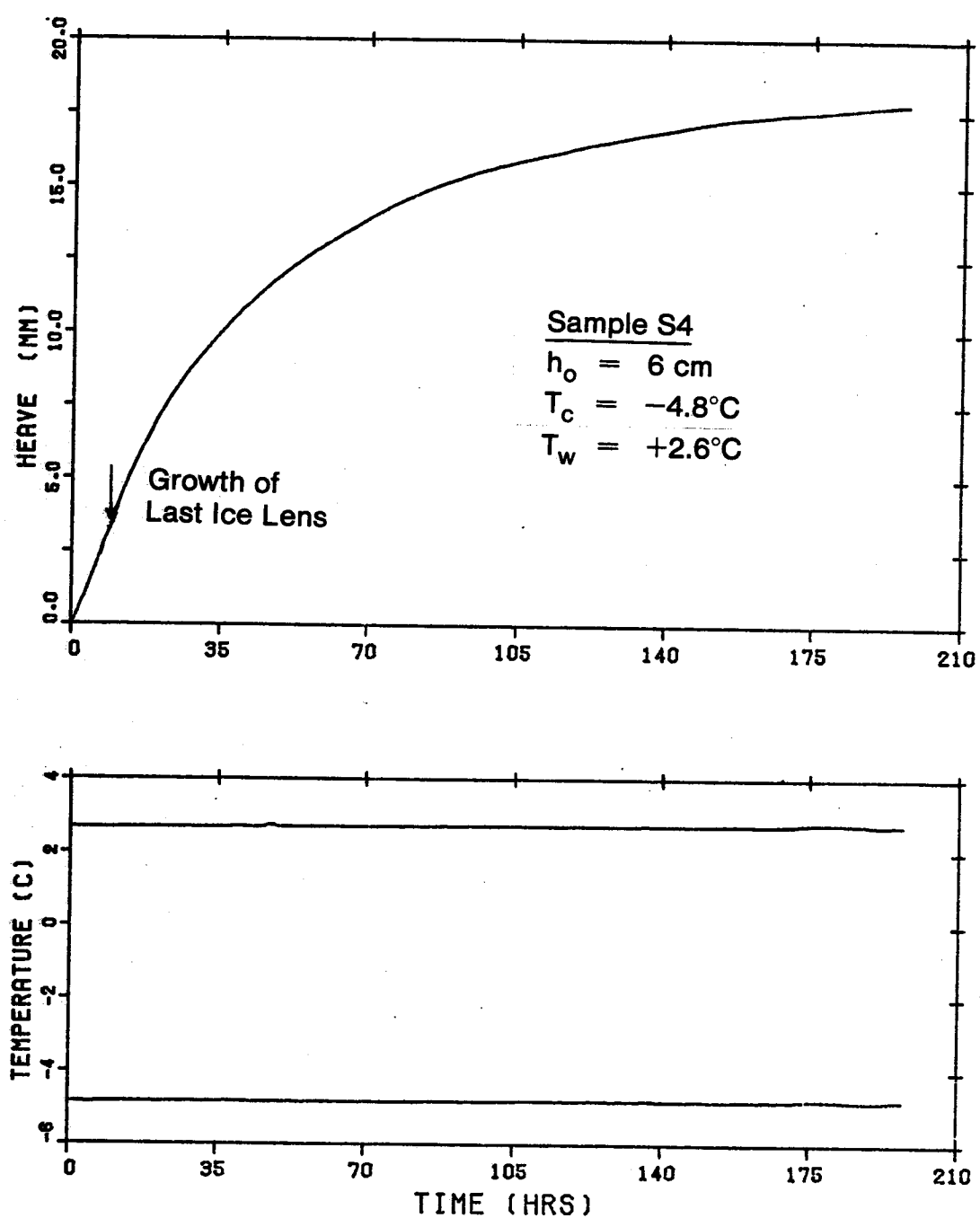
Figure 2.8   Sustained Freezing with Fixed Temperature
Boundary Conditions. Test S-4
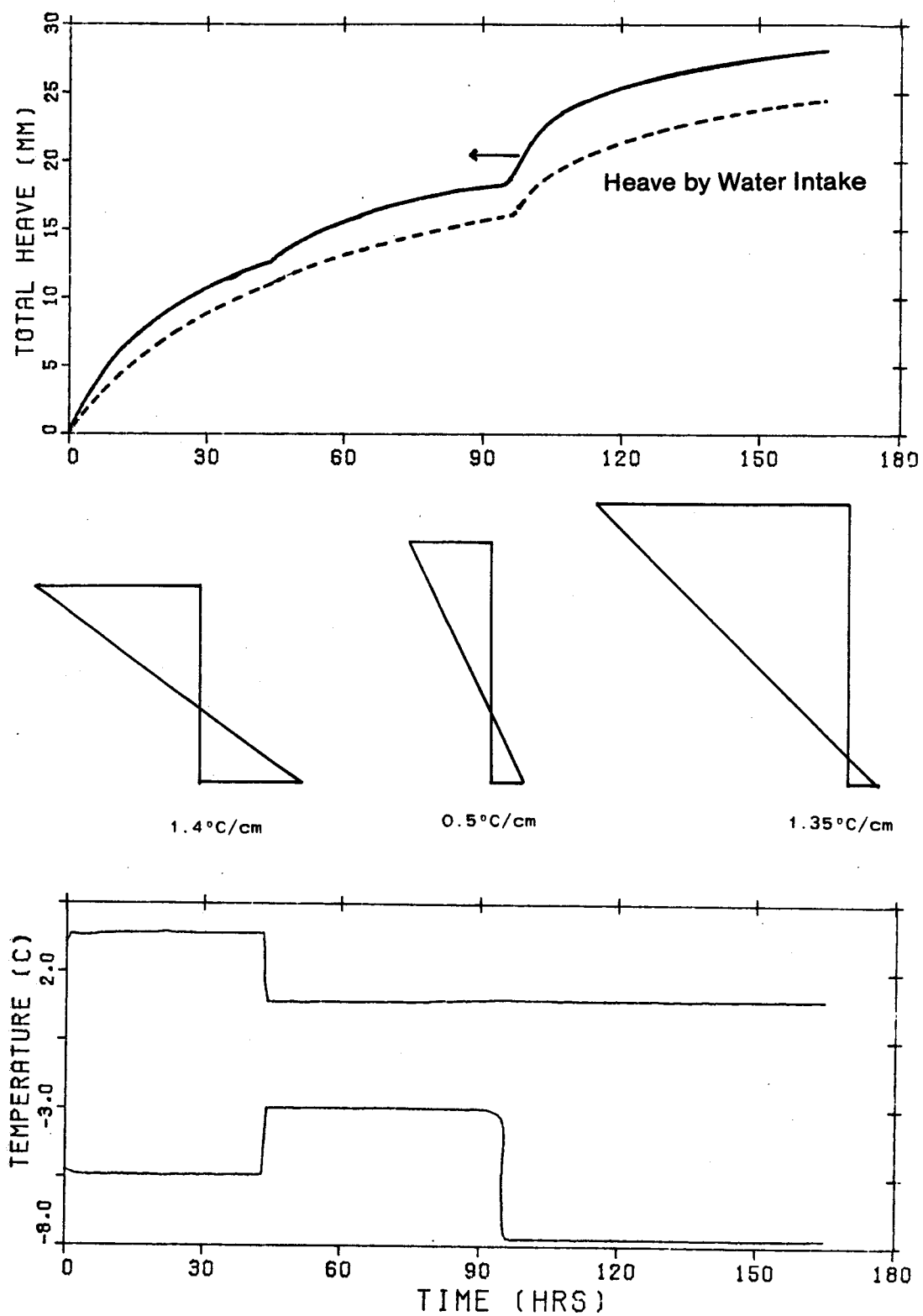
Figure 2.9 Influence of Temperature Gradient. Test S-5

Figure 2.10 Typical Results at the End of an Open System
Freezing Test. Test S-7
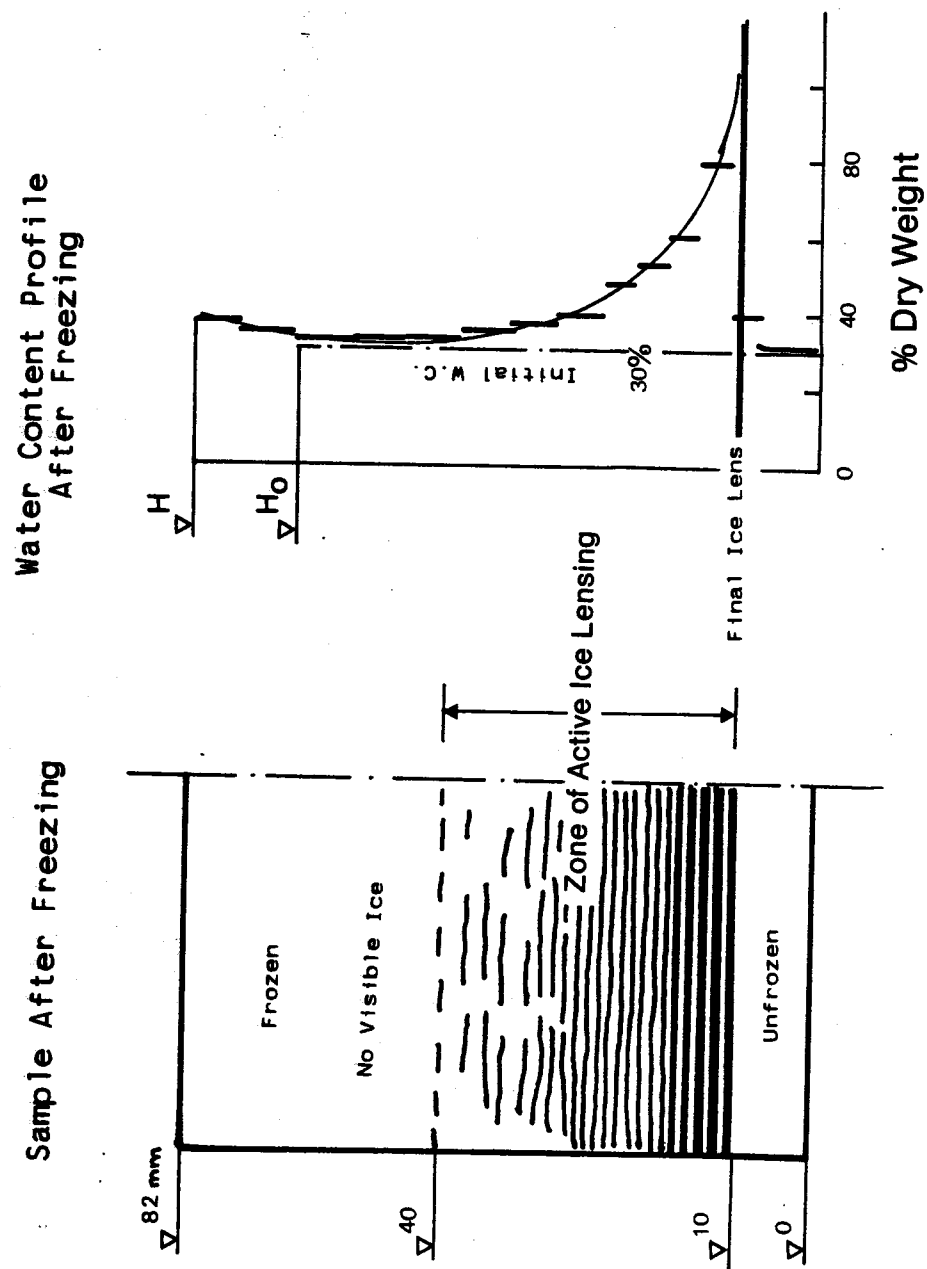
extended to an ice lens that forms in freezing soils. As a consequence, the author decided that these two basic propositions, i.e. the existence of a frozen fringe in any freezing soil and the validity of the Clausius-Clapeyron equation at the base of any discrete ice lens, should be the two special considerations in a comprehensive frost heave theory.

Recalling the results established in Chapter 1, the whole system can be separated into a passive one defined as the frozen soil between the temperatures Tc and Ts and an active system composed of the frozen fringe and the unfrozen soil. In the passive system moisture transfer is strongly reduced due to very low frozen soil permeabilities and the contribution to the final heave has been found to be negligible under both laboratory conditions and under field conditions, at least over a period of several years. This representation of the freezing soil will be used throughout this thesis and is illustrated in Figure 2.11.

From the previous tests, it appears to be of value to separate a freezing situation into two distinct phases.

The initial phase during a freezing test is characterized by an advancing frost front during the whole transient heat flow period. The second phase coincides with the growth of the final ice lens under fixed temperature boundary conditions. Because the temperature at the base of the ice lens is thought to warm up with time during this latter phase, it is referred to here as a retreating frost
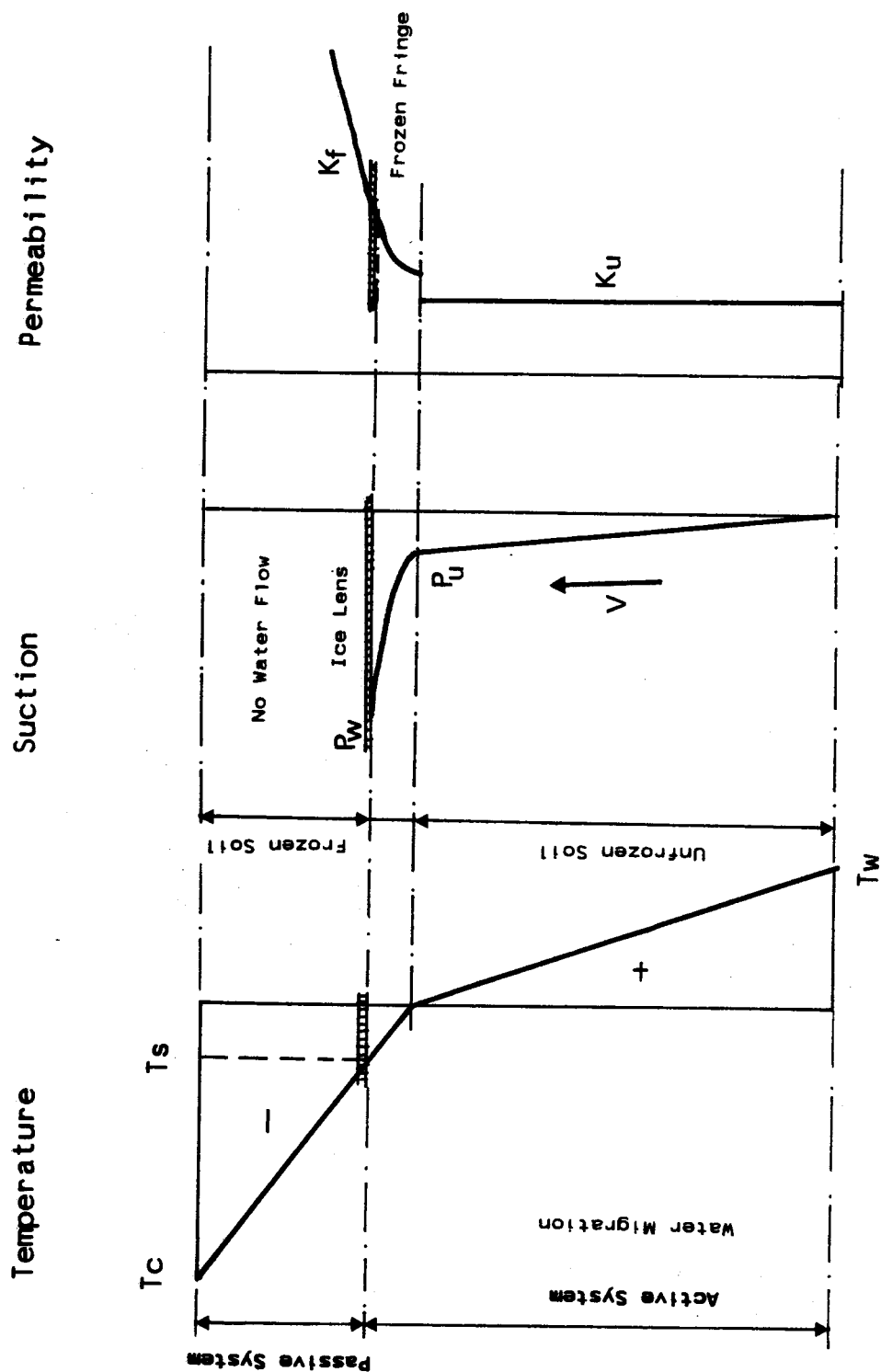
Figure 2.11 Schematic Representation of a Freezing Soil

front.

Under certain conditions, for example variable temperatures at the boundaries, a stationary frost front can be obtained when the net heat extraction rate is zero.

The experimental results obtained in the present study will be presented and discussed in the following manner:

Chapter 3 establishes the governing equations of an engineering frost heave theory. This theory is then applied to a freezing soil at the onset of the formation of the final ice lens. Special consideration is given to the physical overall properties of the frozen fringe developed under zero externally applied load. Experimental results are presented that support theoretical propositions and demonstrate that unique frost heave parameters for a given soil exist for these freezing conditions.

In the light of the results reported in Chapter 3, Chapter 4 presents a critical review of existing frost heave models. The freezing parameters, defined at the formation of the final ice lens, are extended to the transient freezing period. These parameters are then used as input to the general frost heave model and the predictions are compared with actual laboratory data.

Chapter 5 establishes the governing equation holding in the retreating frost front phase. A model for this situation is also presented and predictions are compared with actual laboratory data. A summary of the results of Chapter 3, 4 and 5 are presented as a mechanistic theory of rhythmic ice

lens formation in fine grained soils.

Chapter 6 extends the previous results, obtained for zero applied load, to the more general situation where external surcharges are applied in freezing soils.

Chapter 7 analyses in the light of the results presented in this thesis the interpretation of laboratory freezing tests found in the literature. A standard freezing tests which assesses easily the basic freezing parameters is also presented.

Chapter 8 summarizes schematically the freezing behavior of different soils and presents two new frost susceptibility criteria.

Finally, Chapter 9 extends the results established under laboratory freezing conditions to field problems. A model to calculate the amount of heave under a chilled pipeline is given. The essential conclusions of this study are summarized in a simple method for predicting frost heave in any situation.

3. THE CHARACTERISTICS OF A FREEZING SOIL AT THE ONSET OF THE FORMATION OF THE FINAL ICE LENS

3.1 INTRODUCTION

In the previous chapter three distinct phases of frost heave have been recognized; an advancing frost front created by a positive net heat extraction rate, a stationary frost front corresponding to a zero net heat extraction rate and a retreating frost front state in which the frozen fringe below the final ice lens thaws. This latter condition always arises when temperature boundary conditions are constant with time.

Freezing tests where temperature boundary conditions are constant with time lead invariably to the formation of a final ice lens in a position which is a function of the temperature profile across the sample. This final ice lens is initiated as the temperatures reach a distribution close to steady state conditions.

It is proposed to analyse a freezing soil at the onset of the formation of the final ice lens, which is a simplified case of frost heave with the effect of frost penetration almost eliminated. A simple model is presented for water transport to an ice lens through a porous medium composed of a layer of unfrozen soil overlain by a thin zone

of frozen soil, referred to herein as the frozen fringe.

In addition, the position is adopted that any theory requiring local highly accurate measurements of temperature, unfrozen water content or permeability of frozen soil cannot result in a theory that will yield practical solutions.

Therefore this study is directed towards demonstrating that unique frost heave characteristics in soils are deducible from controlled laboratory freezing tests. Furthermore, these laboratory frost heave characteristics constitute input parameters to a more general theoretical formulation involving coupled heat and mass transfer.

3.2 MASS AND HEAT TRANSFER IN FREEZING SOIL

3.2.1 Mass Transfer

As demonstrated in Chapters 1 and 2, frost heave can be treated as a problem of impeded drainage to an ice lens. Suction is generated at the ice-water interface and causes water to flow to the base of the ice lens. However, the amount of water that can flow to this interface is moderated by a thin zone of low permeability frozen soil that lies between the ice lens and the unfrozen soil. Adopting the view that the water transport is occurring in the films of unfrozen water in the frozen fringe, Darcy's law may then be used to represent the relationship between the flow rate of water and the appropriate driving potential. The general formation for the case of one dimensional flow can be

expressed as:

$$d[K(z) \, dH/dz]/dz = dW/dt \dots\dots\dots\dots\dots 3.1$$

where   H is the potential

             K is the permeability

             dW/dt represents water accumulation (positive or negative)

Equation 3.1 can be reduced to a form involving the velocity of water flow to the ice lens by assuming that the unfrozen soil is saturated and incompressible and that water flows through the frozen fringe to the base of the ice lens where it then freezes. The reduced version of Equation 3.1 is given as Equation 3.2 which demonstrates that the average flow rate through the active system is proportional to the potential gradient:

$$v = -K(z) \, dH/dz \dots\dots\dots\dots\dots\dots 3.2$$

Within the frozen fringe, the driving potential is related to pressure in the ice (atmospheric for the case of zero surcharge), the temperature and the permeability of the frozen soil. This rather complex interaction will be investigated fully in Section 3.5. Recent studies by Vignes and Dijkema (1974) and Biermans et al (1978) establish that below a discrete ice lens under zero external load the suction potential is related solely to the temperature by virtue of the Clausius-Clapeyron equation. In soils, the segregation – freezing temperature $Ts*$ is generally very close to $To*$ and $\ln(Ts*/To*) = (Ts*-To*)/To*$. If no external pressure is applied and if the self weight of the soil can

be neglected, Equation 1.6 reduces to

$$Pw = L(Ts*-To*)/(Vw.To*) = M.Ts \dots\dots\dots 3.3$$

where   Ts*-To* represents the negative temperature at

the base of the ice lens in degrees Celsius.

M is a constant equal to L/Vw.To*

Dissolved salts are not considered in this Equation.
Equation 3.3 establishes that for temperature close to 0°C,
there is a linear relationship between suction and negative
temperature of the water film beneath the ice lens.

In terms of total potential, Equation 3.3 becomes:

$$Hw = Pw/\gamma w + Z \dots\dots\dots\dots 3.4$$

where γw is the unit weight of water

Z is the elevation head.

In most laboratory situations the gravity head part of the
potential can be neglected:

$$Hw = Pw/\gamma w = M.Ts/\gamma w = M'.Ts \dots\dots\dots 3.5$$

The total potential, Hw, is negative due to values of Ts
below 0°C and it is therefore convenient to refer to Hw as a
suction potential. Flow of water towards the ice lens is
caused by the difference in total potential between the base
of the sample, where it is usually zero or positive, and the
base of the ice lens. Considering a two layered system
consisting of the unfrozen soil and the frozen fringe, the
mean flow rate of water towards the base of the ice lens
assuming zero pressure at the base of the sample is given
by:

$$V = |Hw|/(lu/Ku + d/Kf) \dots\dots\dots 3.6$$

where   lu is the unfrozen soil thickness

Ku is the unfrozen soil permeability

d is the frozen fringe thickness

Kf is the overall permeability of the frozen fringe
given by:

$$Kf = d/(\int_o^d dz/Kf(z))\dots\dots\dots\dots\dots\dots\dots3.7$$

Finally, taking into account the volume increase as water changes to ice, the segregational heave rate is related to the water intake velocity by following equation:

$$dhs/dt = 1.09\ V(t)\dots\dots\dots\dots\dots\dots\dots3.8$$

Integration of the segregational heave rate over the freezing time then provides the segregational heave:

$$hs(t) = \int_o^t (dhs/dt)\ dt = 1.09 \int_o^t V(t)dt\dots\dots\dots3.9$$

The total heave of a freezing soil is given by Equation 3.10

$$h(t) = hs(t) + hi(t)\dots\dots\dots\dots\dots\dots\dots3.10$$

where   hi is the heave corresponding to the volume change

upon freezing of *in-situ* water of the soil.

3.2.2 Heat Transfer

Fourier's general equation expresses the conditions which govern the flow of heat in the unsteady state. Convective transport is neglected here. For one dimensional heat flow, Fourier's equation reduces to:

$$d(k\ dT/dz)/dz + Q = CdT/dt\dots\dots\dots\dots\dots3.11$$

where   C is the volumetric heat capacity

k is the thermal conductivity

Q is an internal heat generation term per unit area and per unit time.

In this analysis, the internal heat is liberated at the base of the ice lens where the segregation-freezing temperature is Ts and at the base of the frozen fringe where the *in-situ* freezing temperature is Ti.

At Ts $Q = V(t) . L$ 3.12

At Ti $Q = \epsilon . n . L . dX/dt$ 3.13

where ϵ is a dimensionless factor taking into account the proportion of water remaining unfrozen in the frozen part of the sample and "lumped" at Ti

n is the porosity of the unfrozen soil

L is the latent heat of freezing of water

dX/dt is the rate of frost front penetration

3.2.3 Equations for the One Dimensional Frost Heave Model

In order to proceed with the analysis of a freezing soil, one has to specify both initial and boundary conditions. Figure 3.1 summarizes all the conditions governing a particular case of one-dimensional frost heave with no externally applied overburden. A step temperature, Tc, is applied at the top of the soil while the base is kept constant at Tw. Separate heat conduction equations hold independently for the frozen soil, the frozen fringe, and the unfrozen soil. Both continuity of temperature and heat flux are satisfied at each boundary. No mass transfer exists
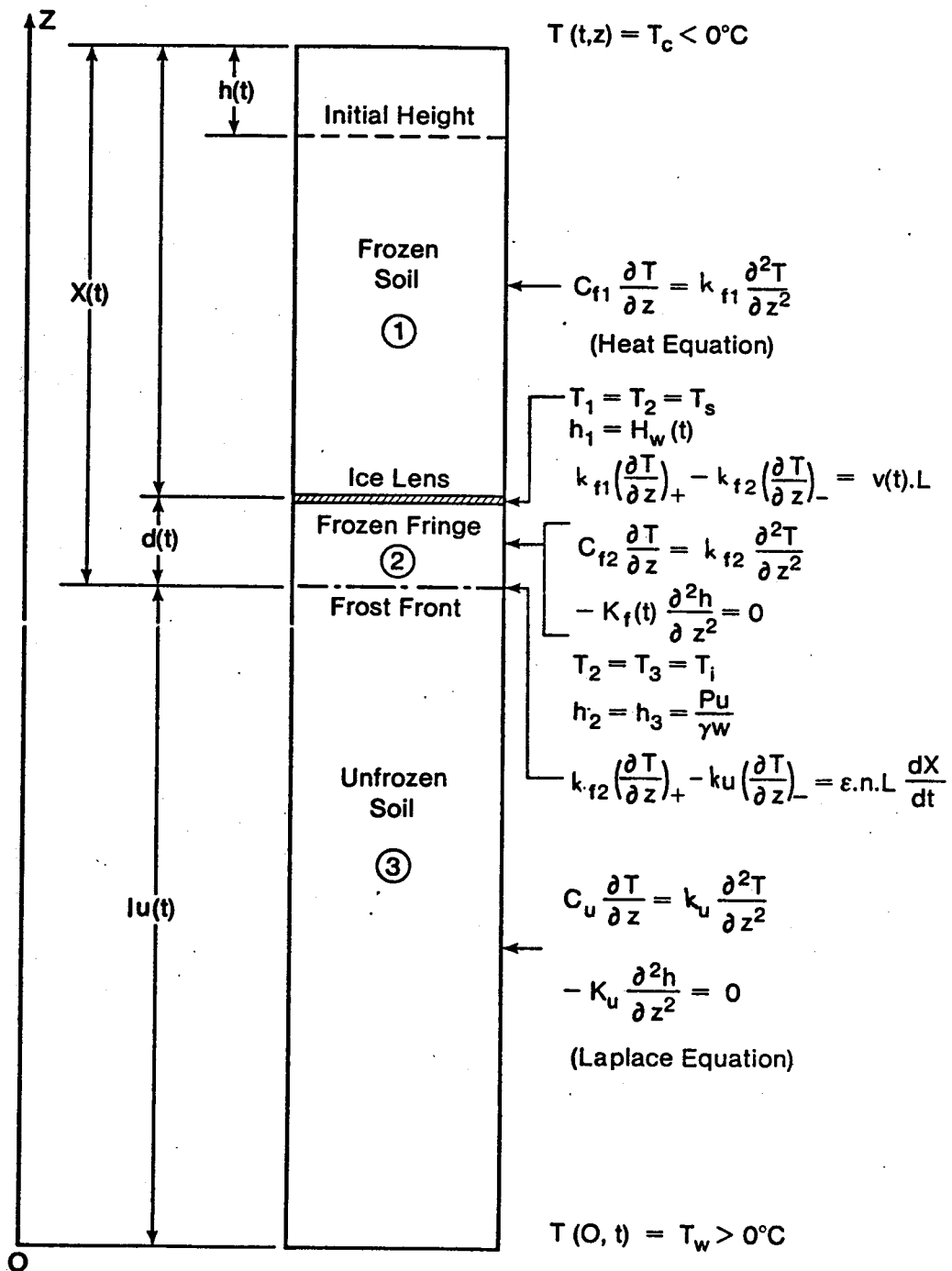
Figure 3.1 Equations For The One Dimensional Frost Heave
Model.
No Externally Applied Load.

within the frozen soil. Water flow within both the frozen
fringe and the unfrozen soil are governed independently by
the Laplace equation, though the theory could be extended to
embrace soil compressibility. Water pressure and discharge
are continuous across the frost front but at the interface
between the ice lens and the frozen fringe the
Clausius-Clapeyron relation holds (Equation 3.5).

The system of equations presented in Figure 3.1 may be
solved with finite difference methods provided the soil
parameters can be specified. In addition to the conventional
geotechnical and thermal parameters, it is also necessary to
characterize the frozen fringe. This is done in terms of two
basic parameters:

1. the overall permeability of the frozen fringe Kf

2. the segregation-freezing temperature Ts.

Both parameters are sensitive to overburden load since
unfrozen water content is affected by changes in ice
pressure. This will be explored in more detail in Chapter 6.

3.3 THEORETICAL ANALYSIS OF THE ACTIVE SYSTEM

Under fixed thermal boundary conditions, i.e., Tw and
Tc constant with time, the temperature profile across the
sample at the onset of the formation of the final ice lens
is shown in Figure 3.2.a. In the active system, the
temperature gradients follow a simple relation:

$$\text{grad } Tu/\text{grad } Tf = ku/kf \dots\dots\dots\dots\dots\dots\dots 3.14$$

where   the subscripts u and f refer respectively to
         unfrozen soil and frozen fringe.

As T_s is very close to 0°C, it is justifiable to assume that
the frozen fringe thermal conductivity is very close to that
of the unfrozen soil. Under these conditions, the
temperature gradient in the frozen fringe is equal to that
in the unfrozen soil. In reality, however, it is clear that
the thermal conductivity of the fringe is different of that
of the unfrozen soil and therefore the temperature gradient
in the fringe is slightly different of that in the unfrozen
soil. A linear model is used herein to describe in a simple
manner the conditions existing close to steady state.

The temperature distribution in the frozen soil above
the ice lens is strongly dependent upon the type of soil for
two major reasons:

1. the amount of water drawn to the base of the ice
   lens and the resulting latent heat release on
   freezing are dependent on the soil type;

2. the variation of the thermal conductivity of frozen
   soil with temperature also depends on soil type.

However, the results to be presented here are not sensitive
to the conditions existing in the passive system since water
migration is restricted to the active system alone.

The theoretical development presented in the previous
sections postulates that T_s and K_f are determinable physical
parameters that characterize a freezing soil. For this to
lead to a useful theory, these parameters must be unique for

a given soil under given conditions and further they must be measurable or inferred from experimental tests. This section is devoted to demonstrating that Ts and Kf are intrinsic parameters of a freezing soil at the onset of the formation of the final ice lens. The next section is dedicated to proving that Ts and Kf can be studied in the laboratory without detailed measurements at the scale of the frozen fringe.

The permeability of a frozen soil is related to the unfrozen water content which is a function of temperature and suction (Harlan, 1973). Further, assuming that the water is flowing to the base of the ice lens through the continuous films of unfrozen water of the frozen fringe, this study takes the view that the location of that ice lens is controlled by the local permeability of the frozen soil. In other words, it is assumed that there is a critical permeability which renders further water migration into the frozen soil materially impossible. Since the permeability of the frozen soil is influenced by temperature, it is expected therefore that for a given soil, the final ice lens is initiated around the same segregation-freezing temperature Tso, independent of the temperature gradient across the frozen zone, i.e., independently of the cold-side step temperature Tc.

Freezing two identical soil samples with different heights under different cold-side temperature and the same warm-side temperature, Tw, leads to temperature profiles at

the onset of the formation of the final ice lens as shown in Figure 3.2.b.

If the segregation-freezing temperatures of final ice lens formation, Tso, are identical, several consequences follow. From Equation 3.5, the suction potential developed at the base of each ice lens is the same in both cases.

$$Hw1 = Hw2 \dots\dots 3.15$$

Geometrical considerations provide the following relations:

$$\frac{d1}{lu1} = \frac{d2}{lu2} = \frac{|Ts|}{Tw} = \frac{1}{p} \dots\dots 3.16$$

Finally, applying Equation 3.6 to the active system, the water intake velocities for the two samples can be expressed as:

$$V1 = |Hw1|/(lu1/Ku + d1/Kf1) \dots\dots 3.17$$

and

$$V2 = |Hw2|/(lu2/Ku + d2/Kf2) \dots\dots 3.18$$

From Equations 3.15 to 3.18, it can be shown that the ratio of both velocities is given by:

$$\frac{V1}{V2} = \frac{lu2.Kf2 + d2.Ku}{lu1.Kf1 + d1.Ku} = \frac{d2(p\,Kf2 + Ku)}{d1(p\,Kf1 + Ku)} \dots\dots 3.19$$

Since the average temperature, (Tso + Ti)/2, is the same in both fringes and if one assumes also that the average suction in each frozen fringe is the same, then the overall unfrozen water content of each fringe is the same. This, in turn, means that the overall permeability of the frozen fringe is identical in both cases. Rewriting Equation 3.19
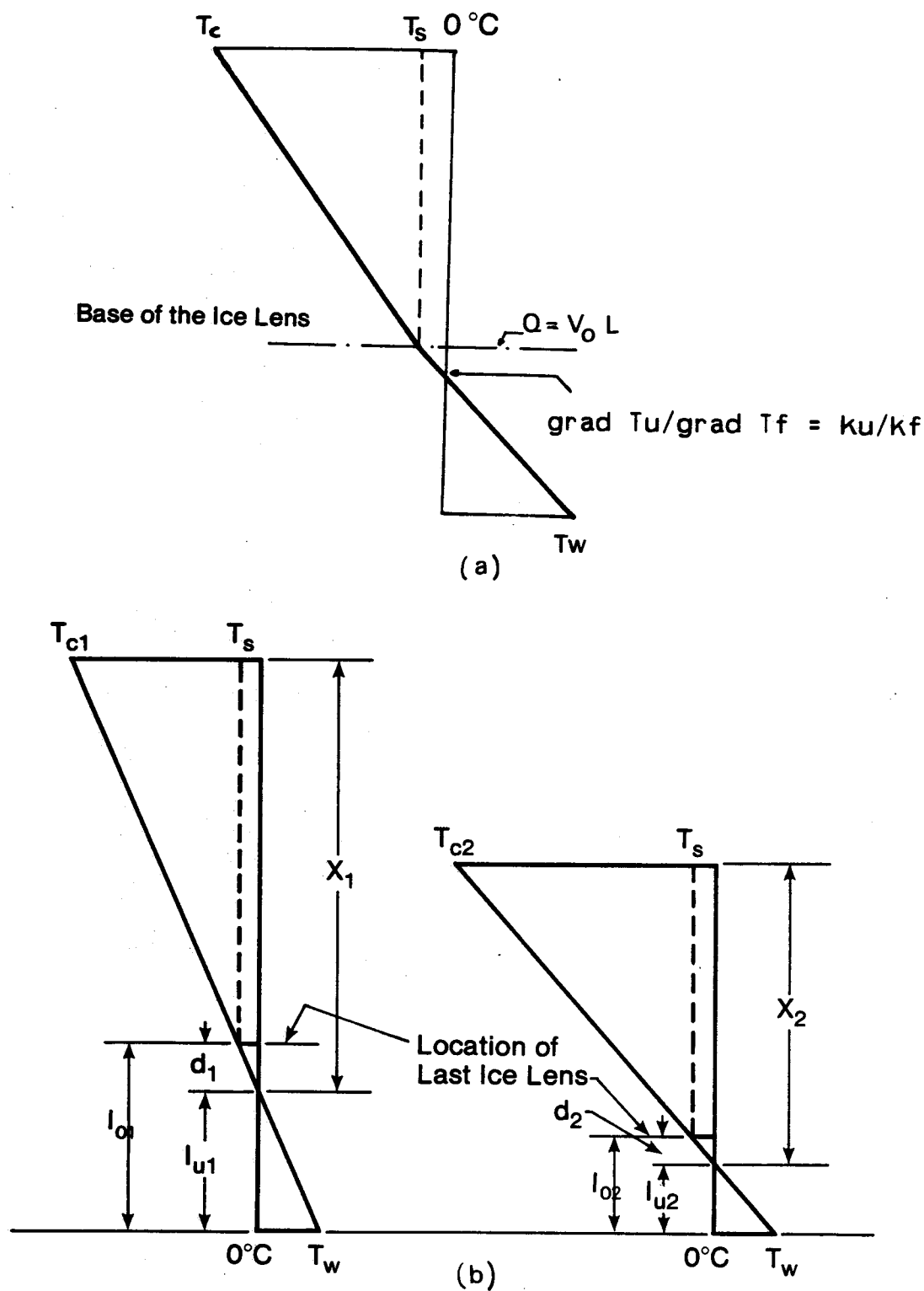
Figure 3.2   Conditions Associated with the Onset of the
             Formation of the final ice lens.

with this additional assumption leads to:

$$\frac{V1}{V2} = \frac{d2}{d1} \quad \dots \dots \dots \dots \dots \dots \dots \dots \dots \dots \dots \dots \dots \dots \dots 3.20$$

This Equation indicates that if the segregation-freezing temperature, Tso, and if the overall permeability of the frozen fringe Kf is the same in both samples, the product of the water intake velocity at the formation of the final ice lens and the fringe thickness is a constant for a given soil, freezing under the above mentioned conditions, i.e.:

$$V1.d1 = V2.d2 = Constant \dots \dots \dots \dots \dots \dots 3.21$$

By combining Darcy's law for the unfrozen soil with Equations 3.19 and 3.21, it can be shown that if Tso is the same in both specimens the suction at the frost front will also be the same:

$$|hu1| = V1.lu1/Ku = V2.lu2/Ku = |hu2| = |hu| \dots 3.22$$

Relating the thickness of the frozen fringe to the temperature gradient by

$$d = |Ts|/grad\ Tf \dots \dots \dots \dots \dots \dots \dots \dots \dots \dots 3.23$$

where   gradTf = gradT(active) = (Tw + |Tso|)/lo = Tw/lu
and combining Equations 3.18, 3.22 and 3.23 results in:

$$Vo = SPo.grad\ Tf \dots \dots \dots \dots \dots \dots \dots \dots \dots \dots 3.24$$

where   SPo is a constant equal to $Kfo.|Hw-hu|/Ts$

The subscript o refers to the onset of the formation of the final ice lens.

Hence, if the segregation-freezing temperature, Ts, under the conditions described herein, is unique at the

formation of the final ice lens, the water intake velocity will be proportional to the temperature gradient across the frozen fringe which is equal, in our case, to that in the active system.

The constant SPo reflects the segregation potential of the soil and is a function of both intrinsic parameters Tso and Kfo. Its experimental determination is relatively simple in a freezing test since SPo is the ratio of two measurable quantities, the water intake rate and the temperature gradient across the active system, both determined at the formation of the final ice lens.

3.4 EXPERIMENTAL RESULTS - INTRINSIC PARAMETERS

In order to investigate the previous statements a series of seven tests were conducted at a constant warm-plate temperature, Tw of about 1.1°C under different cold-side temperatures. All the samples were overconsolidated to 210 kPa and were not subjected to any surcharge during freezing. Their heights varied between 6 and 12 cm. Later tests in a different series permitted the addition of more data.

After freezing, the samples were carefully inspected, cut into two parts and water contents were taken from one. The other half was used to determine the precise location of the base of the final ice lens and to measure its thickness. This permitted a check on the validity of the assumption

that water flow to the ice lens is continuous with no accumulation within the frozen fringe. Further, those measurements allow one to backcalculate very accurately the time at which the final ice lens was initiated. Finally, the position of the frost front obtained from thermistor readings could be compared with the measured height of unfrozen soil. In order to evaluate the influence of the side friction developed during tests when frozen from top downwards, test NS-7 was frozen from the bottom upwards.

3.4.1 Results

The experimental results are shown in graphic form in Figures C.1 to C.9 in Appendix C. Inspection of these figures illustrates that for almost all the tests radial heat flow did not occur. Some samples, however, experienced heat gain from their sides in the frozen part where the temperature gradient across the insulation and cell wall is very steep. As a consequence, the temperature distribution is no longer linear in the passive system as seen in Figure 4.23. In the vicinity of the active system, where the temperatures lie between $+1^{\circ}C$ and $0^{\circ}C$, very little radial heat flow can occur since the room temperature was kept constant at around $+0.5^{\circ}C$. The temperature distribution is, therefore, essentially linear in the active system.

At the end of any freezing test, the location of the base of the final ice lens is measured and the height of the sample at the initiation of this ice lens is backcalculated.

Superposition of the measured temperature distribution provides the value of the segregation-freezing temperature Ts, which was found for Devon silt to be approximately -0.10°C. Special freezing tests conducted with a back-pressure device, described in Chapter 2, confirmed this average value as shown in Figure 3.9. These tests provide further experimental evidence that ice lens formation occurs some distance behind the freezing front.

Furthermore, the thickness of the warmest ice lens compared well with the amount of water drawn into the sample during the freezing time associated with it's formation. It is, therefore, concluded that accumulation of water does not occur within the frozen fringe and that the water flow is continuous to the base of the final ice lens justifying the premise stated in Section 3.3.

Both visual observations and the magnitude of the suction inferred from special freezing tests suggest that the final ice lens grows somewhat behind the frost line, at around -0.10°C. This segregation-freezing temperature for Devon silt is in the range of those found by Loch and Kay (1978) who inferred values of about -0.30°C ± 0.10°C for New Hampshire silt. Considering Equation 3.23, it appears that an accurate determination of Ts does not influence significantly the value of grad Tf since Ts may be neglected with respect to Tw.

The results of the analysis of tests obtained in this series at the onset of the growth of the final ice lens are

reported in Table 3.1. It is considered that the error in measuring the length of the sample below the warmest ice ·lens was no more than ± 1mm. Although the warm-end side temperature, Tw, was known within ±0.01°C an error of ±0.05°C was considered in order to take into account any possible error in the determination of Tso. Combining those variations, a lower and upper bound for the temperature gradient across the active system can be calculated.

Figure 3.3 presents the relation obtained in these tests between the water intake velocity, Vo, and the temperature gradient across the fringe, grad Tf, at the onset of the formation of the final ice lens. As seen, the water intake rate is linearly proportional to the temperature gradient, confirming the results of the theoretical analysis developed in the previous section (Equation 3.24). Since the conclusions of the previous analysis are validated by experimental results, it can be concluded that the basic assumptions made in the previous derivation, namely that Tso is unique for a given soil freezing under the conditions described earlier, and that the overall permeablity of the frozen fringe developed between Tso and Ti is a constant, are also verified.

These experimental results give strong support to the view that for a given soil which freezes under conditions such that the warm-plate temperature Tw is always constant and that the temperature distribution in the active system is linear at the formation of the final ice lens, the final

TEST	Tw (°C)	Tc (°C)	INITIAL HEIGHT (CM)	PERMEA- BILITY (CM/S)	LENGTH l_o (CM)	GRAD Tf (°C/CM)	INTAKE VELOCITY (10^{-6}MM/S)
NS-1	+1.1	-3.4	10.4	10^{-7}	3.20	0.37	31.5
NS-2	+1.1	-4.8	10.4	$.9\times10^{-7}$	2.35	0.51	41.5
NS-4	+1.1	-2.5	7.6	1.1×10^{-7}	3.00	0.40	40.0
NS-5	+1.1	-6.2	10.0	-	1.80	0.67	60.0
NS-6	+1.1	-3.4	6.4	$.95\times10^{-7}$	1.80	0.67	59.0
NS-7	+1.1	-3.5	12.0	-	3.25	0.37	36.0
E-8	+1.1	-4.2	8.3	-	2.80	0.43	40.7
NS-9	+1.0	-6.0	28.0	-	10.60	0.10	9.0
NS-10	+1.0	-6.0	18.0	-	4.50	0.24	18.5

Table 3.1   Conditions of the Different Tests at the
Onset of the Formation of the Final Ice Lens
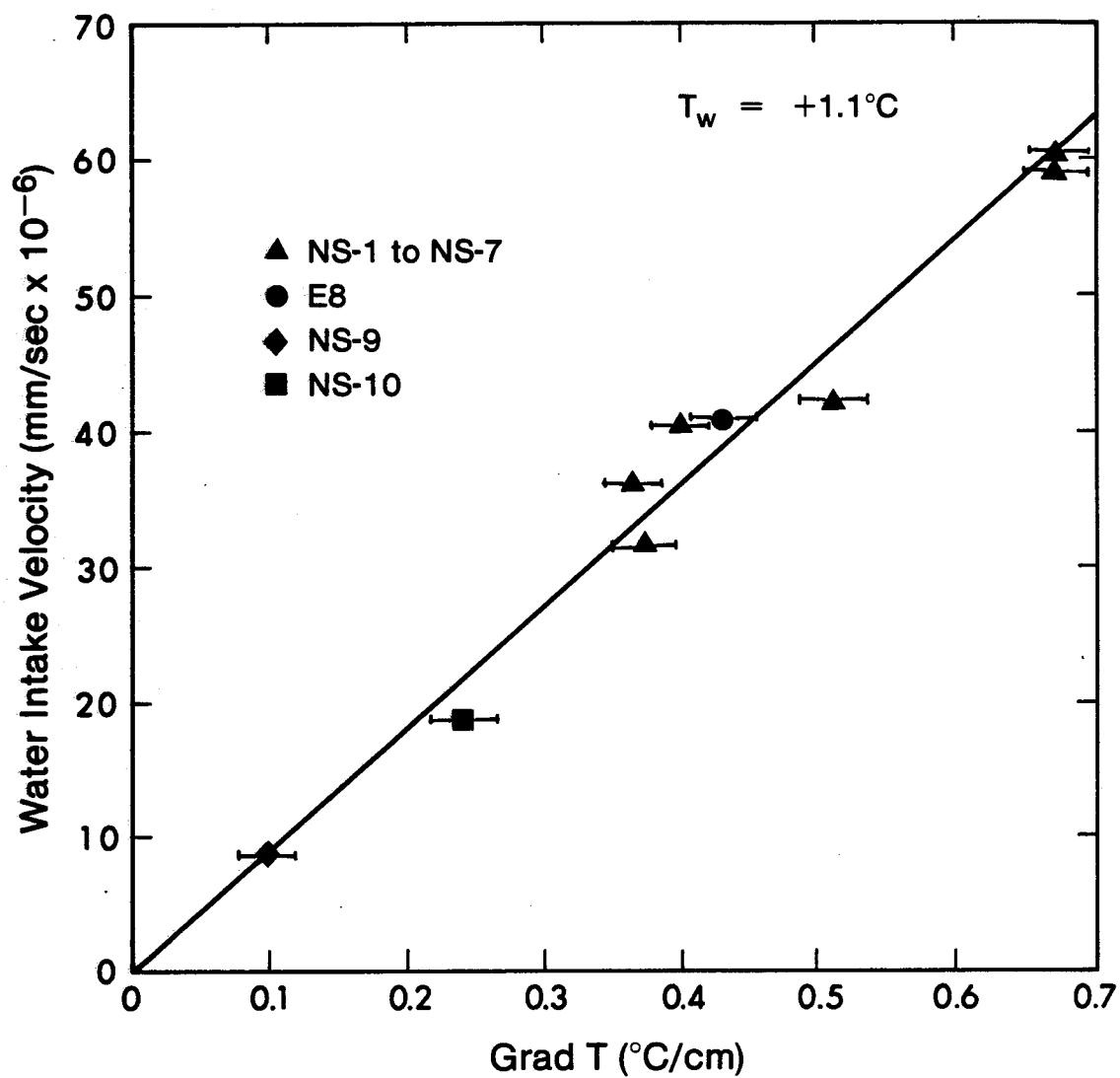
Figure 3.3   Relation Between Water Intake Velocity and
              Temperature Gradient Across the Frozen Fringe at
              the Initiation of the Final Ice Lens

ice lens grows at a unique segregation-freezing temperature, independent of cold-side step temperature, Tc. Tso can, therefore, be considered as an intrinsic parameter of a freezing soil. Since the permeability of the frozen fringe is also constant in those tests, Kfo can also be considered as an intrinsic parameter of the freezing soil.

It should be emphasized that the following assumptions made in the theory are implicitly supported:

1. the validity of the Clausius-Clapeyron equation at the base of the ice lens.

2. Negligible thermal conductivity changes from the unfrozen soil to the frozen fringe.

Furthermore, it is fully acceptable for an engineering approach to treat frost heave as a problem of impeded drainage to an ice lens through a layered system with overall constant properties, Ku, Kfo, lu and d.

The value of the overall permeability of the frozen fringe can be determined from the results of one of the freezing tests shown in Table 3.1. Expressing both suction potential and frozen fringe thickness as a function of Ts (Equation 3.5 and 3.2), Equation 3.6 can be recast as follows:

$$Kfo = (|Tso|Vo/gradTf)/(|M'.Tso/\gamma w|-Vo.luo/Ku)..3.25$$

In this equation, it is important to notice that Vo, gradTf, and luo are measured parameters in a freezing test, affected only by small experimental errors. The unfrozen soil permeability, even though determined by a very delicate

operation, proved to be very consistent for different soil samples, as can be seen in Table 3.1. The results of the permeability tests are found in Appendix A.

Therefore, at first sight, the only term that could affect significantly the value of the overall permeability is Tso. Hence, it is of value to perform a sensitivity analysis on Kfo with respect to variations of Tso. Taking the derivative of Kfo with respect to Ts yields:

$$dKfo/Kfo = -((Vo.lu/Ku)/(|M'.Ts/\gamma w|-Vo.lu/Ku))d|Ts|/|Ts|..$$
3.26

Rewriting Equation 3.26 in terms of total potential gives:

$$dKfo/Kfo = -|hu/(Hw-hu)|.d|Ts|/|Ts| = -X.d|Ts|/|Ts|....3.27$$

Table 3.2 indicates that the suctions at the frost front, obtained using Darcy's law are more or less identical for all of the tests reported here. This was also predicted in Section 3.3. As a consequence, the quantity can be calculated for different values of Tso as Hw is directly related to the value of the segregation-freezing temperature. The relationship between X and Tso is shown in Figure 3.4. Interpretation of that graph reveals that for Tso=-0.10°C a 100% relative error in Tso, i.e., assuming Tso=-0.20°C, would only result in a corresponding error in Kfo of about 7%. However, as Tso tends toward 0°C, Figure 3.4 shows a significant increase of X as a result of the decreasing value of Hw and hence the increasing importance

of hu with regard to Hw in the expression |Hw - hu|. Since Tso was inferred to be around -0.10°C for Devon silt, it is reasonable to assume that the values of Tso for the silt investigated here are within -0.05°C and -0.15°C. In this range, Figure 3.4 clearly shows the insensitivity of Kfo with respect to Tso. Figure 3.5 illustrates the variation of the calculated overall permeability with Tso. The input parameters for Figure 3.5 have been obtained from test NS-1. As stated previously, the permeability of the frozen fringe does not show any significant variation for temperatures, Ts, colder than -0.05°C; its value dropping monotically from 0.84×10^{-9} cm/s to 0.67×10^{-9} cm/s.

Adopting a value of -0.10°C for the segregation-freezing temperature Tso, which implies a suction potential of -125 kPa (or 1250 cm of water), the overall permeability of the frozen fringe can be determined from:

$$Kfo = Vo.do/|Hw-hu| \dotfill 3.28$$

where   do is the thickness of the frozen fringe obtained with Equation 3.23

hu is the suction at the frost front obtained with Darcy's law, assuming a constant permeability of the unfrozen soil of 10^{-7}cm/s.

The results as summarized in Table 3.2 reveal that, for a given soil, the values of hu and Kfo at the onset of the formation of the final ice lens are constant and independent of the cold-side temperature, Tc. The slight variations in
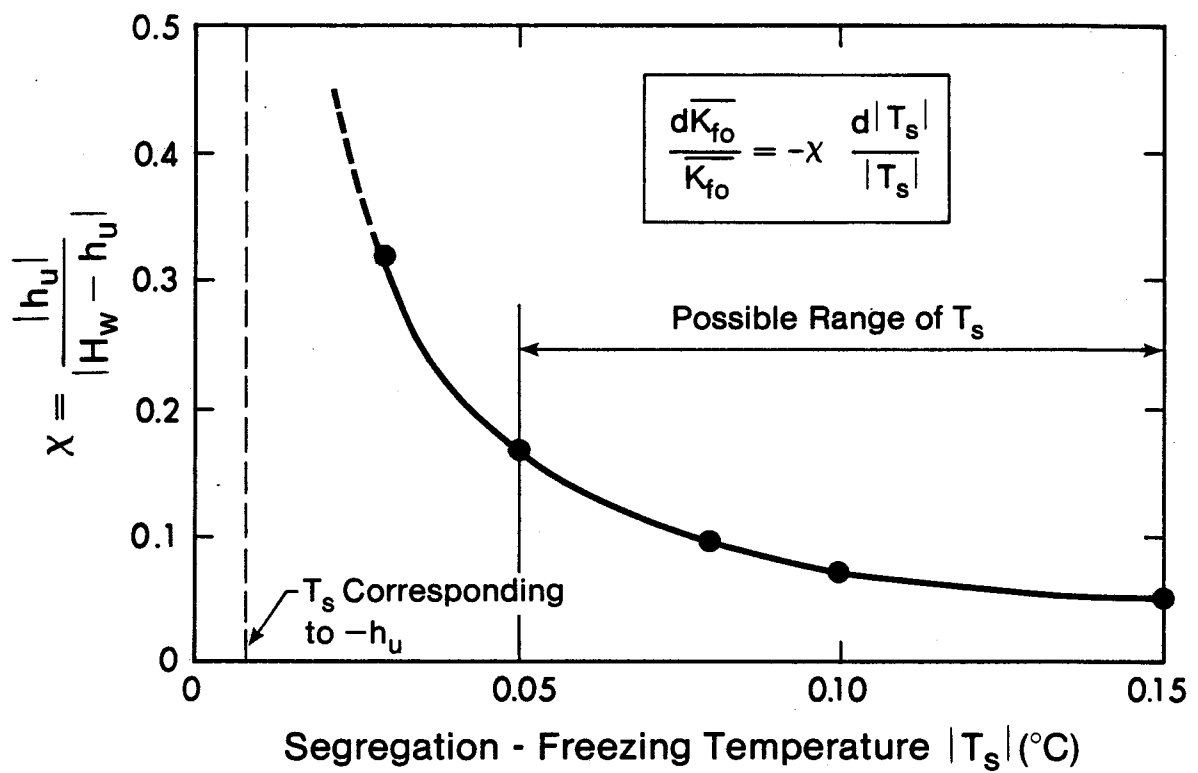
Figure 3.4   Sensitivity Analysis for the Frozen Fringe
            Permeability with Respect to the Segregation
            Freezing Temperature

The y-axis is labeled "Frozen Fringe Permeability (10^{-10} cm/s)" with values 0, 4, 8, 12, 16, 20.

The x-axis is labeled "Segregation - Freezing Temperature $|T_s|$ (°C)" with values 0, 0.04, 0.08, 0.12, 0.16.

An arrow points to "T_s Corresponding to $-h_u$"

$$K_{fo} = \frac{v_o d}{|H_w - h_u|}$$
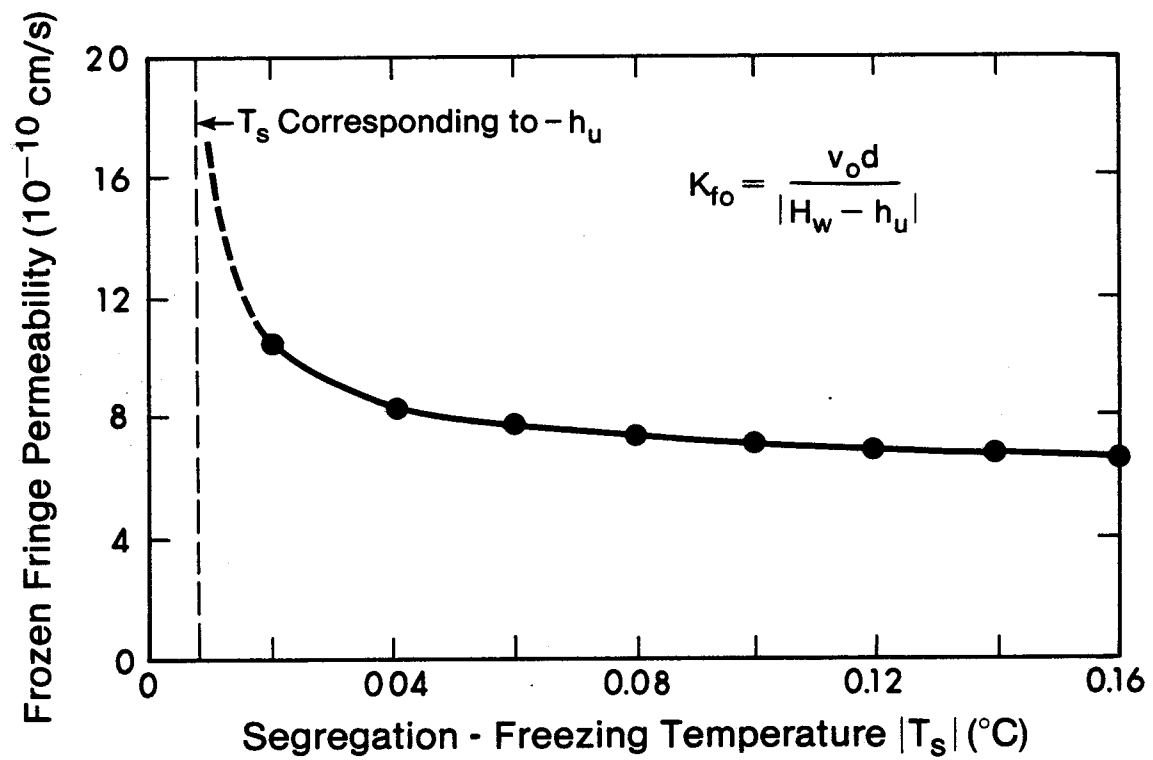
Figure 3.5 Variation of Calculated Permeability of the Frozen Fringe for Different Segregation Freezing Temperatures

hu and Kfo are considered to be a consequence of the experimental error involved in using different samples.

Furthermore, Tables 3.1 and 3.2 show that to steady state lateral friction did not materially influence the heave rate since the measured parameters, Ts and Kfo, do not vary significantly.

If a freezing soil under zero external load reaches a temperature distribution close to steady state such that the final ice lens is created and if the surrounding conditions are such that the suction at the frost front is identical for different freezing tests, its fundamental freezing characteristics, Tso and Kfo and its segregation potential SPo are unique and independent of the cold-step temperature Tc. It must be emphasized that a linear temperature profile in the active system associated with the same warm-end temperature Tw led to the above mentioned conditions. The fore mentioned conditions represent a special case and the more general one, i.e., variation in suction at the frost front, will be investigated in Section 3.6.

3.5 THERMODYNAMIC ANALYSIS OF THE FROZEN FRINGE

The predictive model for flow rate of water to the base of the ice lens implies that the frozen fringe is characterized by a linear temperature variation from Ti to Tso, an equivalent constant permeability and potential boundary conditions Pw and Pu as shown in Figure 3.6.a.

TABLE 3.2.   CALCULATED OVERALL PERMEABILITY OF THE FROZEN
FRINGE FOR DEVON SILT

TEST	FROZEN FRINGE THICKNESS (MM)	SUCTION AT 0°C INTERFACE (CM H20)	PERMEABILITY (10^{-10}CM/S)
NS-1	2.70	-92.0	7.34
NS-1	2.70	-92.0	7.34
NS-4	2.50	-110.0	8.77
NS-5	1.50	-99.0	7.82
NS-6	1.50	-97.0	7.68
NS-7	2.70	-107.0	8.50
E-8	2.30	-104.0	8.27
NS-9	9.60	-89.0	7.44
NS-10	4.20	-75.0	6.61

Moreover, when Pu is the same in different samples, the velocity of water migration is proportional to the inverse of the thickness of the fringe (Eq. 3.21) and these characteristics can then be normalized for a fringe thickness of unity. Thus, a freezing soil reaching the conditions described in the previous section is fully described by the following set of parameters: V_n, K_{fo}, T_{so} and T_i. V_n represents the normalized water intake velocity through a fringe of thickness unity and is given by:

$$V_n = V_o.d_o \dots\dots\dots\dots\dots\dots\dots\dots\dots\dots\dots\dots\dots\dots\dots 3.29$$

The proposed model for mass transfer overcomes the enormous difficulty created by the complexity of the physical properties of frozen soils, especially the lack of knowledge of detailed variation of the permeability with temperature below $0^\circ C$. Nevertheless, qualitative considerations reveal that the permeability decreases with decreasing temperatures as a direct consequence of changes in the unfrozen water content of the soil. The actual permeability profile within the fringe adopts, therefore, a non linear profile since the temperatures vary linearly within the frozen fringe. Figure 3.6.b illustrates this point. The basic assumption, made in this model and corroborated by the experimental results, that there is no accumulation within the fringe will be satisfied only if the suction profile also adopts a non-linear shape. The more general set of parameters describing the frozen fringe is therefore given by V_n, $K_f(T,P)$, T_{so} and T_i.

Considering that the pressure in the ice crystals is atmospheric for samples subjected to zero overburden, i.e., Pi=0, the theoretical suction profile developed in the fringe in response to linear temperature profiles, obtained from the Clausius-Clapeyron equation (Equation 3.3) is also linear and passes through the origin as shown in Figure 3.6.c. A comparison of actual and theoretical suction profiles establishes that there is a considerable difference in their shapes as well as in their values at a given temperature warmer than Ts. Several questions may be raised at this point:

1. Is the temperature profile within the fringe linear?
2. Is it justified to consider phase equilibrium conditions within the frozen fringe?
3. Does the Clausius-Clapeyron equation hold within the fringe?
4. Is it justified to consider atmospheric pressure in the ice or is there a pressure developed in the pore ice due to curvature of the ice-water interfaces within the soil matrix of the fringe?

In response to the first question, it should be reiterated that the temperature conditions examined thus far refer to the initiation of the final ice lens and therefore correspond to a temperature distribution which closely approximates the equilibrium temperature distribution across the sample. Furthermore, there is very little variation of thermal conductivity within the frozen fringe. It follows

Temperature Profile   Permeability   Suction Profile
                          Profile

T_s Pw

$d=1$

K_{fg}

                                              Pu
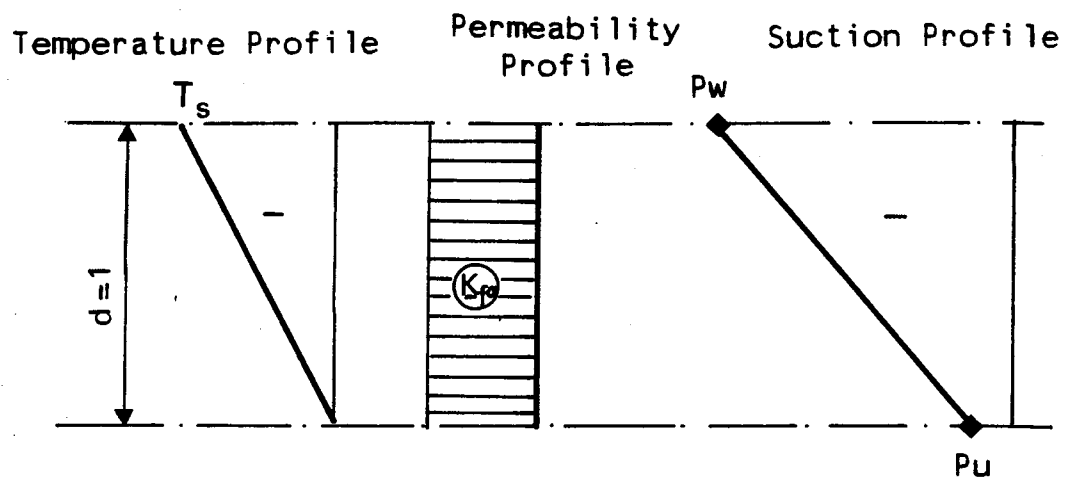
a) Simplified Characteristics of the Frozen Fringe

T_s Pw

$K_f(T)$

                                              Pu
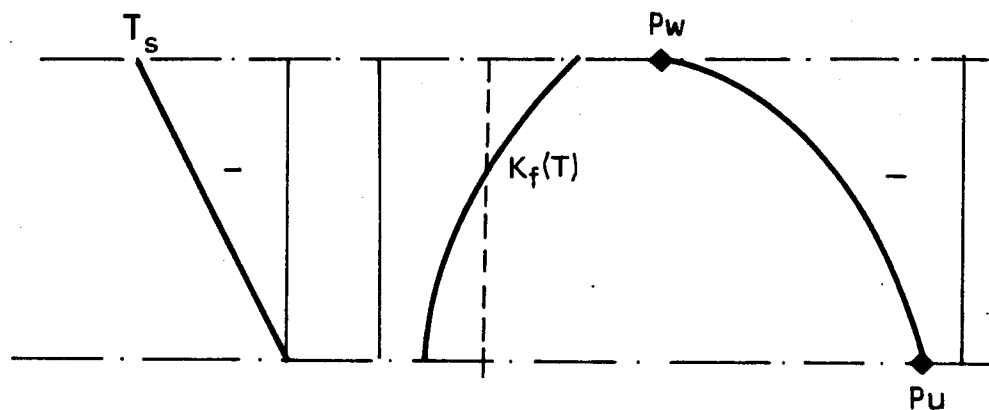
b) Shape of Actual Characteristics of the Frozen Fringe

T_s Pw   Ice Pressure

−   −   +

Pu   −
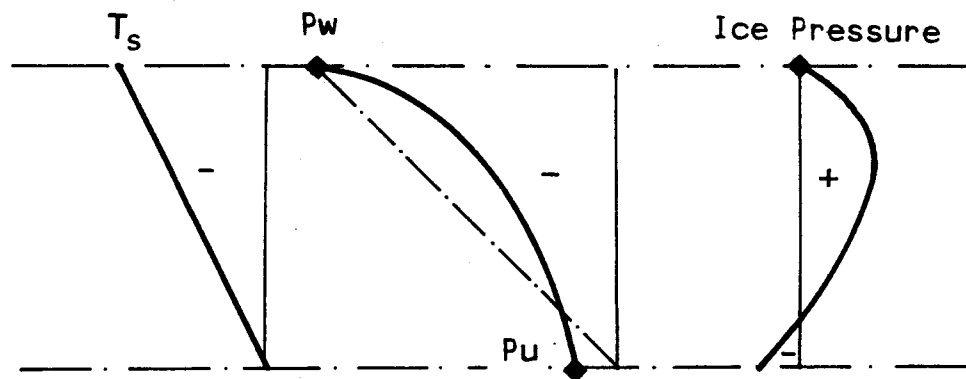
c) Pore Ice Pressure From the Generalized
   Clausius-Clapeyron Equation

Figure 3.6 Physical Characteristics of the Frozen Fringe

that it is reasonable to assume that the temperature profile will be approximately linear.

In response to the second question, it can be considered that the rate of change of temperature and suction is very small at the formation of the final ice lens and therefore the assumption of phase equilibrium is fully justified.

Recognizing the difference in suction profiles, Miller (1978) proposed that the pore ice in the fringe is under pressure due to curvature and surface energy effects, even when no load is applied to the soil. It will be shown in Chapter 6 that pressure develops in the pore ice as well as the ice lenses when an external load is applied. However, the load transfer mechanism is complicated by the complex nature of the composite medium of ice and soil grains. The assumption of pore ice pressure has an effect on the calculated suction in the water phase of a frozen soil. The generalized Clausius-Clapeyron equation (1.6) shows that pressure in the ice increases pressure in the water and thereby reduces the suction developed in the soil at a given temperature. Therefore, adopting a convenient ice pressure profile, the suctions derived from the generalized Clausius-Clapeyron equation can be matched with the actual suctions in the frozen fringe. In the case of no overburden pressure, the ice pressure would have to develop a parobolic shape as shown in Figure 3.6.c with negative pressure or tension close to the frozen-unfrozen interface, a maximum

positive pressure somewhere within the fringe and zero pressure at the ice lens. It is doubtful that this profile could ever occur in reality.

A more realistic approach to the explanation for this difference in the suction profiles is to consider that phase equilibrium within the frozen fringe can be described by a free energy-moisture content relationship. Williams (1976) established a unique relationship between the free energy of soil water and unfrozen water content for a given soil. The free energy of soil water is equal to the sum of capillary, osmostic, surface adsorbtion components and other minor components as given in the following equation:

$$DG = DGcap + DGosm + DGads + \dots\dots\dots\dots\dots 3.30$$

At temperatures down to about -1.5°C, in many soils, capillarity is the dominant effect in DG. In that range, the free energy of soil water is essentially that of the negative pore water pressure in the unfrozen water. The unfrozen water content variation with temperature below 0°C can be determined using several experimental techniques (Anderson and Morgenstern, 1973). Although the methods are quite different, all do not allow water flow in or out the sample during testing since the soil samples are frozen under closed system conditions. The results obtained by several investigators are very consistent and establish a unique relation between the unfrozen moisture content, W_u, and the temperature for a given soil. The hysteresis effect observed during warming and cooling cycles in unfrozen water

content is believed to be primarily due to changes in soil structure during freeze-thaw cycles. It will be assumed that any hysteresis effects are negligible. With this assumption and for a closed system, equilibrium of ice and water within the sample is allowed to establish in those special tests at a given temperature T. The use of the Clausius-Clapeyron equation is then fully justified as a condition of no water flow identical to that existing at the base of any ice lens is obtained. The temperature T is related uniquely to the free energy DG. A unique relationship between DG and Wu is consequently expected in the case of frozen soils with no water flow.

Open system freezing is basically very different from the previous situation since water flowing through the frozen fringe interacts with the surrounding medium. To describe from a thermodynamic point of view this open system situation, it is convenient to go from the initial or reference state (Pw=Pi=0,T=To) to the final state (Pw,Pi=0,T) in two steps as shown in Figure 3.7.a:

1. A temperature change from To to T with no water flow, i.e. similar to a closed system

2. Pore water pressure change from the value obtained at the end of step 1 to the final value, corresponding to the actual value of the suction developed in an open system, under isothermal conditions, i.e. dT=0.
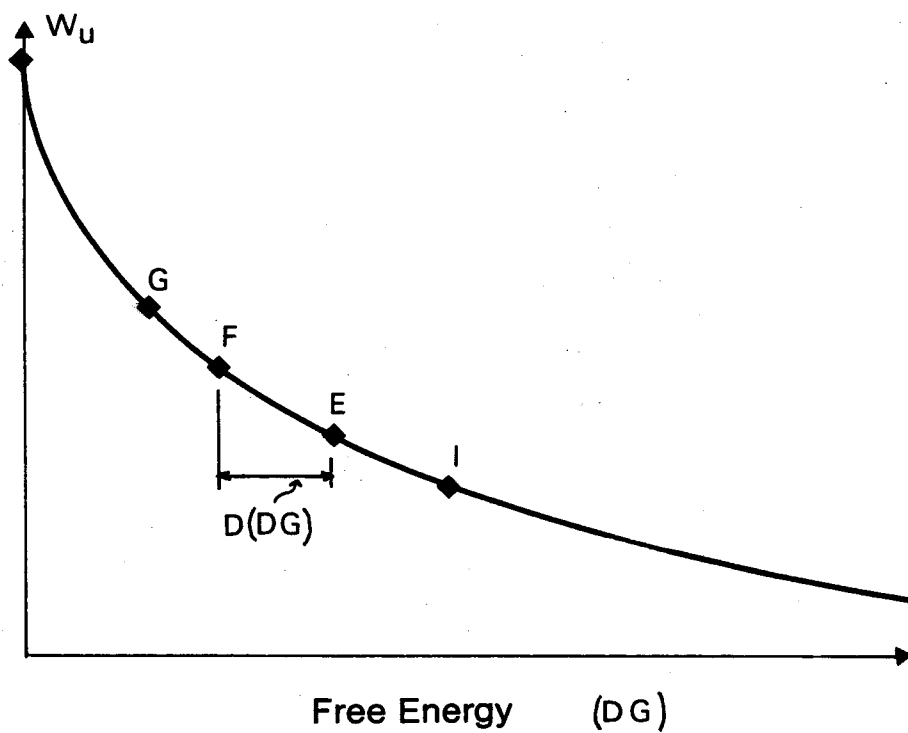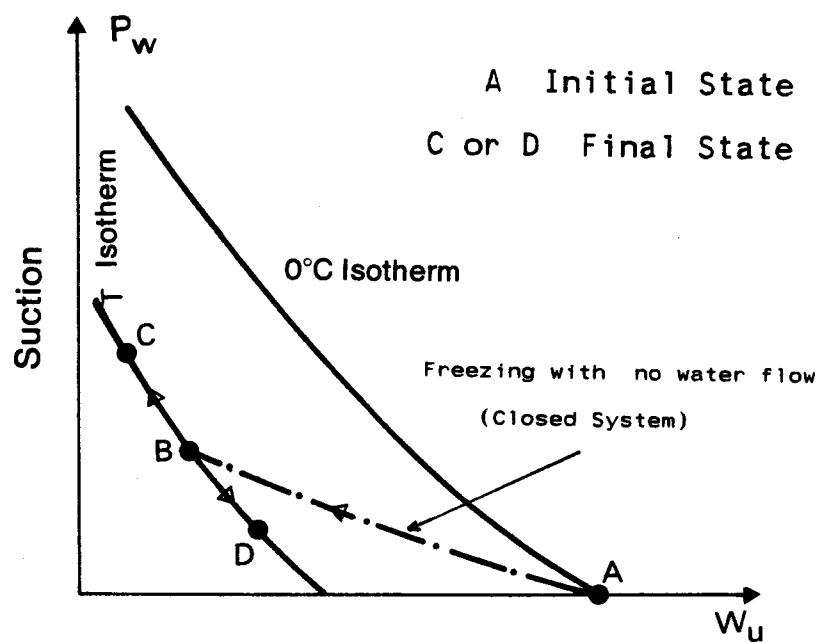
Figure 3.7   Relationship Between Unfrozen Water Content and
            Free Energy State

During the first step, the relative free energy is given by the value of the suction obtained from the Clausius-Clapeyron equation. At the end of that step, ice and water are in equilibrium by definition.

The change in free energy of soil water during the second step is:

$$D(DG)w = DPw.Vw \dots\dots\dots\dots\dots\dots\dots\dots\dots\dots\dots 3.31$$

where   DPw represents the difference in pore water pressure

between the actual value and that for the

closed-system situation

The restoration of equilibrium requires a free energy change in the ice of an equal amount given by:

$$D(DG)i = DPi.Vi = DPw.Vi \dots\dots\dots\dots\dots\dots\dots 3.32$$

This implies a pressure in the ice which is contrary to our assumptions.

However, thermodynamically, some melting or freezing is likely. Melting of ice increases the unfrozen water content, Wu, with a concomitant increase in its free energy while formation of ice reduces the amount of unfrozen water and its free energy. Restoration of equilibrium requires, therefore, additional melting of the ice in the case of a positive pore water pressure change. The free energy of an element of frozen soil at a given temperature T is (DG)ws under no flow conditions. This state is represented by point E on Figure 3.7.b. A negative pore water pressure change at the same temperature T, an increase in suction, would shift the representative point from E to I on a graph relating Wu

and DG. The unfrozen water content decreases and results in a change in permeability at the same temperature. Identically, a positive pore water pressure change at a given temperature, a decrease in suction, would shift the representative point from E to either F or K with a concomitant increase in unfrozen water content depending on the magnitude of the pressure change in the water films.

This simple thermodynamic approach using the free energy concept has demonstrated that a freezing system with a linear temperature profile will develop a compatible permeability and suction profile by melting or freezing some of the pore ice. Furthermore, it is clear that the Clausius-Clapeyron equation which does not consider different amounts of unfrozen water and ice at a given temperature does not hold within the frozen fringe since water flow interacts directly with suction and phase composition. However, equilibrium between both phases is a realistic assumption close to steady state conditions.

The understanding of the physical properties of the frozen fringe in an open system freezing led to the extension of the well-known relationship between unfrozen water content and temperature to the more general relation between unfrozen water content and free energy state of the unfrozen water as suggested by Harlan (1973) and Williams (1976).

When no water flow occurs in frozen soils, i.e. in the passive system, the unfrozen water is solely related to

temperature. However, when water flows through frozen soil, the suction in the frozen medium is no longer solely related to temperature and the unfrozen water content is now a function of both temperature and suction.

For a given value of the suction at the frost front, the previous analysis demonstrates that the normalized water intake flux, corresponding to a fringe thickness of unity, is then unique. Furthermore, since the average permeability of the frozen fringe is constant for these conditions, the average suction is any of the frozen fringes created with the above freezing conditions is also unique since the average temperature in each fringe is the same.

In addition, it may also be concluded that if different suction profiles, i.e. different average suctions, develop within a normalized frozen fringe, different freezing characteristics of that given soil should be expected although the average temperature in each fringe remains constant. This can easily be inferred from Figure 3.7.b since for a given average temperature of the frozen fringe, different average suctions result in different average unfrozen water contents and hence in different average permeabilities of the frozen fringe.

These considerations led to another series of tests in order to investigate the validity of the previous, rather novel, statements.

3.6 EFFECT OF SUCTION ON THE INTRINSIC FREEZING PARAMETERS

3.6.1 Introduction

By recognizing the effect of different temperature boundary conditions on the location of the final ice lens and bearing in mind the fundamental results obtained in the first part of this chapter, it can readily be shown that the warm-end temperature alone affects the value of the suction developed at the frost front. Figure 3.8 presents simplified temperature distributions across a sample for different temperature boundary conditions. As established previously, a freezing system is characterized by its normalized water intake rate, a unique suction profile and a unique overall permeability of the frozen fringe provided the warm-end temperature is the same in each test and that the temperature distribution in the active system is linear. It has also been demonstrated that those characteristics were independent of the cold-side temperature. Consequently, temperature profiles with identical numbers on Figure 3.8 result in identical characteristics of the frozen fringe whereas different warm-end temperatures give different suction profiles in the fringe as seen in the bottom part of Figure 3.8. From geometrical considerations and assuming, for example, a given value of Vn in each case a simple relation between hu and Tw can be established:

$$\frac{|hu1|}{Tw1} = \frac{|hu2|}{Tw2} = \frac{|hu3|}{Tw3} \quad \dots\dots\dots\dots\dots\dots\dots\dots 3.33$$
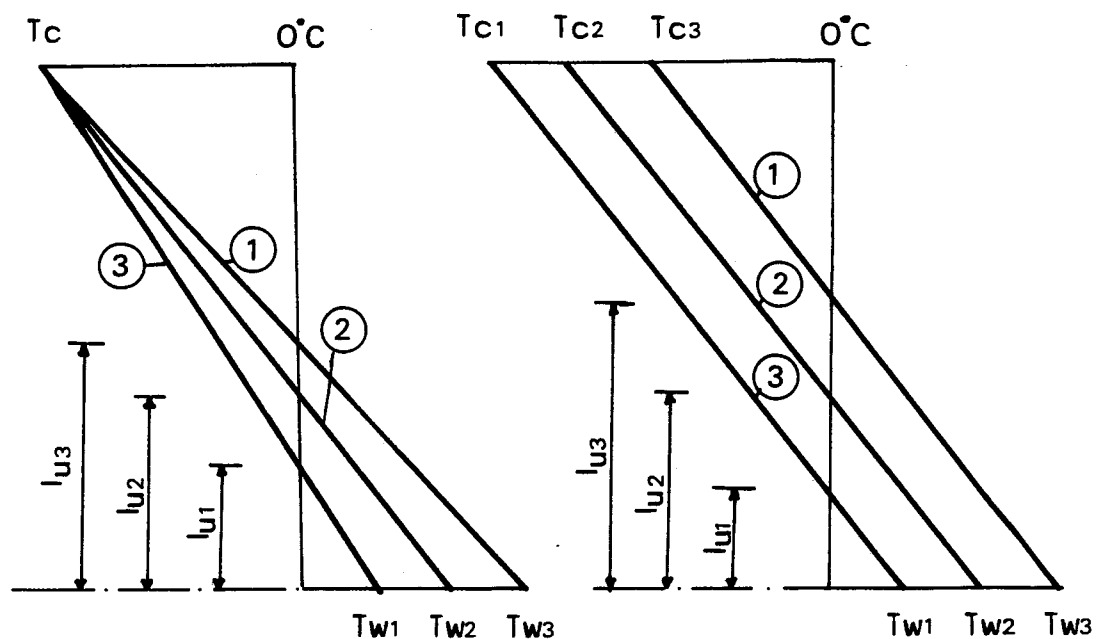
Simplified Conditions at the Initiation of the Final
Ice Lens with Different Thermal Boundary Conditions
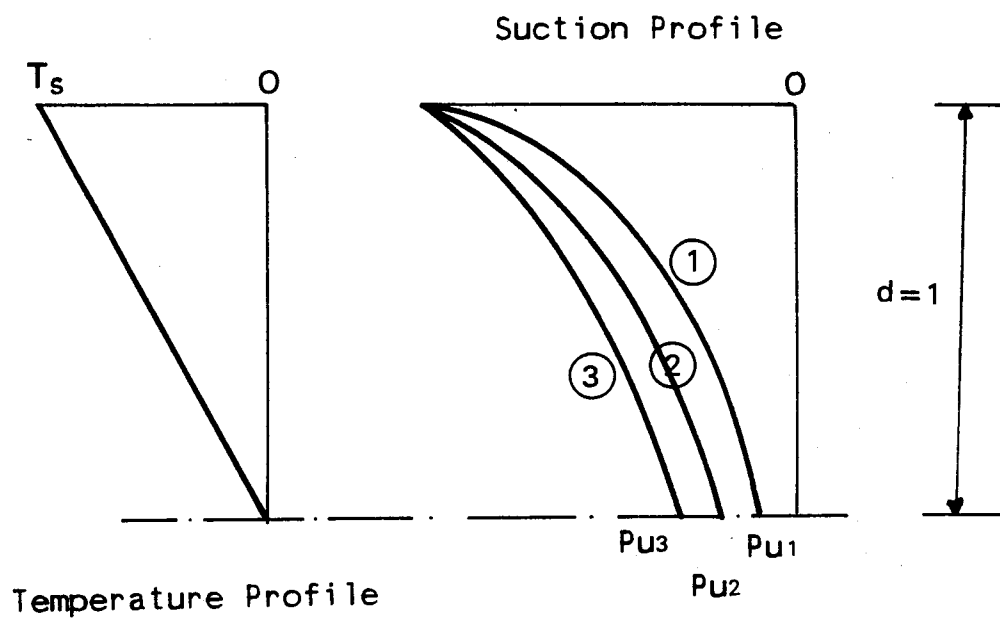
Figure 3.8   Effect of Warm-Plate Temperature on Suction
Profile in the Frozen Fringe

For Tw1 < Tw2 < Tw3, Equation 3.33 yields |hu1| < |hu2| < |hu3|

Further, assuming that the segregation-freezing temperature Ts does not change drastically with different warm-end temperatures, the shape of the suction profile can be drawn qualitatively as shown in Figure 3.8.

It was, therefore, decided to run several freezing tests with no applied load where the warm-plate temperature was varied in each test. The freezing characteristics, Tso, Kfo and SPo, were determined at the onset of the formation of the final ice lens in each test. The samples were prepared from the same Devon silt, preconsolidated to 210KPa is that the initial conditions were as close as possible to those obtained in the first NS series. This investigation was conducted with two types of testing:

1. The freezing characteristics were obtained from a conventional freezing test under fixed thermal boundary conditions with free access of water (open system).

2. Variations in the segregation-freezing temperature Ts were investigated with tests where a back pressure was applied to the pore water. The samples were frozen in an open system to the formation of the final ice lens. The water intake line was then closed and the pore water pressure change was monitored with time. The pore water pressure drop from the initial value equal to the applied back

pressure to the final stable value is related to the temperature at the base of the ice lens through the Clausius-Clapeyron equation. Interpretation of these tests is given in Chapter 2.

3.6.2 Results

Section 3.5 was concluded by presenting the actual engineering parameters of a freezing soil as the average temperature, the average permeability and the average suction of the frozen fringe. The first two parameters can be ascertained quite simply from a conventional freezing test. However, since the average suction is strongly related to the shape of the suction profile which in turn depends on the actual shape of the permeability profile, it is impossible to determine with any satisfactory degree of accuracy the value of that average suction. Recalling that for a given warm-plate temperature, the suction profile in the frozen fringe and particularly the suction at the frost front are unique for a given soil, it appears to be acceptable to consider Pu as a reflection of the average suction Pw of the frozen fringe. The advantage of using Pu instead of *Pw* lies in the ease with which it can be determined by applying Darcy's Equation to the unfrozen soil alone.

The results of series E are shown in graphic form in Figure C.13 to C.20 in Appendix C. A summary of the conditions obtained at the onset of the formation of the final ice lens is presented in Tables 3.3 and 3.4. In most

of the tests, measured temperatures reveal a linear distribution across the samples, confirming the assumption of one dimensional heat flow. Table 3.3 summarizes data where the radial heat flow into the samples was negligible. However, for some samples, especially the longer ones, the recorded temperatures are non linear across the sample. This was nevertheless beneficial to our investigation since both the temperature gradient in the frozen fringe and the length of the unfrozen soil are affected by temperature distribution. This in turn leads to different water intake velocities and different suctions at the frost front. Tests E8 and E9 were both two layered system in which the permeability of the bottom layer was respectively higher, 2cm of porous stone, and lower, 5.1cm of Devon silt preconsolidated to 420 KPa, than that of the reference unfrozen soil of 10^{-7} cm/s. The aim of these two tests was to prove that suction at the frost front is a primary parameter of the freezing soil. They were also used to prove that the warm-plate temperature Tw is only an indirect parameter since one can obtain different suctions at the frost line depending on whether the unfrozen soil of the active system is uniform or layered for the same Tw. All the initial conditions of each test are contained in Appendix C. A summary of data obtained under the prediscribed conditions is presented in Table 3.4.

Four samples were frozen with a back pressure and the resulting drop of the pore water pressure as the system was

Table 3.3 Conditions at the Formation of the Final Ice Lens
for Different Tw

Test	T_w(°C)	T_c(°C)	Initial Height (cm)	l_o (mm)	grad T_f °C/cm	V_o 10^{-6}mm/s
E4	+3.0	-5.5	7.8	30.0	1.03	63.0
E5	+0.4	-4.2	6.0	9.0	0.56	74.0
E6	+0.4	-3.5	7.1	12.0	0.42	58.0
E7	+2.0	-3.5	7.0	32.0	0.66	48.0

Table 3.4 Conditions at the Formation of the Final
Ice Lens

E8	+2.0	-4.2	10.3	48.0	0.43	40.7
					layered medium	
E9	+3.5	-4.1	13.5	77.0	0.61	29.3
					layered medium	
E2	+3.5	-3.6	13.5	82.0	0.50	27.6
					radial heat flow	
NS-8	+2.0	-6.0	17.5	105.0	0.39	20.0
					radial heat flow	

closed was recorded. If the maximum drop in pressure is directly related to temperature as in the Clausius-Clapeyron equation, this would yield the maximum temperature below 0°C, Tm, reached at the base of the ice lens. This can be explained by the fact that, as the system is closed, thermal equilibrium is altered by the sudden removal of the latent heat of phase change of the up flowing water. The restoration of thermal equilibrium requires, therefore, *in situ* freezing of the unfrozen soil. Further advance of the frost front occurs and the temperature distribution is affected as described in Chapter 2. The segregation-freezing temperature, Ts, existing as the ice lens was initiated is therefore warmer than Tm. The relation used to estimate Ts from Tm and the prevailing conditions is given in Chapter 2.

Table 3.5 presents the relevant information from these tests. Figure 3.9 shows the shape of the pore water pressure drop with time and the variation of the calculated maximum and segregation-freezing temperature with warm-end step temperature. This indicates that the time required for thermal equilibrium is around 30 hours. Also the measured drop of pore pressure is around 250 KPa, which indirectly confirms the existence of a frozen fringe since if such a high suction would develop in the unfrozen soil cavitation is most likely to occur. Finally Figure 3.9 clearly shows that the segregation-freezing temperature, Ts, is relatively insensitive to changes in the warm-plate temperature, at least for temperatures warmer than +1.0°C.
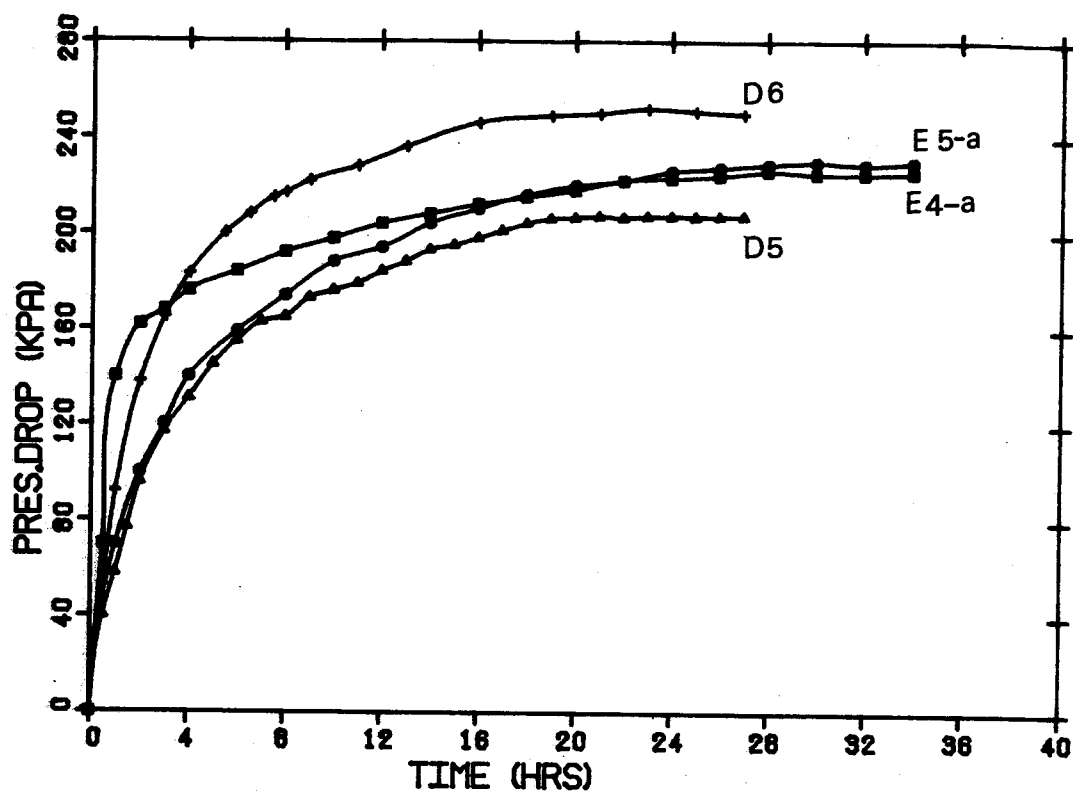
FREEZING TESTS WITH BACK-PRESSURE
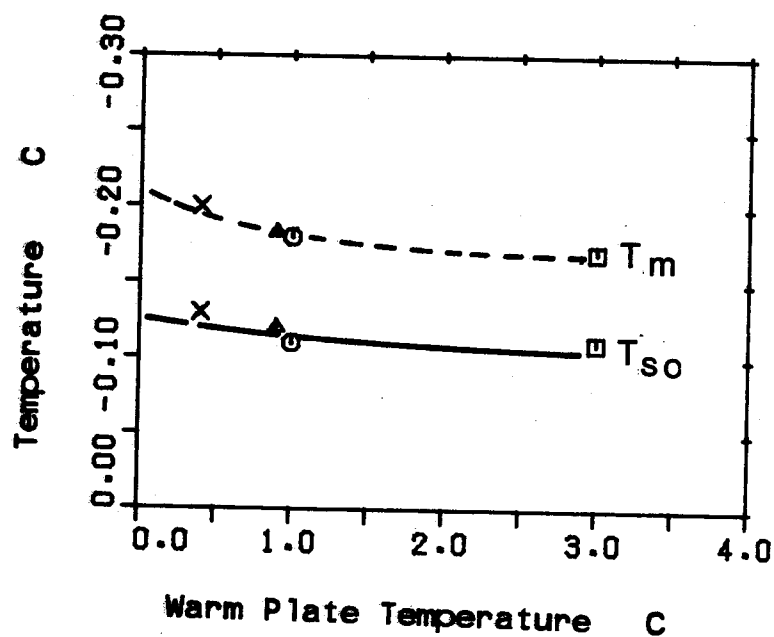
Figure 3.9   Results of Freezing Tests with Applied Back
             Pressure

Table 3.5 Results of the freezing tests with applied
back pressure

Test	Tw(°C)	Tc(°C)	lo(mm)	Ho(mm)	Vo 10^{-6}mm/s
E4a	+3.0	-6.0	13.2	44.0	100.0
E5a	+0.4	-3.0	5.0	32.0	110.0
D5	+1.0	-3.0	23.0	85.0	48.0
D6	+0.9	-3.0	16.0	59.0	60.0

Analysis of data obtained with the conventional freezing tests were performed using Equation 3.28 with a value of -0.10°C for Tso. The overall permeability of the frozen fringe was calculated in each test. The results obtained at the growth of the final ice lens are summarized in Table 3.6. A distinct relationship between the average permeability of the frozen fringes and the suctions at the frost front emerges and is shown in Figure 3.10.

This confirms the concluding statements made in Section 3.5 and gives strong support to the thermodynamic reasoning used to describe a freezing system.

A similar relationship is obtained between the segregation potential and the suction at the frost front of each sample. It is noteworthy to recall that the segregation potential of a freezing soil has been defined as the ratio of the water intake rate and the temperature gradient in the

Table 3.6 Variation of the Characteristics of the Frozen Fringe with Pu

Test	$-Pu(KPa)$	$do(mm)$	$Kfo(10^{-10}cm/s)$	$SPo(10^{-5}mm^2s^{-1}\ {}^{\circ}C^{-1})$
E4	-18.2	.97	5.72	61.2
E5	-5.3	1.80	11.10	132.1
E6	-5.6	2.40	11.60	138.0
E7	-14.6	1.52	6.60	72.7
E8	-10.4	2.30	8.30	94.6
E9	-29.3	1.64	4.90	48.0
E2	-22.0	2.00	5.36	55.2
NS-8	-21.0	2.56	4.90	51.3
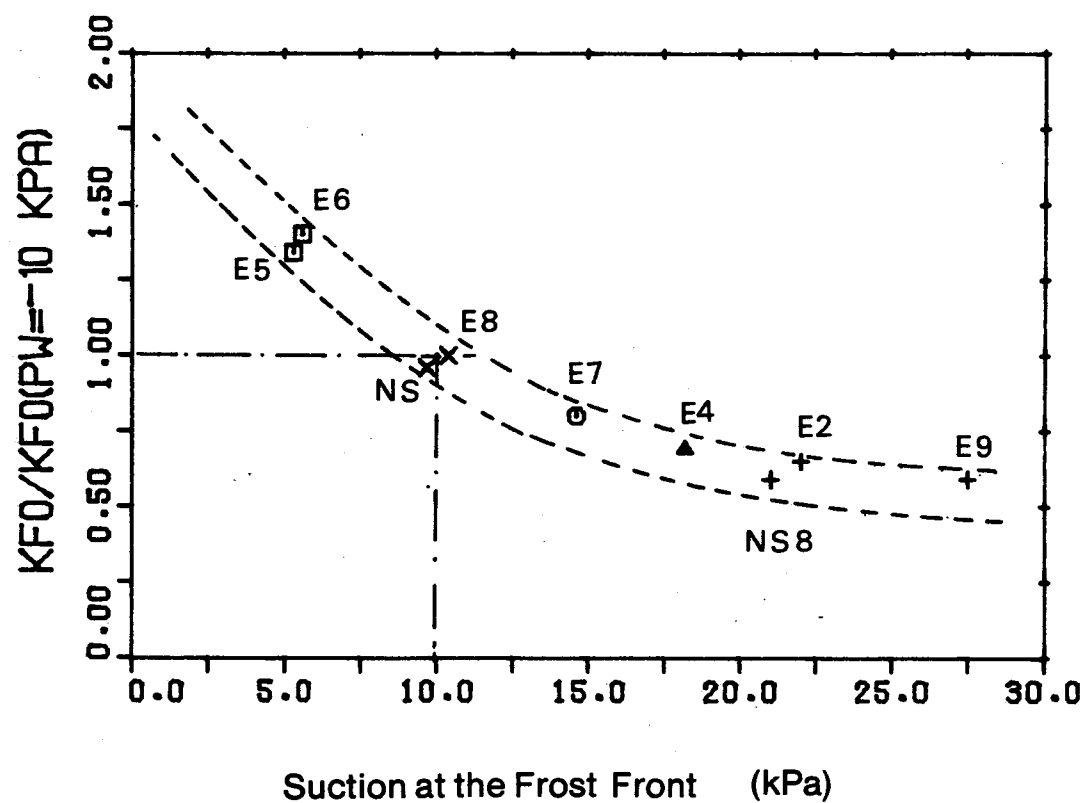
$$Kfo(Pu=-10 \text{ kPa}) = 0.8 \times 10^{-10} \text{ cm/s}$$

Figure 3.10 Overall Permeability of the Frozen Fringe versus
Suction at the Frost Front for Devon Silt

frozen fringe. The segregation potential is, therefore, a direct measurable parameter and is not subjected to any limiting assumptions. This relationship is presented in Figure 3.11.

Again, this demonstrates that the segregation potential of a soil decreases with increasing suction at the frost line. Also for a given suction at the frost front, tests E5 and E6 confirm the uniqueness of the segregation potential as it was established previously from the series NS at a different suction. The results obtained from tests NS-8, E2 and E9 fall remarkably well on the same curve obtained from the tests where the heat flow was primarily one dimensional and the samples uniform. This proves the validity of the premise that the average suction in the fringe is a fundamental parameter of a freezing soil.

3.7 CONCLUSIONS

It has been established that a freezing system can develop different suction profiles within the frozen fringe, dependent on the thickness of the unfrozen soil and the temperature gradient in the frozen fringe. It has also been demonstrated that the suction at the frost front significantly affects the frozen fringe permeability, Kfo, and the segregation potential, SPo. However, the segregation-freezing temperature, Tso, is only slightly affected.
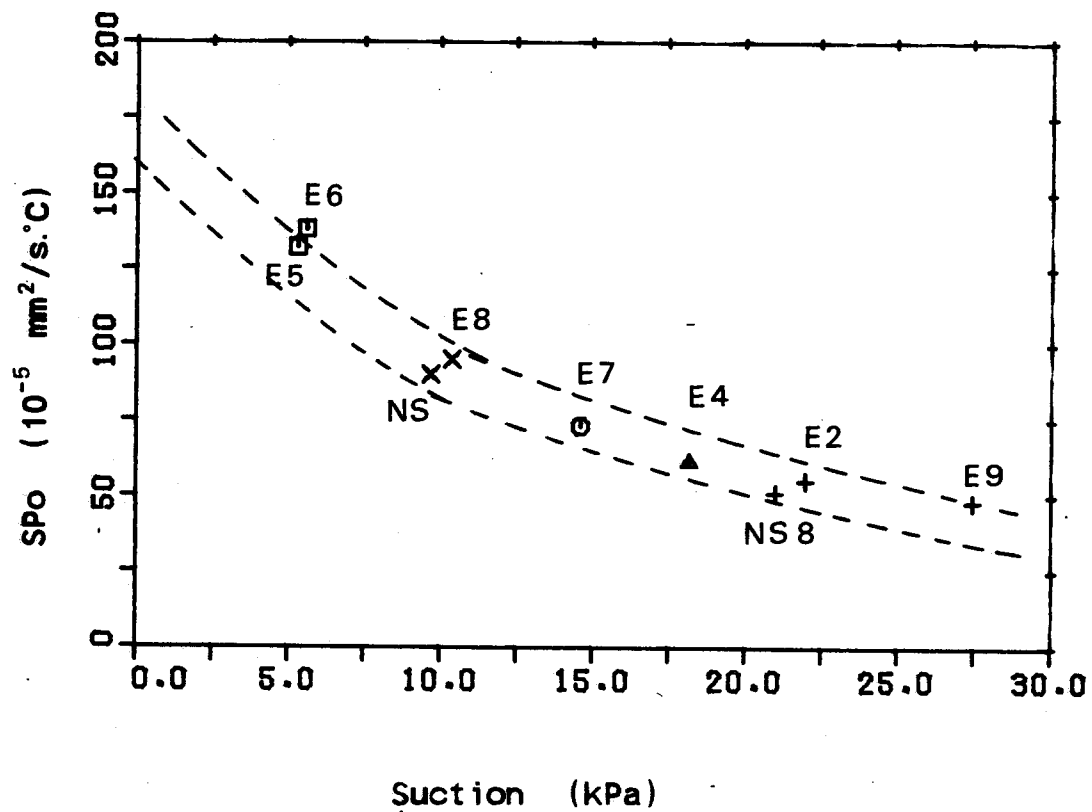
Figure 3.11 Segregation Potential versus Suction at the
Frost Front for Devon Silt

Figure 3.12 summarizes the characteristics of the frozen fringe obtained from the testing program. The suction profile, although qualitative, has been plotted as passing through experimentally determined points, Pw at the top of the fringe and Pu at the bottom. The average permeability of the fringe has been deduced from the freezing tests as described earlier. It is clear that the lower the average suction in the frozen fringe the lower will be the overall permeability of that fringe at a given average temperature Ts. The average temperature is considered herein as a constant since it was proven that Ts is very insensitive to suction changes. The previous analysis also establishes that for a given suction at the frost front, the water intake flux is linearly proportional to the temperature gradient across the frozen fringe. It is, therefore, possible to characterize any freezing soil at the onset of the formation of the final ice lens by a set of straight lines passing through the origin. Each line corresponds to a given suction developed at the frozen-unfrozen interface. The slope of each line represents the segregation potential for the freezing conditions that produce the corresponding suction at the frost front as the final ice lens is initiated. This conceptual characterization of a freezing soil at the formation of the final ice lens are summarized in Figure 3.13. When the suction at the frost front becomes greater, the segregation potential decreases with a concomittant decrease of the slope of the locus of the water intake flux

vs temperature gradient.

Figure 3.13 reveals also that the measured water intake rate at the formation of the final ice lens is dependent on the freezing path. This is striking since for a given temperature gradient across the frozen fringe, different water intake velocities will be obtained at the onset of the formation of the final ice in a given soil for different suctions at the frost front. In other words, one may obtain the same water intake velocity for different temperature gradients in the frozen fringe provided that the suctions at the frost front are also different.

From this simple conceptual model, it is clear that if one reports experimental results on such a plot, i.e. Vo versus grad Tf, either a simple relationship may appear or a more complex relationship may be obtained. This will be investigatedfully in Chapter 7 with different results published in the available literature.
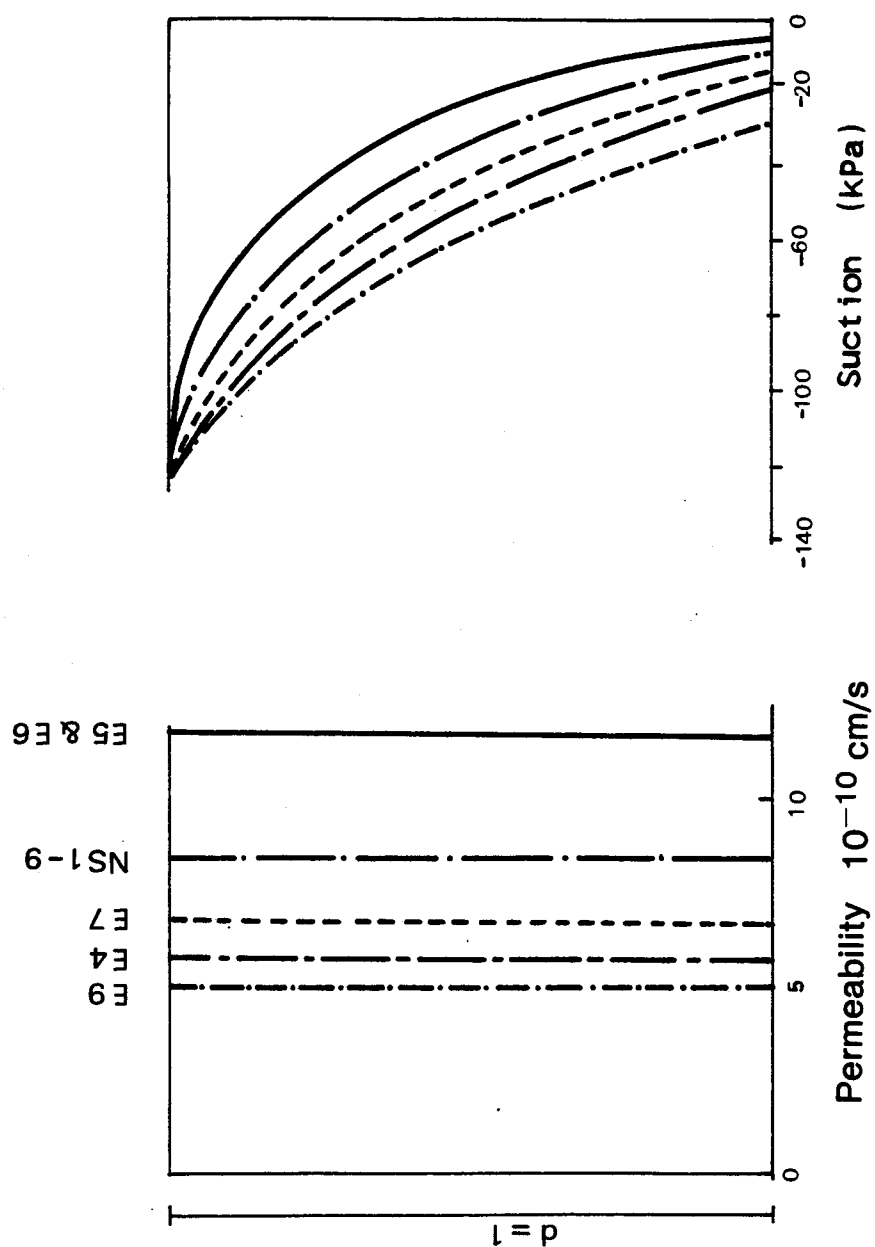
Figure 3.12 Relation Between Suction Profile and Overall
Permeability of the Frozen Fringe of Devon Silt
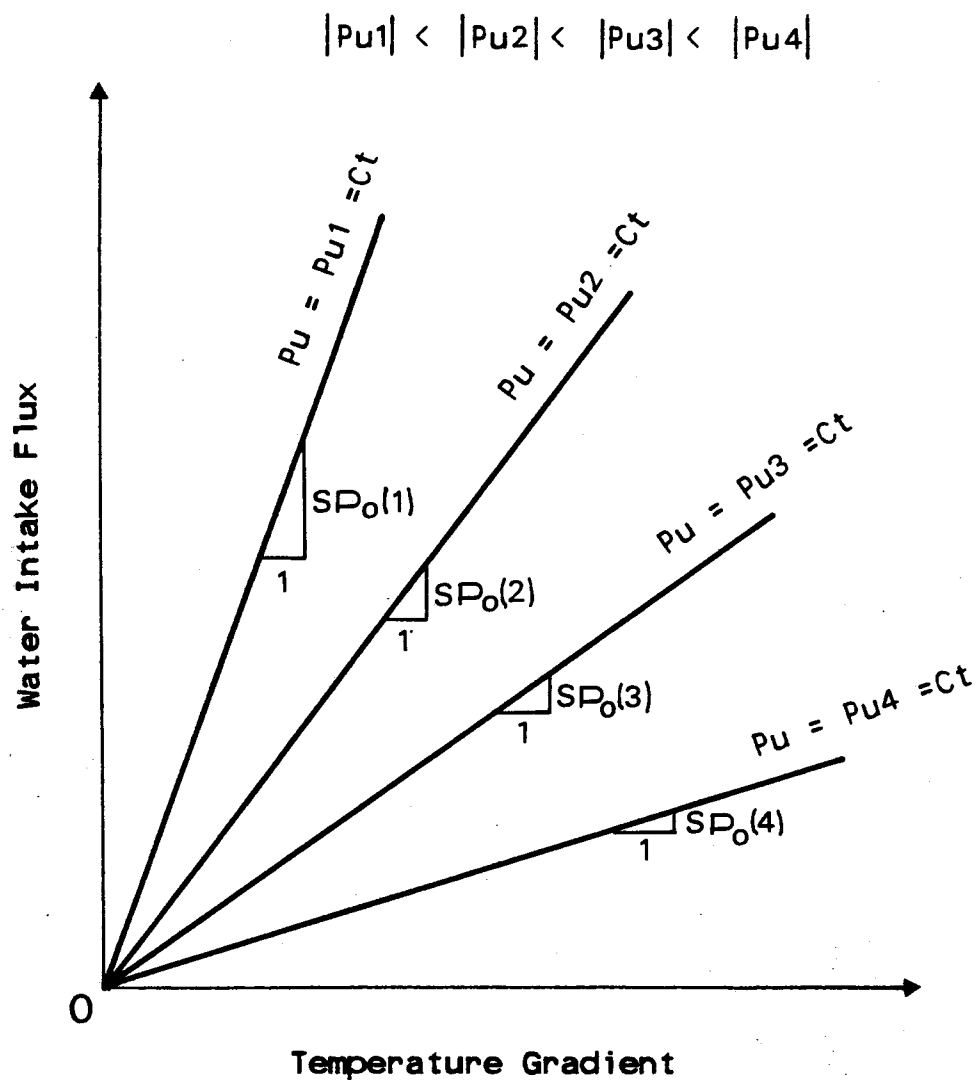
Figure 3.13 Conceptual Characterizationof a Freezing Soil
at the Formation of the Final Ice Lens

4. CHARACTERIZATION OF A FREEZING SOIL DURING AN ADVANCING FROST FRONT

4.1 INTRODUCTION

Chapter 3 explored the characteristics of a freezing soil as the final ice lens was initiated, i.e. when the effect of frost front penetration is almost eliminated. This Chapter is devoted to developing a frost heave model that considers conditions of unsteady heat flow, when the frost penetrates into the unfrozen soil. In the light of the results discussed in Chapter 3, a review of existing models. for freezing soils is presented. Emphasis is given to mass transfer.

Then, the characteristics of the freezing soil are explored in order to develop a comprehensive frost heave model. Comparison of predicted freezing behavior with actual laboratory freezing tests are presented in order to evaluate the performance of the model developed here.

4.2 REVIEW OF PREVIOUS MODELS WITH EMPHASIS ON MASS TRANSFER

Frost heave results from a complex interaction between heat and mass transfer in freezing soils. Fourier's general

equation (3.11) is widely used to model heat transfer in freezing ground when conduction dominates. Several simplifications have been made by different investigators to deal with thermal properties of frozen soils, unfrozen water content and heat transfer by convection. Although these parameters influence slightly the position of the 0°C isotherm and the rate of frost front penetration, the most important factor with regard to frost heave remains the accuracy of mass transfer modelling. Consequently, in the light of the results reported in Chapter 3, it was thought appropriate to analyse different existing models with respect to mass transfer, the type of driving force and the parameters used to describe the frozen soil. Only those models considering simultaneous flux of fluid and heat will be considered.

In essence, laminar fluid transport in any porous media is fully described if the driving force and the transmission and storage properties of the medium are known. These parameters are well understood for the unfrozen part of the freezing system. However, for the frozen part, they represent the key features that differentiate each model. The hydraulic conductivity of the frozen soil is the most controversial parameter within existing models.

Harlan (1973) considered that the storage and transmission characteristics of frozen and partially frozen soils are directly analogous to those of unfrozen soil at similar energy states as represented by the soil-water

pressure head. That is, for a given soil, the soil-water potential -- unfrozen water content and the soil-water potential -- hydraulic conductivity functional relationships of the frozen soil are assumed to be equivalent to the pressure-head -- water content and the pressure-head -- permeability functional relationships for the unfrozen soil.

The driving force is essentially Gibb's free energy of soil-water in the frozen soil and is related to temperature and pressure conditions through the following relation:

$$DGw = (RT*/m) \ln Aw \dots\dots\dots\dots\dots\dots\dots 4.1$$

where   R is the ideal gas constant

   m is the molecular weight of water

   Aw is the activity of liquid water

Assuming that water vapor is an ideal gas, the activity Aw of water is equal to the relative vapor pressure of water in equilibrium with soil at the temperature and pressure conditions of the system (Kijne and Taylor, 1964).

$$DGw = (RT*/m) \ln P/Po \dots\dots\dots\dots\dots\dots\dots 4.2$$

where   P is the vapor pressure of soil water

   Po is the vapor pressure of pure water

Since ice and unfrozen water are in equilibrium in the frozen medium, the vapor pressure of the unfrozen water must equal the vapor pressure of pure bulk ice.

As shown in Figure 4.1, Equation 4.2 predicts free energy differences of the same magnitude as Equation 3.3 which is the Clausius-Clapeyron equation applied to a closed system (no water flow) with zero external pressure.

The generalized mass transport equation for one dimensional unsteady flow in a saturated or unsaturated porous medium combined with the previous parameters gives:

$$d[K(z,T,p) \ d\phi/dz]/dz = dW/dt + DS \dots \dots \dots \dots 4.3$$

where   W is the water content (liquid state)

   p is the matrix pressure or capillary pressure head

   T is the temperature

   ϕ is the potential (ϕ = DGw + Z)

   Z is the elevation head

   DS is the change in ice per unit time and per unit volume

Harlan (op.cit.) adopts a relationship between permeability of frozen soil and free energy of soil-water which leads to a functional relationship between permeability, temperature and suction. As established in Chapter 3, this is the most suitable and complete characterization of a freezing soil.

Equation 4.3 can easily be solved in terms of soil-water potential with a fully implicit finite difference scheme. However, Harlan using this approach does not specify the boundary conditions with regard to mass transfer. It would be reasonable to consider zero potential at the level of the free water table and to specify a single value for the driving potential using Equation 4.2 somewhere within the frozen soil.

Harlan's model adequately describes the physical properties of a freezing soil under quasi steady state

conditions. However, it does not lead easily to the establishment of a functional relationship between permeability of frozen soil and free energy of the unfrozen water. Identical difficulties are encountered in the determination of permeability of unsaturated unfrozen soils and pressure-head functional relationships.

The model presented by Kay et al (1977) uses the assumption that the pressure in the unfrozen water films of the frozen soil is related solely to temperature by the Clausius-Clapeyron equation, with the ice pressure term equal to zero in the case of zero overburden load. The frozen soil permeability, on the other hand, is a function of the pressure in the unfrozen water films. The following relationship was adopted by Kay et al:

$$K = Ko(exp(-gp**2) + f/Ko) \dots\dots\dots\dots\dots 4.4$$

where   g and f are constants determined from laboratory

tests

Ko is the unfrozen soil permeability

Equation 4.4 reveals that there is a minimum permeability of the frozen soil as p approaches infinity, i.e. as the temperature becomes more and more negative. This minimum permeability was taken from test data presented by Williams and Burt (1974) and was assigned a value of 10^{-6} cm^2 / (sec bar) in calculations.

Mass transfer to the frozen soil was described by the following realtion:

$$C.dT/dt + \rho i/\rho l.(dS/dt) = d[K.(\rho l.L'/To).dT/dz]..4.5$$
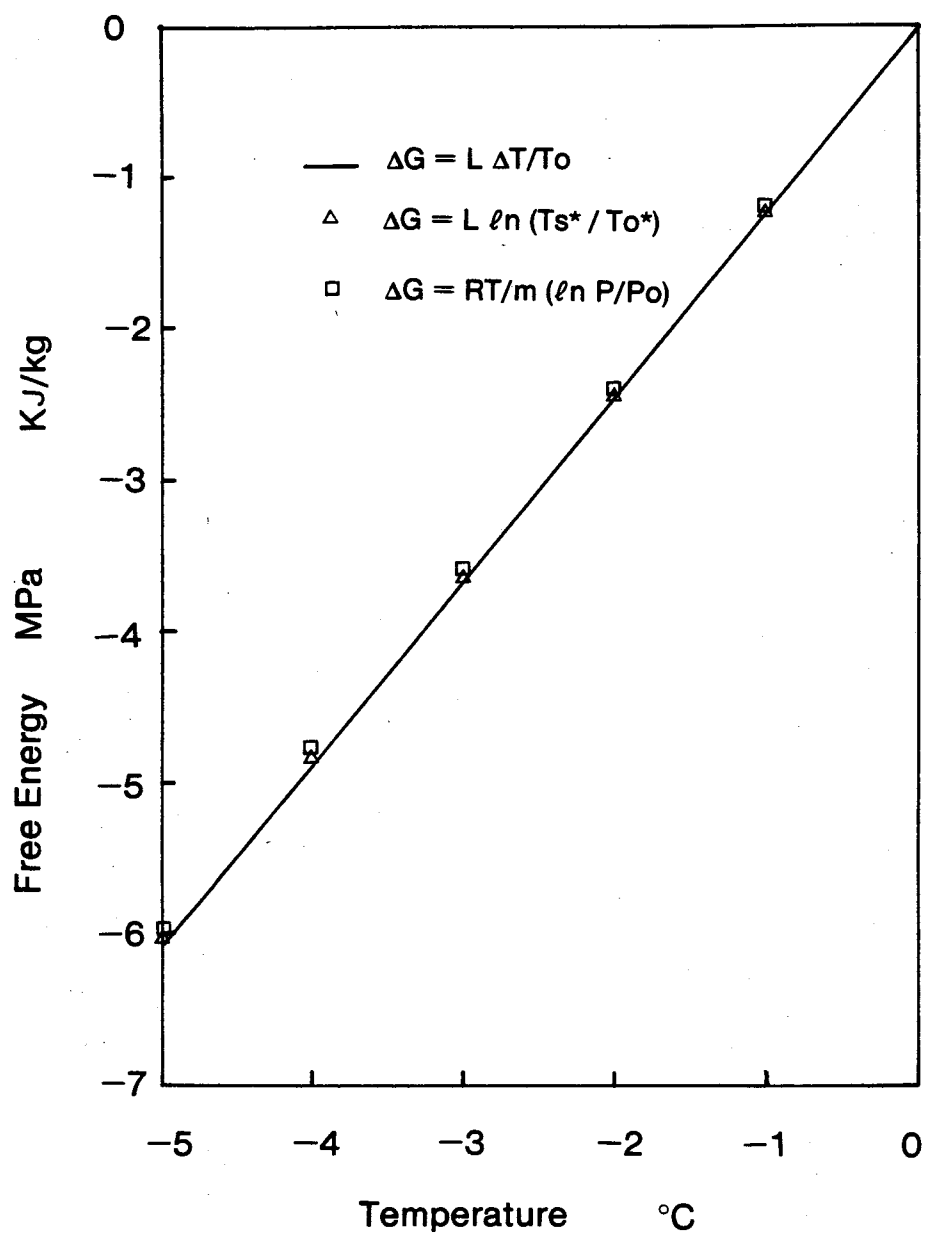
Figure 4.1   Free Energy of Frozen Soil in Relation to
             Temperature
             (after Johanson, 1977)

This equation establishes clearly that the driving potential is related to the temperature by the Clausius-Clapeyron equation everywhere within the frozen soil. As discussed in Chapter 3, this results in a linear suction profile in the case of a linear temperature distribution. While this is most likely the case at quasi steady state conditions, it has been argued in Chapter 3 that the Clausius-Clapeyron equation does not hold within the fringe. Therefore, the constitutive equation for water transport adopted by Kay et al (op. cit.) does not adequately describe the segregation process in a freezing soil. Moreover, since the pressure is directly related to the temperature in their model, the permeability of the frozen soil is implicitly related solely to temperature as well, which is obviously not the case for freezing soil with free access of water.

Good agreement between the volume of water intake predicted from Equation 4.5 and a laboratory test were reported by Kay et al. However, the agreement may be fortuitous as the results were only quoted for the first 20 minutes of the test when the system is highly unsteady. Furthermore, the sample size of 3 cm is believed to be too small to carry out a meaningful freezing test.

Aguirre-Puente et al (1977) proposed that suction is an intrinsic characteristic of a freezing soil, fully independent of the rate of heat flow and the rate of frost front advance. An attempt was made to measure this suction from laboratory tests where tensiometers were placed in the

unfrozen soil. During freezing, the suctions were recorded
at their respective locations. The suction at the frost
front is then obtained by extrapolating. In their model,
this suction is applied at the freezing front throughout the
simulation. Furthermore, it is also assumed that the
freezing front may lie within the frozen zone, allowing for
the existence of a frozen fringe. The position of the
freezing front is defined by the -DT isotherm which was
determined by matching experimental heave and frost
penetration with those obtained from the computer model.
Once a given value of -DT is adopted, a variable
permeability is assigned to the frozen fringe confined
between -DT and 0°C through a functional relationship
depending upon temperature only. The values of the
permeability of the frozen fringe were extrapolated from
test data given by Williams and Burt (1974).

This model, although closer to an engineering approach
to frost heave, since Darcy's law is used to describe the
flow through a two layered porous medium composed of the
unfrozen part and the frozen fringe, possesses two
inconsistencies. The suction potential considered as the
driving force for water migration is actually Pu, the
suction at the frost line since its value is obtained from
the extrapolation of tensiometer readings in the unfrozen
soil(Aguirre-Puente et al,1971).It is clear that treating
frost heave as a problem of impeded drainage through a zone
of reduced permeability requires a knowledge of the driving

potential at the base of the ice lens, Pw, which is approximately one order of magnitude larger than Pu as demonstrated in Chapter 3. This, in turn, leads to an underestimate of the permeability of the frozen fringe and conversely -DT. However, it is possible to match their experimental results by taking an adequate value for -Dt, but this is not relevant to a rational approach. Furthermore, changing the value of -DT should result in changes in suction potential which is not the case in their model. Moreover, the permeability of the frozen soil is related solely to temperature which is not the case for freezing soil with free water supply.

More recently, Taylor and Luthin (1978) considered the water content gradient as the driving force for water movement to the frozen zone in freezing soils. The governing equation for this formulation may then be expressed as:

$$d[D \, dW/dz]/dz = (pi/\rho w)(dS/dt) + dW/dt \ldots \ldots \ldots 4.6$$

where   D is the soil-water diffusivity

          S is the volumetric ice content

          W is the volumetric soil water content

In the frozen soil, the soil-water content refers to the unfrozen water content at a given temperature obtained from laboratory tests. Since these laboratory tests are closed system freezing tests, the model proposed by Taylor and Luthin fails also to adequately describe a freezing system since it has been shown in Chapter 3 that the unfrozen water content is a function of free energy which is dependent upon

temperature and suction.

The closed system freezing tests reported by Jame and Norum (1972,1976) and Dirksen and Miller (1966) were simulated by Taylor and Luthin (op. cit.) using their model. The frozen soil diffusivity was obtained by introducing an impedence factor I which is a function of ice content. By varying this factor, Taylor and Luthin predicted the experimental results quite well.

Although their model appears to be adequate for prediction of closed-freezing tests, it has not been used to simulate heave and water redistribution in open-system freezing tests. One might expect more divergence in the latter case since the characteristics of the freezing soil are not adequately taken into account in their model.

Guymon et al (1980) assume that Darcy's law describes water transport to the freezing front. The physical characteristics of the freezing soil are estimated using Gardner's (1958) relationship:

For the unfrozen water content:

$$Wu = no/(A'.|P|.\exp(m) + 1) \ldots\ldots\ldots\ldots\ldots 4.7$$

For the hydraulic conductivity of frozen soil:

$$Kf = Ko/(B'.|P|.\exp(n) + 1) \ldots\ldots\ldots\ldots\ldots 4.8$$

where   no and Ko are respectively the porosity and

                permeability of the unfrozen soil

                A',B',m,n are constants for a particular soil

                P is the soil-water pressure head of the unsaturated

                unfrozen soil.

As in Harlan's model, the permeability of the frozen soil during freezing with free water supply is correctly accounted for in Guymon et al's model.

The driving force is a suction potential acting somewhere in the frozen soil. In their paper (op. cit.), lack of information with respect to its location and magnitude make careful scrutiny of their analysis difficult. More recently, Berg et al (1980) give a complete description of the previous model. The suction-potential is related to the equivalent critical pore radius of the soil, rc, which is estimated from the soil moisture characteristic curve (desorption portion). They state that the critical pore radius corresponds to the critical suction Pc. Pc is the suction at the point where the slope of the tension vs percent saturation curve decreases rapidly. The following equation is used to determine the radius:

$$rc = - 2 \, \delta aw/Pc \dots\dots\dots\dots\dots 4.9$$

where δaw is the air/water surface tension

Furthermore, the authors adopt the view that Pc is also an indication of the maximum heaving pressure of a freezing soil. By adopting Penner's (1959) statement, based on results from laboratory tests, that the maximum overburden pressure to stop heaving appeared to be about twice as great as the maximum soil water tension required to stop heaving, the following equation for computing the maximum suction potential is obtained:

$$2Pw = Pc = -2 \, \delta iw/rc \dots\dots\dots\dots 4.10$$

where δiw is the ice/water surface tension

Unfortunately, Equation 4.10 has no physical meaning since for a given critical pore radius and for the case of atmospheric pressure in the ice, the Kelvin equation gives:

$$Pw = -2\ \delta iw/rc\dots\dots\dots\dots\dots\dots\dots\dots\dots\dots\dots4.11$$

Although a valuable attempt to embrace the microphysics of a frozen soil has been made, the model presented by Guymon et al (1980) does not correctly consider the suction potential at the freezing front which, in turn, affects the water intake flux.

In order to predict heaving forces and the effect of overburden, Hopke (1980) proposed the adoption of the generalized Clausius-Clapeyron equation (1.6) to describe the freezing system with respect to temperature, pore water pressure and ice pressure. The frozen fringe is indirectly introduced as Hopke assumes that lensing occurs whenever the ice pressure is at least equal to overburden. In order to match experimental data, it appears that it is necessary to introduce an extra length to the predicted thickness of the fringe. This extra distance is a totally empirical variable and is ambiguous in meaning.

The behavior of the model with respect to overburden will be discussed in Chapter 6. Here, only the assumptions made concerning mass transfer will be evaluated.

Soil-water characteristic curves of the unfrozen soil are used in Hopke's simulation. The permeability of the unsaturated medium is related to the water content through

Mualem's (1976) correlation. As pointed out by Koopmans and Miller (1966), the standard data for the drying and wetting of certain soils (the soil water characteristic curves that show water content as a function of pore water pressure) can be used to predict unfrozen water content as a function of temperature and pore pressure. The temperature and the pore pressure are related through the Clausius-Clapeyron equation with $P_i = 0$. This method is adopted by Hopke and therefore yields the unfrozen water content which would be obtained in a closed-system freezing test. The hydraulic conductivity for frozen soils is assumed to be equal to that of the unfrozen soil at the same liquid water content, which results in an inadequate description of the freezing soil with free access to water.

Finally, Gilpin (1980) developed a simple frost heave model which includes the effect of overburden load. His primary interest was to provide an explanation for all the mechanisms associated with frost heave such as heaving pressure, rhythmic ice banding and the nature of the driving force. Although these phenomena and their understanding are of great importance to frost heave, they are not relevant to the purposes of this section and will be discussed in Chapter 5.

Gilpin's model is different from the previous ones because thermal and mass balance at the boundaries defined by T_i and T_f are solved analytically with an iterative method. If the soil parameters and the boundary conditions

are specified, the basic equation of his model can be used to evaluate the remaining four unknowns dhs/dt, Pu, Ts and dX/dt. The advantage of this model over that proposed by Hopke (1980) lies in the fact that no arbitrary value of Ts has to be defined in order to account for the reality. Ts is established by satisfying the thermal balance at the segregation freezing level and the compatibility between the suction related to Ts by virtue of the generalized Clausius-Clapeyron equation and the water flux induced by this suction. Water flux is obviously strongly dependent upon the permeability of the frozen fringe. Therefore, an adequate description of the freezing soil with respect to its permeability is vital to the success of this model which basically is entirely acceptable. In his model, Gilpin considers the soil as a packing of uniform spheres which enables the derivation of a functional relationship between permeability and water content. Extending this relationship to the case of frozen soil, Gilpin adopts an expression between the permeability and the temperature, which is only valid for the case of no water flow and is not relevant for the case of freezing soils with free water supply. The same limitation as for Harlan's (1973) and Guymon's et al (1980) models again hold: the need to characterize the freezing system by a functional relationship between the permeability of the frozen soil and the free energy of the unfrozen water. Furthermore, this is aggravated by the fact, as shown in the next two sections, that the freezing characteristics

4.3 PREDICTIVE CAPABILITY WITH THE INTRINSIC PARAMETERS

One of the most serious drawbacks of Harlan's and Gilpin's models is the requirement of a functional relationship which relates the permeability of the frozen soil to the free energy of it's unfrozen water. This is further aggravated by the fact that, to date, no satisfactory methods for measuring the permeability of frozen soil have been developed.

The model presented in Chapter 3 overcomes the difficulties associated with Harlan's model. It has been demonstrated that the microphysical parameters of the frozen fringe can be replaced by a measurable macrophysical parameter, its overall permeability, Kf. Moreover, this parameter is characteristic of a given soil since laboratory data demonstrated that a unique value of Kf was obtained for a given suction at the frost front. The overall permeability of the frozen fringe may be found from controlled freezing tests with constant temperature boundary conditions as discussed in Chapter 3.

In order to extend the analysis of frost heave to conditions with an advancing frost front, i.e. unsteady heat flow, the governing equations presented in Figure 3.1 are formulated with the following assumptions.

The application of the governing equations may be simplified if one assumes that the thermal properties of the

frozen zone are independent of the temperature. Furthermore, this study takes the view that the amount of unfrozen water remaining in the frozen soil is "lumped" at the frost front by the dimensionless parameter c defined in Chapter 3. It should be stressed that the program could take into account non linear variations of the properties of the frozen soil as well as a relationship between the unfrozen water content and temperature.

Parametric studies, discussed in Section 4.6, which deal with variations in the thermal conductivity of the frozen and unfrozen soil and variations in c strongly support the above assumptions.

As shown in Figure 3.1, the model accounts for variable values of the segregation-freezing temperature, Ts, and the overall permeability of the fringe, Kf, with time. This formulation permits the description of the more general case where the frozen fringe exhibits variable properties in response to the degree of thermal imbalance of the freezing system. Recalling that Ts and Kf have been determined at the formation of the final ice lens, i.e. close to steady state conditions, the assumption that little changes in those parameters occur during unsteady heat flow appears attractive as a first trial and permits a test of the model. The frozen fringe characteristics are considered constant with time and their values are assigned those measured at the onset of the formation of the final ice lens.

The model also assumes implicitly that the

Clausius-Clapeyron equation holds throughout the freezing process at the segregation-freezing level. As discussed in Chapters 1, 2 and 3 this can be verified at the base of any ice lens. However, at the beginning of freezing, no visible discrete ice lenses are created in freezing soils due to rapid frost front penetration. However, water flow into the frozen soil above the segregation-freezing front is not possible because of reduced permeability. The use of the Clausius-Clapeyron equation is then valid for this situation since it is analogous to the case of closed-system freezing with no water flow where the use of that equation has been justified in Chapter 3.

The governing equations for one dimensional frost heave which are summarized in Figure 3.1 may be written in finite difference form using a scheme proposed by Crank and Nicholson (1947). The moving boundary condition is accounted for by either of the methods described by Murray and Landis (1959). The advantage of the Crank-Nicholson scheme is that it remains unconditionally stable for all values of the time step, Dt, which improves the accuracy beyond that in other somewhat simpler methods. The simultaneous equations so generated are tridiagonal when written in matrix form. A simple algorithm derived from the Gaussian elimination technique for simultaneous equations provides a fast, efficient solution. The details of the finite difference scheme are summarized in Appendix F. The finite difference computer program evaluates the total, segregational and

in-situ heave with time, the temperature distribution with time and the change in moisture content as a function of depth and time.

Data obtained from freezing tests in series NS were compared with the results produced by the predictive program. The input parameters used for this analysis are as follows:

1. Overall permeability of the frozen fringe: $Kf = 0.8 \times 10^{-9}$ cm/s

2. Segregation-freezing temperature: $Ts = -0.10°C$

3. Unfrozen soil permeability: $Ku = 10^{-7}$ cm/s

4. Thermal conductivities:

   $ku = 0.35$ mcal/(mm.s.°C) = 1.47 mW/(mm.°C)

   $kfr = 0.36$ mcal/(mm.s.°C) = 1.51 mW/(mm.°C)

   $kf = 0.43$ mcal/(mm.s.°C) = 1.76 mW/(mm.°C)

The thermal and geometrical boundary conditions have to be specified for each test.

The volume of water drawn into the sample is transformed to segregational heave by:

$$hs = 1.09 \; VOL/A \dotfill 4.12$$

where A is the cross-area of the specimen.

Figure 4.2 compares the measured total and segregational heave in tests NS-1 and NS-2 with the predicted values. It appears that good agreement is obtained at the beginning of freezing for about 12 hours, after which a systematic difference is obtained. However, the computed rate of heave compares well with the measured value as

steady state conditions are approached. This is not surprising since the input parameters characterizing the freezing system are representative of quasi steady state conditions corresponding to the growth of the final ice lens. The predicted total heave is approximately 85% of the observed value at the onset of the formation of the final ice lens. Although this may be sufficient for an engineering approach, the simulation does not model the shape of the actual curves satisfactorily. This is best illustrated in Figure 4.3 where the water intake velocity, both observed and computed, is plotted with time for test NS-4. The measured water intake flux is constant for a period of about 9 hours, then drops slowly with time. The computed velocity for water migration, on the contrary, shows a drastic change during the first 10 hours due to rapid frost front penetration and concomittant changes in the frozen fringe thickness as the temperature gradient in the frozen zone decreases. After that period, the change in temperature gradient shows down, which leads to an almost constant water intake velocity.

Figures 4.4 and 4.5 present a summary of observed and computed results for the series NS. Each symbol is associated with a number which represents the time, in hours, at which the parameters are compared. If the predicted values are equal to the measured for a given parameter, then the representative point would lie on a line at 45° passing through the origin. Figure 4.4 reveals that
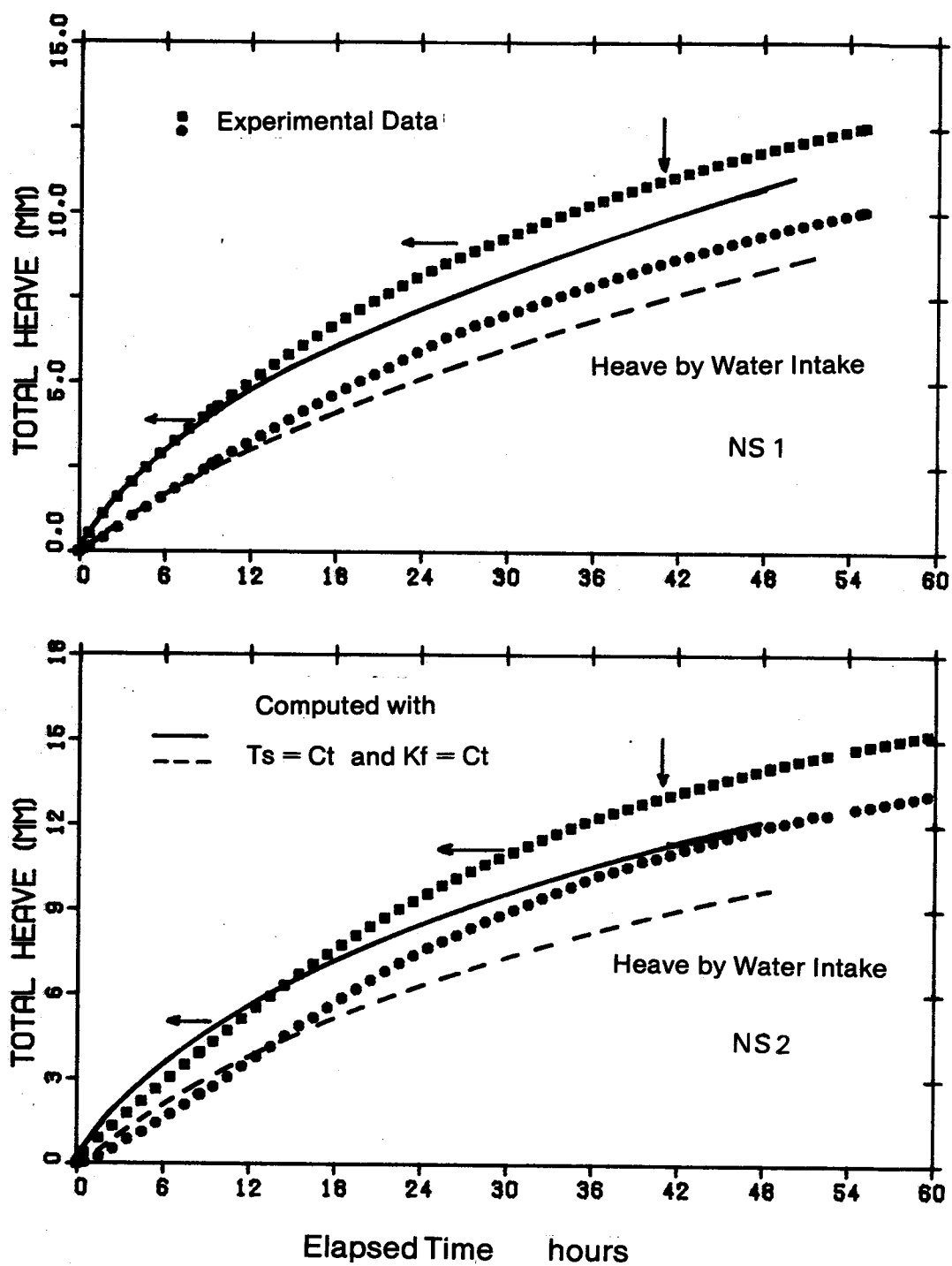
Figure 4.2   Comparison of Prediction Using Constant Freezing
Parameters with Actual Data
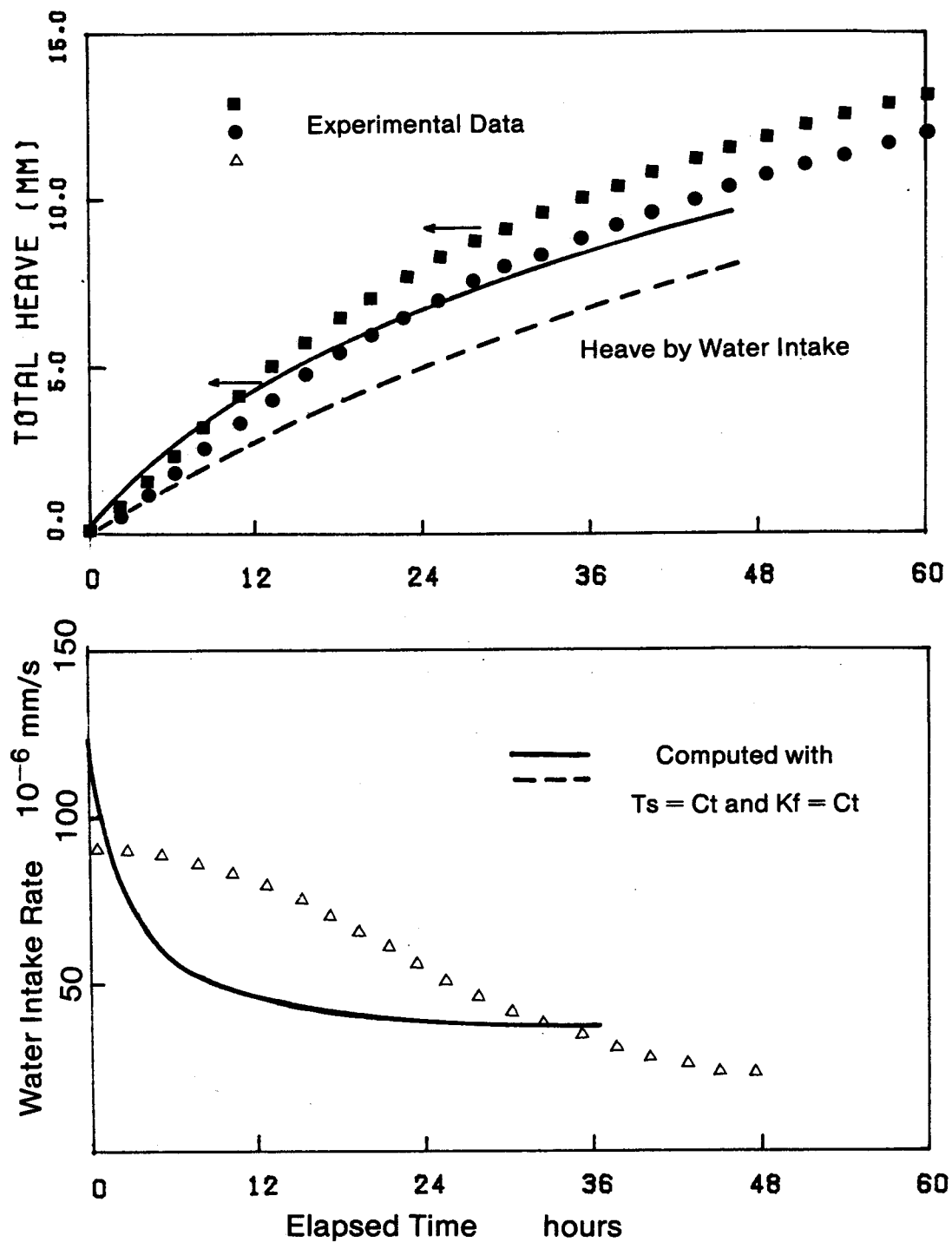
Figure 4.3 Comparison of Prediction Using Constant Freezing
Parameters with Actual Data

the model with the assumption that Ts and Kf are constant during unsteady heat flow overestimates total heave at the beginning of freezing for about 6 to 10 hours and then systematically underestimates its value. Remarkably, a constant trend is observed and the best fit line has a slope steeper than 45° with an intercept on the abcissa at a positive value. Figure 4.5 demonstrates also that water intake velocity deviates from observed values at the beginning of freezing. However, after a period of approximately 12 hours and especially close to quasi steady state conditions, good agreement is observed. This arises from the fact that the characteristics of the frozen fringe used for the simulation are those measured at the onset of the growth of the final ice lens.

It is not surprising that a relatively poor prediction results from the model which assumes that Ts and Kf are constant throughout the freezing tests. As discussed in Chapter 3, the shape of the suction profile and more specifically the suction developed at the frost line influences significantly the characteristics of the frozen fringe. During a laboratory freezing test, the suction at the frost front continually changes. Initially, relatively long flow paths in the unfrozen soil associated with high flow velocities give rise to quite high suctions at the frozen-unfrozen interface. With time, the length of unfrozen soil decreases as does the water flux leading thus to decreasing suctions at the frost line. This, in turn,

influences the characteristics of the developed frozen fringes and is one of the major reasons for the divergence between prediction and actual measurements observed during the early stages of a freezing test.

4.4 VARIATIONS OF THE BASIC FREEZING PARAMETERS DURING TRANSIENT FREEZING

The experimental results obtained in test series NS can be fitted by varying the intrinsic parameters, i.e. the segregation-freezing temperature and the permeability of the frozen fringe with time. If the variation of the segregation-freezing temperature with time is arbitrarily chosen within reasonable bounds, it is then possible to back calculate the value of the overall permeability of the fringe with time that matches the water intake flux . The obvious drawback to this approach is the large member of sets (Ts, Kf) that can be chosen. To explore the dependence of frozen fringe permeability on temperature, three reasonable segregation-freezing temperature variations with time were chosen and the resulting overall permeabilities were calculated. The results are presented in Figure 4.6.

The first two temperature variations, Ts monotonically increasing from a colder temperature than -0.10°C to -0.10°C at steady state and Ts constant, both result in similar frozen fringe permeabilities with time. Both permeability variations increase slowly to the same maximum between 10

number represents the time, in hours
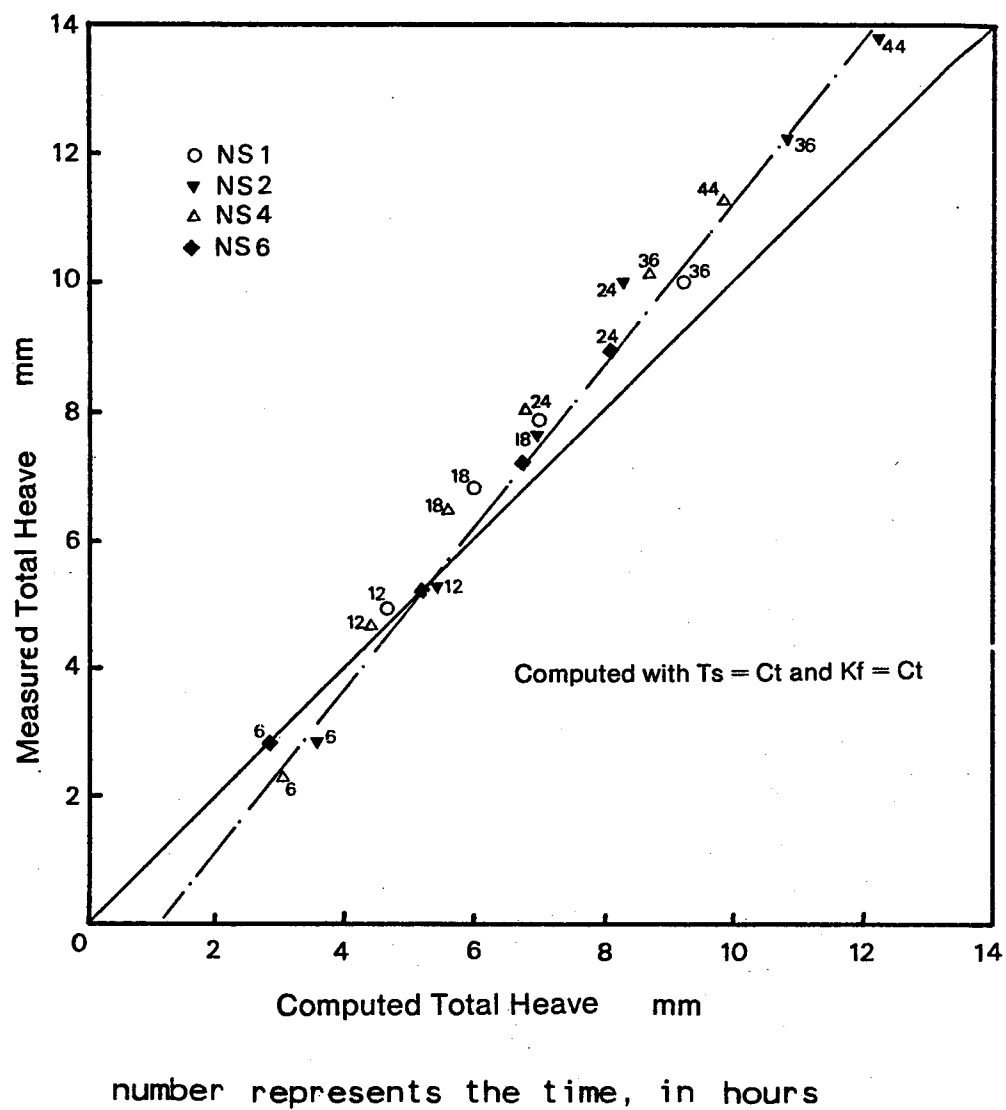
Figure 4.4   Comparison of Predicted Total Heave with Actual
             Data of Series NS
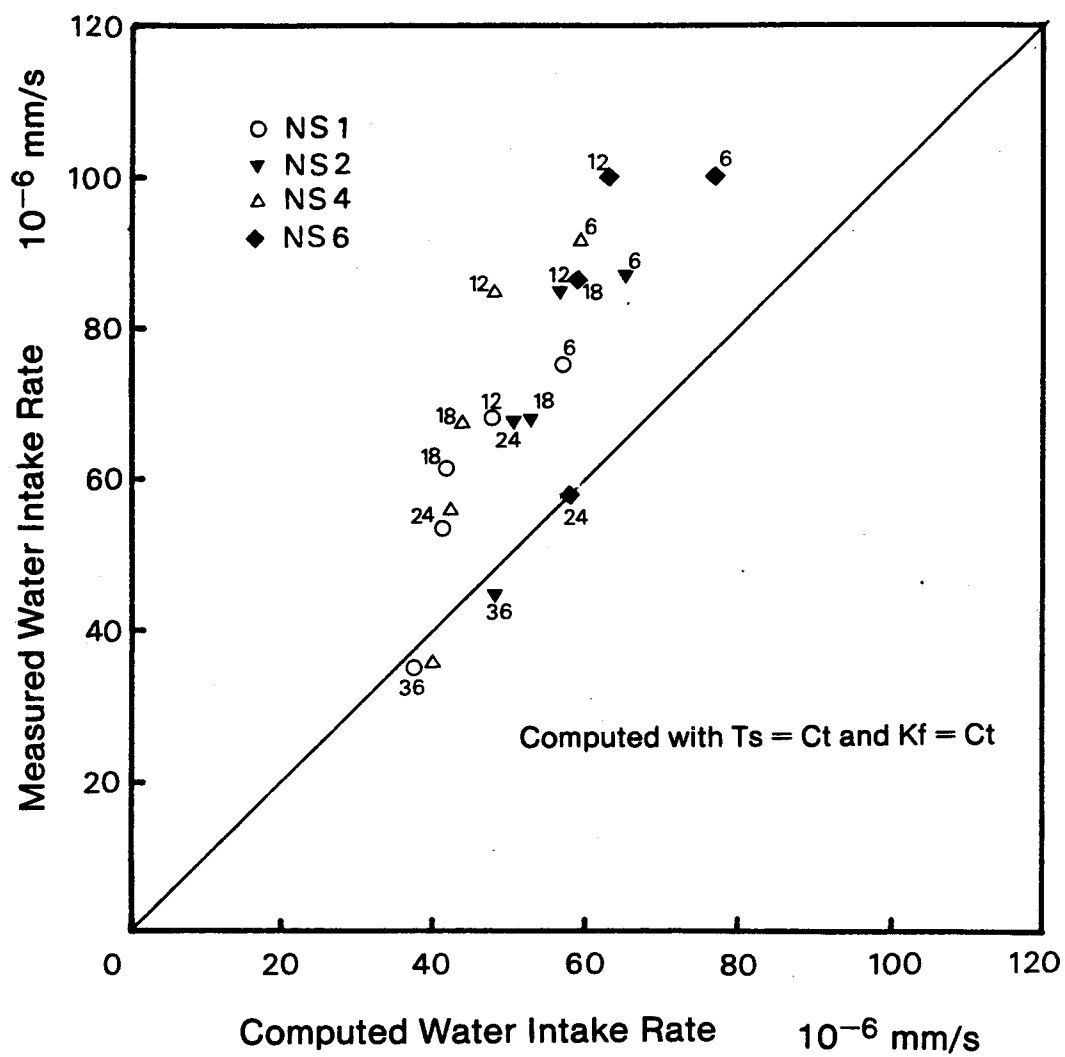
Figure 4.5   Comparison of Predicted Water Intake Flux with
             Actual Data of Series NS

and 20 hours and then decrease to the same steady state values. The similarity and proximity of the two curves clearly indicates once again for Ts less than -0.10°C the overall permeability of the fringe is insensitive to segregation-freezing temperature.

The third temperature variation, Ts monotonically decreasing to -0.10°C results in a somewhat different frozen fringe permeability variation than the first two curves. The backcalculated permeability is approximately constant during the first hours of the freezing test, increases slightly to a maximum and then slowly drops to the same value as the previous cases. The maximum is greater than the previous two situations but is reached at approximately the same time. Full investigation of the freezing tests in series NS and E reveals that the time at which the maximum permeability of the fringe is observed with the previous analysis corresponds more or less to the time at which the zone of active lensing preceding the final ice lens is initiated. In other words, it corresponds to the time at which the temperature changes in the freezing system have slowed down allowing for water to accumulate at a given level for a longer period of time and subsequently to form visible ice lenses. This is discussed in detail in Chapter 5.

It is of value to report here some recent Russian work by Ershov et al (1978) where processes of ice segregation and formation of frozen soil texture were studied using methods of time-lapse photography and scanning microscopy.
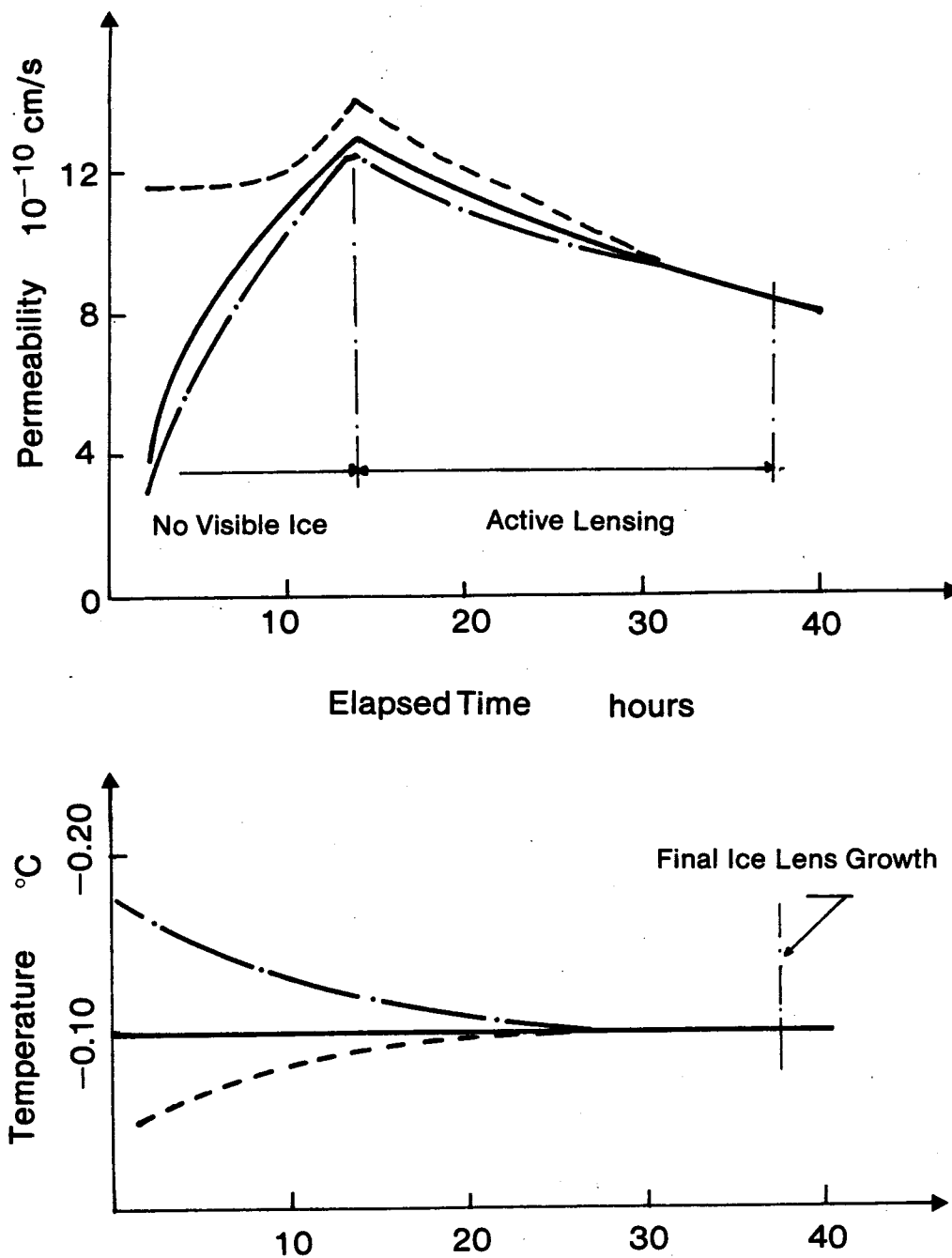
Figure 4.6   Relations between Calculated Permeability of the
             Frozen Fringe and Segregation Freezing
             Temperature

Their results showed that the segregation-freezing temperature increased continuously from a colder temperature than 0°C at the beginning of freezing to 0°C at the end of the test. During the first hours of freezing, the system is highly unstable with respect to temperature and, in most soils, no visible ice lenses form during that period. It is therefore very difficult to estimate the segregation - freezing temperature during the early phase of a freezing test. However, after a while, the system may produce visible ice lenses and the temperature within the sample changes less rapidly. Consequently, the measurements performed by Ershov et al are more reliable during the latter phase of freezing. Nevertheless, their investigation casts light on the physical processes associated with frost heave by demonstrating that variable segregation-freezing temperatures occur during an advancing freezing front. It is reasonable to assume that, as visible ice lenses form, Ts of each new ice lens increases with decreasing rate of frost front advance. At the beginning of freezing, it can be argued that the method used by Ersov et al overestimates the actual value of the segregation-freezing temperature because the actual level of water accumulation is very difficult to assess as the ice content changes are not very significant.

On the other hand, it appears that the water flowing into the frozen soil is not able to accumulate as far as it is supposed to because of drastic changes in temperature and consequently in permeability of the frozen soil.

Accordingly, it is also acceptable to consider that when the temperature change across the specimen is less intense, the intake water may penetrate deeper into the frozen zone. It is therefore speculated that the segregation freezing temperature starts at a temperature warmer than that corresponding to the growth of the final ice lens, decreases during the early phase of freezing to a colder temperature than Ts at steady state conditions and then increases towards the temperature at which the final ice lens is initiated as the system becomes more and more stable. A mechanistic theory of ice lens formation in fine grained soils, presented in Chapter 5, accounts for the change in Ts in the second phase of a freezing test, during the process of active lensing. This theory supports strongly the previous statement that Ts increases during that phase of active lensing. The variation in permeability associated with a segregation-freezing temperature variation of this type has been calculated for test NS-1 and plotted in Figure 4.7. It is shown that during rapid frost front advance, the permeability is approximately constant. As the zone of active lensing is initiated, the permeability drops continuously and ultimately reaches the value determined at the onset of the formation of the final ice lens. It is necessary to emphasize the tentative nature of this argument.
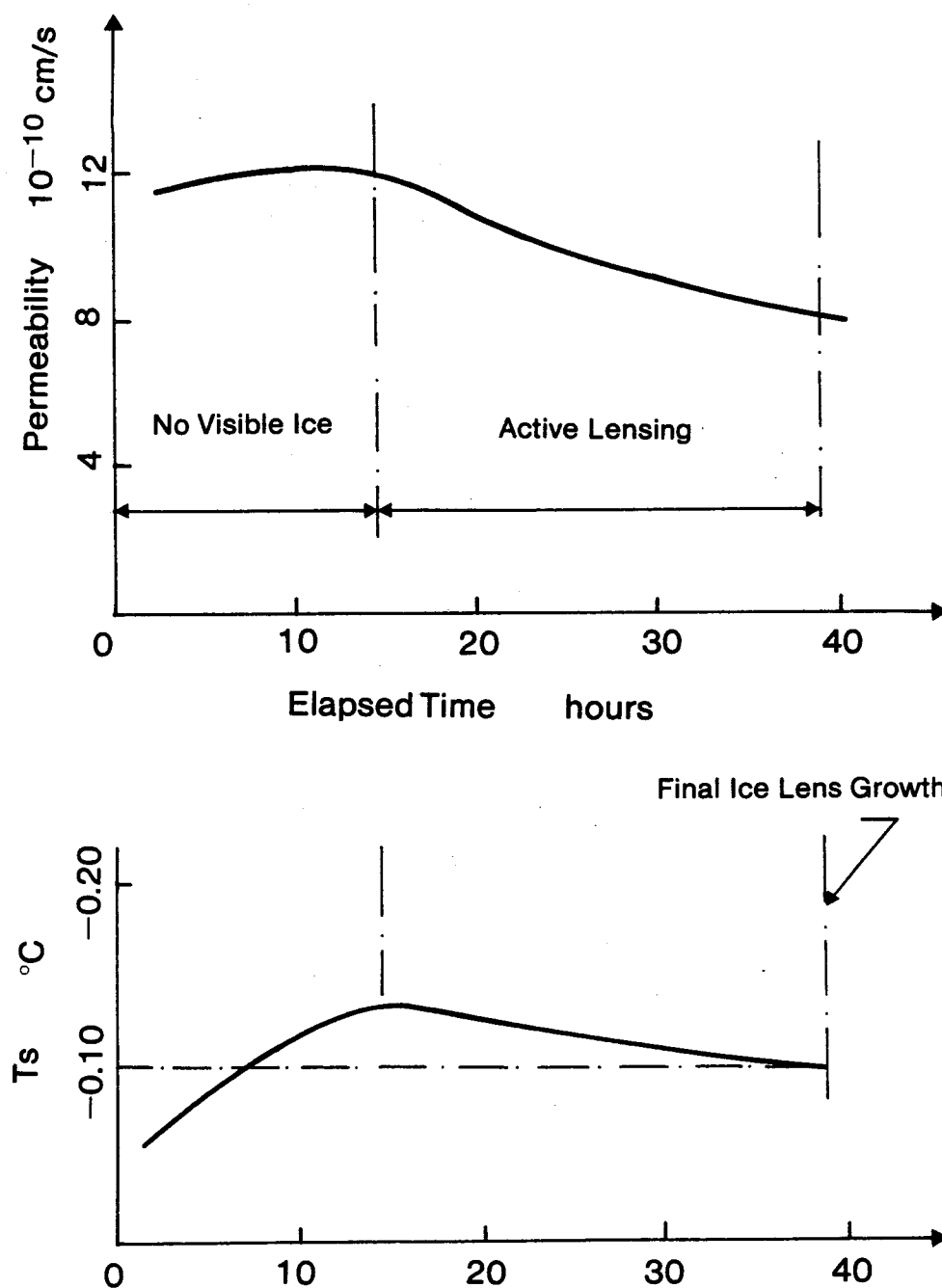
Figure 4.7   Possible Variation of Frozen Fringe
Characteristics during Transient Freezing (Test
NS-1)

4.5 ANALYSIS OF FREEZING TESTS USING THE SEGREGATION POTENTIAL

4.5.1 The Segregation Potential During Transient Freezing

Although the previous analysis provides insight into the basic processes involved during freezing of soils, a more attractive approach is to consider the segregation potential of the freezing soil during an advancing frost front.

The segregation potential was defined in Chapter 3 at the initiation of the final ice lens. It can be defined in general to be the ratio of the water intake flux and the temperature gradient across the frozen fringe at any instant t:

$$SP(t) = V(t)/grad\ Tf(t) \dots\dots\dots\dots\dots\dots 4.13$$

Equation 4.13 demonstrates that SP of any freezing soil can be easily ascertained at any time because it is possible to measure quite accurately both water intake flux and temperature variations with time in any well instrumented freezing test. Furthermore, no limiting assumptions on the nature of the fringe are required.

In order to proceed with an analysis of a freezing system in terms of SP, it is necessary to assess the factors that affect this parameter. Results in Chapter 3 demonstrated that at the formation of the final ice lens, close to steady state conditions, the suction developed at the frost front strongly influences the segregation

potential. Figure 3.10 shows that SP decreases with increasing suctions. It is important to remember that it is the average suction within the frozen fringe which is the basic parameter. However, since it is impossible to date to measure directly this suction, the present study will employ the suction at the frost line instead of the average suction. This can be justified by the fact that for a given soil, the suction at the frozen-unfrozen interface is uniquely related to the average suction as demonstrated in Chapter 3.

The application of the relationship between SP and Pu obtained at quasi steady state conditions to the unsteady heat flow condition when the frost front is advancing, does not seem to be acceptable. This is deduced from the fact that for a given suction, Pu, different values of SP can be obtained depending on the state of thermal imbalance in the sample. For example, in the case of Devon silt, the value of SP at the onset of the growth of the final ice lens is approximately 50×10^{-5} mm^2/(s $^{\circ}$C) at a suction of -20kPa. Whereas, another test in which the same suction at the frost line is obtained during an advancing frost front results in a higher value of the segregation potential.

This leads to the view that the segregation potential is not related solely to Pu, the suction at the frozen-unfrozen interface, but is also a function of the degree of thermal imbalance.

Attempts to establish a relationship between the

variables of rate of heat extraction, rate of frost penetration, and rate of heave, have been made by different researchers. Conclusions from these studies are contradictory.

Beskow (1935) demonstrated, with experiments in which the air temperature above the specimen varied between -2°C and -10°C, that the heaving rate is not always influenced significantly by the rate of frost penetration. However, careful inspection of the frost heaving-time relationship reveals slight variations in the slopes as the air temperature is changed.

Later, more controlled freezing tests have confirmed a definite relationship between heaving rate and frost front penetration rate (Penner, 1958, 1972) and (Kaplar (1968, 1970). Kaplar (1968) concludes that

"The heave rate is dependent on or controlled by the rate of heat extraction (up to some unknown critical rate dependent upon the availability of water and the capability of the soil to conduct the water)"

It has also been shown that the dependence of the heave rate on frost line penetration rate is different for each soil.

Thermal imbalance can therefore be represented by the rate of frost penetration. It is tempting to relate the segregation potential of a freezing soil to the suction and the rate of frost-line advance. However, since the frozen fringe is the seat of the segregational process, it can be shown that, under certain circumstances, a given frost front

penetration over a given time interval does not necessarily induce identical changes in the anatomy of the frozen fringe. This is illustrated very clearly in Figure 4.8. If two samples of a given soil are subjected to different geometrical and thermal boundary conditions and compared upon reaching a given frost penetration rate, there will be differences in temperature gradients in the frozen and unfrozen soil. This, in turn, affects the size of the frozen fringe. If, for simplicity, it is assumed that Ts is the same in both specimens, the frozen fringe thickness is then fully defined at time t in both samples. If the frost front advances in both cases an identical length, DX, during a period Dt, the result is a change in temperature distribution in both samples as shown by the dotted line in Figure 4.8. In this Figure, the ratio of the hatched area and the area defined by the frozen fringe at time t can be interpreted as a measure of the degree of cooling of the fringe. This illustrates that the frozen fringe cooled by a different amount in each case. It is therefore proposed to relate the degree of thermal imbalance to the rate of cooling of the frozen fringe during freezing. The rate of cooling is defined herein as the change in average temperature of the fringe per unit time and can be determined as:

$$dTf/dt = (grad\ Tf(t+dt)\ (dX+d(t)/2))-Ts/2 \ldots\ldots 4.14$$

This equation assumes that Ts is known during the freezing process at any time t. As discussed earlier, this is not the
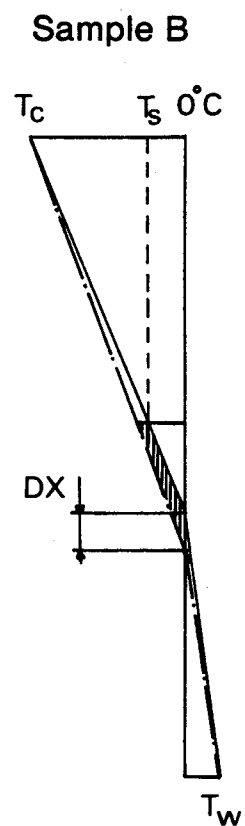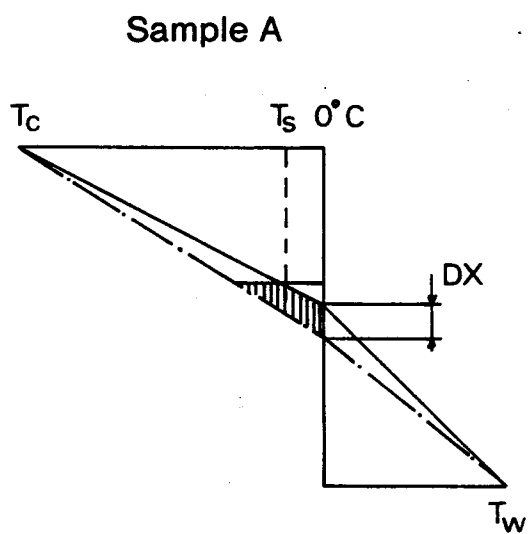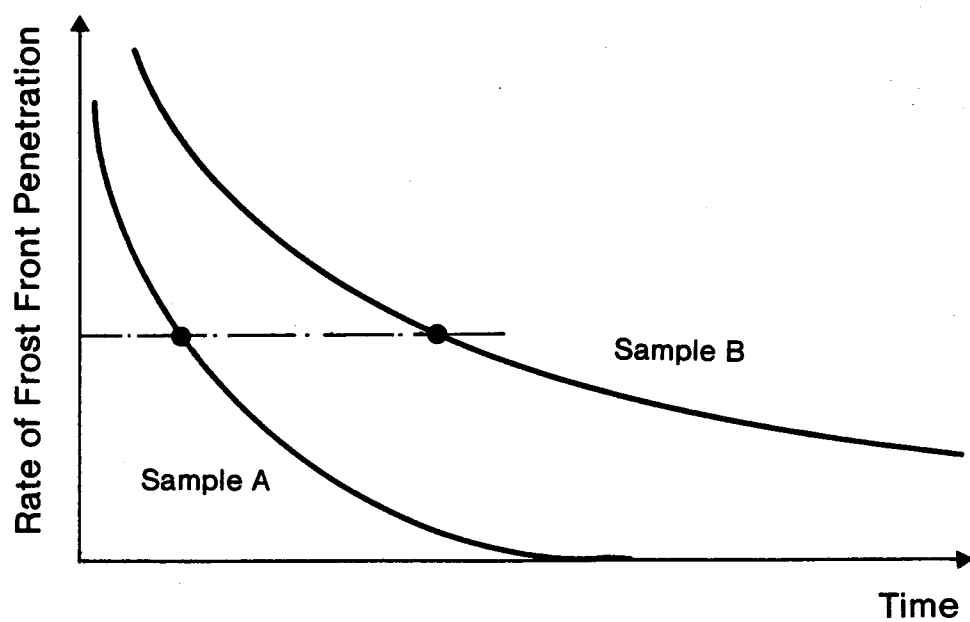
Figure 4.8   Changes in Frozen Fringe at a Given Rate of
Frost Front Advance

case. However, assuming a constant value of about -0.10°C does not affect significantly the value of the rate of cooling. Furthermore, Figure 4.9 reveals that the average rate of cooling can also be approximated by considering the change of temperature per unit time at the level of the *in-situ* freezing temperature. This is given by:

$$dTf/dt = grad\ Tf(t+dt)\ dX ....4.15$$

It should be stressed that these equations hold for any temperature distribution within the frozen soil provided it can be assumed that the gradient temperature in the fringe is constant, at least for short fringes.

This study now takes the view that a freezing soil can be characterized during an advancing frost front by the segregation potential which is a function of two independent parameters, the suction at the frost line, P_u and the rate of cooling of the fringe, dTf/dt. Reanalysis of test data from series NS and E should demonstrate the uniqueness of such a relationship for a given soil. This, in turn, would then result in acceptable input for frost heave characterization in the more general heat and mass transfer formulation.

4.5.2 Freezing Characteristics of Devon Silt

The frost heave characteristic surface $(SP, P_u, dTf/dt)$ can be determined from experimental data using the following procedure. A given freezing test, properly instrumented, yields the variation of the length of unfrozen soil with
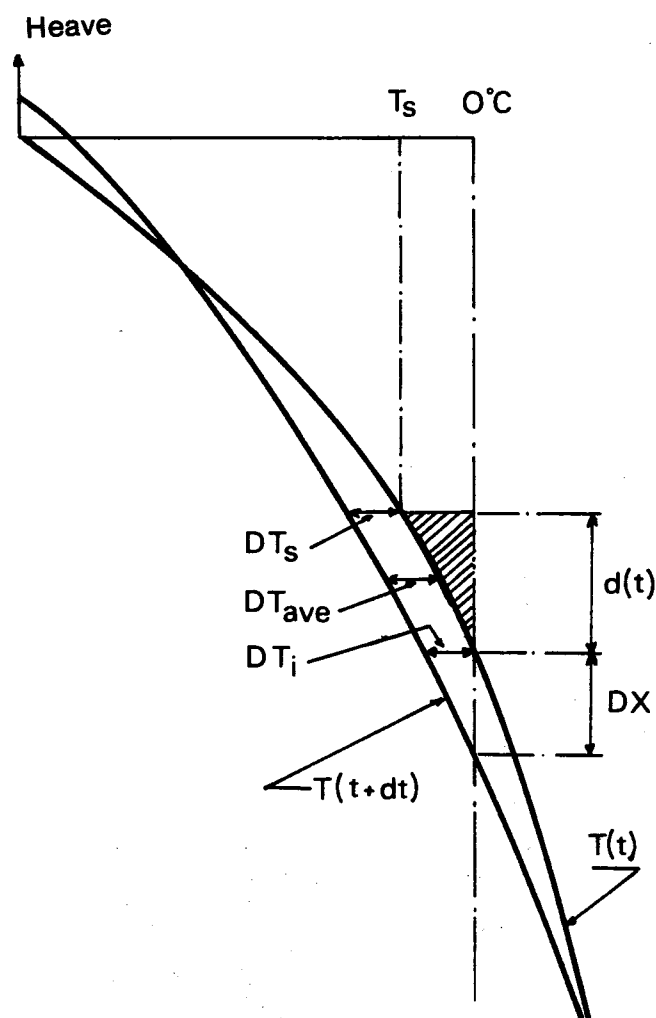
Figure 4.9   Cooling of the Frozen Fringe During Transient
            Freezing

time. Also, the variation in the thickness of the frozen soil can be evaluated with time. Combining this information with the measured temperatures on the side of the sample, it is possible to calculate the temperature gradient across the fringe (or near it) at any time t. Equations 4.14 or 4.15, reformulated for a finite time interval, Dt, yields then the variation of the cooling rate of the fringe with time. Typical data reduction obtained for test E4 is shown in Figure 4.10. It appears that the rate of cooling of the fringe is very high at the beginning of freezing, decreases rapidly with time and approaches zero asymptotically, which represents the steady state temperature distribution. It is worthwhile to mention here that a freezing test with fixed temperature boundary conditions provides a complete range of heat extraction rates. The time corresponding to specific rates of cooling is then determined from these graphs. The corresponding measured water intake velocity combined with the measured length of the unfrozen soil allow the assessment of the suction at the frost line by application of Darcy's law. Finally, the segregation potential at that specific rate of cooling is computed using Equation 4.13.

Figures 4.11 to 4.13 summarize the data for values of the rate of cooling of 1°C/hour, 0.50°C/hour, 0.20°C/hour, 0.10°C/hour, 0.05°C/hour and at the onset of the formation of the final ice lens. This last relationship has already been established in Chapter 3. For high rates of cooling, 1°C/hour and 0.5°C/hour some data points do not fit the

surface. This is not surprising if it is considered that a minimum time is required to establish steady state conditions for water flow through the unfrozen soil as a change in potential is suddenly applied at one boundary. The time required for steady state water flow is identical to the time required to achieve primary consolidation with an initial triangular pore pressure distribution. This time is dependent upon the coefficient of consolidation and the height of the samples. For samples from 5 cm to 10 cm high, the time for steady state water flow ranges from 1 hour to 5 hours for Devon silt. It should also be stressed that the height of the unfrozen soil varies as freezing progresses, accelerating therefore the equalization process. Furthermore, since SP and Pu are both related to the measured water flux, the data points will lie inside the surface, since the water flux is less important than for steady conditions corresponding to the maximum hydraulic gradient. This phenomenon only occurs for relatively short samples in which rates of cooling of $1^{\circ}C/hour$ and $0.5^{\circ}C/hour$ are obtained after a relatively short period of freezing, when the water flow is transient. With time, however, this phenomenon disappears completely.

The results, shown in Figures 4.11 to 4.13, obtained for different tests where different boundary conditions were applied strongly support the view that a freezing soil is characterized during an advancing frost front by the fundamental parameters SP, Pu and dTf/dt. Finally it should
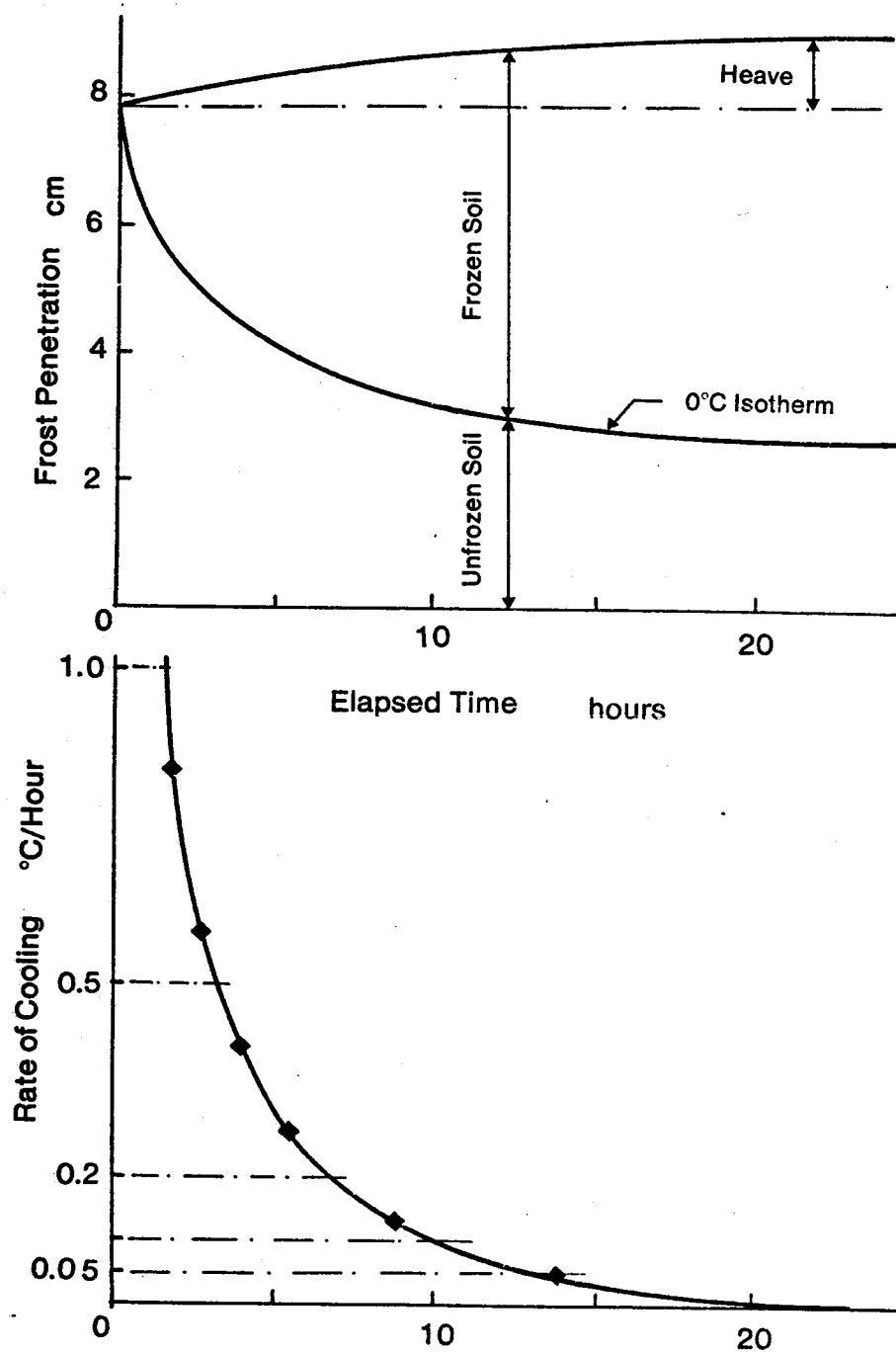
Figure 4.10 Example of Data Reduction for Test E4
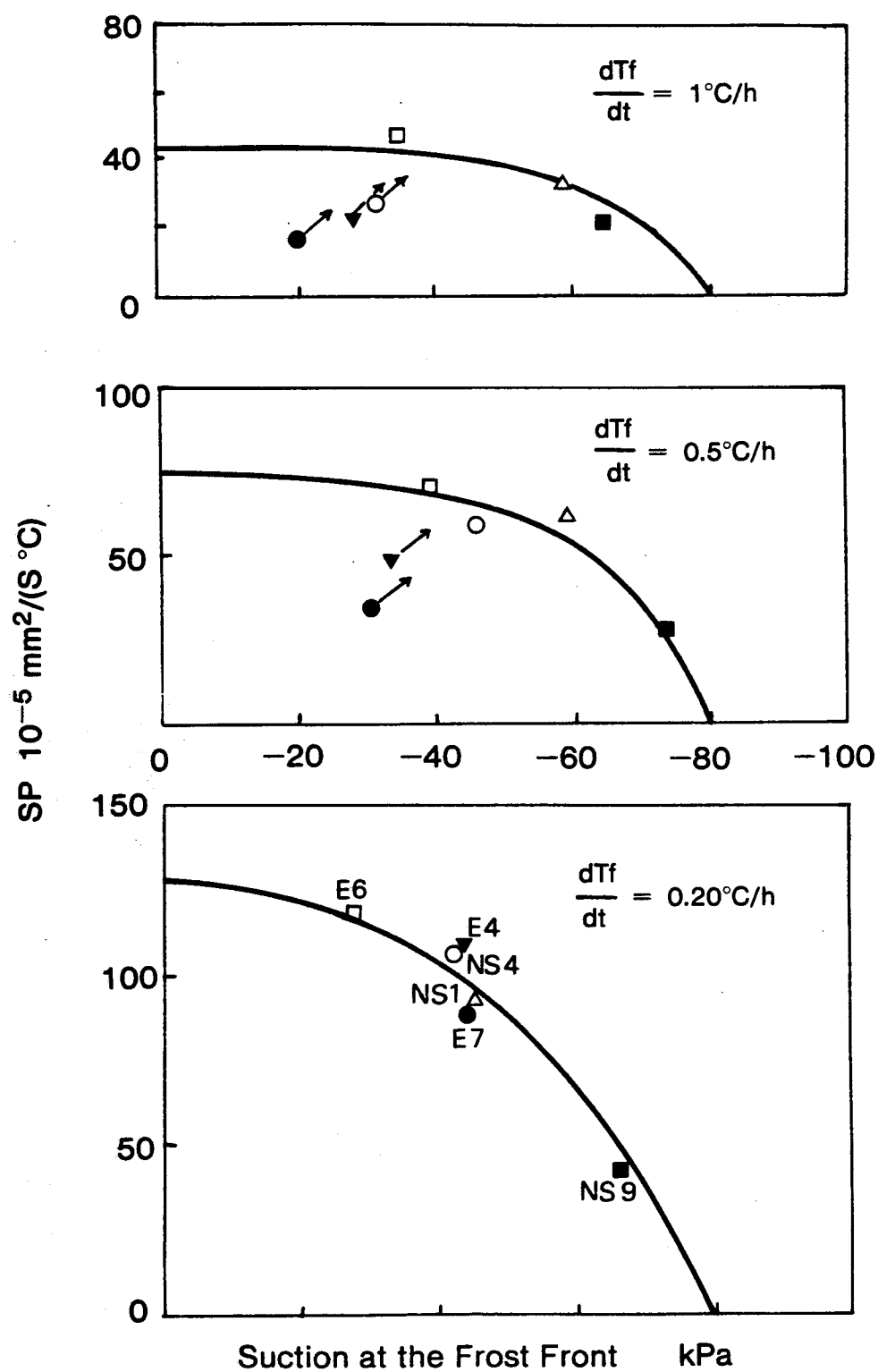
Figure 4.11 Freezing Characteristics for Devon Silt
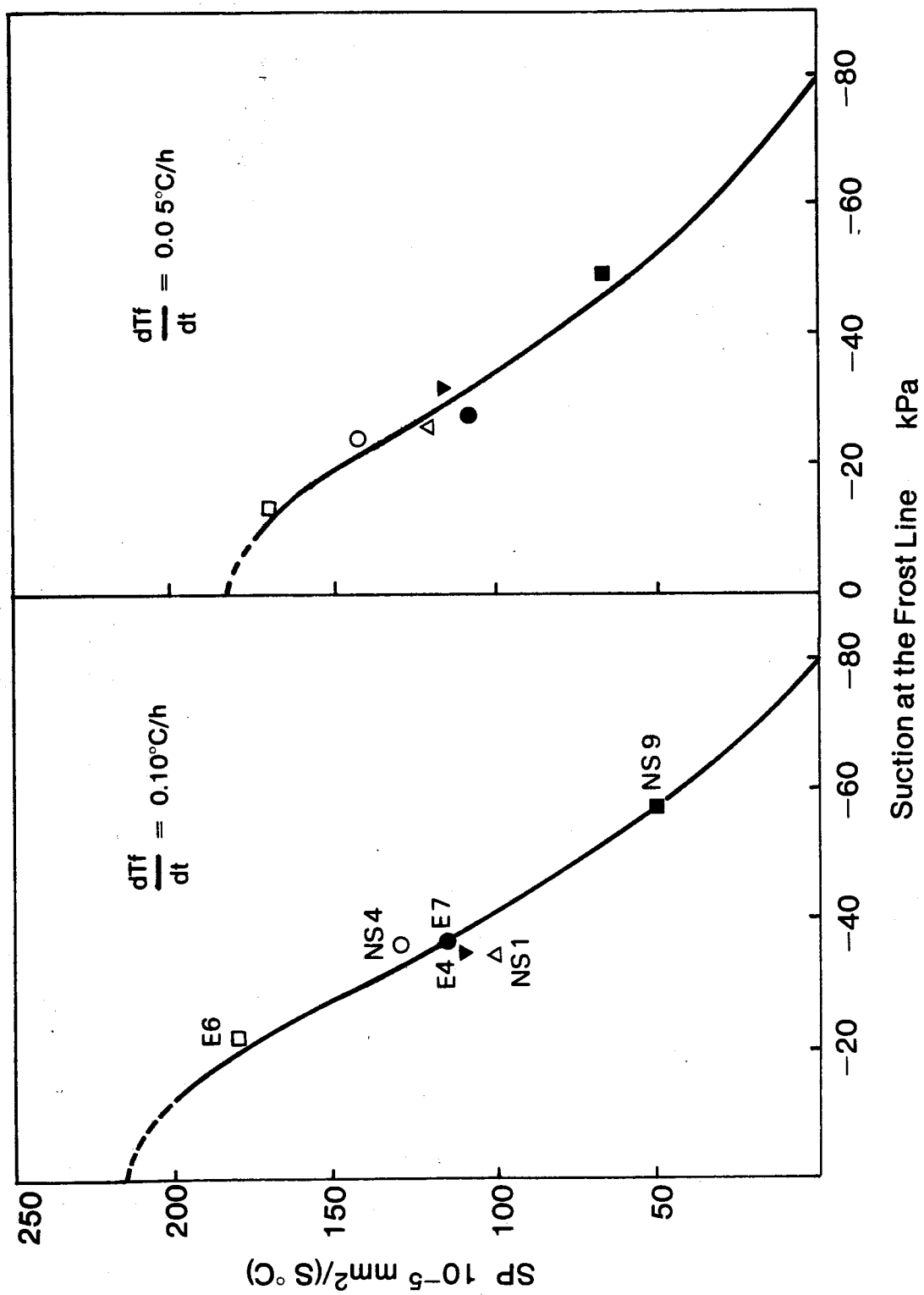
Figure 4.12 Freezing Characteristics for Devon Silt
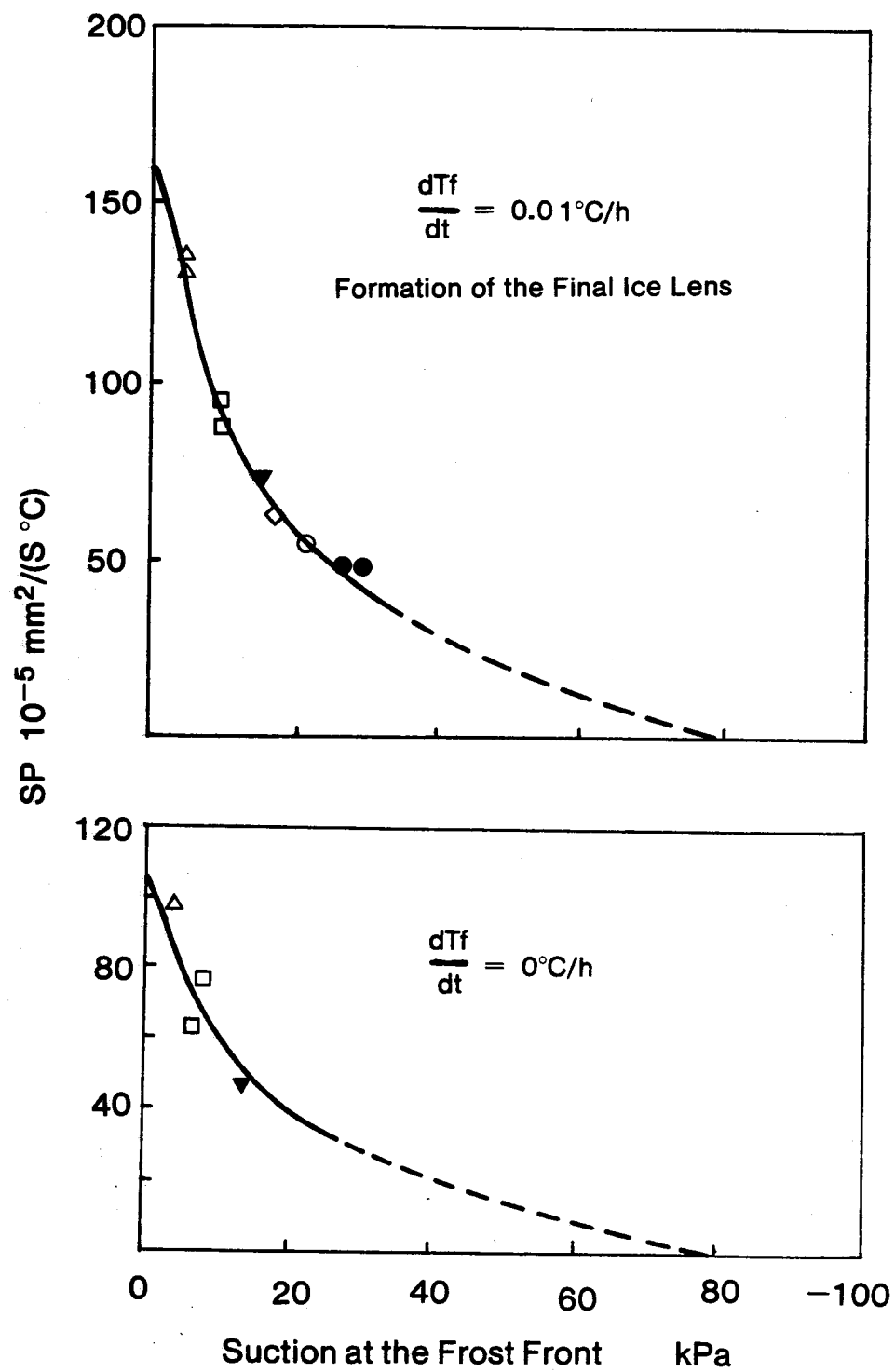
Figure 4.13 Freezing Characteristics for Devon Silt

be stressed that all parameters are directly measurable or deducible from freezing tests with fixed temperature boundary conditions. Moreover, no limiting assumptions are required as was the case for the other basic parameters Ts and Kf.

4.6 PREDICTIVE CAPABILITY WITH THE CHARACTERISTIC FREEZING SURFACE OF DEVON SILT

This section is devoted to demonstrate that the characteristic surface (SP, Pu, dTf/dt) of a given soil can be used as input to the general formulation of simultaneous heat and mass transfer in freezing soils. This is achieved by simulating with the resulting model all the freezing tests performed in Series NS and E. Furthermore, the validity and applicability of this model is tested for variable temperature boundary conditions with time and for layered samples composed of two different media. Hence, the effects of freezing path and impeded drainage are investigated both with the proposed model and experimentally.

4.6.1 Description of the Frost Heave Computer Model

The mathematical model for heat transfer is identical to that described in Chapter 3. The formulation of mass transfer, however, is changed slightly in order to use the characteristic surface of the freezing soil. In order to be

able to use this surface in the computer model, it must be defined with functional relationships. This is done by fitting the experimental curves SP-Pu (Figure 4.11 to 4.13) obtained at different specified rates of cooling with polynomial functions. The segregation potential at any rate of cooling is approximated by linear interpolation of known values of SP for the two closest rates of cooling bounding the actual rate of temperature change.

The flow chart presented in Table 4.2 illustrates the solution procedure used in this model. Unsteady heat flow is first solved respectively in the unfrozen and frozen part of the specimen. From the resulting temperature distributions, the temperature gradients at the frost front, grad Tu and grad Tfr are determined. This, in turn, leads to the rate of cooling to the frozen fringe over the time interval, Dt. The next step is then the evaluation of mass transfer during that time interval. For the current rate of cooling of the fringe, SP can be evaluated as a function of Pu as discussed previously. The water intake velocity is then related to SP by Equation 4.10. This results in a variation of water intake flux with the suction at the frost line for the current rate of cooling as shown in Figure 4.14a. On the other hand, for a given length of unfrozen soil, the velocity of water flow is linearly proportional to the difference in total potential across the unfrozen soil. For zero potential at the base of the specimen, this implies:

$$V = lu(t).Pu/Ku = Constant.Pu \dots\dots\dots\dots\dots 4.16$$
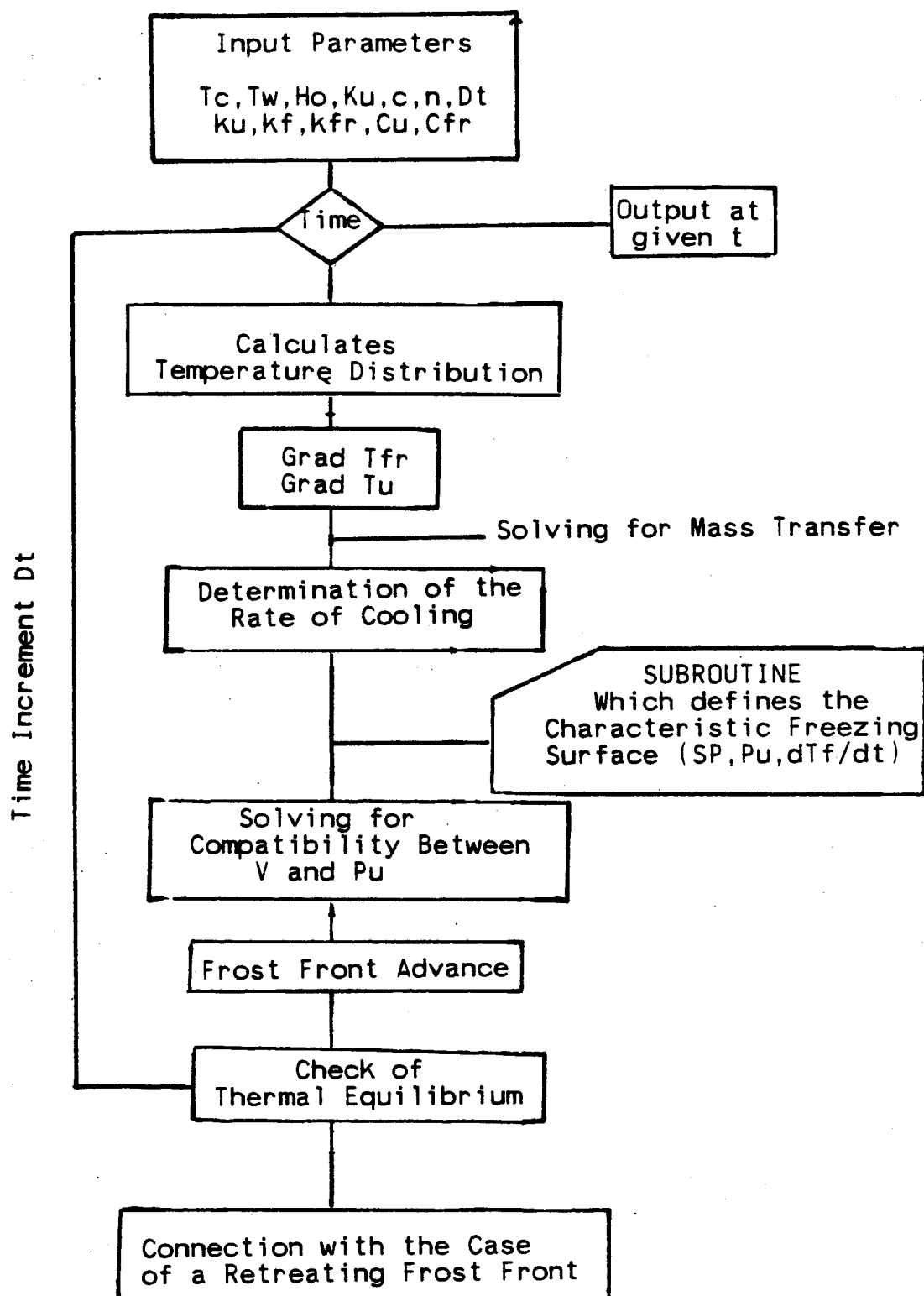
Table 4.2   Flow Chart of the Computer Model
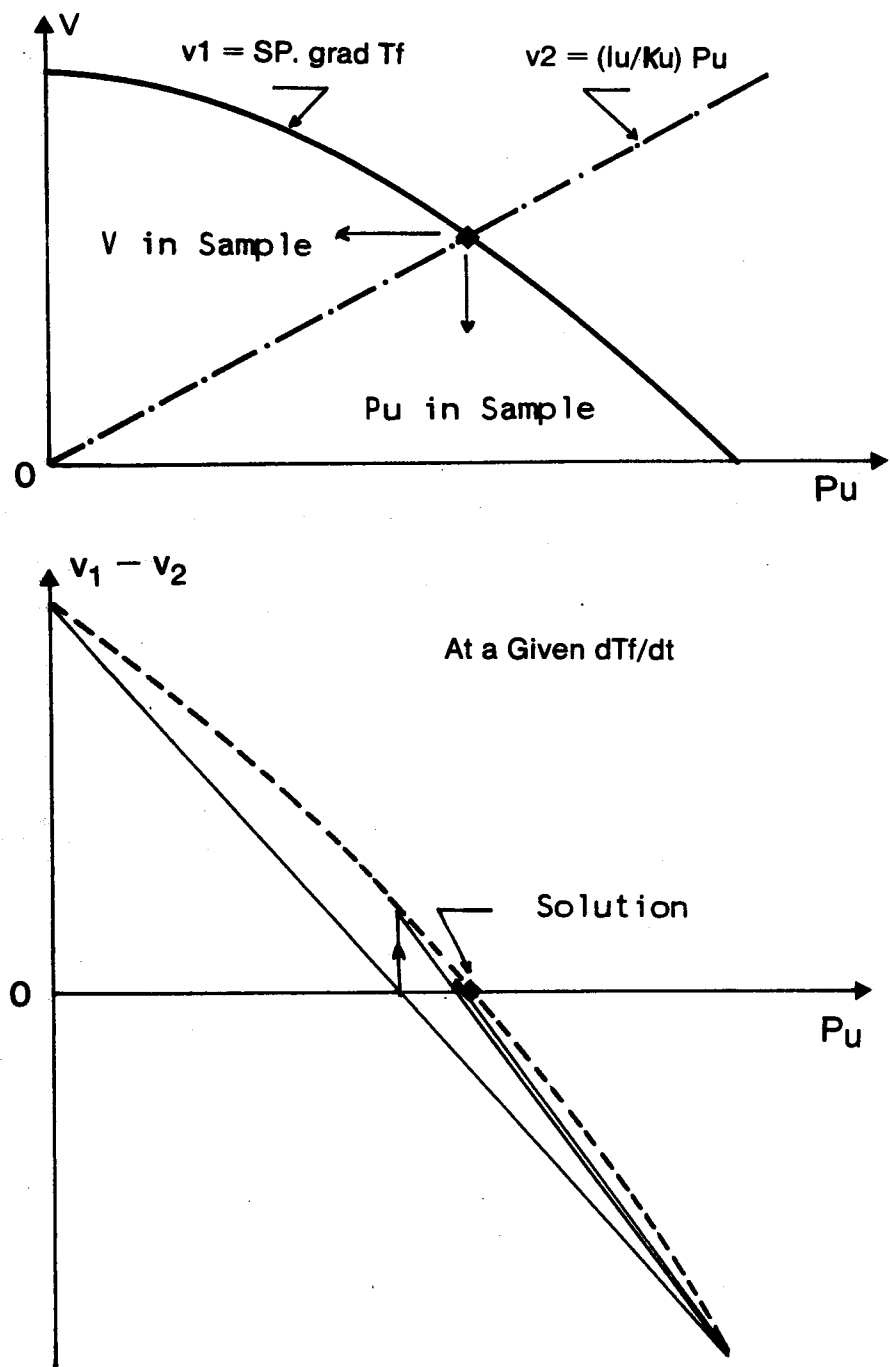
Figure 4.14 Determination of the Water Intake Rate with the Computer Analysis

This relationship is also plotted on Figure 4.14a. It is clear that compatibility between water flux and suction at the frost front must be safisfied with respect to Darcy's law in the unfrozen soil. This is obtained when the water intake velocity calculated with SP and Pu is equal to that obtained with Darcy's equation applied to the unfrozen soil only. In graphic form, the compatibility condition is represented by the intersection of the two curves defined by Equations 4.13 and 4.16. From a computational point of view, the unique solution (V,Pu) is obtained with an iterative method in which the difference V(freezing) - V(Darcy) is calculated for different suctions and the suction for which this difference approaches zero is determined with a false-position method as illustrated in Figure 4.14b.

Finally, the frost front advance during the time interval, Dt, is computed in order to satisfy thermal balance at the 0°C isotherm. The time is increased by another increment and the sequence of operations are repeated until a stationary frost front is attained.

It is generally accepted that the final ice lens is created when the frost front becomes stationary. The time at which the final ice lens was effectively initiated can be determined from experimental data by subtracting the thickness of the final ice lens from the total heave obtained at the end of the freezing test and determine the time at which the total heave corresponds to that value. However, the time of unsteady heat flow predicted by the

model for different freezing tests is always significantly longer than the respective time at which the final ice lens was initiated in the freezing specimens. This observation led to the view that the final ice lens may form slightly before a stationary frost front is reached. Furthermore, subsequent advance of the 0°C isotherm results in further chilling of the frozen fringe reducing the segregational potential. This view is supported by the mechanistic theory of ice lens formation presented in the next chapter.

The analysis of the freezing tests used to determine the characteristic freezing surface reveals that the final ice lens is initiated in our tests at a rate of cooling of the fringe of about 0.01°C/hour. The characteristic surface for Devon silt is consequently completed by determining the relationship SP-Pu at dTf/dt equal to zero, i.e. for a stationary frost front. This is done with the same procedure as discussed in section 4.4 but the time at which the basic parameters are evaluated corresponds to the computed time required to reach a stationary frost front situation. This relationship is shown in Figure 4.13.

Figure 4.15 represents a three dimensional view plotted by the computer using the functional relationships characterizing saturated Devon silt at a given porosity and freezing under zero applied load. This surface is being used as input for the freezing soil in the frost heave model.

4.6.2 Results Predicted with the Frost Heave Model

The results obtained by this model are summarized in Appendix D. In order to judge the effectiveness and predictability of this model, it is convenient to report on the same plot the measured and computed values of given parameters at a given time.

Similarly to Figures 4.4 and 4.5, total heave and water intake flux are again used as key parameters in order to evaluate the adequacy of the proposed model. Each symbol represents a given freezing test and is associated with a number which gives the time, in hours, at which the parameter is compared. Excellent agreement is now obtained for both total heave and water intake velocity for almost all the tests carried out in the present investigation as shown in Figure 4.16 and 4.17.

So far, the frost heave model has only been tested for uniform specimens of Devon silt. If the suction at the frost front is a fundamental parameter then the model should be able to predict total heave with time for a freezing sample composed of a layer of Devon silt of properties similar to those existing in Series NS and E and a second layer of different permeability, provided that the frozen fringe remains in Devon silt. A two layered medium results in a change in the slope of the relation between water flux and suction at the frost front for a given flow path. Consequently, as shown Figure 4.15, the velocity of water sucked to the freezing front is changing as well.
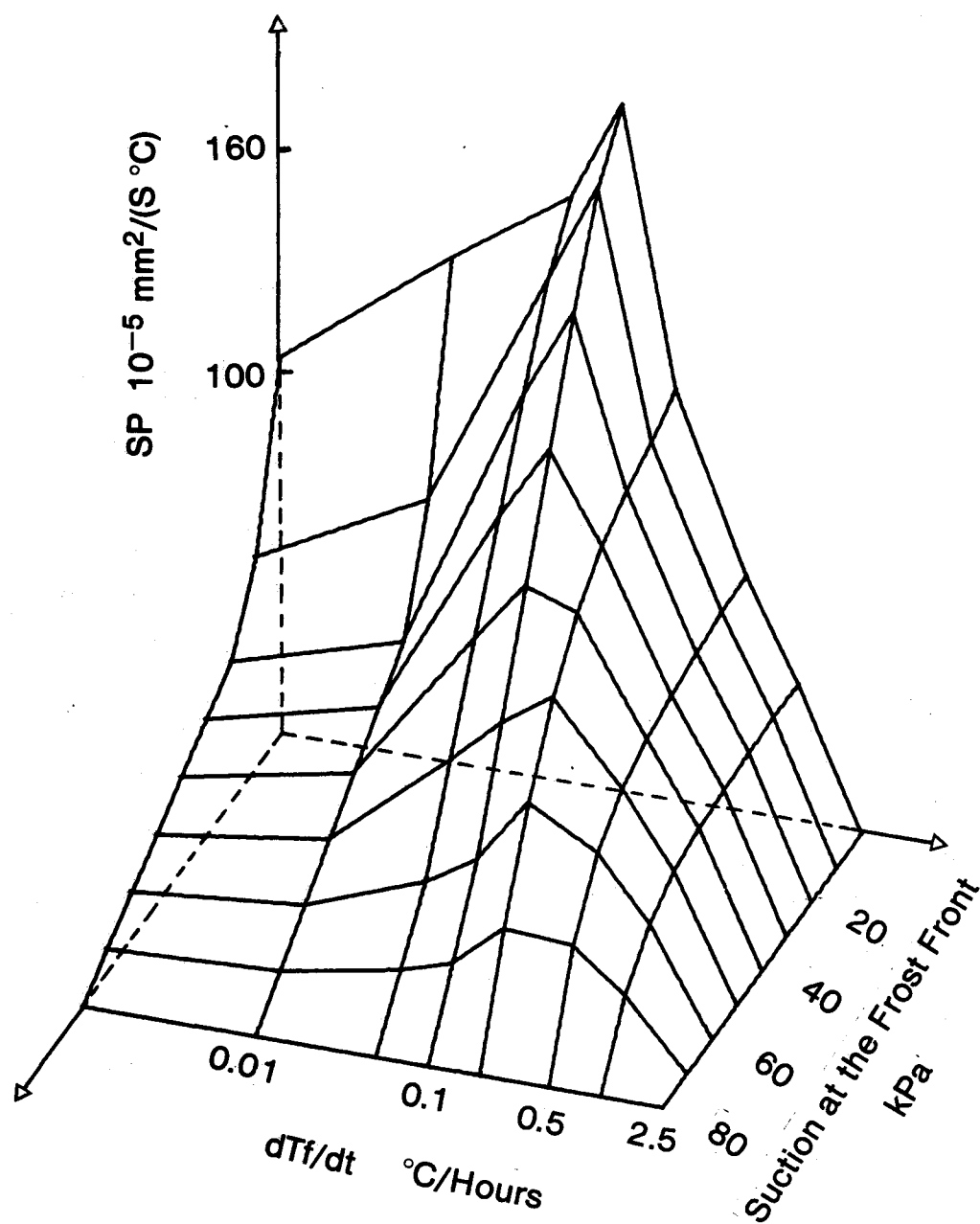
Figure 4.15 Characteristic Freezing Surface for Devon Silt
Used for Simulation
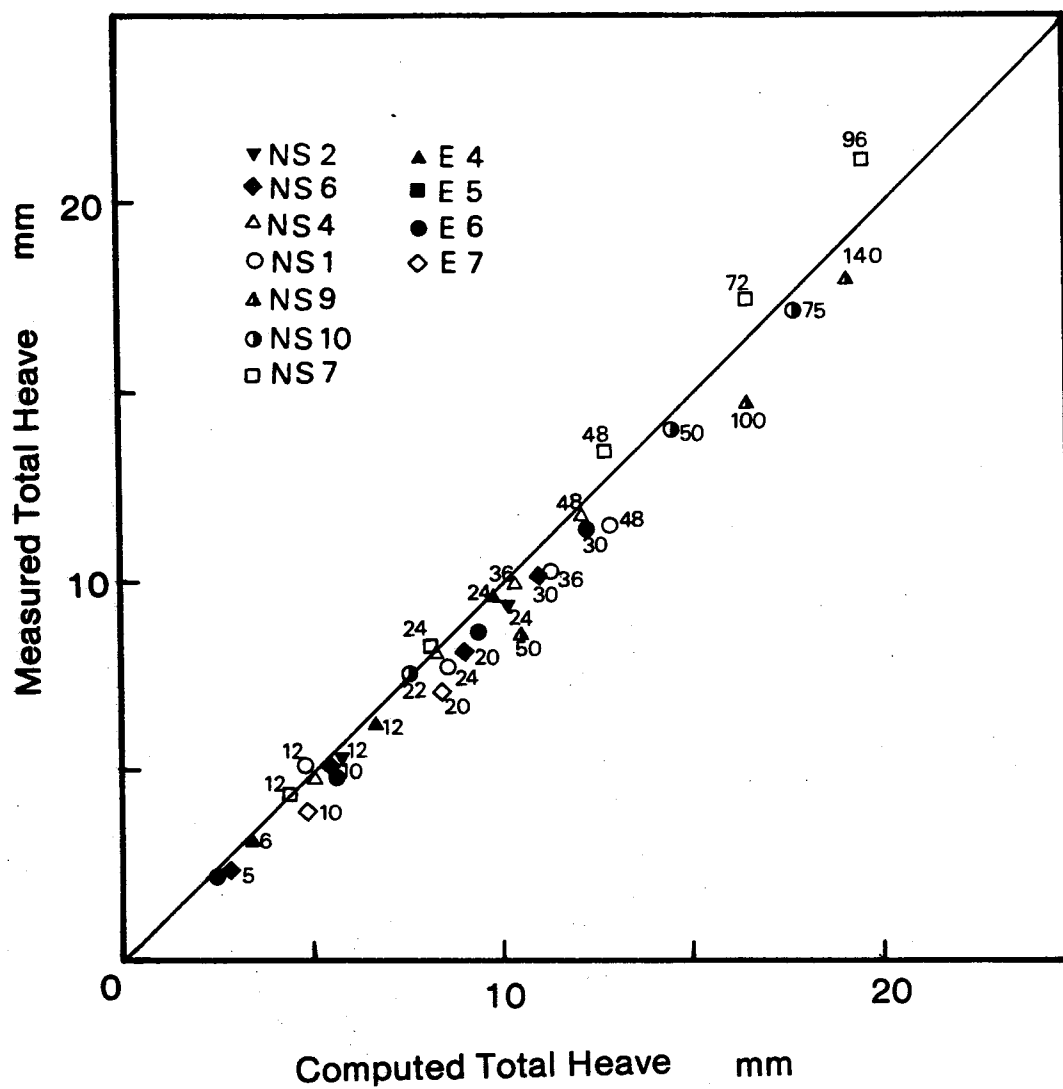
Figure 4.16 Comparison of Predicted Total Heave with Actual
Laboratory Data Using (SP,Pu,dTf/dt)
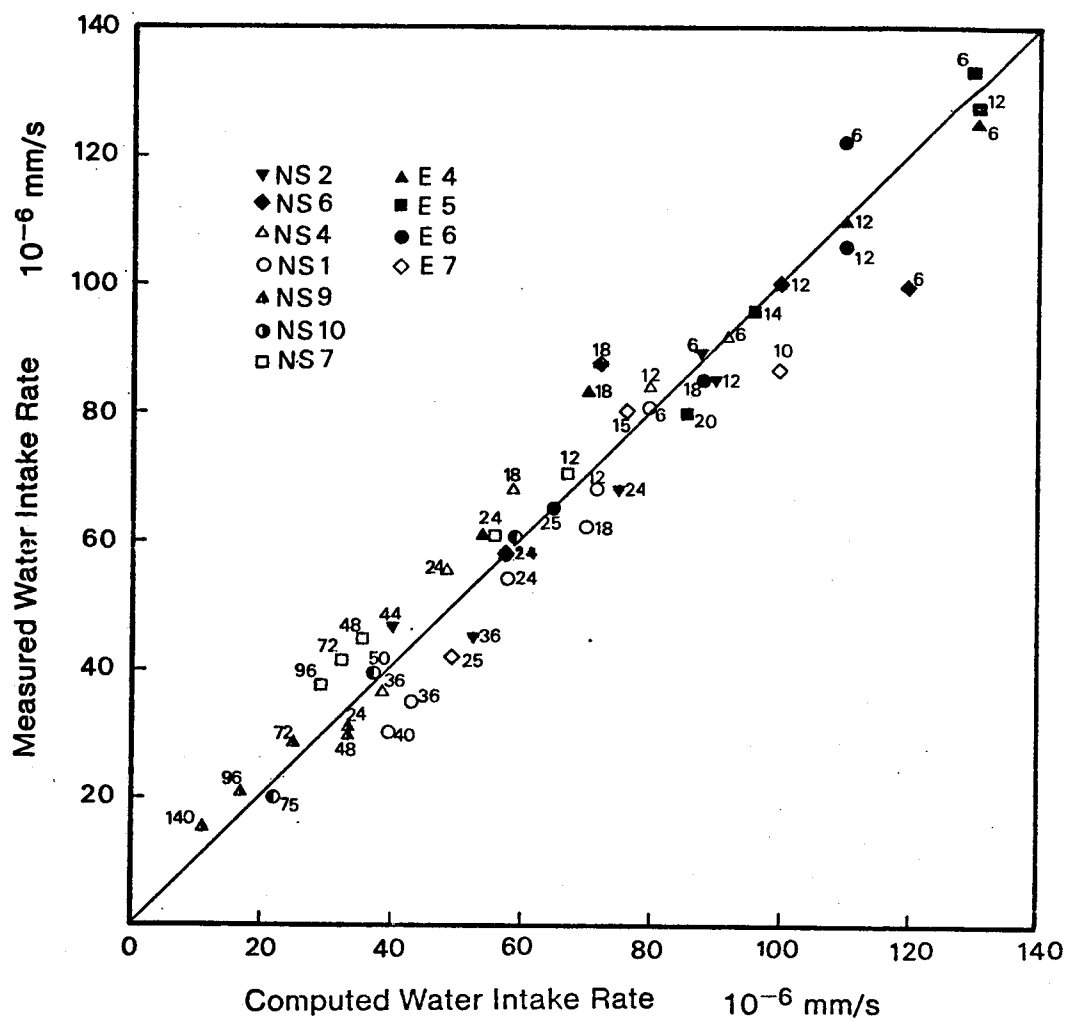
Figure 4.17 Comparison of Predicted Water Intake Flux with Actual Laboratory Data Using (SP,Pu,dTf/dt)

Sample E8 was composed of a 8.3 cm thick Devon silt layer, preconsolidated to 210 kPa and a 2 cm thick porous stone of relatively high permeability. Sample E9 was composed of a 8.4 cm thick Devon silt layer, preconsolidated to 210 kPa and a 5.1 cm thick Devon silt layer preconsolidated to 420 kPa. This higher preconsolidation pressure leads even after rebound under zero applied load, to a lower void ratio and therefore to a lower permeability. This latter was determined prior to freezing by a constant-head permeability test at a temperature of about $+1^oC$ and was found to be approximately $.6x10^{-7}$ cm/s.

In both tests, the temperature boundary conditions were such that the final position of the 0^oC isotherm remained within Devon silt preconsolidated to 210 kPa. This, in turn, insured that, the frozen fringe is developed in identical soil (as in series NS and E) whose freezing characteristics are known.

The computed total heave and heave by water intake are compared with actual test data. Also the penetration of the 0^oC isotherm with time is compared to measured data. The results for test E8 and E9 are shown in Figures 4.18 and 4.19. Excellent agreement is obtained in both cases, confirming thus that the suction at the frozen-unfrozen interface is a fundamental parameter for a freezing soil.

So far, all the simulated freezing tests were frozen with fixed temperature boundary conditions during the whole freezing period. It is tempting to conclude that the

validity of the proposed characterization of a freezing soil is therefore restricted to those thermal conditions.

In order to prove that the characteristic freezing surface, although determined from freezing tests with fixed temperature boundary conditions, is independent of the freezing path, freezing tests with variable temperature boundary conditions were conducted.

Sample E1 was frozen in two stages. During the first stage, the temperatures at the top and the bottom of the specimen were maintained constant for 24 hours. During that period, the frost front penetrated approximately to the middle of the sample. Then, the second stage was initiated by changing the temperatures at both ends in order to force further penetration of the frost front. During that second phase, the temperatures were also maintained constant with time. The warm plate temperature was lowered from $+6^{\circ}C$ to $+1^{\circ}C$. This results, in the early stage of that phase, in heat flow to both ends of the specimen since the temperature distribution presents a maximum temperature somewhere within the unfrozen soil. Temperature distribution in sample E1 are given in Figure C13 in Appendix C. It is worthwhile to stress again the importance of temperature distribution in the determination of the rate of cooling of the frozen fringe which, in turn, influences the segregation potential.

Figure 4.20 shows the comparison between computed and measured results for test E1. It is obvious that the model predicts remarkably well the change and magnitude of the
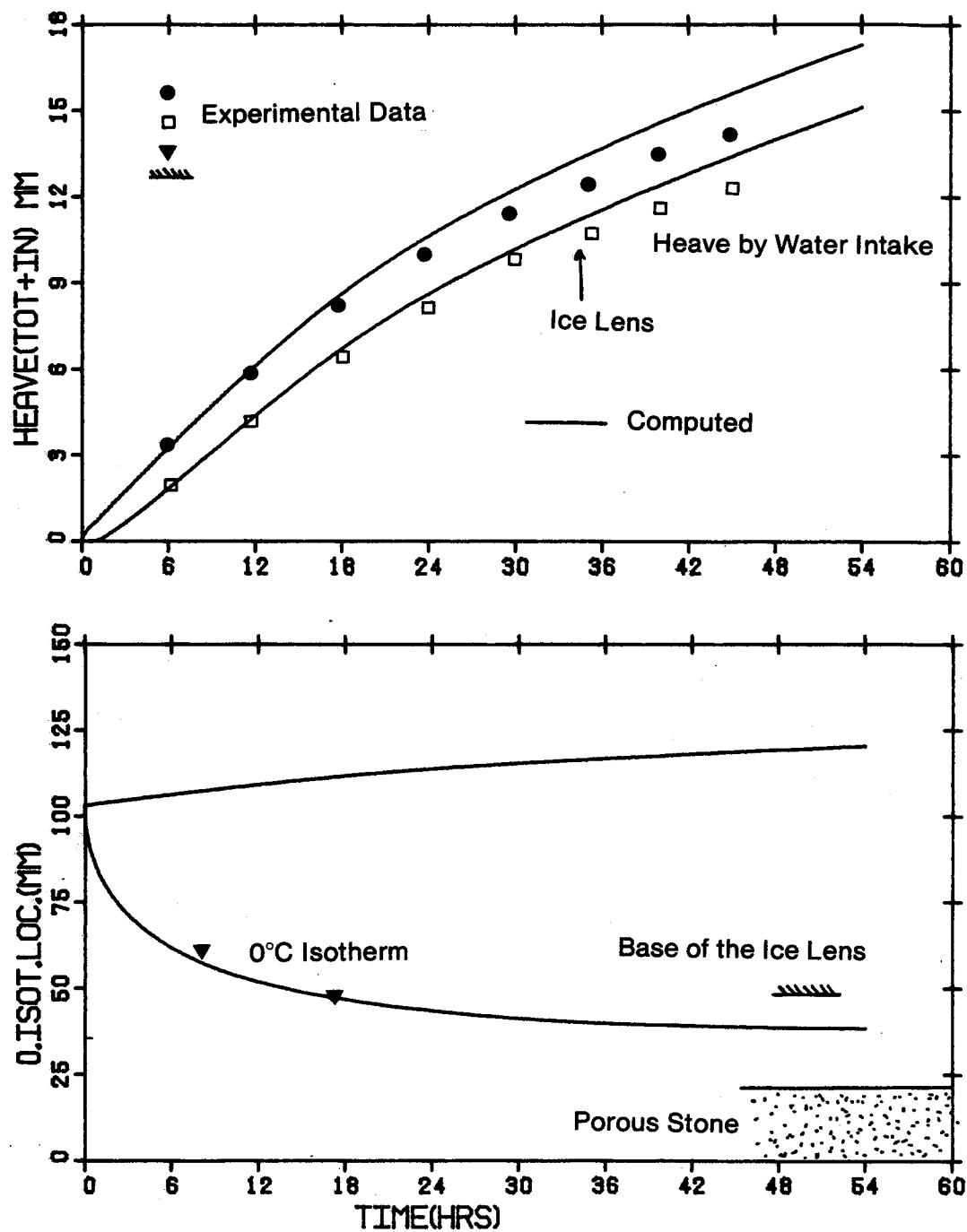
TEST   E-8   (P=0.0;TW=+2.0,TC=-4.20 C)

Figure 4.18 Comparison of Prediction with Actual Data for
            Test E-8
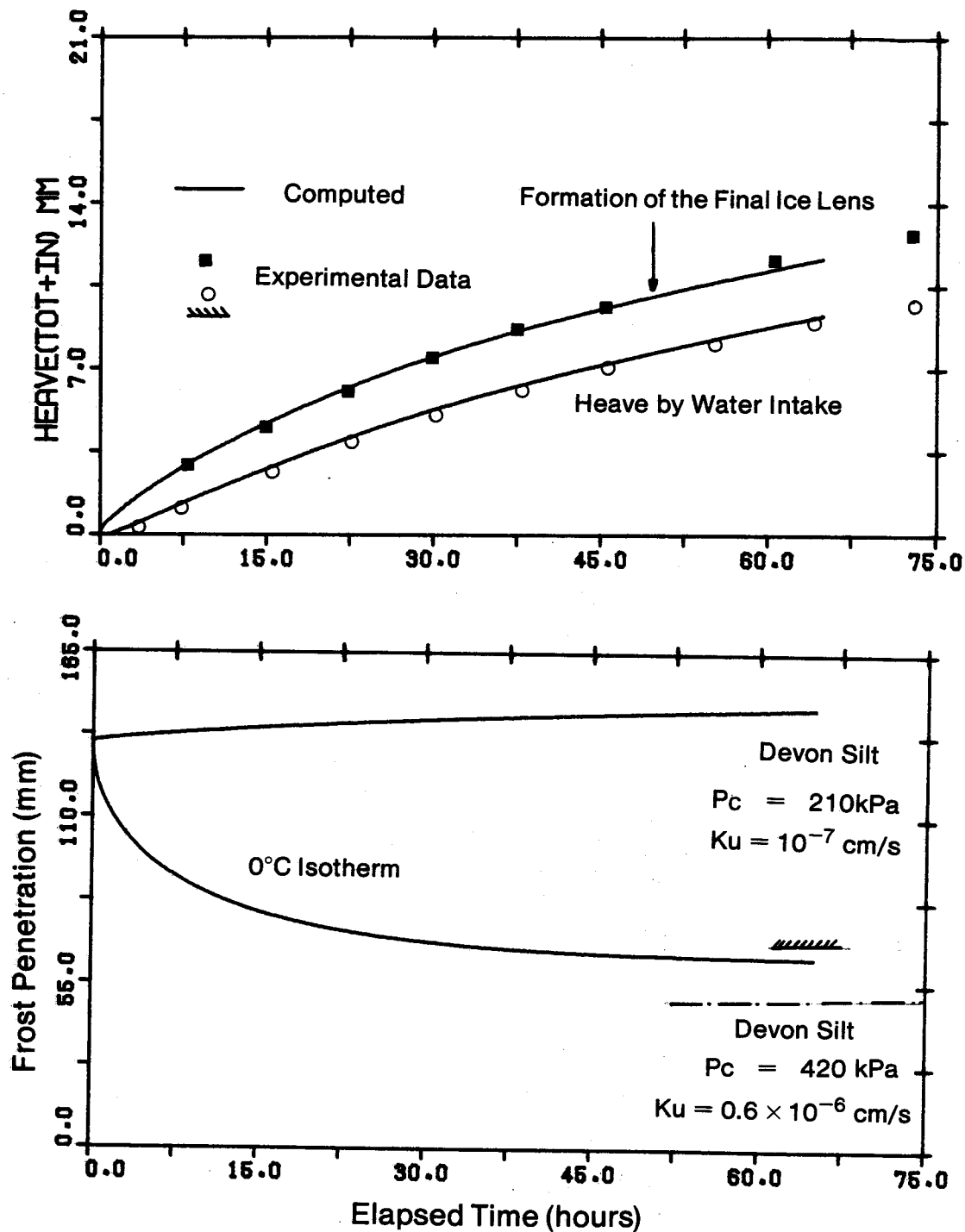
Figure 4.19 Comparison of Prediction with Actual Data for Test E-9

rate of heaving that occurred as the temperature boundary conditions were changed. Furthermore, the computed frost front penetration is also in agreement with the measured temperature profile and the visual observations made after freezing was completed. Figure 4.21 illustrates that the model also predicts very well the increase in water content in the frozen soil. The water content after freezing was measured for thin slices of the frozen soil as discussed in Chapter 2.

During test NS-7, the temperatures at both ends of the sample changed accidentaly by a minor amount as shown in Figure 4.22. The model predicts relatively well the shape of the heaving curve with time when used with fixed temperature boundary conditions. However, the prediction is improved when the actual variation in thermal boundary conditions is taken into account during the simulation. Figure 4.22 illustrates clearly the importance of adequate simulation of thermal boundary conditions, especially when the warm-plate temperature is close to 0°C. In these conditions, the suction at the frost line ranges from atmospheric pressure to about -10 kPa as shown in Figure 3.10. In that domain, the segregation potential varies significantly.

The results presented in Figures 4.20 to 4.22 confirm that the characteristic soil freezing surface (SP, Pu, dTf/dt) is independent of the freezing path.
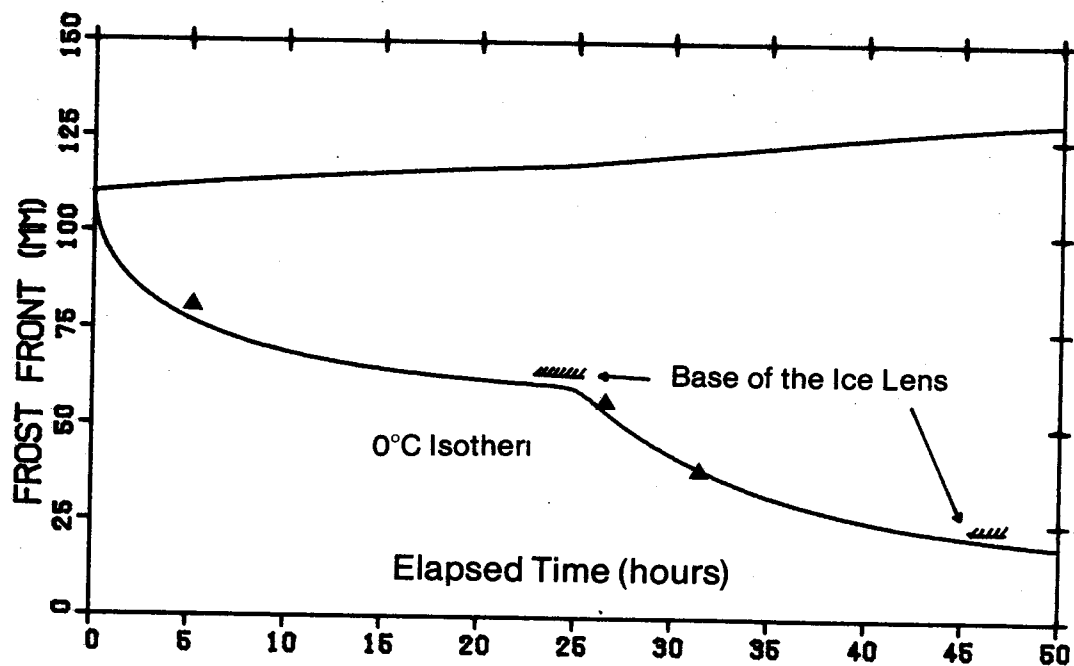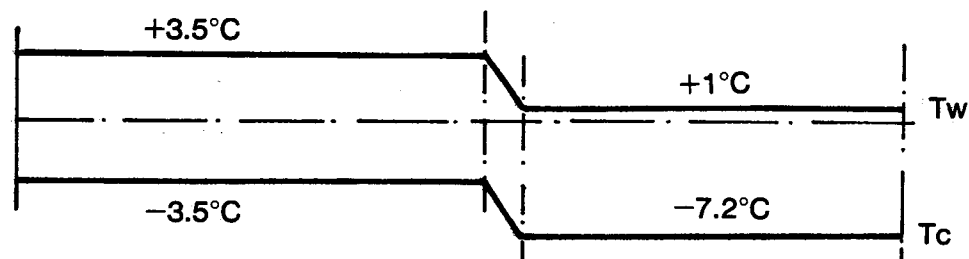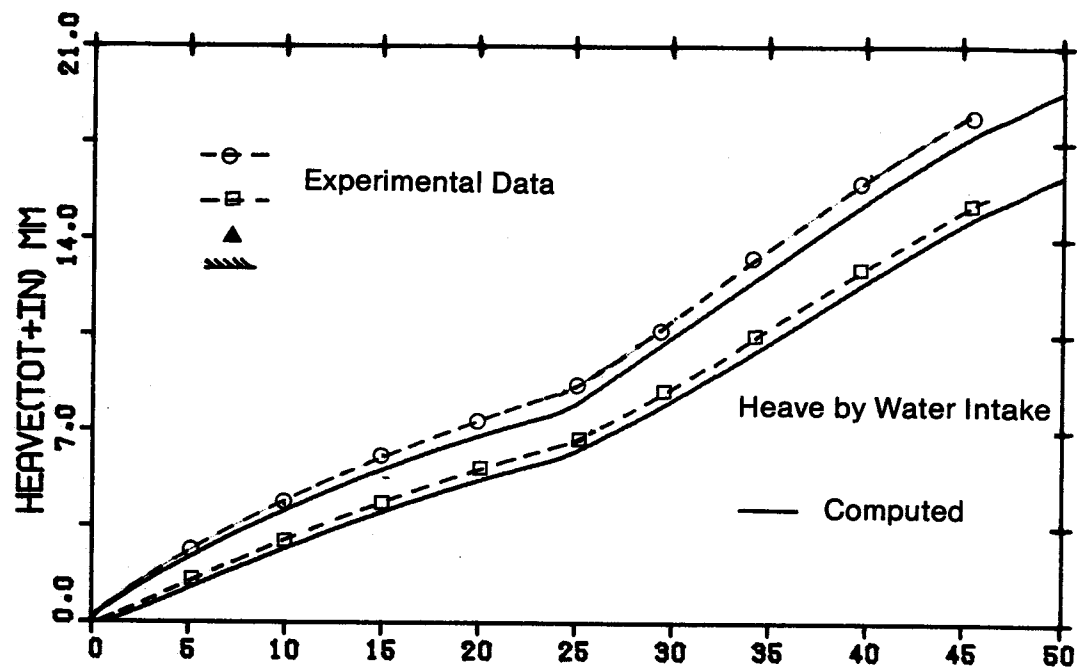
Figure 4.20 Comparison of Prediction with Actual Data for Test E-1
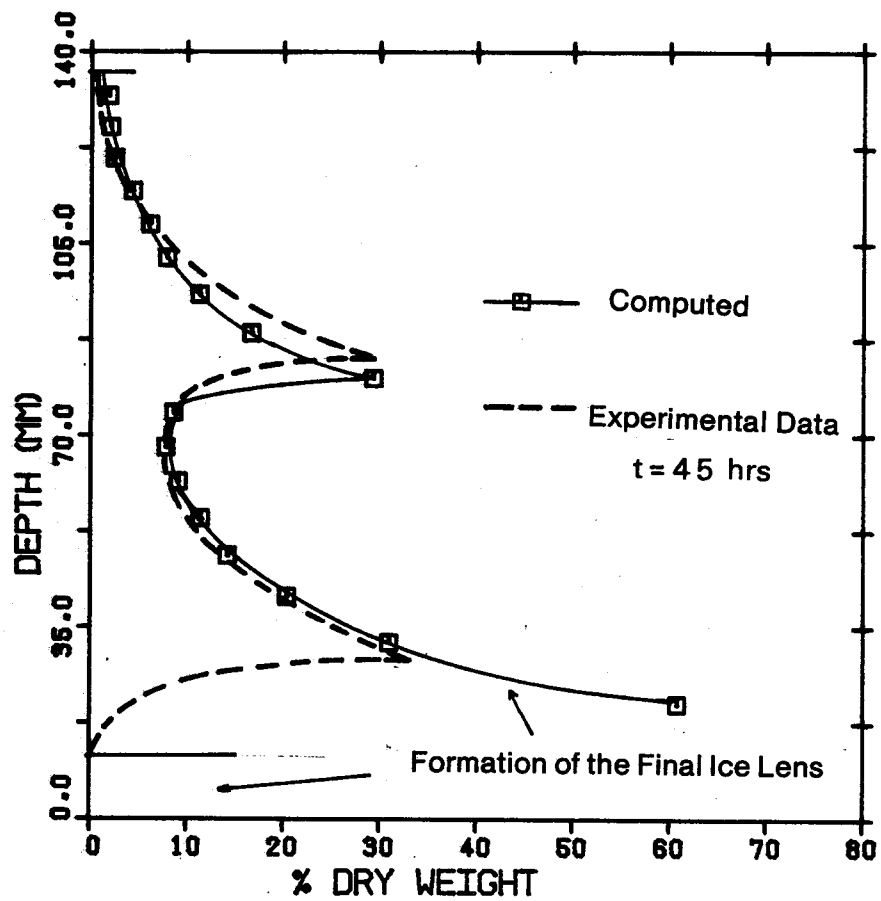
Figure 4.21 Water Content Profile at the End of Freezing for Test E-1
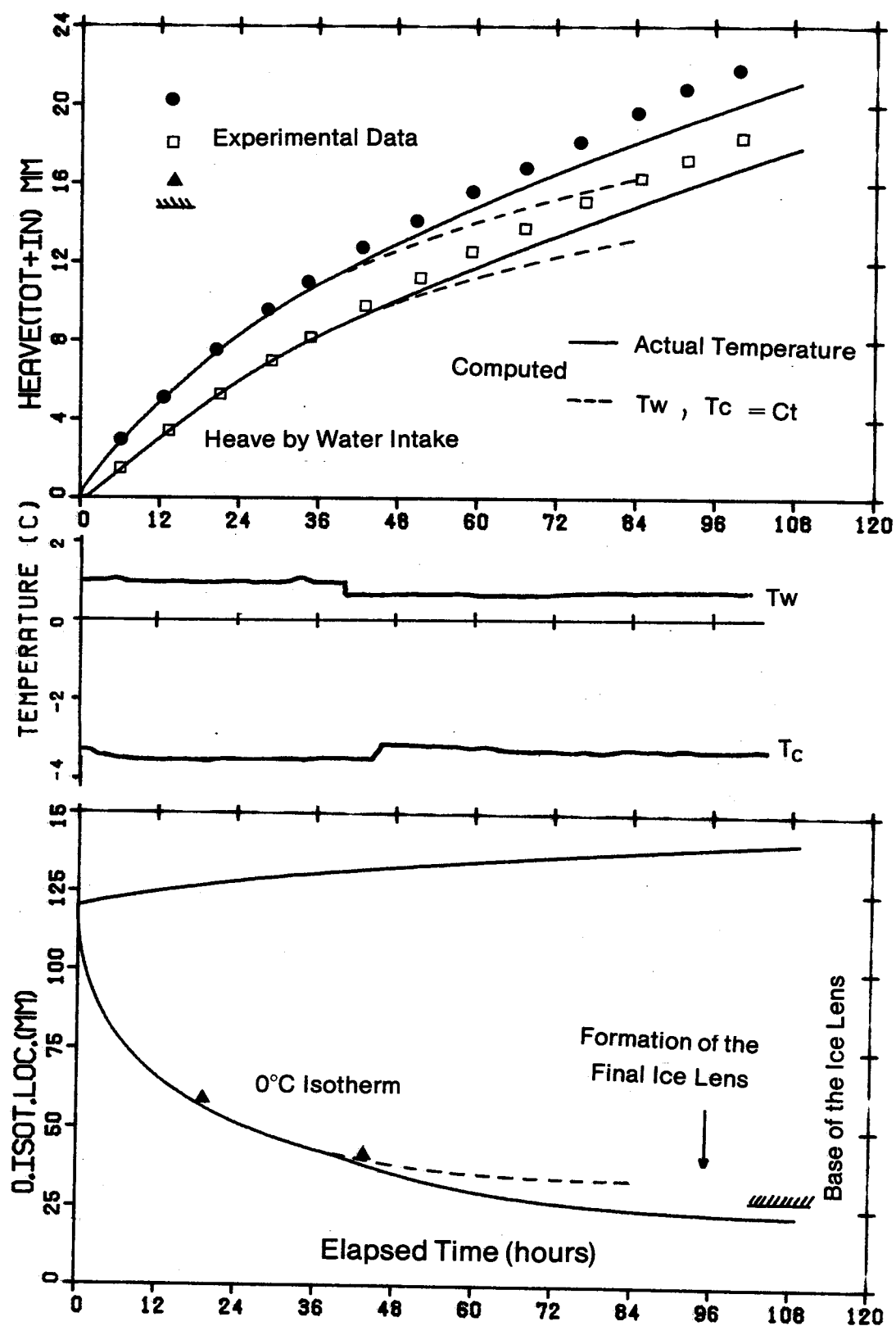
Figure 4.22 Comparison of Prediction with Actual Data for Test NS-7

4.6.3 Prediction of Frost Heave in Long Samples

So far, the frost heave model predicts fairly well the behavior of relatively short samples, less than 15 cm, during freezing with free water supply and no applied load. It was decided to freeze longer specimens in order to investigate the influence, if any, of the initial length of the sample upon the freezing behavior. Theoretically, since the characteristic freezing surface remains the same, the model should predict heave and water intake with the same accuracy as for the previous tests.

Two samples were consolidated to 210 kPa and a height of respectively 28.0 cm for NS-9 and 18.0 cm for NS-10. The freezing cell was obtained by assembling three 10 cm high individual freezing cells. The surrounding insulation was also composed of three individual foam cylinders. This resulted in bad contact and preferential thermal flow paths. Consequently, radial heat flow into the specimens could not be avoided as shown by the temperature distributions obtained as the final ice lens was initiated in both samples (Figure 4.23).

From a theoretical point of view, the radial heat flow component has to be accounted for in the global heat budget within the sample. This requires the derivation of governing equations of two dimensional heat transfer in cylindrical coordinates. It requires furthermore the evaluation of the thermal conductivities of the cell wall, insulation and in general of the whole system. This rather tedious task can be
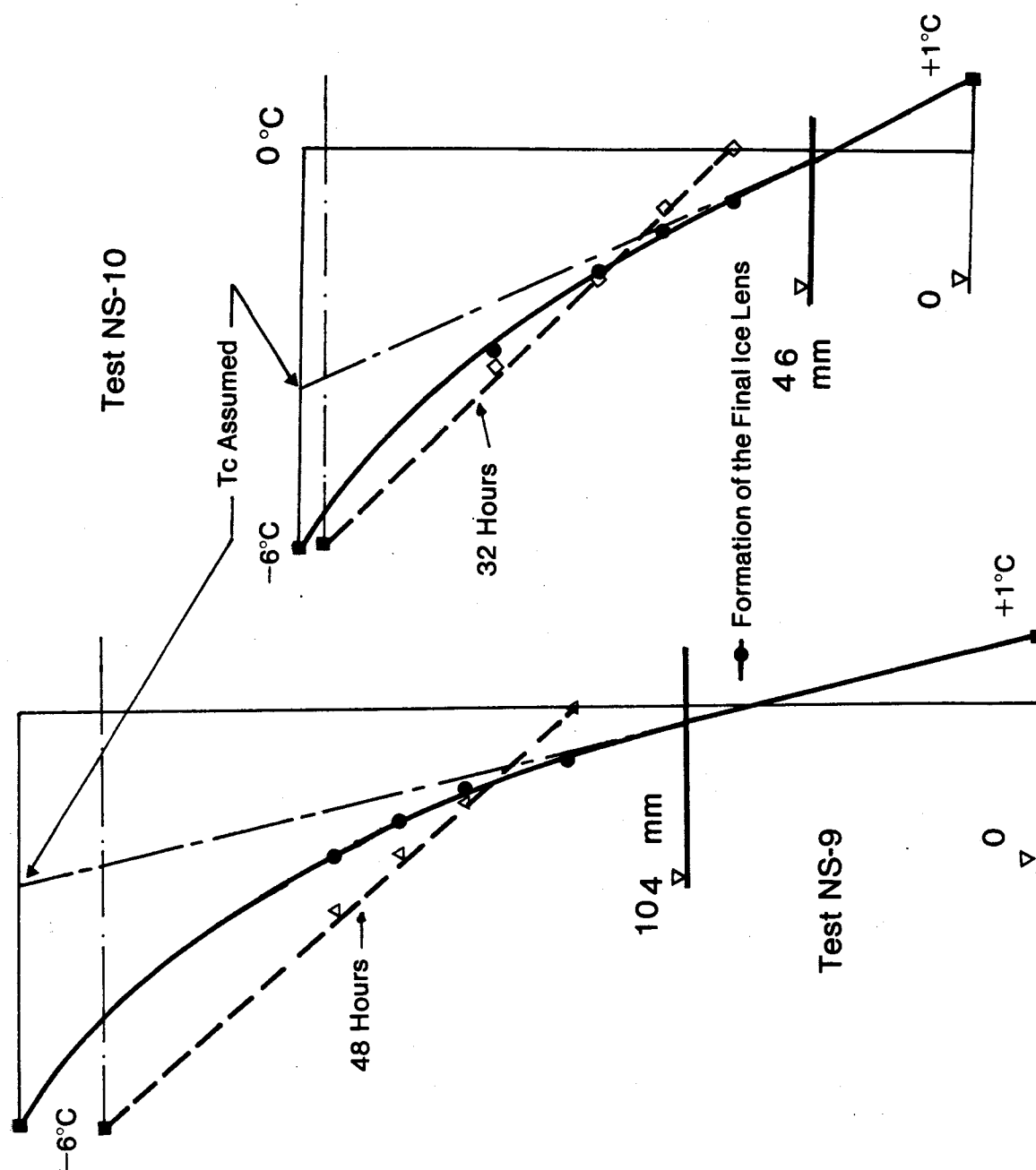
Figure 4.23 Temperature Profile in Sample NS-9 and NS-10

avoided if one treats the problem as a one dimensional heat flow in which the cold-side temperature is assumed to vary so that the temperature gradient across the frozen zone is equal to that measured across the fringe at any time t.

With this approximation, the previous model can be used to simulate tests NS-9 and NS-10. The basic parameters are identical to those used to model the freezing of shorter samples. The variation of the assumed cold side temperature, shown in Figures 4.24 and 4.25 respectively for NS-9 and NS-10, was assessed from Figure 4.23. The assumed temperature corresponds to the intersection of the tangent at 0°C to the actual temperature distribution with the top surface of the specimen. Since the length of frozen soil varies with time and because the influence of radial heat flow increases with increasing height, the assumed temperature decreases with time.

The simulation of tests NS-9 and NS-10 have been performed with the condition of constant Tc and with the assumed variation of Tc with time for both cases. It is clear, as shown in Figures 4.24 and 4.25 that better agreement computed and measured heave is obtained if the cold step temperature varies in order to match the actual slope of the temperature distribution at the 0°C isotherm with time. It is also clear, that the characteristic soil freezing surface is independent of the geometrical boundary conditions and that the model can be used for any length of soil.
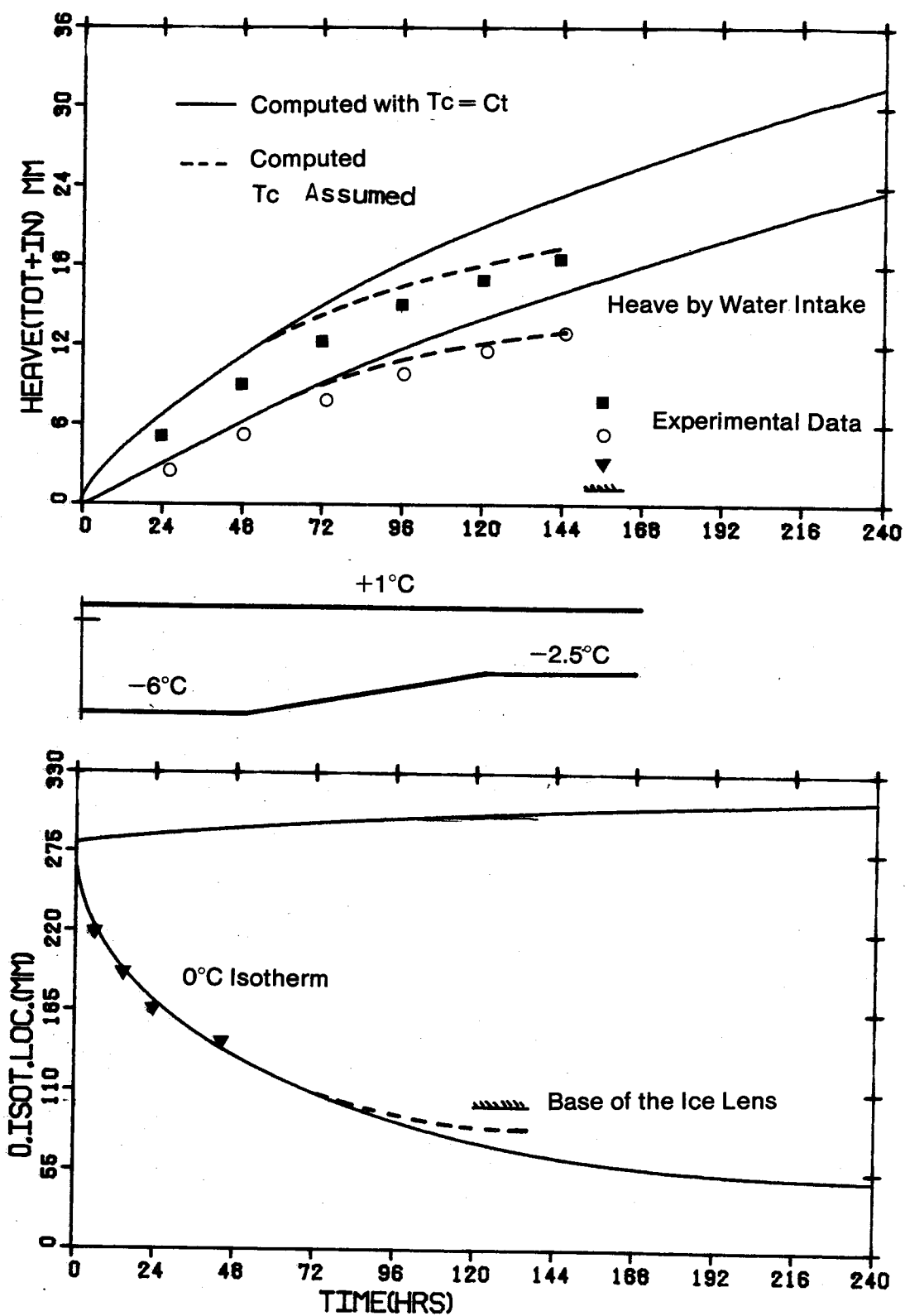
Figure 4.24 Comparison of Prediction with Actual Data for Test NS-9

University of Alberta
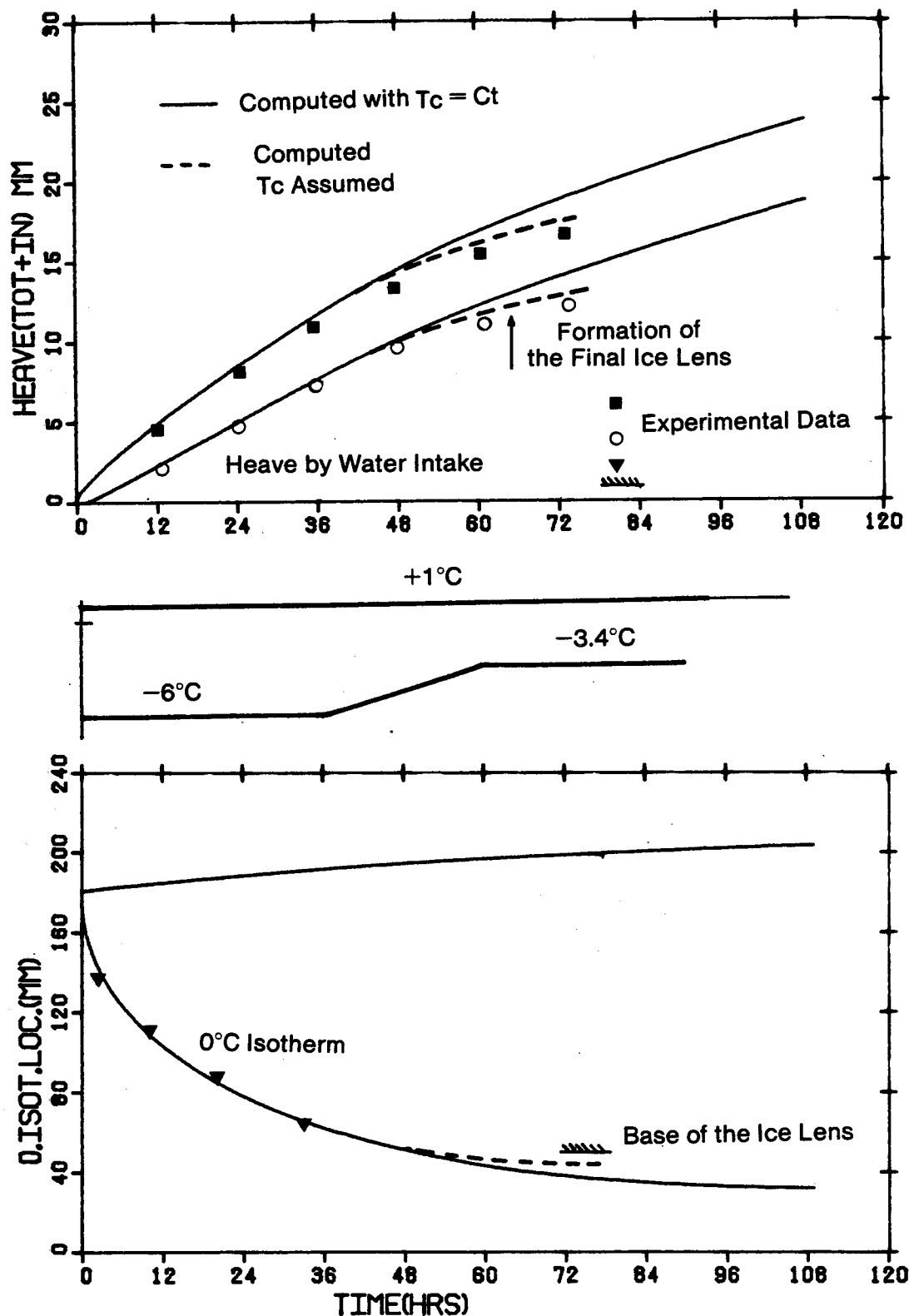
Figure 4.25 Comparison of Prediction with Actual Data for Test NS-10

4.6.4 Sensitivity Analysis

Finally, it is of value to discuss the results obtained from a parametric study where the sensitivity of the prediction of total heave and water migration flux in freezing soils has been determined in response to changes in the hydraulic and thermal characteristics used as input data. This analysis was carried out for test NS-1.

As a first step, the permeability of the saturated unfrozen soil is kept constant. However, the thermal conductivities of the frozen and unfrozen soil and of the frozen fringe are varied. Figure 4.26a reveals that total and segregational heave are sensitive to minor changes in the thermal parameters of the freezing system. The resulting variations are, however, not very significant and remain within an acceptable range of about ±10% for ±25% variation in the thermal properties. The variations in the position of the 0°C isotherm and the time of unsteady heat flow are more significant. If the ratio of the chosen thermal conductivities of the frozen soil and the unfrozen soil is larger than the actual one, the model overestimates heave and water intake and predicts deeper frost front penetration and shorter time of unsteady heat flow. On the other hand, if the adopted values of the conductivities yield a smaller ratio than the actual one, the frost heave model underestimates heave and results in a longer unfrozen part and also a longer time of unsteady heat flow.

Matching therefore one freezing test with respect to

depth of frozen soil and water intake rate, can result in an accurate determination of the thermal characteristics of a given soil.

The second parametric study deals with changes in the permeability of the unfrozen soil. The thermal parameters are constant in that analysis. As seen in Section 4.4, the frost heave model is based upon the relationship between SP and Pu at different cooling rates. Variations in permeability result inevitably in variations of the suction at the frost front of the same order of magnitude. It is, therefore, expected that changes in permeability of the unfrozen soil have an enormous effect on the behavior of a given freezing soil. This is confirmed by the analysis and shown in Figure 4.26b. A change of one order of magnitude in Ku is associated with a dramatic variation in total heave, approximately ±150%.

Such large variations in permeability are, however, unrealistic for laboratory conditions. Moreover, it must be stressed that the characteristic freezing surface was established by assuming a given permeability of the unfrozen soil in order to infer the value of Pu by Darcy's law. The use of this surface as input is only valid if the simulations are performed for identical soil with identical physical properties. If the parametric study is conducted with a variation of ±15% in Ku, the heave is also found to vary within ±15%. Slight variations in permeability due to soil compressibility are most likely to occur close to the
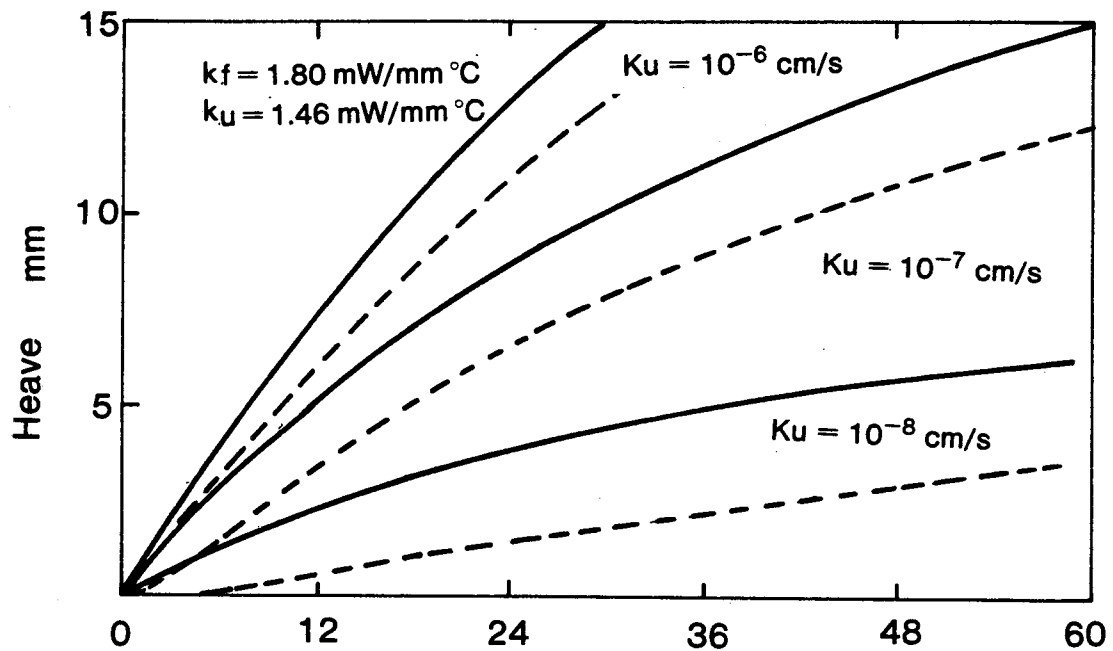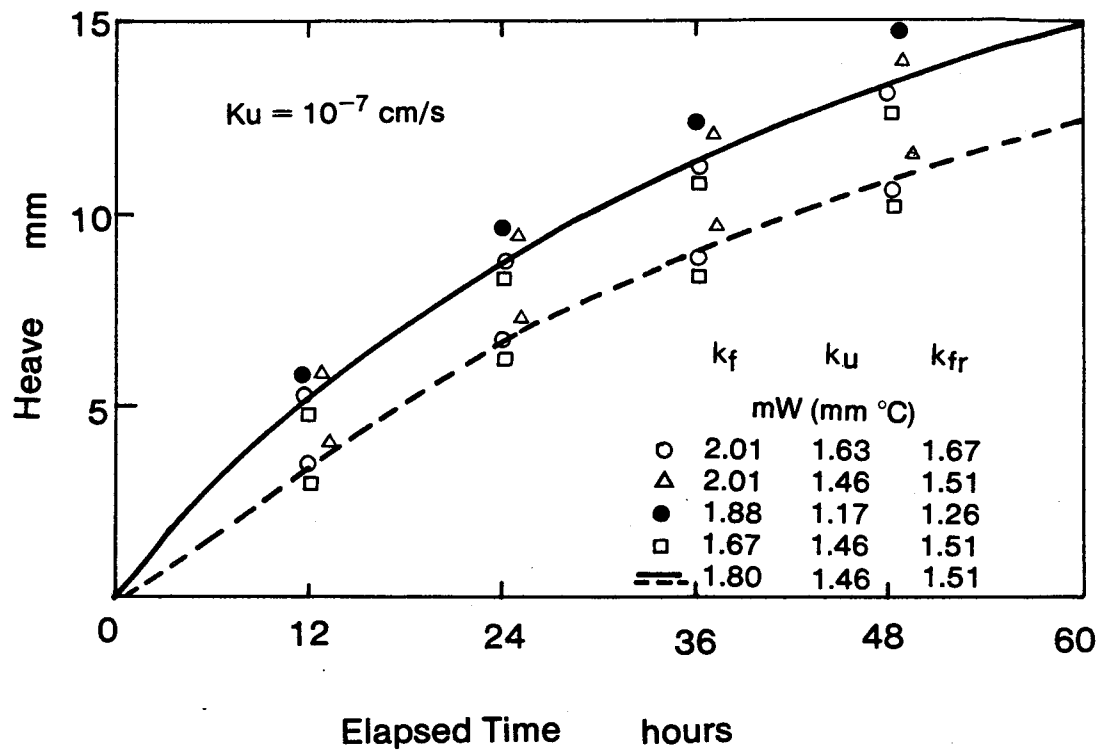
Figure 4.26 Sensitivity Analysis

frost front where the effective stresses in the unfrozen soil are increased due to negative pore water pressures. This, in turn, produces slight variations in the average permeability of the unfrozen soil. The accuracy of the predictions would certainly improve if those minor variations in permeability were accounted for in the frost heave model.

It may be concluded that the sensitivity study demonstrates clearly that the small differences between computed and measured values presented in Figures 4.16 and 4.17 are easily accountable for by minor changes in the hydraulic and thermal parameters of the soil.

4.7 FEATURES OF THE CHARACTERISTIC FREEZING SURFACE OF DEVON SILT

A saturated soil at a given porosity that freezes under zero applied load can be characterized by a unique relationship between the segregation potential, the suction at the frost front and the rate of cooling of the frozen fringe. Figure 4.15 illustrates in three dimensions the shape of this relationship.

It is of interest to discuss some important features of this characteristic freezing surface. As shown in Figures 4.10 to 4.13, the experimental data suggest that a unique maximum suction at the frost front at which no water flow is occurring exists at any rate of cooling of the fringe. This

limiting suction is approximately -80 kPa. For silts, in general, cavitation is most likely to occur at suctions of about -100 kPa. It is, therefore, suggested that the limiting suction inferred from the freezing tests corresponds to the critical suction at which cavitation of water occurs in the unfrozen Devon silt. This explains furthermore that the observed limiting suctions are more or less constant since the soil properties were identical for all the freezing tests used to determine the freezing surface.

Figure 4.15 reveals also that there is a maximum rate of cooling of the fringe for any suction at the frost front at which no water flow to the freezing front is possible. The limiting rate of cooling for Devon silt is approximately 2.5°C/hour. In other words, the frost front penetration is so fast that the time allowed for water to flow to the freezing frost is practically zero, and no segregation heave can occur.

Kaplar (1970) and Penner (1972) suspected that a limiting rate of frost front penetration at which only "in situ" water freezing should occur, exists for any soil. Kaplar found that for gravelly sand this rate was about 1.6 cm/hour. Moreover, it can be deduced from the results presented in his paper that this parameter seems to be dependent on the type of soil. This is also inferred from the present investigation since the characteristic freezing surface is unique for a given soil and is most likely

different for different soils, leading thus to different values of the limiting rate of cooling.

4.8 SUMMARY

It has been demonstrated that during an advancing frost front phase, the freezing characteristics of a given soil under zero applied load are defined by the segregation potential, the suction at the frozen-unfrozen interface and the rate of cooling of the fringe. Moreover, there is a unique relationship between these parameters. In the light of these results, it has been concluded that all the frost heave models that have been proposed in the past are not complete in describing the freezing soil for unsteady heat flow conditions since no considerations are given either to the degree of thermal imbalance, or, in some cases, to the suction developed within the fringe.

A frost heave model has been proposed for the simulation of laboratory freezing tests for one dimensional heat flow. The input to mass transfer is the characteristic freezing surface which is determinable from controlled laboratory freezing tests. The model predicts very well all the freezing tests conducted during this investigation.

It transpires, moreover, that the suction at the frost front cannot exceed a limiting suction of about -80 kPa. This is thought to represent the critical suction at which cavitation occurs in Devon silt.

Evidence of a limiting rate of cooling of the fringe is also provided by the experimental results. For Devon silt, this limiting rate of cooling is approximately 2.5°C/hour. For higher rates of cooling, water flow to the freezing front does not occur.

A parametric study reveals that the model is very sensitive to variations in permeability of the unfrozen soil. This, however, can be minimized by careful sample preparation so that the soil properties of different samples are constant. Variations in thermal properties of the freezing system affect to a lesser extent the results predicted by the proposed frost heave model.

5. FROST HEAVE IN FINE GRAINED SOILS UNDER ZERO APPLIED LOAD

5.1 INTRODUCTION

The first part of this chapter deals with the analysis of frost heave during retreat of the frost front and when it is stationary. Both situations can be obtained during the growth of the final ice lens. A predictive model is proposed for heave and heave rate during the terminal phase of a freezing test.

The second part of the chapter summarizes the different mechanisms operative during freezing of fine grained soils with no applied overburden. A mechanistic theory of rhythmic ice lens formation is also presented.

5.2 FROST HEAVE MODEL DURING A RETREATING FROST FRONT
5.2.1 Maximum Thickness of the Final Ice Lens

It was shown in Chapter 2 that the heave reaches an ultimate value where soil samples are frozen under fixed temperature conditions with the proviso that sufficient freezing time is available. This is thought to be associated primarily with the change in temperature distribution within the sample in response to changes in height of the specimen as the growth of the final ice lens continues with time.

Fixed temperature boundary conditions result then in a decrease in the overall temperature gradient in the sample and a warming of the base of the ice lens and the frozen fringe. During this process, thawing of the bottom part of the frozen fringe also occurs. For this reason, the terminal phase of freezing tests in which the frozen fringe thaws progressively with time has been referred to herein as a retreating frost front. It is clear that as the 0°C isotherm touches the base of the ice lens the frozen fringe will be completely thawed. Furthermore when the temperature at the base of that ice lens becomes 0°C, Equation 1.7 indicates that no suction can be developed in the water film beneath the ice lens. This, in turn, signifies no further water flow to the ice lens and hence cessation of heave. Moreover, the freezing system, i.e. the active and the passive system, is also in a state of thermal equilibrium provided the temperature boundary conditions remain stable in time.

At the end of the advancing frost front phase, the position of the final ice lens is given by lo as seen in Figure 5.1. During the freezing period, the height of the specimen increases from Ho to H. The difference, H-Ho, is a result of the heave which occurred during the freezing process. From the previous discussion, it follows that the ultimate height of the sample results when the temperature is 0°C at the base of the final ice lens, i.e. when the distance between the 0°C isotherm and the base of the sample is equal to lo. For one dimensional heat flow, the

Figure 5.1   Maximum Ice Lens Thickness with Fixed
Temperature Boundary Conditions

temperature gradient in the unfrozen soil is then equal to Tw/lo. The temperature distribution in the frozen part is influenced by the presence of the continually growing ice lens whose thermal conductivity is higher than that of the frozen soil by about 20 to 25%. If no radial heat flow occurs, the temperature profile within the frozen zone can be approximated by two lines of different slopes, one for the frozen soil and a steeper slope for the ice lens.

When heave stops, thermal equilibrium anywhere within the specimen is expressed by:

$$ku.grad\ Tu = ki.grad\ Ti = kfr.grad\ Tfr \quad\dots\dots\dots\dots 5.1$$

This condition can be rewritten if one considers the equivalent thermal conductivity of the medium composed of the frozen soil and the final ice lens as

$$ku.Tw/lo = kfe.Tc/(X+e) \quad\dots\dots\dots\dots\dots\dots 5.2$$

where $kfe = (X+e)/(X/kfr + e/ki)$ $\quad\dots\dots\dots\dots\dots\dots 5.3$

X is the thickness of the frozen soil above the ice lens

e is the thickness of the ice lens

Combining equations 5.2 and 5.3 and solving for e gives:

$$e = \frac{ki}{ku}\ \frac{|Tc|}{Tw}\ lo - \frac{ki}{kfe}\ X \quad\dots\dots\dots\dots\dots\dots 5.4$$

Equation 5.4 yields the maximum thickness that the final ice lens can grow to during a retreating frost front phase for the case of one dimensional heat flow. Adding this value to the height of the specimen prevailing at the end of the

advancing frost front phase provides the ultimate height of the sample under the specified temperature boundary conditions.

Unfortunately, it has been found that as the temperatures reach steady state, the influence of the ambient temperature of the cold room becomes increasingly more significant. Heat flows into the sample through the walls of the freezing cell. Since the heat balance is nearly achieved, any other heat supply becomes important. Therefore, another expression for the maximum thickness of the final ice lens must be derived which includes radial heat flow. One approach to this problem is to lump the radial heat flow, Q_r, to the level of the ice lens and to express the new heat balance for the one dimensional case as:

$$ku.grad\ Tu + Qr = kfe.grad\ Tfe \dots\dots\dots\dots\dots\dots 5.5$$

Equation 5.5 is rewritten as

$$ku'.grad\ Tu = kfe.grad\ Tfe \dots\dots\dots\dots\dots\dots 5.6$$

where $\quad ku' = ku + kr$

$$kr = Qr/(A.grad\ Tu)$$

Then Equations 5.4 and 5.6 yield the maximum thickness of the final ice lens as:

$$e = \frac{ki}{ku'}\ \frac{|Tc|}{Tw}\ lo - \frac{ki}{kfe}\ X \dots\dots\dots\dots\dots\dots\dots\dots 5.7$$

The total amount of heat flowing radially into the sample per unit time can be approximated by:

$$Qr = (kins/ln\ Re/Ri)\sum_{i=1}^{p}(To(i)-Tr).Dh \dots\dots\dots\dots 5.8$$

No Radial Heat Flow

$0\ °C$

Actual Temperature Profile

With Radial Heat Flow

$V = 0$

Final Ice Lens

V_o

Actual Conditions

h max

$0\ °C$

Equivalent Conditions

$V = 0$

$k'_u = k_u + k'_r$

V_o
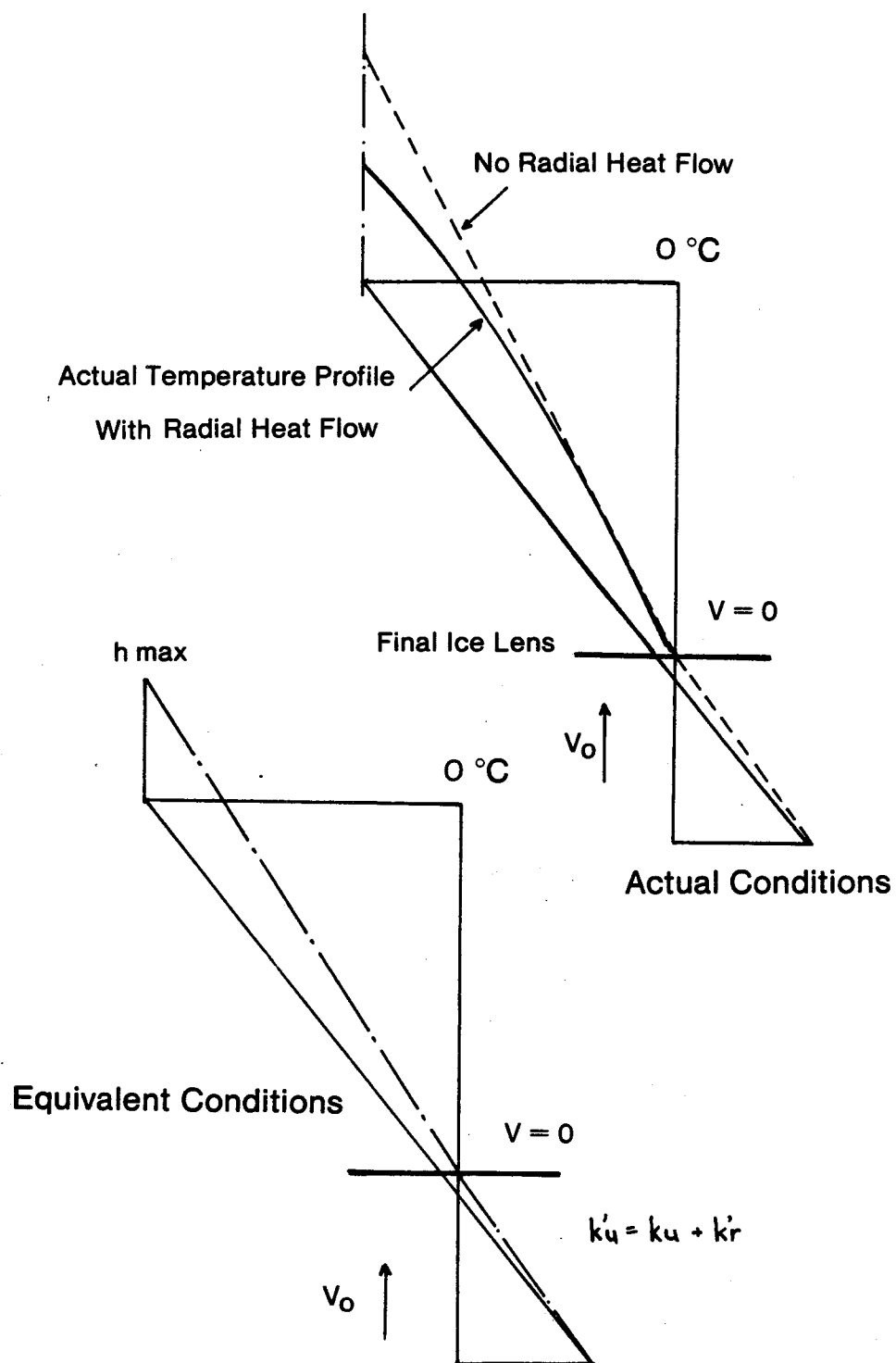
Figure 5.2   Effect of Radial Heat Flow

where   kins is the thermal conductivity of the insulation

and the cell wall

Ri is the inner radius of the cell

Re is the outer radius of the cell

To(i) is the temperature of the sample for each

element

Tr is the cold room temperature

Dh is the height of each element of soil

Figure 5.2 illustrates the effect of radial heat flow on the ultimate heave of the soil sample.

5.2.2 Physical Phenomena Occurring During the Terminal Phase

So far, only heat transfer has been used to assess the ultimate thickness of the final ice lens. No consideration has been given to the physical mechanisms governing mass transfer and to the heave - time relationship developed during the terminal phase.

Freezing tests in which the temperature boundary conditions are maintained constant with time lead, as discussed earlier, invariably to a progressive warming of the base of the ice lens. Equation 1.7 or 3.6 demonstrates that a concomittant decrease in suction in the waterfilm beneath the ice lens then occurs. Moreover, this process is associated simultaneously with a warming of the frozen fringe coupled with some melting of its warmest part. These mechanisms, in turn, influence the overall permeability of the current frozen fringe. Most likely, since the average

temperature of the frozen fringe increases, the overall permeability should also increase in response to a higher unfrozen water content in the fringe.

Furthermore, these processes may be accompanied by selective rejection of solutes into the melt by the growing solid phase (Hallet, 1978). As the soil freezes from top down, solutes are selectively rejected by the ice phase. They tend to accumulate at the freezing front but also diffuse downward, driven by concentration gradients. With continued preferential rejection of solutes by the growing ice, the solute concentration in the unfrozen soil increases progressively. Therefore, it is clear that the growth of the final ice lens contributes to solute enrichment in the unfrozen soil with time. Through their effect on the osmotic pressure, solutes will then affect mass transport during that phase. Increasing solute concentration below the ice lens results in a decrease in the suction potential and an associated decrease in the rate of water migration to the ice lens.

In this study, the suction potential was determined at the beginning of the terminal phase from freezing tests with applied back-pressure. Those suctions compared well with suctions obtained by virtue of the Clausius-Clapeyron equation when the temperature at the ice lens, T_s, was inferred from a measured temperature profile. It is, therefore, concluded that the influence of solute rejection can be neglected during the advancing frost front phase in

our tests. Nevertheless, one should bear in mind that a
stationary frost front for long periods of time could induce
important changes in solute concentration beneath the ice
lens and consequently changes in driving potential.
Neglecting the effect of increasing solute concentration
results in an upper bound of the thickness of the final ice
lens. For engineering purposes, this approximation is quite
justified.

In summary, the terminal phase is characterized by a
decreasing suction potential whose effect on water transport
is moderated by an increasing permeability of the frozen
fringe as thawing proceeds.

The change in height of the specimen during the
terminal phase produces changes in the temperature
distribution and consequently in its gradient. The heat
deficit or the net heat extraction rate at the ice lens will
therefore also change with time. Since heat is released when
upflowing water changes to ice, it is clear that this amount
of heat will be limited by the current heat deficit at the
ice lens.

This study therefore, takes the view that, although the
suction generated beneath the ice lens in response to
negative temperatures and, in some cases, damped by the
effect of increasing solute concentration drives water to
the ice lens, the dominant mechanism governing the rate of
water changing to ice is the current heat deficit existing
at the level of the final ice lens.

5.2.3 Heave Rate During the Terminal Phase

In order to proceed with analysis, Equation 5.4 or 5.7 can be used to predict the maximum thickness of the ice lens during the terminal phase. The position of its base, lo, is predicted using the model developed in Chapter 4. It has been shown that for Devon silt under zero external load, the final ice lens forms at a rate of cooling of the fringe equal to about 0.01°C/hour and at a segregation freezing temperature, Tso, of approximately - 0.10°C. This, in turn, allows one to deduce the length, lo, from the temperature distribution across the active system. The thickness of the frozen soil above the final ice lens is also determined from the model analysis. This thickness is constant during the terminal phase of the freezing test since it is assumed that the warmest ice lens acts like a cutoff with respect to water flow. In the frozen soil, water redistribution is likely to occur over longer freezing periods, but this process, the importance of which is thought to be minor as discussed in Chapter 1, does not affect the value of total heave.

The prediction of the heave - time relationship can be approximated by the following incremental procedure.

The amount of heat necessary to thaw the frozen fringe is neglected in this analysis. For one dimensional heat flow, the water migration flux or rate of heaving is obtained simply by:

$$V = (k_{fe}.grad\ T_{fe} - k_u.grad\ T_u)/L \dots\dots\dots\dots 5.8$$

This equation can be rewritten as:

$$V = \frac{1}{L} \left(\frac{|Tc|-|Ts|}{X+e} \, kfr - \frac{Tw+|Ts|}{Pu} \, ku \right) \dots\dots\dots\dots 5.9$$

However, Ts being unknown during the terminal phase, it is impossible to solve Equation 5.9 directly. The indeterminancy of the previous equation is eliminated if it is possible to find a relationship between the amount of heave occurring during this phase and the amount of thawing of the frozen fringe.

It can readily be shown that when a given percent of the maximum ice lens thickness has occurred, then the same percentage of the frozen fringe has thawed if one assumes that the thermal conductivity of the frozen soil is constant and that the heat released upon freezing is not taken into account. This is obviously not the case in freezing tests. Nevertheless, these assumptions approach reality as the end of the terminal phase is reached since the heave rate is significantly reduced which in turn, reduces the change in the geometrical configuration. During the early stages of frost front retreat, the assumptions are most critical. However they lead to a slight overestimate of the rate of growth of the ice lens since the frozen fringe would disappear faster with the previous assumptions than in the case where the heat released during ice formation is taken into account. The previous assumptions are illustrated in Figure 5.3.

The time required to reach a given percent of heave, x,
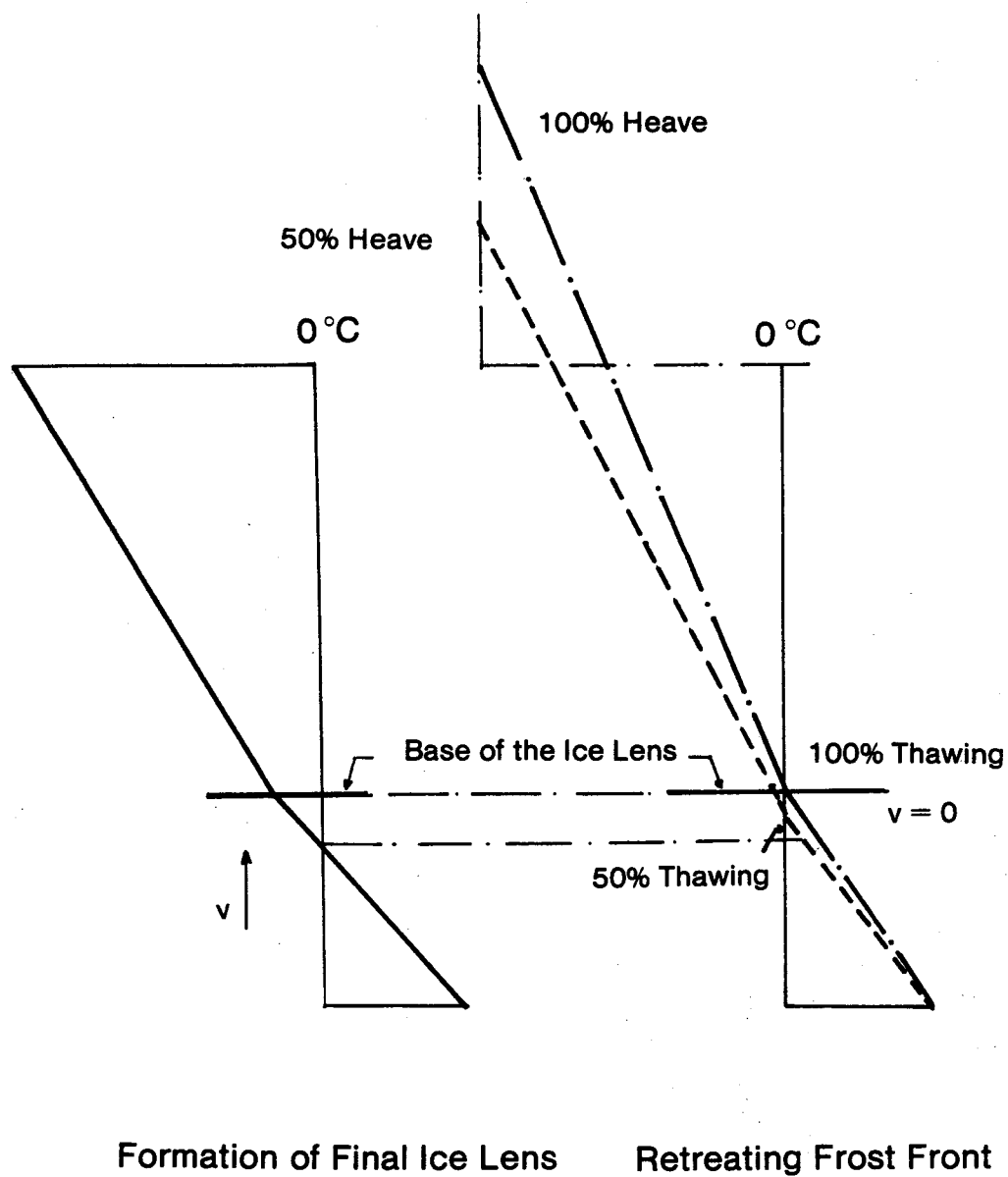
Figure 5.3   Assumptions of the Model During a Retreating Frost Front

can be calculated in the following manner:

$$t(x) = h(x) / 1.09V \dots\dots\dots\dots\dots 5.10$$

where $x = h(t) / h(max)$

$$V = (V(h) + V(h+Dh)) / 2 \dots\dots\dots\dots 5.11$$

where $V(h)$ and $V(h+Dh)$ are obtained from Equations 5.4 and 5.8 and corespond respectively to a thickness of the final ice lens of h and h+Dh.

In the case of parasitic radial heat flow, Equation 5.4 is replaced by Equation 5.7.

5.3 EXPERIMENTAL RESULTS

The previous section postulates that the relationship between heave and time during the terminal phase is determined solely from the thermal balance within the soil sample. This section is devoted to demonstrating that the behavior of laboratory freezing tests can be predicted with these theoretical considerations.

Test S1, described in Chapter 2, was frozen with an applied back pressure to the water reservoir. One of the objectives of this test was to investigate the warming of the base of the ice lens with change in height of the specimen. Freezing was consequently allowed with free access of water until the time at which the final ice lens was initiated. Then, the water line was closed and the change in pore pressure monitored with time. Since it was the first test conducted, the system was closed for only 8 minutes in

order to minimize disturbance. Thereafter, the water intake
line was reopened and the ice lens continued to grow at a
steadily decreasing rate as seen in Figure 5.4. After 18
hours of freezing the waterline was closed a second time and
the pore pressure drop was recorded for about 25 minutes.
Freezing in open system conditions then followed until the
water line was closed for a third time, 65 hours after the
beginning of the test. As discussed in Chapter 2, the effect
of cooling the base of the ice lens was also investigated.
For this reason, under open system freezing, the warm-side
temperature was lowered and a simultaneous increase in heave
rate was induced. In the second phase, the freezing system
was closed two more times, for longer periods than during
the first phase, 60 minutes and 120 minutes. Figure B1 in
Appendix B proves that thermal disturbance does not affect
the characteristics of the freezing system over such a
period since the rate of heaving obtained shortly after the
water line was reopened is identical to that developed
before it was closed.

Figure 5.4 clearly demonstrates that different pore
water pressure changes are obtained at different stages of
the termination phase. It is possible to evaluate the
approximate maximum drop of the pore pressures for each
closed-system test. By relating the maximum drop of the pore
pressures to the temperature at the base of the ice lens
using the Clausius-Clapeyron equation, it becomes evident
that the temperature at the base of the final ice lens
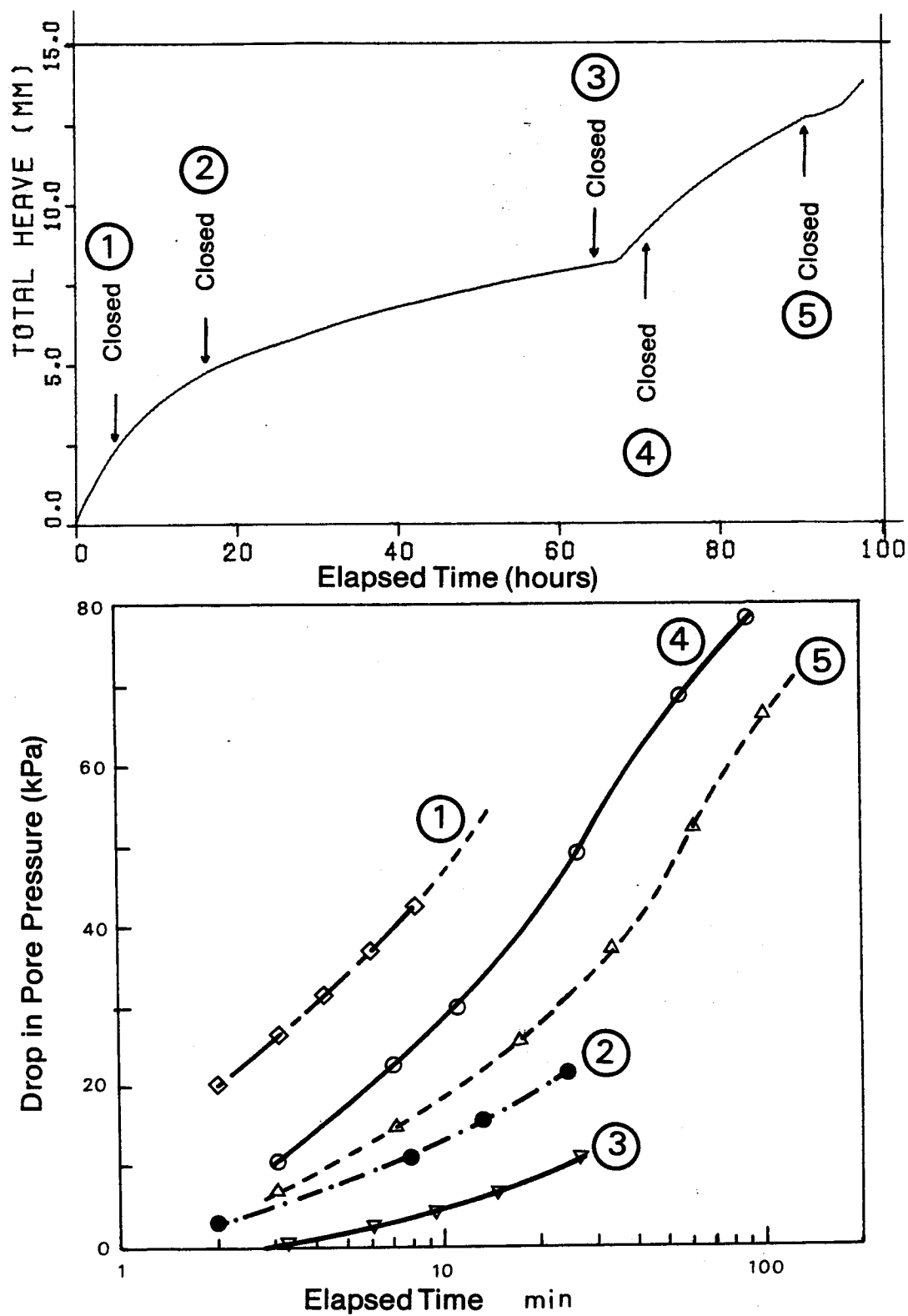
Figure 5.4   Pore Pressure Measurements in Test S1

increases, i.e. becomes warmer, with increasing height of the specimen since the drop in pore pressure decreases. Using X-ray photographs, Penner and Goodrich(1980) also established that the temperature at the base of the final ice lens increases with increasing height of the specimen when the temperature boundary conditions remain constant.

In order to prove that the heat deficit governs the amount of water changing to ice is a valid assumption, test S3 was performed. The soil was frozen under fixed temperature boundary conditions for about 24 hours. At that time, the freezing system had been in the terminal phase for about 10 hours and the final ice lens was about 3mm thick. During the following 24 hours, the temperature gradient in the frozen zone was maintained constant by manually lowering the cold-side temperature according to the amount of measured heave. The warm-end temperature was maintained constant during the entire process. Provided that the change in thickness of the ice lens is not too significant, Equation 5.8 reveals that the water intake rate, and consequently, the heave rate are constant under these conditions. Figure 5.5 shows that the measured heave rate during that second phase, in which the heat flux out of the sample was maintained constant, is constant. Moreover, as soon as the temperature boundary conditions are again constant with time the system goes back to the terminal phase and the rate of heaving decreases slowly with time.

In order to test the validity of the proposed model for
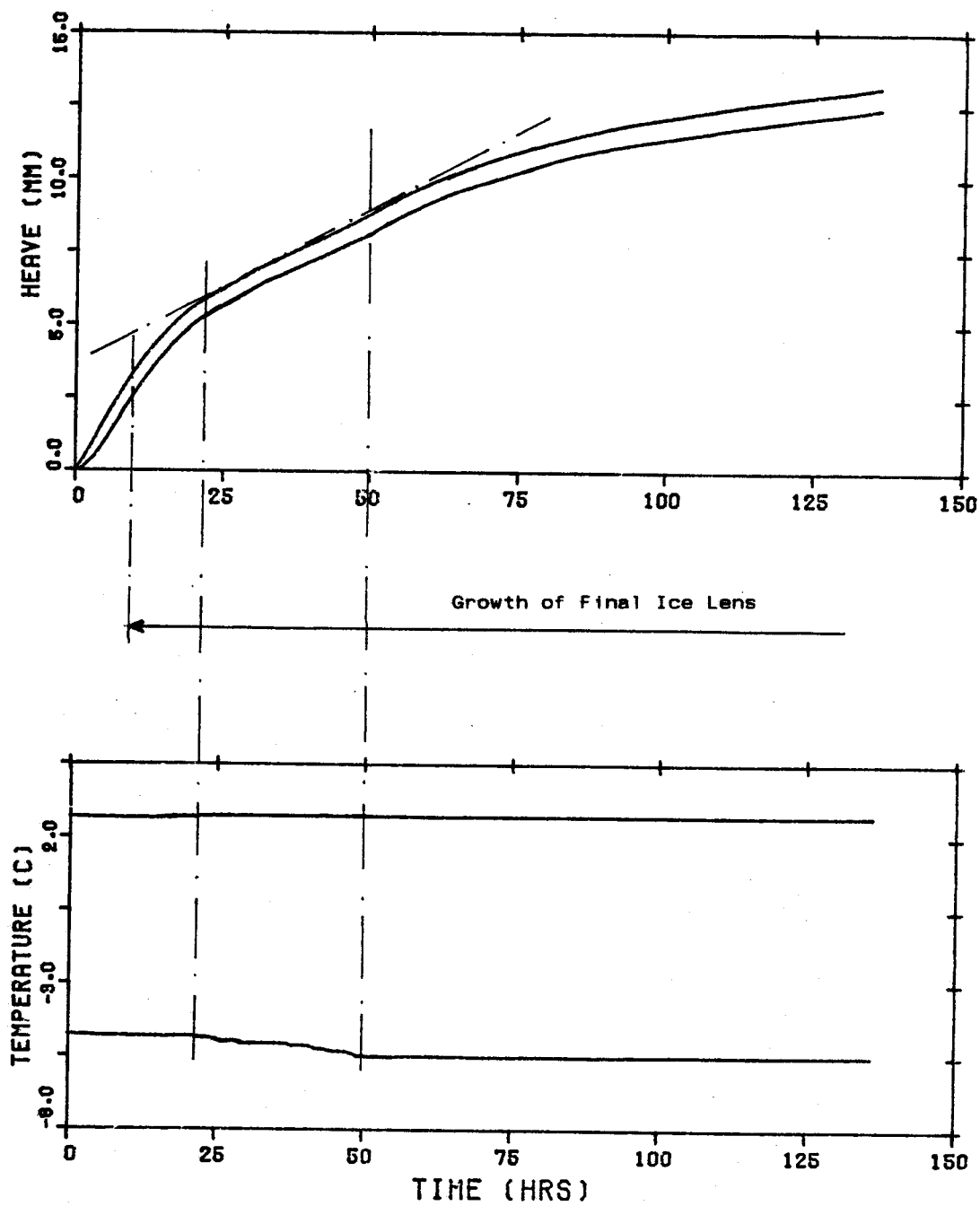
Figure 5.5 Effect of Net Heat Extraction Rate in Test S3

the terminal phase, four freezing tests were performed in which the final ice lens was allowed to grow close to its ultimate thickness. Tests NS-11, NS-12, NS-13 show that fluctuations in cold room temperature as defrost cycles were initiated influence the heaving rate when the temperature distribution is close to its final state. This is illustrated in Figure 5.6. It is clear, when plotting the variation in room temperature, that the warmer the cold-room, the lower is the heave rate and vice versa. These changes in heave rate are induced by minor changes in temperature distribution as a result of radial heat flow variations through the sides of the cell. In view of this phenomenon and since cyclic fluctuations in the cold-room temperature could neither be avoided nor minimized, the insulation method was changed. Instead of using two styrofoam hollow semi-cylinders which are perforated locally to allow the connection with thermistors placed along the cell wall, it was decided to spray a thick layer of urethane foam on the cell. This procedure results in good contacts everywhere around the cell and significantly reduces any preferential heat flow along bad contact areas. As shown in Figure 5.7 the effect of room temperature oscillations has almost disappeared for test G1 where the new insulation was used. The measured temperature profile, however, indicates clearly that radial heat flow, although reduced, is still occurring as shown in Figure C11 in Appendix C. The equivalent thermal conductivity resulting in the same amount
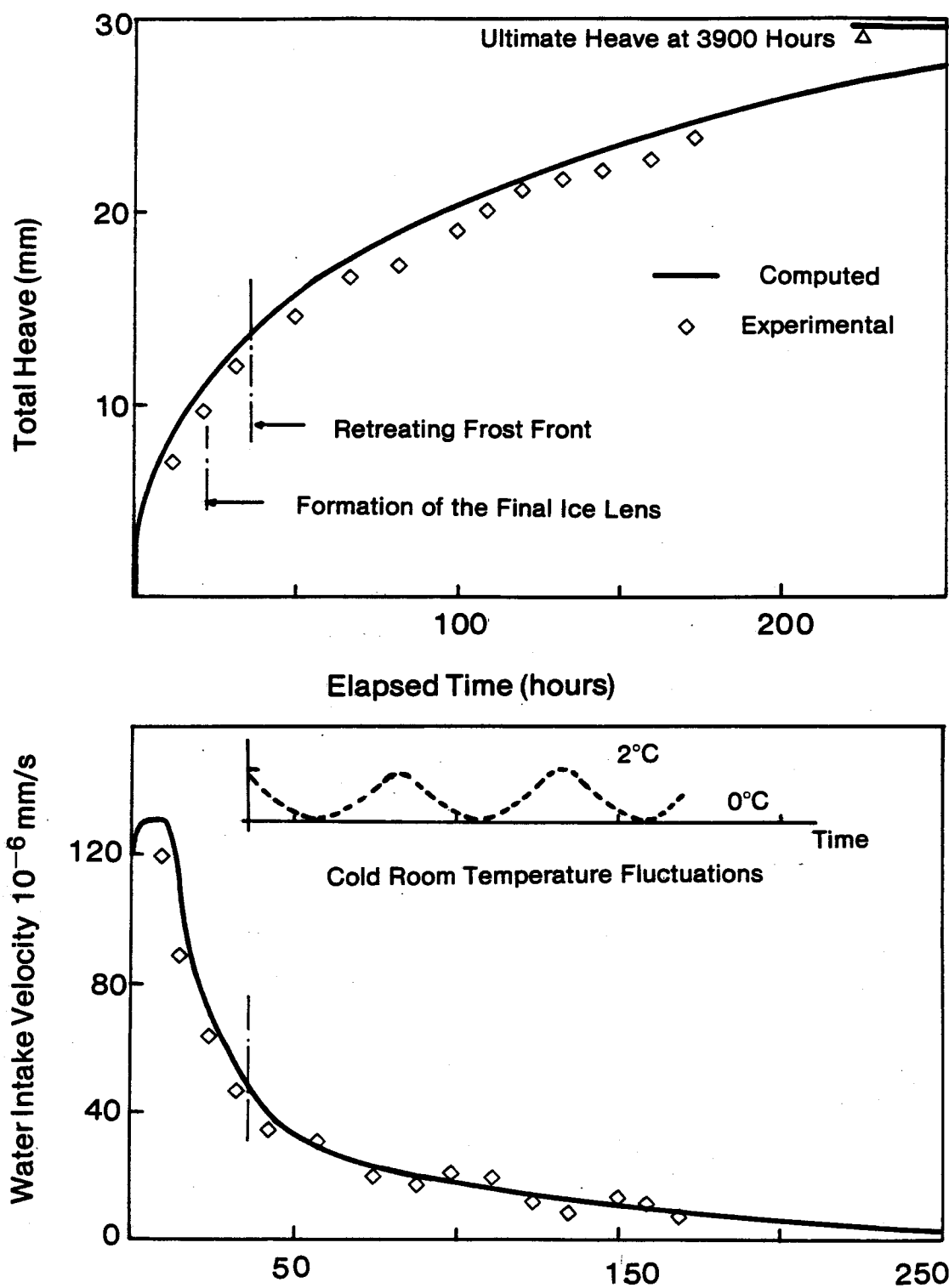
Figure 5.6   Comparison Between Predicted and Observed Data
            for Test NS-12

of heat flow through the sides of the cell is then evaluated with Equation 5.8 and 5.6. For thermal conductivities of the insulation in the range of 0.029 to 0.063 W/m°C,kr varies between 0.34 W/(m°C) and 0.71 W/(m°C) for tests NS-12 and G1.

The unsteady heat flow phase or the advancing frost front phase is simulated with the model presented in Chapter 4. It is possible to predict the depth at which the final ice lens is initiated for each test. Equations 5.7 to 5.11 are used to calculate the maximum heave and the rate of heaving during the terminal phase. Test NS-12 was simulated with an equivalent thermal conductivity of the unfrozen soil equal to 0.45 mcal/(mm.s.°C) or 1.88 mW/(mm.°C).

Figure 5.6 compares actual data with predicted results for test NS-12. The model predicts reasonably the heave during both the advancing and retreating frost front phases. The model predicts stable conditions at about 3950 hours and an ultimate heave of 29.7 mm. Test NS-12 was performed for only 170 hours and resulted in approximately 24 mm of heave. At 170 hours, the model predicts a heave of about 24.8 mm. The rate of water intake compares quite well too, despite its great sensitivity to cold-room temperature fluctuations.

Figure 5.7 shows computed and measured results for test G1. A parametric study with different Ts was undertaken for this test to evaluate the sensitivity of the position of the ice lens which is a function not only of the segregation freezing temperature but the time of its initiation. This
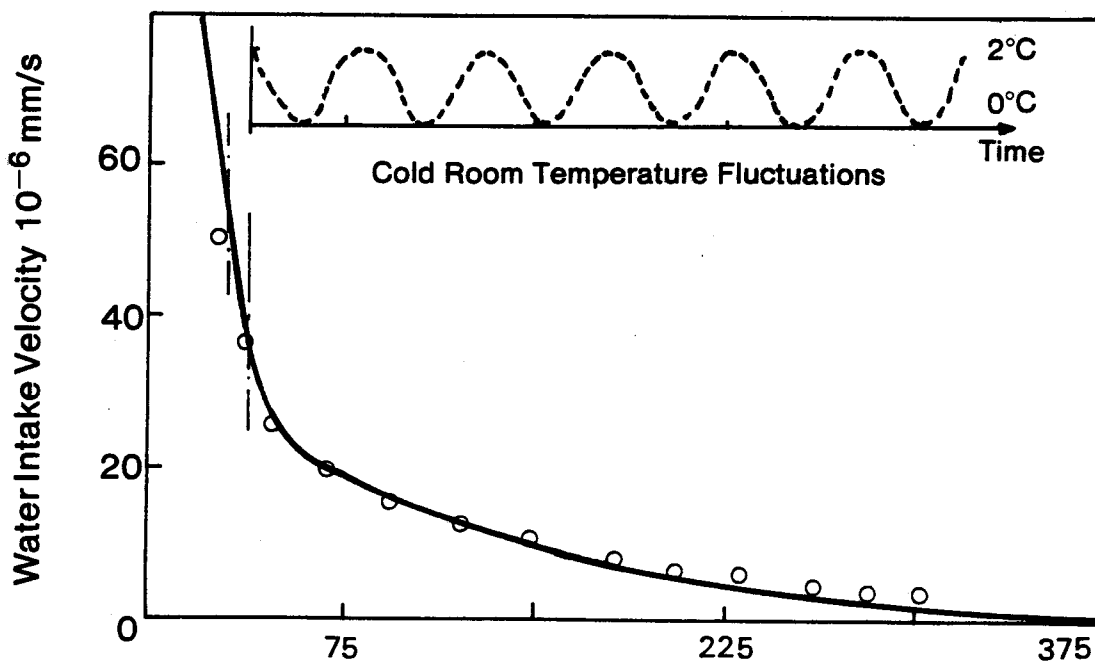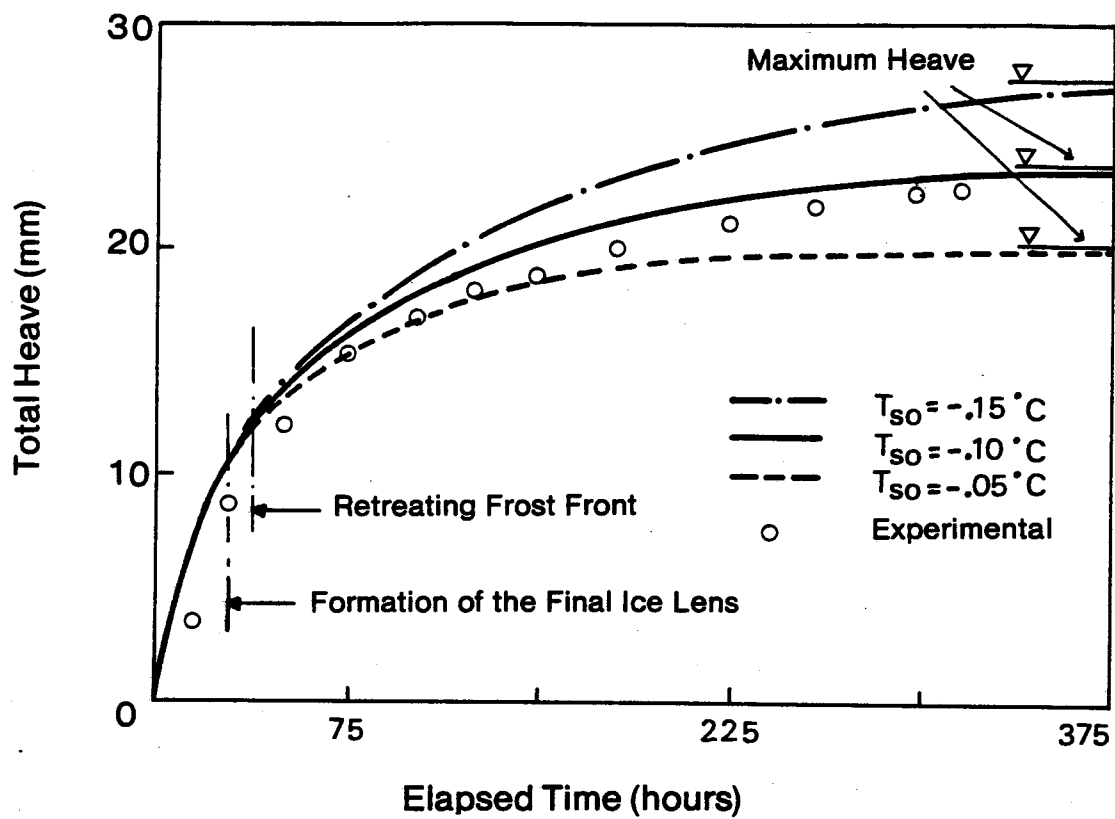
Figure 5.7 Comparison Between Predicted and Observed Data for Test G1

parametric study reveals that the ultimate heave is very sensitive to the position of the base of the final ice lens. However, it is expected that for field conditions, this sensitivity is significantly reduced due to greater thicknesses of frozen and unfrozen soil. Nevertheless, the model closely predicts heave and heave rate for test G1 for a segregation-freezing temperature of $-0.10°C$. The agreement is optimum for this value of T_s because the computed position of the ice lens is 23.6 mm from the base of the sample which is close to the value of 23.5 mm observed in the test (Plate 5.1) The segregation freezing temperature variation of $\pm0.05°C$ resulted in a variation of about ±1 mm in the position of the ice lens and about ±3 mm in the maximum heave for the freezing conditions of test G1.

The equivalent thermal conductivity of the unfrozen soil is 0.42 mcal/(mm s°C) or 1.76 mW/(mm°C) which is less than for test NS-12 due to the improved insulation. According to Equation 5.6, k_r is about 0.29 mW/(mm °C) which corresponds to a low thermal conductivity of the insulation of about 0.03 W/(m °C). Furthermore, Equation 5.8 demonstrates that the total radial heat flow increases with increasing height of the sample. A concomittant decrease in grad T_u during the terminal phase results in a maximum value of k_r towards the end of the terminal phase. The model therefore accounts for variable k_r during the retreating frost front phase. The value of k_r or k_u' given previously for tests NS-12 and G1 correspond to the maximum obtained at

the end of the freezing test.

Figures 5.5 and 5.4 also demonstrate that, provided the geometrical conditions at the beginning of the terminal phase are very close to those obtained in a freezing test, the model predicts closely the relationship between heave rate and time. This supports strongly the approximation made to render Equation 5.9 determinable by assuming that any percent heave was related to the same percent of fringe thawing. Moreover, it can be concluded that the rate of heaving depends solely upon the net heat extraction rate at the level of the final ice. Finally, radial heat flow significantly affects the heat balance within the sample. This, in turn, reduces the heat deficit at the ice lens and consequently the heave rate. By approximating the total amount of radial heat flow lumped to the level of phase change with an equivalent thermal conductivity of the unfrozen soil, it is possible to predict closely the results obtained during the terminal phase of a laboratory freezing test with a simple one dimensional heat flow formulation.

5.4 THE PROCESS OF SOIL FREEZING - A SUMMARY

This section is devoted to the summary and generalization of the different processes operative during fine grained soil freezing with no applied surcharge.

When a sudden step temperature below freezing is applied to the surface of a soil sample, unsteady heat flow
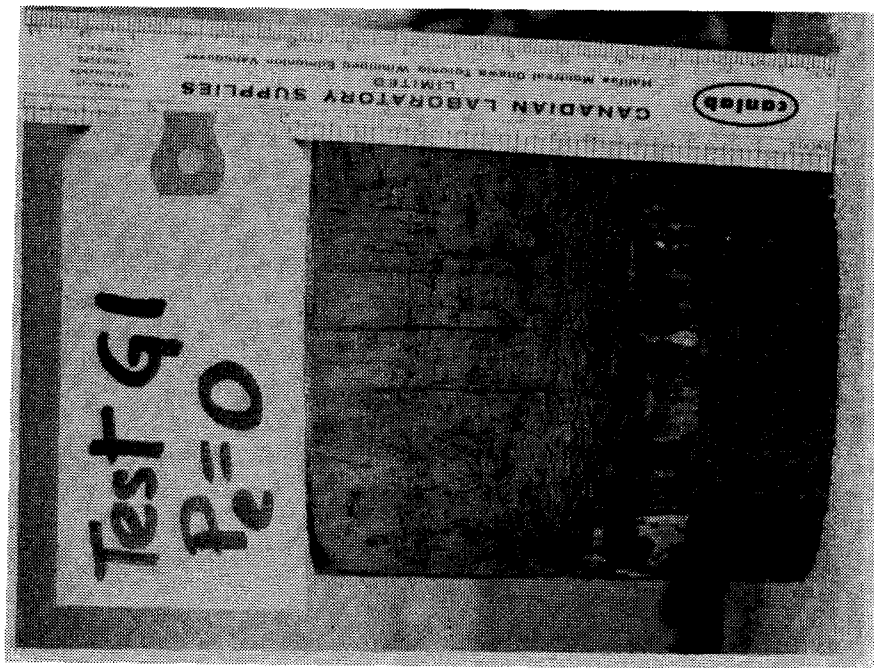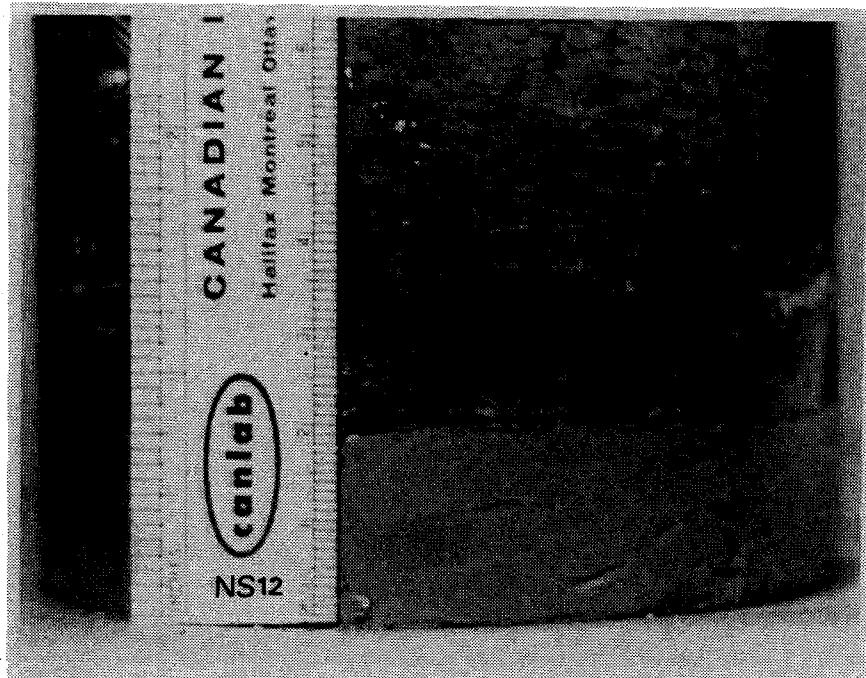
Plate 5.1   Final Ice Lenses in Test G1 and NS-12

is initiated. The frost front progresses into the soil as a function of the imbalance of the heat supplied to the heat removed. The heat deficit forces water to freeze simultaneously at two different temperatures. Pore water freezes *in-situ* at the *in-situ* freezing temperature, T_i, and water from an outside source is attracted to the freezing front where it freezes at the segregation-freezing temperature, T_s. For fine grained soils, T_s is found to be approximately between $-0.05°C$ and $-0.30°C$. The *in-situ* freezing temperature is close to $0°C$ and is primarily affected by pore size as T_i refers to the warmest temperature at which ice can penetrate a pore. Both T_s and T_i are also dependent on solute concentration in the soil.

The unsteady heat flow period is characterized by an advancing frost front. During this phase, the freezing soil is characterized by the segregation potential, SP, the suction at the frost front, P_u, and the rate of cooling of the frozen fringe, dT_f/dt. Once the relationship (SP, P_u, dT_f/dt) is determined from laboratory freezing tests for a given soil, it can be used as input to the general heat and mass transfer formulation governing freezing soils and any freezing condition can then be simulated very accurately.

For a given freezing condition, the advancing frost front phase can also be represented by a relationship between the net heat extraction rate and the total heave rate or the water intake rate. However, this representation is not unique for a given soil and depends on the boundary

conditions as discussed in Chapter 7. Nevertheless, it is entirely valid to represent a single freezing test with such relationships.

During an advancing frost front phase, when the freezing step temperature is constant the net heat extraction rate decreases steadily with time. The representative point of the freezing soil is then moving on two loci, one defining total heave rate changes, the other, water intake flux variations as shown in Figure 5.8. At a given rate of cooling of the fringe, close to maximum frost front penetration, the final ice lens is initiated. The rate of cooling corresponding to the final ice growth is thought to be dependent on soil type. When the frost front reaches its maximum penetration, the representative point of the freezing system is A (Figure 5.8). During the advancing frost front phase, the rate of water migration affects the thermal balance within the soil as latent heat is released during freezing. Thermal equilibrium considerations allow then the determination of the rate of *in-situ* water freezing. This means that high water intake rates retard the frost front penetration whereas small water migration rates increase the speed of frost front advance.

However, at point A, thermal balance is such that no further *in-situ* water freezing is required. The frost front is then at its maximum penetration in the soil. If the rate of heat extraction obtained at this point is maintained constant by changing the cold step temperature for example,
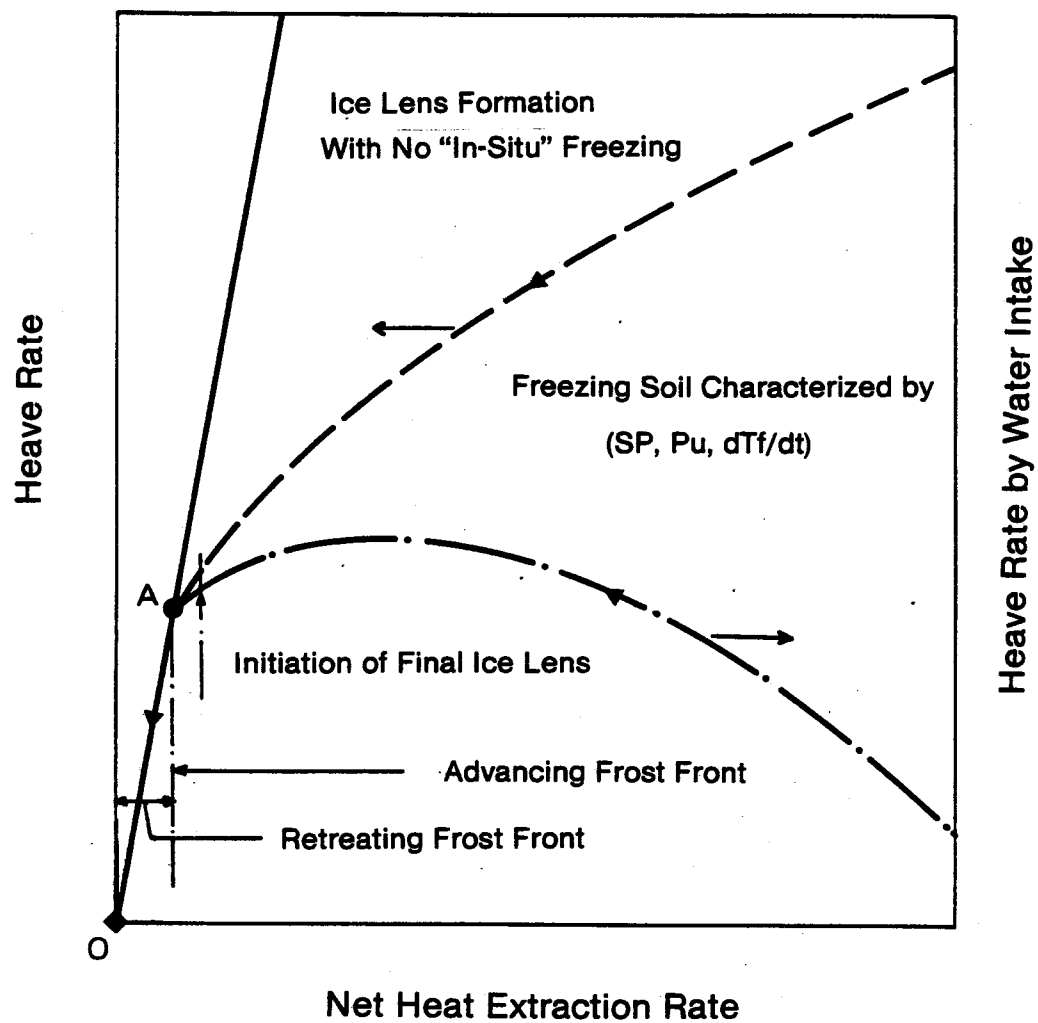
Figure 5.8   Characterization of a Freezing Soil with
              Respect to Net Heat Extraction Rate

the rate of heave will also remain constant. The representative point of this freezing condition is then still point A.

On the other hand, if the temperature boundary conditions are maintained constant with time, water migration and growth of the final ice lens contribute to changes in height of the specimen. This, in turn, affects the temperature profile within the sample and the net heat extraction rate decreases with increasing height of the specimen. The representative point of the terminal phase or retreating frost front situation is then moving on the straight line which is the locus of heave rates for the hypothetical case where all heat extracted comes from ice lens formation with no frost penetration. The slope of this particular line is $1/L$. With time, the representative point of the freezing system reaches 0 where the net heat extraction rate and the heave rate are both zero. This means that the temperature at the base of the ice lens is $0°C$ with atmospheric pressure in the water film beneath the ice lens. It must be emphasized that effects of solute beneath the ice lens are neglected in this conceptual model of freezing. It also means that the sample is in steady thermal state.

During a stationary frost front situation or during a retreating frost front phase, the amount of intake water changing to ice is governed solely by the heat deficit at the base of the ice lens. However, because the temperature at the ice lens is always negative during these phases, a

suction potential still exits at the ice lens and forces
water to flow to the segregation freezing level.

5.5 RHYTHMIC ICE LENS FORMATION IN FINE GRAINED SOILS

The analytical frost heave model presented in Chapter 4
considers that segregational heave is "lumped" at the 0°C
isotherm during unsteady heat flow. Since the frost front
penetrates continuously into the sample, segregational heave
is uniformly distributed within the frozen soil. In other
words, the model does not predict discrete ice lenses but
predicts the average ice content at any location.

In reality, however, and depending on the type of soil,
it often happens that the soil does not freeze homogeneously
but instead lenses of almost pure ice form, separated by
frozen soil with no visible ice structure
(Taber,1929;Palmer,1967). The thickness of these lenses may
vary from less than 1 mm to several centimeters. They are
also roughly parallel to the 0°C isotherm. The distance
between consecutive lenses increases with increasing depth.
This special ice structure formation in freezing soils has
been referred to as rhythmic ice banding.

Martin (1959) presented a theory to explain rhythmic
ice banding. It is based on unsteady heat flow conditions
combined with a nucleation temperature appreciably lower
than the temperature required for freezing the most easily
frozen soil water. Furthermore, he stipulates that the

permeability of the unfrozen soil is such that a steady state heat flow condition can be maintained temporarily, thus allowing the frost front to stabilize for a while and the ice lens to thicken. Further frost front penetration is initiated as the water flux to the ice lens decreases in response to decreasing permeability of the unfrozen soil. Martin states that the decreased permeability arises from the increased negative pressure in the water ahead of the ice front. Ice nucleates again when the actual temperature is lowered to the nucleation temperature. Thereafter, the processes described before repeat.

In summary, this model basically assumes that the ice lens formation corresponds to temporarily steady state heat flow conditions with temperature changes but no further freezing in the unfrozen soil below the ice lens. After a while, water supply is reduced due to decreased permeability of the unfrozen soil and thermal imbalance forces ice to nucleate somewhere below the former ice lens.

More recently, Miller (1978) proposed that ice lens initiation occurs when the effective stress in the frozen soil is zero. This effective stress is equal to $P_e - \sigma_n$ where P_e is the applied surcharge and σ_n is the neutral stress defined as:

$$\sigma_n = X(\psi) \, u + [1-X(\psi)] \, u_i \dots\dots\dots\dots\dots\dots 5.12$$

where $X(\psi)$ is a stress partition function varying with ice content

u_i is the pore ice pressure

u is the pore water pressure

This model fails in the case of zero applied load where it is justifiable to consider ui = 0 everywhere in the frozen soil. This, in turn, implies that δn is negative and that the effective stress is then equal to -δn in the case of Pe = 0. This conceptual model predicts therefore no ice lenses in a freezing soil under zero applied load which is obviously not the case in reality.

In the light of recent developments in frost heave research, that indicate that the ice lens forms somewhere behind the 0°C isotherm and that there is a frozen fringe between the ice lens and the unfrozen soil, Martin's theory is no longer adequate to describe the mechanism of rhythmic ice banding.

In the following, a new mechanistic theory of ice lens formation in fine-grained soils is proposed that is based upon continuous frost front penetration during unsteady heat flow and properties within the frozen fringe that vary in response to temperature changes.

When a sudden temperature well below freezing is applied to the surface of moist soil, nucleation of ice crystals is initiated. Once nucleated, ice propagation into the unfrozen soil does not require further nucleation as established in Chapter 1. The ice crystals therefore grow continuously in the direction of heat removal and apply pressure against any restraining boundary. This pressure is relieved by heaving of the soil in the direction of least

resistance (Kaplar, 1970). If no overburden pressure is imposed and if the self-weight of the overlying soil is neglected, the ice crystals will be under atmospheric pressure.

At the beginning of freezing, when the rate of frost front penetration is high, the water drawn into the sample flows to an accumulation zone whose location is controlled by the local permeability. This thickens locally the thin unfrozen water layers surrounding the soil particles. Thermodynamic equilibrium is altered and the free energy of the water is then higher than that of the adjacent ice. Equilibrium is re-established by freezing some of the water. In other words, the thickness of the unfrozen water films is maintained constant at a given temperature by freezing incoming water. The fast advancing frost front does not allow water to accumulate at a given level for enough time to create a continuous ice lens. Assuming no accumulation of water within the frozen fringe, the suction in the fringe develops a non-linear profile due to decreasing permeability of the frozen soil as the temperature decreases (Figure 5.9a and 5.9b). In the absence of a continuous ice lens, segregational freezing will occur preferentially along the top of the soil particles which is a direction of least resistance. Locally, this will result in non-homogeneous heave and strain the ice matrix at the top of the frozen fringe. As seen in Figure 5.9, the continuous ice in the frozen fringe adopts a rather tortuous and root-like aspect

in a freezing soil due to the soil structure. The ice matrix may be considered as anchored within the soil matrix and the ice is forced to elongate. The non-uniform straining is thought to develop high strains only locally in the ice at the top of the fringe and the rest of the ice is essentially unaffected. The stress condition in the ice at the level of accumulation is very complicated since ice above soil grains is most likely unstressed whereas ice between soil grains is highly stressed. This, in turn, affects thermodynamic equilibrium and the application of the Clausius-Clapeyron equation becomes difficult for these conditions.

When the segregational heave is small, i.e., at the beginning of freezing, the ice may strain without breaking. However, as the frost front penetration rate decreases, the rate of temperature change across the sample is also reduced. Water is then able to accumulate at a given level for a longer period of time. The adjacent ice is now strained to a higher degree leading to failure of the ice grains. Further water accumulation and freezing result in the formation of a discrete ice lens. This ice lens is now unstressed and grows onto a roughly planar substrate composed of soil particles, unfrozen water and the pore ice at the top of the frozen fringe. The ice of the frozen fringe is also unstressed for the case of zero overburden. Under these new conditions, identical to those of Biermans et al (Chapter 1) the Clausius-Clapeyron equation describes the thermodynamic equilibrium at the base of the ice lens

(Figure 5.9c) with the ice pressure equal to atmospheric.

Figure 5.10 represents schematically the process of initiation and growth of a single ice lens and of the formation of the subsequent ice lens. Let us consider the time t at which one or more ice lenses have formed in the specimen. At this time, another ice lens is initiated at a given location defined by its particular segregation freezing temperature, Tsf. Because unsteady heat flow is still occurring, the frost front advances at some rate dX/dt. This, in turn, produces changes in the temperature profile across the sample and more specifically across the current frozen fringe. During a time interval, Dt, the base of the ice lens cools below Tsf and the extent of the frozen fringe increases by DX. In other words, the frozen fringe existing at the onset of formation of the ice lens increases in length with time and the temperature across it becomes colder. Consequently, the overall permeability of the fringe decreases, the flow path increases and the suction potential developed at the base of the ice lens becomes greater. As shown in Equation 1.7, for temperatures close to 0°C, the suction varies linearly with temperature below 0°C. In contrast, the unfrozen water content and hence the frozen soil permeability decay more or less exponentially with decreasing temperature (Johanson, 1977). As long as the relation between suction and frozen fringe permeability is such that the water flow entering the fringe is able to traverse it, water will be drawn to the base of the ice lens
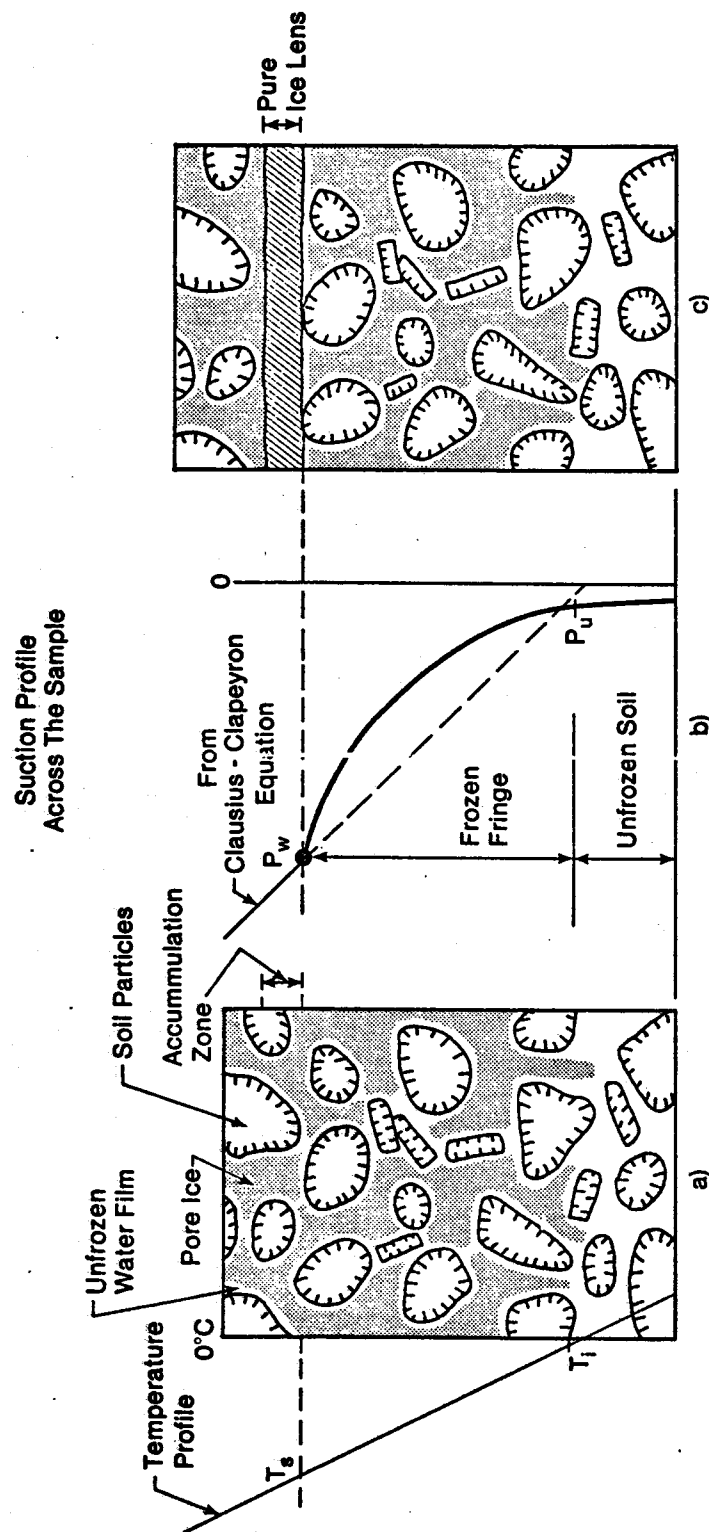
Figure 5.9   The Mechanism of Ice Lens Formation
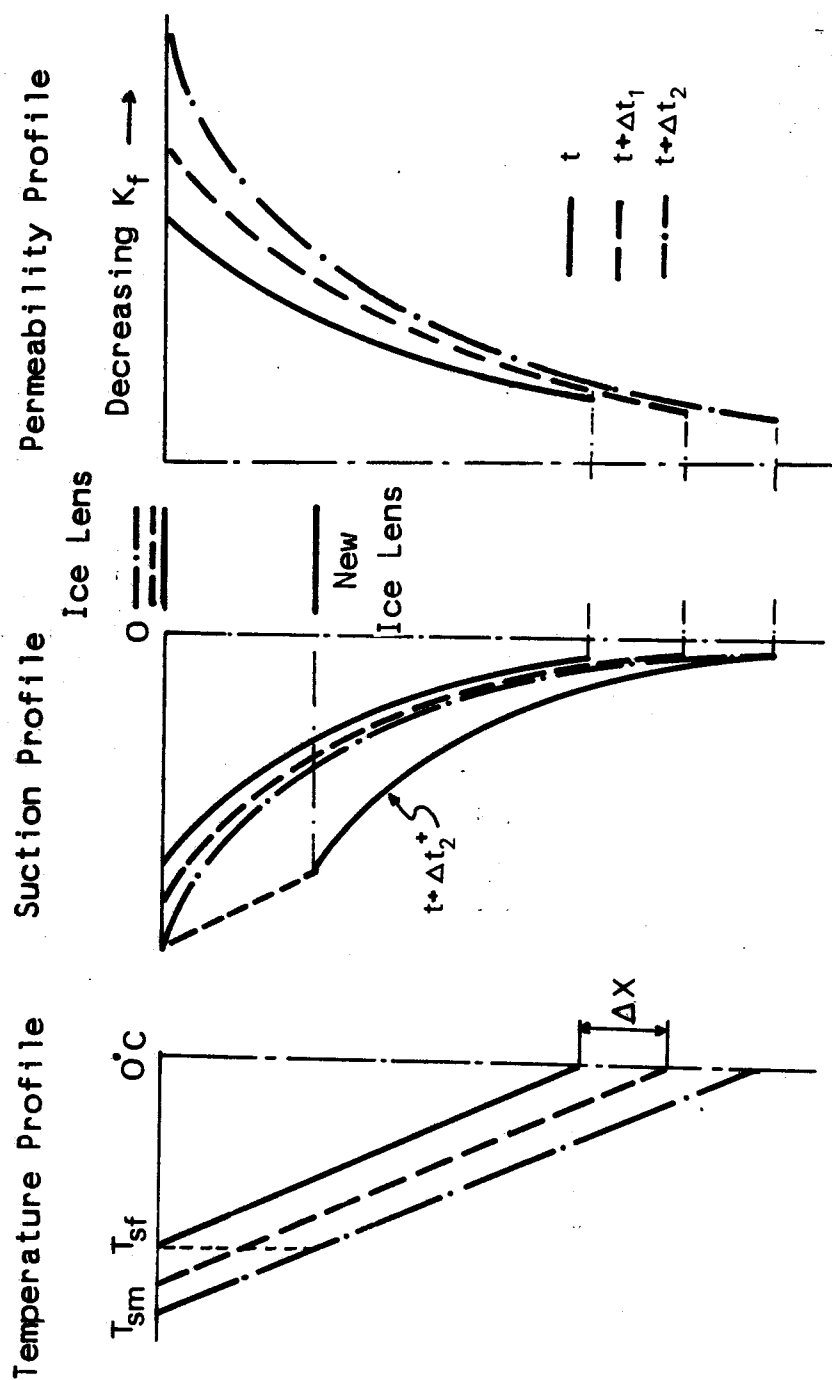
Figure 5.10 Change in the Characteristics of the Current
Frozen Fringe During an Advancing Frost Front

and thus contribute to its growth. Therefore, during the time interval Dt the ice lens grows to a thickness equal to 1.09 V.Dt where V is the average water intake flux. Further penetration of the frost front results in further chilling of the current frozen fringe. After a while, the temperature at the base of the warmest ice lens reaches a value, Tsm, at which, the permeability of the upper part of the fringe is so small that water flow is essentially stopped in the zone of extremely low permeability. Water now accumulates somewhere below the base of the former ice lens. The new level of accumulation is governed by the local permeability of the current frozen fringe which can be associated with a segregation-freezing temperature of ice lens formation, Tsf.

This process is repeated periodically until steady state conditions are reached and the final ice lens is formed at a temperature, Tso.

The results of Section 4.3 demonstrated that during the period of formation of the zone of active lensing, the overall permeability of the frozen fringe decreases steadily with decreasing rate of cooling of the fringe. During that particular period, the overall permeability of the frozen fringe is insensitive to the chosen value of Ts. The previous result implies therefore that the unfrozen water content is also dependent upon the rate of cooling. Hence, it can be argued that the critical permeability governing the position of the different ice lenses is not solely a function of temperature. In other words, it is plausible to

consider that Tsf is not a constant during unsteady heat flow. Furthermore, since the overall permeability of the current frozen fringe decreases steadily during the formation of the zone of active lensing, one can expect that the temperature of ice lens formation, Tsf, becomes warmer as the rate of cooling decreases. This postulate, which is very difficult to verify experimentally, is nevertheless supported by recent work reported by Ershov et al (1978).

The application of the previous mechanism to uni-directional freezing of a fine-grained soil predicts at the outset a frozen zone with increasing ice enrichment but no visible ice lenses due to the rapid change of temperature across the sample. Then, as the front frost penetration slows down, very thin and barely visible ice lenses appear. Their vertical spacing is relatively small due to the high temperature gradient in the frozen soil. With time, this temperature gradient decreases as a result of further advance of the freezing front. The frozen fringe thickness increases and the ice lenses grow thicker with increasing spacing. As the steady state condition is approached, the fringe tends to its maximum thickness. This process is represented schematically in Figure 5.11. For fixed temperature boundary conditions, this final ice lens will continue to grow until its suction potential at the base is atmospheric and no further water flow to the ice lens is possible. If the water beneath the ice lens is pure, the end of the ice lens growth corresponds to a temperature of its

base of 0°C for the case of atmospheric pressure in the ice lens.
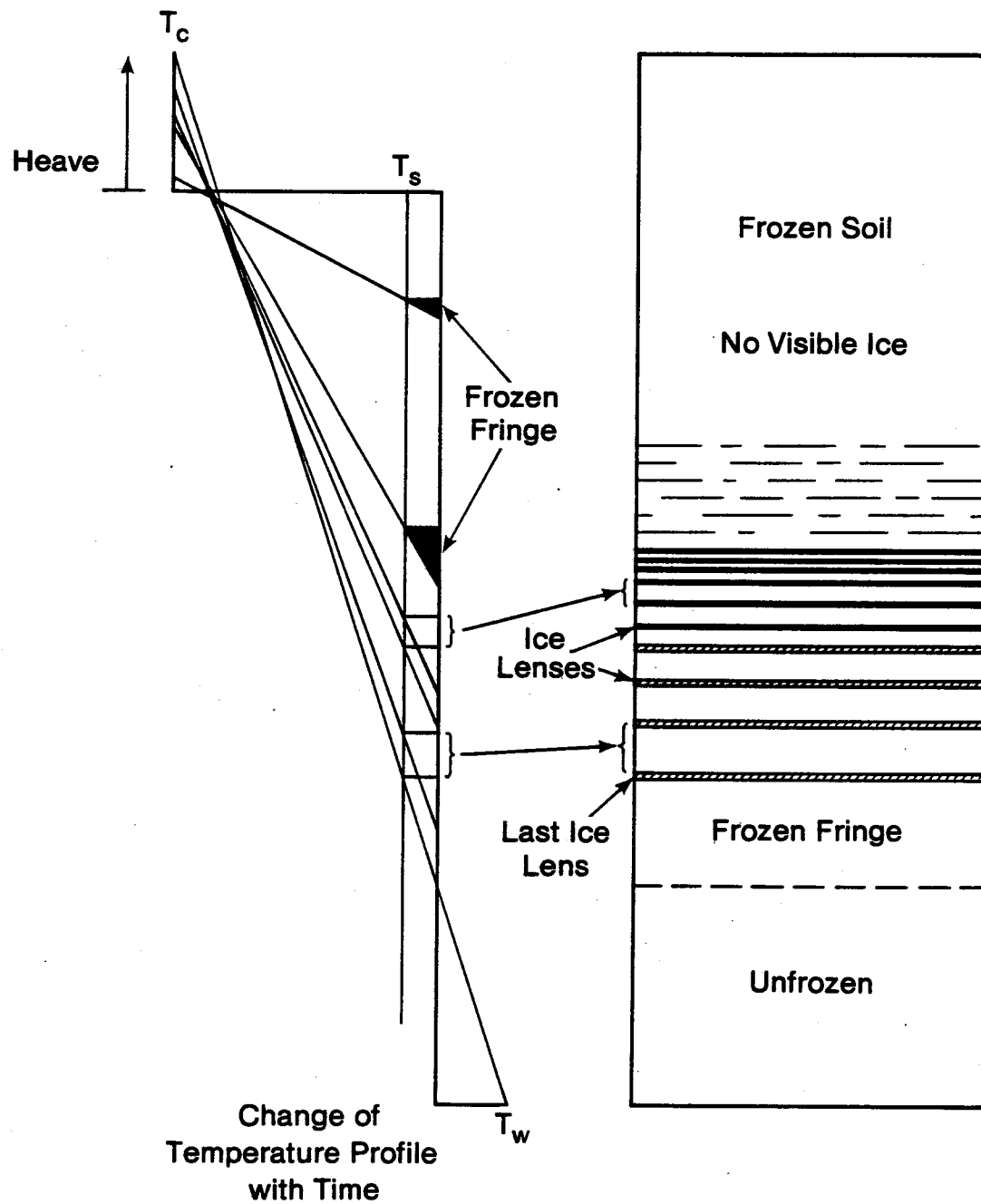
Figure 5.11 Schematic Rhythmic Ice Lens Formation

6. EFFECTS OF APPLIED PRESSURE

6.1 INTRODUCTION

It has been appreciated by workers in the field of frost action for some 50 years that increased load on a freezing soil can reduce the heave rate. There are several well documented case records which illustrate the phenomenon. Beskow (1935) was the first to document that increased applied pressures cause a decrease in heaving rates in silty soils.

However, opposing views are found in the literature concerning the exact mechanism that is operative in the reduction of frost heave as increasing stresses are applied to a freezing soil.

One school of thought developed the concept of the "shut off" pressure, for which no flow into or out of the sample will occur. Linell and Kaplar (1959) showed that such a pressure was found for a variety of soils. Other supporting laboratory evidence was presented by Arvidson (1973). These tests showed that when the applied load was lower than the shut-off pressure water was attracted to the freezing front and when the applied pressure exceeded the shut-off pressure, water was expelled. Takashi et al (1974) in a series of experiments in which the rate of frost front

penetration was kept constant, also established two different modes of behavior of moisture migration due to changes in applied load. Hill (1977) obtained results similar to those found by Takashi et al (op. cit.).

Despite the fact that there is an enormous amount of data reported in the literature to support the concept of the "shut off" pressure, a second school of thought promulgates the view that it is not possible to control independently frost heaving arising from in situ water freezing and from the ice segregation process by loading the soil. Penner and Ueda (1977), who subscribe to this second view, demonstrated that expulsion of water can be followed by water intake provided sufficient freezing time is allowed.

This chapter will analyse freezing tests with applied pressure in the same way as freezing tests with no applied surcharge. The characteristics of the frozen fringe are investigated for a given stress in the sample during an advancing frost front, at the onset of formation of the final ice lens and during the retreating frost front phase.

Finally the concept of "shut off" pressure is evaluated in the light of the results obtained with the general approach described in this thesis.

6.2 THE EFFECT OF PRESSURE FROM A THERMODYNAMIC PERSPECTIVE

The application or removal of pressure on the frozen soil clearly changes the free energy of the ice. This alters thermodynamic equilibrium and restoration of equilibrium requires an equal change in the free energy of the unfrozen water.

The equality of the free energies can be expressed by the following general equation (Chapter 1):

$$Vi.dPi - Si.dT = Vw.dPw - Sw.dT \dots \dots \dots \dots 6.1$$

If the process is isothermal, i.e. dT=0, the change in free energy in the ice is DPi. Vi on applying the pressure DP = DPi. Thermodynamic equilibrium thus requires a change in the free energy of the bulk soil water equal to

$$D(DG)w = DPw.Vw = DPi.Vi \dots \dots \dots \dots \dots 6.2$$

Equation 6.2 reveals therefore that for thermodynamic equilibrium, the change in water pressure must be about 9% greater than the change in ice pressure.

As shown on Figure 6.1, the unfrozen water can be separated into two different types. The unfrozen water that is relatively far from the soil particle surfaces can be considered as capillary water or bulk water. This type of water is not affected significantly by the solid surface of the soil particles. It is assumed that the pressure in that type of free water is related to the ice pressure through the Laplace Equation. For the simplified case of a spherical interface, this equation reduces to:

$$P_i - P_w = 2.\delta_{iw}/r \dotfill 6.3$$

where r is the radius of the ice-water interface

δ_{iw} is the interfacial energy of ice/water

If the pressure in the ice is atmospheric, Equation 6.3 gives:

$$P_{wo} = - 2.\delta_{iw}/r_o \dotfill 6.4$$

If an applied pressure results in an increase in the ice pressure from zero to P_i, Equation 6.2 establishes that the change in pore water pressure in the bulk soil water is $(V_i/V_w)P_i$. Equation 6.3 now yields:

$$P_{wo} = P_e.(V_i-V_w) + 2.\delta_{iw}/r \dotfill 6.5$$

Substitution of P_{wo} by its value given in Equation 6.4 results in

$$2.\delta_{iw} (1/r_o - 1/r) = P_e (V_i-V_w)/V_w \dotfill 6.6$$

Since the right side of Equation 6.6 is postive, the term $1/r_o - 1/r$ must also be positive. This implies then that $r > r_o$.

This simple analysis demonstrates that a change in external pressure on a frozen soil is also associated with a change in the unfrozen water content. This change is however very small since it is only induced by $0.09 P_e/2.o_{iw}$. Moreover, increasing pressures result in increasing unfrozen water contents since the radius of the ice water interface increases with increasing pressures. Experimental evidence for this relationship is given by Williams (1976), where changes in water content determined from volume changes of frozen Tanzania Clay were related to pressure changes. Only

slight variations in the unfrozen water content were observed in response to substantial pressure changes.

The second type of unfrozen water can be considered as being strongly influenced by the solid surface of the soil particles. Gilpin (1979) proposed a model that includes the effect of a solid surface in the formulation of the free energy of that type of water. Thermodynamic equilibrium provides then the variation of the state variables with distance from the solid surface. It was demonstrated that pressure and temperature affect the thickness of that liquid film layer. Increasing pressure at constant temperature results in increasing thickness of the liquid water layer.

For the special case of a discrete ice lens, the relationship between Pw, Pi and Ts given in Chapter 1 reduces to

$$Pw = L.\ln(Ts*/To*) \; / \; (VwTo*) + (Vi/Vw)Pe.....6.7$$

since it is appropriate to put Pi equal to the applied external pressure. Freezing tests in which the soil is prevented from heaving induce heaving pressures. These heaving pressures build up with time and reach ultimately a maximum stable value, corresponding to a condition of no water flow to the ice lens. It is therefore assumed that for these ultimate conditions, Pw is equal to zero. Such tests provide therefore an excellent check of the validity of Equation 6.7. Rewriting this equation for Pw=0 results in:

$$- L.\ln(Ts*/To*)/(Vw.To*) = (Vi/Vw)Pe = 1.09 \; Pe...6.8$$

Several investigators, (Radd and Ortle, 1973; Hoekstra,
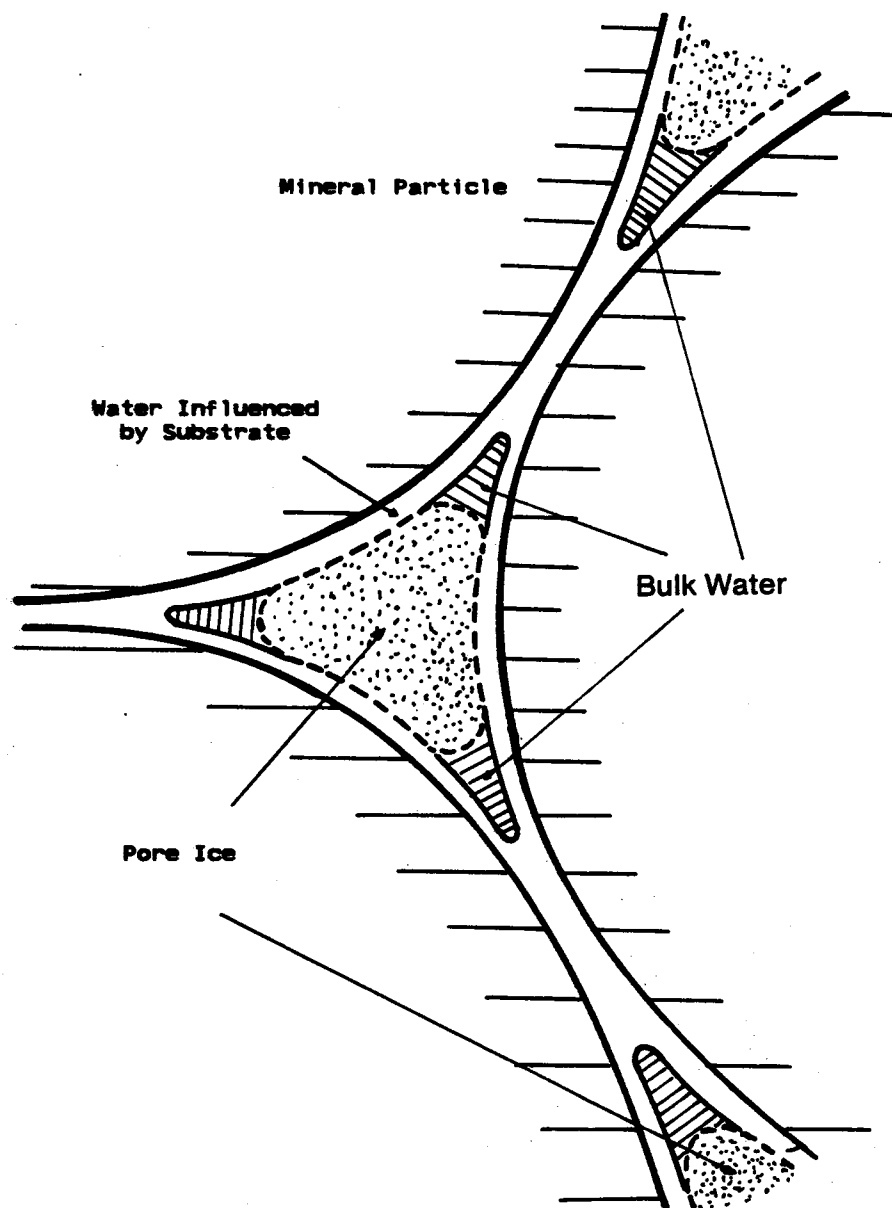
Figure 6.1   The Water Phase in Frozen Soil

1969) conducted this type of freezing test and demonstrated that the relation given in Equation 6.8 was closely verified in their experiments.

Finally the application of pressure also influences the freezing point depression. Equations for different pressure conditions were given by Edelfson and Anderson (1943) and more recently by Everett (1961).

For the case where the total pressure change on the ice equals the total change in pressure on the water, the following relation is obtained:

$$dT/dP = (Vw-Vi)To*/L \dots\dots\dots\dots\dots\dots\dots\dots 6.9$$

where   dT is the change in freezing point

dP is the change in pressure

Equation 6.9 reveals that for a change in pressure of 100 kPa, the freezing point is depressed by -0.0072°C. However, in a freezing soil, once nucleation has occurred the pore ice penetrates into the soil as a continuous medium. Therefore, this latter aspect of pressure effect is not relevant to frost heave problems.

6.3 THE EFFECT OF PRESSURE ON THE SEGREGATION FREEZING TEMPERATURE

The previous section has demonstrated that the effect of overburden pressure on a freezing soil is twofold. Firstly, the suction potential established beneath the warmest ice lens is reduced by an amount equal to (Vi/Vw)Pe.

This, in turn, affects certainly the rate of water migration and the rate of heave. Secondly, changes in pressure affect the unfrozen water content of the frozen soil. Increasing the pressure results in a small increase in the amount of unfrozen water which, in turn, produces changes in the local permeability of the frozen soil, especially in the frozen fringe. It is therefore expected that the frozen fringe characteristics, Ts and Kf, change with applied pressure changes.

6.3.1 Closed System Freezing

A series of closed freezing tests with applied backpressure were performed in order to investigate changes in maximum drop of the pore water pressure with applied external pressure. The initial pore water pressure, which is equal to the back pressure, drops during freezing as a result of the lower pressure that is generated within the frozen soil. The maximum drop of the pore pressure corresponds to equilibrium conditions in the sample. The pore pressure in the unfrozen soil is then equal to that generated at a given temperature in the frozen soil and no water flow to that zone occurs. The maximum drop of pore water pressure is therefore an indirect measure of the extent of the active zone in the frozen soil.

The initial and final conditions of the tests in this series are summarized in Appendix E. The experimental apparatus is described in Appendix A. An insulated triaxial

cell was used in order to apply the back pressure to a 10 cm diameter soil sample. The cell pressure was applied through air and was about 700 kPa. The top cap served to maintain a constant negative temperature at the surface of the specimen. Pressure was applied by means of a bellofram. The bottom plate was maintained at a constant temperature above freezing.

To start with, the sample was frozen in a closed system, i.e. no external water source, under zero additional pressure. During this stage, a transducer measured the change in water pressure with time. The pore pressure initially dropped and after a while stabilized. The second phase was initiated by applying an additional vertical pressure. This produced instantaneously a change in pore pressure which was also monitored with time.

During the first stage of the test unsteady heat flow occurs. However, after a while, the temperature profile reaches steady state conditions and the frost front becomes stationary. The pore water pressure approaches an ultimate value during stationary frost front freezing as shown in Figures 6.2 and 6.3. Those figures also reveal that if the maximum drop of pore water pressure is related to temperature through the Clausius-Clapeyron equation, the maximum temperatures corresponding to the maximum drop in pore pressure are colder than those obtained in tests where an ice lens was formed prior to closed system conditions. As demonstrated in Chapter 1, an ice lens acts like a cutoff to

water migration and probably also to suction generated behind that ice lens, in the frozen soil. It is therefore plausible that in a closed freezing system, the zone of frozen soil which influences the pore water pressure in the unfrozen soil extends deeper into the frozen soil than when an ice lens forms during open system freezing.

The application of an additional vertical stress to the specimen produces in both tests an almost instantaneous equal change in the pore fluid pressure. In test D1, 75 kPa was applied which resulted in an increase of 71 kPa in pore pressure, shown by a decrease in the pore pressure drop in Figure 6.2. For test D3, a pressure of 225 kPa produced an equivalent change in the pore water pressure as shown in Figure 6.3.

At this stage, if the seat of the suction potential in the frozen soil remains at the same location, no change in the pore water pressure should occur with time. The experimental results establish clearly that a further drop of pore pressure with time occurs and reaches ultimately a new stable value. Since thermal equilibrium was already attained during the first stage of these tests, the change in pore water pressure is thought to be related to a change in the position of the level producing the maximum suction developed in the frozen soil that influences the pore water pressure in the unfrozen soil. In other words, this study takes the view that the segregation freezing temperature becomes colder with increasing pressure on the soil. This is
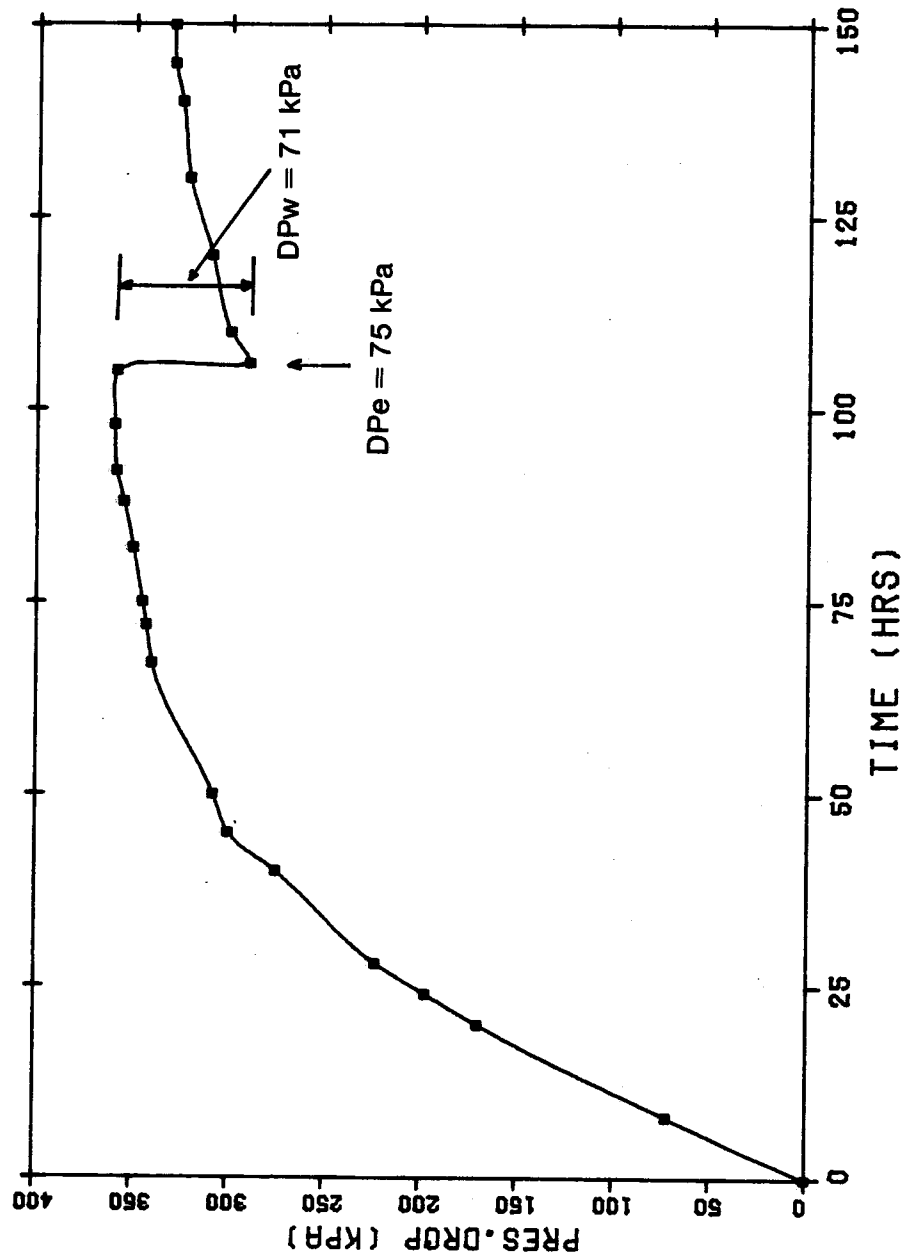
Figure 6.2   Closed Freezing Test with Applied Back Pressure
Drop in Pore Water Pressure

best illustrated in Figure 6.4 where the temperatures required to produce the maximum pore pressure drop are calculated with Equation 6.7 and plotted as a function of applied vertical stress.

6.3.2 Open System Freezing

The drop in the maximum negative temperature of the active zone, as a result of applied load has been confirmed for closed freezing conditions only. The next step is to investigate the general validity of this finding in a freezing system with free access of water where ice lenses are most likely to form in the freezing soil. An elegant way to prove the validity of this proposition is to consider that for a given temperature profile across the sample, ice lenses should occur at different levels with different applied pressures. The higher the surcharge, the colder should be the segregation freezing temperature of final ice lens formation.

A test of this type was test C1 which was frozen with an applied pressure of 160 kPa with free water access and under fixed temperature boundary conditions. The final ice lens was allowed to grow until visible. Then, keeping the temperatures constant at both ends, the sample was unloaded to 85 kPa. If the segregation freezing temperature is warmer, as shown in Figure 6.4, this hypothesis predicts that the new ice lens should grow somewhere below the first one. After this second ice lens reached a reasonable
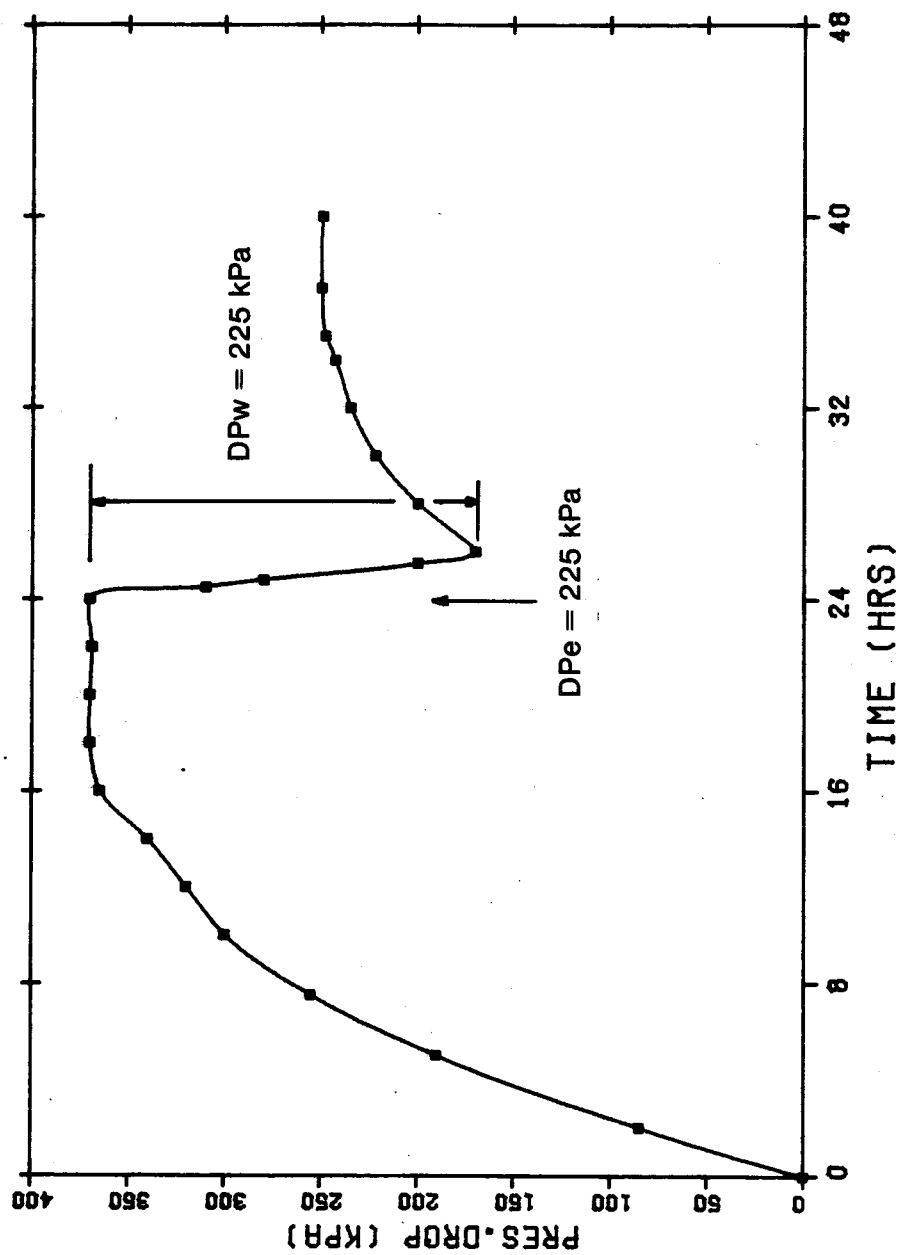
Figure 6.3 Closed Freezing Test with Applied Back Pressure
          Drop in Pore Water Pressure
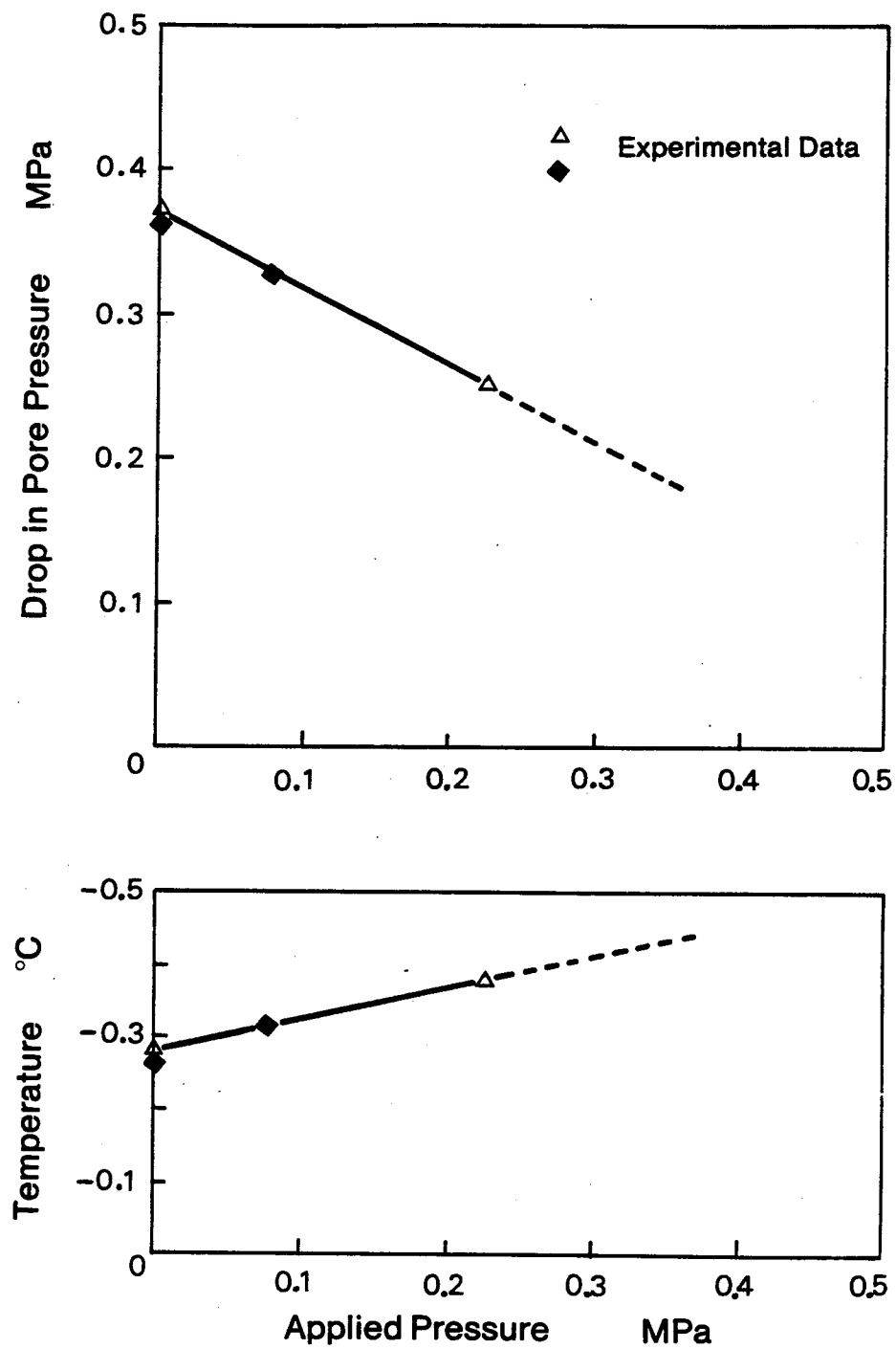
Figure 6.4 Effect of Applied Pressure on Pore Pressure and Temperature in the Active Zone in Closed System Freezing

thickness, the sample was completely unloaded. The results shown visually in Plate 6.1 confirm the validity of the proposed mechanism of ice lens formation with applied pressure. Three distinct ice lenses were created under an approximately constant temperature profile by successive unloadings. It is therefore confirmed that the segregation freezing temperature becomes colder with increasing applied pressure. In other words, the freezing front moves further into the frozen soil with increasing surcharge. This has two further ramifications. Firstly, the length of the frozen fringe increases. Secondly, the overall hydraulic gradient across the fringe is also reduced due to increased length of the fringe and smaller suction potential beneath the ice lens.

It is appropriate at this juncture to comment on recent work by Penner and Walton (1978). Results of the investigation by Penner and Ueda (1977) are summarized by Penner and Walton (1978) in graphical form where total heave rate for given applied loads is plotted against cold-side freezing temperature. Their results are shown in Figure 6.5a. Since a freezing soil is characterized by a frozen fringe whose segregation - freezing temperature is a function of applied pressure, one has to ensure that the cold side freezing temperature is colder than that segregation freezing temperature in order to allow the full development of the frozen fringe in that freezing soil. Careful inspection of Figure 6.5a reveals a drastic change
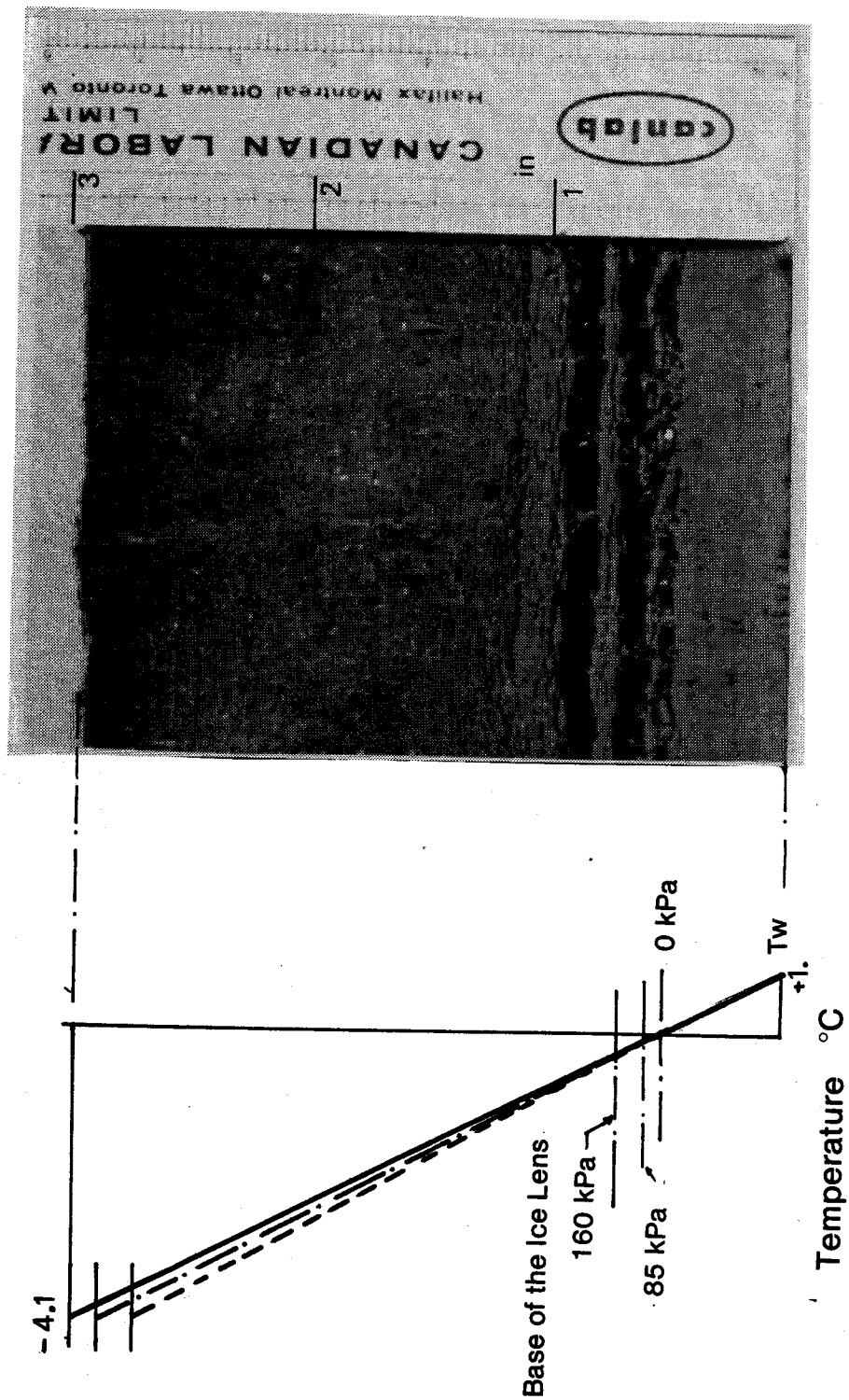
Plate 6.1   Formation of Different Ice Lenses During
Unloading Under the Same Temperature Gradient

in the slope of total heave rate vs temperature curves for cold side temperatures close to 0°C dependent on the applied surcharge. It is found that the higher the applied load, the colder the step temperature at which the change in total heave rate occurs. If it is argued that this drastic change in slope is related to the minimum negative freezing temperature required to develop the full frozen fringe, the value of this specific cold side temperature can also be taken as an indication of the segregation freezing temperature that exists in the freezing soil for a given applied load. By taking the derivative of the total heave rate with respect to cold side temperature. Penner and Walton concluded that the greatest rate change in ice accumulation occurs at colder temperatures as the overburden pressure is increased. Figure 6.5b summarizes their results. They concluded furthermore that since the temperature gradient in the frozen soil was essentially linear, the temperature axis in Figure 6.5b may be thought as a measure of the distance from the location of the 0°C isotherm where the heave phenomenon is occurring. It follows from this that the greatest rate change in ice accumulation moves further into the colder zone as overburden pressure is increased. Although this result confirms the results found in our study, one should be careful in the interpretation of freezing tests in terms of derived parameters such as cold side temperature and total heave rate and especially in their generalization. A critical analysis of Penner and
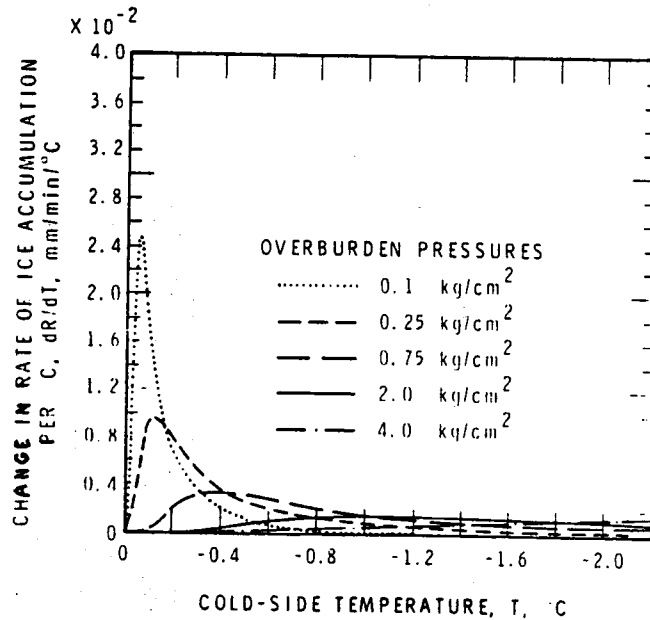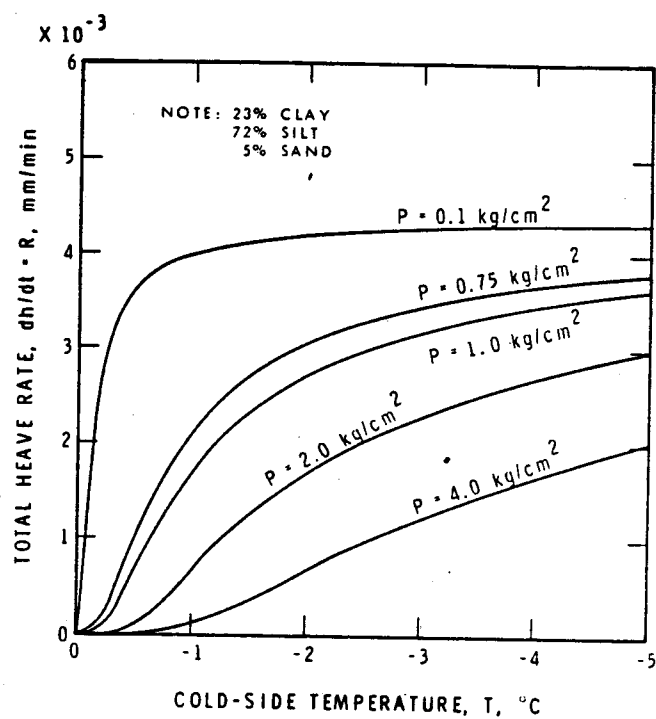
Figure 6.5   Results from Penner and Walton (1978)

Ueda's (1977) testing procedure and test results is given in Chapter 7.

6.4 INTRINSIC FREEZING PARAMETERS AT THE GROWTH OF THE FINAL ICE LENS

As discussed in Chapter 3, a freezing soil can be characterized by either Ts and Kf or SP. From a practical point of view, the latter is more appealing since it can be determined directly from measurable quantities such as water intake flux and temperature profile. The determination of the first set of intrinsic parameters requires additional tests from which the value of Ts can be inferred. However, the knowledge of the variation of these parameters gives a better insight into the processes involved during freezing with or without applied pressure.

The results of the laboratory freezing tests with applied surcharge are therefore presented firstly with respect to the segregation potential and secondly with respect to Ts and Kf in order to emphasize physical mechanisms occurring as pressure is applied.

6.4.1 Variation of the Segregation Potential with Applied Pressure

The effect of applied pressure on water migration rate during freezing was investigated in series C. All samples in that series were frozen with free water supply. The

temperature boundary conditions were held constant throughout each freezing test. The samples were prepared by consolidating a slurry to a consolidation pressure of 210 kPa. After primary consolidation was complete, the sample was placed in the freezing cell where it rebounded under applied pressures less than 210 kPa and consolidated further for applied surcharges higher than the preconsolidation pressure. In Chapter 3, it was demonstrated that lateral friction is not significant for no externally applied load. However, as load is applied on the sample, horizontal pressure is induced due to a no lateral strain condition. This, in turn, increases the actual vertical stress at the freezing front during heaving. To minimize the effect of friction, most of the specimens were frozen from the bottom upwards so that as the frost front becomes stable, only the unfrozen part has to be pushed upwards by the heaving soil. Since the warm plate temperature is about +1°C, the unfrozen soil length is relatively short and the total lateral friction is then minimized. Initial geometrical and thermal boundary conditions and the results obtained in series C are summarized in Appendix E.

Table 6.1 presents the conditions of the freezing tests at the onset of the formation of the final ice lens. Figure 6.6 illustrates the variation in segregation potential with applied pressure for Devon silt. Experimental data show that SPo decreases with increasing stress at the freezing front. Furthermore, it is clear that samples frozen

Test	Pe (kPa)	Vo 10^{-6}cm/s	grad Tf $^{\circ}$C/cm	SPo 10^{-5}mm^2/(s$^{\circ}$C)	
NS&E	0			92	
C8	45	43	0.63	68	Tw=+1°C
C9	45	60	1.50	40	Tw=+4.5°C
C7	60	47.0	0.80	58.7	
C3	90	56.0	1.29	43.4	
C10	100	26.0	0.67	38.8	
C11	120	26.0	1.0	26.0	
C12	120	43.3	1.33	32.6	
C5	120	25	0.88	28.4	
C6	120	22.4	1.0	22.4	
C4	170	10.0	0.56	17.9	
C2	190	11.7	0.83	14.1	
C13	265	8.8	0.71	12.4	
C14	400	3.75	1.11	3.4	

Table 6.1 Conditions at the Onset of the Formation of the Final Ice Lens for Series C

from the bottom upwards exhibit no significant lateral friction. This is inferred from the fact that the results obtained from a freezing test performed on a sample placed inside a cell composed of superposed 1 cm high rings compares well with the results of a freezing test under the same applied pressure where the sample froze from the bottom upwards in a normal cell. The superposed lucite rings reduce the total lateral friction at the freezing front to that developed over an individual ring, i.e. over only 1 cm. Freezing identical samples from the top downwards indicates that a lower SP is obtained for the same external surcharge. However, this is expected since the actual stress acting on the freezing front is increased due to the influence of lateral friction. The side friction can be evaluated by the amount of additional pressure needed to shift the experimental data points to the SP vs Pe curves on Figure 6.6 obtained for the case of negligible side friction.

As SPo is a function of Pu, Figure 6.6 is only a partial representation of a freezing soil when external pressures are applied. The complete characterization of a freezing soil under different applied surcharges is given in Figure 6.7, Figure 6.6 represents the intersection of the general set of curves defined in Figure 6.7 with approximately a line passing through the origin. For Figure 6.6, the variation in suctions at the frost front is rather small for the different applied loads. It must also be emphasized that only a limited amount of data is available

for the complete characterization of a freezing soil at the formation of the final ice lens. For this reason, the relationship between SPo and Pu obtained for zero applied surcharge is extended to the case with applied pressure. Therefore, it is assumed that for any applied surcharge, the critical suction, which is thought to correspond to cavitation in the unfrozen soil, remains constant.

Figure 6.7 also indicates that the effect of suction at the frost front is reduced with increasing applied pressures since the slopes of the different curves decrease with increasing pressure. As pointed out in Chapter 3, the suction at the frost front can be directly related to warm plate temperature provided the temperature distribution in the active system is linear. In this case, the effect of warm end temperature will be progressively reduced as pressure is increased.

6.4.2 Variations of Tso and Kfo with Applied Pressure

The analysis of the freezing test results obtained in Series C with respect to Tso and Kfo requires the determination of Tso for each surcharge. Section 6.3 establishes that the final ice lens forms at colder segregation freezing temperatures with increasing pressures. Two different procedures were used to infer the value of Tso. Firstly, visual observation at the end of the freezing test and application of the measured temperature profile result in the value of the temperature at the base of the
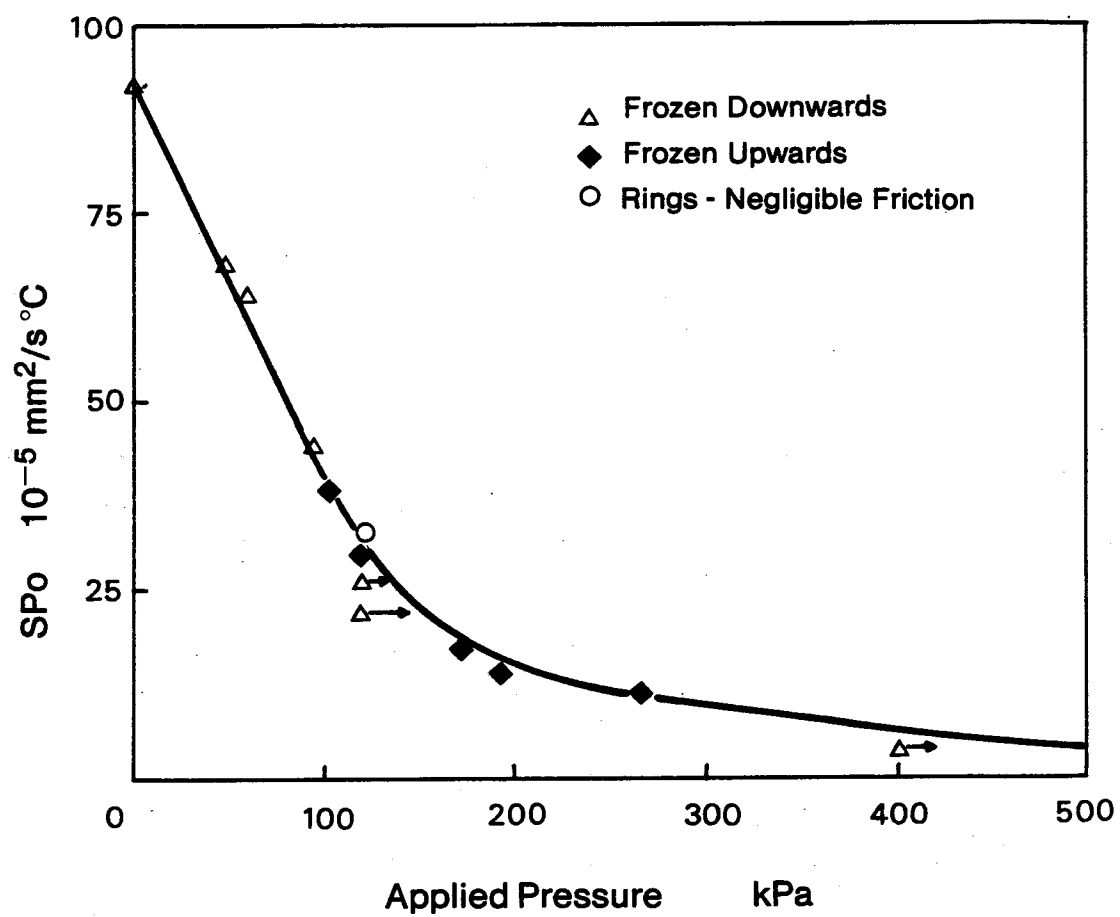
Figure 6.6   Segregation Potential for Devon Silt under
Different Applied Loads.(Series C).
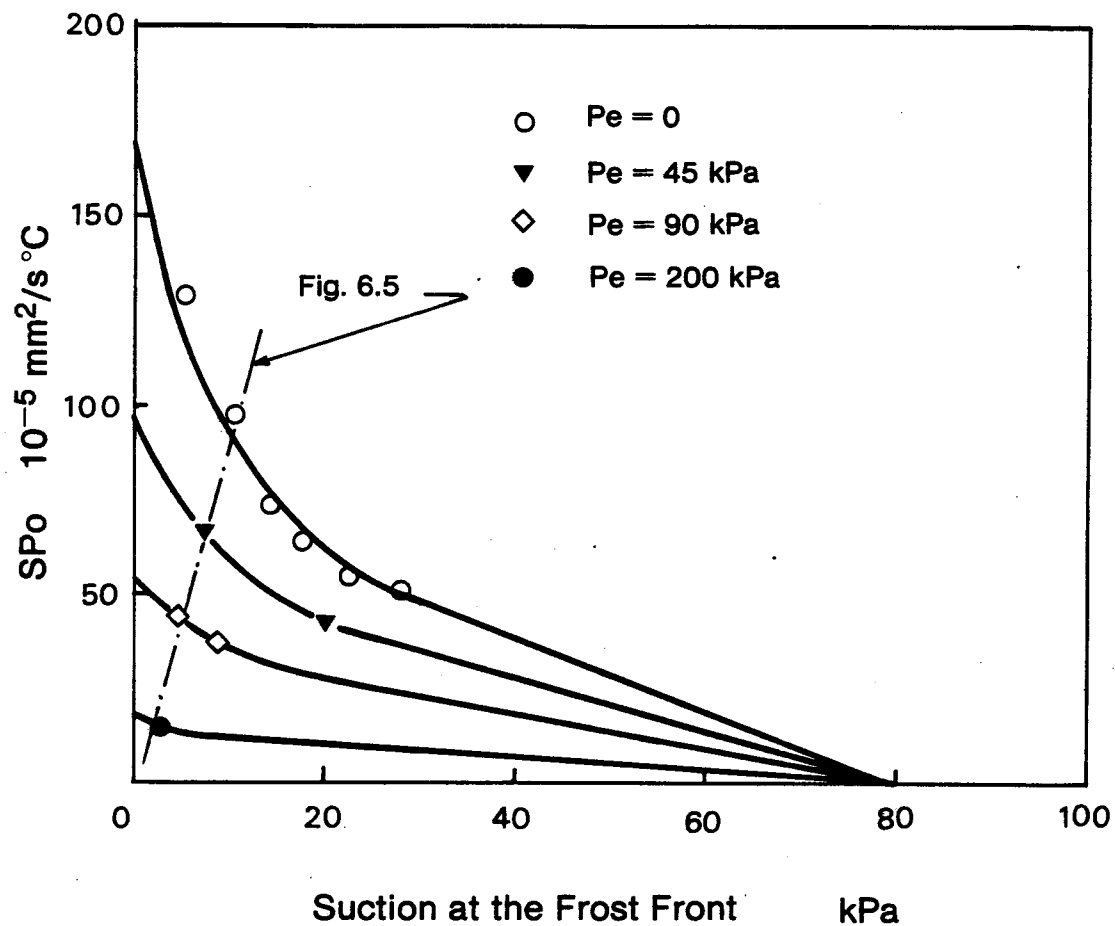
Figure 6.7   Variation of the Segregation Potential at the
             Formation of the Final Ice Lens With Applied
             Pressure and Suction at the Frost Front.

final ice lens. Since the frozen fringe grows thicker with increasing pressures, this method provides fair accuracy with higher loads. Plate 6.2 illustrates the extent of the frozen fringe for an applied surcharge of 265 kPa and 400 kPa. The darker color corresponds to the unfrozen soil and the lighter to frozen soil.

The second method is to freeze a sample with applied back-pressure in an open-system until the final ice lens is initiated. The subsequent drop in pore pressure is recorded as the water line is closed. The temperature at the base of the ice lens is then obtained by Equation 6.7.

The segregation freezing temperatures were determined for 3 tests, C10, C13, and C14. The results are presented in Figure 6.8. Remarkably, for the testing pressure range, the variation of Tso with respect to applied pressure can be approximated by a straight line. This study takes therefore the simplified view that Tso of the other tests in this series can be interpolated from this straight line. Comparison of the interpolated values from the line with values obtained from visual observations at the end of each test support fully this assumption.

The overall permeability of the frozen fringe can be calculated by a combination of Equation 6.7 and 3.36. It should be emphasized that the suction potential below the ice lens is reduced as a consequence of applied pressure. Implicitly, it is assumed that there is no accumulation of water within the frozen fringe as external pressure is
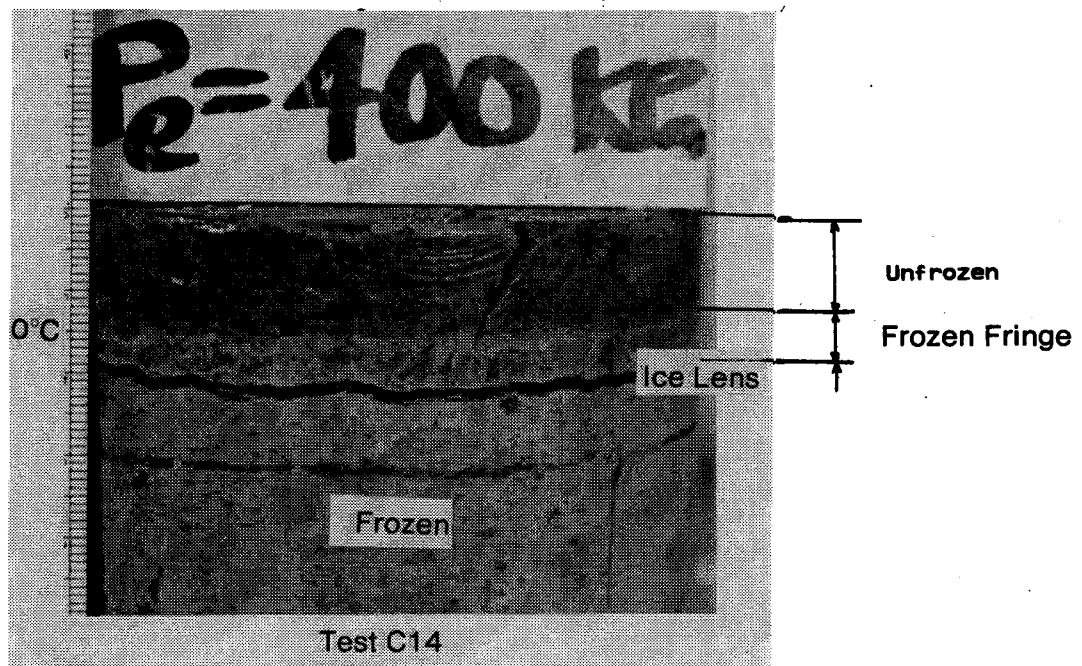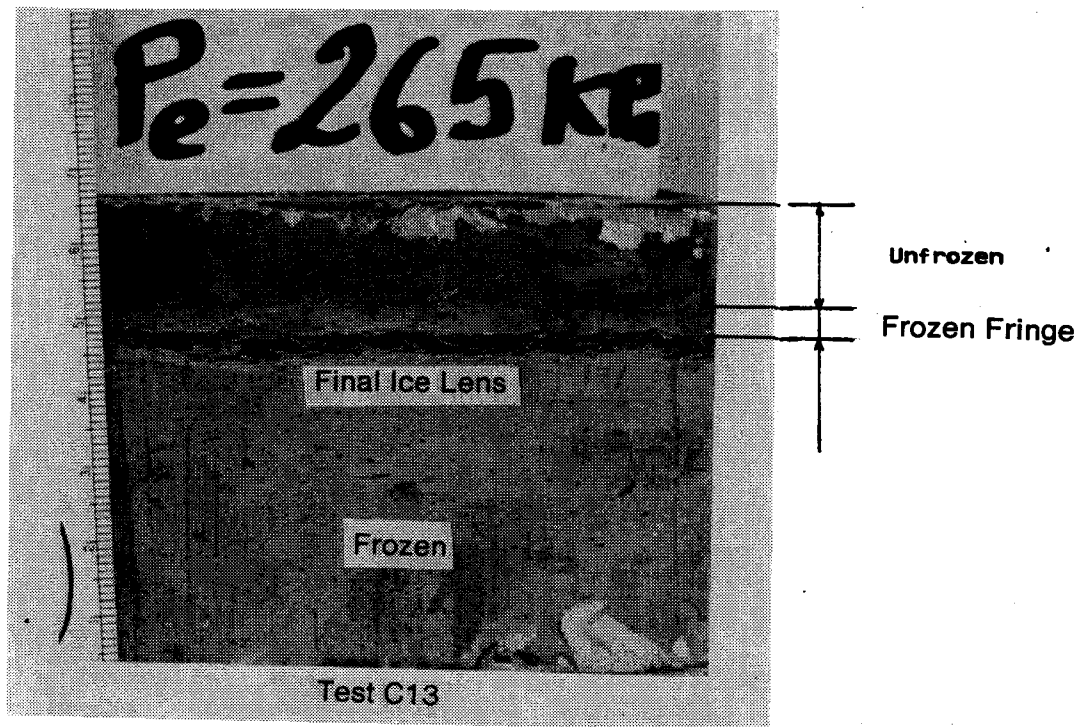
Plate 6.2   Evidence of Frozen Fringe in Devon Silt

applied. All the water entering the frozen fringe freezes at the segregation freezing level, i.e. at the base of the ice lens. The results obtained in series C in terms of Kfo are easily deducible from Table 6.1 and are summarized in graphical form on Figure 6.8. Note that the overall permeability at different pressures has been normalized with respect to the permeability obtained for zero external load. Figure 6.8 shows that the average permeability of the frozen fringe decreases with increasing pressures and tends asymptotically towards the abscissa axis. At 400 kPa, the overall permeability is approximately 25% of that obtained under zero external pressure.

This result may initially cause some consternation since it is expected that the permeability should increase in response to higher unfrozen water contents as pressure is applied. However, the fact that the segregation freezing temperature decreases with increasing pressures results in colder average temperatures in the fringe. Therefore, the average unfrozen water content in the fringe decreases as pressure is applied, despite the moderating effect of increasing pressures in the ice. This, in turn, results in decreasing permeability of the frozen fringe with increasing applied load.

Figure 6.9 illustrates the variation in suction potential at the base of the final ice lens with increasing surcharge during the freezing tests in series C with free water supply. The change in segregation-freezing temperature
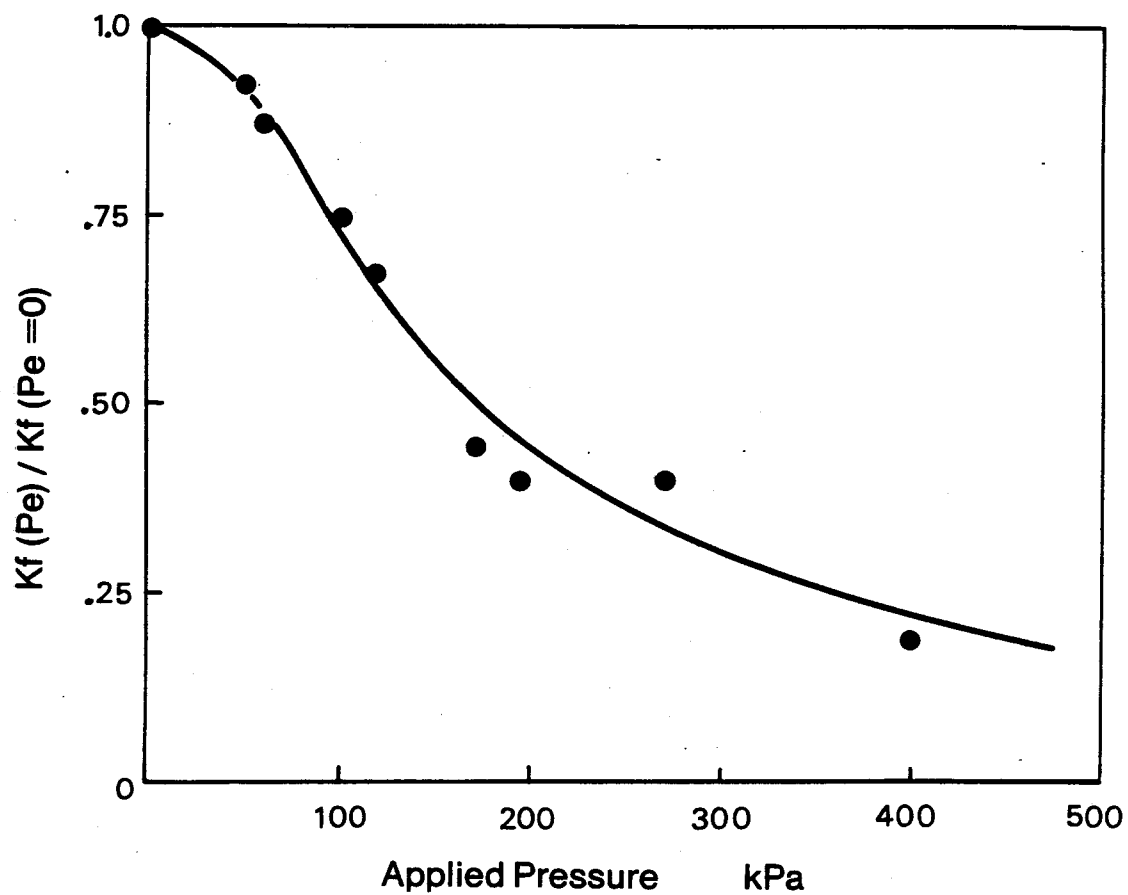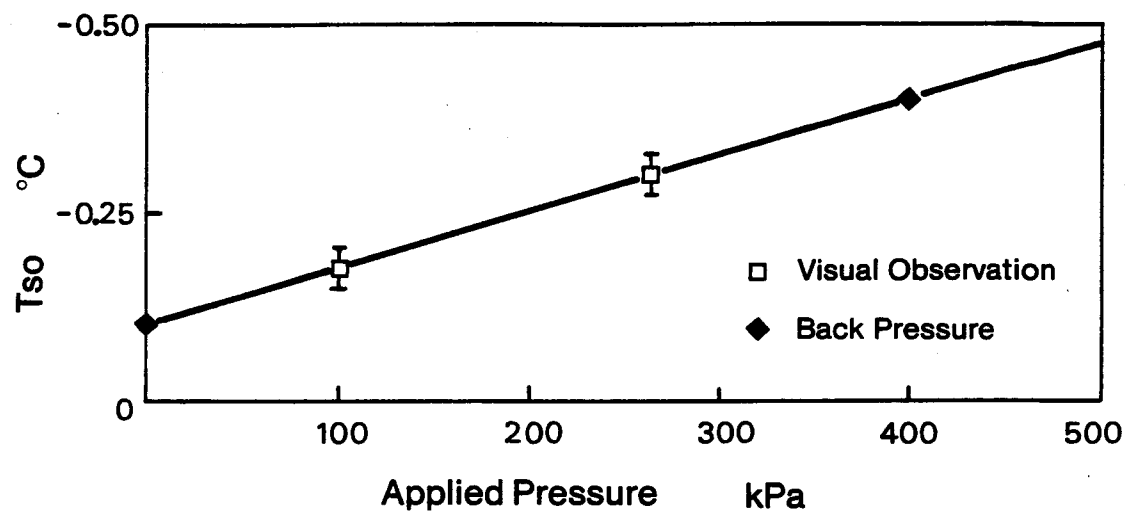
Figure 6.8   Intrinsic Parameters at the Formation of the
Final Ice Lens for Different Applied Surcharges

moderates significantly the variation in suction-potential. A variation of 100 kPa in the external pressure results in only a variation of 10 kPa in the pore water pressure beneath the ice lens.

The combination of reduced permeability of the frozen fringe and reduced overall hydraulic gradient is then responsible for the reduced heave rates as load is applied.

6.5 THE TERMINAL PHASE OF FREEZING WITH APPLIED PRESSURE

Chapter 5 has established the governing equations for the terminal phase or the retreating frost front situation in the case of zero overburden. No water flow towards the ice lens occurs when the suction potential at the ice lens becomes zero. This happens when the temperature at the base of the ice lens is 0°C for zero applied surcharge. The no flow condition for zero applied load can be generalized for the case of externally applied pressures. Equation 6.5 yields for Pw = 0:

$$Ts* = To* \exp(-Pe.Vi/L) \dotfill 6.10$$

For engineering purposes, Pe is relatively small and Equation 6.10 reduces to:

$$Ts* = To* (1 - Pe.Vi/L) \dotfill 6.11$$

Expressing the segregation freezing temperature in degrees Celsius, it can readily be shown that the locus of the points corresponding to atmospheric pressure in the water film beneath the ice lens is a straight line passing through
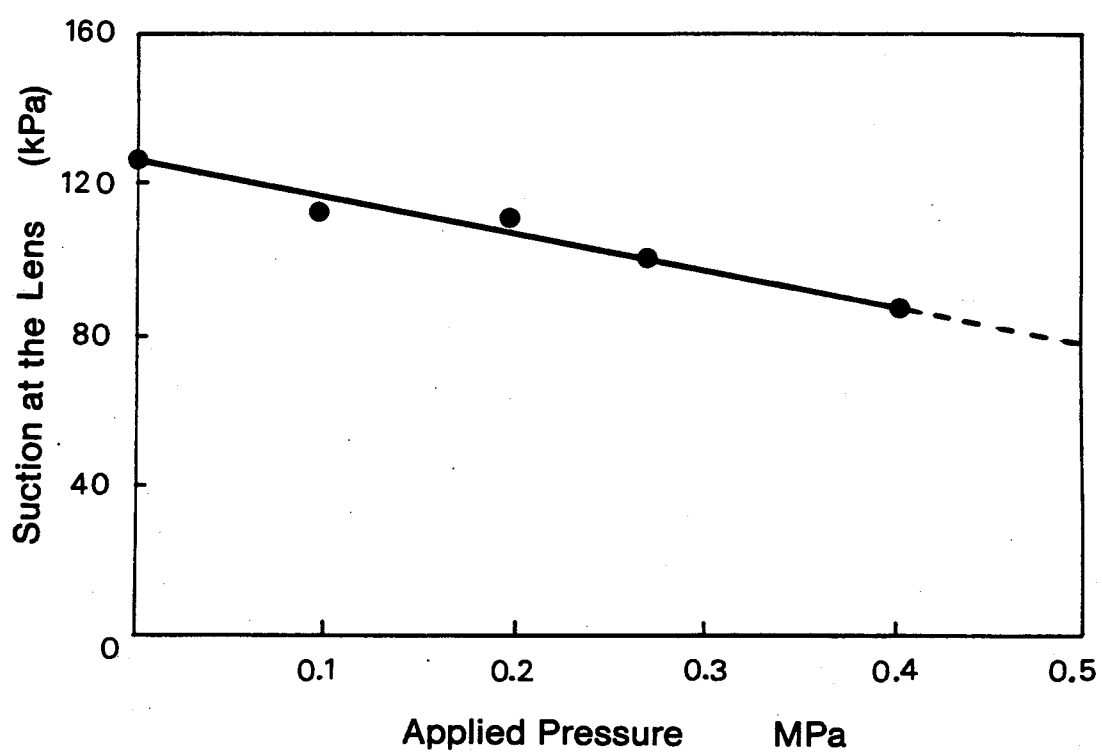
Figure 6.9   Variation in Suction Potential at the Final Ice
Lens with Applied Pressure

the origin given by the following equation:

$$Ts = Ts* - To* = -(Vi.To*/L)Pe\dots\dots\dots\dots6.12$$

It is of value to plot on the same graph the previous line, corresponding to zero pressure in the water film beneath the final ice lens at different applied surcharges, and the locus of Tso when the applied pressure varies from experimental data. This latter locus is associated with the initiation of the final ice lens. As shown in Figure 6.10, the two lines converge at a high applied pressure. Unfortunately, data points were not obtained for pressures higher than 400 kPa. Nevertheless, it seems reasonable that linear extrapolation of the experimental results yields an upper bound to the value of the pressure and of the temperature corresponding to the intersection of the two lines. At this specific point, the segregation freezing temperature of final ice lens formation induces zero suction. Consequently, the hypothetical ice lens cannot grow since no water flow is possible. In other words, this intersection point corresponds to the real "shut off" pressure for which there is no ice lens growth. As shown in Figure 6.10, this "shut off" pressure is very high for Devon silt, in the range of 800 to 1000 kPa.

Arguments in Chapter 5 have demonstrated furthermore that the retreating frost front phase is associated with a warming of the base of the final ice lens. During this terminal phase, the locus of this temperature change can be represented by a vertical line on Figure 6.10. The end of
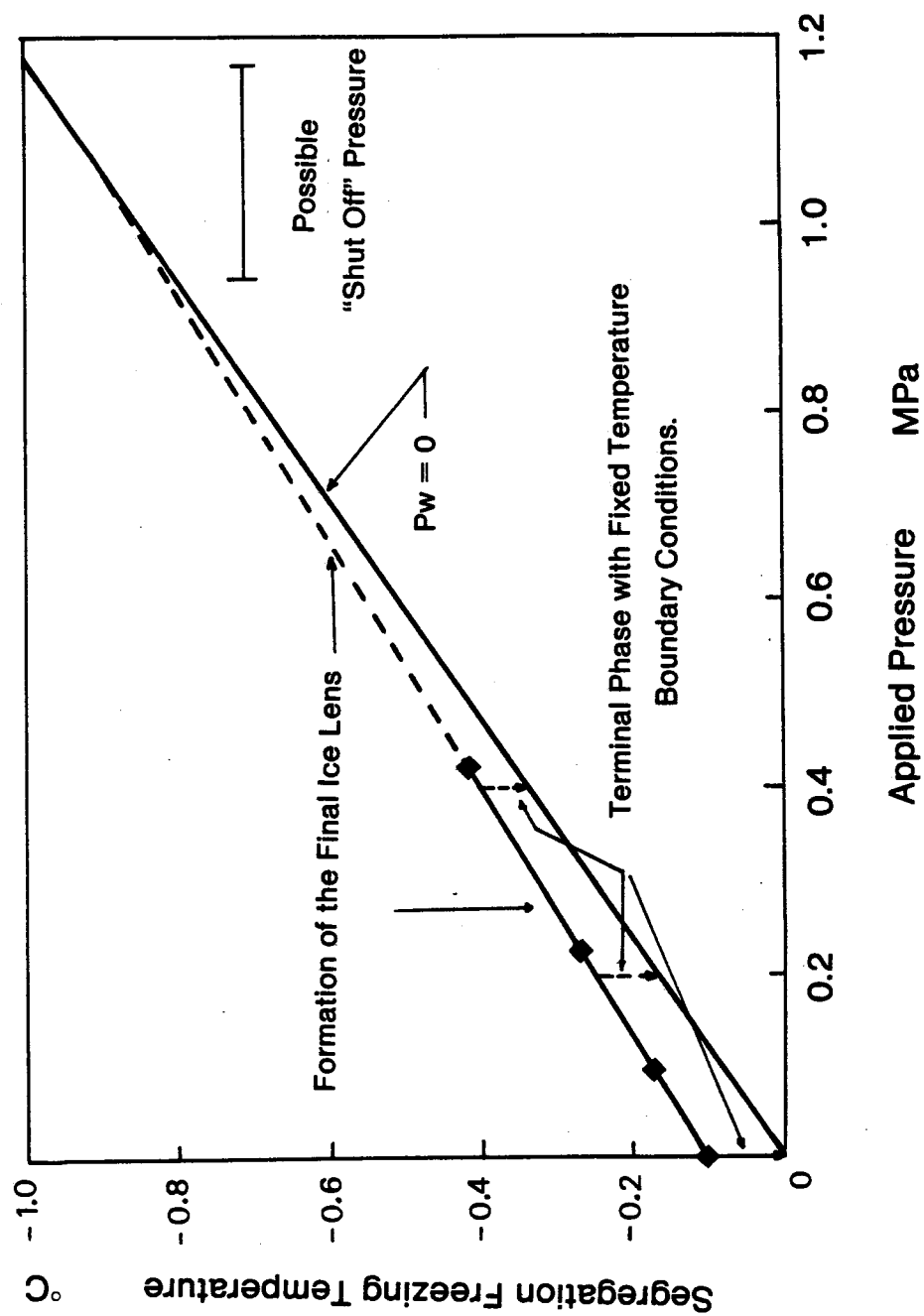
Figure 6.10 The Shut-off Pressure in Freezing Soils

the retreating frost front phase is then given by the intersection of these vertical lines and the Pw = 0 line. For zero overburden pressure, the intersection point is the origin which means that the terminal phase ends when the temperature at the base of the final ice lens is 0°C. This result can be extended to any applied pressure. As shown in Figure 6.10, for an applied surcharge of 200 kPa, the final ice lens is initiated at a temperature of -0.25°C and the heaving will stop when the temperature at the base of the ice lens reaches about -0.175°C. It should be emphasized that the retreating frost front situation exists for fixed temperature boundary conditions.

Because the line corresponding to the segregation freezing temperatures at the onset of the formation of the final ice lens and the envelope of zero pressure in the water film beneath the final ice lens converge, the change in temperature during the terminal phase is maximum for Pe = 0. It decreases steadily as the pressure is increased. This, in turn, influences the maximum thickness of the final ice lens. Conversely, since the water intake rate decreases with increasing pressure, the time needed to reach the same amount of heave increases considerably with increasing pressure. This explains why the rate of heave in test C13 is constant over about 100 hours as shown in Figure E.12 in Appendix E.

The heat balance at the ice lens still governs the rate of phase change at its base and consequently the rate of

growth of the final ice lens. Effect of solute rejection is more important when the frost front is stationary for longer periods. However, increasing solute concentration beneath the ice lens does not affect the suction potential at the level of the final ice lens. This results in an upper bound for the maximum thickness of the final ice lens and is therefore on the safe side for engineering applications.

Theoretical analysis simulating the conditions obtained as the final ice lens is initiated in tests C10, C13 and C14 reveal that steady state heat transfer describes adequately the observed behavior of the freezing soil during the retreating frost front phase. The maximum thickness of the final ice lens can be predicted from:

$$e = \frac{k_i.|T_c - T_{se}|}{k_u.(T_w + |T_{se}|)} l_o - \frac{k_i}{k_{fr}} X \ldots\ldots\ldots\ldots(6.10)$$

where   Tse is the value of the segregation freezing temperature at which Pw is atmospheric for the given external pressure.

To predict the heave rate, the method proposed in Chapter 5 for Pe = 0 is adopted. The results obtained with this analysis are summarized in Figure 6.11. The analytical method predicts a maximum thickness of the final ice lens for test C13 of about 11 mm after 1200 hours of sustained temperature boundary conditions during the retreating frost front. For test C14, the thickness of the final ice lens also approximately 11 mm but the analysis predicts that the length of the terminal phase is almost twice as long as for

test C13. Unfortunately, it is not practical to run freezing tests for such a long period and the actual final ice lens was only grown for about 120 hours in both tests. Nevertheless, the observed data agree very well with the predicted values of ice lens thickness.

6.6 PHYSICAL PROCESSES DURING FREEZING WITH AN ADVANCING FROST FRONT

The complexity of the freezing process during the advancing frost front phase emerges from the well known observation that, for the same soil, water is either attracted to or expelled from the freezing front during the early stage of this phase. This has also been observed in the tests performed in series C. As shown in Appendix E, it is clear that attraction occurs when the applied load is small and that expulsion occurs when the external pressure is higher. However, despite the fact that water is expelled during the early stage of freezing, it has been observed that expulsion of water is only the primary mode of behavior, and that, after a while, expulsion stops and water intake occurs. It has also been observed that, in each case, the volume of expelled water is relatively small.

This bi-modal behavior of a freezing soil with applied load is very puzzling. No satisfactory explanation for this phenomenon has yet been proposed.
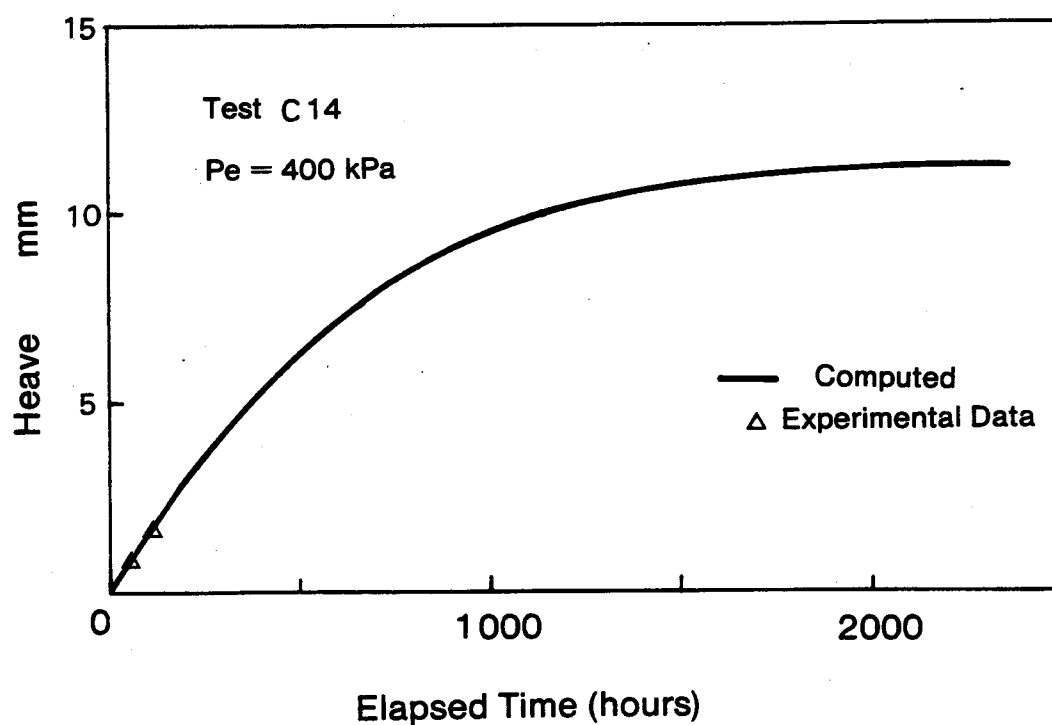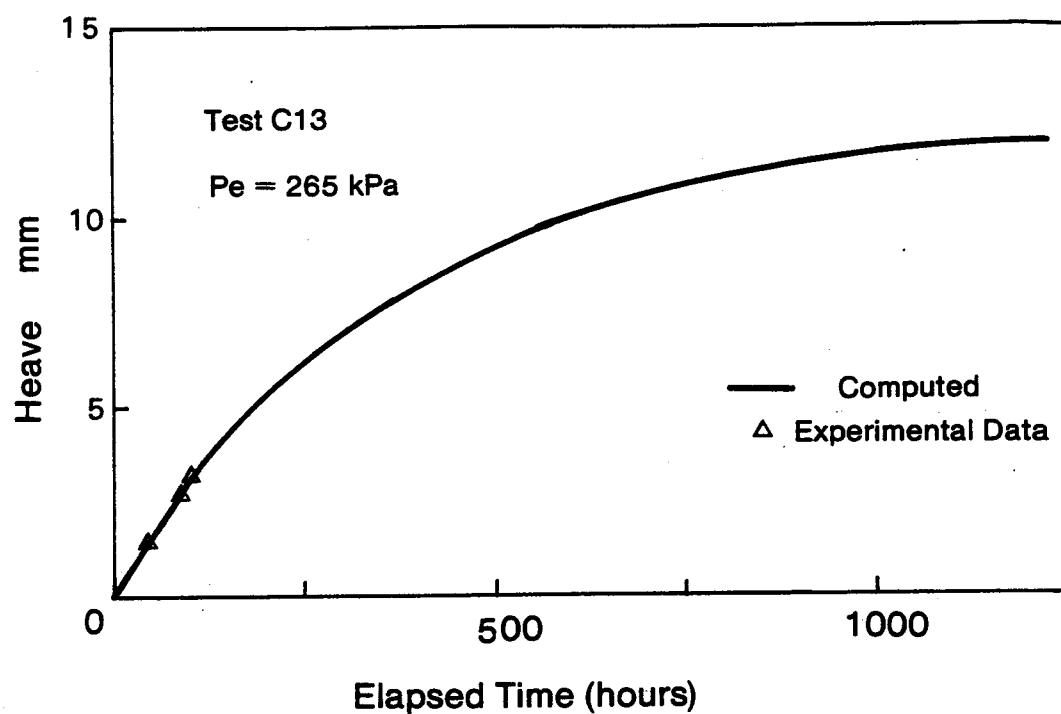
Figure 6.11 Predicted and Measured Thickness of the Final
Ice Lens in Tests C13 and C14

It is possible to gain more insight into the freezing mechanism with applied pressure by considering the results obtained in Chapter 4. It has been proposed that Ts varies during the advancing frost front phase for zero applied load. Furthermore, it has been established that the rate of cooling of the frozen fringe, which is indirectly a measure of the rate of frost front advance, influences the segregation potential. Since SP embraces both Ts and Kf, it can be argued that the rate of frost front advance also influences the value of Ts.

Another important consideration is the evaluation of the ice pressure within the frozen fringe. This problem is easily solved for zero applied load since the ice pressure is then atmospheric everywhere in the frozen soil. However, with an applied surcharge, stresses are created in the sample.

In the unfrozen part, all the load is carried by grain to grain contacts, i.e. effective stress. In the frozen part, a stress partition most likely occurs. If ice can fill a soil pore without pushing apart the surrounding soil grains, it can be assumed that the ice pressure is still atmospheric since the soil grains still carry the load. This case most likely happens close to 0°C where appreciable unfrozen water is present in the frozen soil. However, as the temperature decreases, the ice content increases and the pore ice in the frozen fringe will carry some of the applied load. The pore ice will therefore be stressed. The stress in

the pore ice is thought to increase with increasing ice content, hence with decreasing temperatures. At the ice lens, the problem is again much simpler since the pressure in the ice is equal to the external pressure Pe. This statement is verified provided the ice lens is created over the whole cross area of the sample. Behind the ice lens, in the passive system, the stress partition is not relevant to the problem of frost heave since water movement occurs solely in the active system.

The ice pressure distribution in the frozen fringe is a function of ice content which has not been determined to date in a freezing system with free water supply. As with the suction profile, only the extreme values of the ice pressure are known, $Pi = 0$ at the base of the fringe (at Ti) and $P = Pe$ at the top of the frozen fringe (at Ts).

A qualitative analysis of the freezing soil with applied load can now be discussed. It may be assumed that at the beginning of freezing, the conditions in the frozen fringe are as shown in Figure 6.12a. It has been established in Chapter 4 that for high rates of cooling, Ts can be warmer than Tso, corresponding to the formation of the final ice lens. The pore water pressure at the segregation freezing level can be calculated by Equation 6.5. If the external pressure Pe is larger than the term containing Ts, a positive pore water pressure is obtained. Therefore, depending on the actual pore ice pressure profile in the frozen fringe and if one assumes that the temperature

profile in the frozen fringe is linear, different pore water profiles can be generated in the frozen fringe. As shown in Figure 6.12a, a typical distribution has been plotted. Water flows to the freezing front in the upper part of the fringe and is pushed out of the lower part of the frozen fringe.

With time, the rate of cooling decreases and the segregation freezing temperature may decrease. Ultimately, there is a segregation freezing temperature for which no positive pore water pressure are generated within the frozen fringe. The freezing system now attracts water to the freezing front and identical processes as those described for zero overburden now occur.

It is necessary to emphasize the tentative nature of this discussion.

The previous analysis led to the view that there is a critical rate of cooling of the fringe at a given applied pressure at which water will be drawn into the sample during freezing. Test data of series C yielded the results summarized on Figure 6.13. For Devon silt, it is clear that for a pressure below 120 kPa, water is always attracted to the freezing front. The conclusions of Chapter 4 establish that there is a maximum rate of cooling for which no water is able to flow to the segregation freezing level. This result has been extended for the case of applied pressure.

For applied surcharges higher than the critical value, e.g. 120 kPa for Devon silt, the rate of cooling at which water is drawn into the sample decreases with increasing
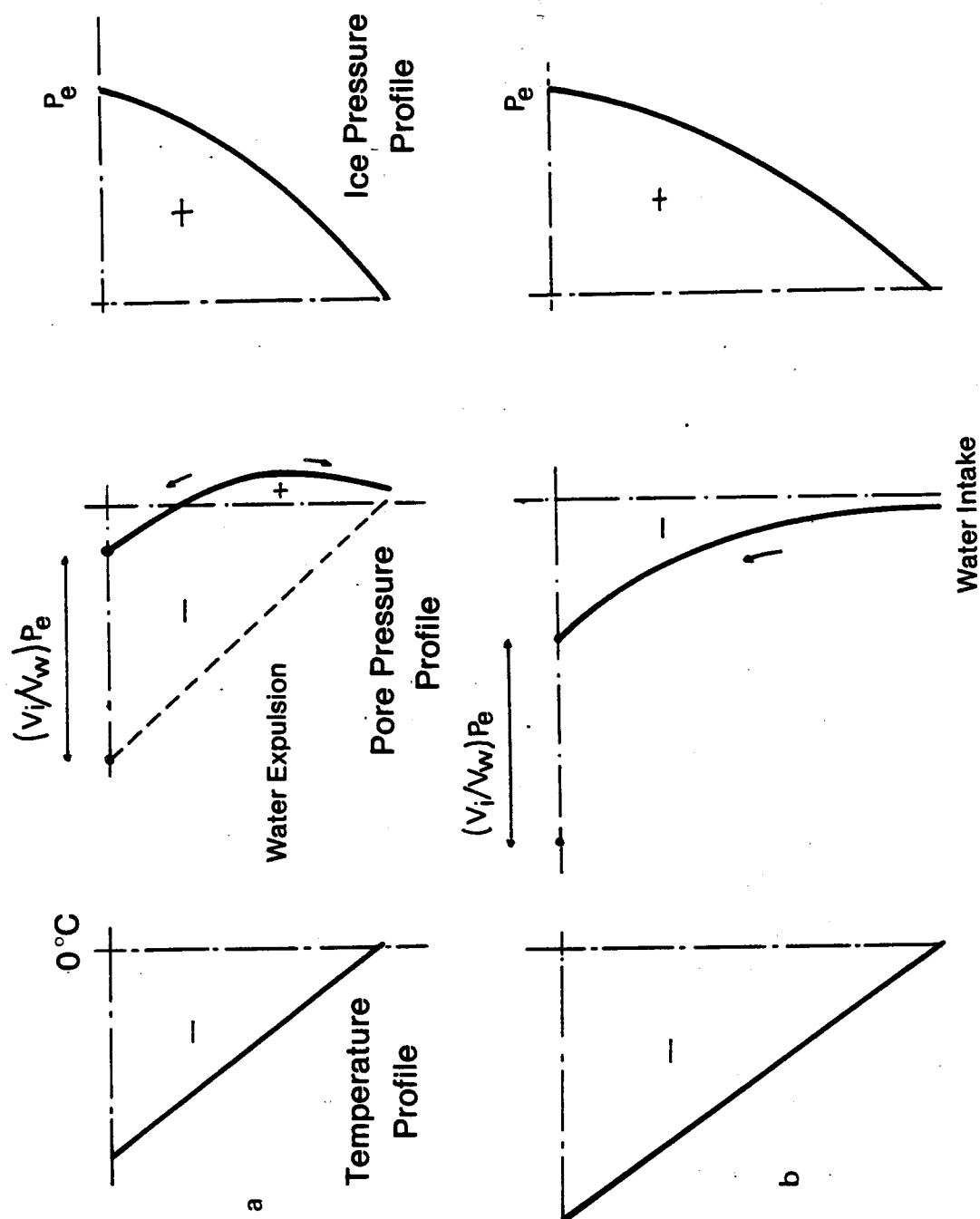
Figure 6.12 Schematic Conditions During an Advancing Frost
Front and Applied Pressure
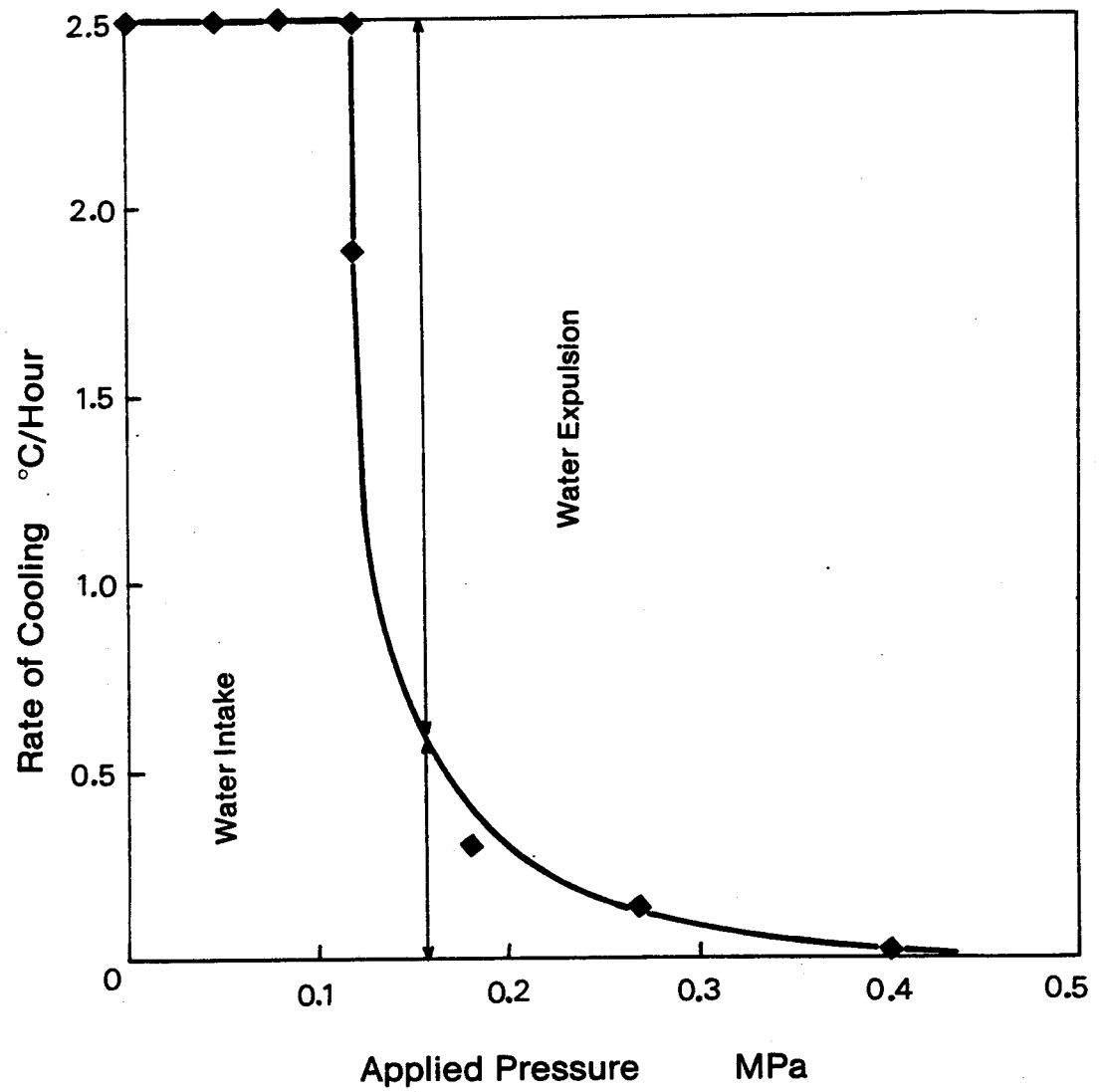
Figure 6.13 Critical Rate of Cooling during Freezing with Applied Load

external pressure. It is believed that the relationship between that critical rate of cooling and applied pressure is unique for a given soil. This statement is based upon the fact that there is a unique relationship between SP, Pu and dTf/dt at a given Pe and that SP embraces Ts.

Figure 6.13 reveals that, at a given pressure water from an outside source is attracted to the freezing front when the rate of cooling is smaller than the critical value of the rate of cooling and is expelled from the sample for higher rates of cooling.

Takashi et al (1974) presented results of freezing tests where expulsion of water occurred at a frost front penetration rate higher than 11 mm/h for an external pressure of 112 kPa. Attraction of water occurred for the same applied pressure when the speed of frost front advance was less than 11 mm/h. Moreover, an identical soil sample under 212 kPa expelled water during freezing with frost front advance rates higher than 1 mm/h.

It is of value to realize that the results published by Takashi et al are identical to those given in the present study. Furthermore, small changes in applied load are associated with drastic changes in the critical rate of cooling.

Since the volume of expelled water is small, it seems reasonable to approximate the heave occurring during an expulsion mode by the heave resulting from the "in situ" water freezing. It is of benefit to note that the unfrozen

water content increases with increasing pressure, which, in turn, affects the heave of "in situ" water freezing. In an analytical approach, a variation in ϵ with applied pressure might be an elegant way to account for the physical process operative during freezing with applied load.

When water is attracted, frost heave with applied load can be treated similarly to frost heave with zero surcharge. The freezing characteristics, either Ts and Kf or SP must be determined from laboratory freezing tests for a range of applied pressures. The analytical model developed in Chapter 4 is still valid if one considers the change in the input characteristic freezing surface with applied load and if one introduces the relationship given in Figure 6.13.

Finally, it is easy to extend the mechanistic theory of ice lens formation for the case of zero external surcharge to the case where an external pressure is applied on the freezing soil. However, Figure 6.12 establishes that the thickness of the zone of active lensing is affected when external pressure is applied. This results from the fact that water expulsion may occur during the early stage of freezing and thus no visible ice lens can form due to lack of sufficient water. An extreme case corresponds, for example, to a freezing situation with a high overburden load in which water is only attracted to the freezing front when the frost front is almost stationary. In these conditions, the sample will exhibit only one ice lens which is the final ice lens and is grown during the retreating frost front

phase if the temperature boundary conditions are constant. This is adequately illustrated in Plate 6.2 where no visible ice can be seen above the final ice lens in both cases. The mechanism of discrete ice lens formation is still valid.

6.7 THE HEAVING PRESSURE IN FREEZING SOILS

This section is devoted to the investigation of the mechanisms which lead to a stable situation at the end of the terminal phase during open-system freezing test in which vertical displacement is prevented. This latter category of freezing tests is widely use to measure the maximum heaving pressure that a freezing soil is able to produce.

When a saturated soil is prevented from heaving, the total volume of water and solids in a particular soil system must remain constant. If no consolidation takes place upon freezing, e.a. a coarse grained material, the constant volume condition requires that some water has to be expelled from the sample when ice forms. When a fine grained soil is frozen under a constant volume condition and a pressure develops, the unfrozen part of the specimen consolidates. Constant volume of the whole sample is maintained by the formation of an ice lens in the frozen part.

The heaving pressure develops slowly with time. Therefore since the ice pressure increases, the frozen fringe also changes continuously with time. The process can be described as a continuous movement of the ice lens

towards colder temperatures as the heaving pressure increases with time. This process takes place under a condition of almost constant temperature gradient once steady state heat flow is almost obtained. In other words, the current warmest ice lens is pushed progressively farther into the frozen soil by a process of melting and refreezing. The thickness of the frozen fringe increases with time under these conditions. It can be argued that when the pressure at the freezing front reaches the "shut off" pressure, as defined of Figure 6.10, the freezing system should reach an ultimate heaving pressure. Experimental evidence is available to confirm the existence of a maximum heaving pressure for a given soil (Penner, 1959; Hoekstra, 1969). However, no direct correlation has yet been made between the measured heaving pressure and the "shut off" pressure determined from open-freezing tests. It should be remembered that heaving pressures are very sensitive to the rigidity of the experimental apparatus, and that the above mentioned comparison requires careful testing.

Let us now consider the characteristics of the frozen fringe as the maximum heaving pressure is approached. The sample is composed of a frozen part above the ice lens, an ice lens, the frozen fringe below the ice lens and the unfrozen part. From a consideration of statics, equilibrium results in an effective stress in the unfrozen soil equal to the heaving pressure. This is achieved by consolidation as mentioned earlier. Furthermore it is clear that the pressure

in the ice lens must also be equal to the heaving pressure.

For equilibrium to exist, the pore ice pressure profile in the frozen fringe must adopt a linear distribution as shown in Figure 6.14. This ice pressure profile associated with a linear temperature distribution in the frozen fringe results in zero pore water pressure throughout the frozen fringe. This pressure state in the frozen fringe is then in equilibrium with that in the unfrozen soil where the pore water pressure is also zero. Through progressive melting of the pore ice of the frozen fringe, the ice content will be such that the pore ice pressure profile will adapt to the existing temperature profile in order to achieve no pore water pressure gradient in the active system.

The situation at the end of the retreating frost front phase in open-system freezing with applied load is identical to the previous case. Final conditions will correspond to a linear pore ice pressure profile in the ultimate frozen fringe. The upper part of the fringe is equal to overburden and the pore ice pressure at the warmest end of the fringe is atmospheric.

6.8 SUMMARY

It has been demonstrated that the segregation freezing temperature of final ice lens formation decreases with increasing applied loads. Since the suction developed beneath the ice lens is a function of both temperature and
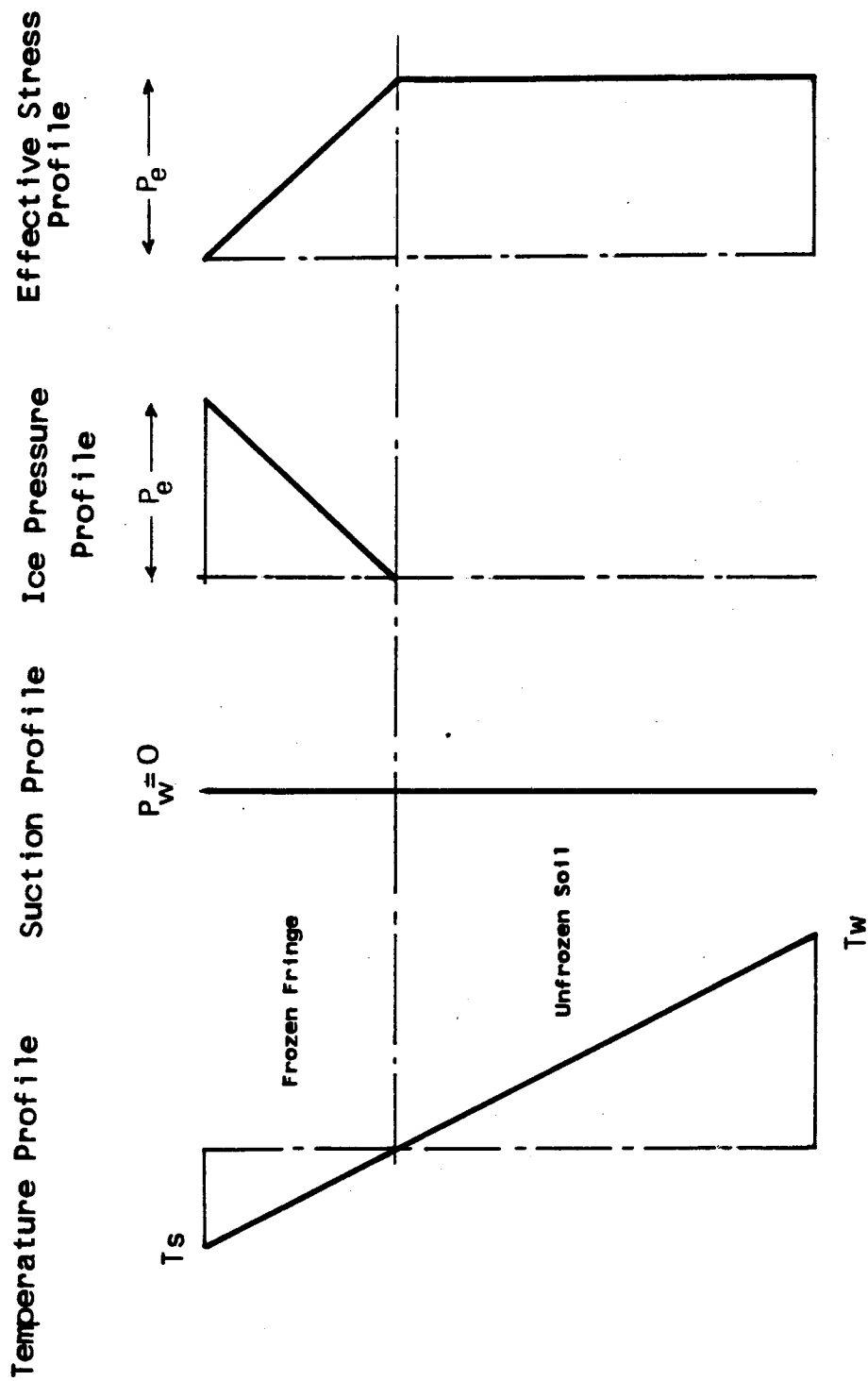
Figure 6.14 Conditions at the End of the Terminal Phase

ice pressure, it has been established experimentally that the suction decreases very slowly as the external pressure increases. Increasing lengths of the frozen fringe and decreasing driving potentials result in a decreasing overall hydraulic gradient in the fringe as applied pressure increases. Moreover, the overall permeability of the frozen fringe also decreases with increasing surcharge. It then follows that increased load depresses the heave rate in agreement with established findings of workers in the field of frost action for some 50 years.

This study takes the view that expulsion of water occurs during the advancing frost front phase. This is a function of applied load and rate of cooling of the frozen fringe. There is a unique relationship between applied pressure and rate of cooling of the fringe for which water is attracted to the freezing front. This relationship defines two regions in the space (Pe, dTf/dt). The left region in figure 6.13 corresponds to freezing with water expulsion and the right region to freezing with water intake if an outside water source is available.

It has also been established that the higher the applied load, the closer to final thermal equilibrium conditions the sample will start to attract water from the outside source.

Finally, evidence has been presented for the existence of a "shut off" pressure for which no water flow to the ice lens is possible. This "shut off" pressure is defined as the

applied pressure which produces zero pore water pressure at the segregation freezing level during steady state heat flow. This "shut off" pressure is extremely high for engineering purposes, in the order of 1000 kPa for Devon silt.

7. INTERPRETATION OF LABORATORY FREEZING TESTS

7.1 INTRODUCTION

In this chapter, attention is directed towards the application of the conceptual frost heave model established previously to the interpretation of various laboratory tests reported in the literature. These different tests are also evaluated with respect to their relevance for the classification of soils with regard to frost susceptibility. A standard freezing test which assesses easily the basic freezing parameters of any soil is presented.

7.2 ANALYSIS OF FREEZING TESTS AT THE FORMATION OF THE FINAL ICE LENS

The water intake rate or the total heave rate during freezing have often been taken as basic freezing parameters. This has led to the pursuit of a relationship between water intake rate or total heave rate and other variables such as cold side step temperature, unfrozen soil length, or rate of heat extraction. It is of value to show how the conceptual approach described in Chapter 3 can account for the shape of these relationships. The next sections deal solely with the

parameters at the formation of the final ice lens, i.e. close to stationary frost front conditions.

At the formation of the final ice lens, the segregation potential is constant for a given suction at the frost front. It is clear therefore, that for a given soil, different relationships between Vo and grad T can be obtained if the suction at the frost front varies. If, for example, the testing program is conducted such that at the formation of the final ice lens the same temperature gradient is obtained with different suctions at the frost front, the locus of the values of the water intake rate then becomes a vertical line as shown on Figure 7.1. Different freezing conditions may therefore result in an infinity of curves. Some typical cases are summarized on Figure 7.1.

7.2.1 Water Intake Flux in Relation to Unfrozen Soil Length

Loch (1979) has recently proposed plotting the water intake rate versus the reciprocal of the length of unfrozen soil as the frost front becomes stationary. He states:

"If the suction (-Pw) at the frost front is a constant for a soil, as is expected, one should find a linear relation between water intake rate and 1/lu."

The suction at the frost front is thought to be constant because Loch assumes that the pressure difference Pi-Pw across the curved ice-water interface at the frost front is solely a function of pore size. However, as demonstrated in
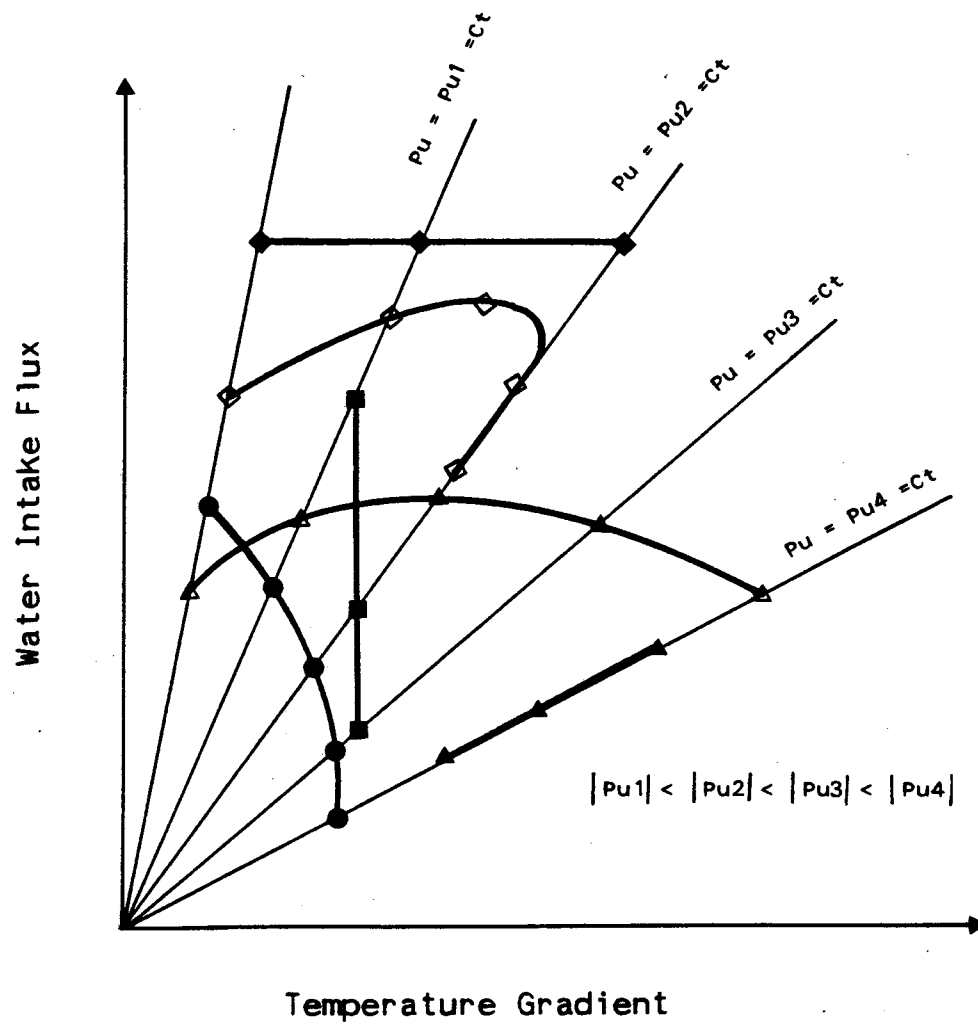
Figure 7.1 Typical Vo-grad T relations at the Final Ice Lens Formation for a Given Soil

Chapter 3, the curvature of the interface is not a constant in a freezing system with free water supply but depends on both temperature and suction. At the frost front it can be argued that the pore ice pressure is always atmospheric.

In the tests under consideration, freezing took place in three stages for each sample. The final ice lens was allowed to grow to an appreciable thickness during each stage. The water intake rate was inferred from the total heave versus time relationship associated with the measured thickness of the ice lenses. This procedure was adopted since the author believes that the measurement of total heave is more accurate than that of the water intake volume in Loch's tests.

The experimental results obtained by Loch (op. cit.), shown in F are not very convincing since some data points deviate seriously from linearity. Moreover, one should expect these lines to pass through the origin which is not always the case. Loch does not present an explanation for that divergence.

However, the results given by Loch support the view that for the same soil, different suctions at the frost front can develop depending on the freezing conditions. This can be inferred from the bottom part of Figure 7.2 where the relationship between Vo and grad T is given for three tests where adequate information was available. If one joins each point with the origin, two different lines are obtained for Gulli disturbed soil which means that different suctions at
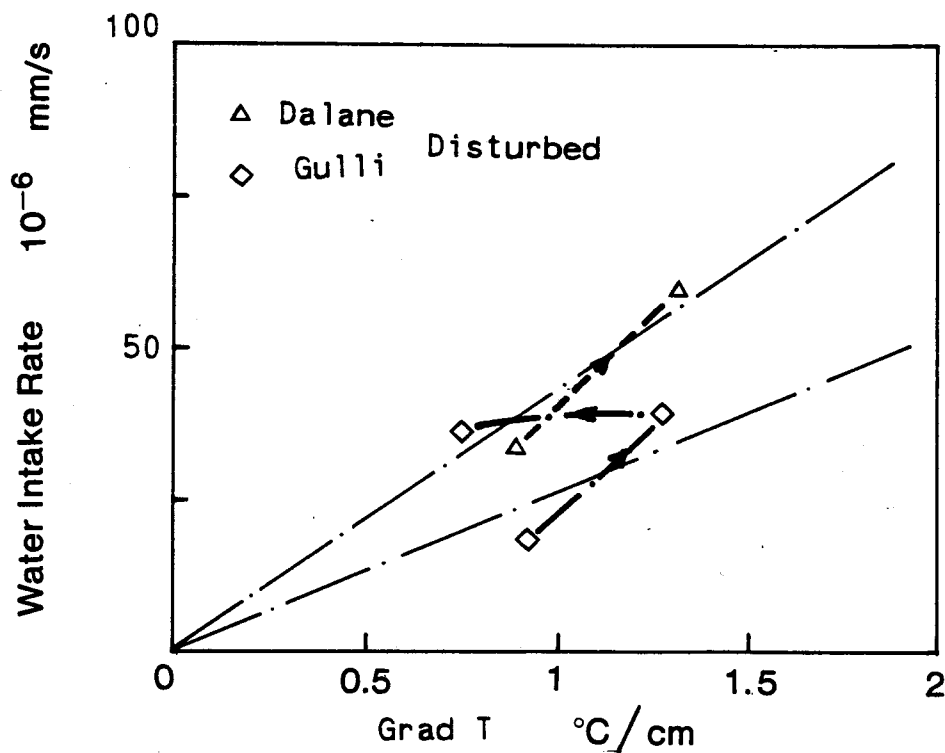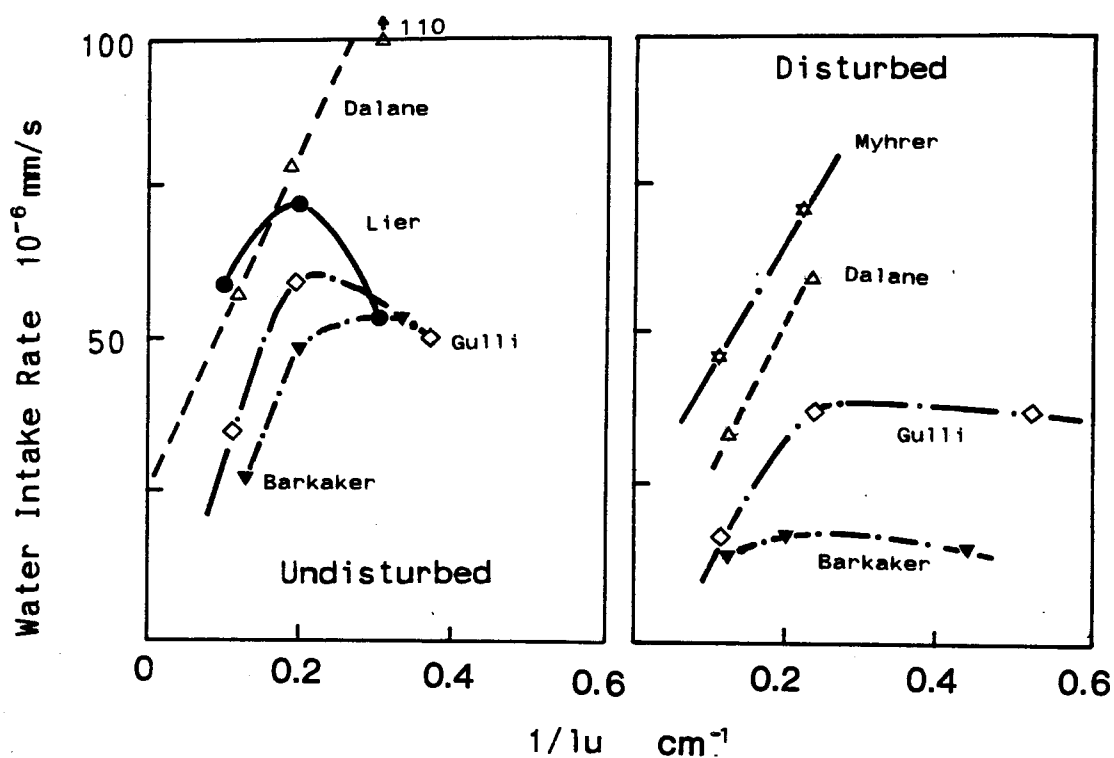
Figure 7.2 Experimental Results Obtained by Loch (1979)

the frost front existed for stage 3 and stages 1 and 2 of this freezing test. Consequently, it is expected that the curve Vo versus 1/lu for Gulli disturbed soil will diverge from linearity because their respective points do not always correspond to the same suction at the frost line. For Dalane disturbed soil, the plot Vo versus grad T reveals that the representative points obtained at the end of stage 1 and 2 are situated on a line passing through the origin. This, in turn, means that the same suction exits at the frost front in these two stages. Therefore, the experimental data should be located on a straight line passing through the origin on a Vo-1/lu plot, which is the case as shown on Figure 7.2.

It can therefore be concluded, in the light of Figure 7.2, that the conceptual model presented in Chapter 3 based on freezing tests with Devon silt can be applied to other soils. Any freezing soil can be characterized by the basic freezing parameters at the onset of the final ice lens, SPo and Pu, determinable from simple laboratory freezing tests.

7.2.2 Water Intake Flux in Relation to Applied Pressure and Cold Step Temperature

Penner and Ueda (1977, 1978) established experimentally that the relation between the logarithm of heaving rate and P/T, the ratio of overburden pressure and cold-side freezing temperature is linear in the case of Leda clay and a silt from the Mackenzie River Valley, N.W.T. This relation is, in fact, a combination of two linear relationships between the
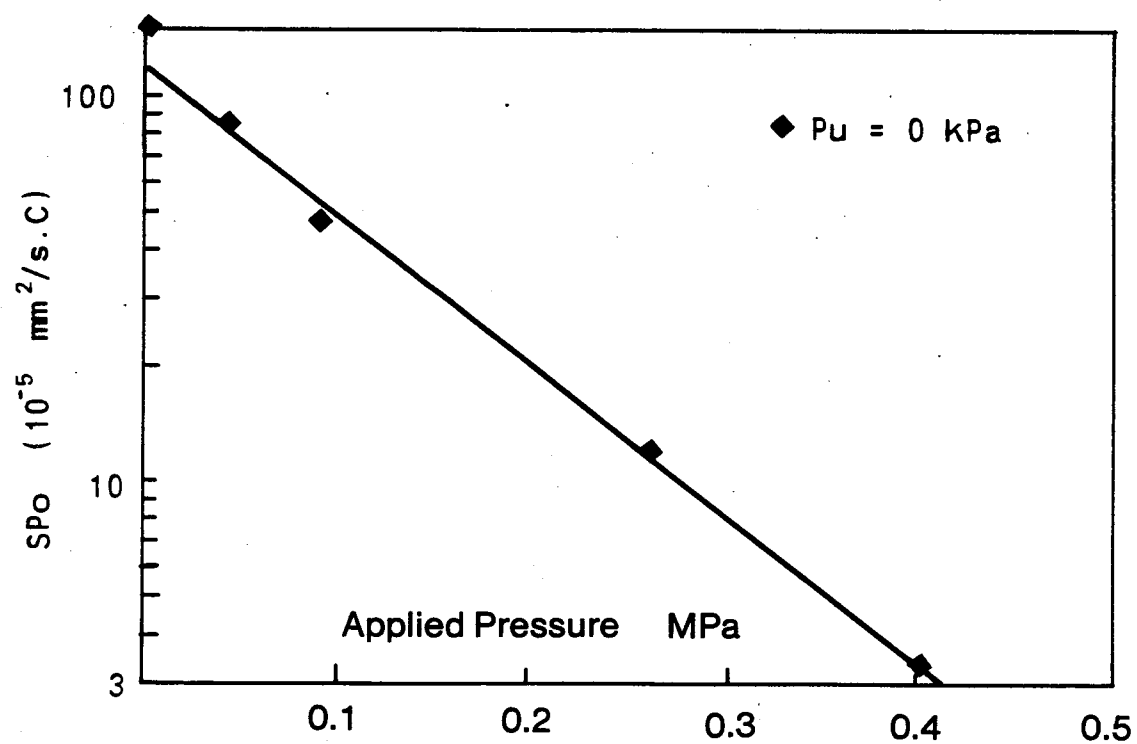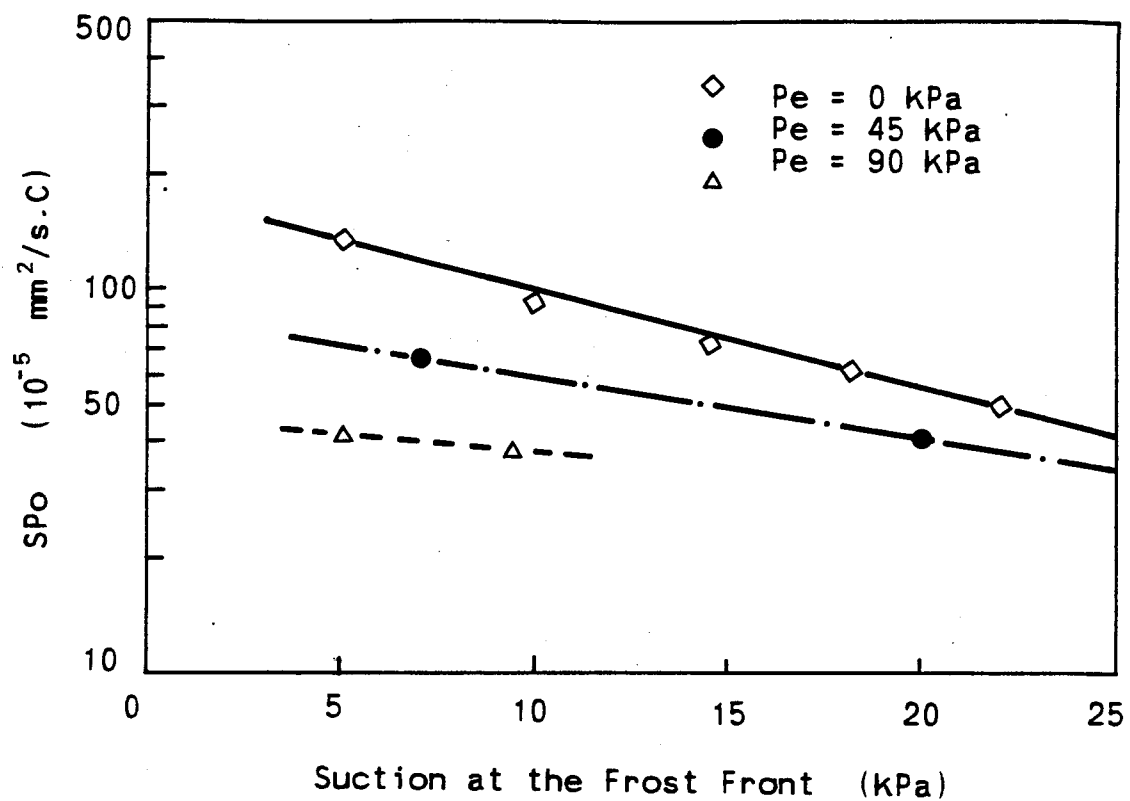
Figure 7.3   Segregation Potential for Devon Silt

logarithm of heave rate and the reciprocal of the cold-step temperature 1/T, and log (dh/dt) and Pe. The values of the heave rate was generally taken close to steady state conditions in the different tests performed by Penner and Ueda . Therefore, one can argue that dh/dt is equal to 1.09 Vo and that a similar relationship would then exist between log (Vo) and Pe/T.

It is of value to analyse their tests in the light of the results presented so far in this thesis. Figure 7.3 summarizes the relationship between the segregation potential, the suction at the frost front and the applied pressure at the initiation of the final ice lens in Devon silt. The plotted results indicate clearly that there is a linear relation within the observed range between the logarithm of the segregation potential and the suction at the frost front. There is also a linear relation between log (SPo) and Pe for a given suction at the frost front.

Since SPo is the ratio of water intake rate and temperature gradient across the frozen fringe when the final ice lens forms, it is clear that if the temperature gradient is a constant in different freezing tests, the variation in Vo in those tests will then adopt a similar shape to the variation of SPo. Furthermore, if the inverse of the cold-step freezing temperature, 1/Tc, is related linearly to the suction at the frost front, a linear relationship between log (Vo) and 1/Tc is to be expected for a given applied load. This follows readily from the results

presented in Figure 7.3.

The testing procedure adopted by Penner and Ueda was as follows. During one freezing test, the cold-step temperature was lowered in stages. The warm-plate temperature was supposed to be constant during the whole freezing procedure. However, as seen in Figure 7.4, it is clear that Tw could not be maintained constant but decreased as the cold side temperature was decreased. This was also noted by Hopke (1980). Each stage was maintained long enough to allow for a stationary frost front to develop at each successive position of the $0^\circ C$ isotherm. This is illustrated in Figure 7.4. Therefore, the rate of water intake at the end of each stage corresponds approximately to the conditions of final ice lens formation. The soil, Leda clay preconsolidated to 400 kPa, was frozen under an external pressure of 200 kPa.

From the results given on Figure 7.4 one can readily obtain the relation between the temperature gradient at the frost front and the water intake velocity at the end of each freezing stage. The representative points of each stage are summarized on Figure 7.5. This plot reveals that different suctions at the frost front were obtained at each freezing stage. Although the permeability of the unfrozen soil is not specified, the suction at the frost front can be estimated · by Vo.lu, the product of water intake flux and length of the unfrozen soil. Darcy's law establishes the equivalence between (V.lu) and ($|Pu|$.Ku). Therefore, if one assumes that the permeability of the unfrozen soil remains constant
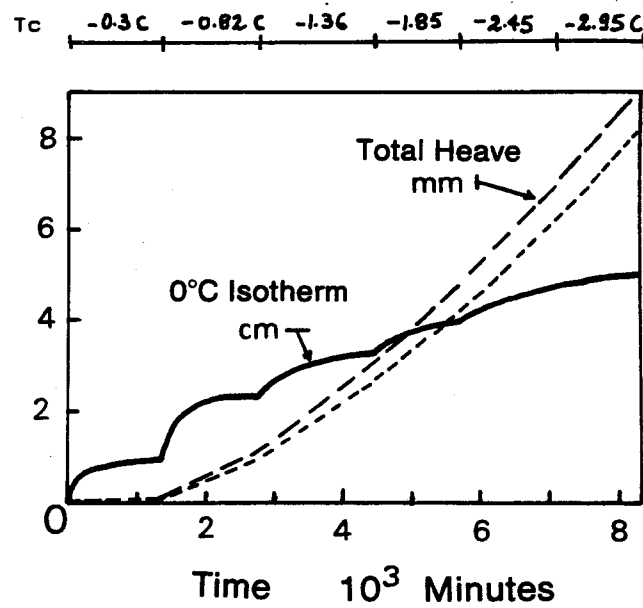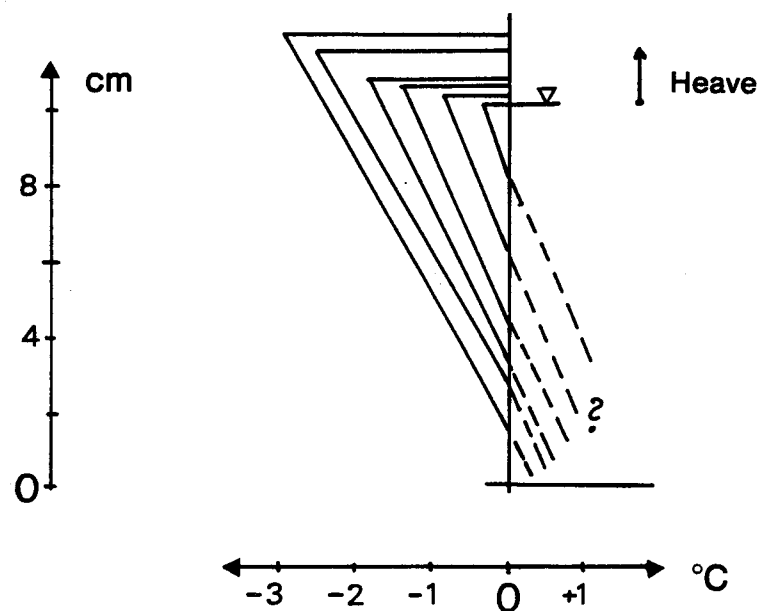
Figure 7.4 Experimental Results Obtained by Penner and Ueda (1978)

during the whole freezing test, Vo.Pu is proportional to the suction at the frost front.

The value of Vo.lu can readily be calculated for each freezing stage. The number beside each representative point on Figure 7.5 indicates the value of Vo.lu, and consequently, is an indication of the relative magnitude of the suction at the frost front. Remarkably, Penner and Ueda's data confirm also that the segregation potential, which is the slope of each line passing through the origin and the representative points of the freezing test, increases when the suction at the frost front is reduced. Furthermore, for a given suction, any freezing condition is represented by a unique line passing through the origin.

Figure 7.5 also establishes that the temperature gradient across the fringe was more or less constant in the four last stages.

Let us now plot Vo.lu, hence the suction at the frost front, versus the inverse of cold-side freezing temperature. As shown on Figure 7.5 a linear relationship is obtained approximately. For these conditions, i.e. constant temperature gradient during freezing and linear variation of Pu with $1/Tc$, a linear relationship between log (Vo) and $1/Tc$ is expected provided that a linear relationship between log (SPo) and Pu for a given applied pressure exists for that soil. Experimental data from the previous test, presented in Figure 7.5, support strongly these arguments. It can be argued furthermore, that the shape of the relationships
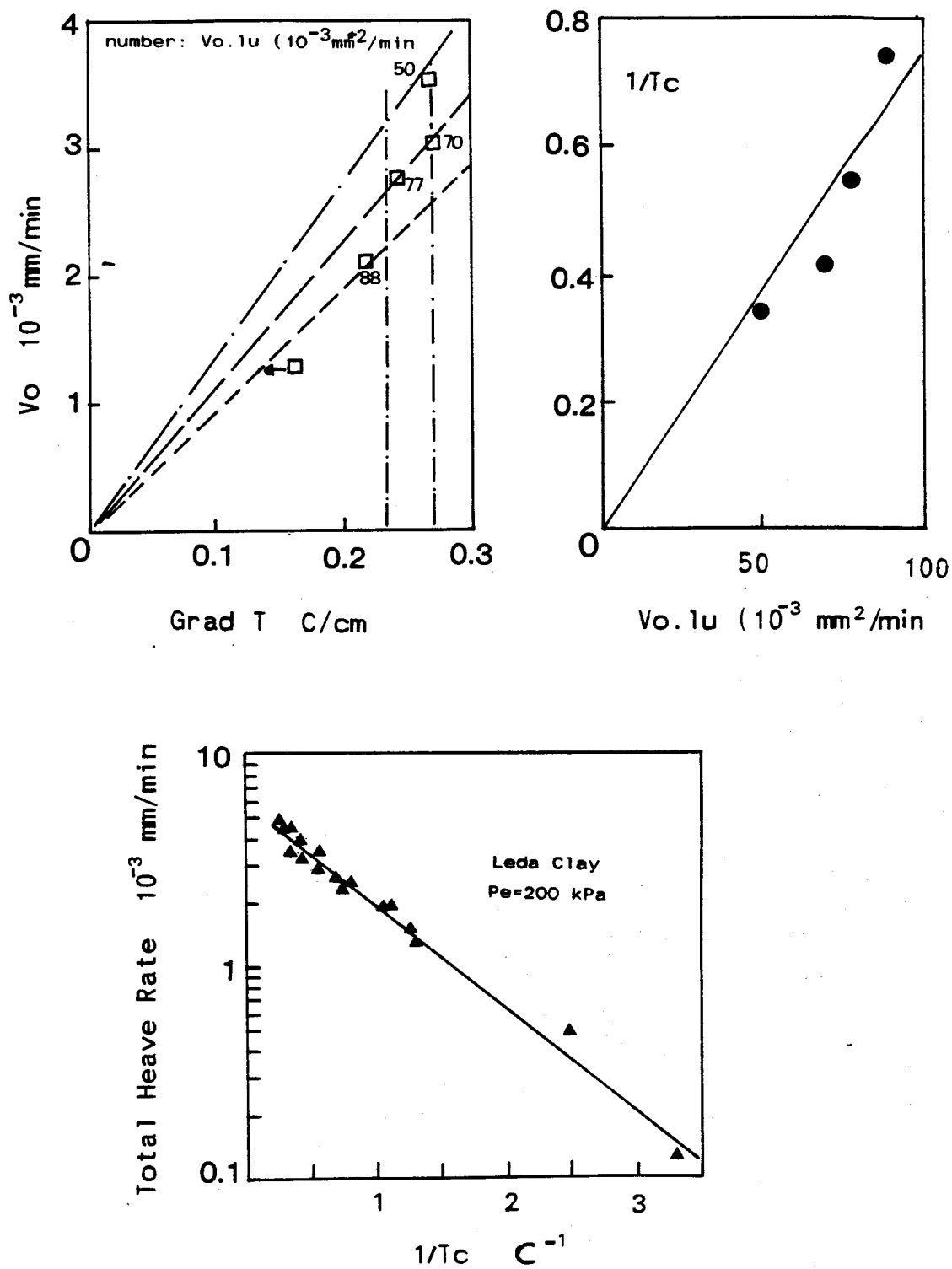
Figure 7.5 Experimental Results Obtained by Penner and Ueda (1978)

between the fundamental freezing parameters for Devon silt are extendable to other soils.

Finally, if the freezing conditions are such that a linear relationship between log (Vo) and 1/Tc is obtained, a linear relationship between log (Vo) and Pe/Tc is then to be expected since it is thought that the relation between log (SPo) and Pe is linear in many soils. However, one should bear in mind the influence of Pu in the relationship between SPo and Pe as demonstrated in Chapter 6.

From the previous analysis it can be deduced that the heave rate or water intake flux existing at the formation of the final ice lens is temperature path or freezing path dependent. It must be emphasized again that the fundamental freezing surface (SP, Pu, dTf/dt) of a given soil embraces the freezing path effect by considering the rate of cooling of the frozen fringe dTf/dt and the suction at the frost front.

If the freezing conditions at the formation of the final ice lens are different from those required to obtain a linear relationship between log (Vo) and 1/Tc, no obvious relationship should be found. This proposition is supported by the results of the freezing tests conducted during this investigation. The freezing data of our tests are summarized in terms of log (Vo) and 1/Tc on Figure 7.6. As shown, the experimental points are all random except for three tests in which the temperature gradient was approximately constant and in which a linear relationship between Pu and 1/Tc

existed. These three data points are situated, as expected, on the same line. However, for the same soil, no definitive relationship can be obtain from the other representative points.

Data given by Loch (1979) provide further support to our views. For Dalane undisturbed soil, the conditions stipulated previously in order to obtain a linear relationship between 1/Tc and log (Vo), are fullfilled as seen in Figure 7.3. As expected, the representative points of the three different stages during the freezing of Dalane undisturbed soil are on a straight line. However, the other data points do not satisfy the required conditions and consequently no specific relationship appears on Figure 7.7 for those freezing tests.

7.2.3 Concluding Remarks

Penner and Ueda (1978) performed freezing two different freezing tests. In the first set, the cold-side temperature was held constant for three successive runs, but the warm-side temperature was changed. The results established that the heave rate was the same for all three runs as shown on Figure 7.8.

In the second test, the warm-side temperature was held constant and in three successive runs the cold-side step temperature was changed. The results demonstrated that the heave rate was very sensitive to the cold-step temperature, as shown on Figure 7.8.
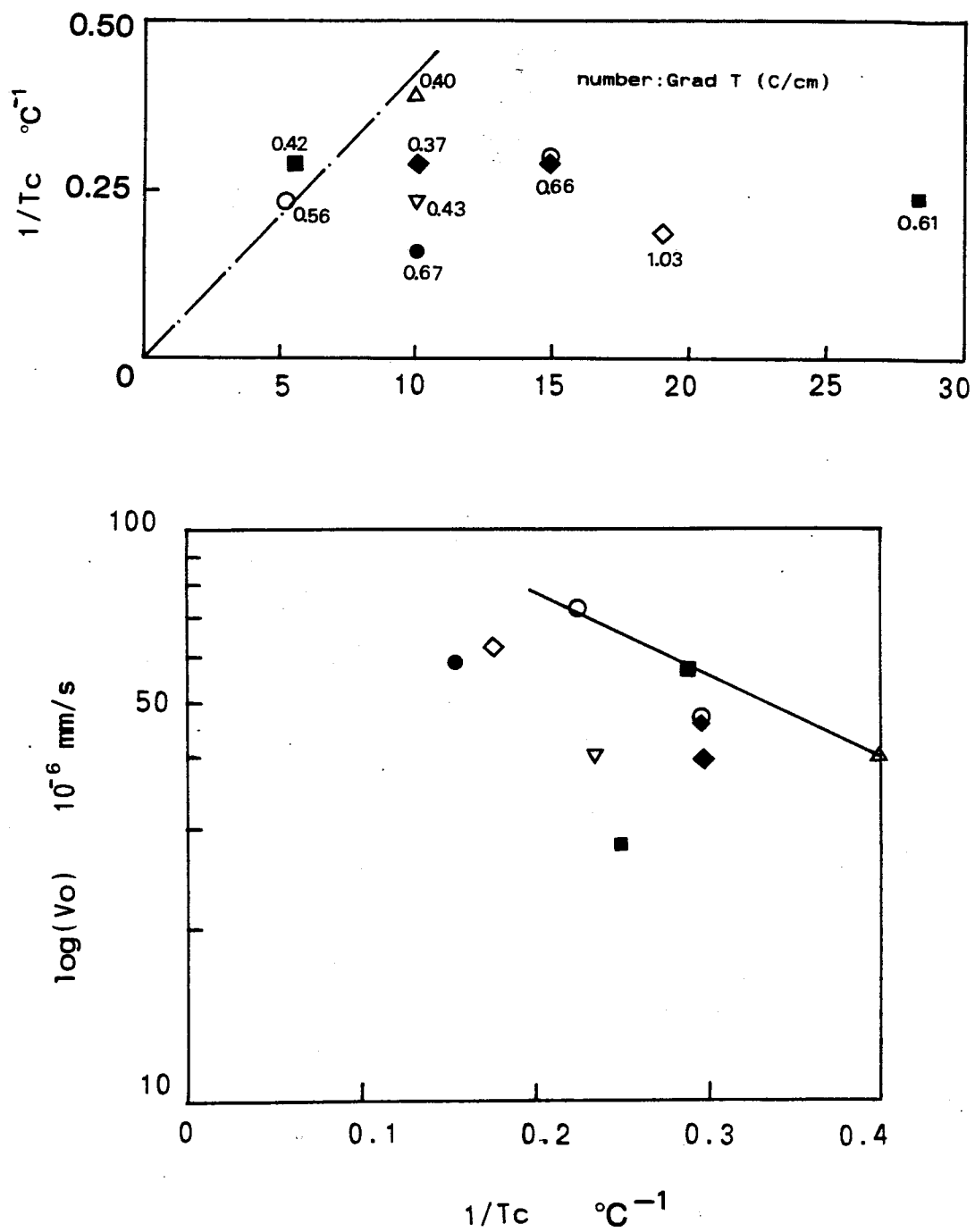
Figure 7.6   Experimental Results Obtained for Devon Silt.
(This Study)
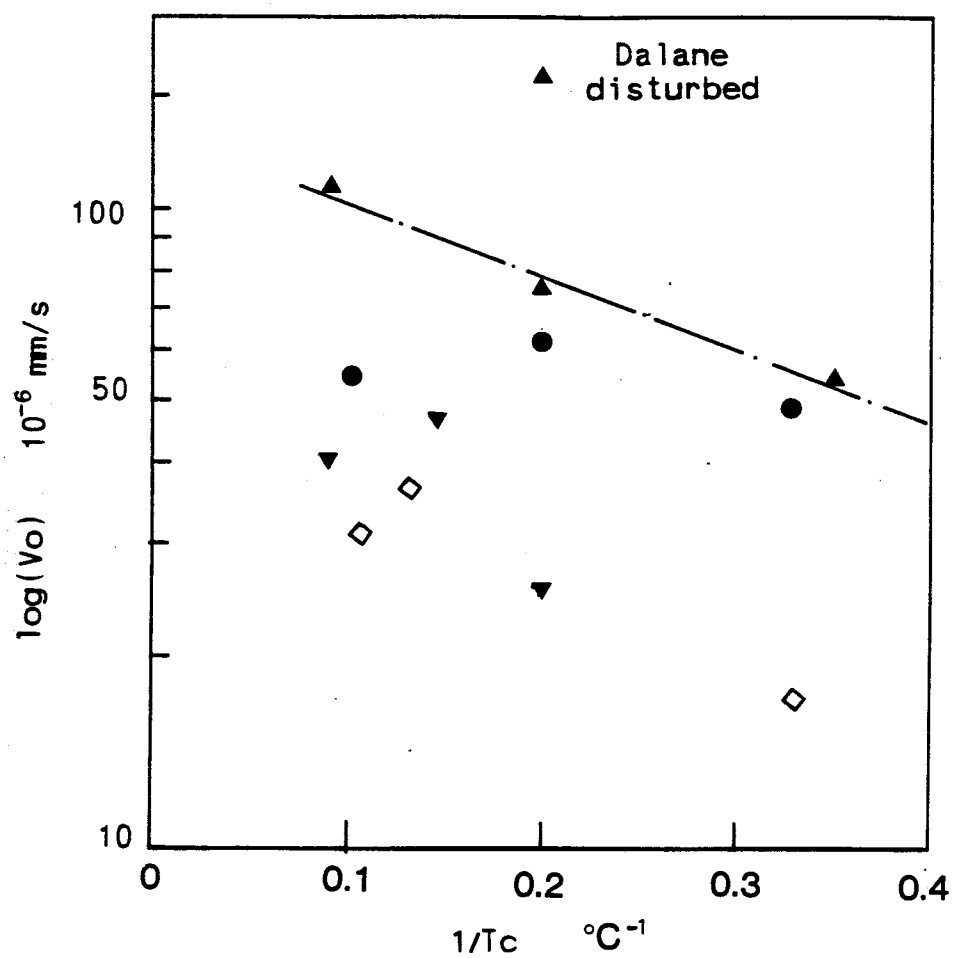
Figure 7.7   Experimental Results Obtained by Loch (1979)
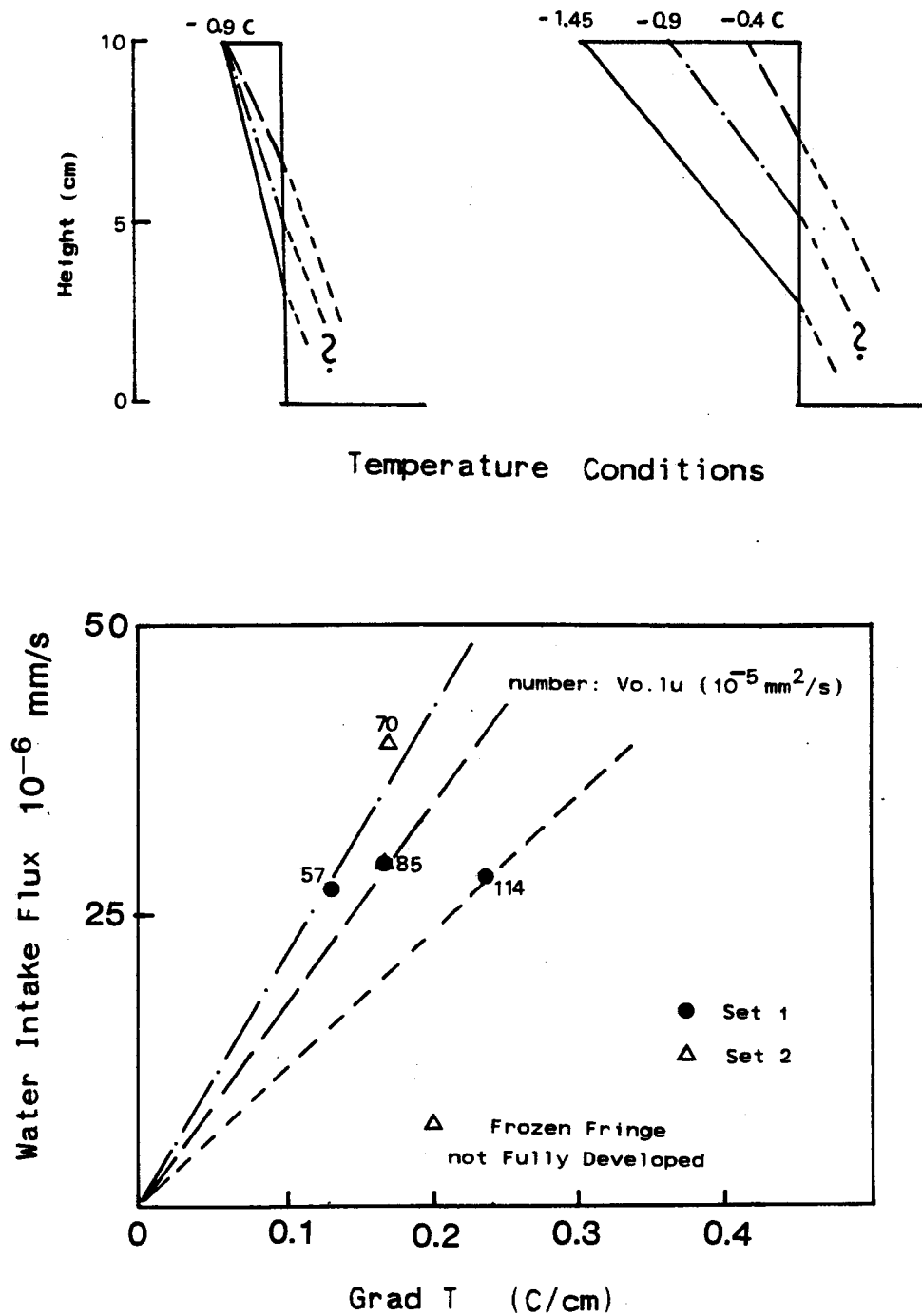
Figure 7.8   Influence of Warm and Cold Side Temperature.
After Penner and Ueda (1978)

Before analysing the results presented by Penner and Ueda, it should be mentioned that the first test of the second set was run with a step freezing temperature of -0.40°C. Considering that the soil is clay and that the external pressure is large, e.g. 200 kPa, it can be argued that the segregation freezing temperature in these conditions could be lower than -0.40°C. This, in turn, would inhibit the development of the frozen fringe in the first test of the second set. It is therefore expected that the results obtained in that freezing test are not comparable with those obtained in the other tests where the step-freezing temperature was colder.

If one calculates the value of Vo.lu for each test in the first set, different values are obtained. As discussed previously this product can be related directly to the suction at the frost front. Since the suction at the frost front is different for each test, the three representive points will be situated on three different lines passing through the origin.

Furthermore, the temperature gradients in the frozen fringe in each test were such that the three representative points on Vo vs Grad T plot are situated on a horizontal line. This is the case of the freezing tests of set 1.

This illustrates very clearly the danger of concluding too hastily that the warm-end temperature has little effect on heave rates. Furthermore, it is predictable from the conceptual model presented in Chapter 3 that the heave rate

should increase when the cold-side temperature increases provided that the suction at the frost front becomes smaller and that the temperature gradient across the active zone either increases or remains constant.

The interpretation of freezing tests in terms of derived parameters such as water intake velocity, heave rate, total heave rate, cold-step freezing temperature, length of unfrozen soil and the generalization of such particular relationships should be avoided since the results are very sensitive to the freezing procedure and the conditions of final ice lens growth. It has been demonstrated that a conceptual model characterizing a freezing soil with two basic parameters at the formation of the final ice lens, the segregation potential and the suction at the frost front accounts for the existing relationships between the derived parameters found in the literature.

7.3 INFLUENCE OF THE HEAT EXTRACTION RATE ON THE ICE SEGREGATION RATE OF SOILS

Several investigators (Kaplar, 1968, 1970; Penner, 1972) emphasized that the heat extraction rate is a fundamental parameter in the freezing process and not the frost front penetration rate. They suggested, therefore, that soils should be tested at the same rate of heat extraction instead of at the same rate of frost penetration.

Loch (1979) also subscribed to that view as he proposed that a comparative heave test should be carried out at a standard rate of heat extraction. Furthermore, Loch stated:

> "If one is able to maintain this fixed rate of heat extraction during a test, then heave will be a straight line with time..."

The model presented in Chapter 4 allows one to calculate the net heat extraction rate at any time. Figure 7.9 summarizes the curves of net heat extraction rate versus water intake flux and total heave rate obtained from the simulation of most of the freezing tests reported in this thesis.

It must be emphasized that all the curves in Figure 7.9 correspond to a given soil freezing under zero applied load. The straight line passing through the origin is the locus of heave rates for the hypothetical case where all heat extracted comes from ice lens formation with no frost penetration. The slope of this particular line is 1/L.

Figure 7.9 reveals that a wide range of heat extraction rates have been covered during each freezing test. Furthermore, it is striking that a limiting rate of heat extraction exists at which no water flow to the freezing front is possible. For Devon silt, this limiting rate of heat extraction is approximately 0.4 mW/(mm^2.s).

As no further frost front advance occurs, all the curves intersect the straight line characterizing the final ice lens formation. As discussed in Chapter 5, the representative point of the freezing soil is then moving on
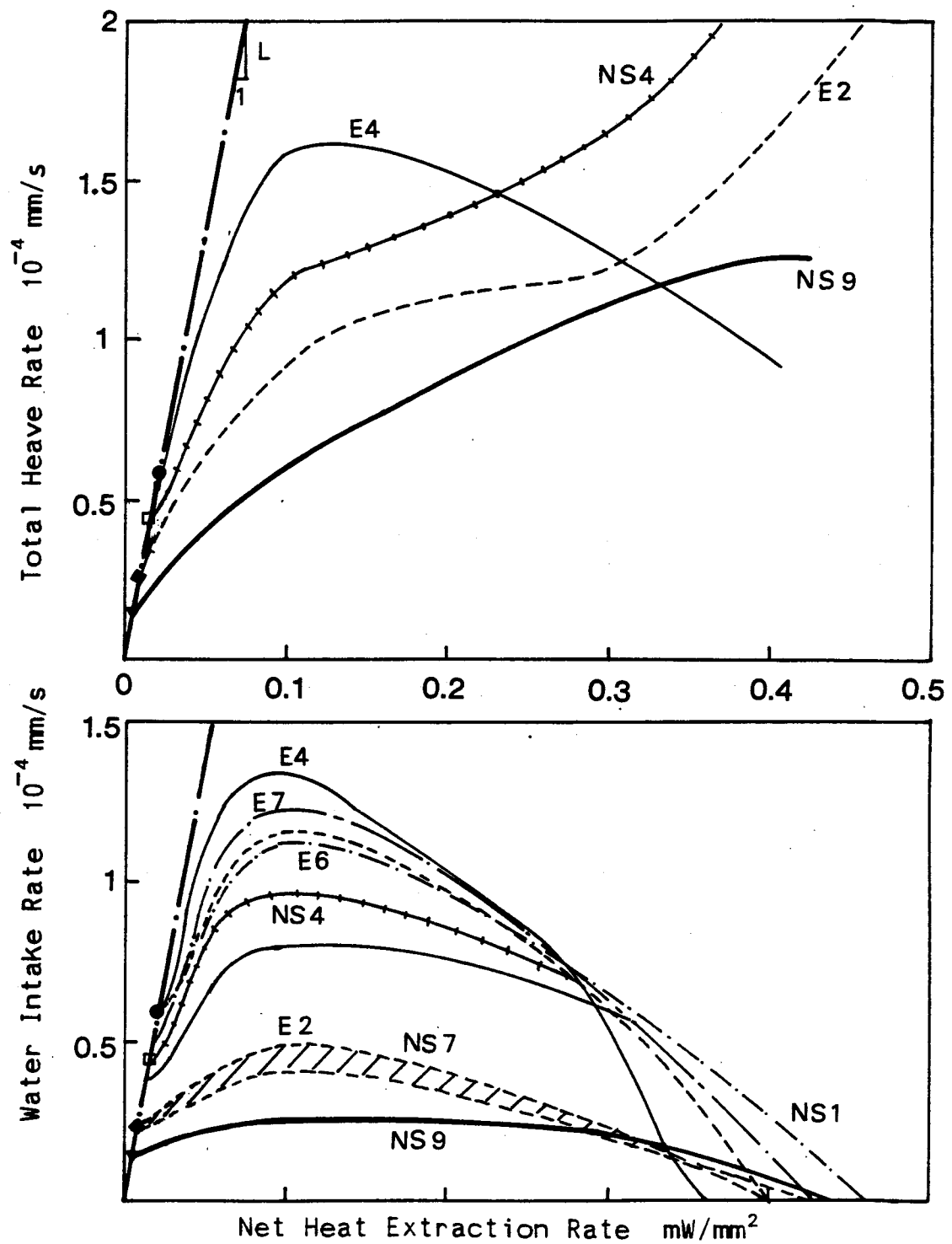
Figure 7.9 Heave Rate vs Heat Extraction Rate for Devon Silt

this line if the temperature boundary conditions are constant with time. It is of value to notice that different freezing conditions result in different positions of the intersection of the representative curves and the straight line, although the unfrozen soil properties are always the same.

Another important feature is the difference in shape of the curves representing total heave rate and those representing water intake flux as a function of net heat extraction rate. This arises from the fact that when the heat extraction rate is high, thermal balance at the frost front requires a large amount of heat, which is liberated by freezing *in situ* pore water. The shape of the total heave versus heat extraction rate depends on the rateof frost front advance and the amount of heat liberated by the intake water as it freezes at the segregation freezing level. These shapes compare quite well with those obtained by Horiguchi (1978) for various types of zeolites.

The results presented on Figure 7.9 demonstrate clearly that the net heat extraction rate is not a fundamental parameter of a freezing soil. This parameter is dependent on the thermal and geometrical conditions existing in the sample at any time. However, it can readily be derived from the basic freezing parameters (SP, Pu, dTf/dt) combined with the heat balance equation and the frost heave model given in Chapter 4.

7.4 ANALYSIS OF FREEZING TESTS IN TERMS OF THE ICE SEGREGATION RATIO

Hwang (1977) proposed to predict total heave in a freezing soil with the total ice segregation ratio, ISR. ISR is equal to the ratio of total heave and frozen soil thickness at the end of a freezing test with constant temperature boundary conditions. Hwang (op. cit.) assumes that this ratio is a fundamental parameter of a freezing soil, which depends upon applied pressure only.

In order to evaluate the relevance of this parameter, the results of the freezing tests performed during the present investigation have been analysed in the following manner. For each test, total heave is plotted against the thickness of the frozen soil. This allows one to visualize the variation of the total ice segregation ratio during a freezing test. Figure 7.10 summarizes the results obtained from various freezing tests with zero applied load. It must be emphasized that all the tests have been performed with constant temperature boundary conditions. However, the initial thermal and geometrical conditions were different for each test. The results presented on Figure 7.10 establish clearly that ISR is not a fundamental parameter for a given soil freezing under laboratory conditions since different ISR are obtained for the same soil. It is noteworthy to realize that the final ice lens forms when the slope of the h-Xf relationship is equal to 1, i.e. when the

increase in frozen soil thickness is equal to the increase in the final ice lens thickness. Figure 7.10 indicates also that there is no apparent relationship between the shape of the different h vs Xf curves which were obtained for the same soil.

Again, it must be stressed that the variation of ISR can be predicted using the frost heave model given in Chapter 4 with the fundamental freezing characteristics (SP, Pu, dTf/dt).

7.5 A STANDARD LABORATORY TEST FOR FREEZING SOILS

This section summarizes four currently proposed or used freezing tests which determine the frost heave susceptibility of various soils. Their analysis and relevance to frost heave characteristics will be critically reviewed in the light of the conceptual model established in this thesis.

The conclusions that have been drawn from the analysis of laboratory data on frost heave testing of Devon silt will lead to the proposal for a standard laboratory test for freezing soils.

7.5.1 Review of Some Existing Standard Freezing Procedures

Three tests currently used in North America are all based upon measurement of the total heave rate of a soil. These tests are:
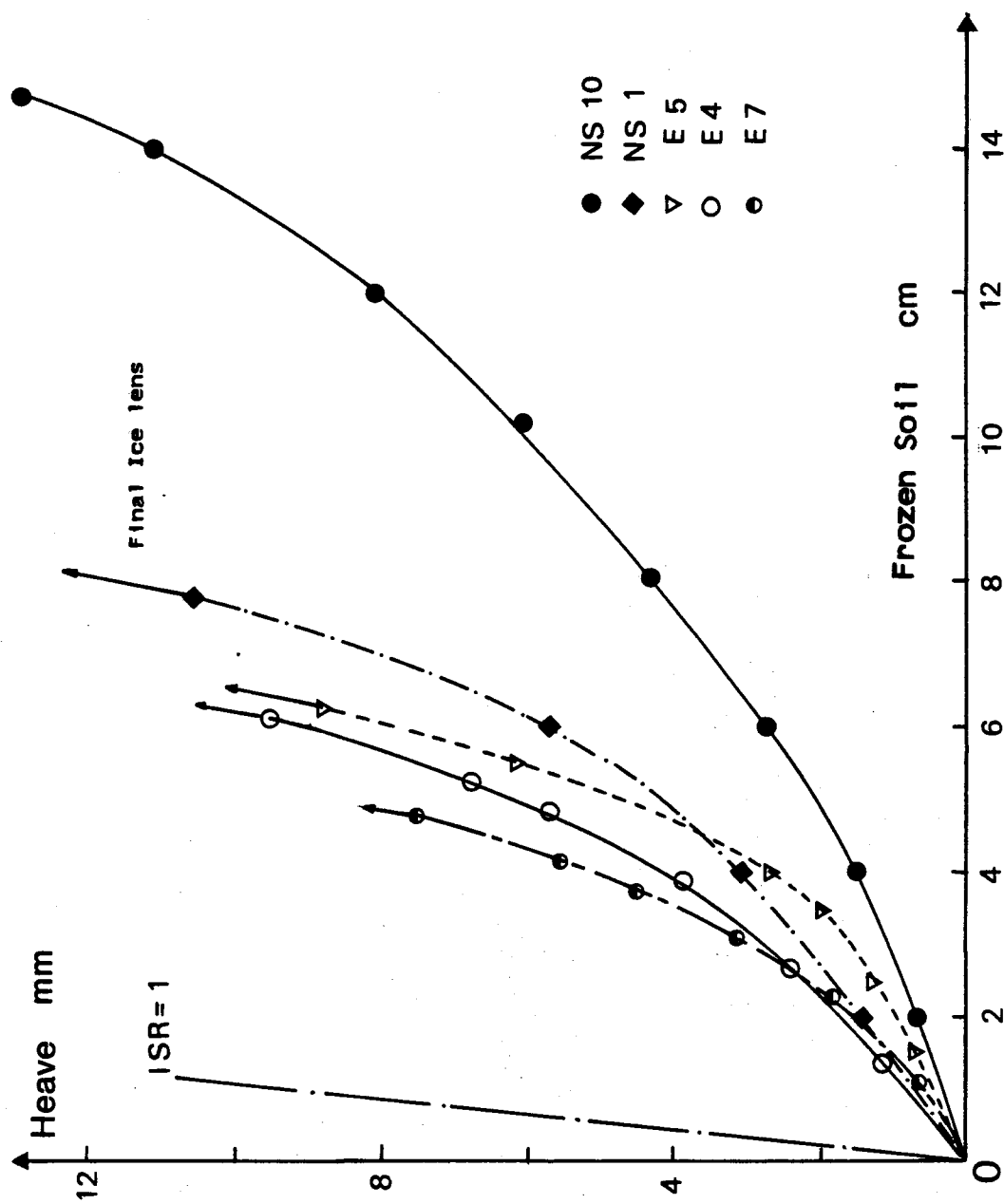
Figure 7.10 Influence of Boundary Conditions on ISR for a
Given Soil Under Zero Overburden

1. the test of the U.S. Army Cold Regions Research and Engineering Laboratory (CRREL) described by Kaplar (1965)

2. the Appropriate Freezing Rates Test, proposed by Penner (1972)

3. the Rapid Frost Heave Test, proposed by Zoller (1973)

The U.S. Army CRREL-Laboratory classifies soils for their susceptibility to frost heave, according to their heave rate in a laboratory test, in which samples are subjected to a constant frost penetration rate of about 1 cm per day.

Soil specimens, 15 cm high, are placed in tapered lucite mold diameter of 15 cm, and frozen from the top, in freezing cabinets placed in a 4°C room. The specimens are subjected to a small surcharge of 3.45 kPa and have a free water supply at their base. At the given frost penetration rate, 2 weeks are required to completely freeze a sample.

Disadvantages of this technique are numerous:

1. the length of time for testing a sample,

2. the necessity for continuous adjustment of the cold-side temperature in order to maintain the constant frost penetration rate

3. bad temperature control of the warm end of the sample

4. wall friction along the mold which has been reported by Kaplar (1968)

5. the interpretation of the data in terms of the fundamental freezing parameters, SP or Ts and K_f are very difficult.

This latter point is illustrated in the following.

Figure 7.11 is the projection of the characteristic freezing surface for Devon silt on a plane defined by SP and dT_f/dt. If one would freeze a sample with a constant rate of cooling of the frozen fringe and if the suction at the frost front decreases with time, Figure 7.11 reveals that the segregation potential increases with time. The freezing path during this particular procedure is indicated by the vertical line on Figure 7.11.

If a freezing test would be conducted with a constant temperature gradient in the sample, a constant rate of cooling implies then a constant rate of frost penetration. This can readily be inferred from Equation 4.14. Furthermore, in these conditions, the variation in water intake flux, hence in total heave rates since the componant of "in situ" pore water freezing is constant, is identical to the variation in SP. This special situation is illustrated in Figure 7.11

An early paper by Hayley and Kaplar (1952) corroborates this special freezing behavior.

The freezing test was started by lowering the temperature in the cabinet to approximately -1.1°C for a period of two days, then to -1.7°C for two more days and to -2.2°C for two other days. After that period of six days,
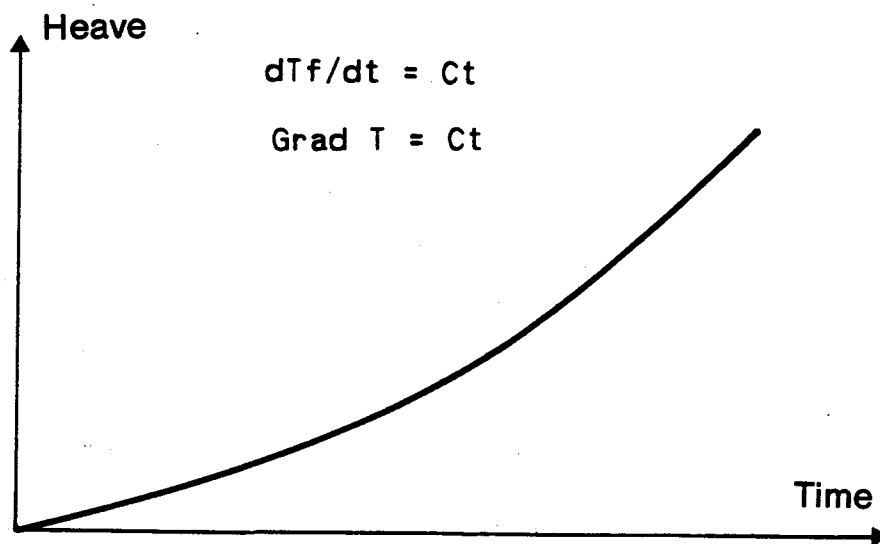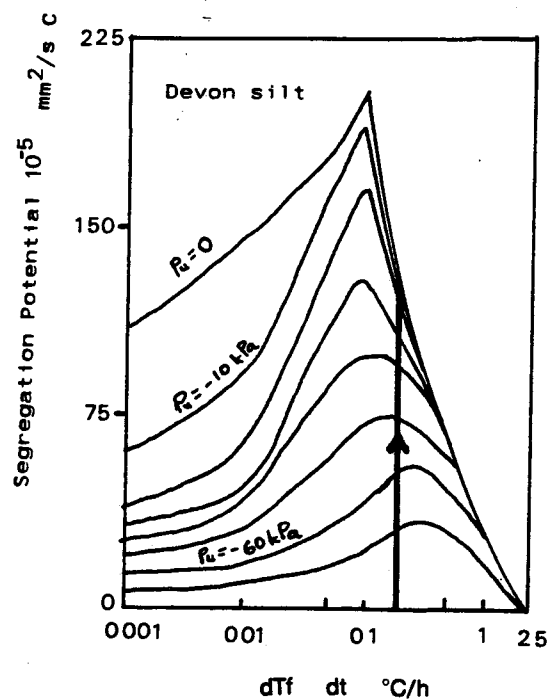
Figure 7.11 Freezing Test with Constant Frost Penetration
Rate and Constant Temperature Gradient

the temperature within the cabinet was changed only by the amount necessary to maintain the rate of penetration of the 0°C isotherm at approximately 6.35 mm/day. Measured temperature profiles reveal that the warm-plate temperature declined with time as the cold-side temperature was lowered. Fortunately, this resulted in a more or less constant temperature gradient in the specimen.

The total heave and the penetration of the frost front with time is summarized in Figure 7.12 for two New Hampshire silt samples.

The frost front penetration rate was constant after 14 days of freezing and approximately 7.5 mm/day. As anticipated, the total heave rate increased as the length of the unfrozen soil decreased with time leading to a decrease in suction at the frost front with time.

This freezing procedure is essentially similar to that adopted by CRREL. The previous example supports again the view that the model presented in this study is extendable to any freezing path. It is also clear that the CRREL freezing technique is inadequate to determine accurately the basic freezing characteristics due to variability and bad control of boundary conditions.

The disadvantage of long freezing periods is overcome in the so-called Rapid Frost Heave Test, as developed by Zoller (1973).

It is claimed that this test can be carried out in a laboratory at normal room temperature by simply insulating
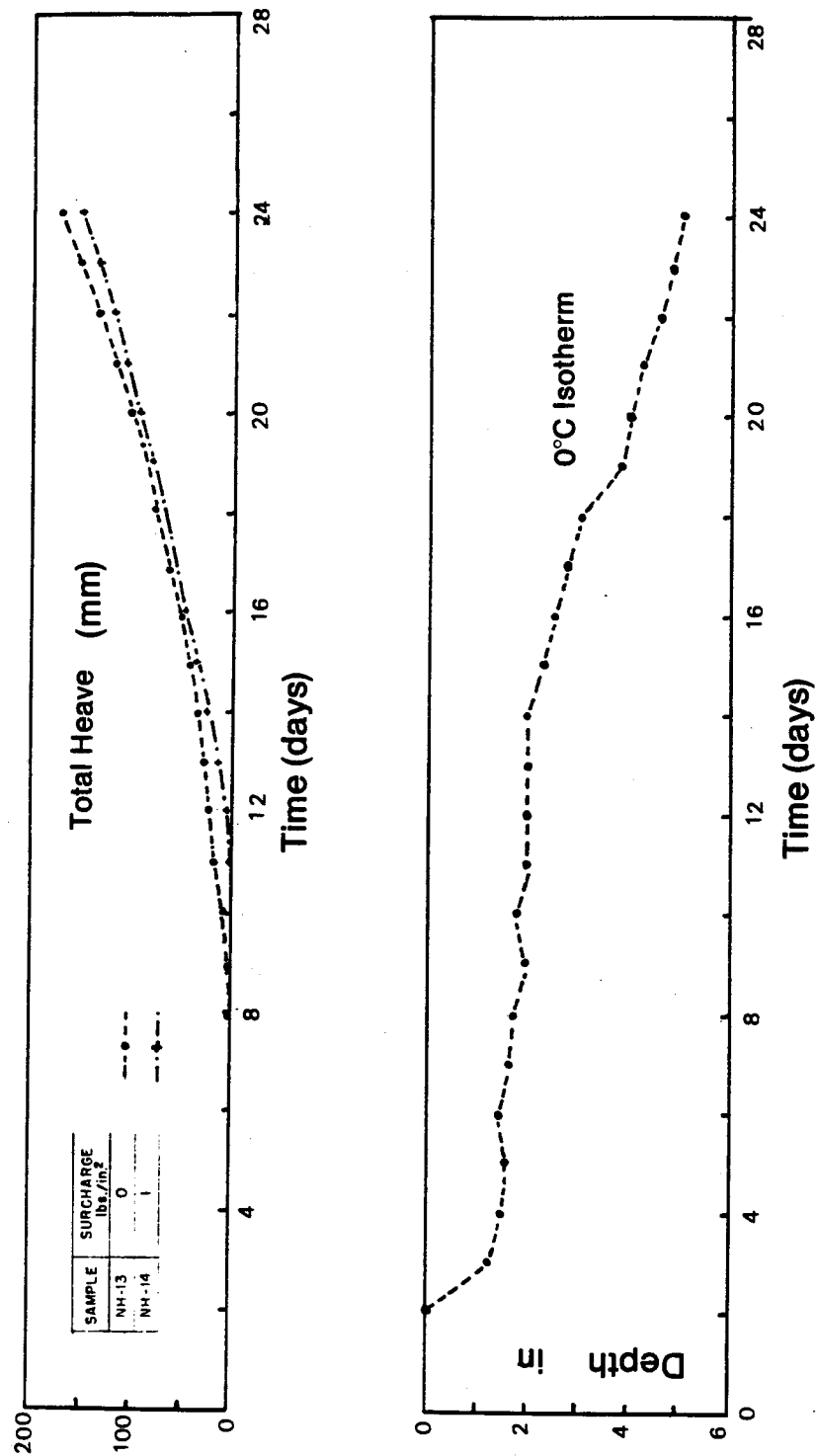
Figure 7.12 Frost Heave for New Hampshire Silt. After Hayley and Kaplar (1952)

the cylindrical side of the sample with foamed plastic. Temperature control at the top of the sample is obtained with a Peltier thermoelectric cooling element of 13.5 cm diameter. Thermoelectric cooling has the advantage that the rate of freezing can be increased substantially and adjustment for constant frost front penetration rate is easily done by adjusting the electric current. Testing time in this technique is reduced drastically by freezing to a depth of 7.5 cm at a frost penetration rate of 7.5 to 17.5 cm/day. The freezing time is less than a day. Friction is reduced by the use of a non-tapered mold of stacked lucite rings, each 2.5 cm high.

One assumption in this test is that the heave rate stays constant with time, and therefore a short testing time is permissible. As seen earlier a constant frost front penetration can result in a constant heave rate depending on the value of the suction at the frost front. However, in reality the freezing conditions are not that well controlled and slight variations in the heave rate are frequently observed.

Another assumption is that the rate of heaving of soils, subjected to a faster freezing rate than those used in the CRREL tests is uniquely related to the heaving rate obtained with the CRREL procedure on the same soil. By subjecting 5 soils to both testing procedure, Zoller produced new heave criteria for the CRREL classification system. The basis of this modification is shown in Figure

7.13. This assumption, however, is not general for most of the soils, since the total heave rate is a function of both geometrical and thermal boundary conditions as shown in Figure 7.9. Loch (1979) expressed identical doubts on the uniqueness of the curve of Figure 7.13.

The test method by Penner (1972) is similar to the rapid frost heave test reported by Zoller, with the major exception that Penner suggests use of rates of freezing that are related to thermal conditions in the field. Because of variability in these conditions he suggests two tests per soil, one at less than the minimum rate of freezing and the other at somewhat faster than the maximum rate of freezing expected in the field.

However, as already discussed in Section 7.3, the total heave rate is not uniquely related to the rate of heat extraction for the same soil. Therefore, one should be cautious when extrapolating laboratory freezing results to field conditions.

A fourth freezing method can be found in the current literature. Its procedure and equipment were described by Loch (1979).

This testing procedure is basically different from the previous category for two reasons. Firstly, the samples are tested in their undisturbed state. This is based on the assumption that degree of disturbance and degree of compaction have an effect on heave rate. Secondly, water intake rate is selected as the criterion for frost heave
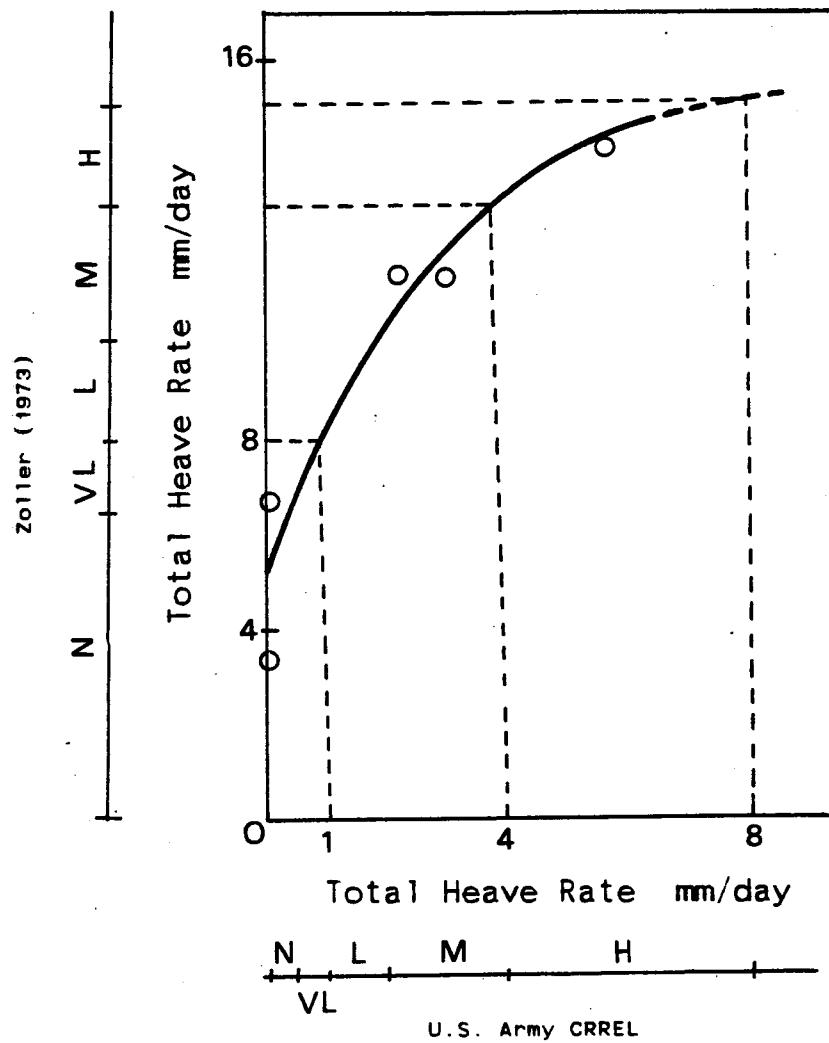
Figure 7.13 Frost Susceptibility Classification. After Zoller (1973)

susceptibility, instead of the total heave rate.

Tests using this procedure have been carried out by Loch at the Norwegian Road Research Laboratory. The cylindrical samples have a height of 10 cm and a diameter of 9.5 cm. Their cylindrical surface is coated by a rubber membrane. The sample is placed in a holder of stacked plastic rings with a height of 2 cm each. This set up is thought to nearly eliminate wall friction.

The test is carried out in a controlled temperature room at about +0.5°C. This, combined with the presence of insulation with styrofoam spheres around the sample, practically eliminates radial heat flow into the samples. The temperatures at the top and base of the sample are controlled by aluminum cooling plates in which cooled alcohol is circulated.

Most tests have been carried out with a fixed base temperature of slightly higher than 0°C and with the temperature of the top cooler dropping and levelling off at about -7°C after 24 hours. No control exists over the rates of heat extraction and frost penetration in this procedure. In this manner all samples were frozen to the bottom within 2 days.

This testing procedure is thought to be the most suitable for the determination of the frost susceptibility of various soils. However, because the thermistors are either fixed to the different rings or actually embedded in the soil, their current positions are not fixed since the

heaving soil displaces them. Despite that minor inconvenience, the procedure proposed by Loch can be used to determine the basic freezing parameters of a soil.

7.5.2 Freezing Tests with Constant Temperature Boundary Conditions

This paragraph summarizes the conclusions from the analysis of the laboratory data obtained with freezing tests carried out under constant temperature boundary conditions. The essential points of the testing procedure will be presented and some important recommendations given that will facilitate obtaining the maximum information out of one single freezing test.

The equipment of the freezing set-up is given in detail in Figures 2.1 and 2.2.

The freezing procedure is the following. Saturated samples of diameter slightly less than the cell diameter are frozen from the bottom upwards in order to reduce the effect of lateral side friction. The samples are coated with a rubber membrane. For Devon silt, it was established that when frozen from the top downwards, lateral friction was noticed when an external pressure was applied on the freezing soil. The samples have a free water supply at their warm side and can heave freely. The freezing cell is placed in a controlled temperature room at approximately $+0.5^\circ C$ to $+1.5^\circ C$. Furthermore, if the freezing cell is heavily insulated with urethane foam, radial heat flow into the

sample is negligible during an advancing frost front.

The cold plate and the warm plate temperatures are maintained constant during the complete freezing test. This procedure results then in a period of decelerating frost penetration followed by a period with a retreating frost front during which the final ice lens can grow. Thus, during one single freezing test, the rate of cooling of the current frozen fringe steadily decreases from a high value to zero.

The criterion on which frost heave susceptibility can be judged has been selected as the segregation potential at the formation of the final ice lens i.e. at a quasi stationary frost front. As established in the previous chapter, this parameter is the ratio between the measured water intake velocity and the temperature gradient across the active system at a quasi stationary frost front.

The soil is characterized by the segregation potential of the final ice lens formation, i.e. for dTf/dt almost zero. This is justified for field freezing situations, since the rate of cooling is very close to zero due to small temperature gradients. This is fully explored in Chapter 9.

However, even though the effect of rate of cooling can be neglected, the suction at the frost front remains an important factor affecting the segregation potential.

To overcome the necessity of conducting several freezing tests in order to investigate the relation between SPo and Pu two procedures can be adopted.

Firstly, if one single freezing test is carried out

with a warm plate temperature close to 0°C and if the length of unfrozen soil at quasi stationary frost front is small, it can be argued that Pu is close to zero and that SPo is very close to its maximum value. This, in turn, results in an upper bound of the heave expected in field conditions.

Secondly, if one freezing test is carried out in stages by varying the temperature boundary conditions and if during each stage, the final ice lens can grow to a visible thickness, Chapter 3 demonstrates that different suctions at the frost fronts are obtained if the warm plate temperature is different and if the temperature profile in the active system is linear. With a single freezing test, a significant range of the relationship SPo vs Pu could therefore be investigated.

It should be emphasized that the porosity of the soil tested in the laboratory should be as close as possible to that in the field. Also, it is not absolutely necessary to perform a permeability test on the unfrozen soil since the product Vo.lu represents indirectly the magnitude of the suction at the frost front.

With an additional assumption on Tso if its value can be inferred from visual observations associated with the temperature profile, it is also possible to determine the permeability of the frozen fringe from a single freezing test. This has been fully investigated in Chapter 3. Finally, it is also noteworthy to point out that if any solutes are present in the field, the segregation potential

determined from a laboratory freezing test on a soil sample with identical properties embraces the effect of solutes on the heaving processes. In general, increasing solute concentrations may be associated with decreasing values of the segregation potential.

8. NEW FROST SUSCEPTIBILITY CRITERIA

8.1 FREEZING BEHAVIOR OF VARIOUS SOILS

The variation in the freezing parameters in different soils can be summarized schematically as shown on Figure 8.1. The wide range of existing soils has been separated into three distinct classes; a coarser material group or sands, medium sized soils or silts, and fine grained plastic soils or clays.

Sands have practically no unfrozen water content below 0°C and the segregation freezing temperature is then very close to 0°C. This results in low suctions at the ice lens or at the accumulation zone. Low unfrozen water contents result also in a very low permeability of the frozen soil. Therefore, the water intake rate is usually small during freezing of sands. Expulsion of water is also possible since the effect of overburden becomes very significant in these conditions.

In general, silty soils present an unfrozen water content of approximately 10% to 20% of the total moisture close to 0°C. The unfrozen water content decreases with decreasing temperatures. The segregation freezing temperature of that class of soils, depending on the value of the permeability of the frozen soil, is much colder than
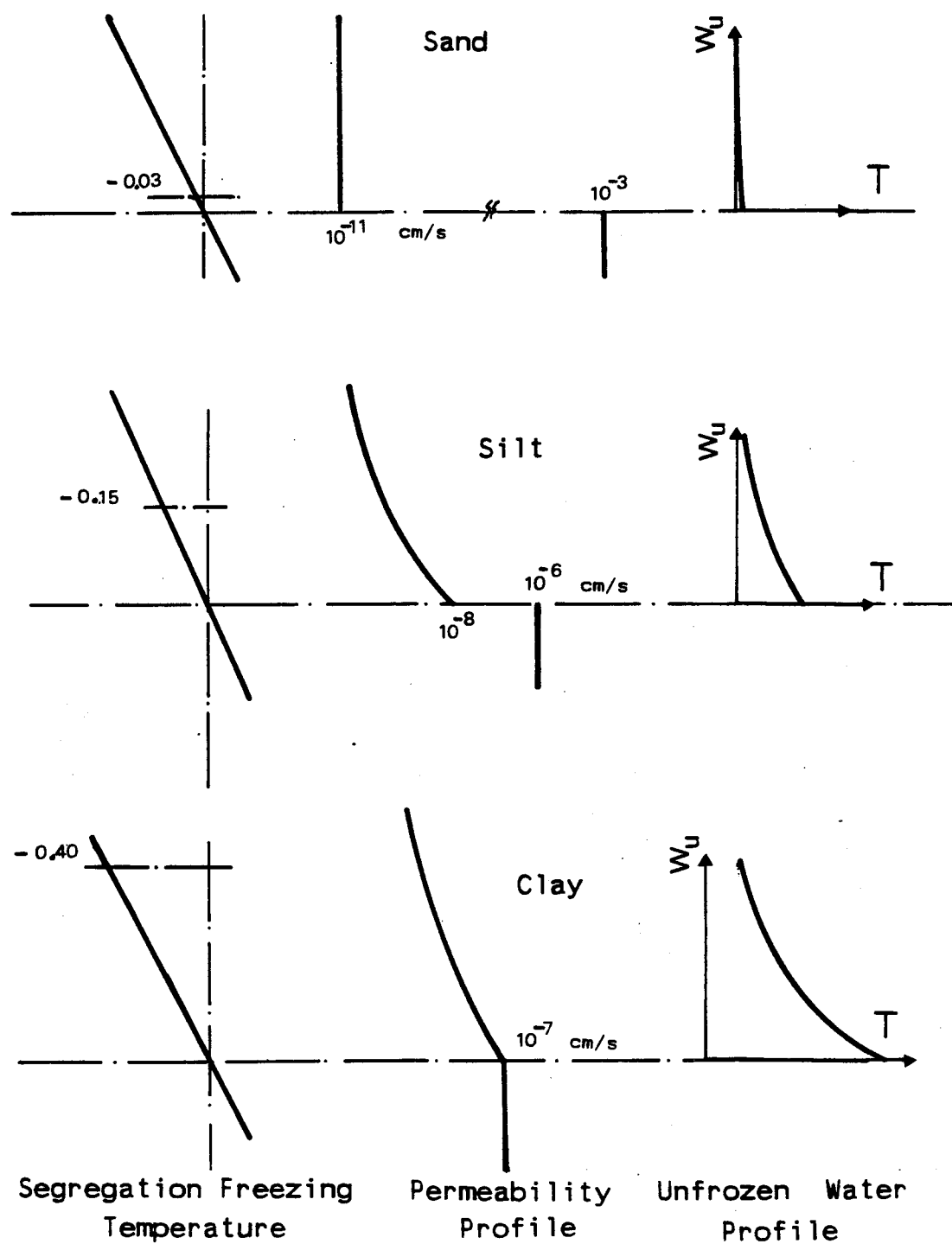
Figure 8.1   Freezing Characteristics for Various Types of Soils

for the previous soil category. The combination of relatively high suctions at the ice lens and high overall hydraulic gradient in the frozen fringe produce high segregation potentials hence highly frost susceptible soils.

In the third class of soils, i.e. clay soils, higher unfrozen water contents with a smooth transition zone over a wide range of negative temperatures result in significant segregation freezing temperatures. These temperatures range between -0.4°C to -0.8°C or may even be colder. The suction at the freezing front is then quite high. However, because of the relative low hydraulic conductivity of the unfrozen soil, the overall hydraulic gradient in the frozen fringe is significantly reduced. This, in turn, affects the water intake flux and hence the segregation potential.

The effect of applied pressure can be extended to these categories of soils. Figure 8.2 illustrates the different behavior of these three soil classes with applied pressure. One should bear in mind that the curves presented in Figure 8.2 are only schematic. Nevertheless, the general aspect that can be grasped from this figure is very close to the reality.

It appears from Figure 8.2 that the maximum heaving pressure, as defined in Chapter 6, increases significantly as the average particles size decreases. In other words, it is expected that the maximum heaving pressure in clays is much higher than that in sands. As shown in Figure 8.2, the maximum heaving pressure is directly related to the
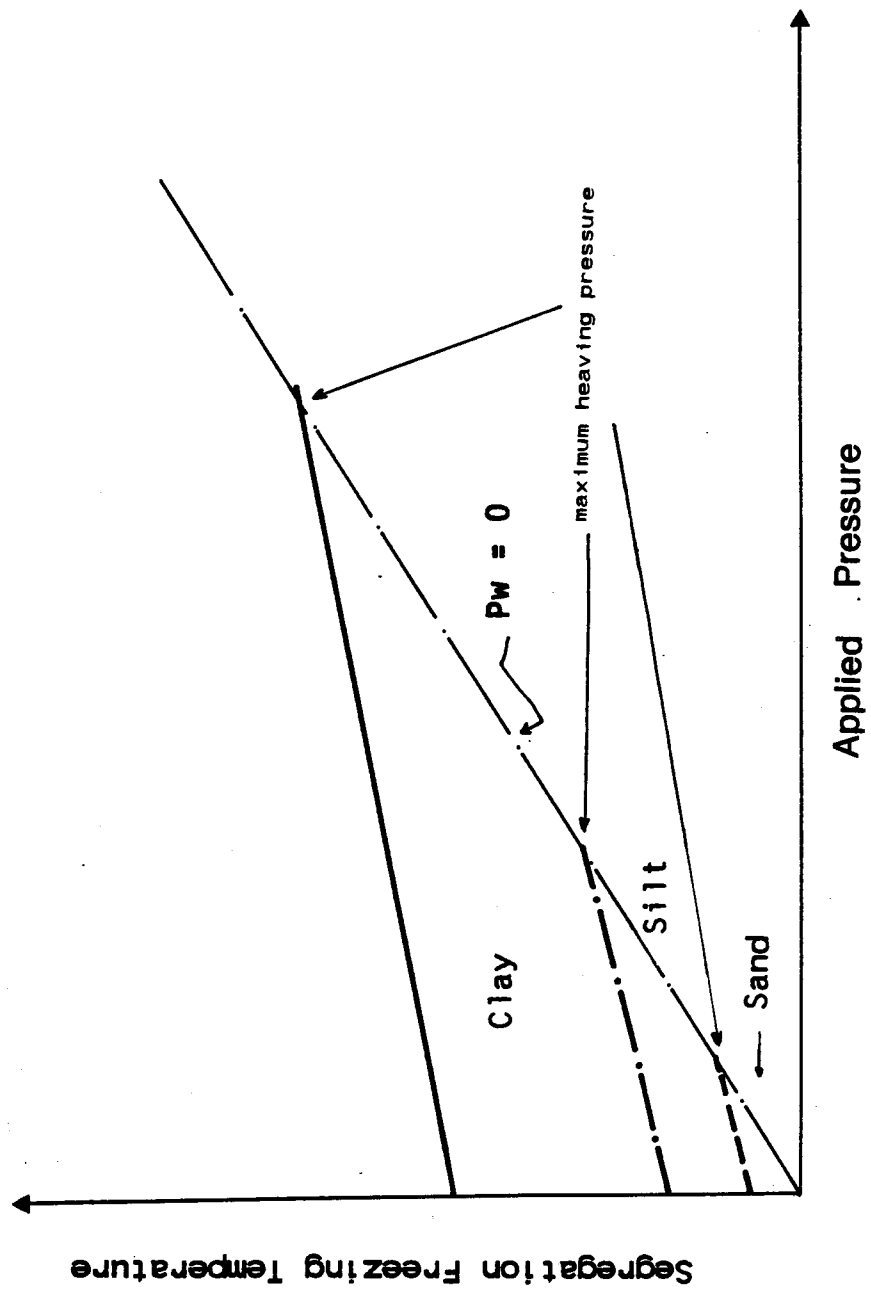
Figure 8.2   Maximum Heaving Pressure for Different Types of
             Soils

segregation freezing temperature at the formation of the final ice lens under zero applied surcharge.

Penner (1967) and Hoekstra (1969) established clearly that the maximum heaving pressure was controlled by pore and particle size, confirming thus the previous concept.

8.2 FROST SUSCEPTIBILITY DURING AN ADVANCING FROST FRONT

As discussed in Chapter 7, the segregation potential at the formation of the final ice lens, measured in a standard laboratory freezing test, is representative of the frost heave susceptibility of a soil. In order to propose a new frost susceptibility classification, the segregation potential of various soils has been calculated from the results of freezing tests reported in the current literature.

The soil used in Series S was sampled from a different location and exhibits slightly different properties as seen in Appendix A than the silt used to perform the quantitative tests in this study (series NS, E, C, D). The permeability of the unfrozen soil was inferred from the consolidation tests. A value of approximately 10^{-7} cm/s was adopted. The conditions obtained at the onset of the formation of the final ice lens are summarized in Table 8.1.
The relationship between SPo and Pu is illustrated in Figure 8.3. By comparing Figure 3.11 and Figure 8.3, it may be concluded that the freezing tests reveal changes in the

Table 8.1   Segregation Potential of the Formation
of the Final Ice Lens in Series S

Test	Tw $^{\circ}$C	Po cm	Vo 10^{-6}mm/s	grad T $^{\circ}$C/cm	SPo 10^{-5}mm^2/(S$^{\circ}$C)
S1	2.85	2.4	73.0	1.23	59
S1	1.20	1.6	61.5	0.81	76
S2	3.6	2.8	80.0	1.32	61
S5	3.4	2.6	78.0	1.35	58
S7	0.41	1.0	52.0	0.51	102

overall properties of the freezing soil. Moreover, minor

changes in the unfrozen soil properties result in quite

appreciable changes in the segregation potential. The soil

used in Series S has a smaller precentage, approximately

20%, of clay size particles than the soil used in Series NS

which contains approximately 28% clay size particles. The

maximum segregation potential obtained for Devon silt of

series S is approximately 130 x 10^{-5} mm^2/(s$^{\circ}$C) and for Devon

silt in series NS SPo is around 160 x 10^{-5} mm^2/(s$^{\circ}$C)

Analysis of the tests reported by Loch (1979) and

summarized on Figure 7.9 permits one to determine the range

of SPo for Gulli soil and Dalane soil, both disturbed

samples. For Gulli soil, which is described as a clayey

silt, SPo is found in the range of 20 x 10^{-5} to 50 x 10^{-5}

mm^2/(s$^{\circ}$C) whereas for Dalane soil, which is given as a silty

clay. SPo varies from 38 x 10^{-5} to 50 x 10^{-5} mm^2/(s$^{\circ}$C) and

over. Different suctions at the frost front are responsible

for that range. Unfortunately, total information is not
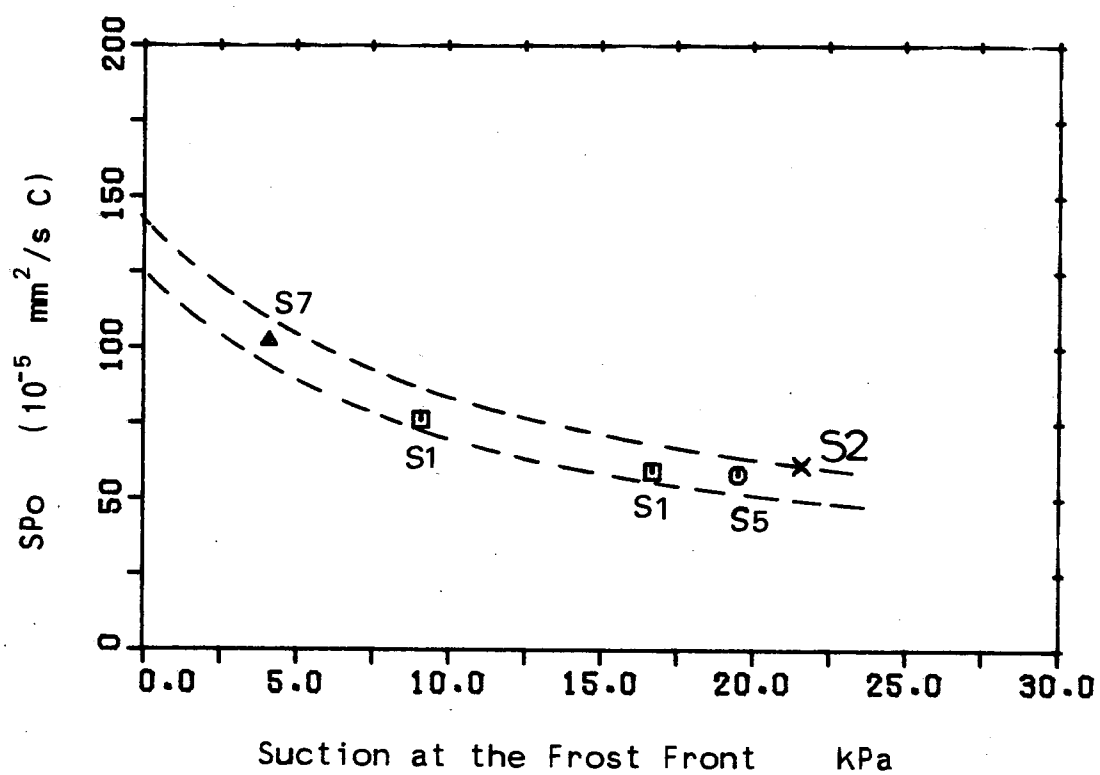
Figure 8.3 Segregation Potential for Devon Silt. Series S

available to back analyse the results of the other freezing tests. Nevertheless, it is felt that SPo is very sensitive to soil type. This is further supported by the results presented in Table 8.2.

This table summarizes some of the results that can be deduced from several freezing tests in which the basic parameters are adequately described. The values of the segregation potential corresponds approximately to the formation of the final ice lens. Since the permeability of the unfrozen soil is not given, the actual suction at the frost front cannot be inferred. However, it may be argued that the suction is close to 0 because the warm plate temperature was close to 0°C in most of the freezing tests. Table 8.2 reveals several important features of freezing soils.

Firstly, analysis of test results reported by Kaplar (1968) on New Hampshire silt, support our experimental findings that the segregation potential is independent of cold side freezing temperature if the suction at the frost front is the same. Since the samples were frozen close to their bottom, the suction at the frost front should be very close to zero in the three tests conducted by Kaplar. For these conditions, the segregation potential, as expected, was more or less constant.

Another striking point is that for the same type of soil, e.g., New Hampshire silt, an extremely wide range of segregation potentials has been found. Careful scrutiny

Table 8.2 Segregation Potential for Various Soils

Soil Type	Properties	SPo $10^{-5}mm^2/(S°C)$	%< 0.005mm	Reference	Remarks
New Hamp. Silt	WC=22%	500	12%	Hayley and Kaplar (1952)	
New Hamp. Silt	γ=100PCF ML non plastic	957 1055 966	7%	Kaplar (1968)	Tc=-3.9°C Tc=-9.5°C Tc=-12.2°C
Hutchinson Gravelly Sand	γ=140PCF SW-SM non plastic	150	2%	Kaplar (1968)	
Gravelly Silty Sand	γ=120PCF WC=12.5%	136-96	5%	Kaplar (1974)	
New Hamp. Silt	WC=45% γ=1.46 g/cm³	50	10%	Loch and Kay (1978)	
Leda Clay		150	55%	Penner and Ueda (1977,1978)	Preconsolidation pressure Pc=400KPo Applied pressure Pe=200KPo
Mackenzie Valley Silt		195	12%	Penner and Ueda(1977)	Pe=100KPe
Calgary Silt	WC=20% γ=130PCF	100-200	20%	Northern Engineering Services(1975)	Pe=14 to 24KPa
Gravels and Sandy Gravels	γ=130PCF WC=10%	5-15	1%	Kapler (1974)	Assumption on grad T

reveals changes in density and initial moisture content. This, in turn, is thought to affect both degree of compaction and amount of fines in the soil. The positive effect of the degree of compaction on heave rate was shown clearly by Penner (1959) and Zoller (1973). It is therefore possible that such a wide range can be obtained for the same, or apparently identical, type of soil. This is further evidence of high sensitivity of the segregation potential to any changes in the structure and in the chemistry of the soil.

Figure 8.4 presents a summary grouping of the few tests reported in Table 8.2 and the tests conducted by the author. It was decided to plot the segregation potential of the final ice lens formation versus the percentage of soil particles finer that 0.005 mm. This value was chosen arbitrarily and corresponds to fine silt sizes and clay sizes in the soil. It can be seen that there is no distinct grouping of the data. One should bear in mind that these points correspond to different degrees of compaction, and different structural compositions. The difficulty associated with the considerable overlap of such a relationship can easily be overcome if a standard freezing test is conducted as described in the previous section.

Based on Figure 8.4, a frost susceptibility classification can be proposed ranging from negligible to extremely high frost susceptible soils.

As pointed out by Penner (1967) the most obvious factor

is the particle size. As seen in Figure 8.4, the domain
bounding the observed data has a parabolic shape with a
maximum for approximately 10% to 20% finer particles than
0.005 mm. This result supports Penner's views. However, it
is clear that this indirect assessment of frost
susceptibility is not sufficiently reliable to overcome the
need for direct testing.
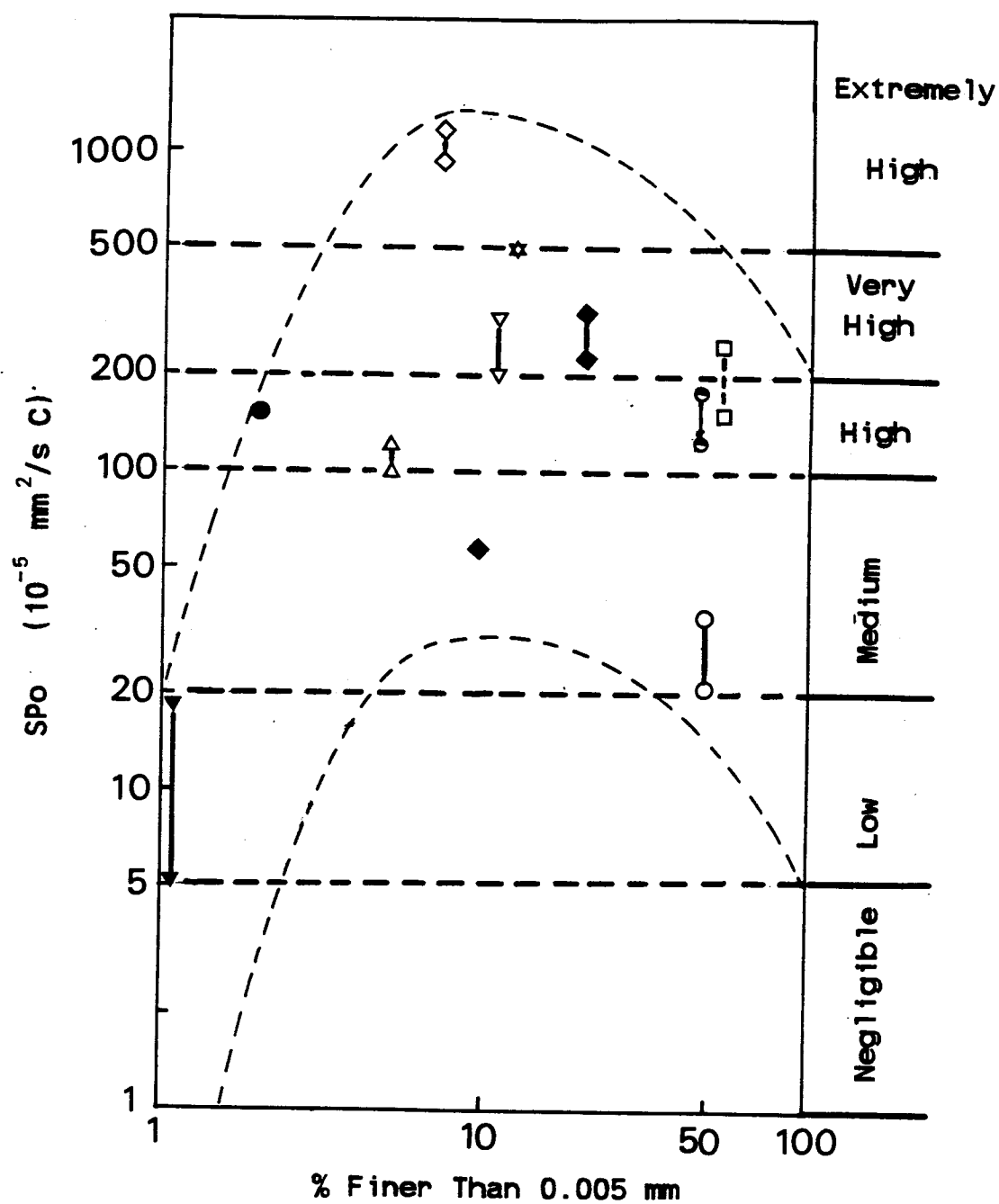
Figure 8.4   New Frost Susceptibility Classification

8.3 FROST SUSCEPTIBILITY DURING A RETREATING FROST FRONT

Figure 8.4 suggests that a silty sand and a silty clay may have the same segregation potential. If these two different types of soil would freeze under the same conditions, it would be expected that the heave at the end of unsteady heat flow would be approximately of the same order of magnitude. Slight variations should be expected due to differences in thermal conductivity and in unfrozen water content.

However, the segregation freezing temperature of the final ice lens formation is different in these two types of soil. From the earlier discussions in this thesis, it emerges that the silty sand soil has a warmer segregation freezing temperature than the silty clay since the unfrozen water contents are strongly dependent on particle size. This, in turn, influences the thickness of the final ice lens grown under fixed temperature boundary conditions , see Equation 5.4. A colder segregation freezing temperature results in a thicker frozen fringe for a given temperature gradient.

It is therefore proposed that there is an additional consideration to the previous frost susceptibility criterion derived for unsteady heat flow only. This supplementary criterion concerns the growth potential of the final ice lens during a stationary or retreating frost front situation.

Figure 8.5 is a schematic representation of the relationship between the growth of the final ice lens and segregation freezing temperatures. It is clear, that although a silty sand and a silty clay possess the same segregation potential, the maximum thickness of the final ice lens in a silty sand is much lower than that in a silty clay. Furthermore, the heaving processes may reach its stable situation, i.e. cessation of heave, much faster in silty sands than in clay soils. In that latter case, heave may continue for tens of years if the temperature boundary conditions could be maintained constant for such a long period.

However, even within a life time of a structure i.e. 30 years, significant differences due to differences in final ice lens growth may be observed.

From Figure 8.2, it transpires that a freezing test in which the maximum heaving pressure is measured indicates, in a relative manner, the magnitude of Tso for zero overburden and hence is an indication of the growth potential of the final ice lens.

Depending on the freezing condition, either natural or artificial, the engineer must decide whether the first criterion or both should be used in order to determine the degree of frost susceptibility of the soil.
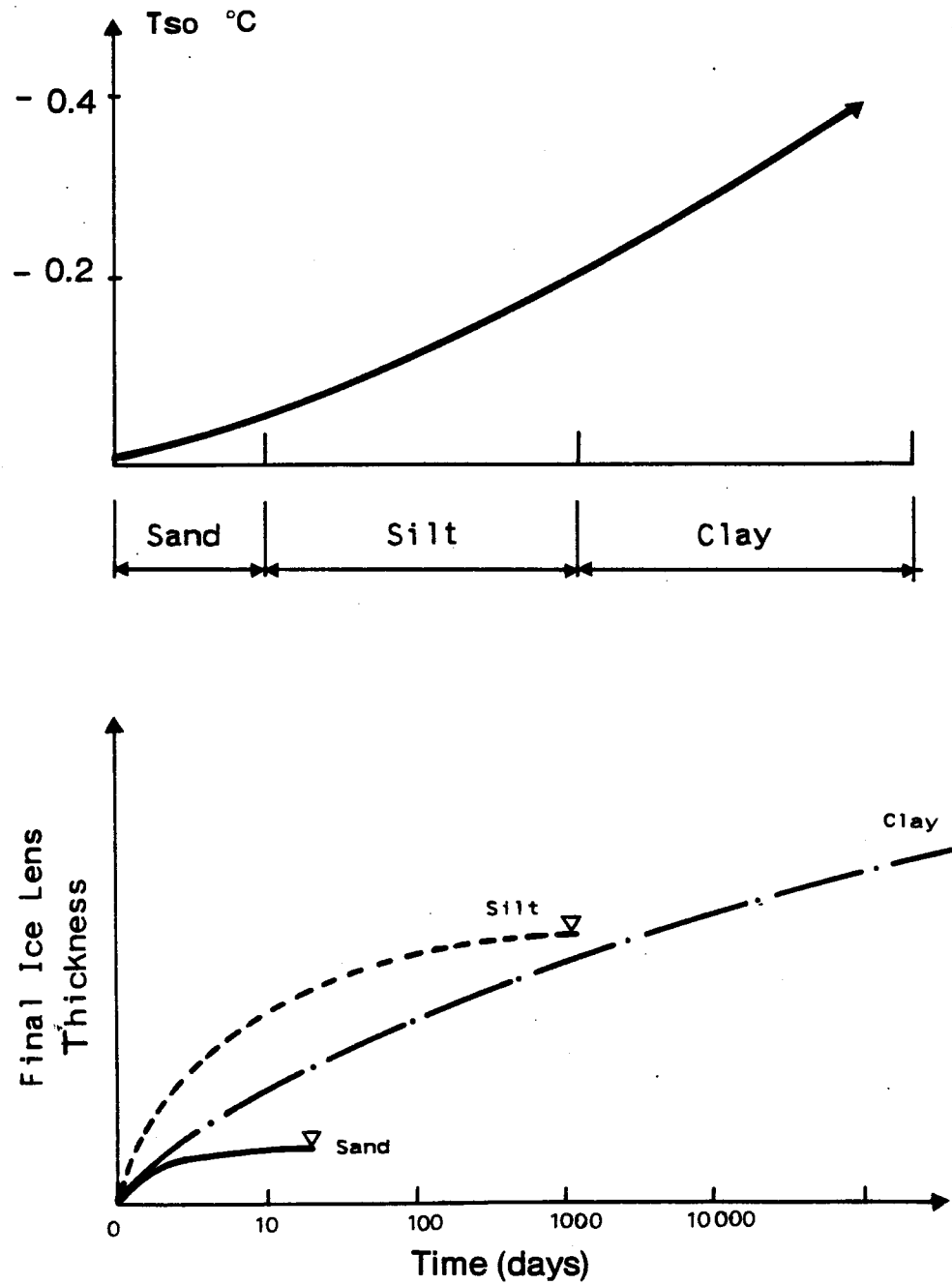
Figure 8.5   Maximum Thickness of Final Ice Lens for Various
                Soils

9. ANALYSIS OF FIELD PROBLEMS

9.1 INTRODUCTION

This chapter is devoted to the application of the results from laboratory freezing tests and the frost heave concepts established previously to some practical problems that might be encountered in the field.

In the first section, simplifications to the theory are introduced which make the solution to freezing problems more amenable. One such field situation where frost heave is of crucial importance is the construction of pipelines in Northern Canada and Alaska to carry chilled natural gas. Freezing of soil beneath the pipeline may occur for tens of years, resulting in pipeline heave in the unfrozen regions of the discontinuous permafrost zone.

A model to calculate the amount of heave under a chilled gas pipeline is presented in the following sections. This model is used to evaluate and to predict the results of a field test program reported by Slusarchuk et al (1978). The test program is concerned with the behavior of four sections under various conditions at the freezing test site.

Finally, a simple method for predicting frost heave is presented at the end of this chapter. This simple model summarizes the main points established by this thesis.

9.2 SIMPLIFIED FREEZING CHARACTERISTICS FOR FIELD CONDITIONS

Chapters 3 to 6 have dealt exclusively with laboratory freezing conditions. As established in these chapters, a freezing soil is characterized either by its segregation potential, SP, or by its segregation-freezing temperature, Ts, and by the overall permeability of the frozen fringe, Kf. These parameters are dependent upon applied pressure, Pe, suction at the frost front, Pu, and rate of cooling of the current frozen fringe, dTf/dt.

Field conditions initially may appear more complicated than controlled laboratory conditions. Many soils are fissured in their upper section and the number of fissures usually decreases rapidly with depth. The mass permeability in fissured soils may be two or more orders of magnitude higher than that of intact soil. Water percolation occurs along the fissures and small potential differences are then sufficient to drive the liquid. Therefore, the presence of fissures affects the suction at the frost front since the length of the flow in intact soil is reduced significantly. During field freezing conditions, the water flux to the freezing front is usually very small and high mass permeability results then in small suctions at the frost front. This study adopts the view that the frost heave characteristcs of a freezing soil in field conditions correspond practically to the case Pu = 0. As discussed in Chapter 3, this leads to an upper-bound for the computed

frost heave and is consequently on the safe side for engineering purposes.

In the field, the frost front may penetrate to significant depth below the water table. This, in turn, implies that high pore water pressures can exist at the frozen - unfrozen interface. This pressure at the frost front can be viewed as a back pressure which increases the free energy of both the water and the ice in the frozen fringe.The phase equilibrium is therefore not significantly affected as discussed in Chapter 2. Consequently, although a positive pore water pressure may exist at the frost front, the freezing characteristics of the current frozen fringe are very close to those obtained in the laboratory when Pu is atmospheric. Furthermore, since water is only driven under a total potential difference, the actual flow rate is not affected by the relative depth of the frost front to the water table because the static pressure or back pressure is applied everywhere in the fringe.

Another simplification for field conditions can be made with regard to the rate of cooling of the fringe. Due to the increased thickness of the frozen soil and to the reduced frost front penetration rate when comparing laboratory with field conditions, it can readily be shown that the rate of cooling of the current fringe is very small soon after the beginning of freezing. For example, if the frozen soil is 1 m thick and if the temperature gradient is 0.1°C/cm, frost penetration rates of 1cm/h and 1mm/h would produce

respectively rates of cooling of 0.1°C/h and 0.01°C/h. It is therefore argued that the soil freezing characteristics in field conditions may be approximated by the characteristics corresponding to the formation of the final ice lens obtained in standard laboratory freezing tests, i.e. when dTf/dt is close to zero.

Finally, the influence of the overburden as the frost front penetrates deeper can no longer be neglected. The effect of overburden becomes even more important if additional berms or other types of surcharge are introduced. The effect of applied load on the freezing parameters is accounted for in the following manner:

$$|Ts| = |Tso| + a.Pe \dots\dots\dots\dots\dots\dots\dots\dots\dots 9.1$$

$$\log Kf = \log Kfo - b.Pe \dots\dots\dots\dots\dots\dots\dots 9.2$$

where   Pe is the pressure at the freezing front in MPa

a is a soil constant relating the decrease in Ts to the increase in Pe.

b is a soil constant relating the decrease in Kf to the increase in Pe.

the subscript o refers to the parameters at Pe=0

Equations 9.1 and 9.2 can be obtained from laboratory freezing tests as discussed in Chapter 6. Furthermore, the constants a and b correspond to freezing tests in which Pu = 0 and to the formation of the final ice lens, i.e. dTf/dt close to zero.

It will be shown that the complex relationships between Ts and Kf or SP and (Pu, dTf/dt, Pe) obtained in laboratory

freezing tests can be reduced to a very simple relationship between the freezing parameters and Pe in the case of field conditions.

9.3 ANALYSIS OF THE PERFORMANCE OF A CHILLED PIPELINE AT CALGARY, ALBERTA

In order to study the behavior of a chilled, large-diameter gas pipeline buried in frozen frost susceptible soil, a field test facility was constructed by Northern Engineering Services in Calgary, Alberta in 1973. Four test sections using 1.22 m diameter pipe were buried in a frost susceptible silt, and have been maintained at a temperature of -8.5°C for about 7 years and is still operating. The results of these full-scale tests are given by Slusarchuk et al (1978) and detailed data can be obtained from the interim report presented by Northern Engineering Services Company limited in (1975).

9.3.1 A Frost Heave Model for Freezing Under a Pipe

9.3.1.1 Advancing Frost Front

The specific geometrical conditions of freezing under a chilled gas pipeline governs the formulation of the heat flow that must be considered in the frost heave model. The general equations of heat and mass transfer should be formulated in a two dimensional space for the case of freezing around a pipe. However, it is convenient to

approximate the total heave occurring beneath the centerline of the pipe by a simplified model which assumes radial heat flow.

The general non-dimensional form of the equation of heat conduction in cylindrical polar co-ordinates (r, θ, z) reduces to the two dimensional equation for the case where T is independent of z:

$$1/\alpha(dT/dt) = d^2T/dr^2 + 1/r(dT/dr) + 1/r^2(d^2T/d\theta^2) \ldots 9.3$$

where α is the thermal diffusivity of the medium.

The sector beneath the pipe shown in Figure 9.1 is one of circular symmetry along the centerline which results in $d^2T/d\theta^2 = 0$ and Equation 8.1 simplifies to:

$$1/\alpha(dT/dt) = d^2T/dr^2 + 1/r(dT/dr) \ldots\ldots\ldots\ldots\ldots\ldots 9.4$$

In a freezing soil, Equation 9.4 holds independently in the frozen soil and in the unfrozen soil. Both continuity of temperature and heat flux must be satisfied at each boundary. For the case of radial heat flow beneath the pipe, the mathematical formulation for the boundary conditions is:

$$T = Tc \text{ for } r = ro$$

$$T = Ti = 0°C \text{ for } r = X(t) + ro$$

$$T = Tw \text{ for } r = ro + X(t) + Z(t)$$

at the 0°C isotherm, per unit area:

$$kf.grad \ Tf = ku.grad \ Tu + V.L + \epsilon.n.L.dX/dt$$

The heat-conduction equations are solved numerically using the finite difference scheme proposed by Crank and Nicholson (1947). The moving boundary condition associated with the penetration of the frost front is accounted for by

a supplementary node at the frozen-unfrozen interface. As illustrated in Figure 9.1, the nodes are unequally spaced in the frozen zone due to frost heave and equally spaced in the unfrozen soil. Tw represents the initial ground temperature which is assumed constant at large depths. The details of the finite difference formulation are summarized in Appendix F.

Water flux to the freezing front is calculated using Darcy's law for the two layered medium composed of the frozen fringe and the intact unfrozen soil:

$$V = (Hw/l)K' \dots\dots\dots\dots\dots\dots\dots\dots\dots\dots\dots\dots\dots 9.5$$

where $K' = 1/(lu/Ku + d/Kf)$

$d = Ts/grad\ Tf$

$Hw = Pw/w = (L/Vw.\gamma w)\ ln\ Ts*/To* + (Vi/Vw.\gamma w)Pe$

l is the length of the active system

lu is the length of intact unfrozen soil between the frost front and the closest fissure.

Ts and Kf are obtained from Equations 9.1 and 9.2. The frost heave model accounts for variable length of the flow path in intact unfrozen soil which allows one to model changes in permeability. However, since Ku is two or three orders of magnitude larger than Kf, the water flux is not very sensitive to variations in lu.

When the soil is not fissured, i.e. fat clays, the length of the flow path in the unfrozen soil significantly increases. Equation 9.5 is still valid but the characteristics of the frozen fringe no longer correspond to
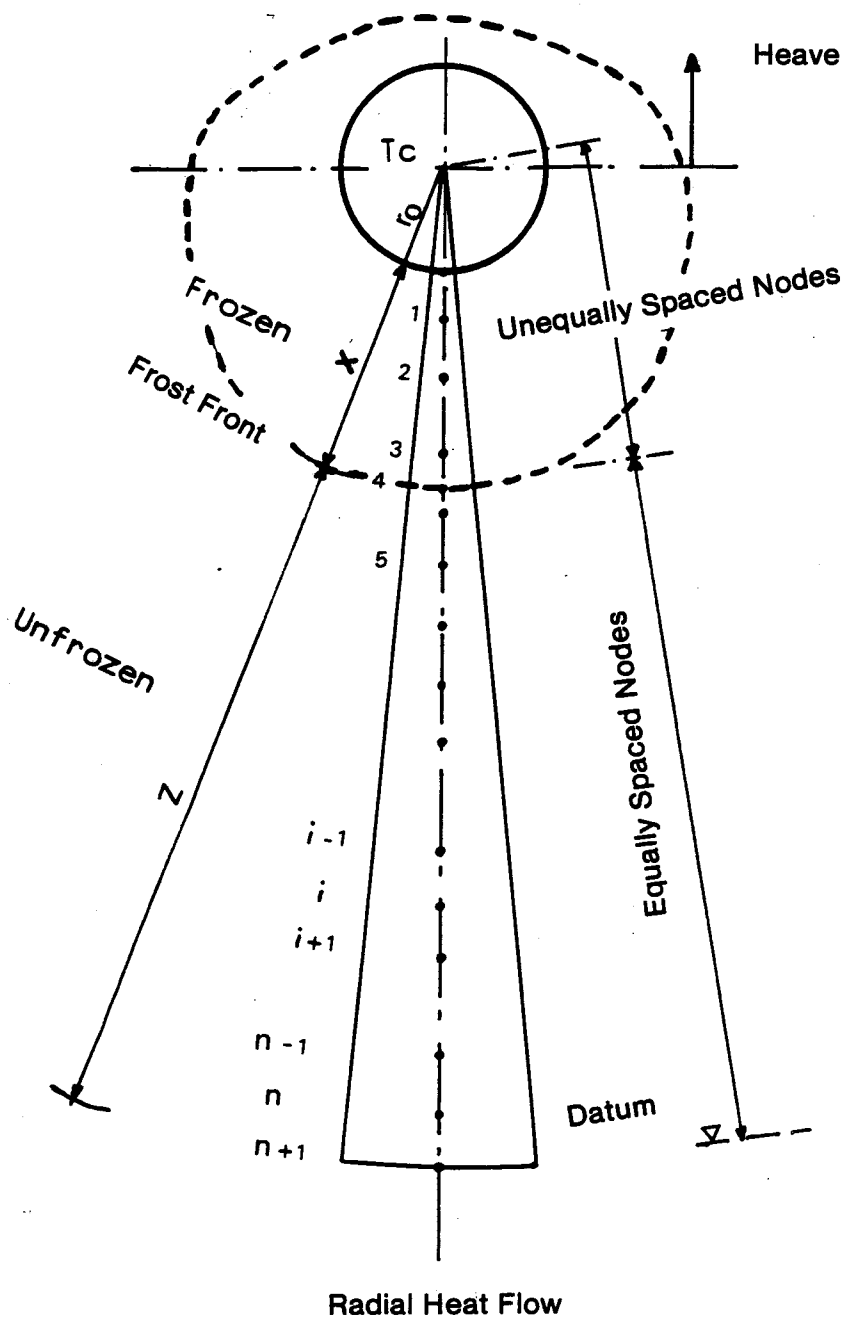
Figure 9.1   Conditions Associated with Freezing Under a Pipeline

Pu=0. An adequate frost heave computation therefore requires use of the freezing characteristics corresponding to the actual suction at the frost front. For complicated geometrical conditions, this suction may be calculated from a conventional seepage analysis and used as input to the frost heave model.

The previous frost heave model evaluates the pressure at the freezing front as follows:

$$Pe(t) = Pov + \gamma_f \cdot X(t) + Pad \dots\dots\dots\dots\dots 9.6$$

where   Pov is the initial overburden pressure

γ_f is the unit weight of the frozen soil

Pad is an additional pressure

This additional pressure must be introduced when the surcharge is increased either by the placement of a berm during freezing or by restraining loads applied during freezing by means of hydraulics jacks and reaction piles. Pad is a function of time since the width of the frost bulb changes with time. The plan area of the bulb, A, also changes and the vertical stress Pad can be calculated from:

$$Pad(t) = External\ Load/A(t) \dots\dots\dots\dots\dots 9.7$$

9.3.1.2 Retreating Frost Front

When the temperature boundary conditions are fixed with time, the frost front reaches a maximum penetration after a given freezing period. This coincides with the growth of the final ice lens during which the frost front retreats.

The results established in Chapter 5, namely that the

heat balance at the ice lens governs the magnitude of the
heave rate, is also adopted for field conditions. However,
due to the geometry of the problem, the equations used to
determine the maximum thickness of the final ice lens are
more complicated.

The temperature distribution in the frozen and unfrozen
zone is given by the steady state distribution around a
cylindrical heat source as a function of radius r as:

$$T = Ta - (Ta-Te) \ln(r/ro)/\ln(Re/ro) \dots\dots\dots\dots 9.8$$

where   Ta is the temperature at the inner surface

Te is the temperature at the outer surface

ro is the inner radius

Re is the outer radius

The temperature gradient at any point within the
cylinder is obtained by taking the derivative of T with
respect to r in Equation 9.8:

$$dT/dr = -(Ta-Te)/(r.\ln Re/ro) \dots\dots\dots\dots 9.9$$

Equation 9.8 gives

$$|grad\ Tf| = -Tc/(Ro.\ln Ro/ro) \dots\dots\dots\dots 9.10$$

where   Ro = ro+X

Te = 0°C

Ta = Tc

$$|grad\ Tu| = -Tw/((ro+X)\ \ln R/ro+X) \dots\dots\dots\dots 9.11$$

where   R = ro+X+Z

Ta = 0°C

Te = Tw

The ultimate heave is obtained when the suction at the base of the ice lens reaches zero. As established in Chapter 6, the temperature at the ice lens is then related solely to the pressure in the ice lens by:

$$Tse = -Pe.Vi.To*/L \dots\dots\dots\dots\dots\dots\dots 9.12$$

Equation 9.12 signifies that when the temperature at the base of the ice lens reaches Tse, the pressure in the liquid film beneath the ice lens is atmospheric and water flow to the ice lens ceases.

Figure 9.2 illustrates the conditions at the beginning and at the end of the retreating frost front phase. The position of the final ice lens is a function of both temperature distribution and applied pressure as indicated in Equation 9.1. The maximum thickness of the final ice lens can be obtained from Equation 9.13 which represents the condition of thermal balance at t of the terminal phase:

$$kf.|Tc-Tse|/(R1.\ln R1/ro) = ku.|-Tw+Tse|/(R1.\ln R2/R1)..9.13$$

where   R1 = ro + Xs +e

R2 = ro + Xs + e + Zs

Zs is the length of unfrozen soil at the beginning of the retreating frost front phase

Xs is the length of frozen soil at the beginning of the retreating frost front phase

e is the maximum thickness of the final ice lens

In Equation 9.13, e is the only unknown and the solution can readily be found with an iterative method using a computer analysis as shown in Appendix F.
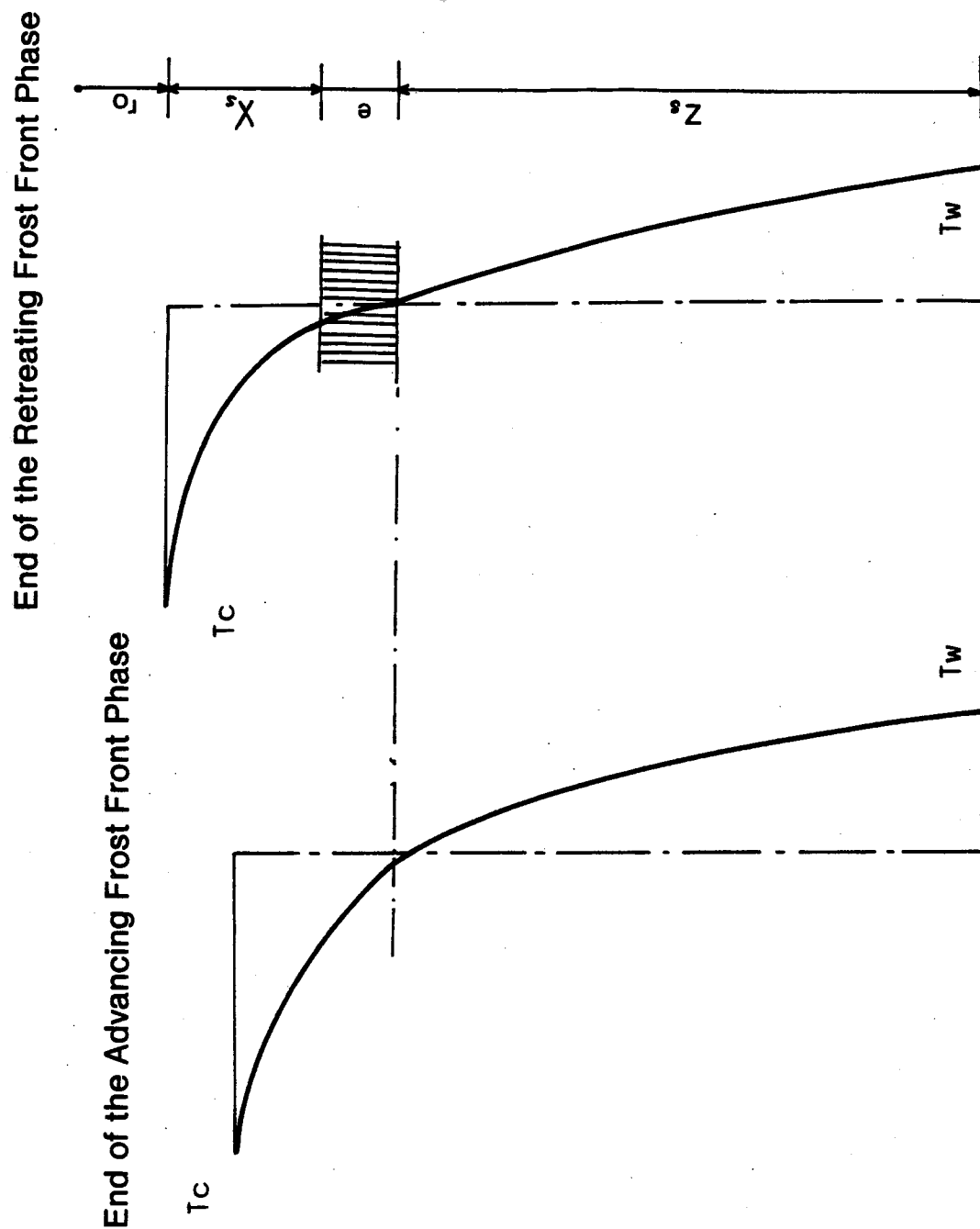
Figure 9.2   Temperature Distribution beneath the Pipe During
the Terminal Phase of Freezing

The heave vs time relationship during the terminal phase is calculated by adopting the same assumptions as those made in the model for one dimensional frost heave in laboratory simulations. This is to say that 100% heave has occurred when the temperature at the ice lens reaches Tse and that 50% heave has occurred when the temperature at the base of the final ice lens is equal to (Ts + Tse)/2.

9.3.2 Site Conditions and Soil Properties

The moisture content of the test facility soil varied between 18 and 22% and the plastic limit of the soil between 14 and 18% with a liquid limit of 24 to 31%. Grain size distributions were determined from samples of soil from different depths and showed that, in general, the soil contained 13% sand sizes, 64% silt sizes and 23% clay sizes.

The depth to the free ground water table was monitored in open standpipes and in August 1973 was found to lie between 2.3 and 2.6 m below original ground surface. The results of *in-situ* field permeability tests indicated that the Darcy coefficient of permeability was between 0.6 and 1.10^{-4} cm/s. Visual inspection of undisturbed Shelby tube samples indicated that a number of fissures were present in the soil.

Northern Eng. Services Ltd. (1975) conducted a series of laboratory freezing tests on remoulded and undisturbed Calgary silt. The freezing temperature, Tc, applied on the surface of the specimen was maintained constant during a

freezing test. However, as in Penner and Ueda's (1977)
tests, the warm plate temperature was not controlled and
decreased with time. This accounts in most tests for the
continuous advance of the frost front. Furthermore, as
established in Chapter 6, an advancing frost front
associated with a pressure at the freezing front may create
water expulsion. Therefore, in some tests where the frost
front did not reach a stable position and where Pe is
relatively high, the tests results should be used with
caution.

Figure 9.3 presents the results of the analysis of the
freezing tests reported by Northern Eng. Services (1975) in
terms of permeability of the frozen fringe at the formation
of the final ice lens. Since the length of unfrozen soil at
the end of freezing was very small, it is argued that the
calculated parameters of the frozen fringe correspond to Pu
= 0. Furthermore, since the properties of Calgary silt are
very close to those of Devon silt and since it was not
possible to infer Ts from the reported results, it is
assumed that the relationship Ts-Pe established for Devon
silt is also very close to that for Calgary silt. It is
clear that this difficulty could be avoided by considering
the segregation potential. However, the model used to
predict the growth of the final ice lens requires the value
of Ts and Tse. Furthermore, it has been demonstrated in
Chapter 3 that the calculated permeability of the frozen
fringe is not sensitive to the value of Ts.
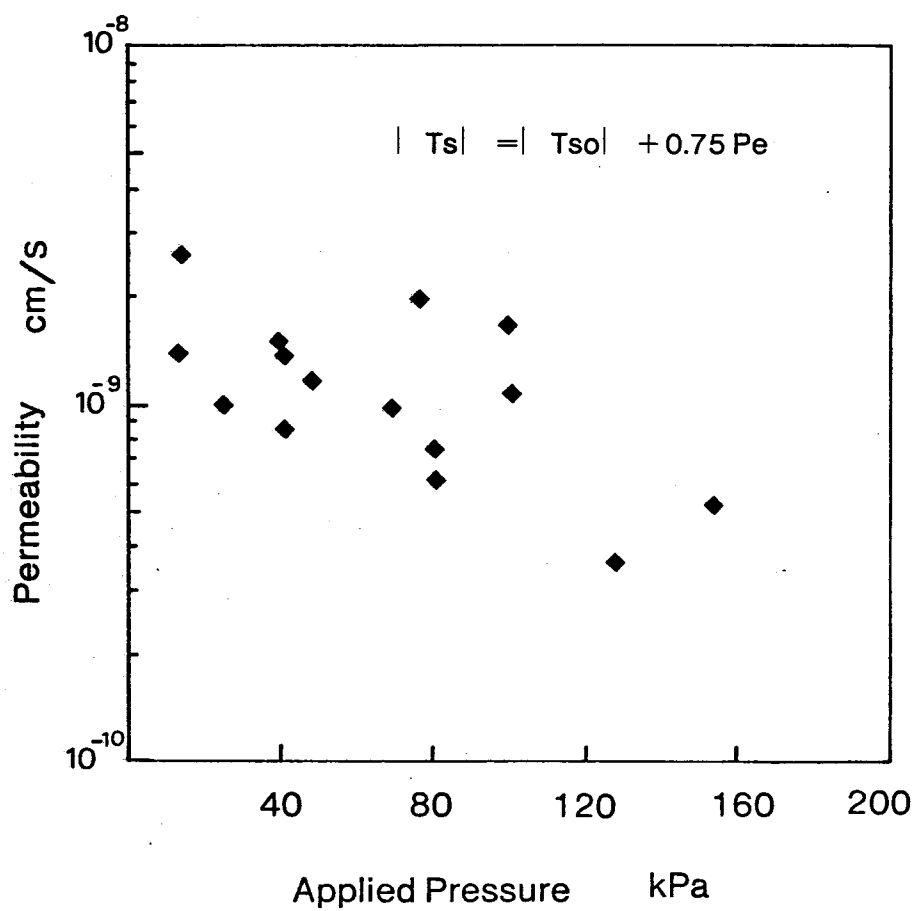
Figure 9.3   Results of the Analysis of Freezing Tests
Reported by Northern Eng. Services (1975)

The results plotted on Figure 9.3 show significant scatter. This scatter arises from several factors. The most important one is the variation of the suction at the frost front in different freezing tests. Another source of this scatter is the variation of type of freezing, i.e. stationary frost front or continually advancing frost front. Finally, the quality of testing and testing procedure may be questionable.

Despite the scatter, the data plotted on Figure 9.3 show a similar trend for the relationship between Kf and Pe obtained for Devon silt, namely that Kf decreases with increasing Pe.

9.3.3 Comparison of the Freezing Characteristics in Field and Laboratory Conditions

This section considers the hypothesis that the characteristics of the frozen fringe under field conditions are identical with those developed under laboratory conditions when Pu = 0 and at the formation of the final ice lens.

In order to verify this previous statement, the freezing conditions of the control section, which was buried 0.75 m below nominal ground surface were simulated using the field frost heave model. The parameters Kfo and b in Equation 9.2 were varied in order to fit best the experimental heave-time relationship. The other input parameters necessary to solve the heat and mass transfer formulation were taken from the

interim report (1975).

The ground temperature was inferred from the thermistors readings and taken as +6.5°C. This temperature was considered constant at a depth of 15 m below the original position of the pipe's base. From Equation 9.8, it can readily be shown that the temperature distribution in the upper part of the soil is not very sensitive to changes in initial length of unfrozen soil greater than 15 m.

The temperature in the pipe was maintained at about -10°C by circulating chilled air through the pipes. In reality, the temperature in the pipe varied between -10°C and -7°C with fluctuations in ambient atmospheric temperature. A mean value of about -8.5°C was adopted for the simulation. Furthermore, during the first 50 days of freezing, the pipe temperature was assumed to decrease linearly from -3.2 to -8.5°C.

The thermal conductivities of the frozen soil and the unfrozen soil were taken respectively as 1.8 W/(m°C) and 1.5W((m°C). The quantity of unfrozen water remaining in the frozen soil was taken as 10% of the initial water content.

The initial overburden pressure was estimated to be approximately 11 kPa. After 400 days, a berm was added on the top of the pipe which increased the stress on the freezing bulb by approximately 6.4 kPa.

Since the water table was at the same level as the base of the pipe, the soil was assumed to be fully saturated with a porosity of about 0.38. The permeability of intact

unfrozen soil was taken as 0.15×10^{-5} cm/s.

The relationship between Ts and Pe is given by Equation 8.1. The coefficient a is identical to that for Devon silt and is 0.75 °C/MPa.

Figure 9.4 summarizes the results obtained from the frost heave simulation with different values of the parameters Kfo and b. An initial conclusion from these results in Figure 9.4 is that the heat-conduction problem has been adequately formulated since the frost front advance with time agrees very well with the measured position of the 0°C isotherm.

It is important to stress that the actual position of the frost front was determined by means of temperature measurements and that a check by drilling was also performed, which increases significantly the reliability of the results of the reported field tests. It is noteworthy to recall that, in this thesis, the position of the frost front is taken with respect to the initial position of the base of the pipeline. This is similar to laboratory tests in which the location of the 0°C isotherm was taken with respect to the initial height of the specimen. The frost front given in the report by Northern Eng. Services refers, in reality, to the thickness of the frozen soil beneath the pipe which includes total heave. The thickness of the frozen soil is easily obtained by adding both total heave and frost penetration. The advantage of taking the depth of the frost front with respect to the original position of the pipe lies
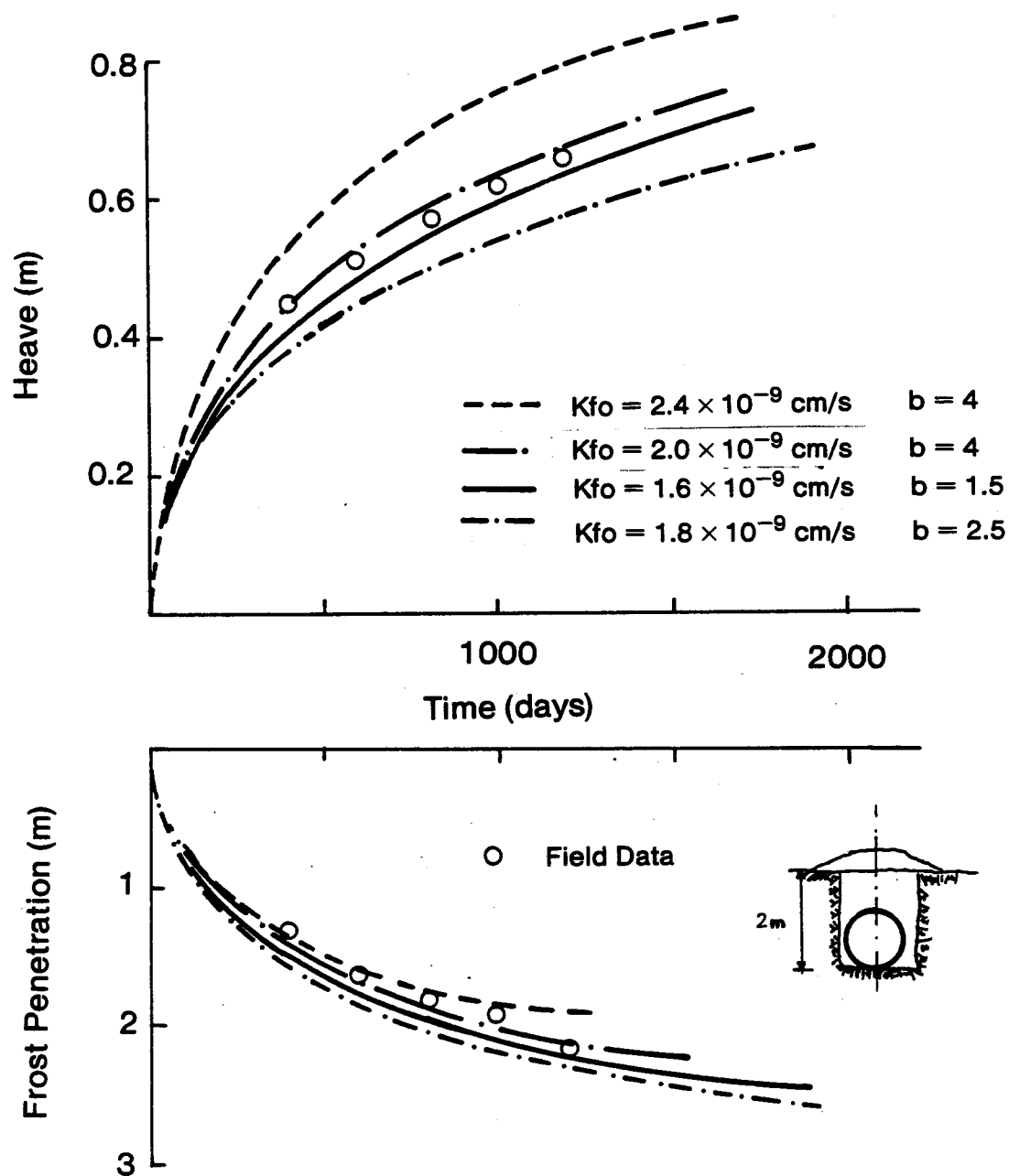
Figure 9.4 Best Fit for the Results at the Control Section

in the fact that the different phases, advancing and retreating frost line, are readily observable.

The model analysis reveals that unsteady heat flow associated with an advancing frost front occurs for about 2000 days or 5.5 years. The maximum frost penetration is approximately 2.3 m. This, in turn, produces a stress at the freezing front of about 52 kPa, which is relatively low. It is interesting to note that in that small stress range, actual frost heave can be fitted by a number of different relationships between Kf and Pe. If the stress range is larger, this is no longer the case as seen in Figure 9.5.

If the relationships Kf - Pe obtained from the back analysis of the results of the control section are plotted on the same graph as an expected laboratory relationship for this material given in Figure 8.3, both the field and laboratory freezing parameters will fall within an acceptable range. This is clearly illustrated on Figure 9.5.

The computer model also indicates that the rate of cooling of the current fringe was less than 0.01°C/h after about 40 days. This result justifies therefore the use of the freezing parameters at the formation of the final ice lens obtained in laboratory freezing tests with constant temperature boundary conditions.

9.3.4 Variations in Freezing Characteristics in Field Conditions

Variable soil conditions along the pipeline
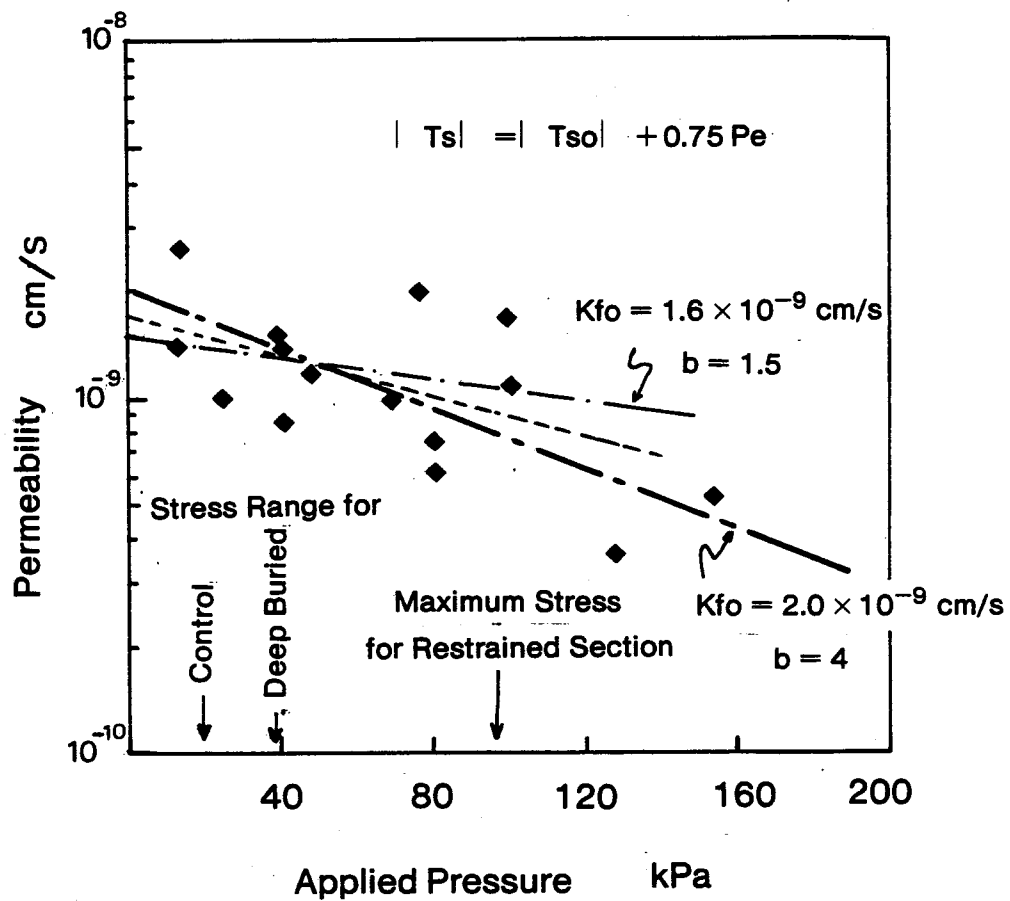
Figure 9.5 Comparison of Frost Heave Characteristics in
Laboratory and Field Conditions

signigicantly influence the amount of heave during the initial freezing period. This is apparent from the results of the control section where total heave profiles along the pipeline show differences at both ends of the pipeline as shown in Figure 9.6. However, it is interesting to note that these heave profiles remain more or less parallel after about 100 days. This indicates that differences occur during the first 100 days and thereafter heave and heave rates are quite uniform along the pipeline. Figure 9.7 illustrates these observations.

This high sensitivity of heave during a short period is thought to be associated mainly to variations in the fissure pattern, which results in variation in the length of flow path in intact unfrozen soil. This, in turn, produces variations in suctions at the frost front and hence in the freezing characteristics. Furthermore, during the early stage of freezing, higher rates of cooling increase the sensitivity of the freezing parameters with respect to suction at the frost front. Therefore, during the early stage of freezing, the simple field frost heave theory will be associated with these limitations.

For these reasons, a maximum value of frost heave or an upper bound can be computed for each case by considering that the permeability of the frozen fringe is given by Equation 9.2. In order to investigate the effect of changes in the permeability of the current fringe during the first 100 days of freezing, it is possible to adopt a simple
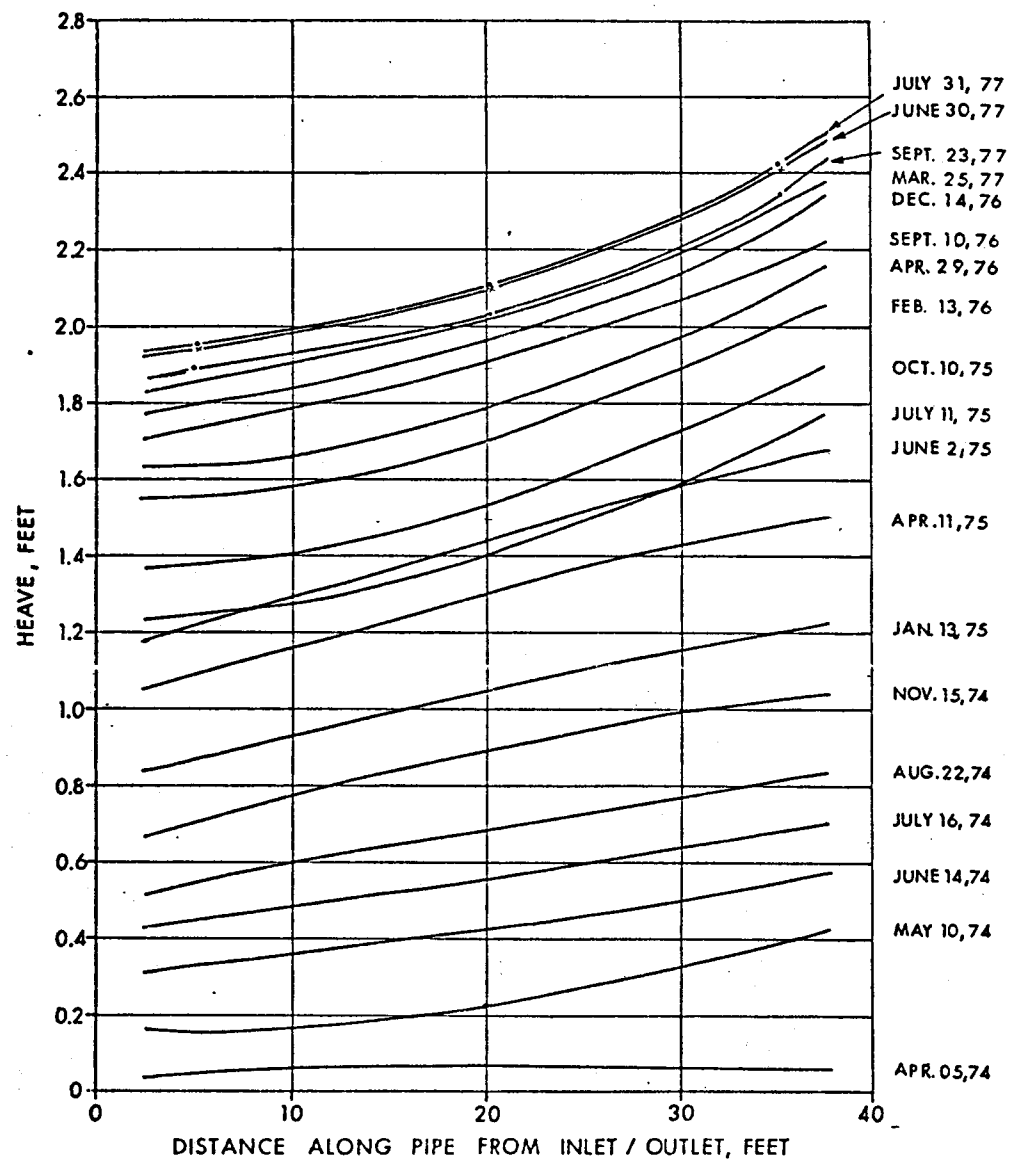
Figure 9.6   Heave Profiles along Pipe at Control Section
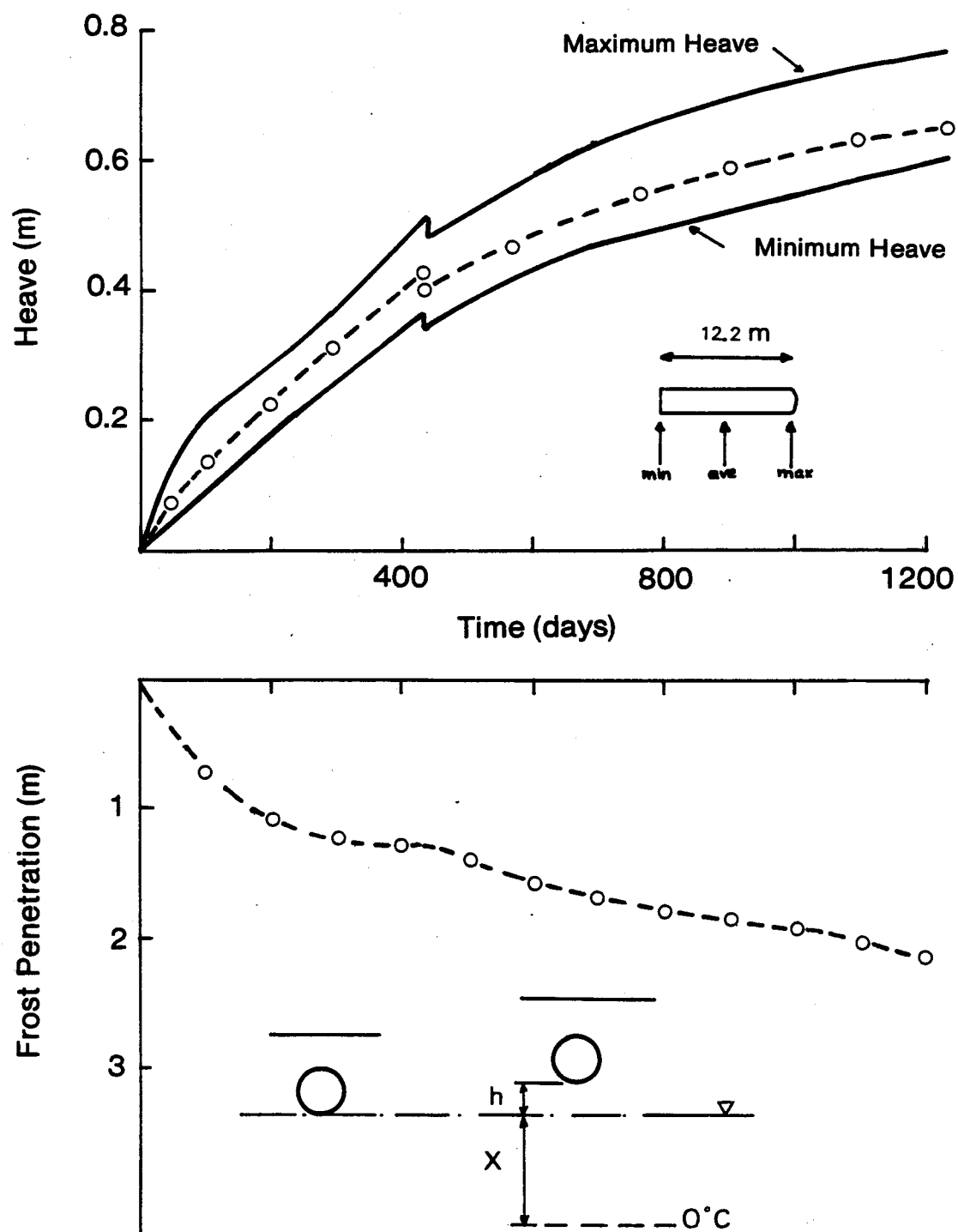
Figure 9.7   Variation in Heave along the Control Section

expression for this variation :

$$Kf(t) = (s + (1-s).t/100)Kf \dots\dots\dots\dots\dots9.13$$

where   t is the elapsed time in days

Kf is obtained from Equation 9.2

s is a dimensionless constant specifying the rate

of change in permeability.

Figure 9.8 shows the variation of total heave and frost penetration for the control section for different values of s. This graph demonstrates that variable freezing characteristics of the frozen fringe during the early stages of freezing can significantly affect the shape of the relationship between total heave and time.

9.3.5 Prediction of Heave in the Case of Deep Burial, Gravel Pad and Restrained Pipeline

It is now of benefit to investigate if the field frost heave model can be used to correctly assess the amount of heave for different test sections. Four separate sections of pipe, each 12.2 m long, were buried under different conditions at the test facility. These conditions were represented by the control, deep burial, restrained and gravel sections.

The pipe at the deep burial section was buried 1.68 m below nominal ground surface. The effect of the additional overburden on the rate of heaving was investigated at this section. At the restrained section, the pipe was buried 0.75 m below nominal ground surface similar to the control
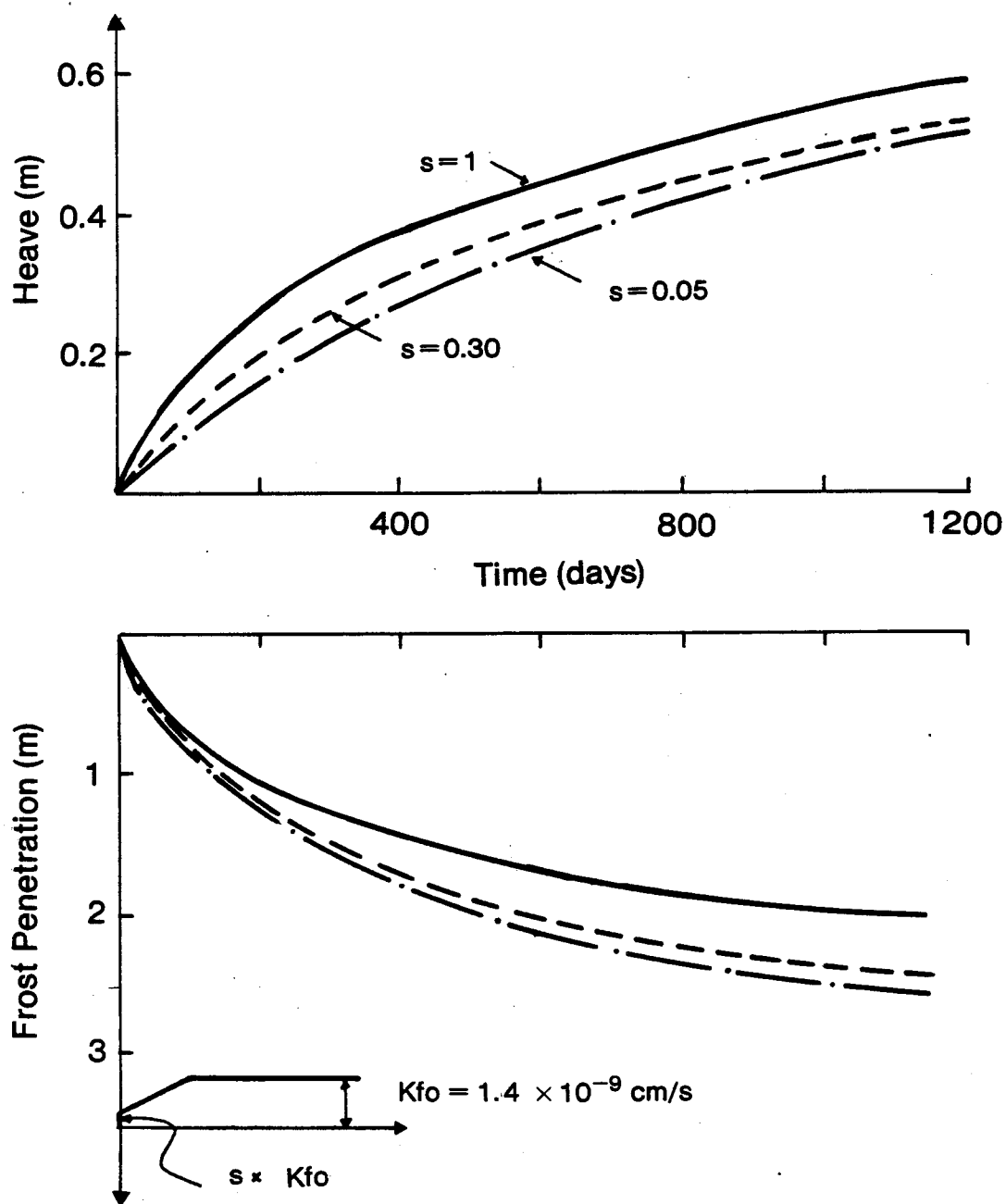
Figure 9.8   Variation in Heave for Different Values of s.
Control Section

section. The pipe at this section could be restrained by any desired constant load. At the gravel section, the pipe was also buried at 0.75 m below ground surface. However, the trench was dug 1m deeper and backfilled with gravel so that the pipe rested on a 1m layer of gravel. The effect of replacing the frost susceptible soil directly under the pipe with non frost susceptible soil was studied at this section.

In those three sections, the stresses at the freezing front are higher than those obtained in the control section and are approximately 60 to 150 kPa. The freezing parameters will therefore be taken as $Kfo = 2.0 \times 10^{-9}$ cm/s and b = 4 cm/s.MPa. As shown on Figure 9.5, this relationship is a good approximation of the laboratory freezing results over this large stress range. Moreover they are also best fit to the Control Section behavior.

The initial overburden for the deep burial section is 18 kPa, for the gravel section 34 kPa, and for the restrained section 11 kPa. The loading history for the restrained section is given in Figure 9.11. For both the gravel and the deep burial sections a surface berm has been added which increases the stress at the frost bulb by about 6.4 kPa after 400 days of freezing.

The results of the computer simulation are summarized on Figures 9.9 to 9.11 and compared with actual field measurements, which correspond to 1600 days of freezing (Morgenstern, 1980). An upper bound is obtained by considering Kfo constant during the whole freezing phase.

However, due to rapid freezing in the early stage, a more realistic heave has been computed by allowing a linear variation of Kf during the first 100 days. This is achieved by taking a value of s between 0 and 1.

Figure 9.11 illustrates the simulation of the restrained section for different freezing parameters. The field data indicate clearly that considerable differential heave along the pipe section occurred. The maximum heave can be closely predicted if, in addition to the freezing parameters deduced from laboratory tests and from the results obtained for the control section, a value of s equal to 0.15 is used. However, the minimum heave is closely predicted if the permeability of the frozen fringe is taken as $Kfo = 1.1 \times 10^{-9}$ cm/s and b = 4 cm/s.MPa.

Inspection of these figures demonstrates that the field frost heave model adequately predicts both total heave and frost front penetration for a variety of conditions.

The previous analysis also reveals that for the temperature conditions at the Calgary test site, an advancing frost front occurs for about 1500 to 2500 days, which also compares well with observations.

The excess pore pressure immediately beneath the frost front along the center line of the pipe can also be predicted by the model. For the control section, the negative excess pore pressure beneath the frost line was calculated to be in the range of -0.8 to -0.2 kPa. The frost heave model predicts that the negative pore pressure reduces
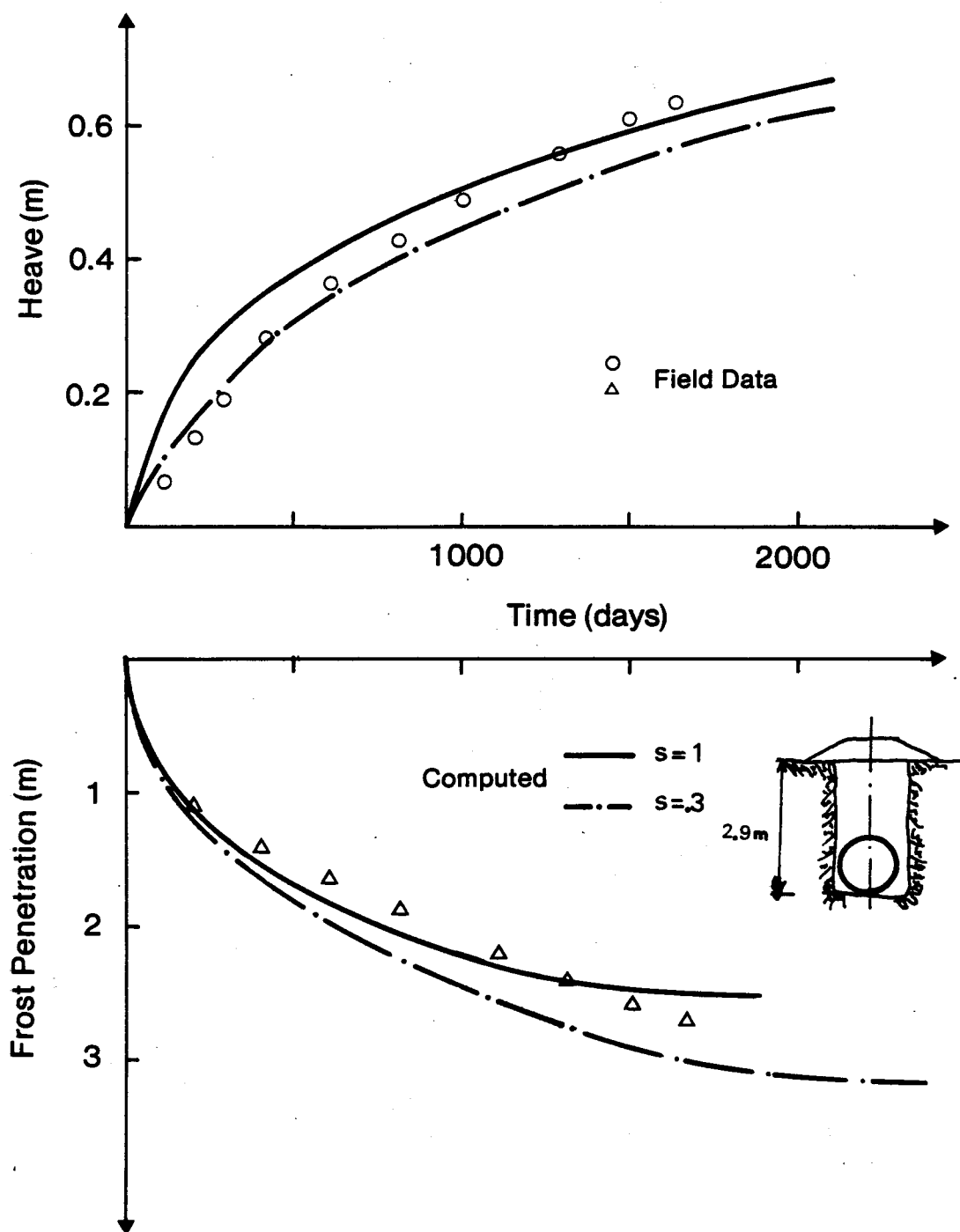
Figure 9.9   Comparison of Prediction with Actual Field Data
at the Deep Burial Section
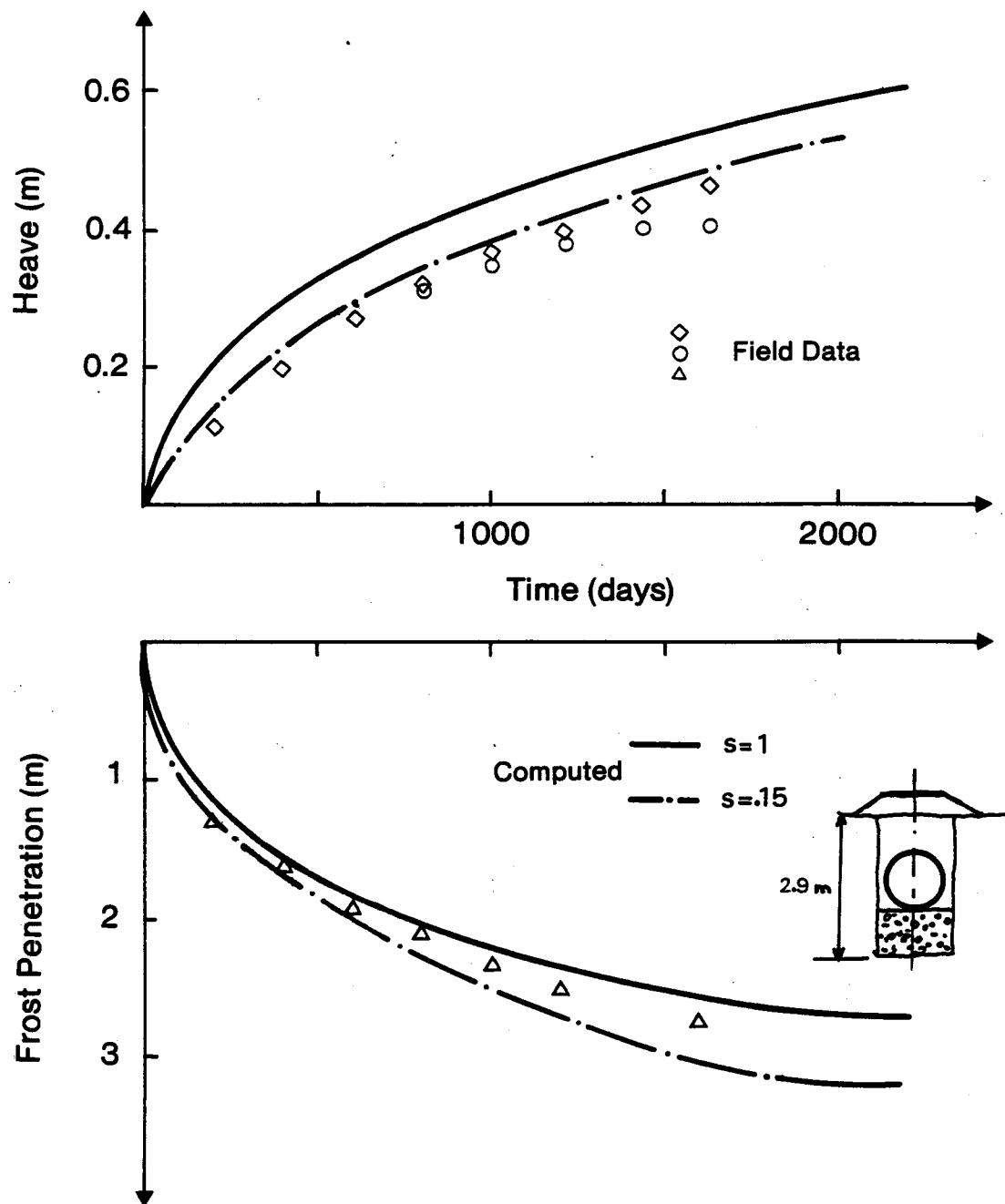
Figure 9.10 Comparison of Prediction with Actual Field Data
at the Gravel Section
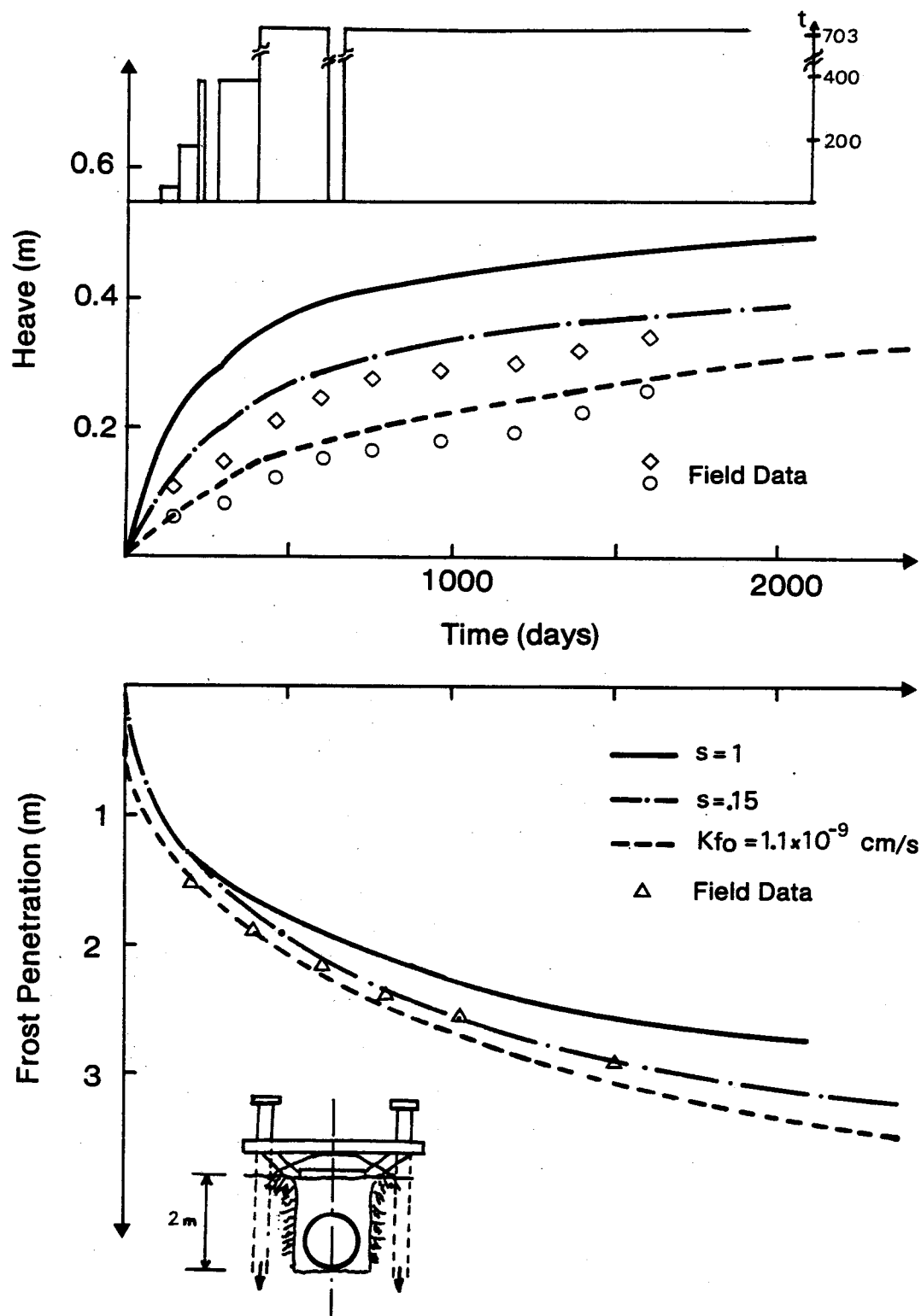
Figure 9.11 Comparison of Prediction with Actual Field Data at the Restrained Section

with frost penetration. Since the piezometers (Terra Tec
Model P-1022) installed at the test site have an accuracy of
0.6 kPa, such small negative pore pressures could not be
measured. This is consistent with the field observations
reported by Slusarchuk et al. (1978).

9.3.6 Maximum Thickness of the Final Ice Lens

When the frost front reaches its maximum depth, further
growth of the final ice lens forces the frost front to
retreat if the temperature boundary conditions are assumed
to remain constant with time. However, in the field total
thawing of the frozen fringe requires much more time than in
the laboratory tests. In this latter situation, Chapter 5
establishes that the terminal phase is approximately 150 to
300 days long. The application of the field frost heave
model to the condition when the frost front retreats yields
the maximum possible heave that can be obtained for each
field test at Calgary. The results are summarized on the
following table:

Section	Ultimate heave (m)	Heave at 30 years (m)
Control	2.0m at 3000 years	0.98m
Deep Burial	2.0m at 3200 years	0.96m
Gravel	2.20m at 3440 years	0.92m
Restrained	1.70m at 3520 years	0.84m

9.3.7 Conclusions

The field frost heave model for simulating frost heave beneath a chilled gas pipeline is in reasonable agreement with the field observations for different pipeline sections. This study establishes that frost heave in field conditions can also be treated as a problem of impeded drainage to a freezing front. The magnitude of the suction generated at the freezing front is related to the segregation freezing temperature, Ts, and to the pressure in the ice, Pe. The water that flows to this front is moderated by a thin frozen zone of low permeability. Furthermore, it has been demonstrated that the permeability of the frozen fringe developed in the field compares well with that determined from laboratory tests when Pu is close to zero. For practical considerations, freezing tests should be carried out with a warm plate temperature close to 0°C. This will result in a small thickness of unfrozen soil at the onset of the formation of the final ice lens and therefore in a small value of the suction at the frost front. In order to eliminate any parasitic effect of friction, it is recommended that freezing takes place from the bottom upwards.

It is noteworthy to stress that a fixed temperature boundary in the unfrozen soil leads invariably to the formation of a final ice lens. This may not be the case in reality since the actual boudary condition is rather a specified geothermal heat flux. Therefore, it is expected

that several thick ice lenses should be observed in the
field as the frost front becomes almost stationary. However,
due to the very small temperature gradient in the frozen
frozen fringe, no significant difference in heave rate
predicted with the simple boundary condition assumed in the
present model or adopting the actual field thermal boundary
conditions should occur.

Finally, it must be emphasized that the previous
analysis of frost heave in terms of Ts and K_f could also be
carried out in terms of SP, at least during the advancing
frost front phase. An example of this alternative method for
heave predictions is given in Section 9.6.

9.4 PRACTICAL RESULTS FOR THE DESIGN OF A CHILLED GAS PIPELINE IN DISCONTINUOUS PERMAFROST

It is now of value to use the field frost heave model
to study the effects of variations in pipeline freezing
temperatures, ground temperatures and the effect on heave of
different thicknesses of insulation around the pipe. The
frost heave model proposed by Hwang (1977) is also evaluated
in this section.

9.4.1 Influence of Pipeline Temperature

Figure 9.12 illustrates the variation in total heave
and frost penetration below the original position of the
base of the pipe for different values of the pipeline

temperature. The ground temperature was taken as +2ºC. The parameters for the freezing soil are:

$$Tso = -0.10ºC \qquad a = 0.75 ~ ºC/MPa·$$

$$Kfo = 2x10^{-9} ~ cm/s \qquad b = 4 ~ cm/s.MPa$$

Several consequences of altering the pipeline temperature can be noticed. Colder freezing temperatures result in higher total heave and larger frost penetration. The time required to initiate the retreating frost front phase increases with decreasing pipe temperatures. For Tc = -1ºC, the frost line will reach its maximum penetration after about 3 years, whereas for Tc=-10ºC the frost front will continue to advance after 30 years of freezing.

Figure 9.12 also reveals that the relationship between Tc and total heave is not linear. A freezing temperature five times colder results only in a heave of 1.35 times larger. This arises from the fact that drastic freezing temperature changes are associated with drastic changes in frost penetration but not in temperature gradients in the frozen fringe. Since the thickness of the current fringe is related to the temperature gradient and recalling Equation 9.4 which demonstrates that the water flux is more or less inversely proportional to the frozen fringe thickness, the previous results then follow readily.

9.4.2 Influence of Ground Temperature

Figure 9.13 illustrates the variations in total heave and frost penetration below the original position of the
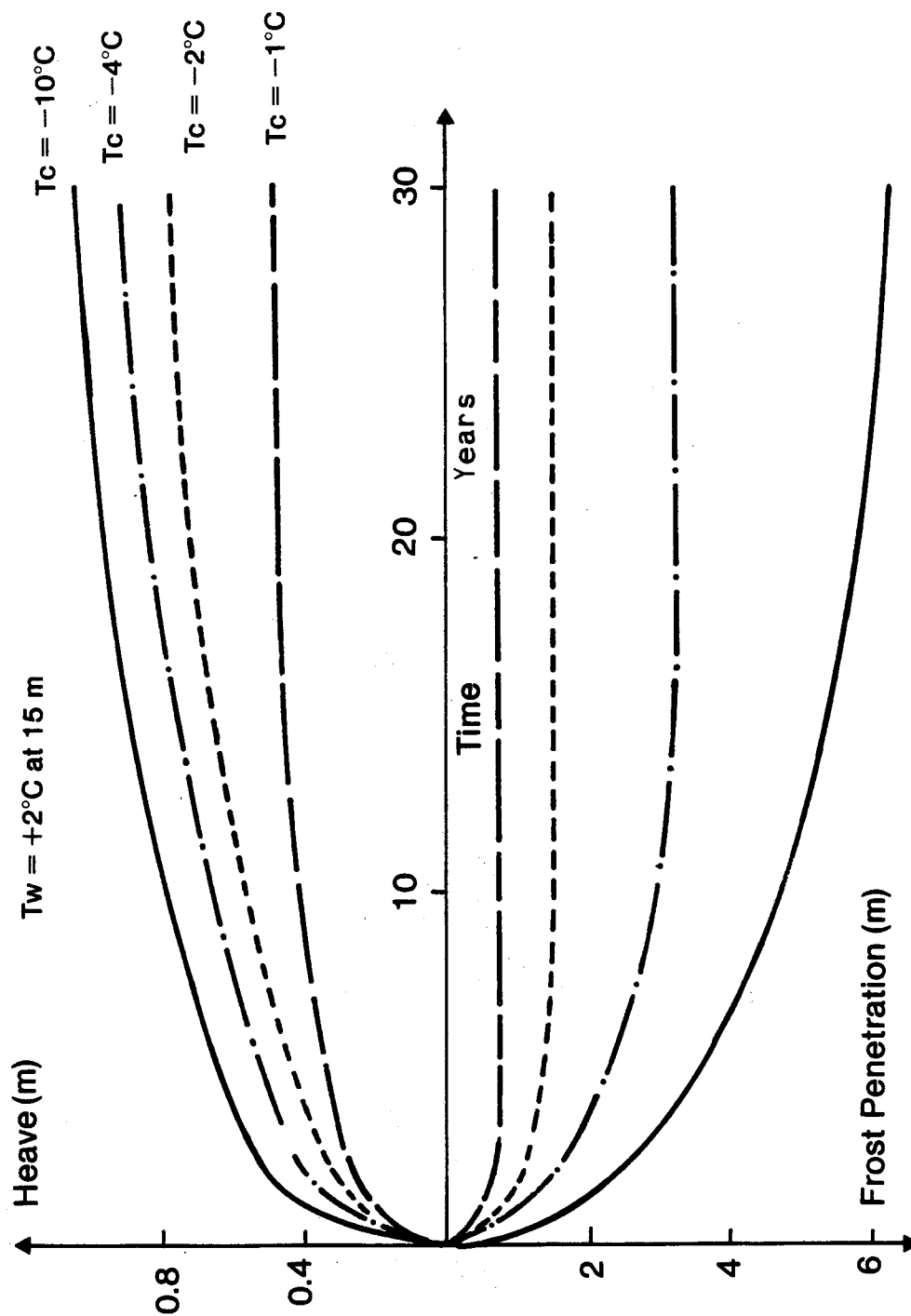
Figure 9.12 Influence of Pipeline Temperature

pipeline's base for different ground temperatures. The
freezing temperature of the pipe is constant for all the
simulated cases and is taken as -8.5°C. The parameters of
the freezing soil have been slightly altered in order to
study the sensitivity of total heave on these parameters.
For this analysis Kfo is 1.4×10^{-9} cm/s and b = 1.5 cm/MPa s.

The results presented in Figure 9.13 warrant further
explanation. The model predicts that the highest heave is
obtained for the warmest ground temperature. This is
contrary to the prediction by the model presented by Hwang
(1977) for the case of the upperbound frost heave of a pipe
based on energy considerations. Hwang (op. cit.) predicts
that the colder the ground temperature, the higher the
resulting frost heave. The field frost heave model predicts
that the colder the ground temperature, the deeper the frost
penetration into the unfrozen soil. Therefore, if the pipe
temperature is the same in all cases, it is clear that the
temperature gradient across the current fringe decreases
with increasing depth, hence when Tw decreases. This, in
turn, increases the length of the frozen fringe with a
concomittant decrease of the overall hydraulic gradient,
which reduces water flux to the freezing front and hence
total heave.

It should also be emphasized that the stresses at the
freezing front increases with depth. Therefore low stresses
are associated with warmer ground temperature whereas higher
stresses develop with colder ground temperature thus also
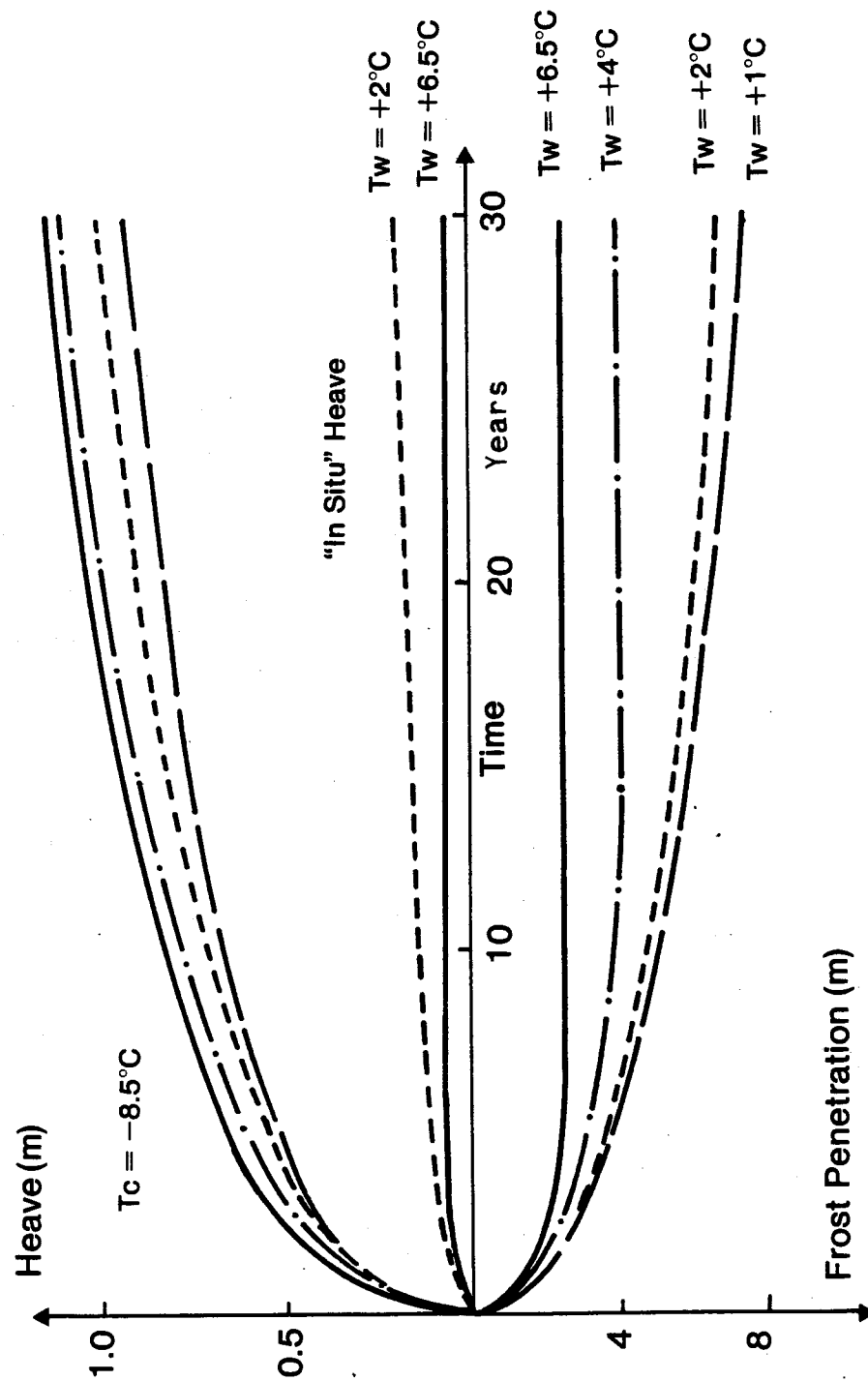
Figure 9.13 Influence of Ground Temperature

affecting heave rate.

For colder ground temperatures, the frost front penetrates deeper and takes longer to reach its maximum depth. As indicated on Figure 9.13, "in situ" water freezing contributes more to the total heave in the case of a colder ground temperature. This explains the fact that total heave is not that sensitive to ground temperature variations.

Before continuing the exploration of different design considerations for a chilled gas pipeline, it is of interest to evaluate the validity of the upper bound solution of frost heave proposed by Hwang (1977). His basic idea is to consider that all the heave comes from the formation of a unique ice lens. During that hypothetical process, the frost front is not penetrating into the unfrozen soil and the thermal balance reduces to:

$$kf.grad\ Tf = ku.grad\ Tu + V.L \dots\dots\dots\dots\dots 9.15$$

This equation is then used to calculate V as time and geometry change. Hwang's simplified theory is represented by a straight line of slope 1/L passing through the origin on a plot V vs net heat extraction rate. If the results of our model are plotted on the same graph (Figure 9.14) it becomes clear that Hwang's model is unrealistic as it leads to a considerable overestimation of the heave. Furthermore, if it is assumed that only one pure ice lens forms below the pipe, it is obvious that the colder the ground temperature, the smaller grad Tu which means that if Tc is constant, the higher V and consequently the higher the heave. (Equation

9.15)

Figure 9.14 also reveals that the range of net heat extraction rates observed shortly after the beginning of freezing beneath the pipe is about two orders of magnitude smaller than those obtained in laboratory conditions(Figure 7.8). This is one more piece of evidence that the characteristics of the frozen fringe are independent of the amount of net heat extraction rate. Therefore, it is justified to assess these freezing characteristics from laboratory tests.

9.4.3 Influence of Pipe Insulation

Figure 9.15 illustrates the effect of insulating the pipeline. The selected ground temperature was +2°C and the pipeline temperature -8.5°C. Frost heave was calculated for different insulation thickness. The thermal conductivity of the insulation was considered to be 10 times smaller than that of the frozen soil. A 5 cm thick insulation reduces total heave by about 20% whereas a 15 cm thick insulation reduces total heave by approximately 45%. Conversly, the frost penetration is also reduced with increasing thickness of the insulation.

9.5 ANALYSIS OF LABORATORY MODEL PIPELINE TESTS

Northern Engineering Services (1975) conducted a number of model pipeline experiments in the laboratory. The aim of
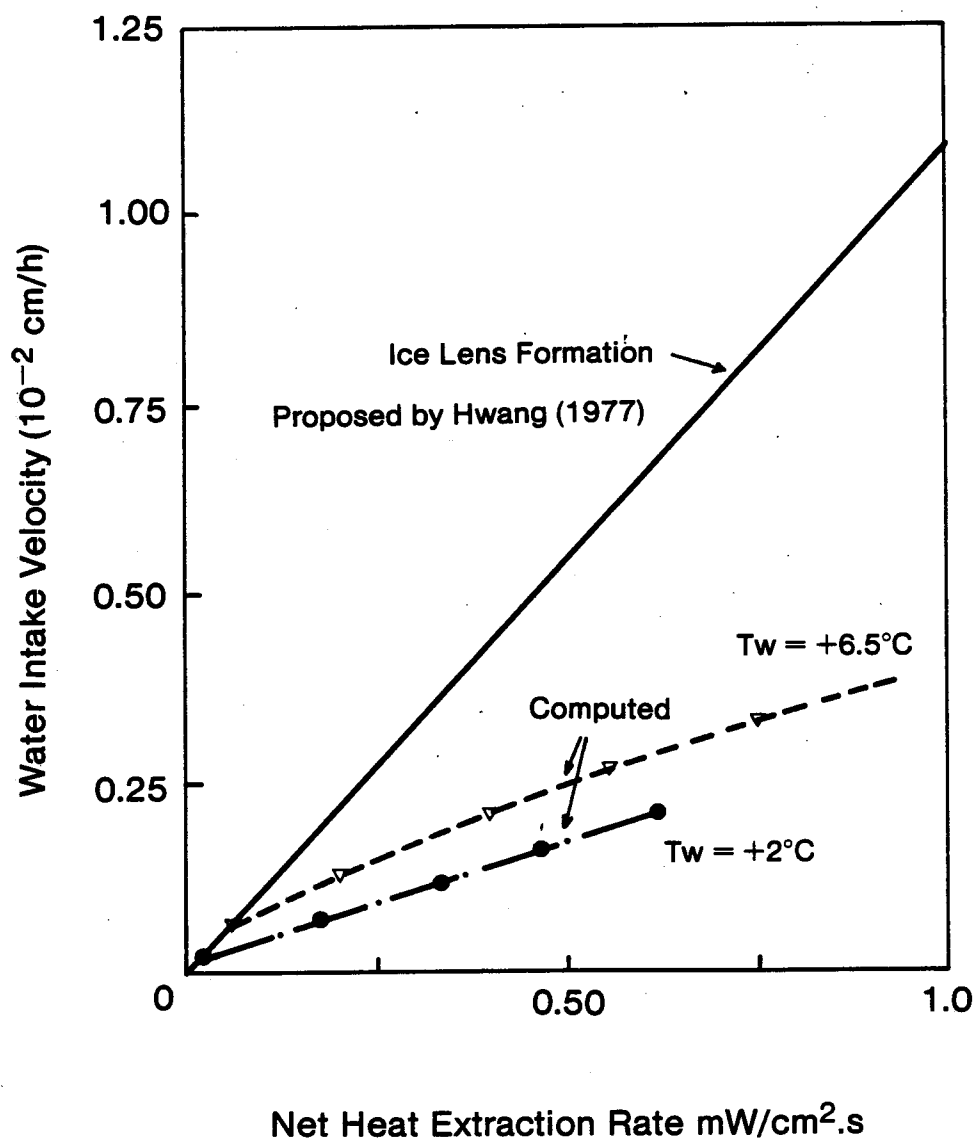
Figure 9.14 Heat Extraction rate Beneath a Pipeline
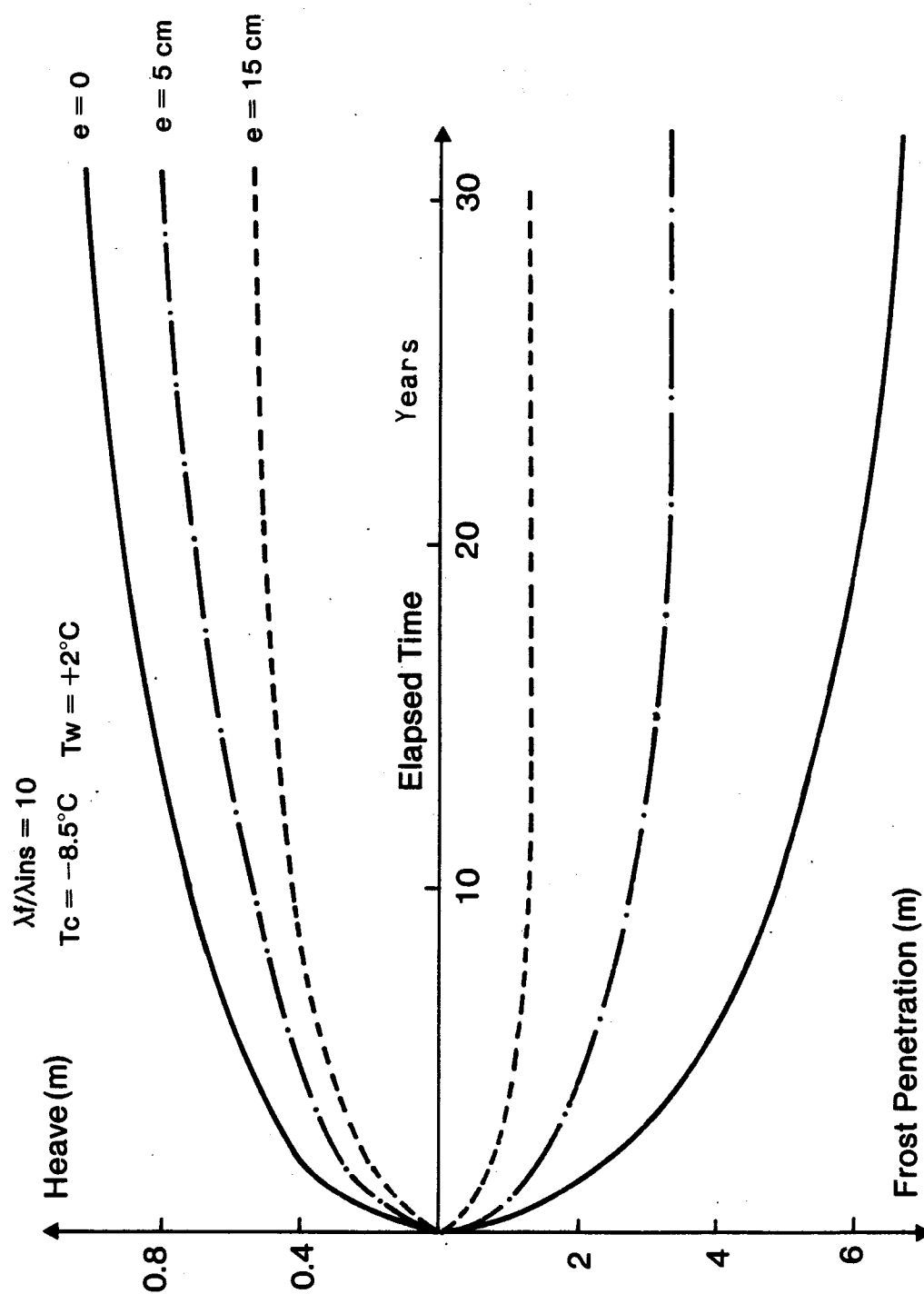
Figure 9.15 Influence of Insulation Thickness

these tests was to obtain qualitative information on the effects of temperature on the development of the frost bulb around a buried pipeline operated at a temperature below 0°C. Qualitative information was also sought with respect to frost heave. The dimensions of the laboratory model are presented in Figure 9.16.

Since the heat flow below the centerline can reasonably be approximated by one dimensional radial heat flow, the model presented in this chapter can be used to simulate frost front penetration and heave for these laboratory models studies. The simulation of the frost penetration required variable pipeline temperatures. This is due to poor temperature control in those tests as reported by N.E.S. (1975). All the tests were conducted on remolded Calgary silt obtained from a depth of 2 to 2.9 m.

Tests U-1, U-2, and U-3 were run consecutively to assess the effect of alternate freezing and thawing on pipeline performance. For tests U-2 and U-3, the initial conditions correspond to the final conditions at the end of the thawing cycle for the previous test, i.e. test U-1 and test U-2. The initial ground temperatures below the pipe are therefore warmer than expected which accounts for shallower frost penetrations. Test U-5 and U-6 are essentially duplicate tests and the soil had not been previously frozen in either case. The results of these tests are summarized in Figure 9.17. Each of these tests was compared with the results of the model presented in this chapter. In order to
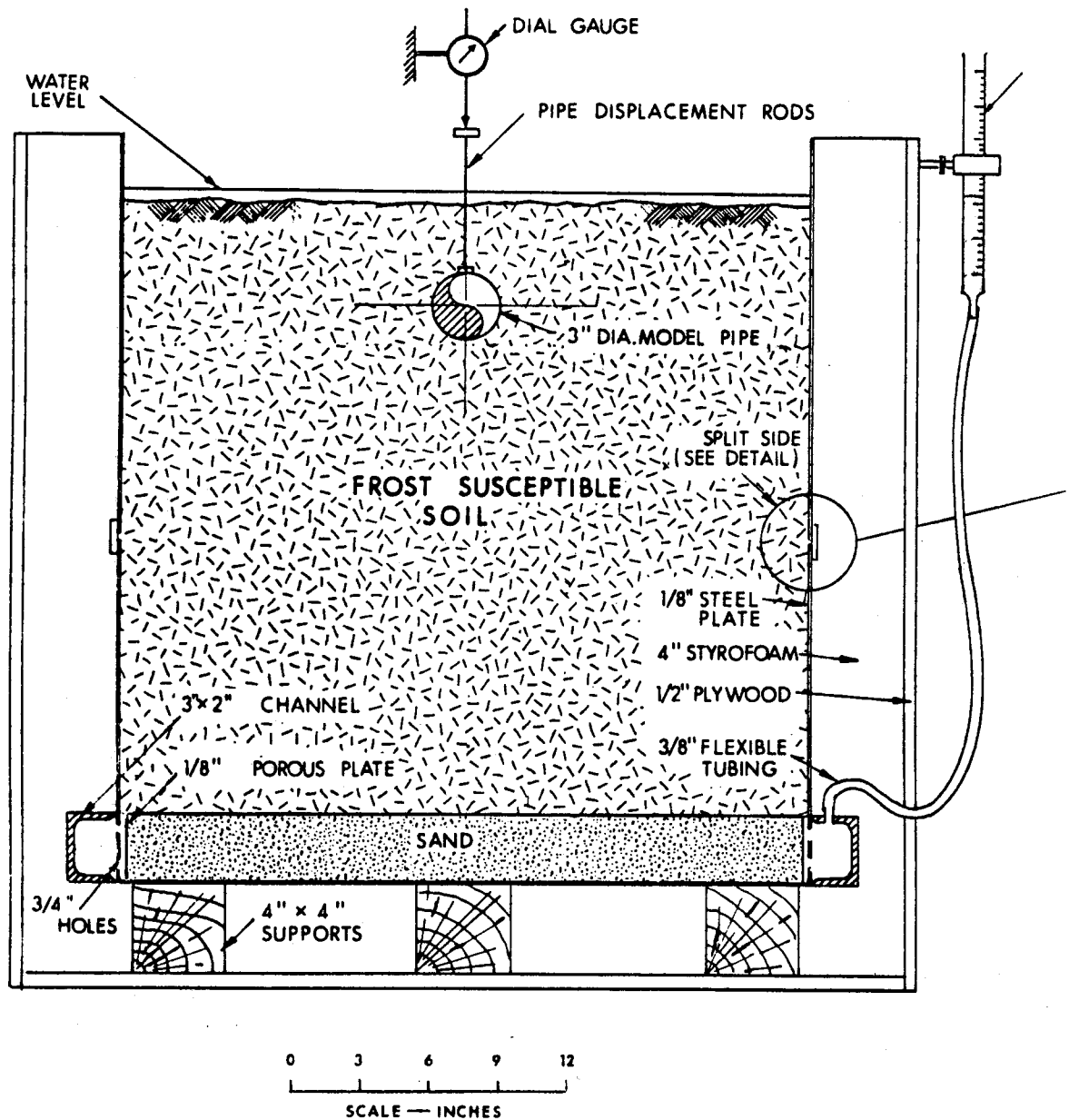
Figure 9.16 Dimensions of the Model Box After Northern Eng.
Services (1975)

fit correctly the frost penetration, both cold side and warm side temperature were varied in the model analysis during the early freezing phase. However, thereafter the temperature remained constant. For test U-2, U-5, and U-6 the pipe temperature was -2.2°C and -6°C for test U-3. The warm side temperature was around +2°C.

The model analysis reveals that the best fit for tests U-2 and U-3 is obtained with a permeability of the frozen fringe of 1.4 x 10^{-9} cm/s and that test U-5 and U-6 are best fitted with Kf = 1 x 10^{-9} cm/s. Comparing these results with those obtained with one dimensional freezing tests on small samples and those inferred from the field tests reported in Figure 9.5, it is remarkable how well the freezing characteristics inferred from the pipe model tests match those deduced from conventional freezing tests.

Another important result is that the properties of the frozen fringe depend upon freeze thaw cycles. It appears that the freezing potential of a soil is increased after one freeze-thaw cycle and remains more or less constant during further freeze thaw cycles. This increase in permeability of the frozen fringe is thought to be associated with a change in structure of the soil.

Finally, tests U-5 and U-6 clearly demonstrate that for the same freezing temperature in the model pipe, the deeper the frost front, the smaller the resulting heave. This result confirms that colder ground temperatures which lead to deeper frost penetrations are actually more favourable
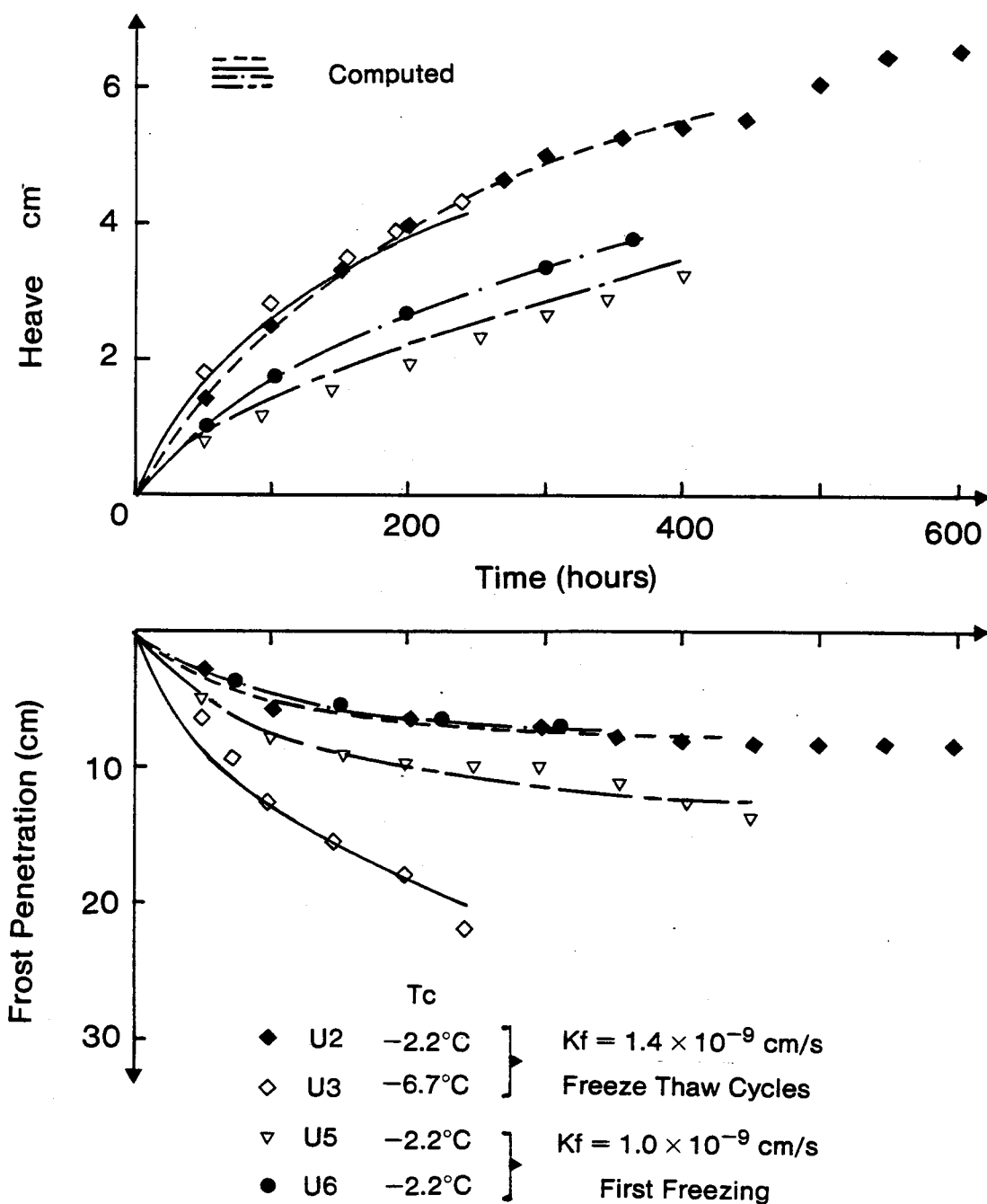
Figure 9.17 Comparison between Prediction and Actual
        Laboratory Data for the Model Pipeline Test

conditions with regard to pipeline heaving than warmer ground temperatures.

9.6 A SIMPLE METHOD FOR PREDICTION OF FROST HEAVE DURING AN ADVANCING FROST FRONT

It is of value to summarize the main points established by this investigation so far and to propose a simple method for predicting frost heave in any soil under various freezing conditions. The objective of this method is to allow the designer to assess approximately but in a straight forward manner the amount of heave that may occur over a given time. The following approach is thought to be very useful to highway design engineers who are faced with problems of seasonal frost heave and shallow frost penetration.

9.6.1 A Simple Frost Heave Calculation

The input data required for a solution are as follows:

1. The relationship between surface freezing temperature and time: $Tc = Tc(t)$

2. The relationship between depth of frost front and time: $X = X(t)$

3. The laboratory relationship between the segregation potential, SP, and the applied pressure at the onset of the formation of the final ice lens: $SP = f(Pe)$

    In the previous laboratory tests, the warm plate

temperature should be close to 0°C in order to
ensure small values of Pu.

Once the above data are known, a frost heave prediction may
be carried out in the following way.

The movement of the frost front may be represented by
the equation

$$X(t) = B.t.\exp(q) \dots\dots\dots\dots 9.16$$

The constants B and q may be determined either from a
geothermal analysis with appropriate boundary conditions, or
from existing solutions for identical problems. Also, for
certain types of problems, the frost line advance may be
obtained readily from either the Stefan Formula or the
modified Berggren Formula.

Knowing the position of the 0°C isotherm at any time,
the temperature gradient across the frozen zone may be
approximated as:

$$\text{grad } T(t) = Tc(t)/(X(t)+h(t)) \dots\dots\dots 9.17$$

where   h(t) is the total heave that occurred at time t

X(t) is the frost penetration below original ground
surface at time t.

Equation 9.17 assumes implicitly that the temperature
distribution in the frozen soil can be approximated by
steady state one dimensional heat flow. Furthermore,
variation in thermal conductivity with temperature is also
neglected.

Finally an upper bound by frost heave is computed by
considering freezing characteristics obtained from

laboratory tests in which Pu is close to zero. Since the segregation potential varies with applied pressure, this latter is evaluated as

$$Pe(t) = Pov + \oint f.(X(t)+h(t)) \dots\dots\dots\dots\dots 9.18$$

and the water intake flux is then given by:

$$V(t) = SP(Pe).grad\ T(t) \dots\dots\dots\dots\dots 9.19$$

The integration of Equation 9.19 over a time interval Dt yields directly the segregational heave:

$$Dhs = 1.09\ V(t).Dt \dots\dots\dots\dots\dots 9.20$$

and the total heave is obtained by adding to this the amount of heave, Dhi, arising from the freezing of in-situ pore water during Dt:

$$Dh = Dhs + Dhi \dots\dots\dots\dots\dots 9.21$$

where $\qquad Dhi = 0.09\ \epsilon.n.Dx$

The total heave developed with time is then simply obtained by adding all the elementary heave amounts.

It must be emphasized that the segregation potential can be easily determined from laboratory freezing tests, as discussed in Chapters 3 and 7. Furthermore, a knowledge of Ts and Kf is not required since SP embraces both of them. Also, it should be stressed that SP takes into consideration all the additional factors affecting heave, such as salt concentration and structure of the soil.

9.6.2 Analysis of Some Field Tests

The analysis of in situ freezing tests reported by Aitkens (1974) and Haas (1962) is presented in the following

to illustrate the utility of the simple frost heave calculation.

Aitkens (op. cit.) conducted an investigation from August 1960 to March 1966 to determine the extent to which seasonal frost heave can be reduced by application of a surcharge stress on the ground surface. The test site was located near Fairbanks, Alaska. Permafrost started at a depth of about 1.4 to 1.8 m beneath the ground surface. The groundwater table was near the surface throughout the summer and at the start of the freezing season. The soil is a gray or brown silt of fairly uniform gradation, containing organic matter in layers or pockets.

The ground freezing temperature for the model analysis was inferred from the air freezing index as follows. The simplest method of introducing an arbitrarily prescribed surface temperature into a method for calculating frost depth in unfrozen soil is by the use of the Stefan solution. This solution assumes a linear temperature profile in the frozen soil, and ignores the temperature distribution in the unfrozen soil. If the surface temperature variation with time is denoted by the function Tc(t), then the depth of the frost front may be given as (Nixon, 1973):

$$X = ((2.kf.\int_0^t Tc(t).dt)/L).exp(0.5) \dots\dots\dots\dots 9.22$$

$\int_0^t Tc(t).dt$ is the area under the surface temperature-time curve and is termed the Freezing Index. (FI)

If, for example, one assumes that seasonal ground surface

temperatures vary as a half sine wave between time 0 and time te and denoting the maximum value by Tmax, the expression for Tc is:

$$Tc = Tmax.sin (\pi.t/te) \dots\dots\dots\dots\dots\dots 9.23$$

where $Tmax = (FI).\pi/2.te$

The frost penetration is then obtained by:

$$X = (kf.FI.(1-cos(\pi.t/te))/L).exp(0.5) \dots\dots\dots 9.24$$

As demonstrated by Nixon (1973), the Stefan solution for the step decrease in surface temperature results in a significant over-estimation of the freezing rate as the Stefan number increases. The Stefan number is defined as Cf.Tc/L and the solution given by Equation 9.24 assumes that the "sensible heat" CfTc is small in comparison with L.

The results presented by Aitken (1974) have been compared with the results computed with the simple frost heave model. The frost front penetration was approximated using Equation 9.24. The actual data were approximated by taking an adequate value for the thermal conductivity of the frozen soil. The freezing index and time (te) were obtained from the data reported by Aitken. Different values of SP are used in order to match the observed heave. Figures 9.18 and 9.19 summarize both experimental and computed heave and frost penetration with time and for different surcharges.

Figure 9.20 represents the relationship between SP obtained from the analysis of the field tests and Pe.

It is of value to compare SP for Fairbank silt obtained in laboratory conditions with those inferred from the field
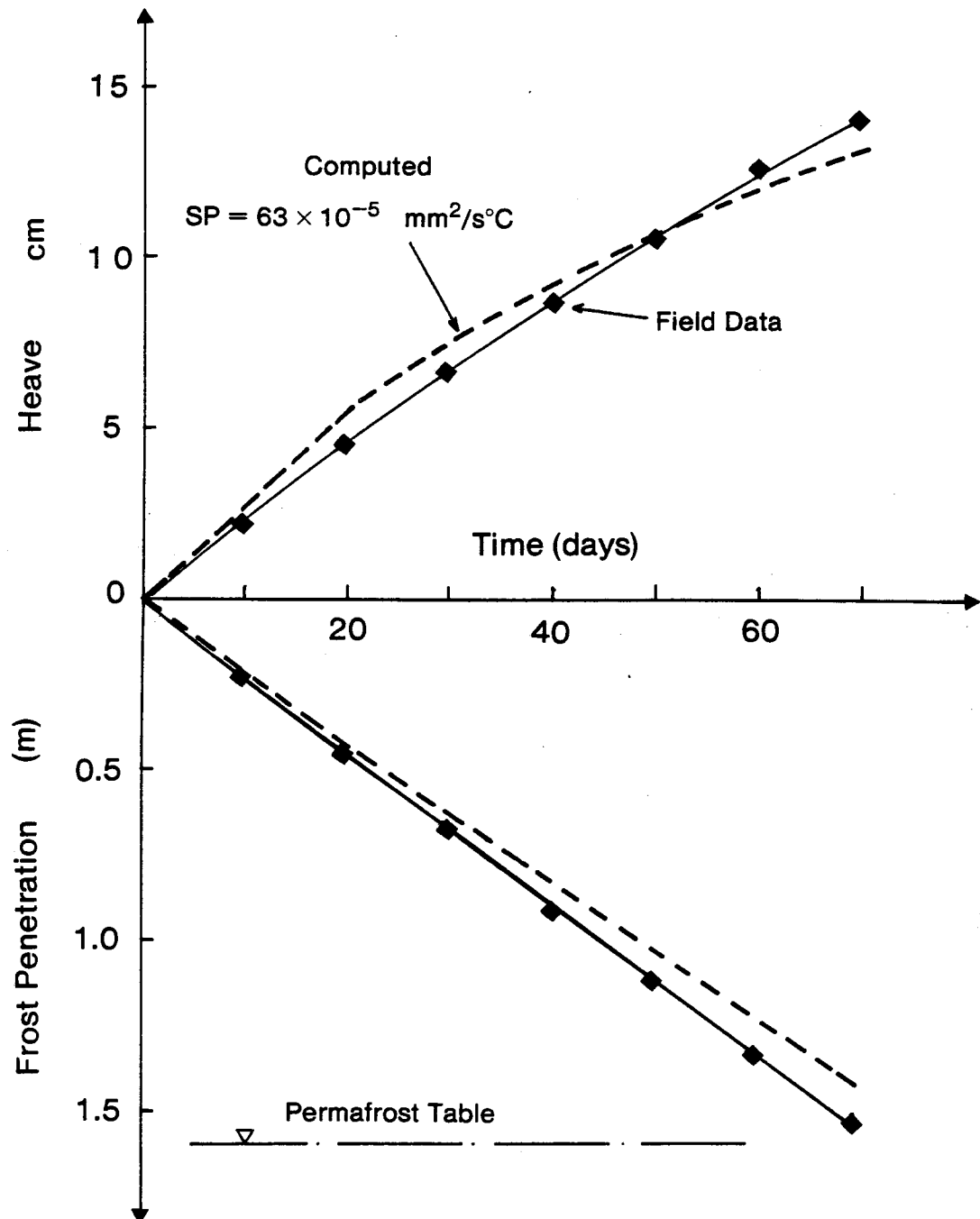
Figure 9.18 Comparison of Prediction with Actual Field Data
with Zero Surcharge (Aitken, 1974)
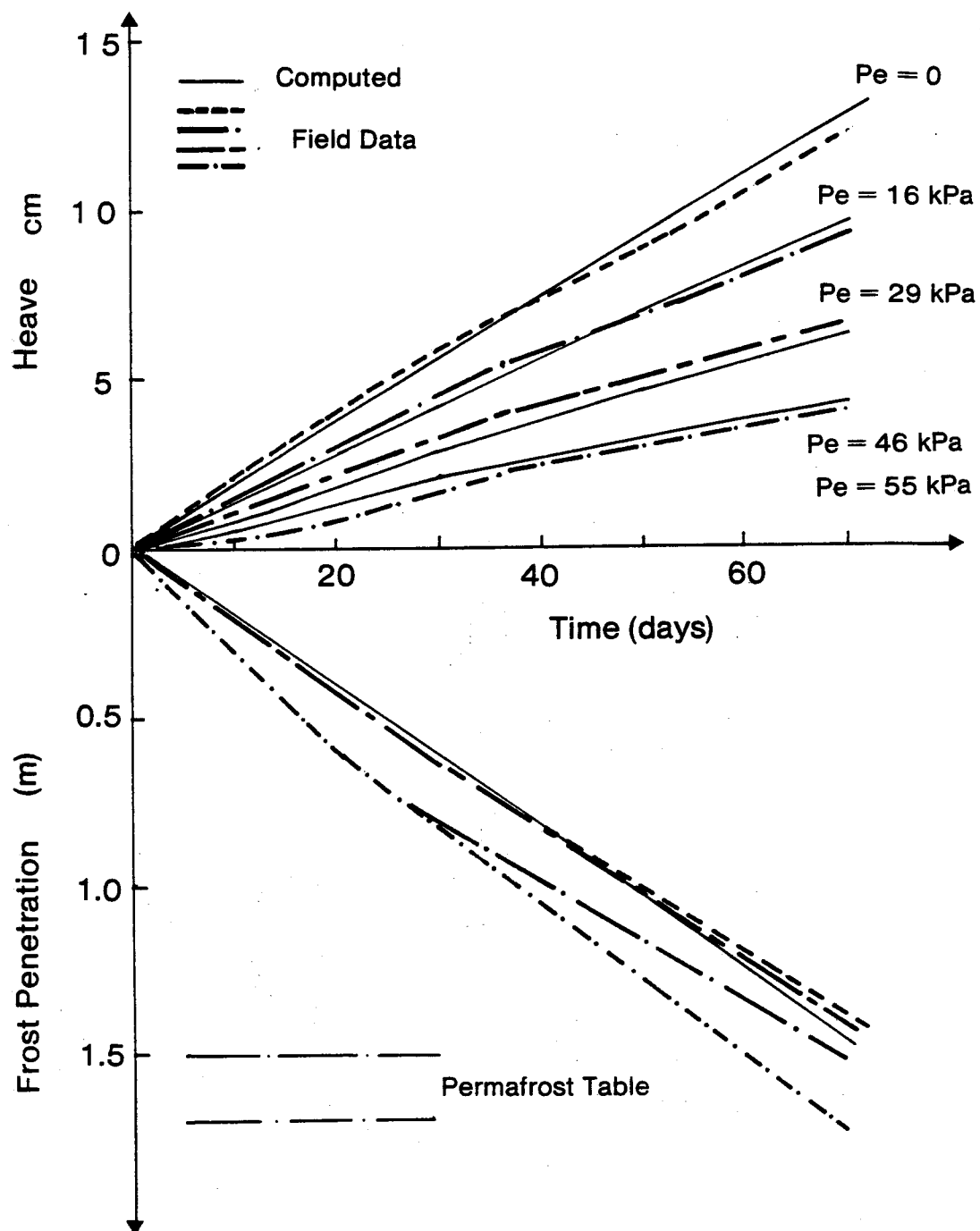Freezing season 1960-61

Figure 9.19 Comparison of Prediction with Actual Field Data
with different Surcharges
Freezing season 1961-62 (Aitken, 1974)
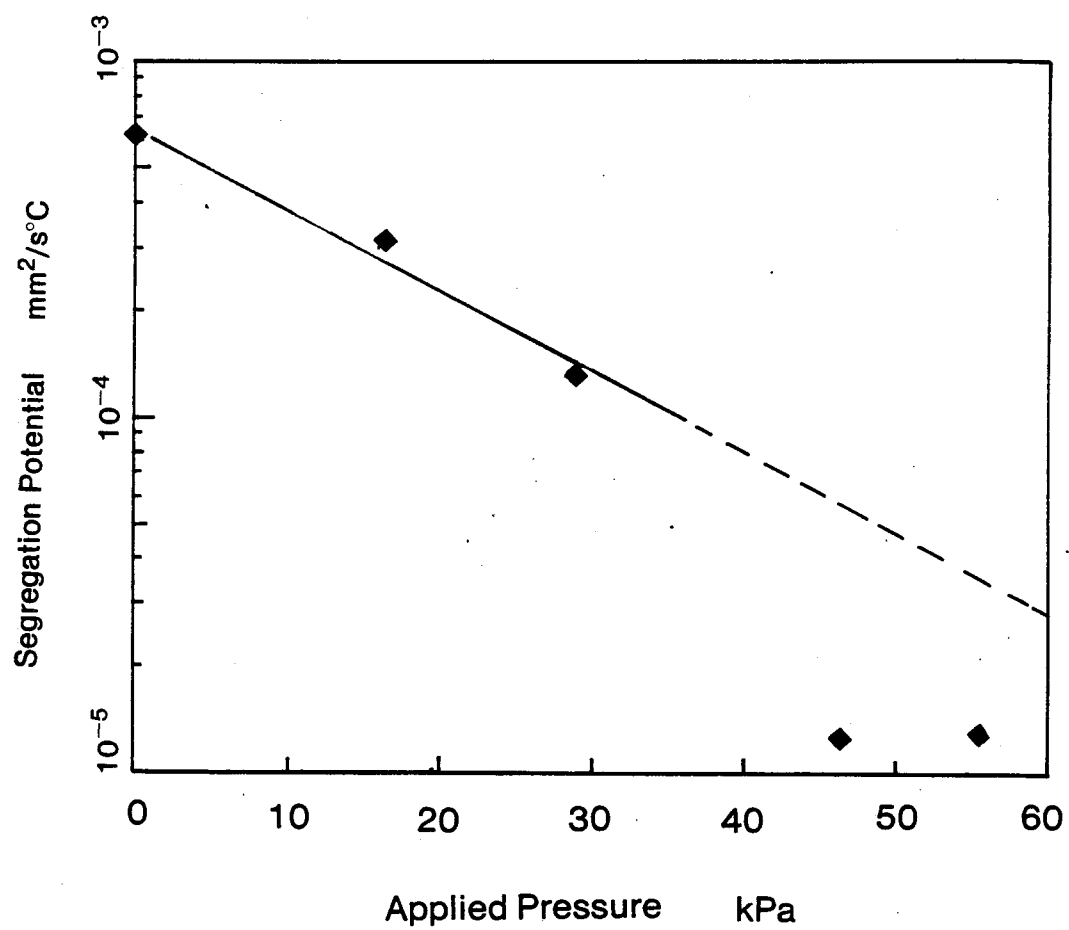
Figure 9.20 Relationship between the Segregation Potential
and Applied Pressure for Fairbanks Silt in Field
Conditions

tests. The segregation potential for Fairbanks silt from various locations were calculated from data reported by Kaplar (1974). The samples were all frozen with a specified rate of frost advance. SP was found to vary between 300.10^{-5} and 27×10^{-5} mm²/s°C. The segregation potential inferred from the field test is approximately 65×10^{-5} mm²/s°C, which is in the lower part of the previous range. It is noteworthy to point out that the amount of organic matter in Fairbanks silt is variable. This is thought most likely to account for the wide range of SP in the laboratory.

The simple frost heave model predicts relatively well the shape of observed heave in Aitken's tests, provided the correct SP is used.

Another verification of the applicability of this simple method can be made by simulating the field tests reported by Haas (1962). His paper reports some results of field observations on suitably prepared field plots. Four soils, ranging from a fat clay to a sand with fines, were used. The freezing temperature also varied like a half sine over the whole freezing period. The freezing index of the second freezing season (1959-60) was approximately 1000°C days. Figure 9.21 to 9.23 compare the field results with those obtained with the simple frost heave model when the frost penetration is matched using Equation 9.24. Again, the model provides a reasonable prediction of the shape of heave vs time for a single value of the segregation potential.

The Unified Soil Classification System defines Pike Bay
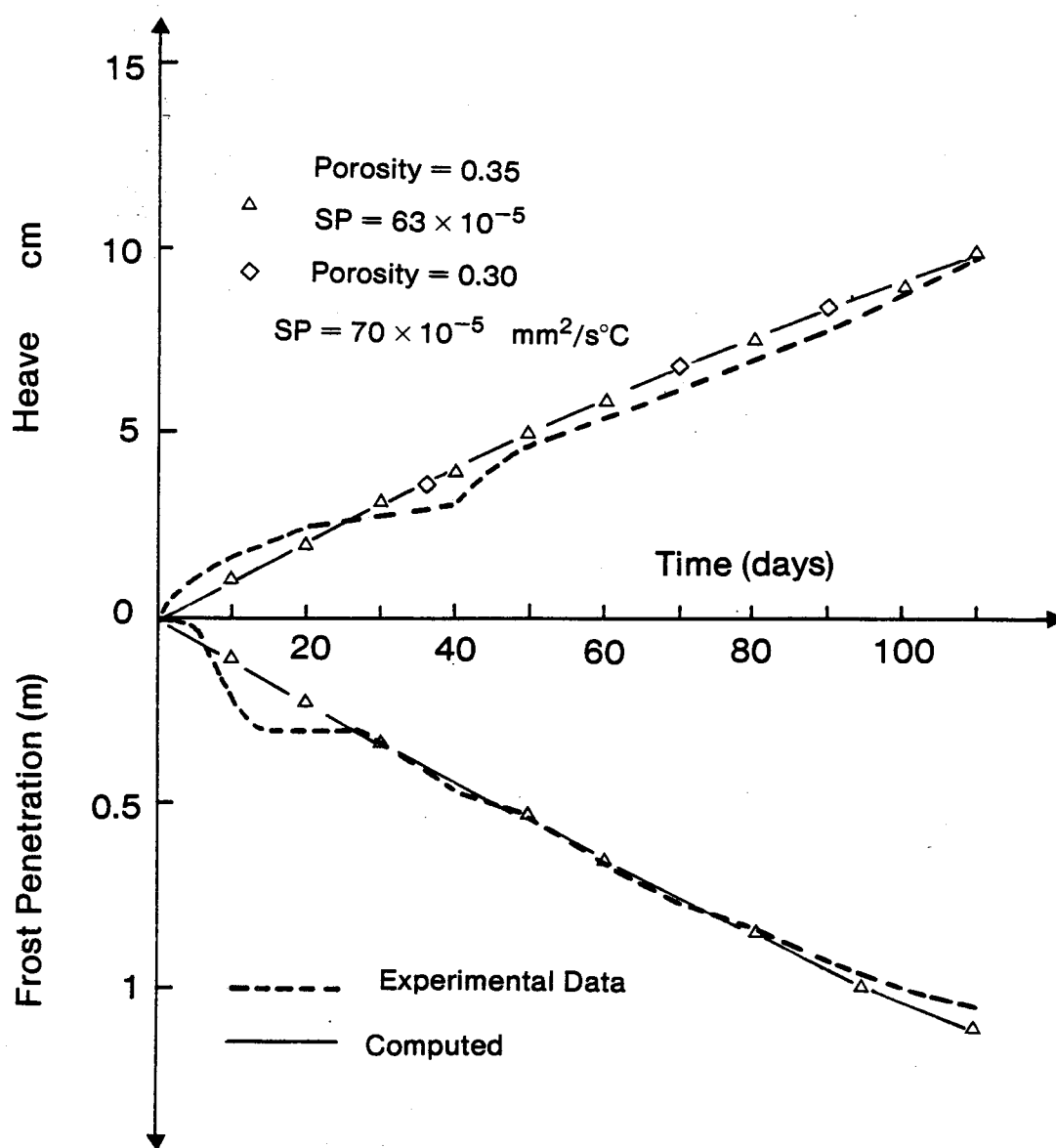
Figure 9.21 Comparison of Prediction with Actual Field Data
for Pike Bay (Haas, 1962)
Freezing Season 1959-60
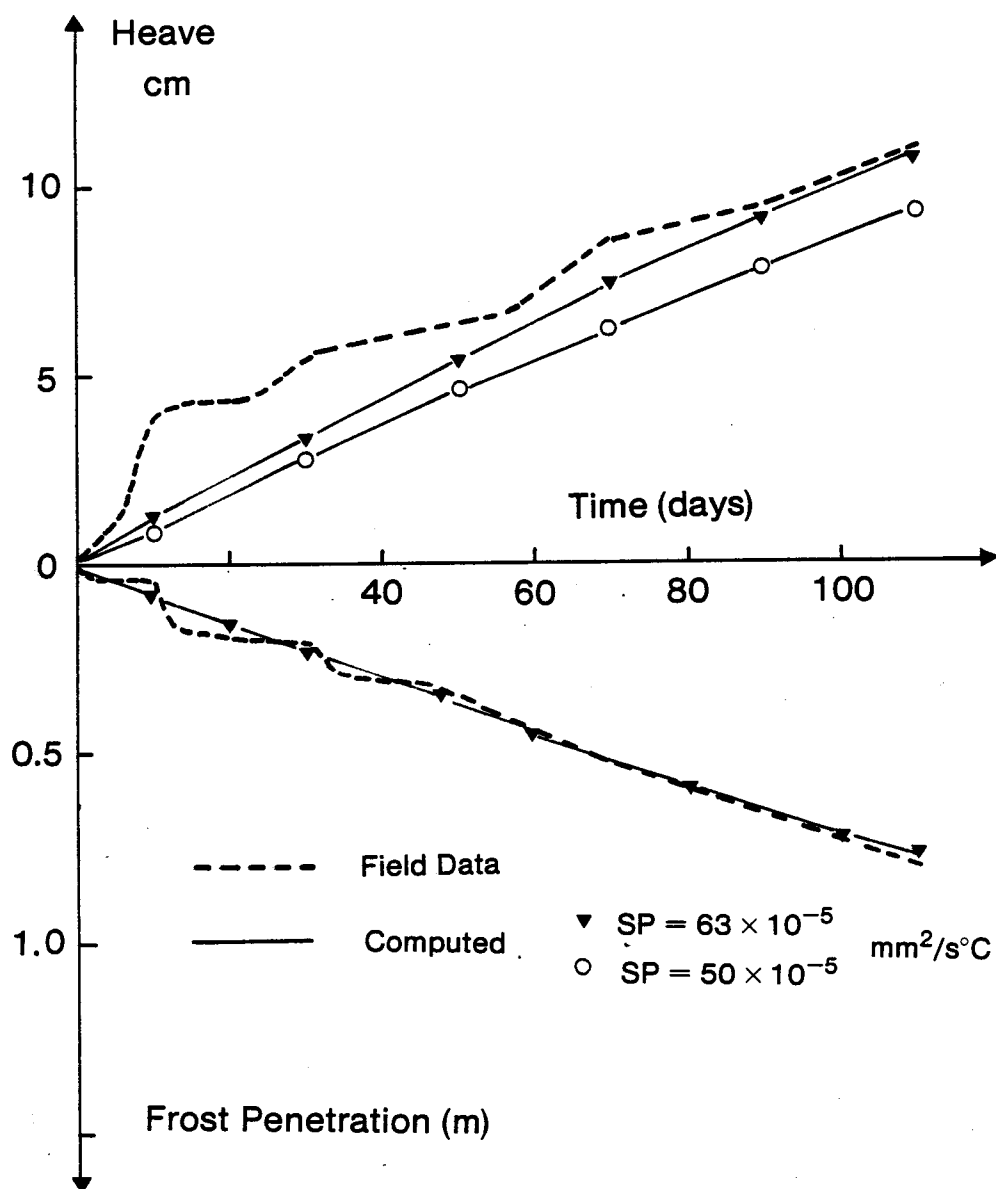
Figure 9.22 Comparison of Prediction with Actual Field Data
for Oneco Sand (Haas, 1962)
Freezing Season 1959-60
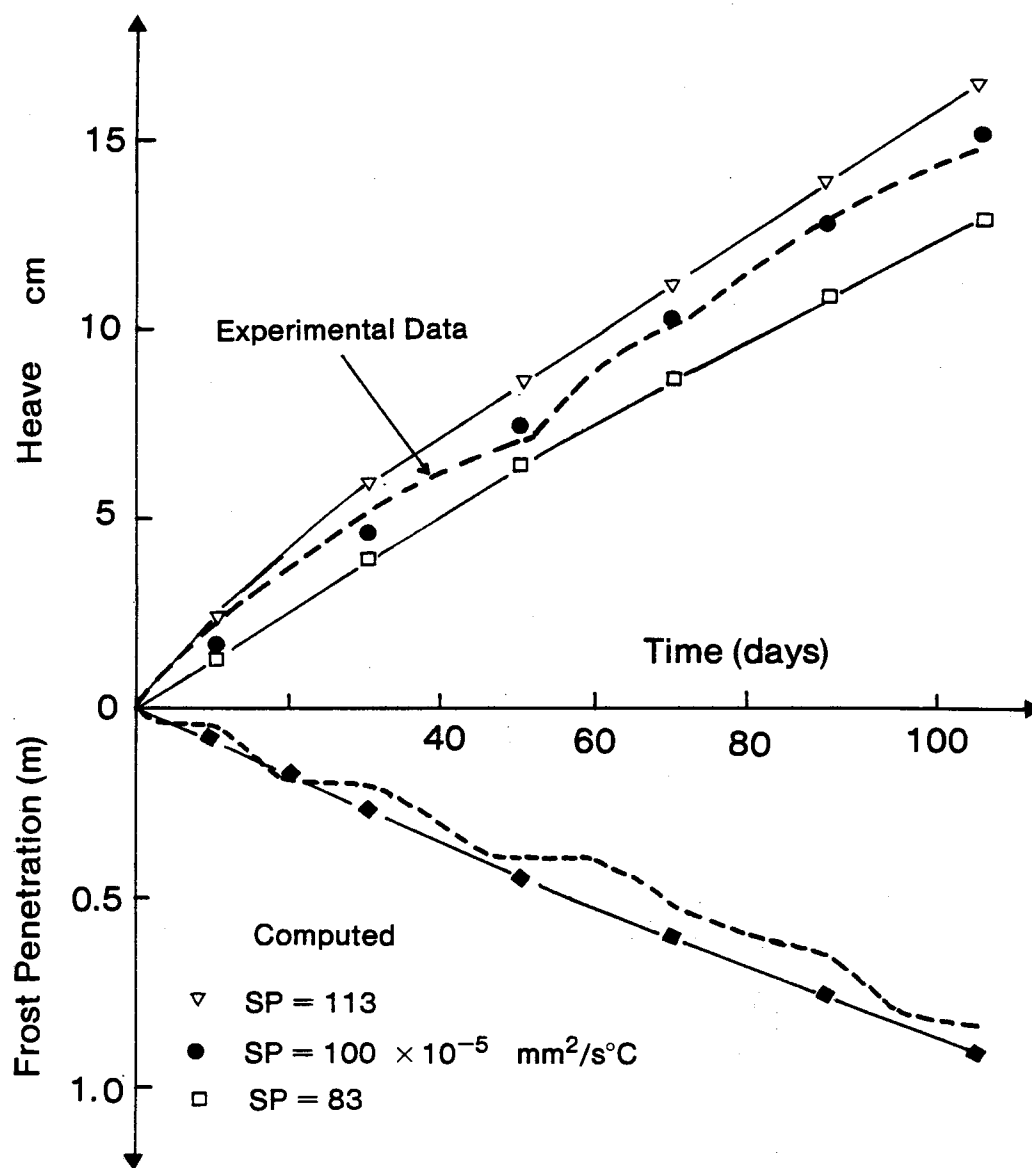
Figure 9.23 Comparison of Prediction with Actual Field Data
for Laminga Silt (Haas, 1962)
Freezing Season 1959-60

soil as a clayey sand, poorly graded sand-clay mixture. From the back-analysis, its SP was about 70×10^{-5} mm²/s°C. The same classification system defines Oneco sand as a poorly graded sand with little or no fines. Its SP was found to lie between 50 to 63×10^{-5} mm²/s°C. Finally Laminga silt is classified as an inorganic silt with low plasiticity and very fine sand particles. Its SP deduced from the field results is about 100×10^{-5} mm²/s°C.

These values of the segregation potential seem reasonable and compare relatively well with the values of SP obtained from laboratory freezing tests on similar types of soils summarized in Chapter 7.

Within the framework of the assumptions made in the formulation of this simple frost heave model, relationships have been derived to calculate readily the amount of frost heaving for various freezing conditions. It has been demonstrated with a number of case histories that the segregation potential, SP, in field situations is of the same order as that determined from laboratory freezing tests. This result considerably increases the confidence in the use of controlled laboratory freezing tests in order to predict frost heave in field conditions.

The fundamental freezing parameters of various soils that have been studied in the present work are summarized in the following tables. Table 9.1 gives the segregation-freezing temperature, the permeability of the frozen fringe and the segregation potential for both

laboratory and field freezing conditions. The values reported in this table have been extrapolated to the case of zero external surcharge, i.e. Pe = 0.

It has been established that the previous freezing parameters vary with applied pressure. The following relationships can be used to calculate the variation of these parameters:

$$|Ts| = |Tso| + a.Pe$$

$$\log Kf = \log Kfo - b.Pe$$

$$\log SP = \log SPo - c.Pe$$

where   a,b,c are constants for a given soil and for a given suction at the frost front. Table 9.2 gives the value of these constants for the case of Pu=0.

Soil Type	Tso °C	Kfo 10^{-10}cm/s	SPo 10^{-5}mm²/(S°C)	Reference
Devon Silt (lab.)	-0.10	16.0 (Pu=0> 8.0 (Pu=-10kPa) 5.2 (Pu=-20kPa)	170 92 55	Konrad (1980)
New Hamshire Silt (lab.)	-0.30 --	4.2 --	50 500	Loch and Kay(1978) Hayley and Kaplar(1952)
Calgary Silt (lab.)	-0.10 (assumed) -0.16 (Pe=34kPa)	10.5-16.7 7.4	100-200 --	N.E.S.(1975) Penner and Goodrich (1980)
Gulli Clayey Silt	-0.65	--	20-40	Loch (1979) (lab.)
Dalane Silty Clay	-0.45	--	40-50	Loch (1979) (lab.)
Calgary Silt Field	-0.10 (assumed)	10.0-20.0	90-250	Slusarchuk et al. (1978)
Fairbanks Silt	--	--	63	Aitken(1974) (Field)
Pike Bay sandy clay	--	--	70	Haas (1962) (Field)
Oneco Sand	--	--	50-63	Haas (1962) (Field)
Laminga Silt	--	--	80-115	Haas (1962) (Field)

Table 9.1 Summary of Typical Values of Freezing Parameters Obtained for Both Laboratory and Field Conditions Under Zero Applied Load.

Soil	a $^oC/MPa$	b $cm/S.MPa$	c $mm^2/S.^oC.MPa$	Reference
Devon Silt	0.75	2.3	4.2	Konrad Laboratory
Calgary Silt	0.75 (assumed)	2.5-4.0	3.8-9.0	NES (1980) Laboratory
	0.81	1.34	--	Penner and Goodrich (1980) Laboratory
	0.75 (assumed)	4.0	7.0-9.0	Slucharchuk et al (1978) Field
Fairbanks Silt	--	--	20.9	Aitkens (1974) Field

Table 9.2 Summary of Typical Values of Parameters a, b, c Obtained for Both Laboratory and Field Conditions.

10. CLOSING REMARKS

The general characteristics of frost heave during the freezing of fine grained soils have been accounted for in a conceptual model that distinguishes between a passive system and an active system. The active system, which is the seat of the segregational process, is composed of the frozen fringe and the unfrozen soil. The passive system is defined as the frozen soil above the segregation freezing level.

It has been established that a quantitative theory of frost heave coupling heat and mass transfer requires the knowledge of the freezing characteristics of the soil. This study also demonstrates that these freezing characteristics are deducible from controlled laboratory freezing tests.

10.1 LABORATORY FREEZING CONDITIONS

Freezing tests where temperature boundary conditions are constant with time lead invariably to the formation of a final ice lens. At the formation of this ice lens, it has been shown that frost heave can be treated as a problem of impeded drainage to this ice lens through a medium which is composed of the unfrozen soil and the frozen fringe. This study also indicates that the frost heave characteristics at the formation of the final ice lens are defined either by

the segregation freezing temperature and the overall permeability of the frozen fringe or by the segregation potential.

It has also been shown that the freezing characteristics are strongly affected by the average suction in the frozen fringe. This suction is related uniquely to the suction at the frozen-unfrozen interface. Since the latter can easily be determined, it has been taken as a fundamental parameter characteristic in freezing soils. The experimental data reveal that the frozen fringe permeability and the segregation potential decrease with increasing suction at the frost front. However, the segregation-freezing temperature is only slightly affected by suction changes.

The present study also establishes that for a given suction at the frost front and under zero load, the water intake flux is proportional to the temperature gradient across the fringe at the formation of the final ice lens. It then follows that the segregation potential at the formation of the final ice lens in a given soil is constant for a given suction at the frost front. The previous result also signifies that the segregation freezing temperature and the permeability of the frozen fringe developed for the previous conditions are independent of temperature gradient and hence of the cold-side temperature.

During an advancing frost front phase, i.e. unsteady heat flow, the previous characteristics of a given soil are

dependent on the degree of thermal imbalance. This second parameter has been introduced by means of the rate of cooling of the frozen fringe which is the rate of change of the average temperature of the current frozen fringe. This parameter embraces both geometrical and thermal conditions. This study establishes that a unique relationship between the segregation potential, the suction at the frost front and the rate of cooling of the fringe exists in a freezing soil.

The frost heave model has been used to simulate laboratory freezing tests for one dimensional heat flow. The input to mass transfer is the characteristic freezing surface (SP, Pu, dTf/dt) which can be determined from controlled laboratory freezing tests. The model was able to predict closely the results of all the freezing tests conducted during this investigation since the characteristic freezing surface is to a first approximation independent of the freezing path. Any attempt to use other less fundamental parameters such as net heat extraction rate, frost penetration rate, or the ratio of heave and frozen soil thickness to predict frost heave in laboratory tests would result in some success for specific freezing paths. However, because the forementioned parameters are freezing path dependent, they cannot predict all freezing paths as this model does. It is possible to deduce these ad hoc parameters from the fundamental ones. It transpires, moreover, that the suction at the frost front cannot exceed a limiting suction

which is thought represents the critical suction at which cavitation occurs in the unfrozen soil.

Evidence of a limiting rate of cooling of the frozen fringe is also revealed by the experimental results. For Devon silt, this limiting rate of cooling is approximately 2.5°C/hour. For higher rates of cooling, water flow to the freezing front does not occur.

The present investigation demonstrates that the freezing characteristics of a soil vary with applied pressure. It has been clearly established that the segregation freezing temperature at final ice lens formation decreases with increasing applied loads. This is associated with a decrease in the overall permeability of the frozen fringe. The segregation potential, at the formation of the final ice lens, decreases also with increasing external surcharge. It then follows that increased load depresses the heave rate, which has been recognized in the field of frost action for some 50 years.

Water expulsion during advancing frost front is a function of applied load and rate of cooling of the fringe. There is a unique relationship between these two parameters for which water is attracted to the freezing front. This relationship predicts that the higher the applied surcharge, the closer to final thermal equilibrium conditions the sample will start to attract water from an outside source.

Evidence of a "shut off" pressure has been presented for which no water flow to the ice lens is possible. This

"shut off" pressure is defined as the applied pressure which produces an atmospheric pressure in the water films at the segregation freezing level. For engineering purposes, this "shut off" pressure is very high, in the order of 1000 KPa for Devon silt.

During a retreating and a stationary frost front, frost heave results from the growth of the final ice lens. In these conditions, the heave and the rate of heave are determined solely by the net heat extraction rate at the freezing front. The growth of the final ice lens stops when the temperature at its base reaches the value that produces an atmospheric pressure in the adjacent water film. This final temperature is a function of applied load and is equal to 0°C when there is zero overburden.

10.2 FIELD FREEZING CONDITIONS

During freezing of a small specimen, there is a substantial variation of rates of cooling and suctions at the frost front. However, due to the larger scale of field conditions and to high mass permeability of the unfrozen soil, these parameters do not vary significantly during field freezing. It has been shown that an upper bound to frost heave can be computed if the freezing characteristics obtained from laboratory testing correspond to the onset of the formation of the final ice lens and to a suction at the frost front close to atmospheric pressure. This is easily

achieved in a constant temperature freezing test in which the warm side temperature is close to 0°C. The characteristics of a freezing soil in field situations reduces simply then to either a relationship between the segregation freezing temperature, the permeability of the fringe and applied load or a relationship between the segregation potential and applied pressure.

The predictive power of the field frost heave theory, in which the freezing soil is characterized by either one of the previous relationships, has been shown through the successful detailed analysis of the performance over several years of a chilled pipeline and of subgrade behavior during seasonal freezing.

10.3 FROST HEAVE SUSCEPTIBILITY CRITERIA

This study of freezing soils led to the proposal for two frost heave susceptibility criteria. The first one is valid during an advancing frost front situation. The segregation potential at the onset of the formation of the final ice lens has been found to reflect the degree of frost heave susceptibility. Furthermore, the segregation potential of a freezing soil is very sensitive to soil structure, unfrozen water content, salt concentration and many other factors. Its determination, however, is extremely simple in a controlled laboratory freezing test.

In general, silty soils have the highest segregation potential whereas sands and fat clays have lower segregation potentials of about the same order of magnitude.

While sands and fat clays may exhibit the same amount of heave during an advancing frost front, the thickness of their final ice lens is much different. For this reason, a second frost heave susceptibility criterion has been introduced which holds only when the frost front retreats. In this final phase, the present investigation establishes that given time the final ice lens will grow thickest in clay, thinner in silts and practically not at all in sands.

10.4 RECOMMENDATIONS

The investigation performed here has been directed towards the establishment of the physics of freezing soils in laboratory one dimensional freezing. Although many field problems are multidimensional in nature, frost heave can be calculated with the freezing characteristics obtained for one dimensional heat flow provided that the thermal problem can be solved using numerical models.

The comparison of the freezing characteristics obtained during laboratory freezing with those inferred from field freezing situations appears to require the highest priority at the present state.

Furthermore, the study of the effect of freeze thaw cycles on the segregation potential of a given soil would be

of great importance to highway engineers who are faced with seasonal freezing and thawing. It would also be of value to study the effect of salt concentration on the segregation potential, since addition of salt to a freezing soil significantly reduces the heave rate.

Finally, the analysis of the tremendous amount of well-documented laboratory tests in the available literature in terms of the segregation potential will certainly greatly enhance the present state of knowledge concerning the behavior of freezing soils.

REFERENCES

Aguirre-Puente, J., B. Khastou et M. Chaloub. 1971. "Etude du gonflement et de l'aspiration d'eau engendre par le gel lors de la congelation des sols fins humides". Proc. 13th Int. Conf. on Cold. Washington, D.C. V.1, pp.759-764

Aguirre-Puente, J., M. Fremont and J.M. Menot. 1977. "Gel dans les milieux poreux permeabilite variable et mouvement d'eau dans la partie a temperature negative." Proc. Int. Symp. on Frost Action in Soils. U. of Lulea, Sweden, pp.5-28

Aitken, G. 1963. "Reduction of frost heaving by surcharge loading." Proceedings 1st International Conference Permafrost, Purdue University, Lafayette, Indiana, pp.319-324

Aitken, G. 1974. "Reduction of frost heave by surcharge stress." Cold Regions Research and Engineering Laboratory Tech. Report 184.

Anderson, D.M. and N.R. Morgenstern. 1973. "Physics, Chemistry and Mechanics of Frozen Ground." Proceedings 2nd International Conference Permafrost, Yakutsk, U.S.S.R., pp.257-288.

Arvidson, W. and N.R. Morgenstern. 1974. "Water flow induced by soil freezing." Proceedings 27th Canadian Geotechnical Conference, Edmonton, Alberta, pp.137-143.

Arvidson, W. 1973. "Water flow induced by soil freezing." M.Sc. Thesis, Dept. of Civil Engineering, University of Alberta.

Berg, R.L., G.L. Guymon and T.C. Johnson. 1980. "Mathematical model to correlate frost heave of pavement with laboratory predictions." Cold Regions Research and Engineering Laboratory Report 80-10.

Beskow, G. 1935. "Soil freezing and frost heaving with special application to roads and railroads." (translated by J. Osterberg), Northwestern University Tech. Inst., 1947.

Biermans, M., K. Dijkema and D.A. de Vries. 1976. "Water movement in porous media towards an ice front." Nature, Vol.264, pp.166-167.

Biermans, M., K. Dijkema and D.A. de Vries. 1978. "Water movement in porous media towards an ice front." J. Hydrology, Vol.37, pp.137-148.

Bouyoucos, G.J. 1916. "The freezing point method as a new

means of measuring the concentration of the soil solution directly in the soil."Mich.Agr.coll.,Tech.Bull.24,pp.1 44.

Crank, J. and P. Nicholson. 1947. "A practical method for the numerical evaluation of solutions of partial differential equations of the heat conduction type." Proceedings Cambridge Phil. Soc. 43, pp.50-67.

Dirksen, C. and R.D. Miller. 1966. "Closed-system freezing of unsaturated soils." Soil Science Soc. Amer. Proceedings, Vol.30, pp.168-178.

Edelfson, D.H. and A.B.C. Anderson. 1943. "Thermodynamics of soil moisture." Hilgardia, Vol.15, pp.30-298.

Ershov, E., V. Cheverev and Y. Lebedenko. 1976. "Experimental study of moisture migration and ice release in the frozen zone of thawing soils." Vestnik, Geol. Moscow Univ., Vol.37, No.1 (In English), pp.111-114.

Ershov, E.D., V.G. Cheverev, Yu. P. Lebedenko and L.V. Shevchenko. 1978. "Water migration, formation of texture and ice segregation in freezing and thawing clayey soils." Proc. 3rd. Int. Conf. Permafrost, Vol. 1, NRC Canada, , pp.174-180.

Everett, D.H. 1961. "The thermodynamics of frost damage to porous solids." Trans. Faraday Soc., Vol.57, pp.1541-1551.

Freden, S. 1965. "Some aspects on the physics of frost heave in mineral soils." Surface Chemistry pp. 79-90.

Gardner, W.R. 1958. "Some steady-state solutions of the unsaturated moisture flow equation with application to evaporation from a water table." Soil Science 85, pp.228-232.

Gilpin, R.R. 1979b. "A model of the "liquid-like" layer between ice and a substrate with application to wire regelation and particle migration." J. of Colloid and International Science, Vol.68, No.2, pp.235-251.

Gilpin, R.R. 1980. "A model for prediction of ice lensing and frost heave in soils." Submitted to the J. Water Resources Research.

Guymon, G.L., T.V. Bromadka II and R.L. Berg. 1980. "A one-dimensional frost heave model based upon simulation of simultaneous heat and water flux." Cold Reg. Science Tech., 2, Vol.3, pp.253-262.

Haas, W.M. 1962. "Frost action theories compared with field

observations." Highway Research Board, Bull. 331, pp.81-97.

Hallet, B. 1978. "Solute redistribution in freezing ground." Proceedings 3rd International Conference on Permafrost. Edmonton, Alberta. pp.85-91.

Harlan, R. 1974. "Dynamics of water movement in permafrost." Proceedings of Workshop Seminar, Canadian Nat. Committee, International Hydr. Decade, pp.69-77.

Harlan, R.L. 1973. "Analysis of coupled heat-fluid transport in partially frozen soil." Water Resour. Research, 9, No.5, pp.1314-1323.

Hayley, J.F. and C.W. Kaplar. 1952. "Cold-room studies of frost action in soils." Highway Research Board, Publ.213, pp.246-267.

Hesstvedt, E. 1964. "The interfacial energy ice/water." Norw. Geotechnical Inst. Publ. No.56, pp.7-10.

Hill, D.W. and N.R. Morgenstern. 1977. "Influence of load and heat extraction on moisture transfer in freezing soils." International Symp. on Frost Action in Soils, Lulea, Sweden, Vol.I, pp.76-91.

Hill, D.W. 1977. "The influence of temperature and load on moisture transfer in freezing soil." M.Sc. Thesis, Dept. Civil Eng., Univ. of Alberta.

Hoekstra, P. and E. Chamberlain. 1964. "Electro-osmosis in frozen soils." Nature, Vol.203, pp.1406-1407.

Hoekstra, P. 1965. "Conductance of frozen bentonite suspensions." Soil. Science Soc. Amer. Proceedings, Vol.29, pp.519-522.

Hoekstra, P. 1966. "Moisture movement in soils under temperature gradients with the cold-side temperature below freezing." Water Resources Research, Vol.2, pp.241-250.,

Hoekstra, P. 1969a. "The physics and chemistry of frozen soils." Highway Research Board, Special Report 103, pp.78-90

Hoekstra, P. 1969b. "Water movement and freezing pressures." Soil Science Soc. Amer. Proceedings, Vol.33, pp.512-518.,

Hopke, S. 1980. "A model for frost heave including overburden." Cold Regions Science and Tech., 2, Vol.3, pp.111-127.

Horiguchi, K. and R.D. Miller. 1980. "Experimental studies

with frozen soil in an ice sandwich permeameter." Cold Regions Science and Tech., 2, Vol.3, pp.177-183.

Horiguchi, K. 1978. "Effects of the rate of heat removal on the rate of frost heaving." Proceedings of the International Symposium on Ground Freezing, Ruhr University, Bochum, FRG, pp.25-30.

Hwang, C.T. 1977. "Frost heave design of a chilled gas pipeline." 30th Canadian Geotechnical Conference, Saskatoon, Sask., Canada.

Jame, Y.W. and Norum, D.I. 1972. "Phase composition of a partially frozen soil." Division of Hydrology Coll. of Eng., Univ. of Saskatchewan, Saskatoon, Research Paper 11.

Jame, Y.W. and Norum, D.I. 1976. "Heat and mass transfer in freezing unsaturated soil in a closed system." Proceedings 2nd Conference on Soil Water Problems in Cold Regions, Edmonton, Alberta.

Johansen, O. 1977. "Frost penetration and ice accumulation in soils." International Symposium on Frost Action in Soils, University of Lulea (Sweden), Feb. 16-18, Vol.1, pp.102-111.

Kaplar, C.W. 1968. "New experiments to simplify frost susceptibility testing of soils." Highw. Research Rec., 215, pp.48-59.

Kaplar, C.W. 1970. "Phenomenon and mechanism of frost heaving." Highway Research Record No. 304, pp.1-13.

Kaplar, C.W. 1974. "Freezing test for evaluating relative frost susceptibility of various soils." Cold Regions Research and Engineering Laboratory Technical Report 250.

Kay, B.C., M.I. Sheppard and J.P.G. Loch. 1977. "A preliminary comparison of simulated and observed water redistribution in soils under laboratory and field conditions." Int. Symp. on Frost Action in Soils. Univ. of Lulea, pp.29-41.

Kay, B.D. and P.H. Groenevelt. 1974. "On the interaction of water and heat transport in frozen and unfrozen soils: I. Basic theory; the vapor phase." Soil Science Soc. Am. Proceedings, 38, pp.395-400.

Kijne, J.W. and S.A. Taylor. 1964. "The temperature dependence of soil water vapor pressure." Soil Sic. Soc. Amer. Proceedings 28, pp.595-599.

Koopmans, R.W.R. and R.D. Miller. 1966. "Soil freezing and

soil water characteristic curves." Soil Science Am. Proceedings, 30, pp.680-685.

Kudryavec, V.A., E. Ershov and V. Cheverev. 1973. "Moisture transfer in frozen soils." Moscow Univ. Geol. Bull. No. 5 (In Russian) pp.26-34.

Linell, K.A. and C.W. Kaplar. 1959. "The factor of soil and material type in frost action." Highway Research Board, Bull. 225, pp.81-126.

Loch, J. 1975. "Secondary heaving: experiments and analysis of frost heaving pressure in soils." Ph.D. Thesis, Dept. of Agronomy, Cornell University.

Loch, J.P.G. and B.D. Kay. 1978. "Water redistribution in partially frozen, saturated silt under several temperature gradients and overburden loads." Soil Science Soc. Am. J., 42, pp.400-406.,

Loch, J.P.G. 1978. "Thermodynamic equilibrium between ice and water in porous media." Soil Science, 126, pp.77-80.,

Loch, J.P.G. 1979a. "Influence of the heat extraction rate on the ice segregation rate of soils. Frost i Jord, 20, pp.19-30.

Loch, J.P.G. 1979b. Suggestions for an improved standard laboratory test for frost heave susceptibility of soils." Frost i Jord, 20, pp.33-38.

Loch, J.P.G. 1980. "Frost action in soils. State of the art." Proceedings 2nd International Symp. on Ground Freezing, Trondheim, Norway, pp.581-596.

Lovell, C. 1957. "Temperature effects on phase composition and strength of partially frozen soil." Hwy. Res. Board Bull. 168.,pp. 74-95.

Mageau, D. and N.R. Morgenstern. 1979. "Observations on moisture migration in frozen soils." Canadian Geotechnical J., Vol.17, No.1, Feb. 1980, pp.54-60.

Mageau, D.W. 1978. "Moisture migration in frozen soil." M.Sc. Thesis, Dept. of Civil Eng., University of Alberta, Edmonton.

Martin, R.T. 1959. "Thythmic ice banding in soil." Highway Research Board Bulletin 218, NAS-NRC, Washington, pp.11-23.

Miller, R.D. 1970. "Ice sandwich functional semipermeable membrane." Science, Vol.169, pp.584-585.

Miller, R.D. 1972. Freezing and heaving of saturated and unsaturated soils." Highway Research Rec. 393, pp.1-11.

Miller, R.D. 1978. "Frost-heaving in non-colloidal soils." Third International Conference Permafrost, Edmonton, Alberta, pp.707-713.

Miller, R.D., J.P. Loch and E. Bresler. 1975. "Transport of water in a frozen permeameter." Soil Science Soc. Amer. Proceedings 39, pp.1029-1036.

Morgenstern, N.R. 1980. Personal Communication.

Mualem, Y. 1976. "A new model for predicting the hydraulic conductivity of unsaturated porous media." Water Resource Research 12, pp.513-521.

Murray, W.D. and Landis, R. 1959. "Numerical and machine solutions of transient heat conduction problems involvng melting or freezing." Trans. Am. Soc. Mech. Eng. 81, pp.106-112.

Nersesova, Z. and N.A. Tsytovich. 1963. "Unfrozen water in frozen soils." Proceedings 1st International Conference Permafrost, Purdue Univ., Lafayette, Indiana, pp.230-234.

Nixon, J.D. 1973. "The consolidation of thawing soils." Ph.D. Thesis, Dept. of Civil Eng., University of Alberta, Edmonton.

Northern Engineering Services. 1975. "Interim report on results from frost effects study.

Palmer, A.C. 1967. "Ice lensing, thermal diffusion and water migration in freezing soil." J. of Glaciology, Vol.6, No.47, pp.681-694.

Penner, E. and L.E. Goodrich. 1980. "Location of segregated ice in frost susceptible soil." Proceedings 2nd International Symp. on Ground Freezing, Trondheim, Norway, pp.626-639.

Penner, E. and T. Ueda. 1977. "The dependence of frost heaving on load application." Symposium on Frost Action in Soils. University of Lulea, Lulea, Sweden, Proceedings, Vol.I, pp.92-101.

Penner, E. and T. Ueda. 1978. "A frost-susceptibility test and a basis for interpreting heaving rates." Proceedings Third International Conference on Permafrost, Edmonton, Alberta, pp.721-727.

Penner, E. and T. Walton. 1978b. "Effects of pressure and temperature on frost heave." Proceedings International

Symposium on Ground Freezing, Ruhr-University Bochum, Germany.

Penner, E. 1958a. "Pressures developed in a porous granular system as a result of ice segregation." Highway Research Board, Special Report 40, pp.191-199.

Penner, E. 1958b. "Soil moisture suction - its importance and measurement." Proceedings American Society for Testing Materials, Vol.58, pp.1205-1217.

Penner, E. 1959. "The mechanism of frost heaving in soils." Highway Research Board., Bull.225, pp.1-22.

Penner, E. 1960. "The importance of freezing rate in frost action in soils." Proceedings American Society for Testing Materials, Vol.60, pp.1151-1165.

Penner, E. 1963. "Frost-heaving in soils." Proceedings First International Conference on Permafrost, Purdue Univ., Lafayatte, Indiana, pp.197-202.

Penner, E. 1967a. "Heaving pressures in soils during unidirectional freezing." Canadian Geotech. J., Vol.IV, No.4, pp.398-408.

Penner, E. 1967b. "Pressures developed during the unidirectional freezing of water-saturated porous materials." Proceedings International Conference on Low Temp. Science, Sapporo, Japan, pp.1401-1412.

Penner, E. 1968. "Particle size as a basis for predicting frost action in soils." Soils and Foundations, Vol.8, No.4, pp.21-18.

Penner, E. 1970. "Frost heaving froces in Leda clay." Canadian Geotech. J., Vol.7, No.8, pp.8-16.

Penner, E. 1972. "Influence of freezing rate on frost heaving." Highway Research Rec. 393, pp.56-64.

Radd, F.J. and D.H. Oertle. 1973. "Experimental pressure studies of frost heave mechanisms and the growth-fusion behavior of ice." Proceedings 2nd International Conference on Permafrost. Yakutsk, USSR, pp.377-384.

Slusarchuk, W., J. Clark, J.F. Nixon, N.R. Morgenstern, P. Gaskin. 1978. "Field test results of a chilled pipeline buried in unfrozen ground." Proceedings 3rd International Conference Permafrost, Edmonton, Alberta, pp.878-890.

Taber, S. 1929. "Frost heaving." J. Geology, Vol.37, pp.428-461.

Takashi, T., H. Yamamoto, T. Ohrai and M. Masuda. 1978. "Effect of penetration rate of freezing and confining stress on the frost heave ratio of soil." Proceedings Third International Conference Permafrost, Vol. I, pp.736-742.

Takashi, T., M. Masuda and H. Yamamoto. 1974. "Experimental study on the influence of freezing speed upon frost heave ratio of soil under constant effective stress." J. Jap. Soc. Snow and Ice, Vol.36, pp.49-67.

Taylor, G.S. and J.N. Luthin. 1976. "Numeric results of coupled heat-mass flow during freezing and thawing." Proceedings Second Conference on Soil Water Problems in Cold Regions, Edmonton, Alberta, pp.155-172.

Taylor, G.S. and J.N. Luthin. 1978. "A model for coupled heat and moisture transfer during soil freezing." Canadian Geotechnical J., Vol.15, p.548.

Vignes, M. and K. Dijkema. 1974. "A model for the freezing of water in a dispersed medium." J. Colloid Interface Science, Vol.49, pp.165-172.

Williams, P.J. and T. Burt. 1974. "Measurement of hydraulic conductivity of frozen soils." Canadian Geotechnical J., Vol.11, pp.647-650.

Williams, P.J. 1968. "Properties and behavior of freezing soils." Norwegian Geotech. Inst. Publ. No.72, Oslo.,

Williams, P.J. 1976. "Volume change in frozen soils. Laurits Bjerrum Memorial Volume." Norwegian Geotech. Inst., pp.233-246.

Wissa, A. and R.T. Martin. 1968. "Behavior of soils under flexible pavements - development of rapid frost susceptibility tests." Mass. Inst. Tech. Research Rep. R68-77, Soils Publ. 224, pp.1-113.

Zoller, J.H. 1973. "Frost heave and the rapid frost heave test." Public Roads, 37, pp.211-0220.

APPENDIX A

Properties of Devon silt of Series S, NS, and E

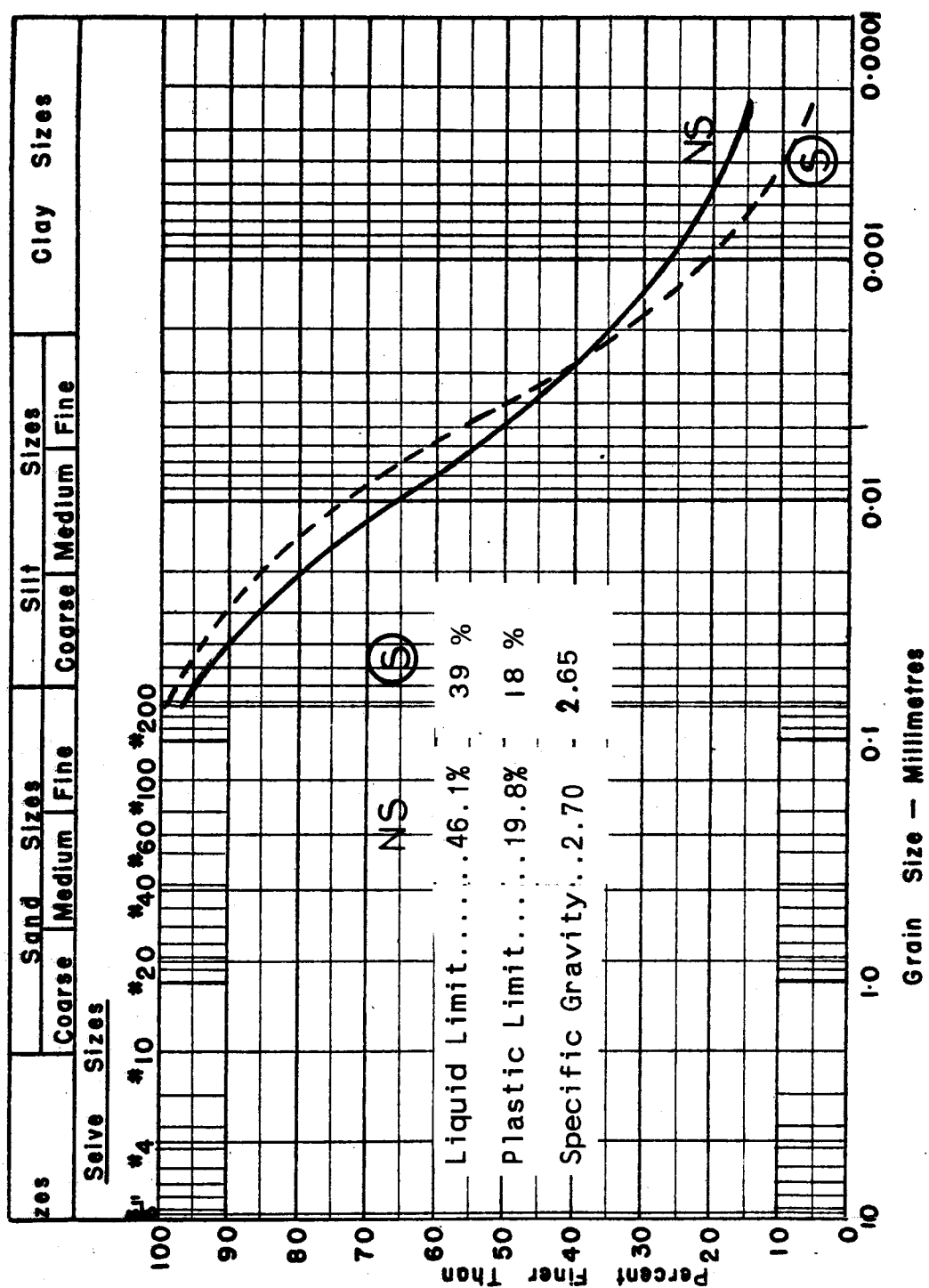Experimental set-up for freezing with applied back pressure

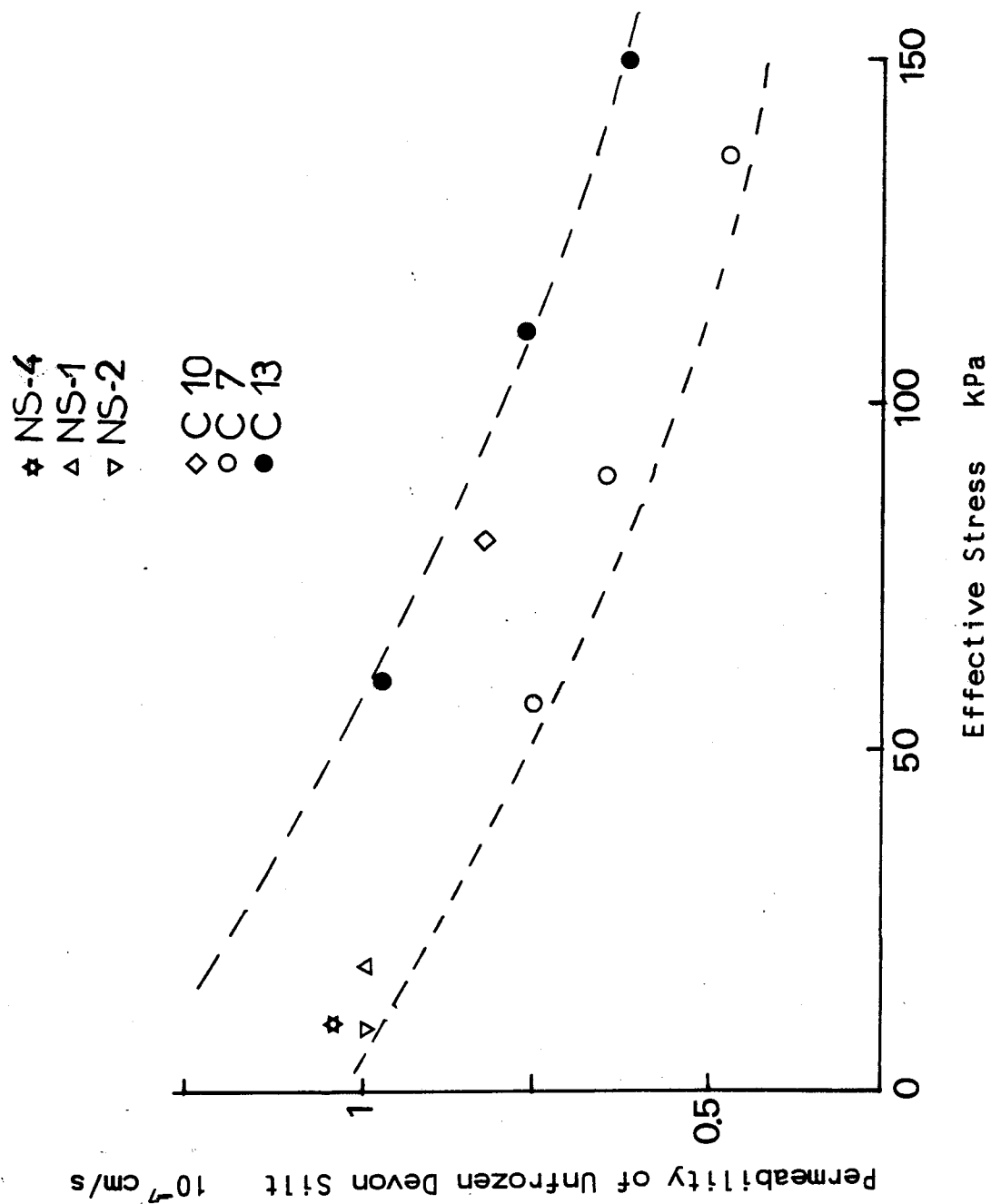Fig. A 1   Properties of Devon Silt From Series S and NS

University of Alberta

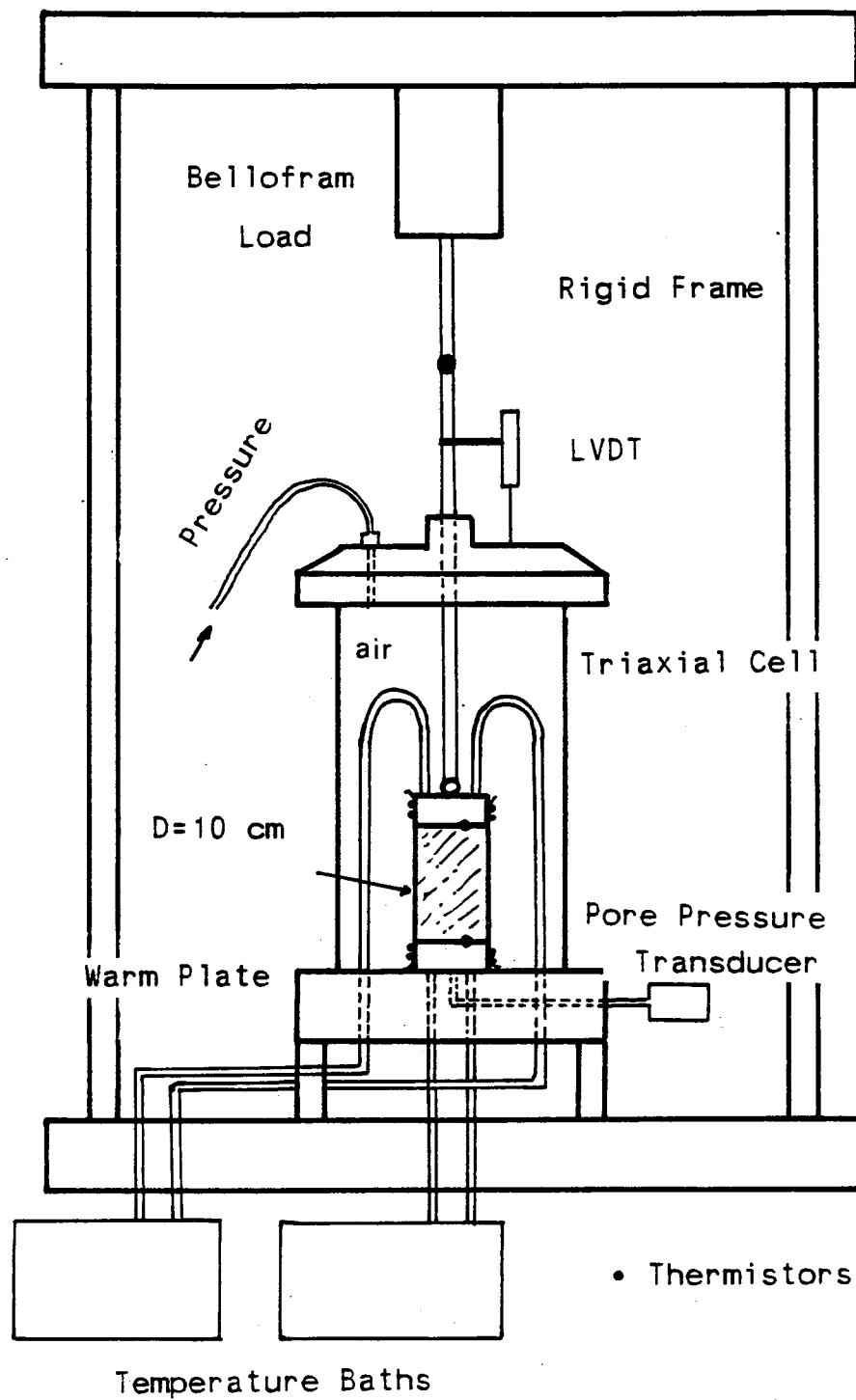Fig. A 2　　　Permeability of Unfrozen Devon Silt. Pc=210 kPa

Fig. A 3   Experimental Set-Up for Freezing Tests with High Applied Back-Pressure

APPENDIX B

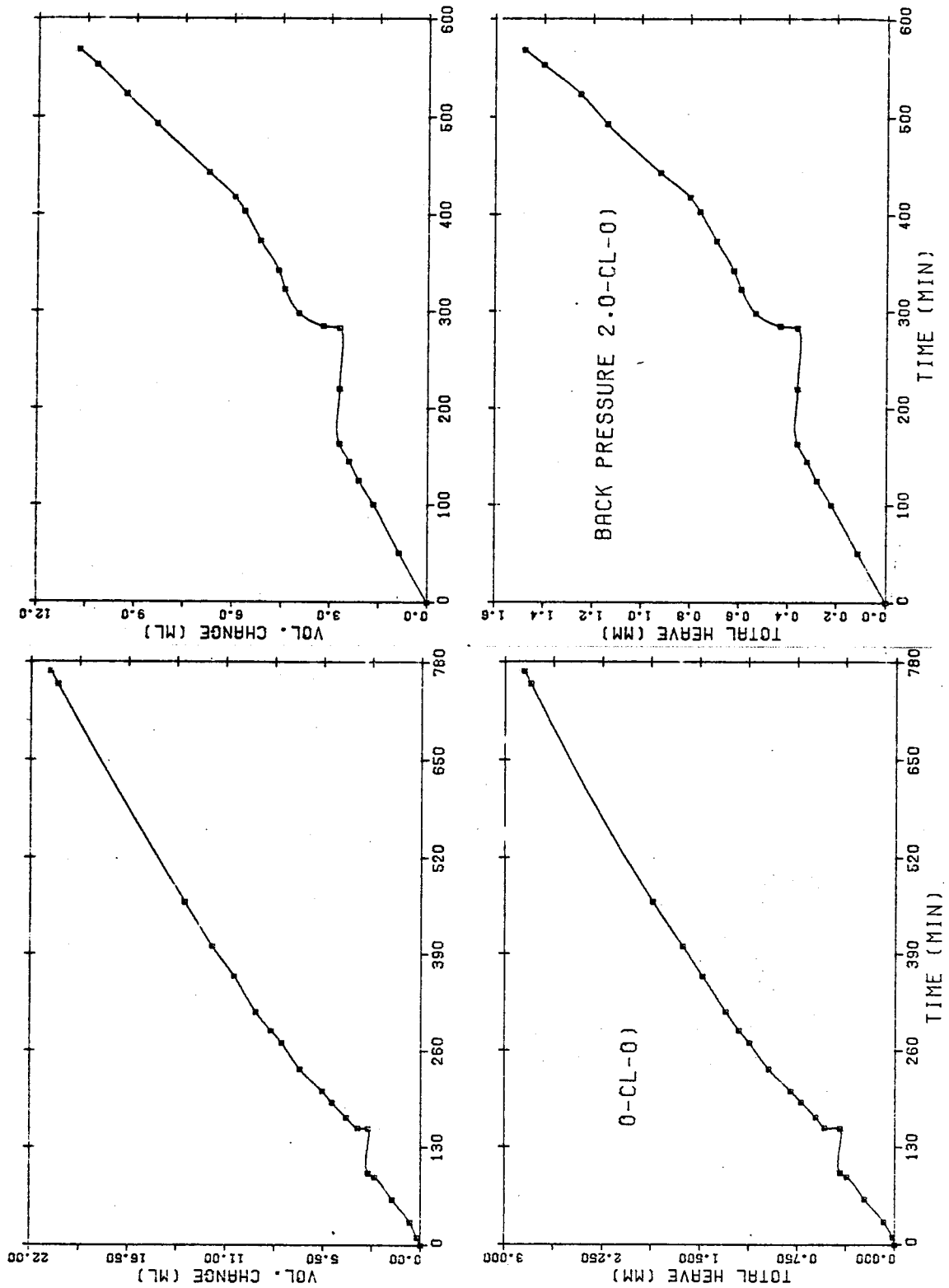# Experimental Results from Series S

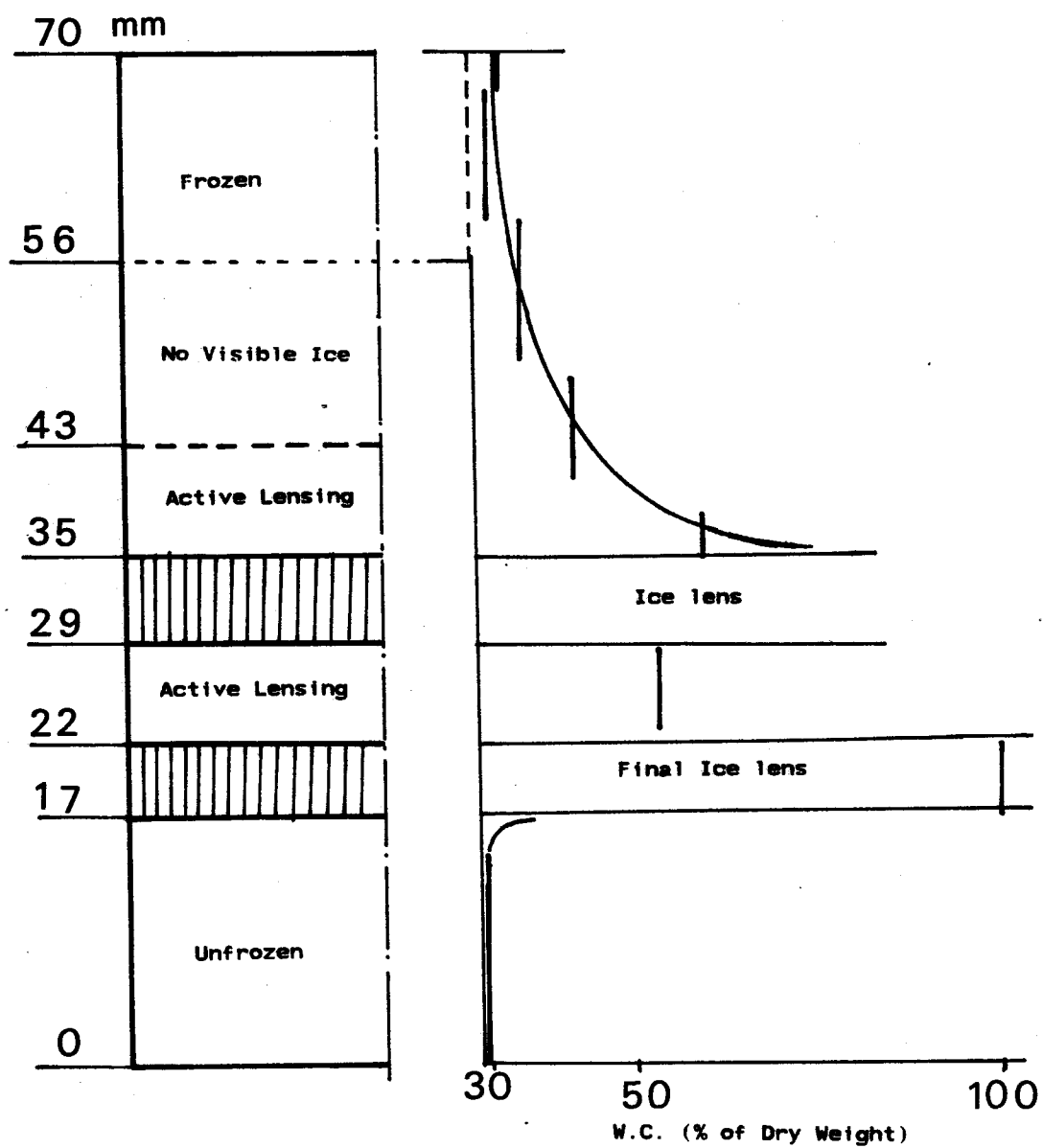Fig. B 1   Water Intake Before and After Closed System
Freezing in Test S 1
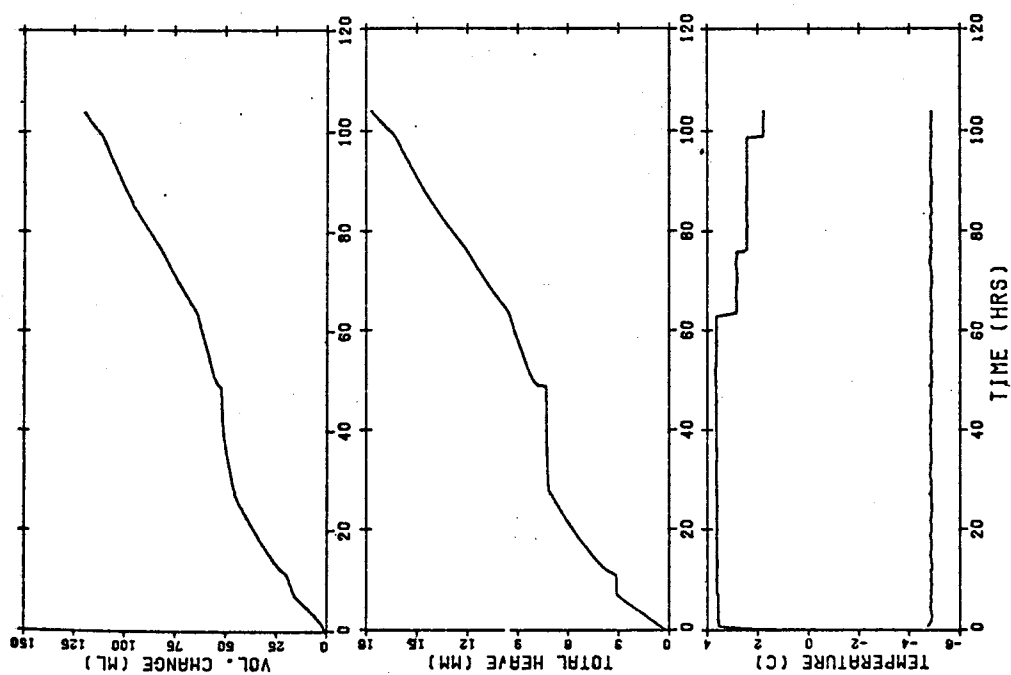
Fig. B 2   Experimental Results from Test S 1

Fig. B 3   Experimental Results from Test S 2

University of Alberta
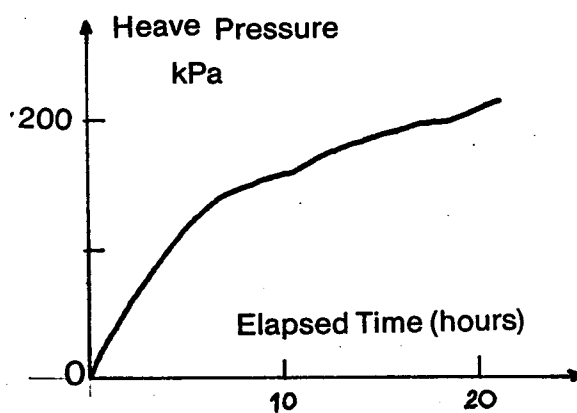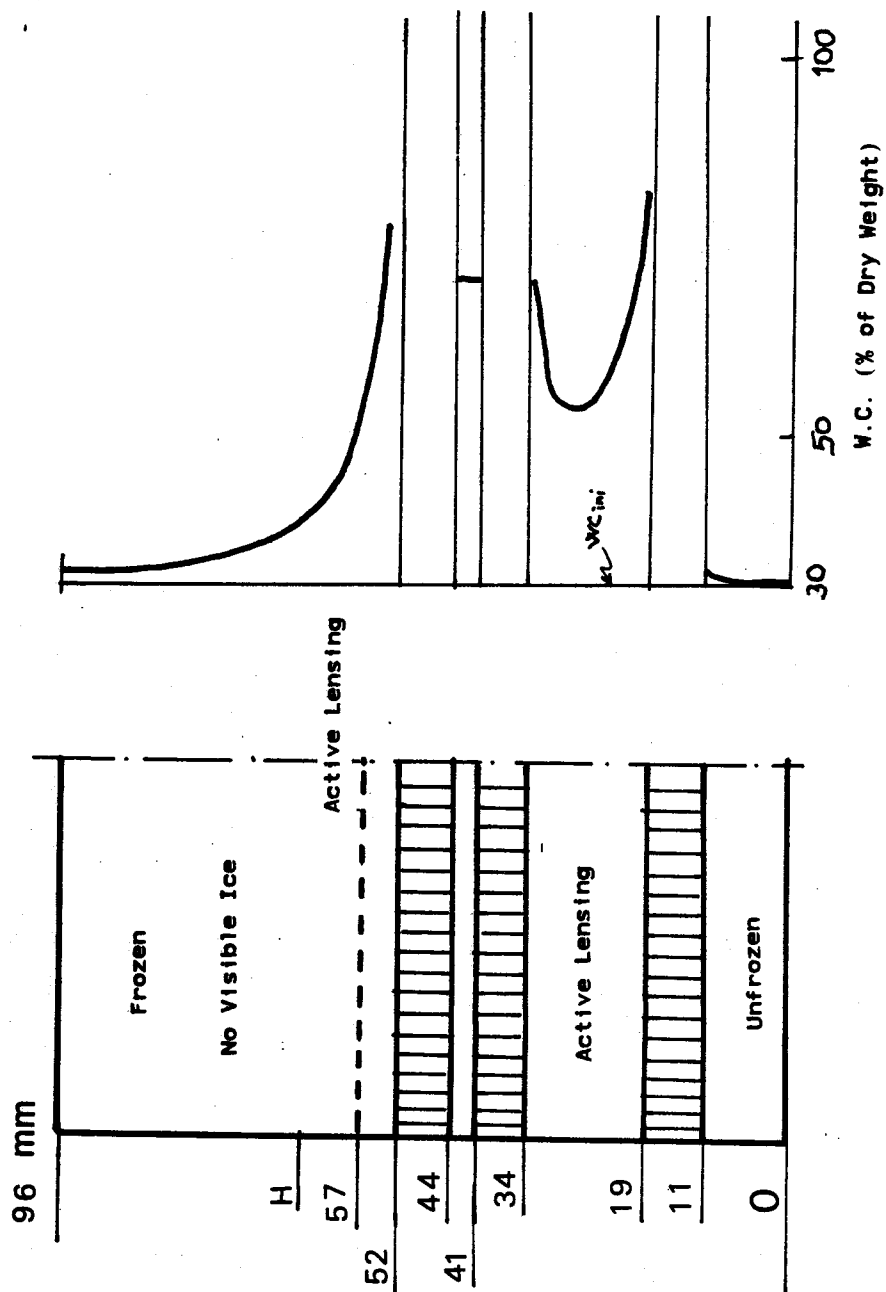

Fig. B 4   Experimental Results from Test S 5
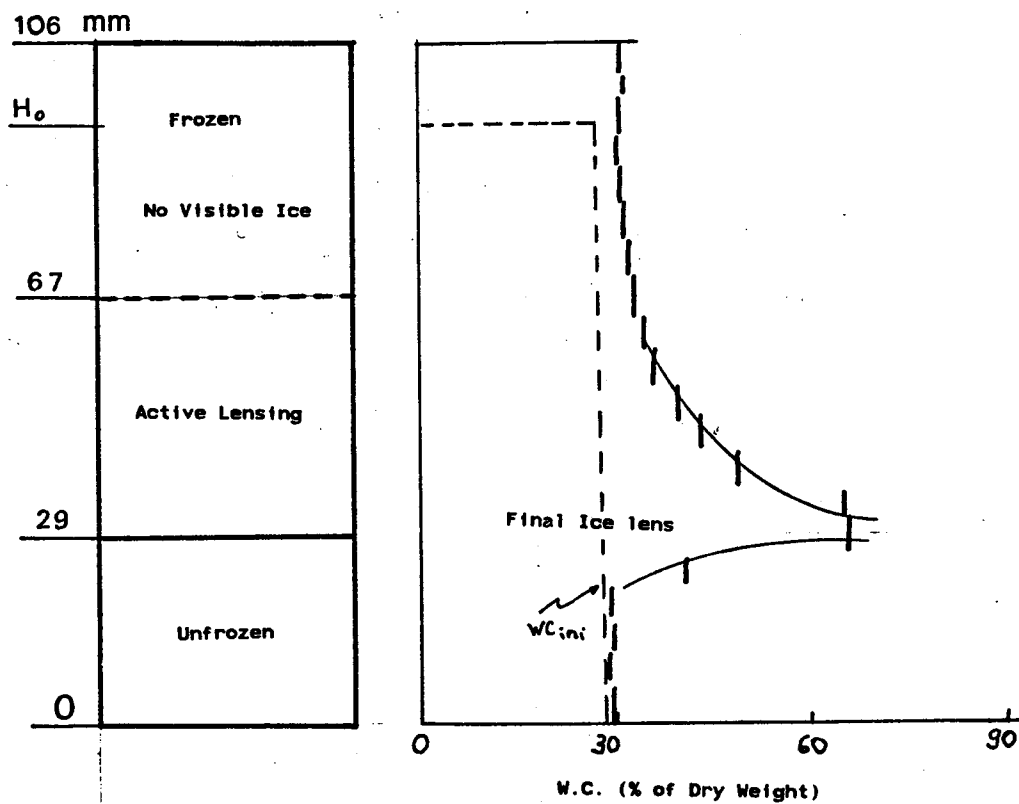
Fig. B 5   Experimental Results from Test S 6
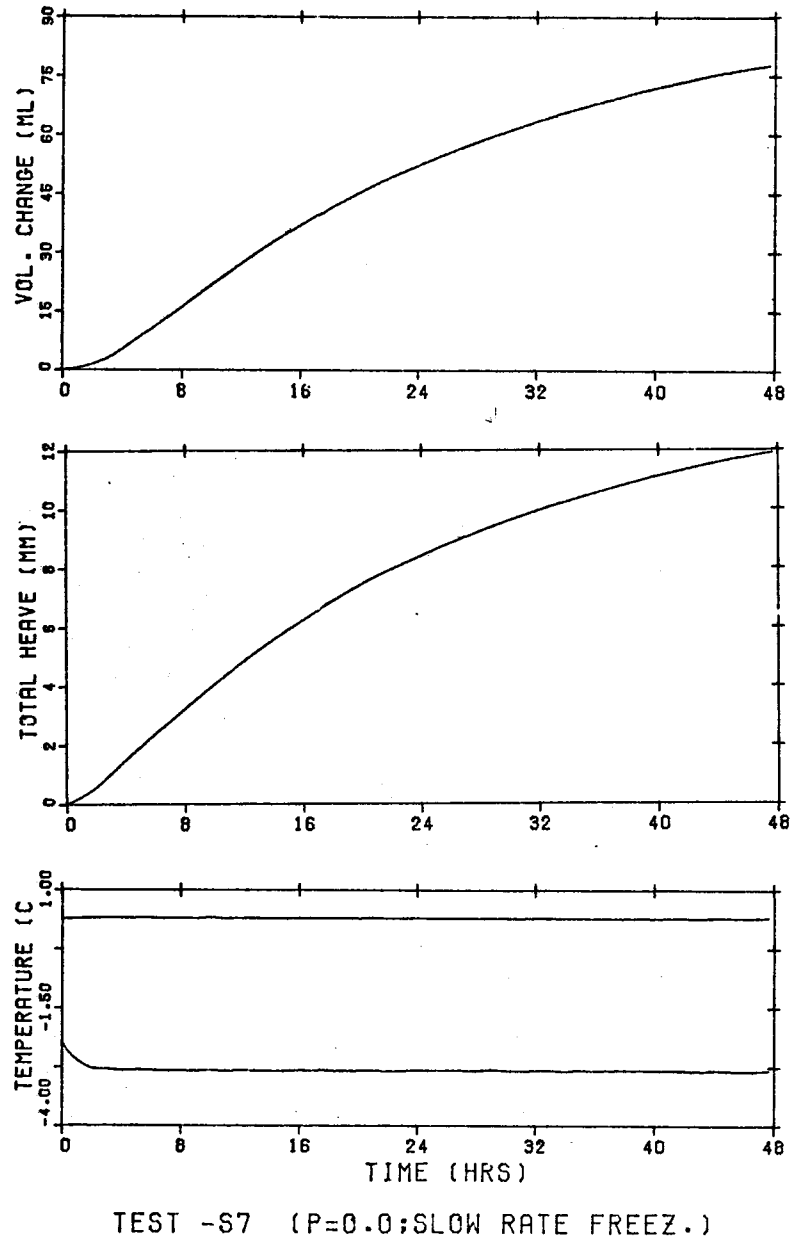
TEST -S7   (P=0.0;SLOW RATE FREEZ.)
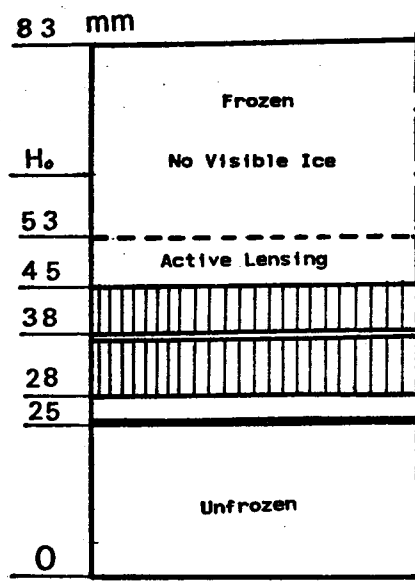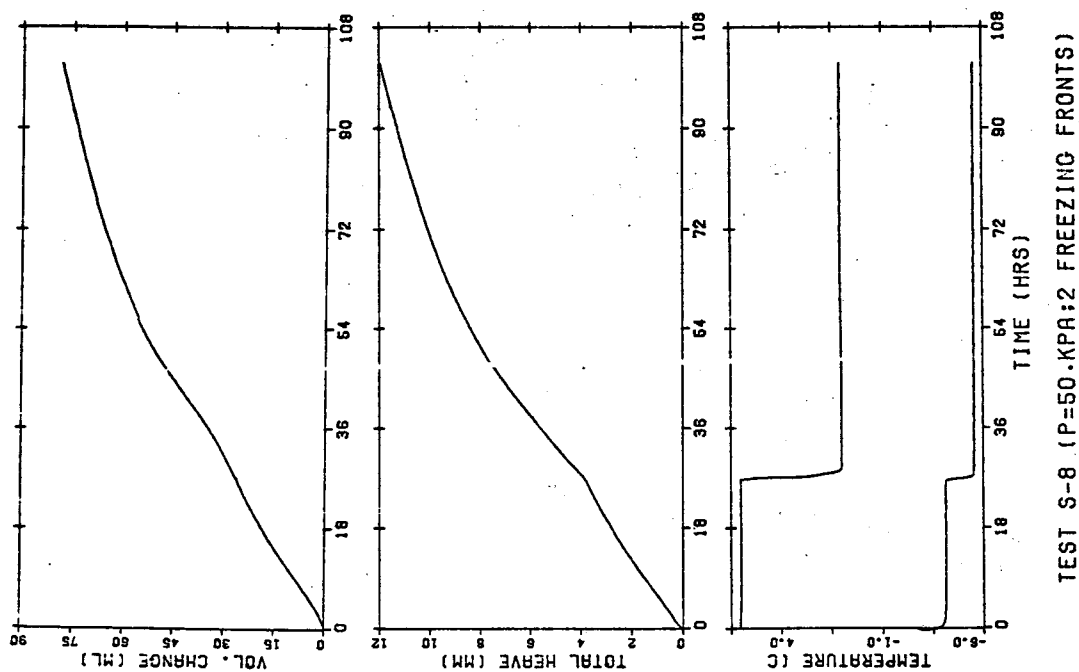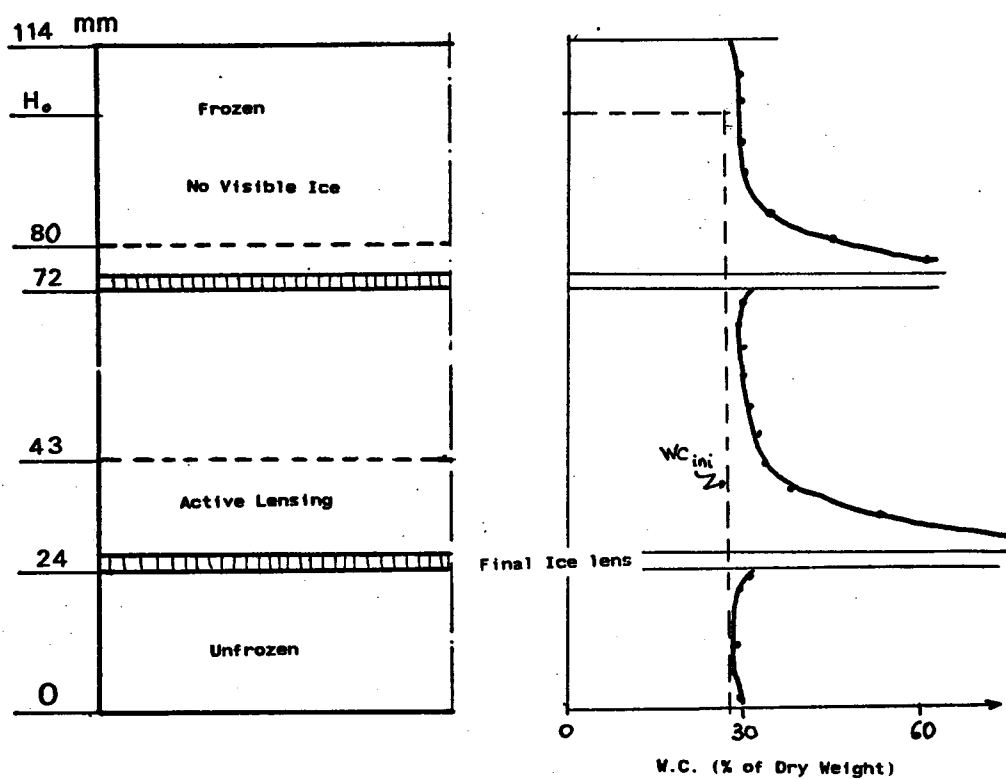
Fig. B 6   Experimental Results from Test S 7

Fig. B 7   Experimental results from Test S 8 - Pe=50 kPa

APPENDIX C

Experimental Results

C1 - C12 Series NS

C13 - C20 Series E

Zero External Surcharge
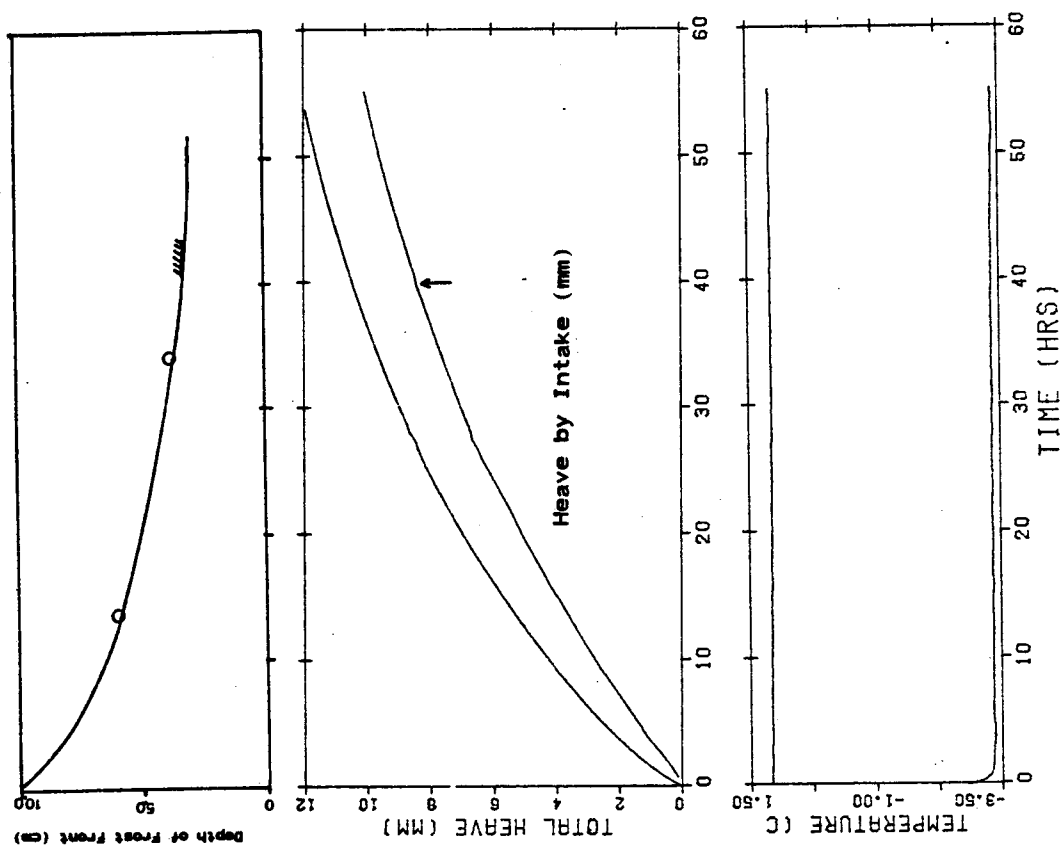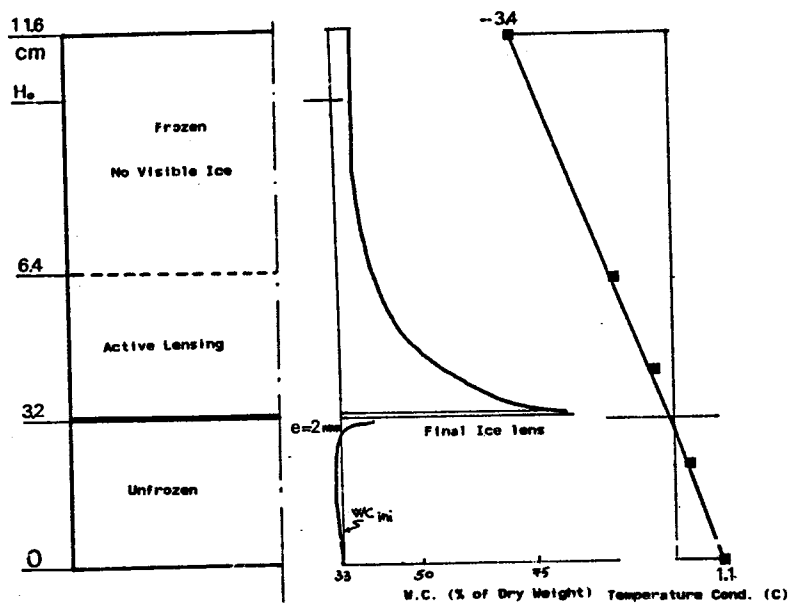
Figure C.1 Experimental Results From Test NS-1
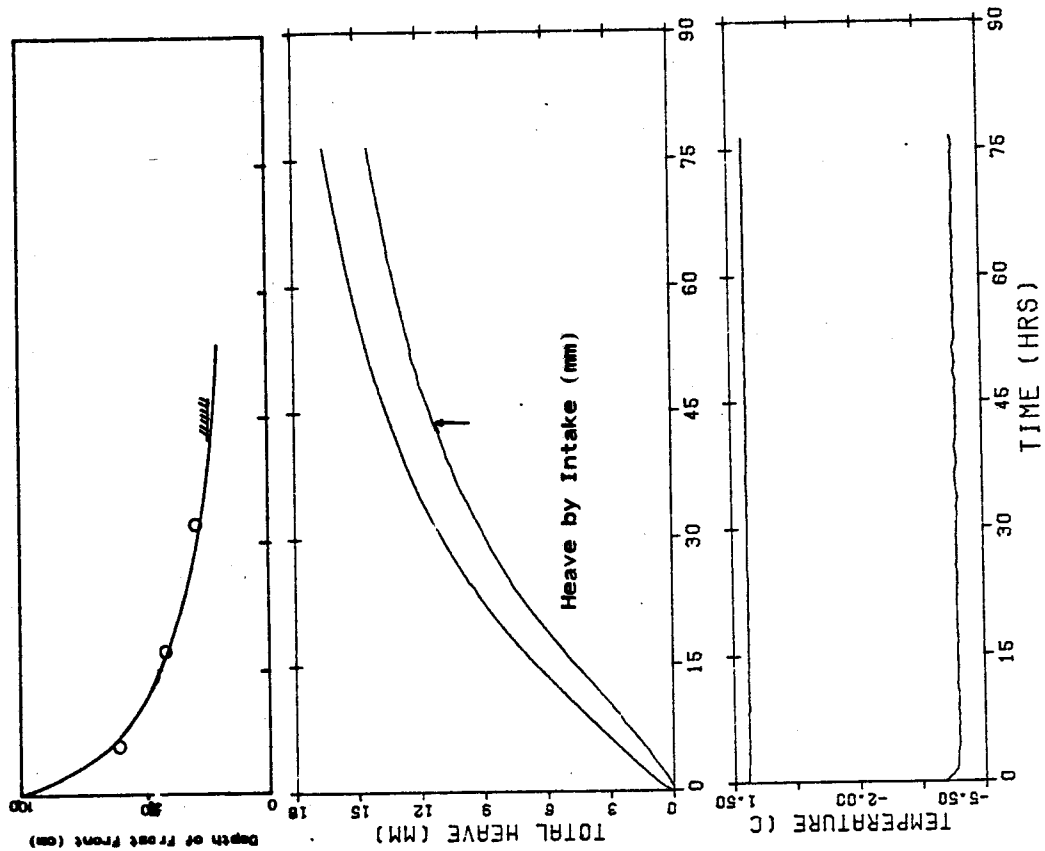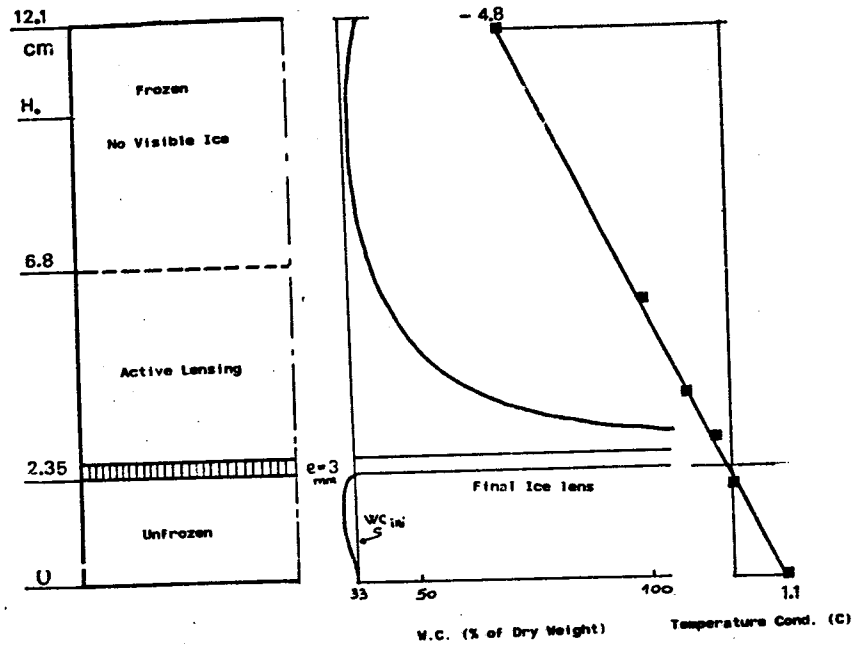
Figure C.2 Experimental Results From Test NS-2
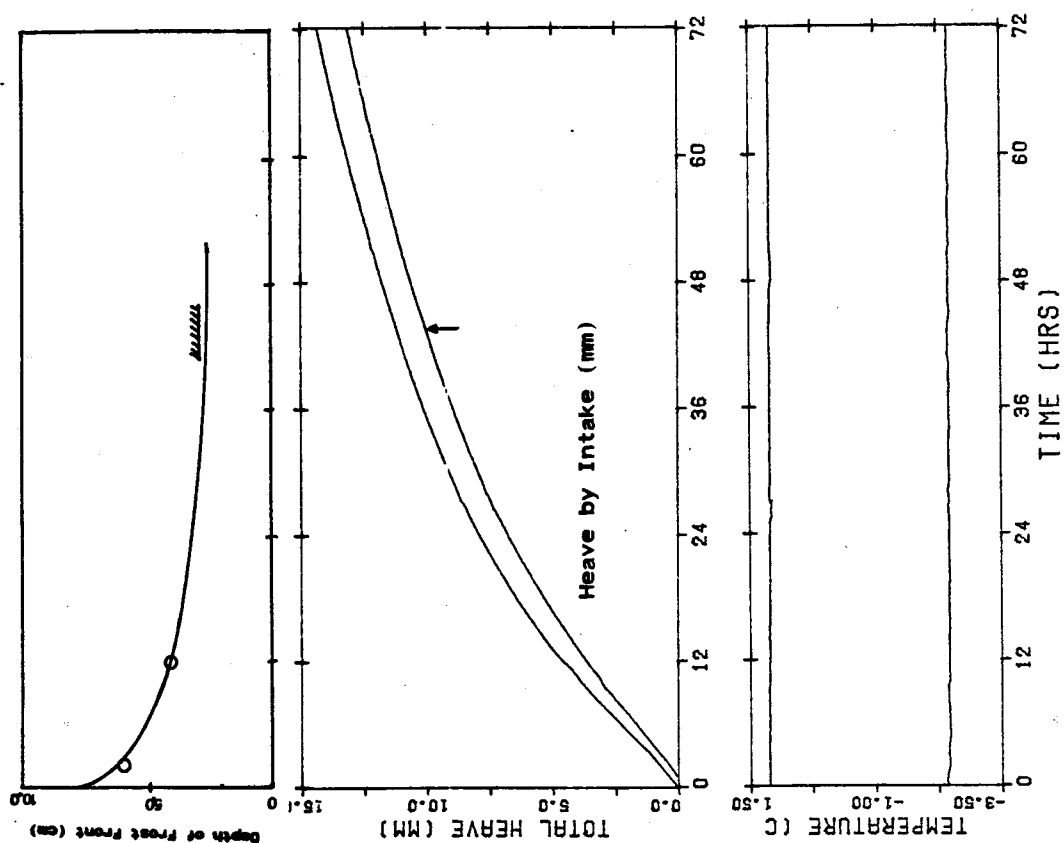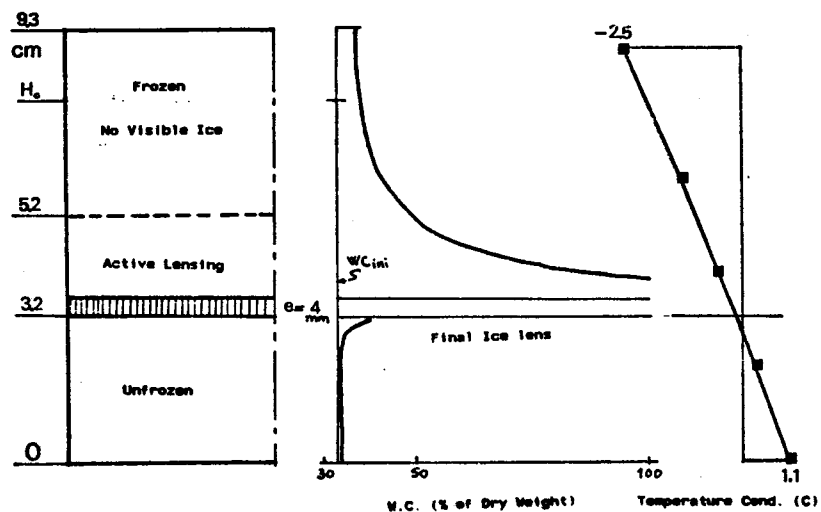
Figure C.3 Experimental Results From Test NS-4
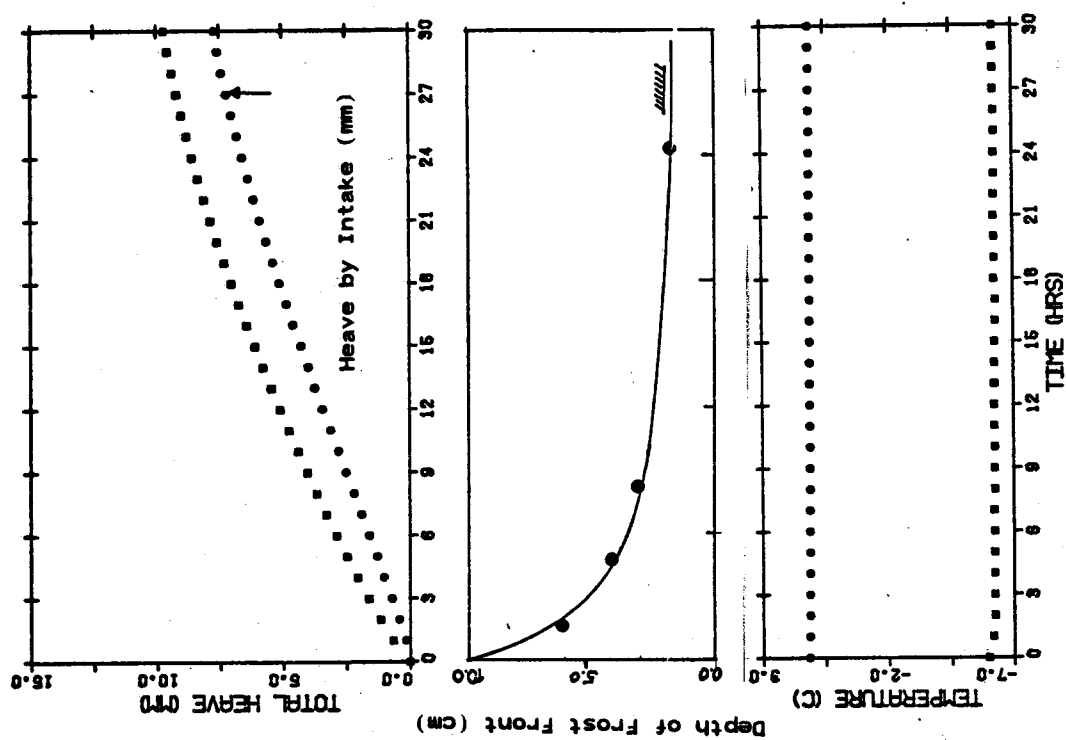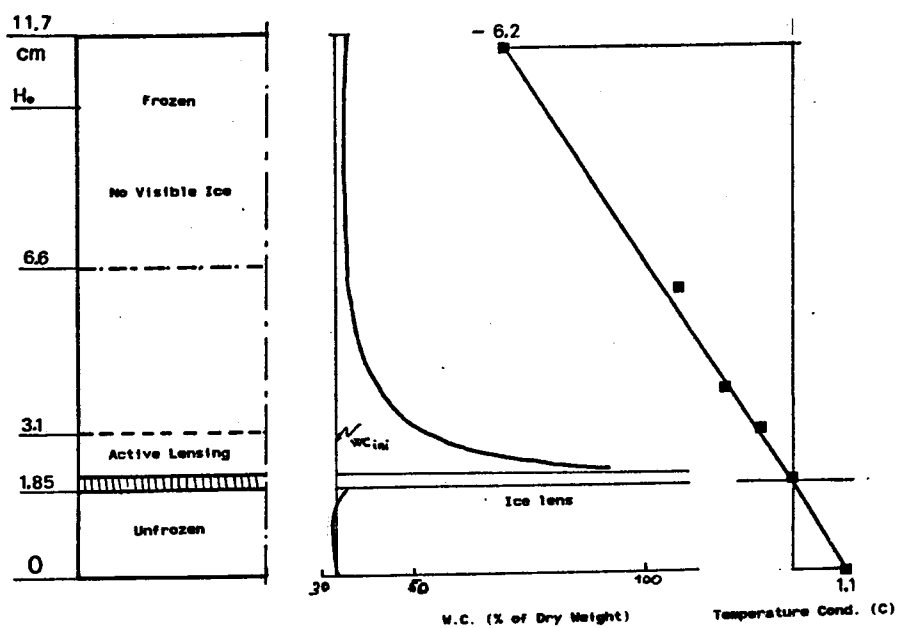
Figure C.4 Experimental Results From Test NS-5
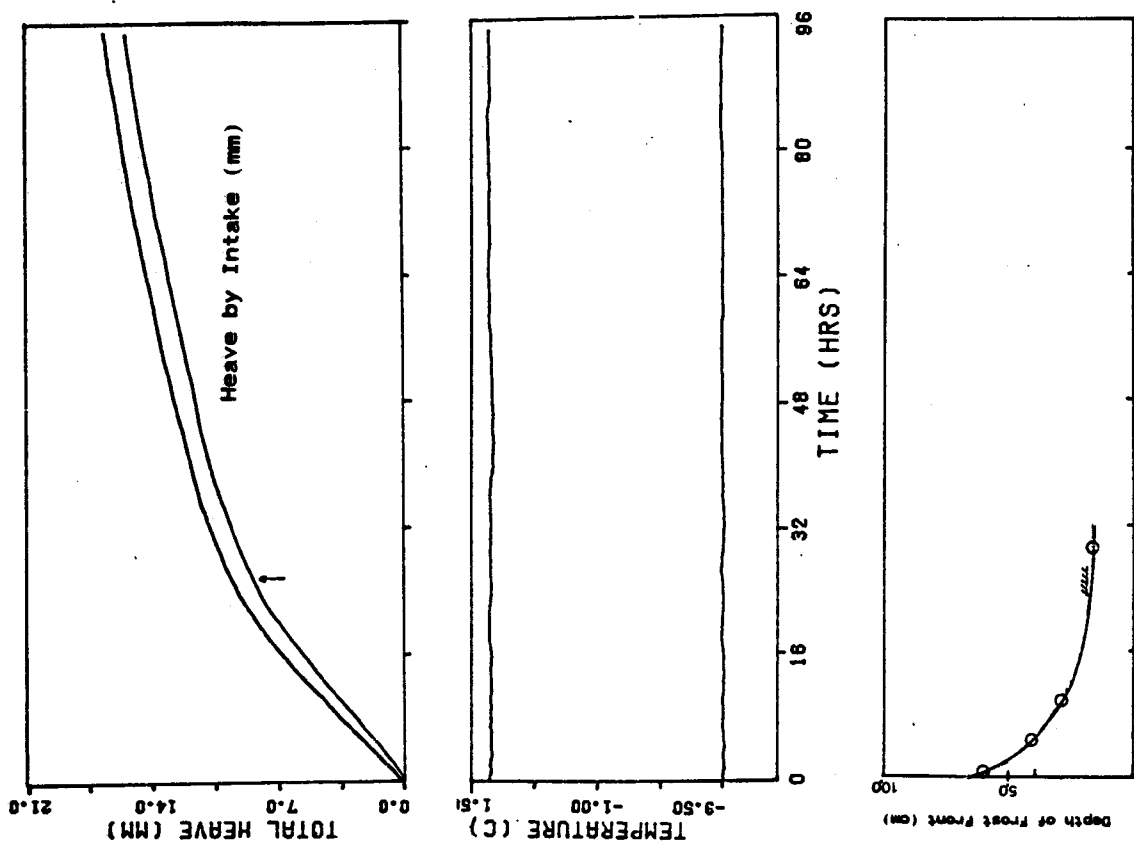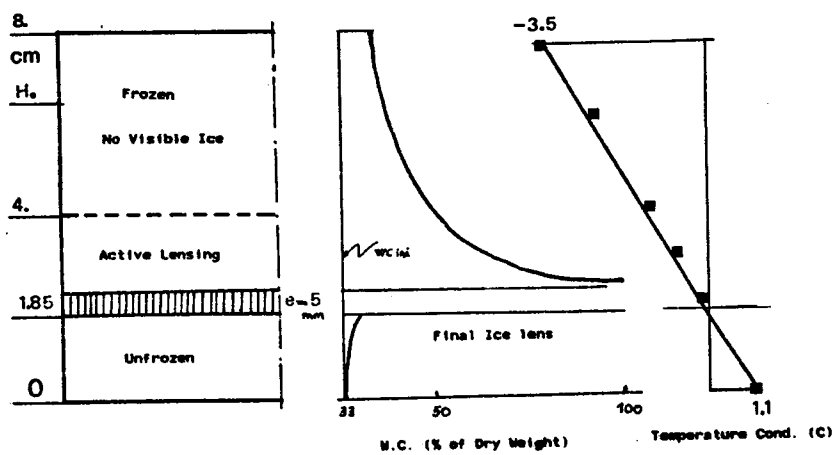
Figure C.5 Experimental Results From Test NS-6

University of Alberta
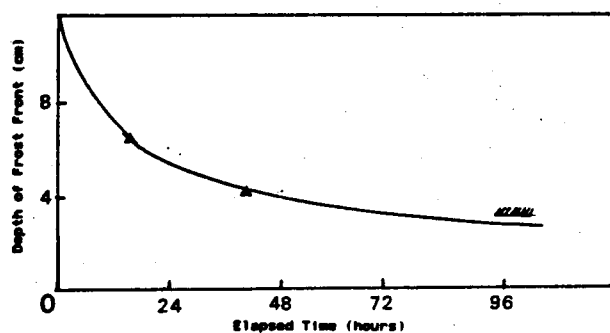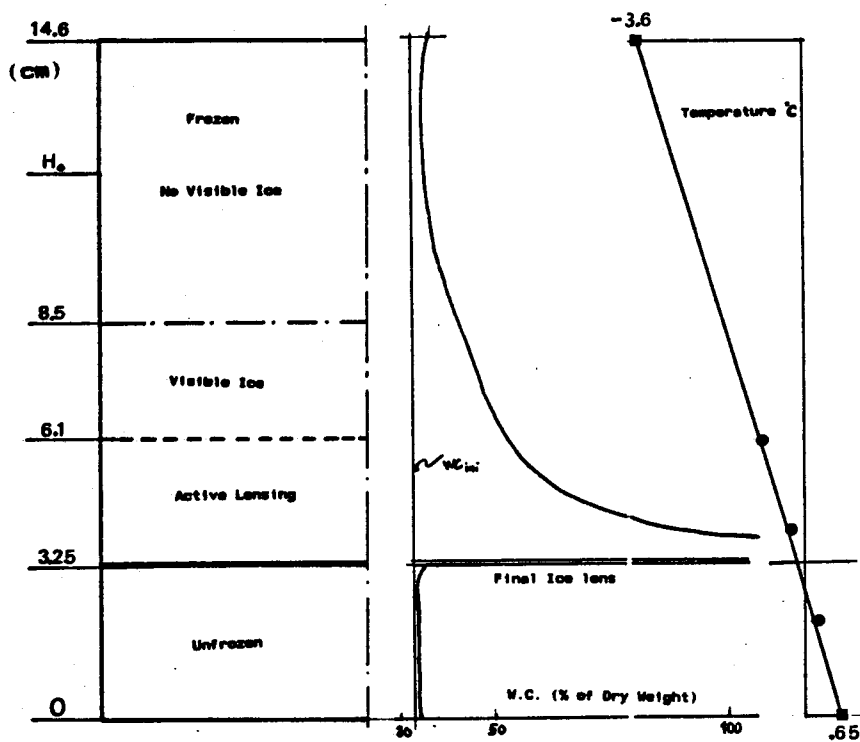
Figure C.6 Experimental Results From Test NS-7
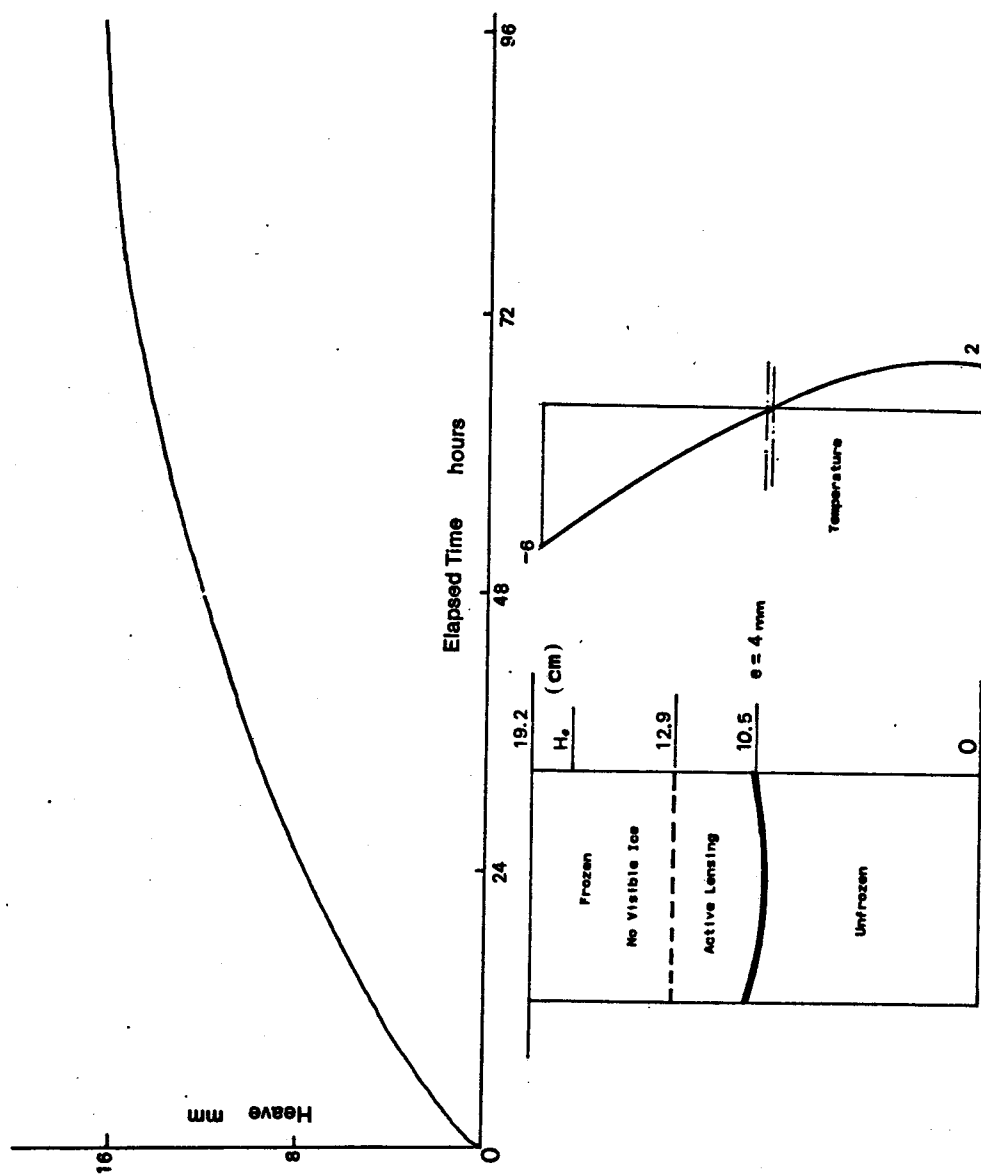
Figure C.7 Experimental Results From Test NS-8
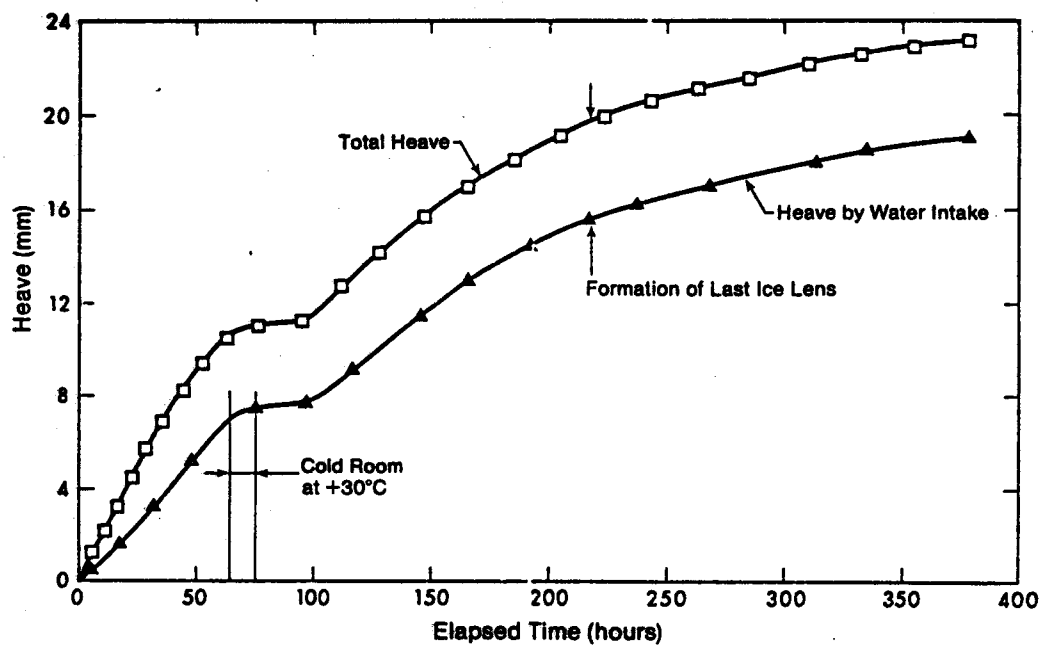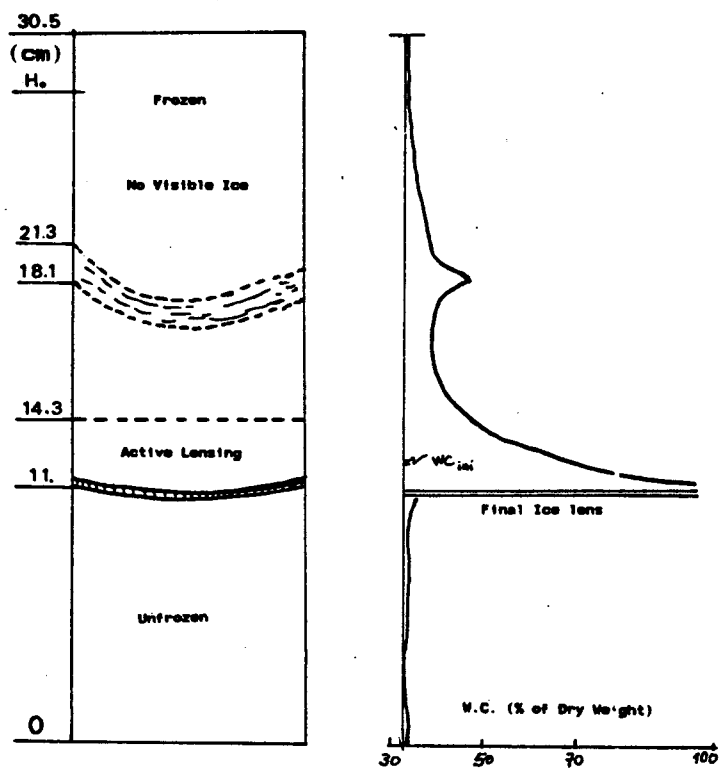
Figure C.8 Experimental Results From Test NS-9

Figure C.9 Experimental Results From Test NS-10
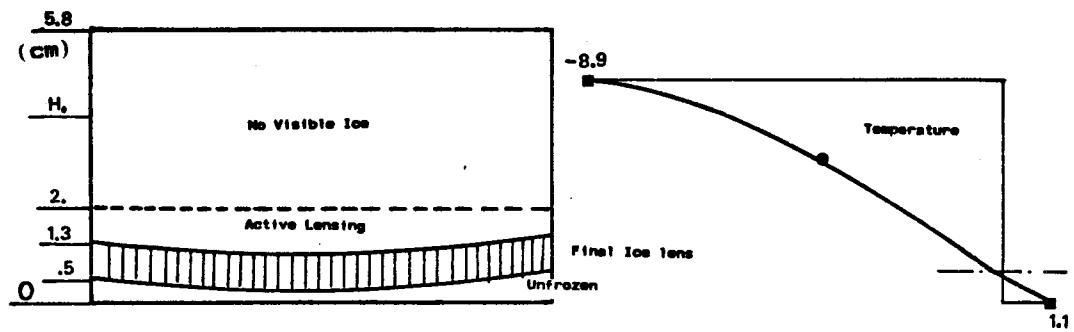
Figure C.10 Experimental Results From Test NS-11
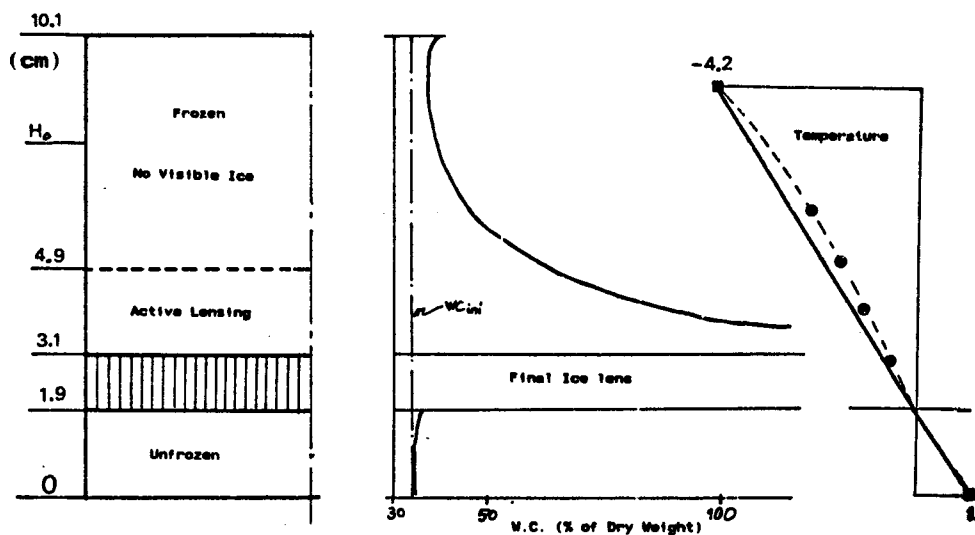
NS 12
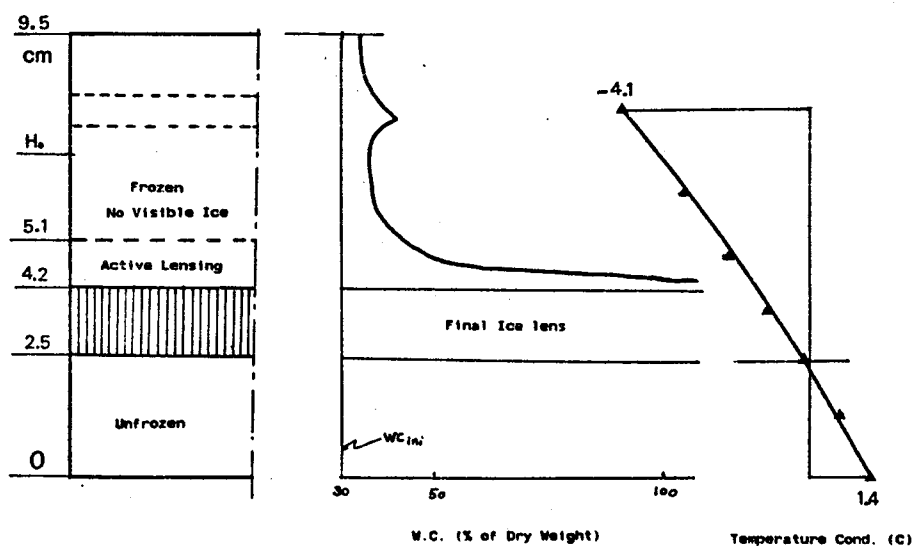
G 1

Figure C.11 Experimental Results From Test NS-12
& Test G-1
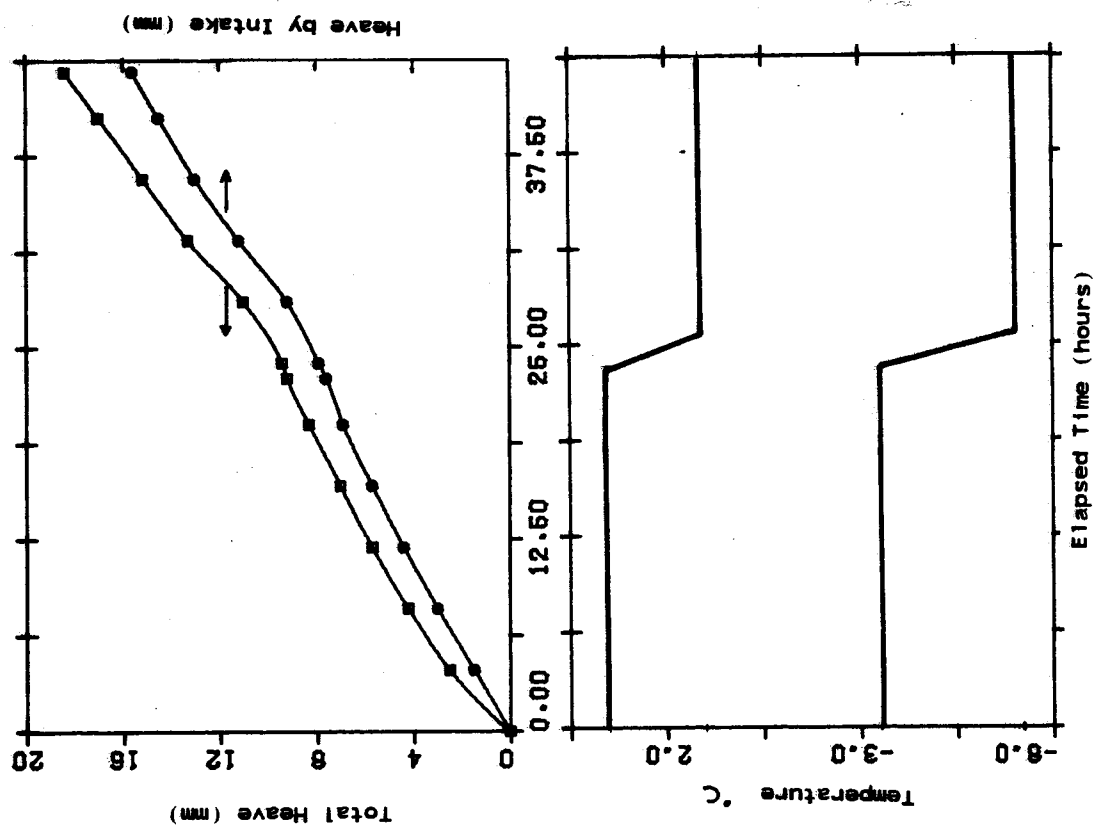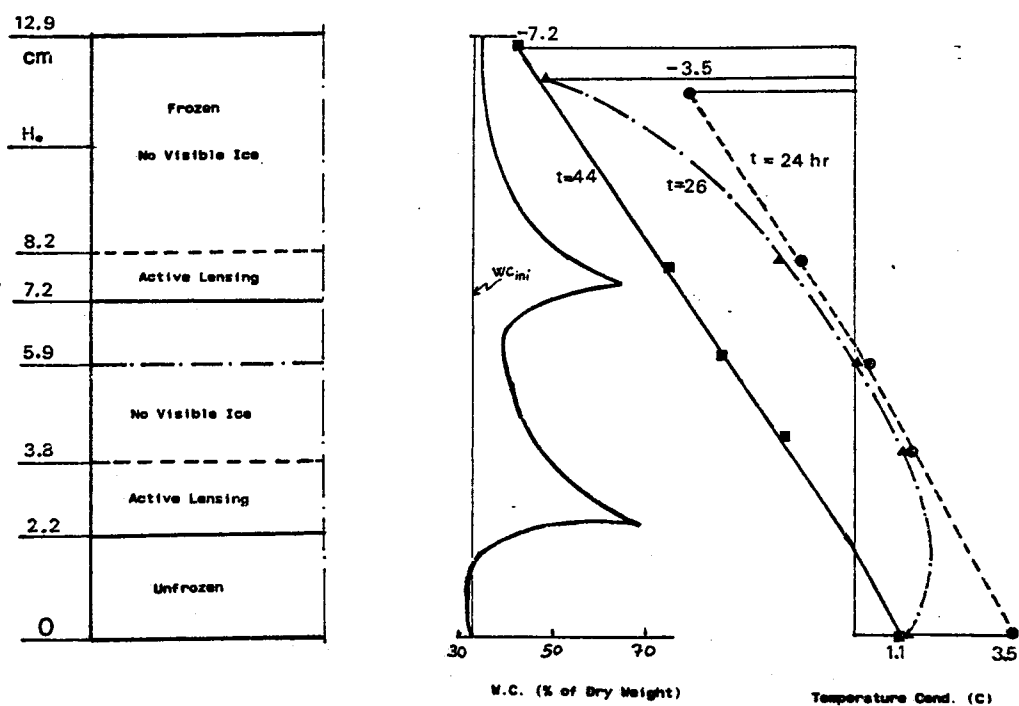
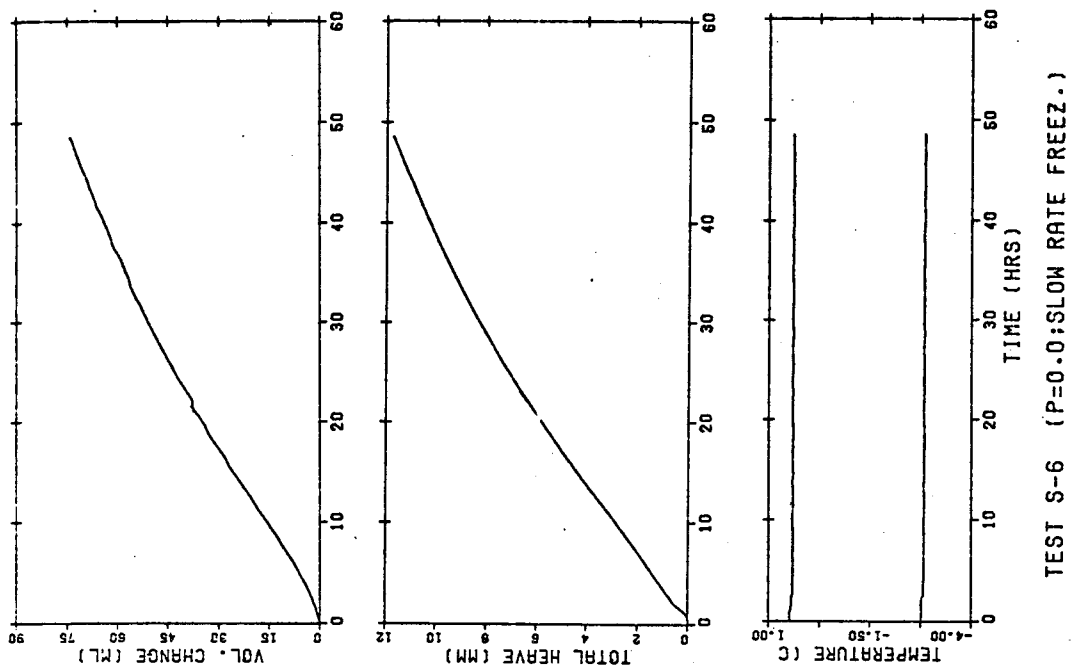Figure C.13 Experimental Results From Test E-1
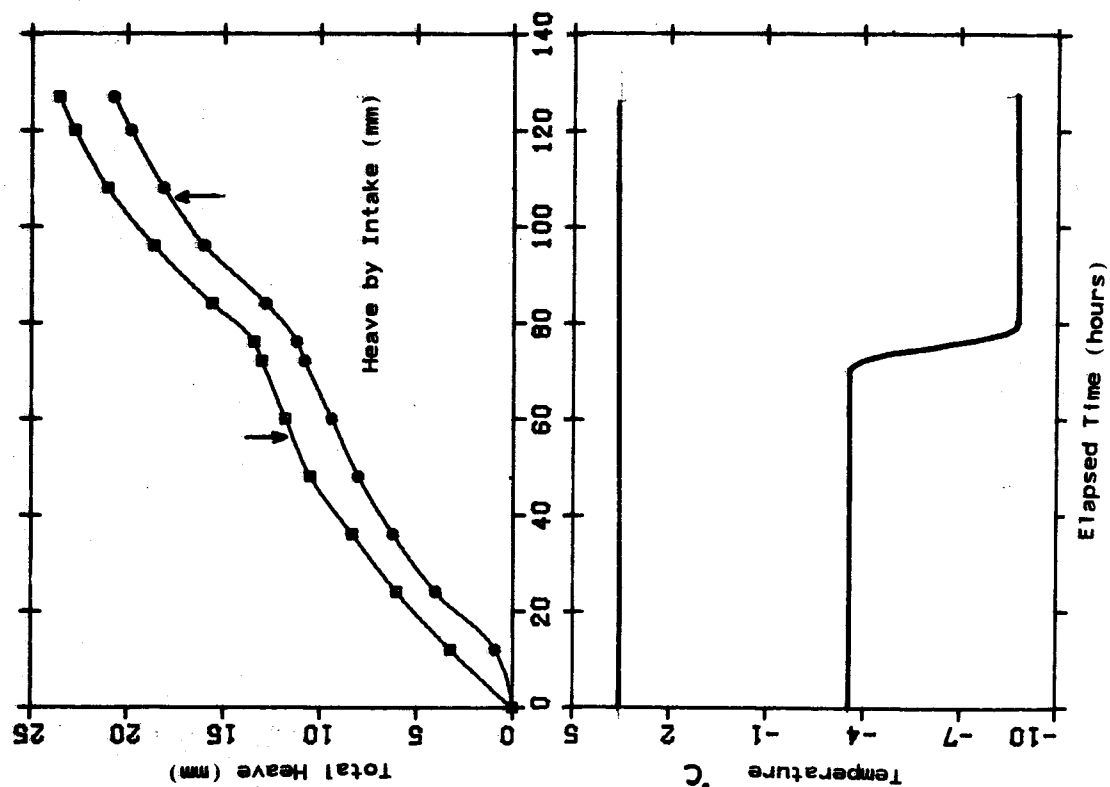
Figure C.14 Experimental Results From Test E-2
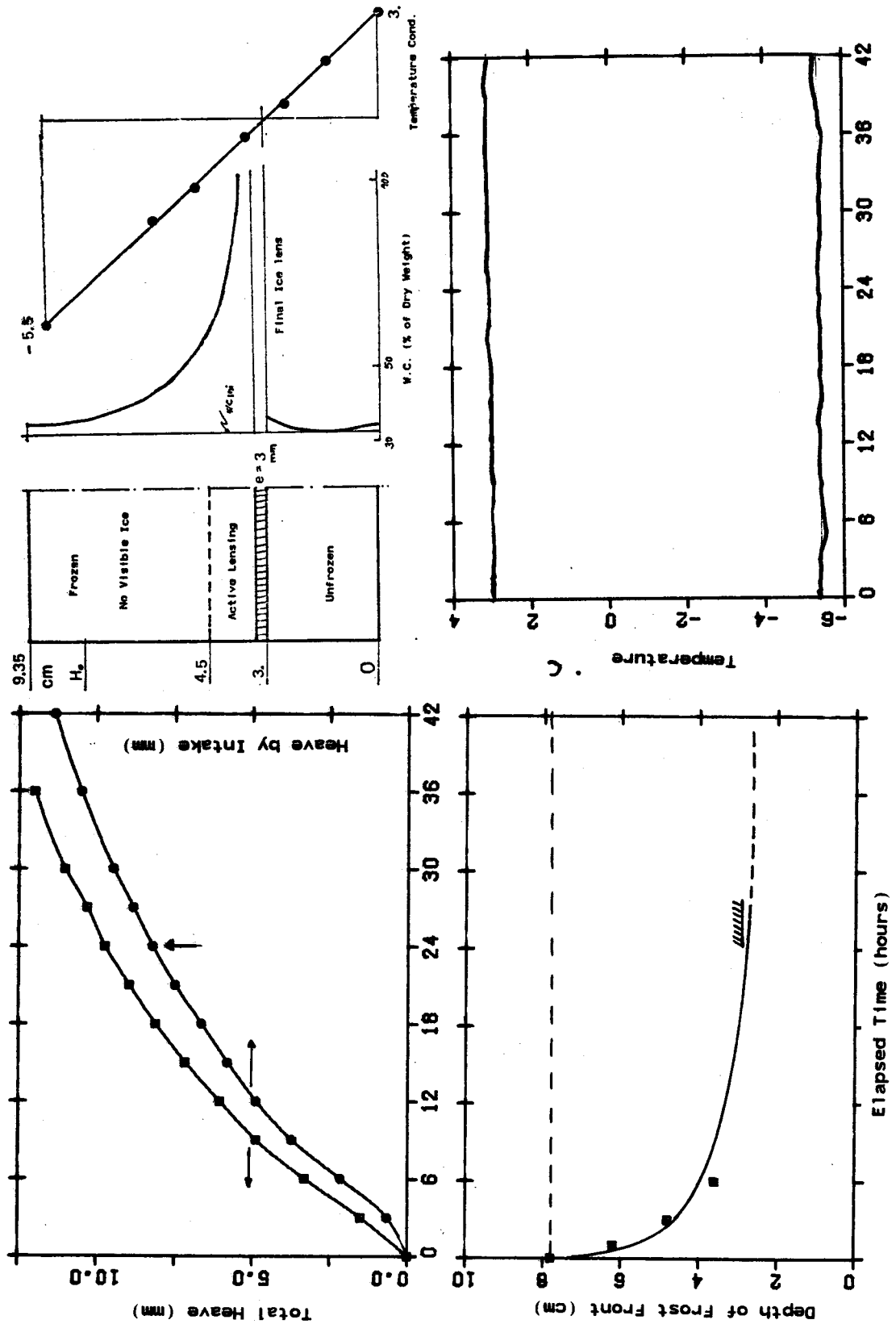
Figure C.15 Experimental Results From Test E-4
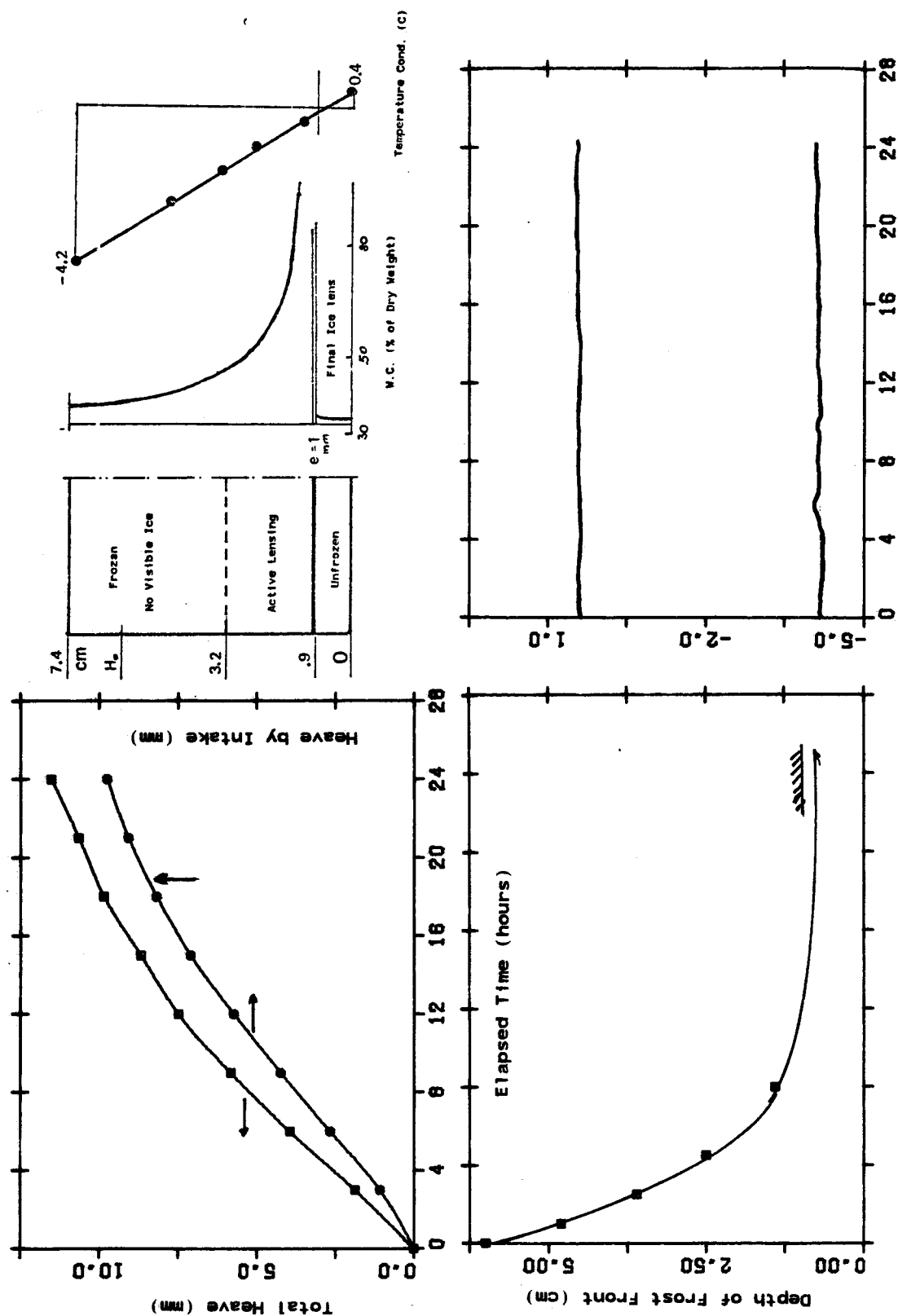
Figure C.16 Experimental Results From Test E-5
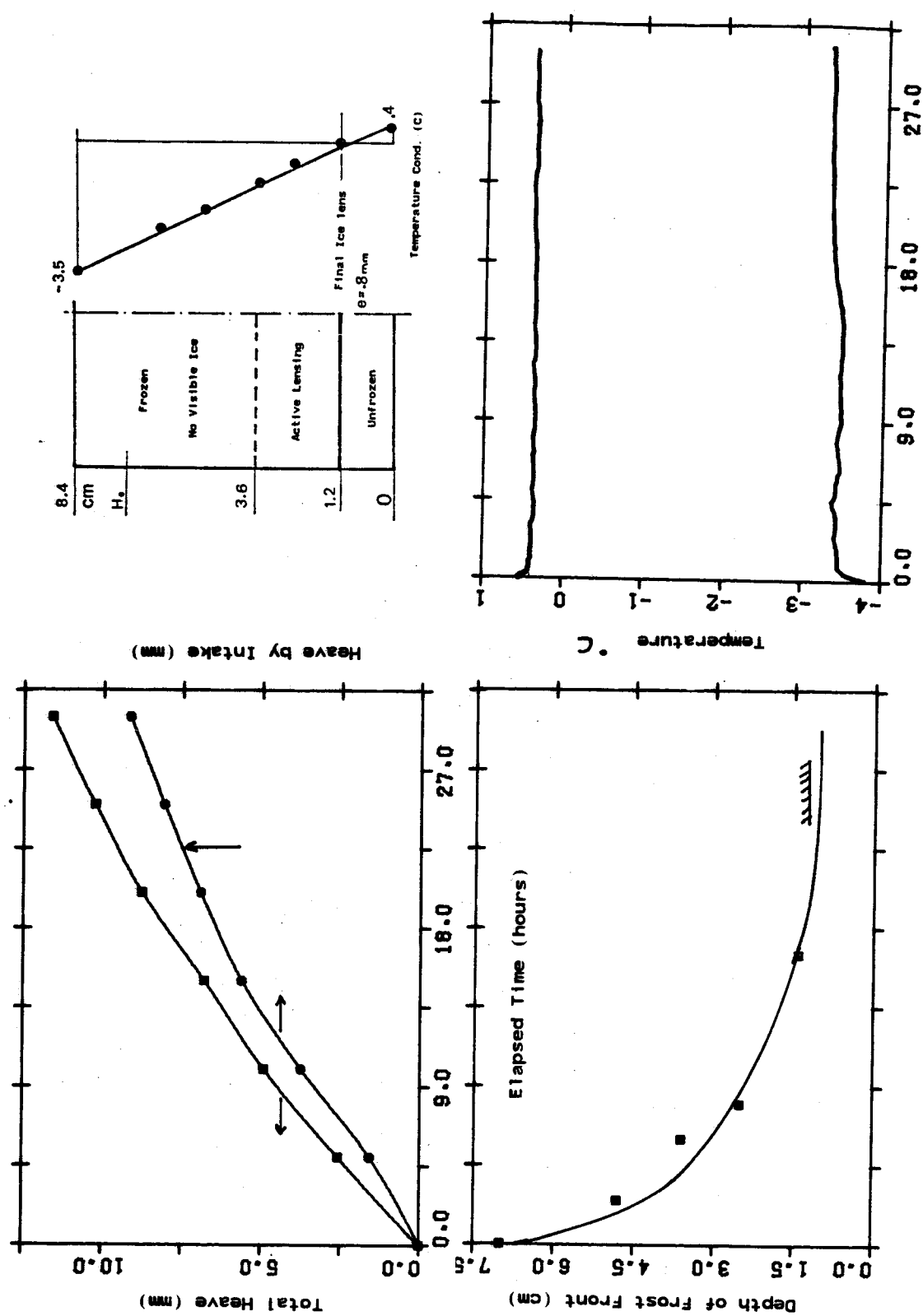
Figure C.17 Experimental Results From Test E-6
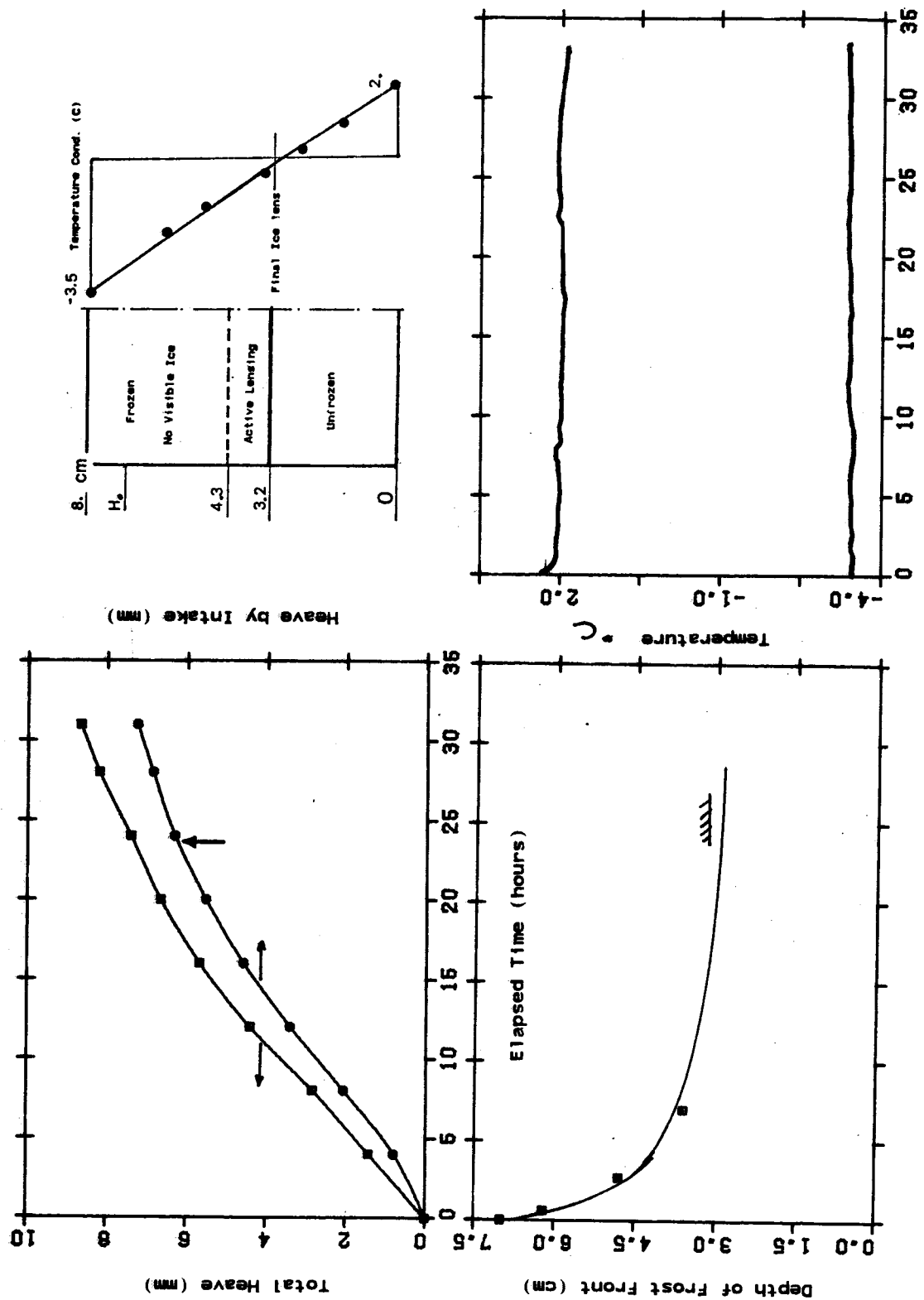
Figure C.18 Experimental Results From Test E-7
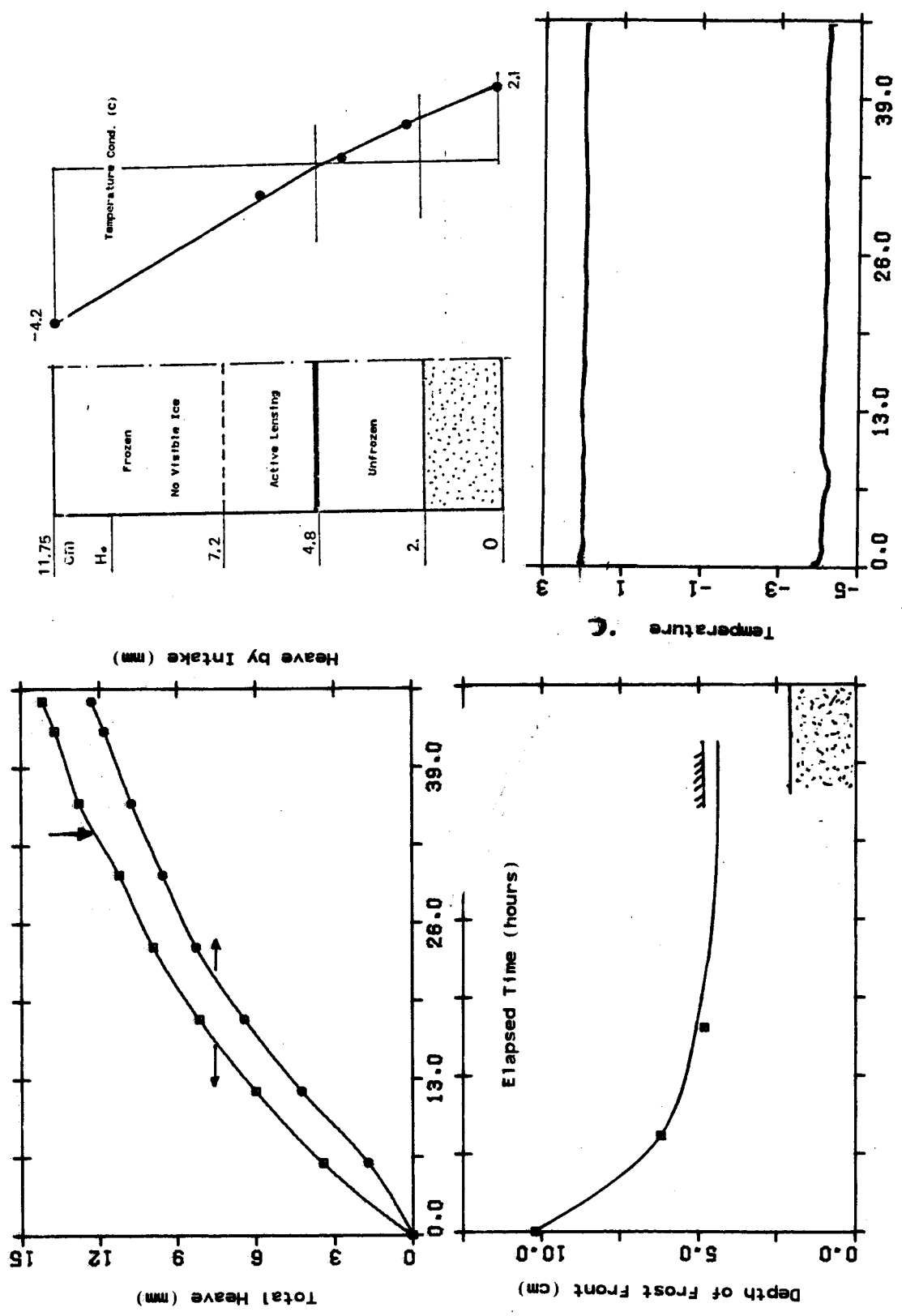
Figure C.19 Experimental Results From Test E-8

438
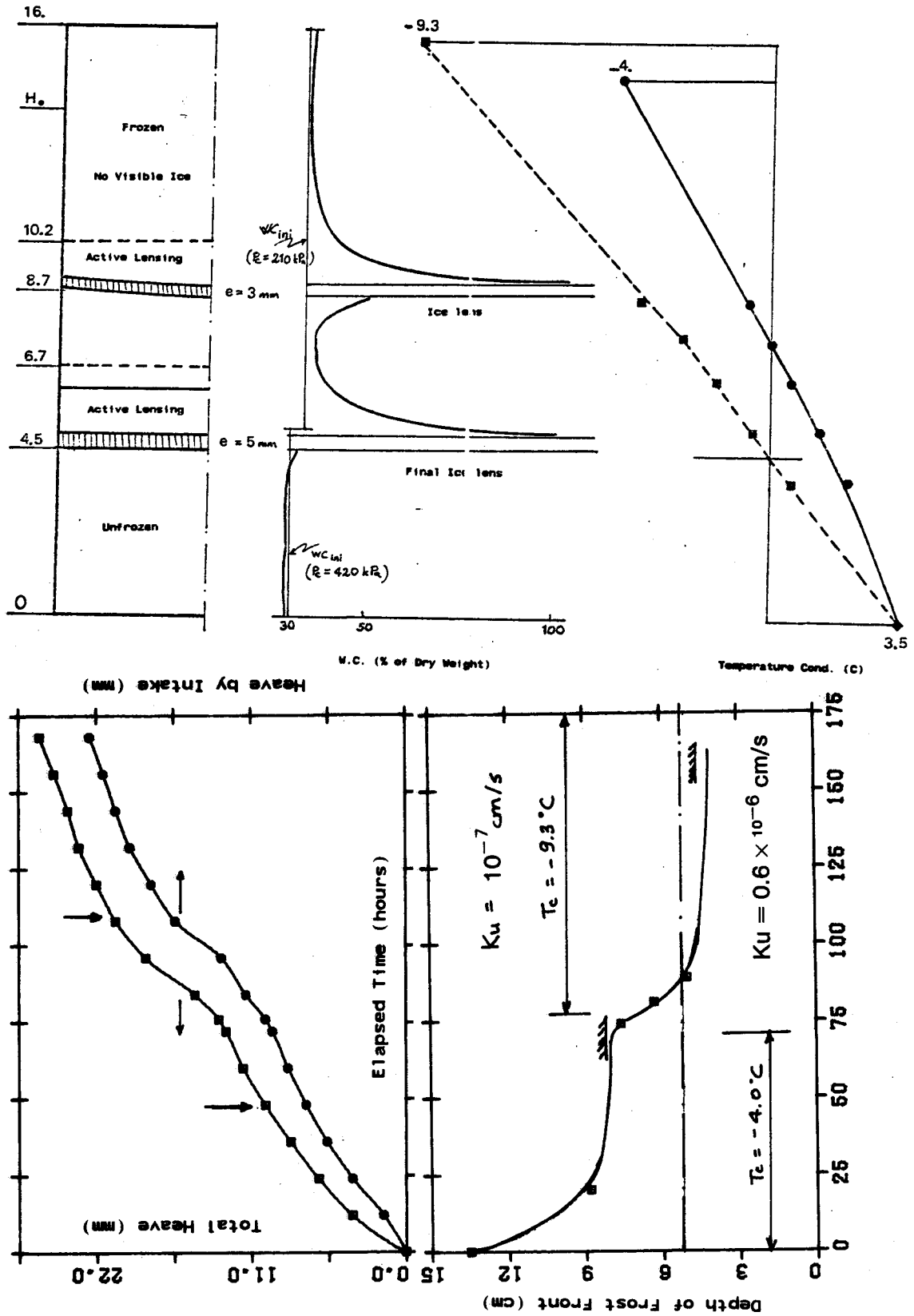
Figure C.20 Experimental Results From Test E-9

APPENDIX D

Results of Computer Simulation for One
Dimensional Laboratory Freezing.
Zero External Applied Surcharge
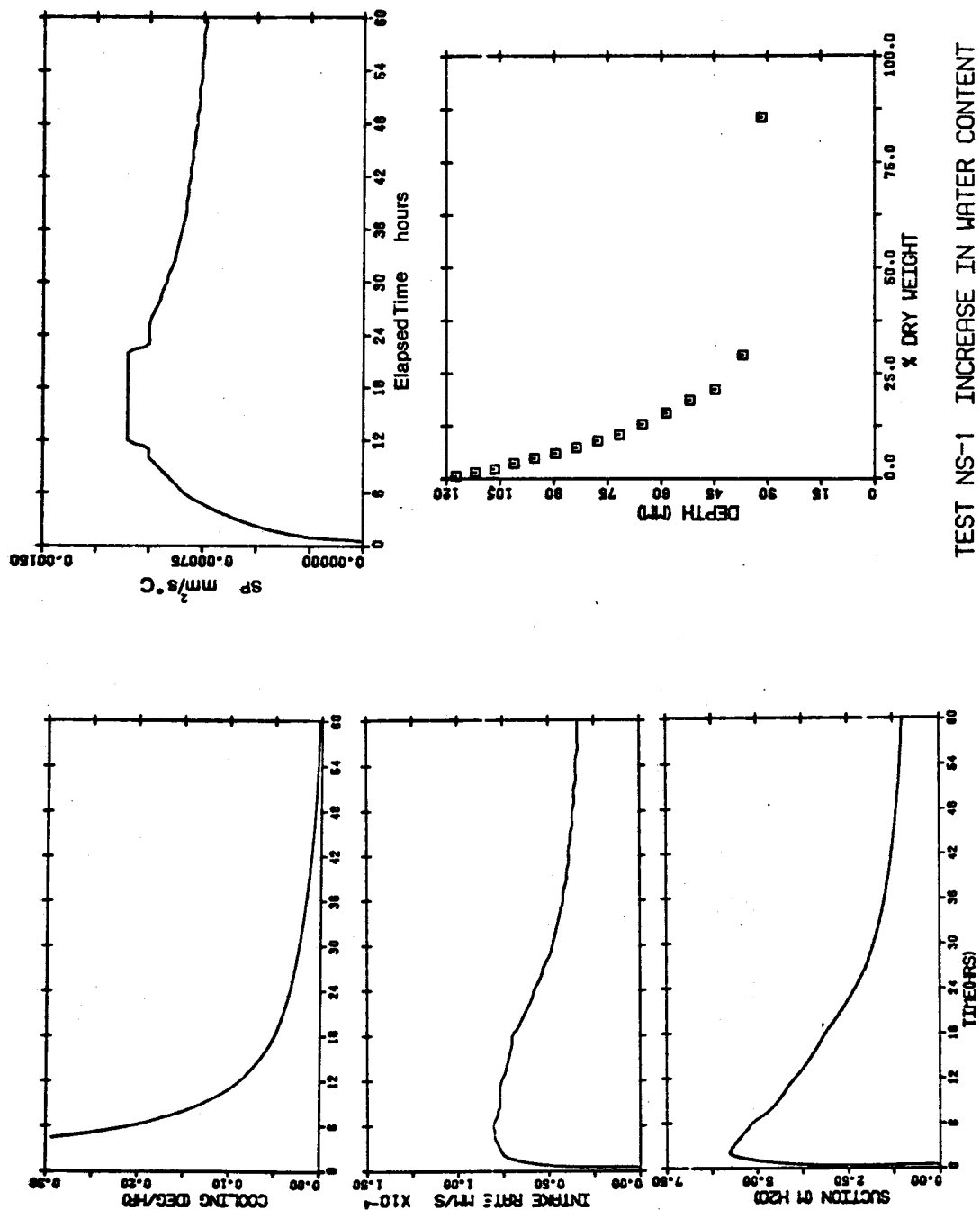
Figure D.1 Example of Computer Output for Test NS-1
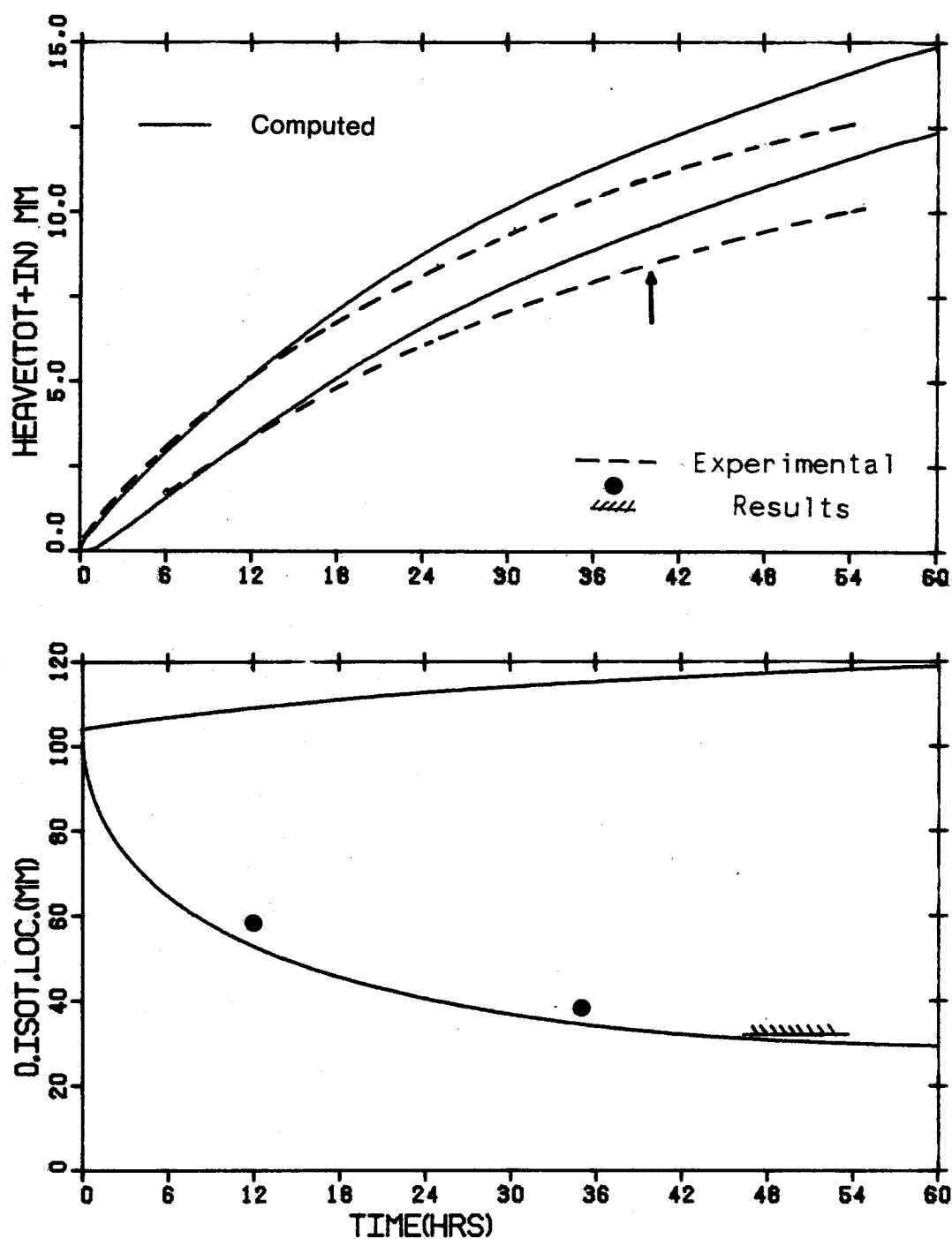
TEST NS-1 (P=0.0;TW=+1.1,TC=-3.40 C)

Figure D.2 Comparison Between Prediction and Experimental
Data for Test NS-1
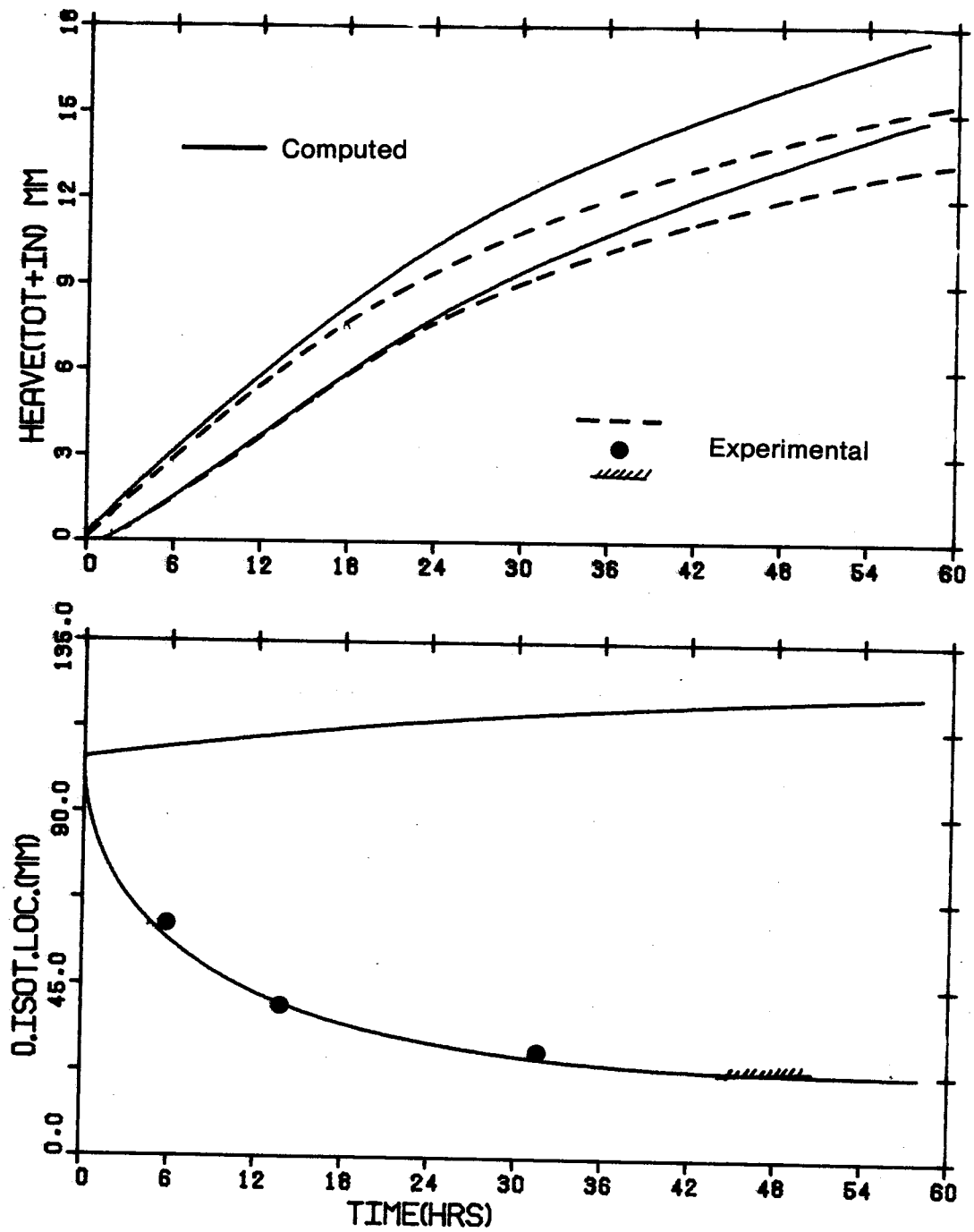
TEST NS-2 (P=0.0;TW=+1.1,TC=-4.80 C)

Figure D.3 Comparison Between Prediction and Experimental
Data for Test NS-2
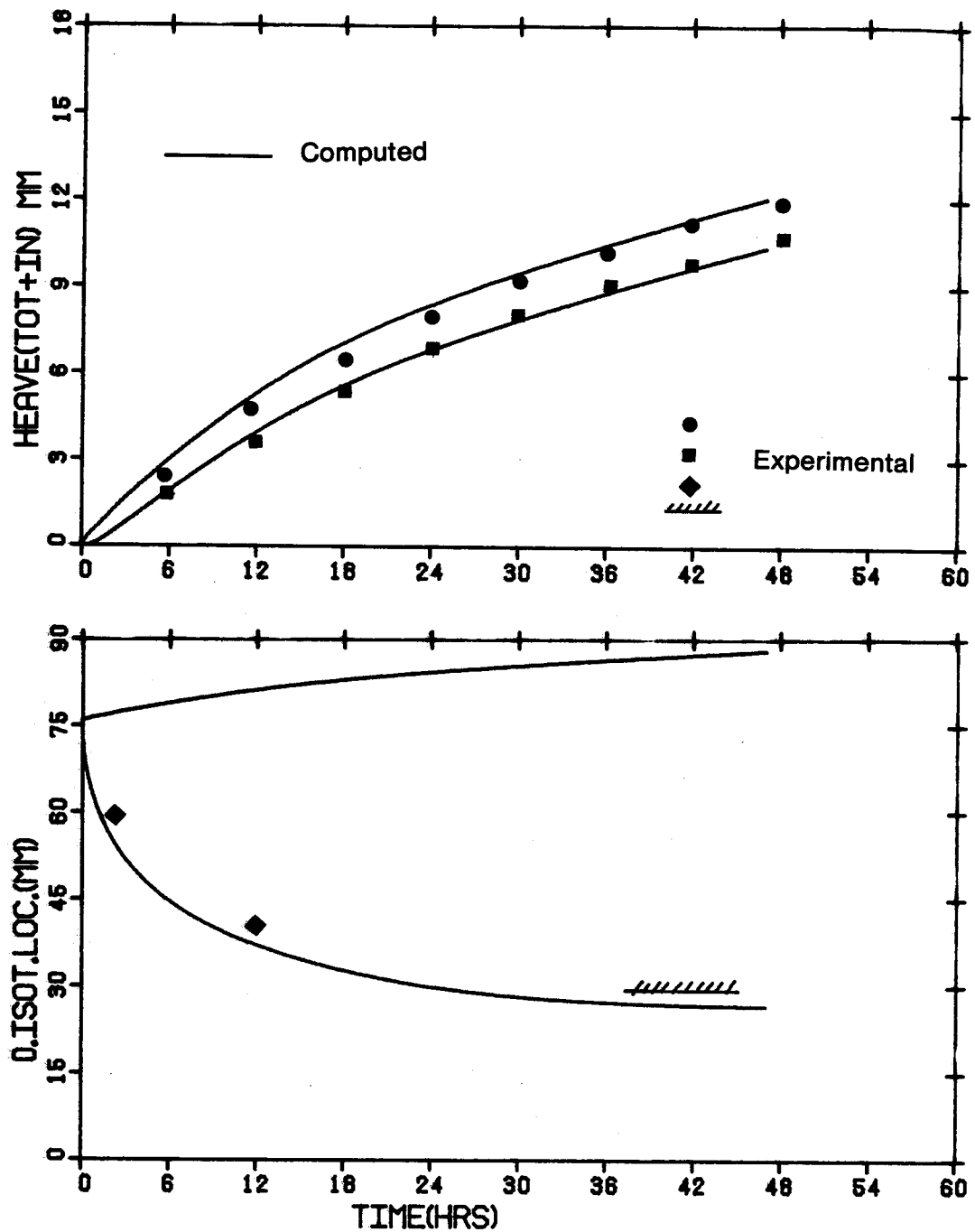
TEST NS-4 (P=0.0;TW=+1.1,TC=-2.50 C)

Figure D.4 Comparison Between Prediction and Experimental
Data for Test NS-4
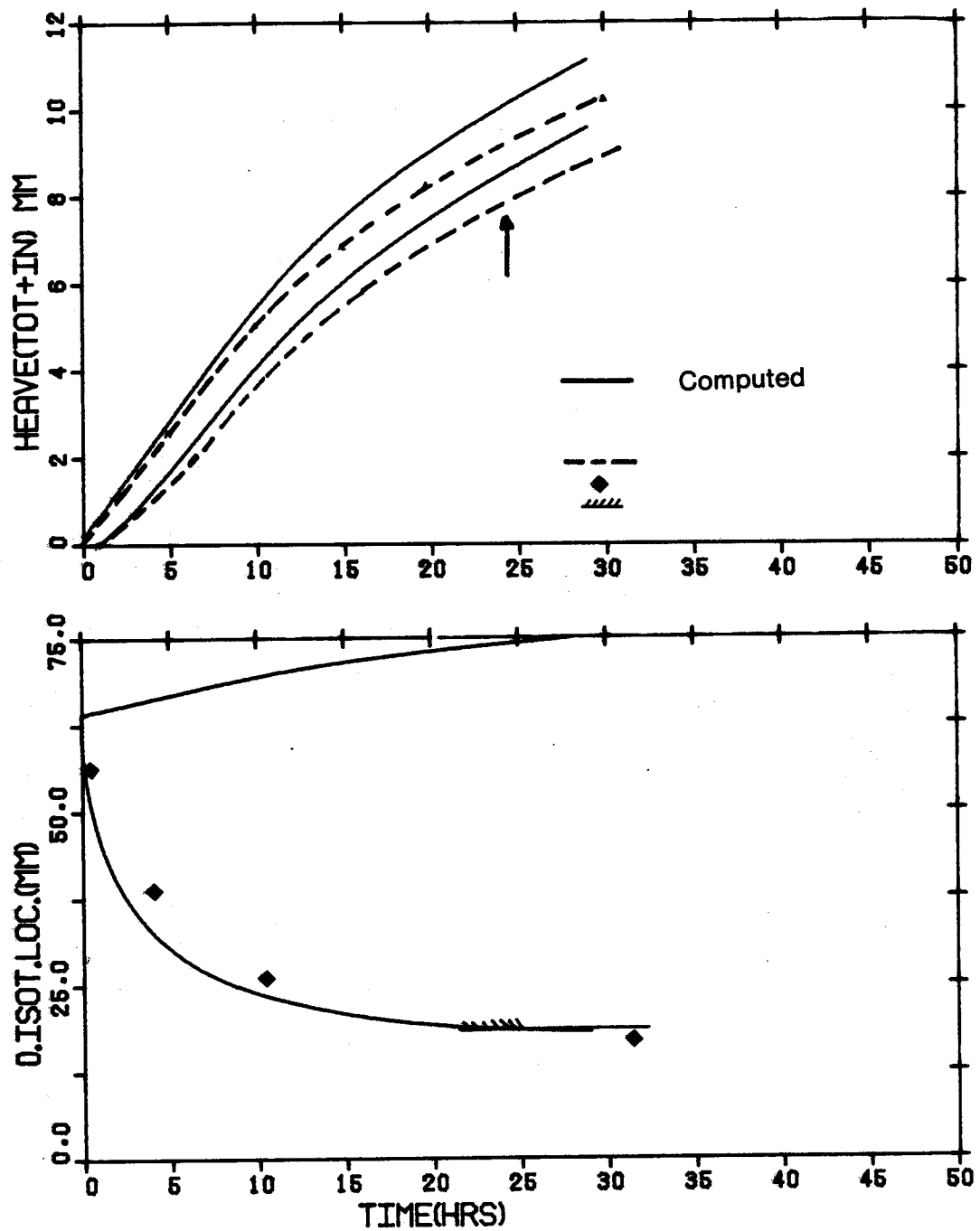
TEST NS-6 (P=0.0;TW=+1.1,TC=-3.40 C)

Figure D.5 Comparison Between Prediction and Experimental
Data for Test NS-6
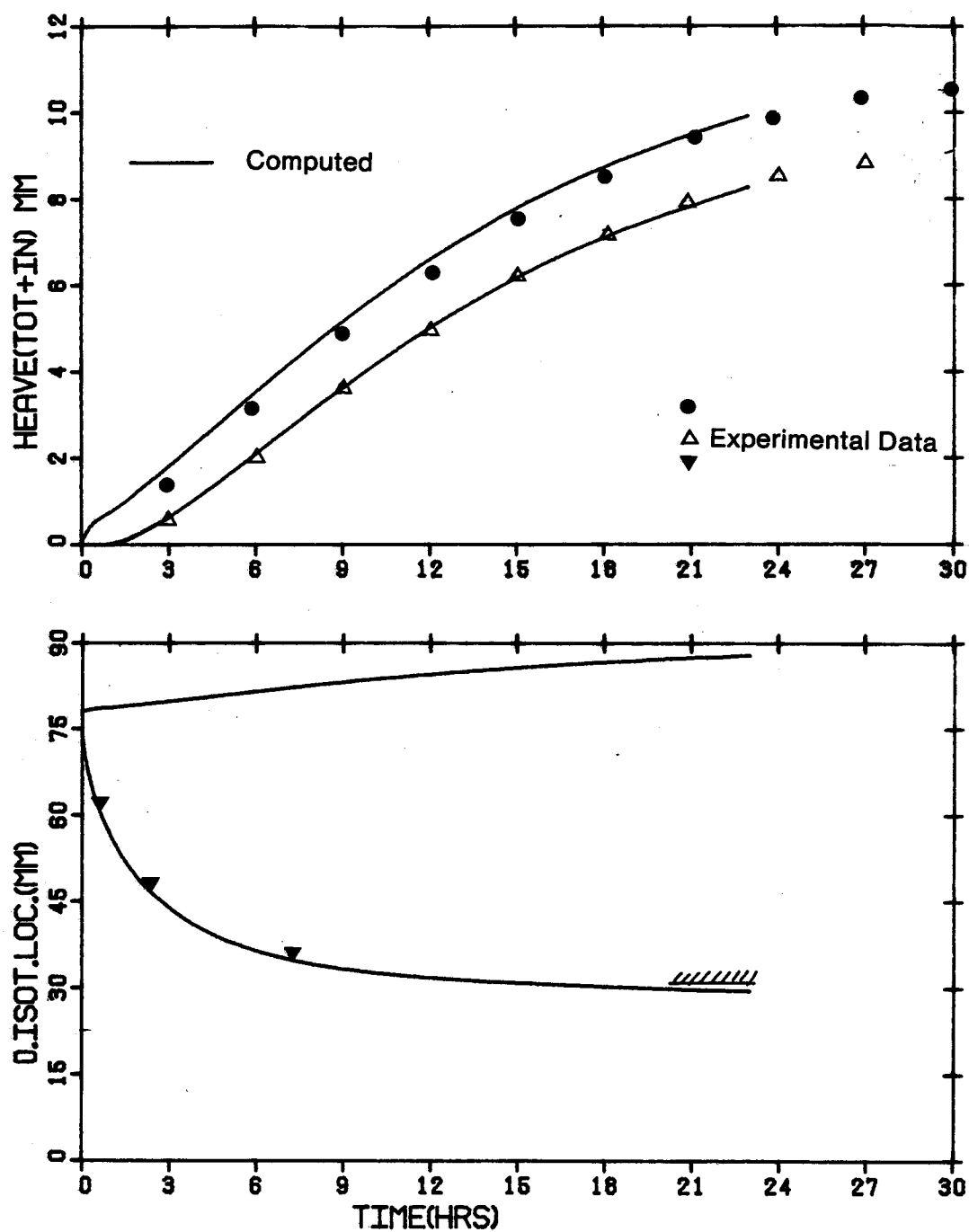
Figure D.6 Comparison Between Prediction and Experimental
Data for Test E-4
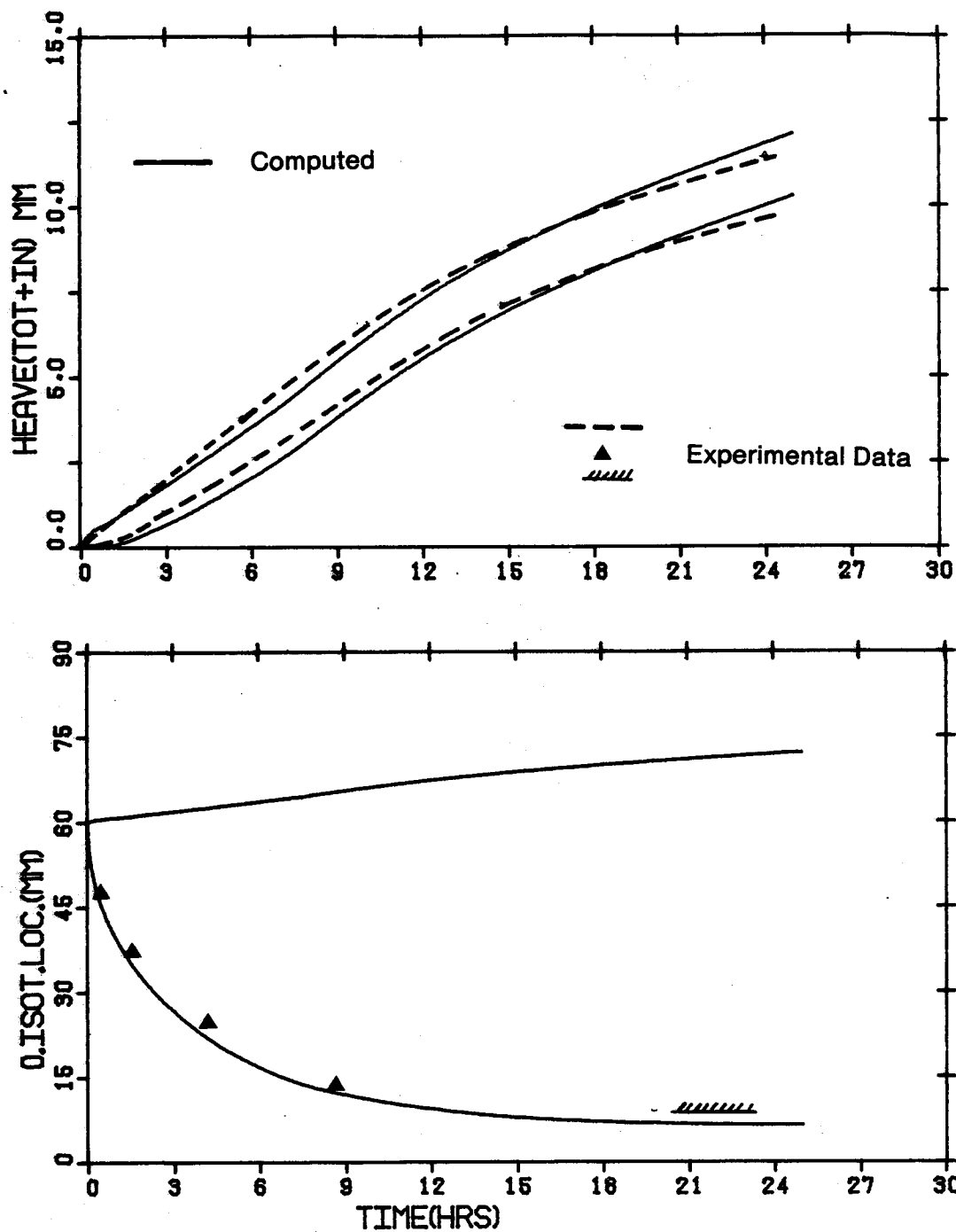
TEST   E-5 (P=0.0;TW=+0.4,TC=-4.20 C)

Figure D.7 Comparison Between Prediction and Experimental
Data for Test E-5
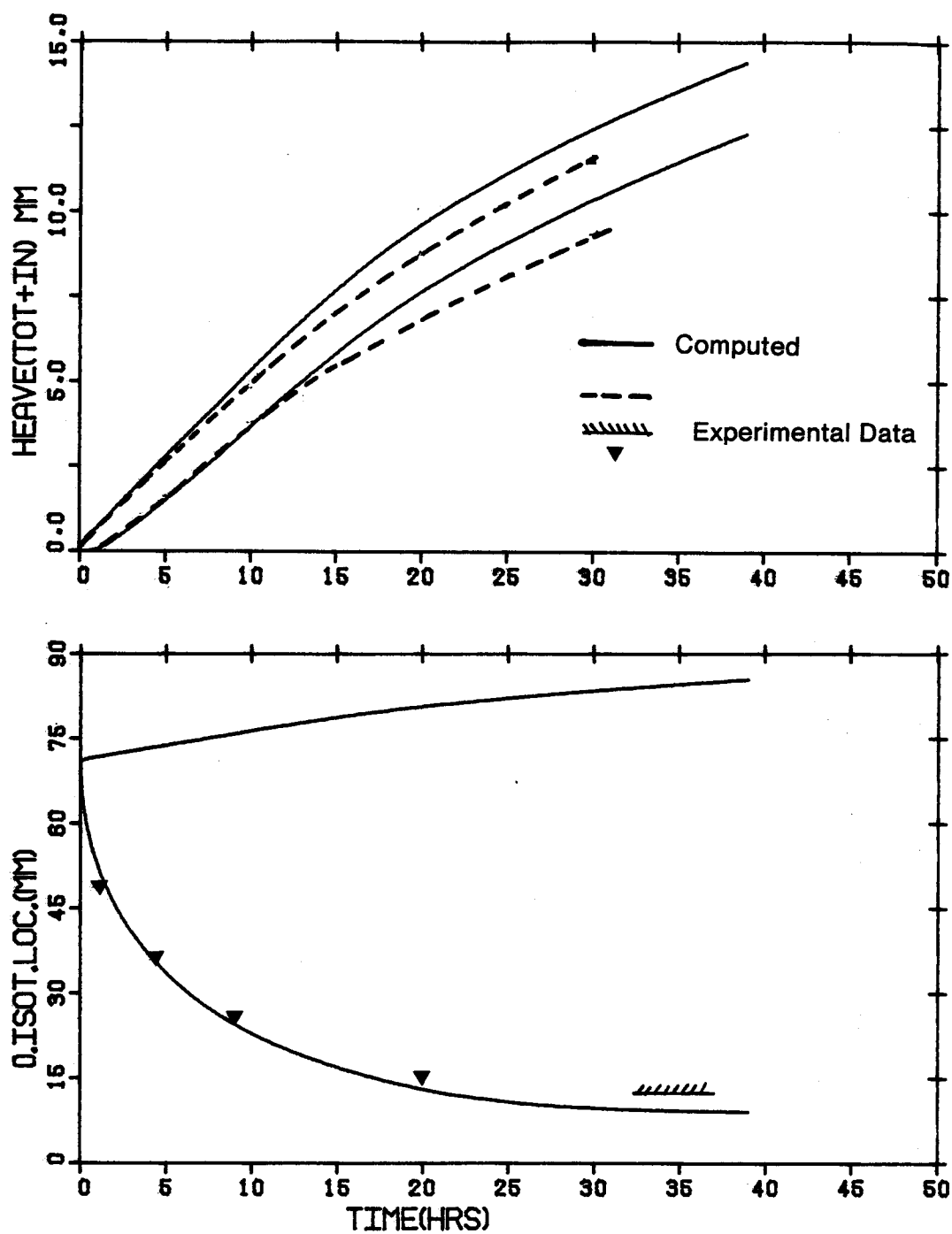
TEST E-6 (P=0.0;TW=+0.4,TC=-3.50 C)

Figure D.8 Comparison Between Prediction and Experimental
Data for Test E-6
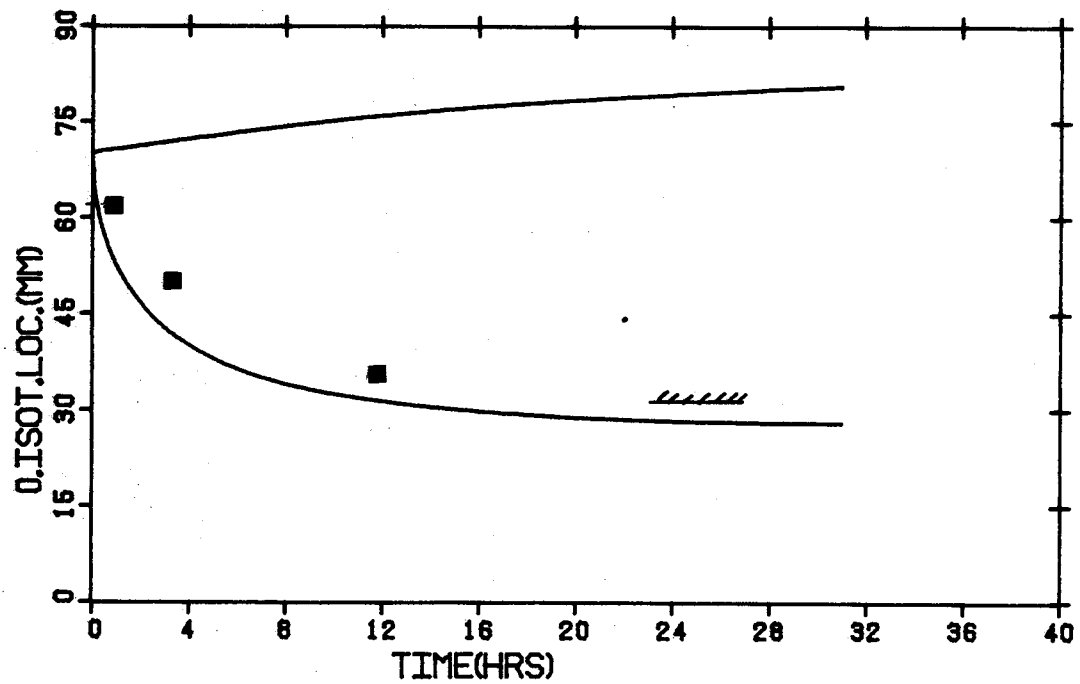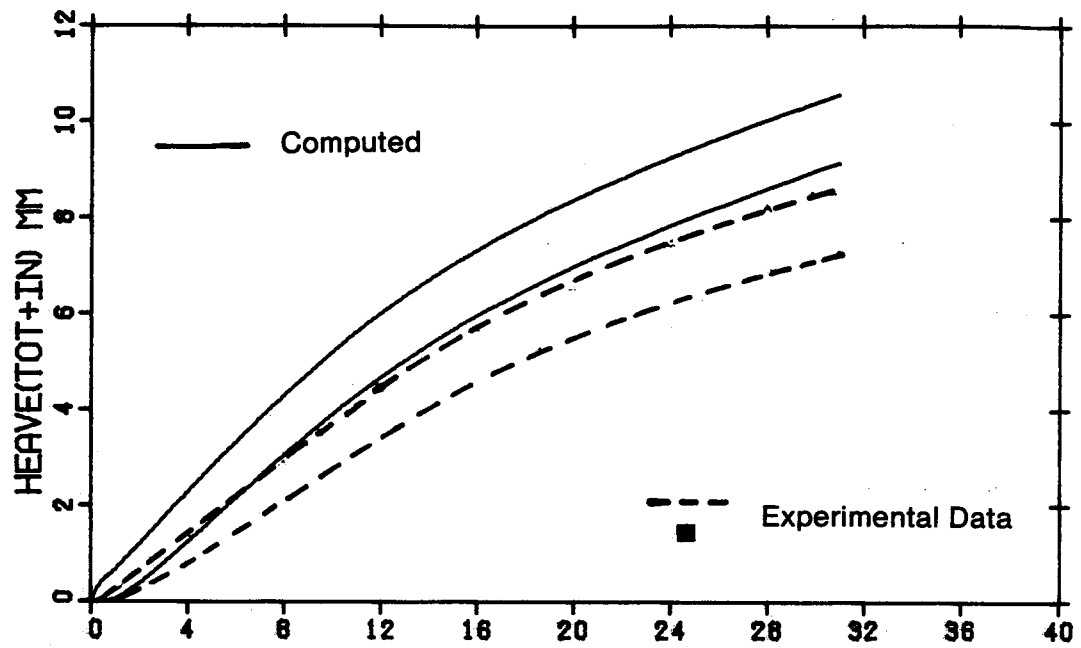
Figure D.9 Comparison Between Prediction and Experimental
Data for Test E-7

APPENDIX E

Experimental Results from Series C

Applied Surcharge
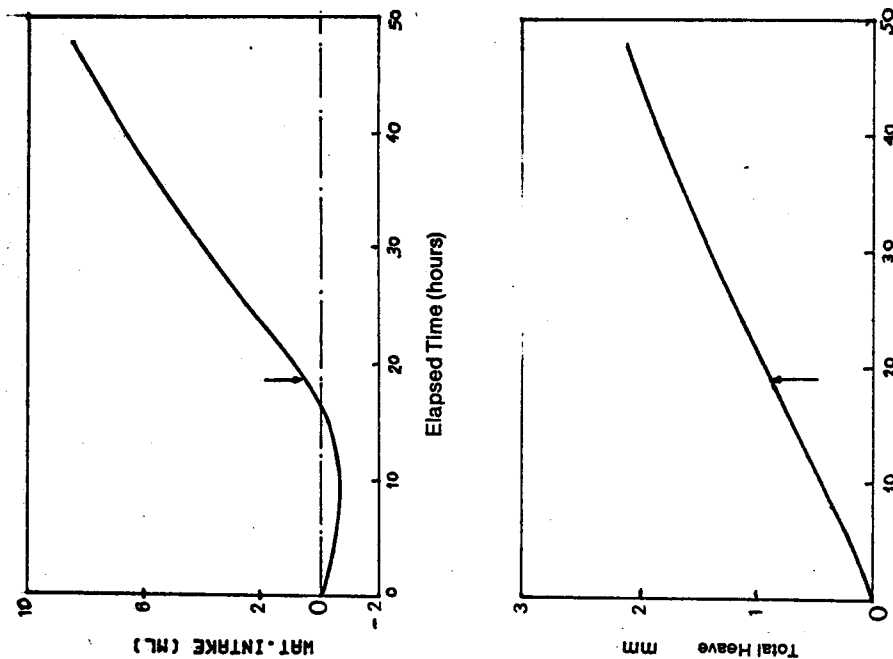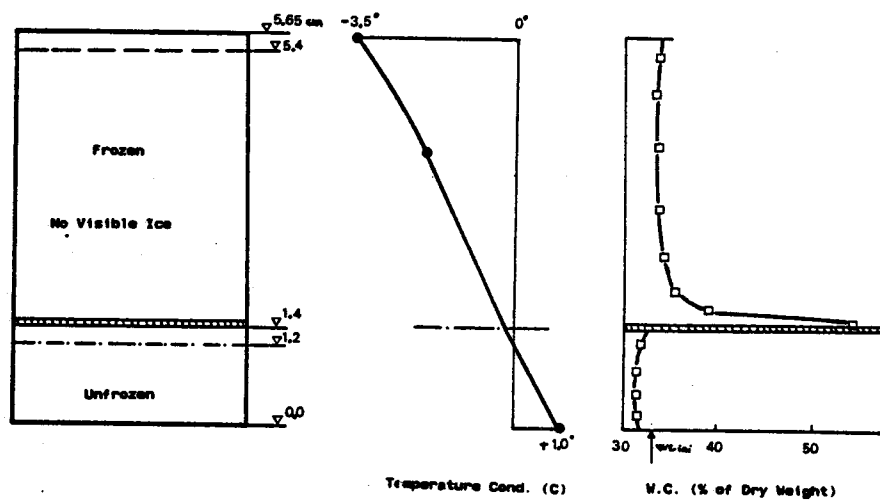
Figure E.1 Experimental Results from Test C-2. Pe=190 kPa
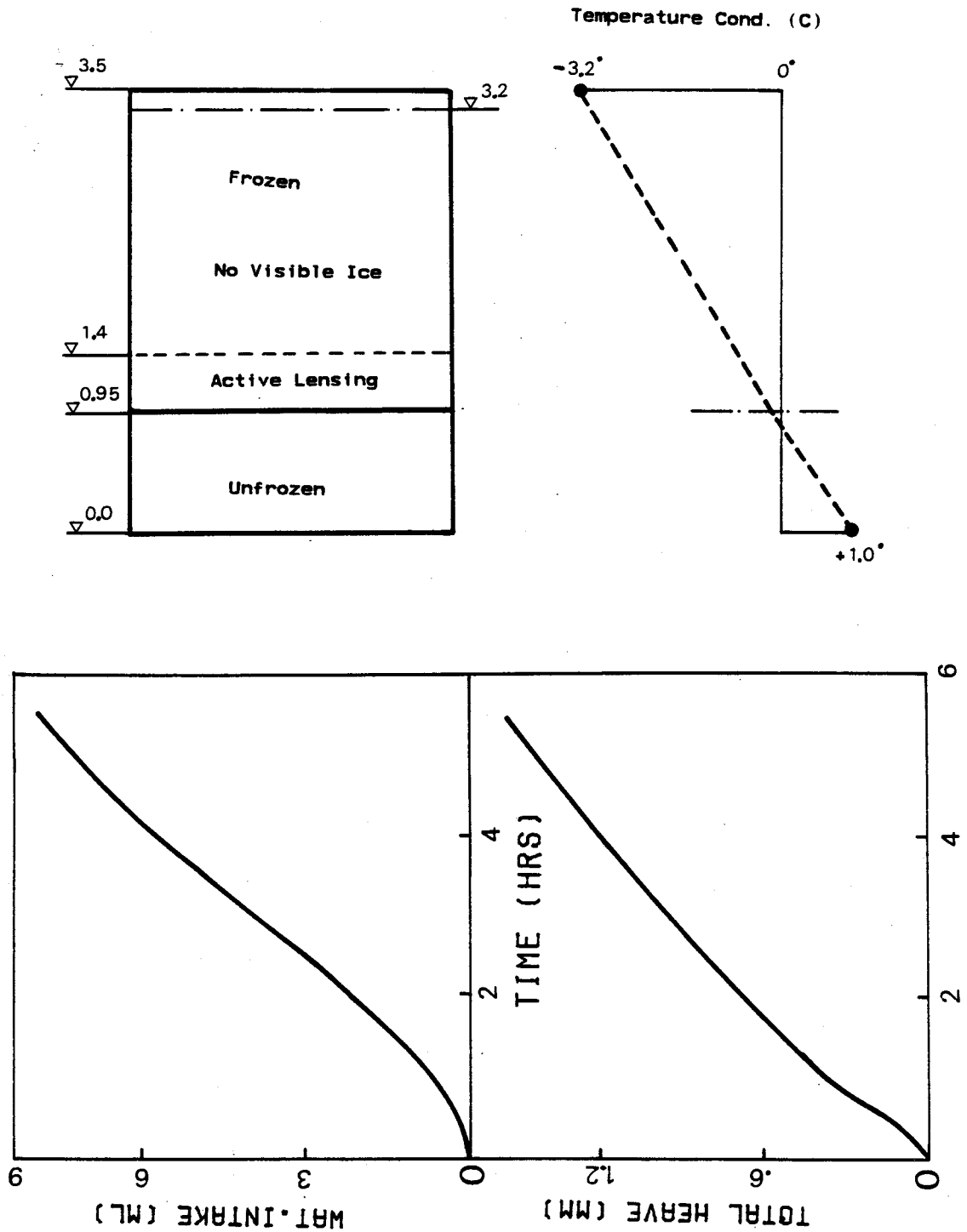
Figure E.2 Experimental Results From Test C-3. Pe=90 kPa
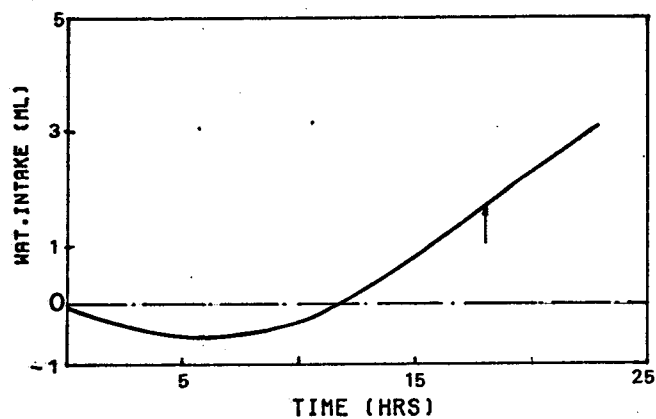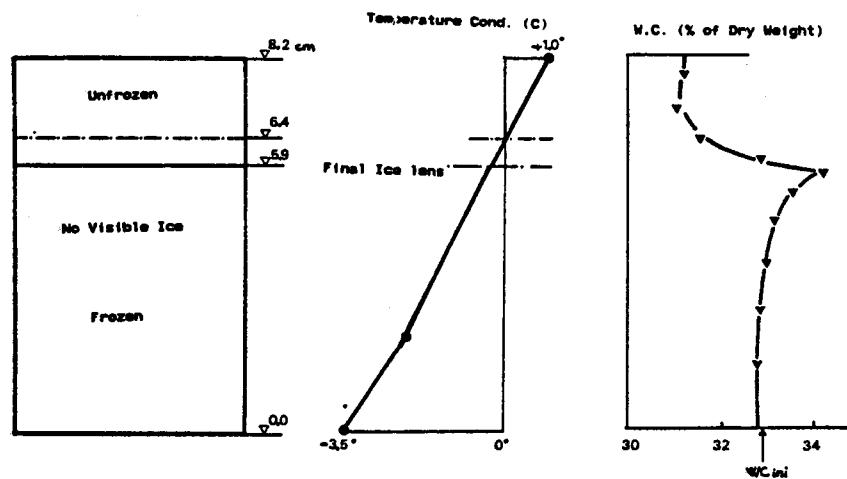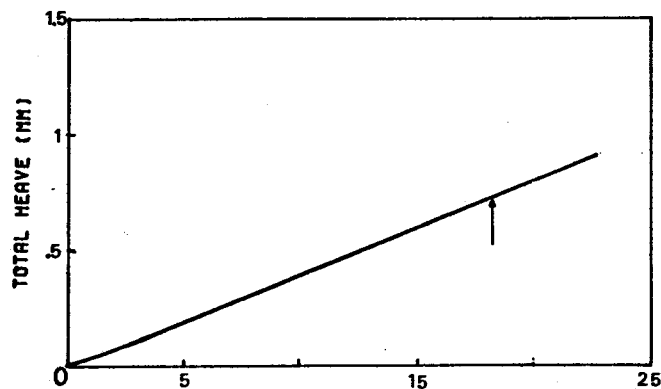
Figure E.3 Experimental Results From Test C-4. Pe=170 kPa
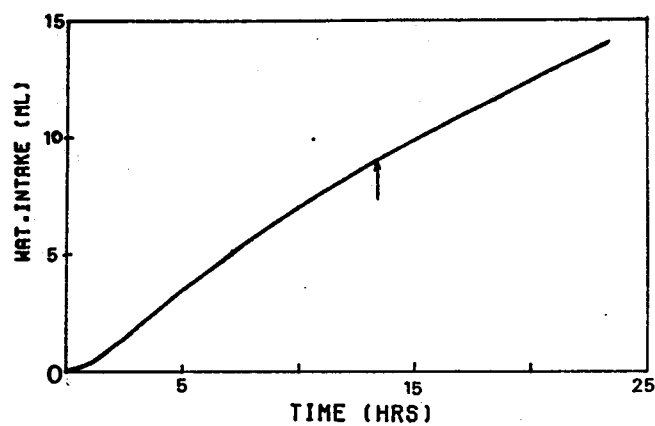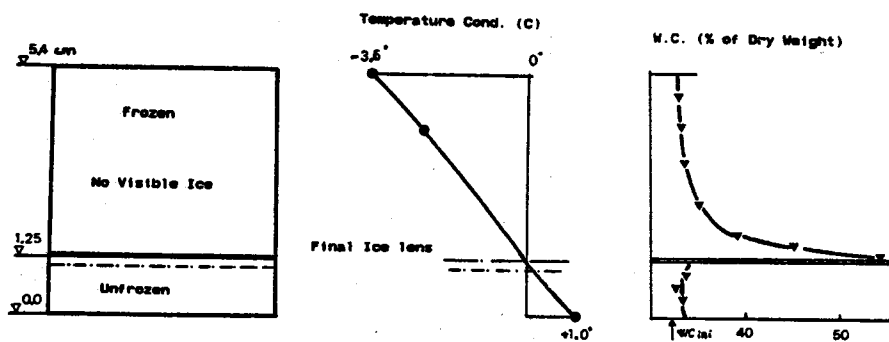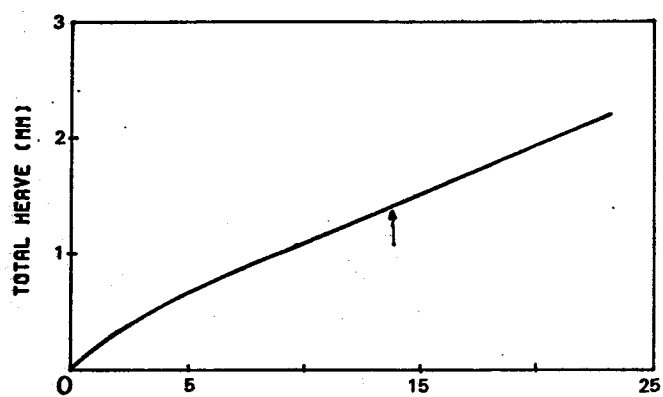
Figure E.4 Experimental Results From Test C-5. Pe=120 kPa
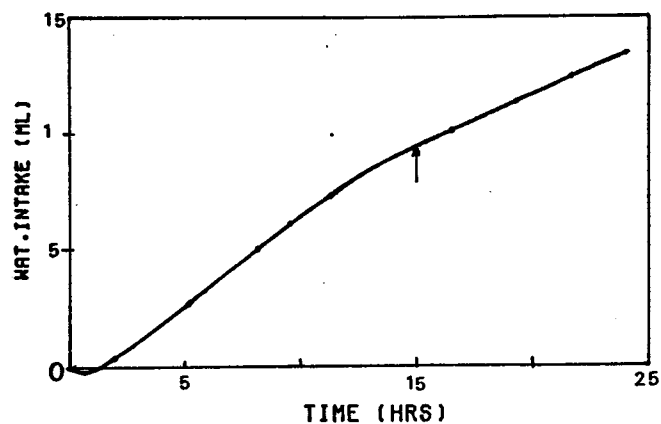
TEST C6 (P=120KPA;TC=-3.5,TW=+1.OC)
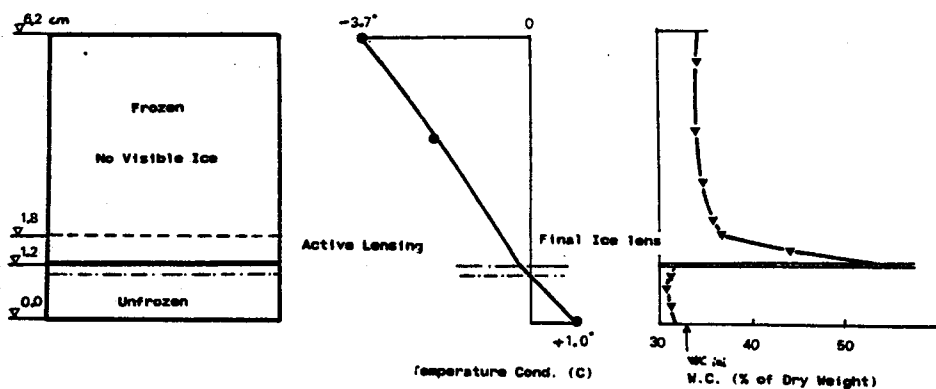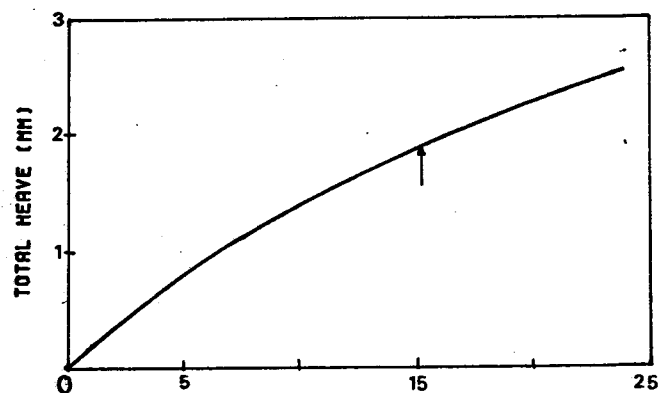
Figure E.5 Experimental Results From Test C-6. Pe=120 kPa
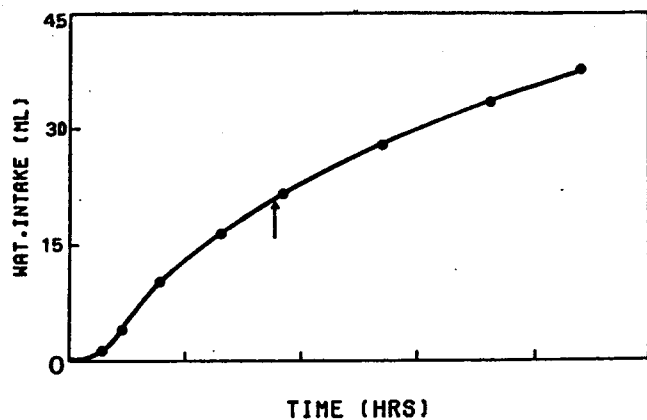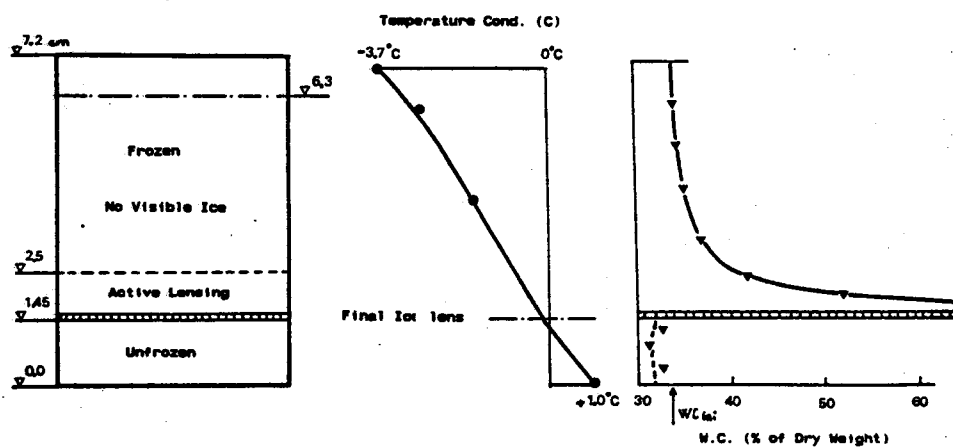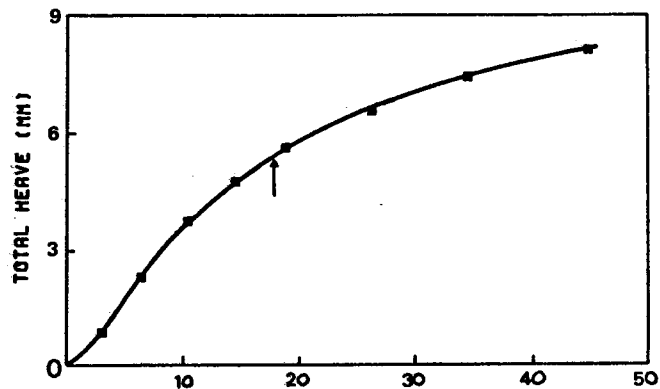
Figure E.6 Experimental Results From Test C-7. Pe=60 kPa
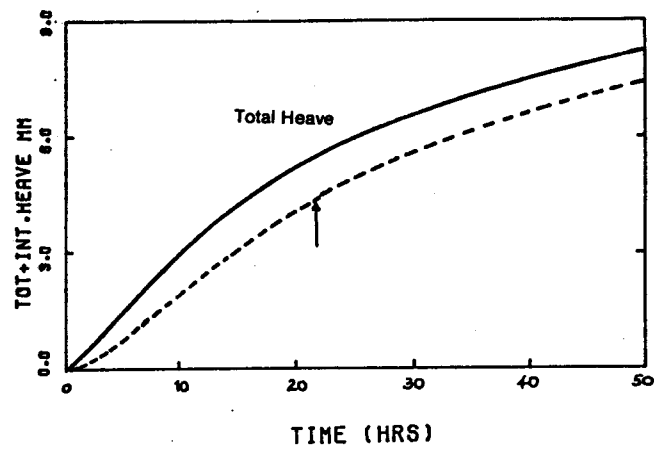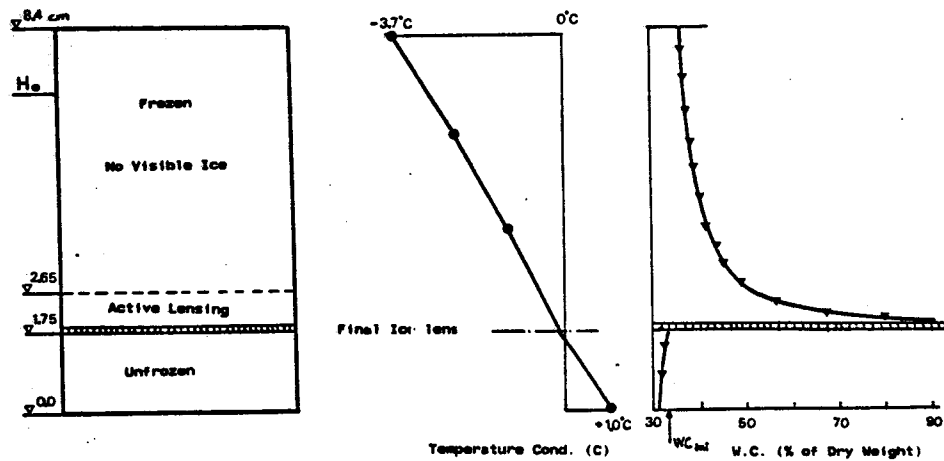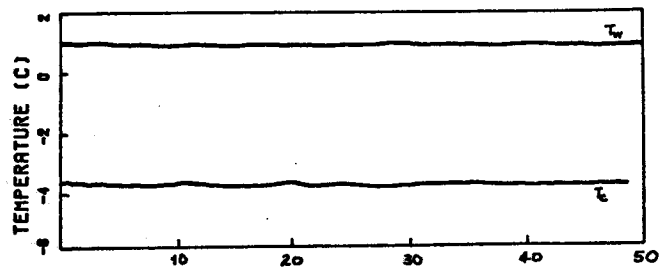
Figure E.7 Experimental Results From Test C-8. Pe=45 kPa
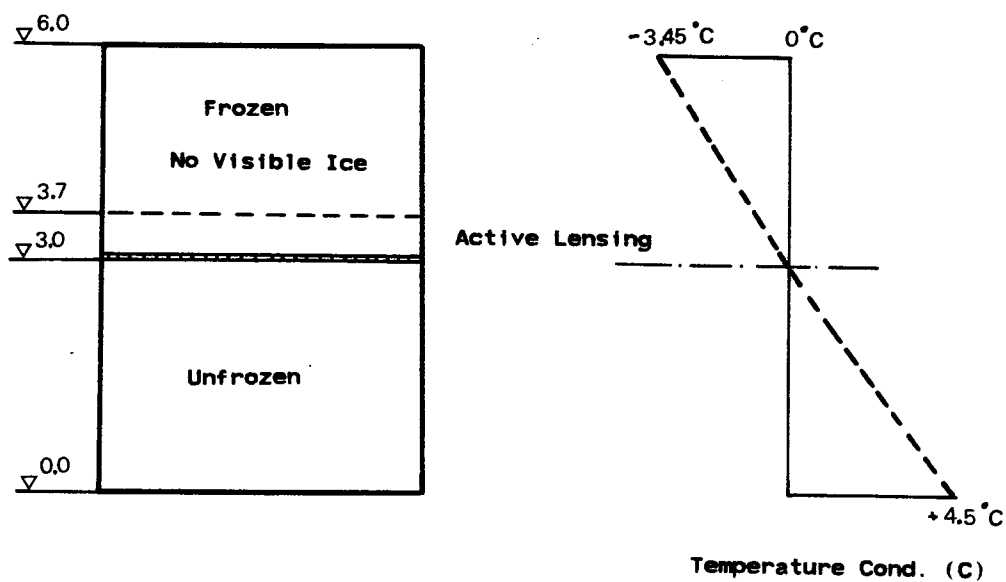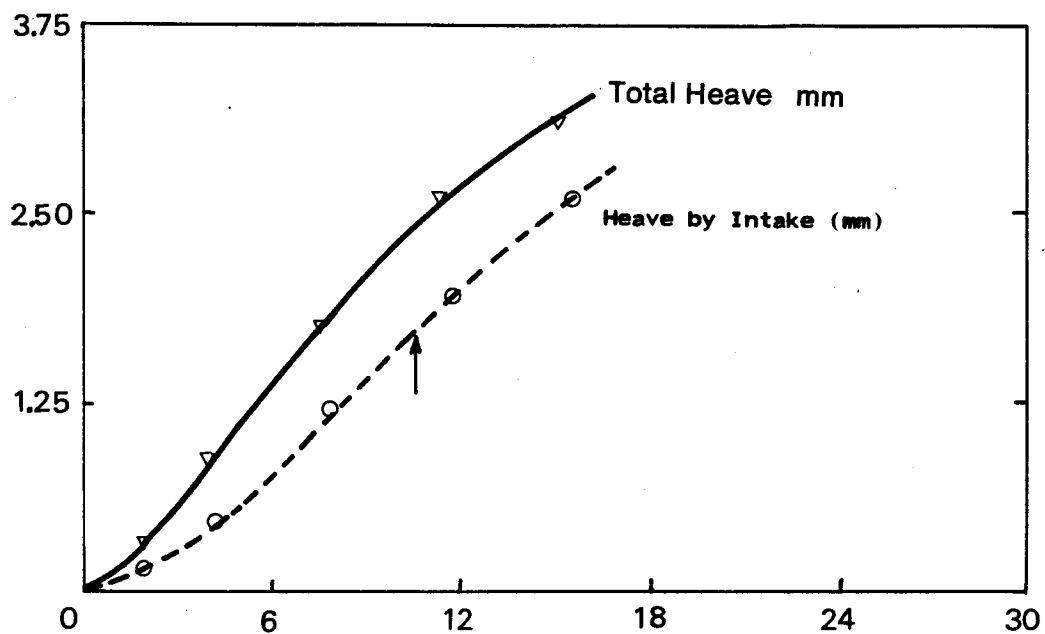
Figure E.8 Experimental Results From Test C-9. Pe=45 kPa

458
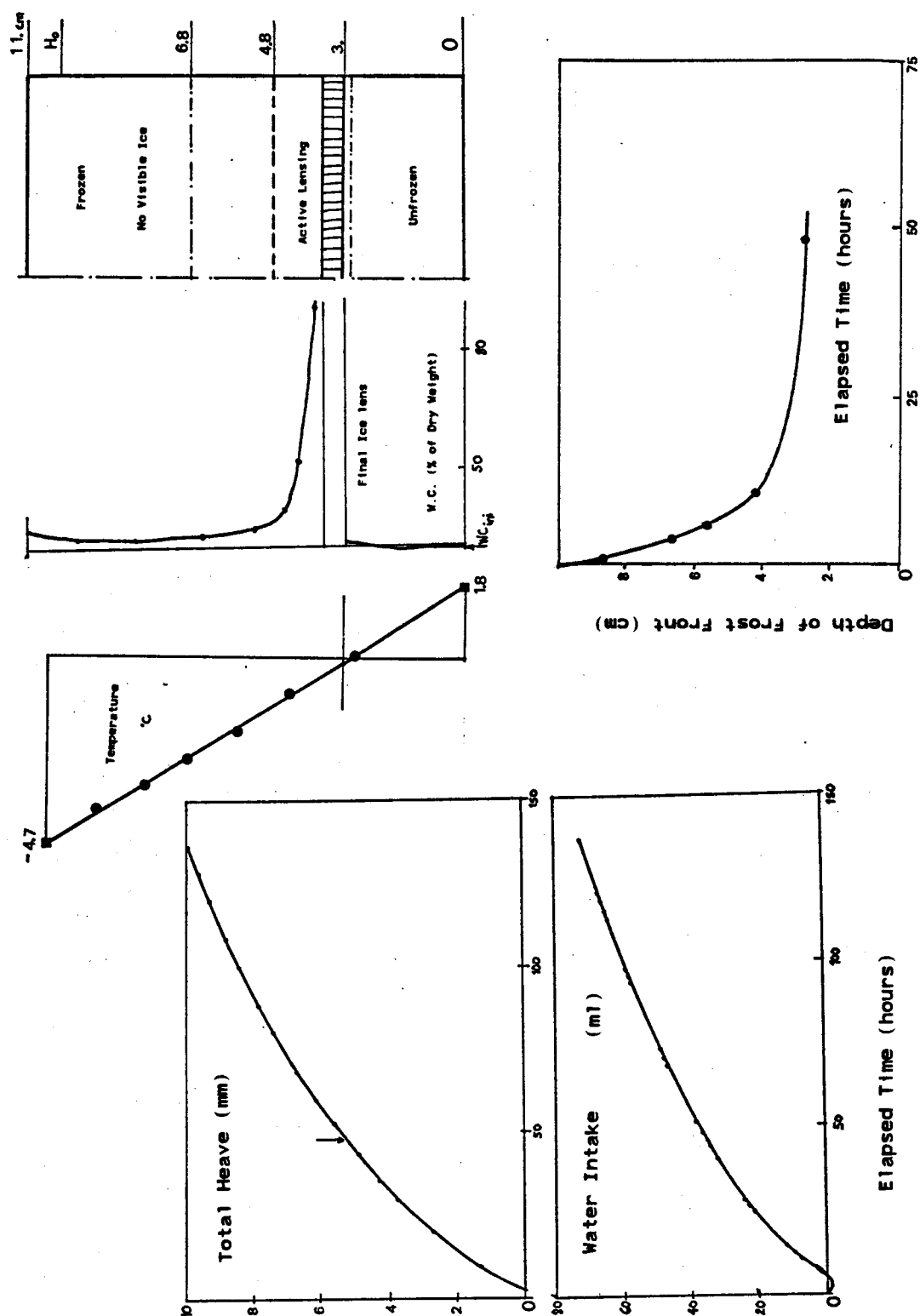
Figure E.9 Experimental Results From Test C-10. Pe=100 kPa
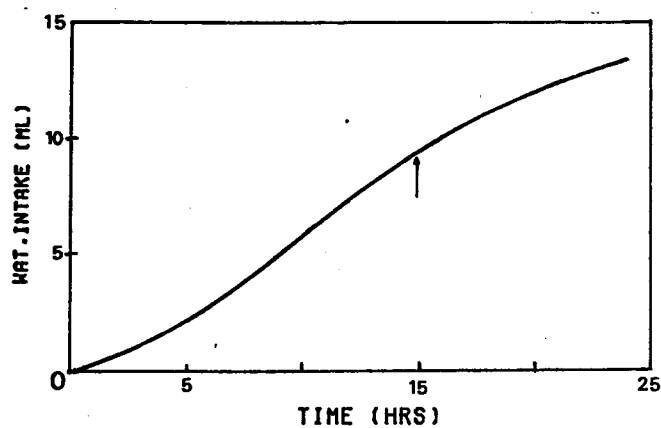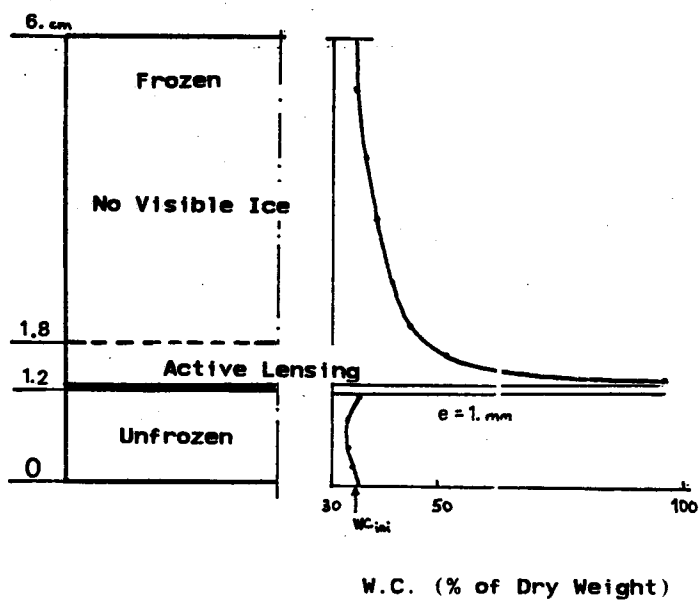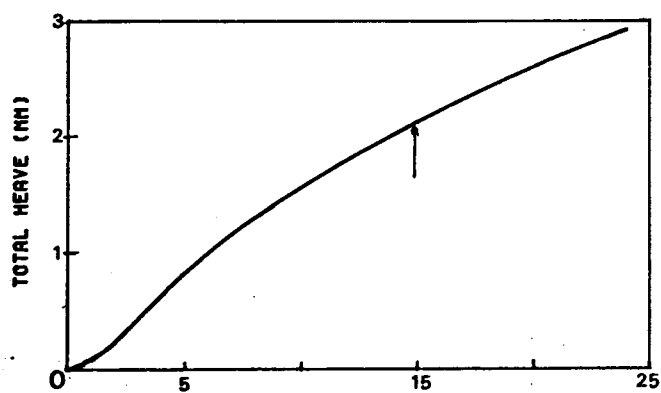
Figure E.10 Experimental Results From Test C-11. Pe=120 kPa
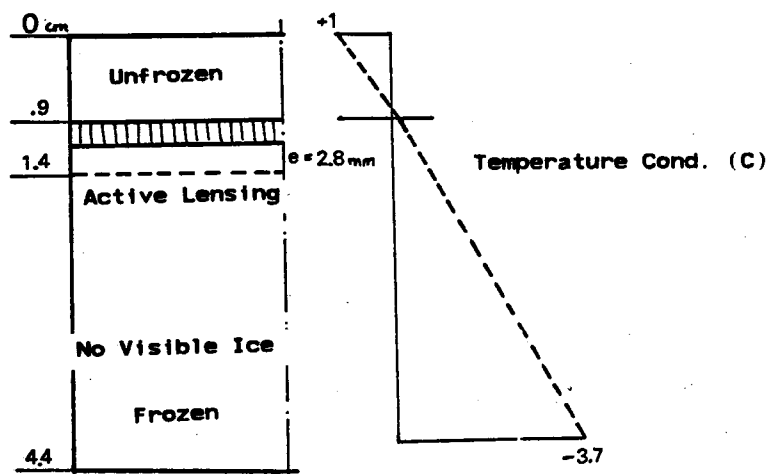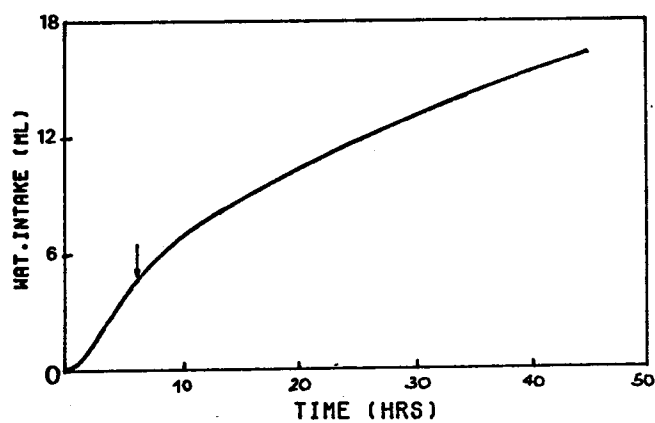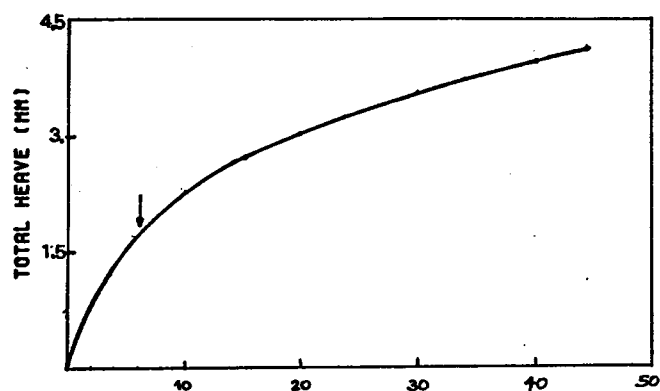
Figure E.11 Experimental Results From Test C-12. Pe=120 kPa
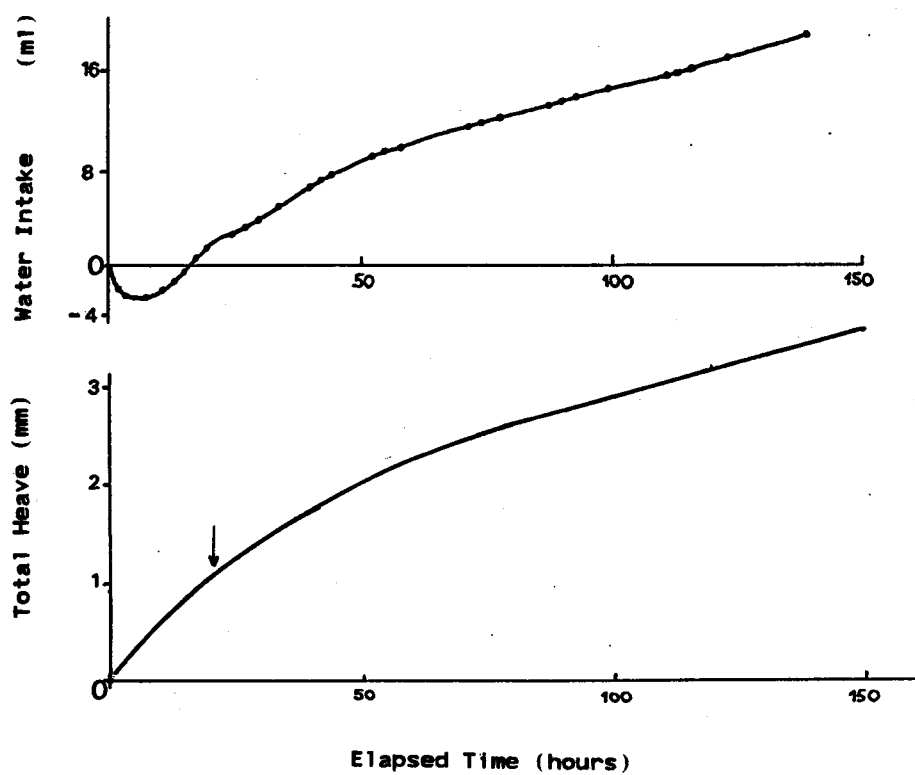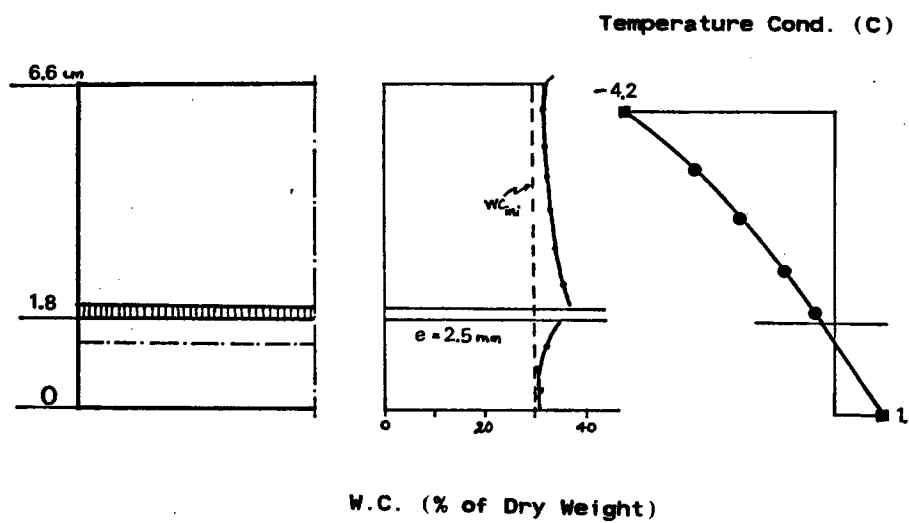
Figure E.12 Experimental Results From Test C-13. Pe=265 kPa

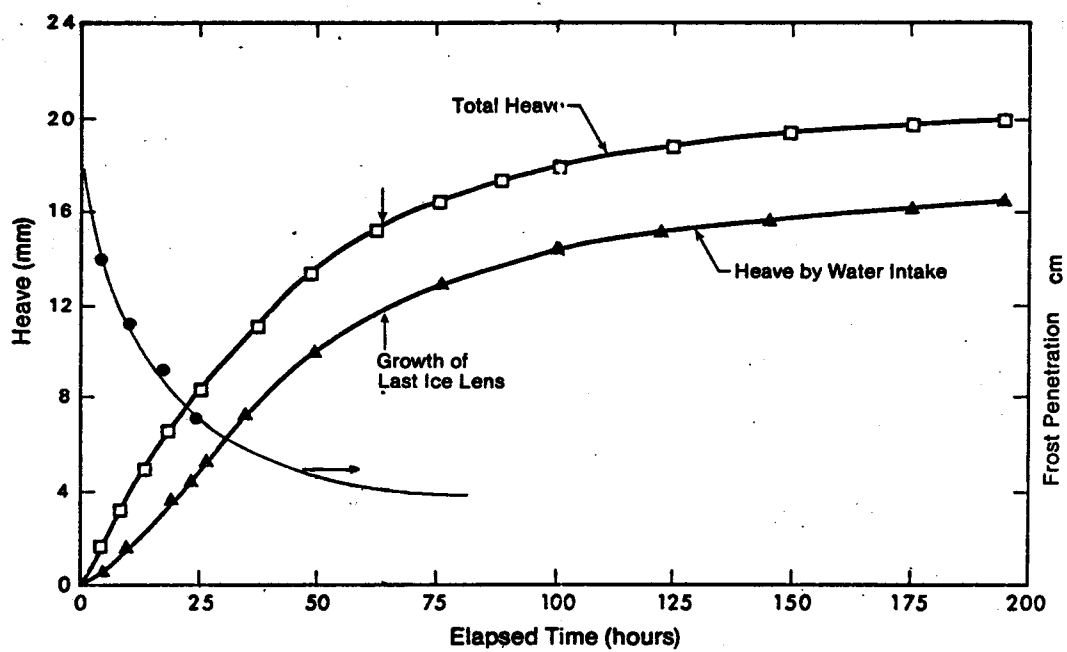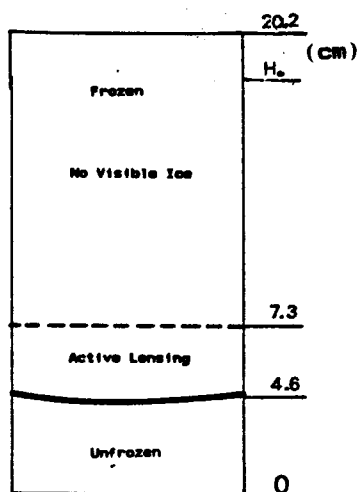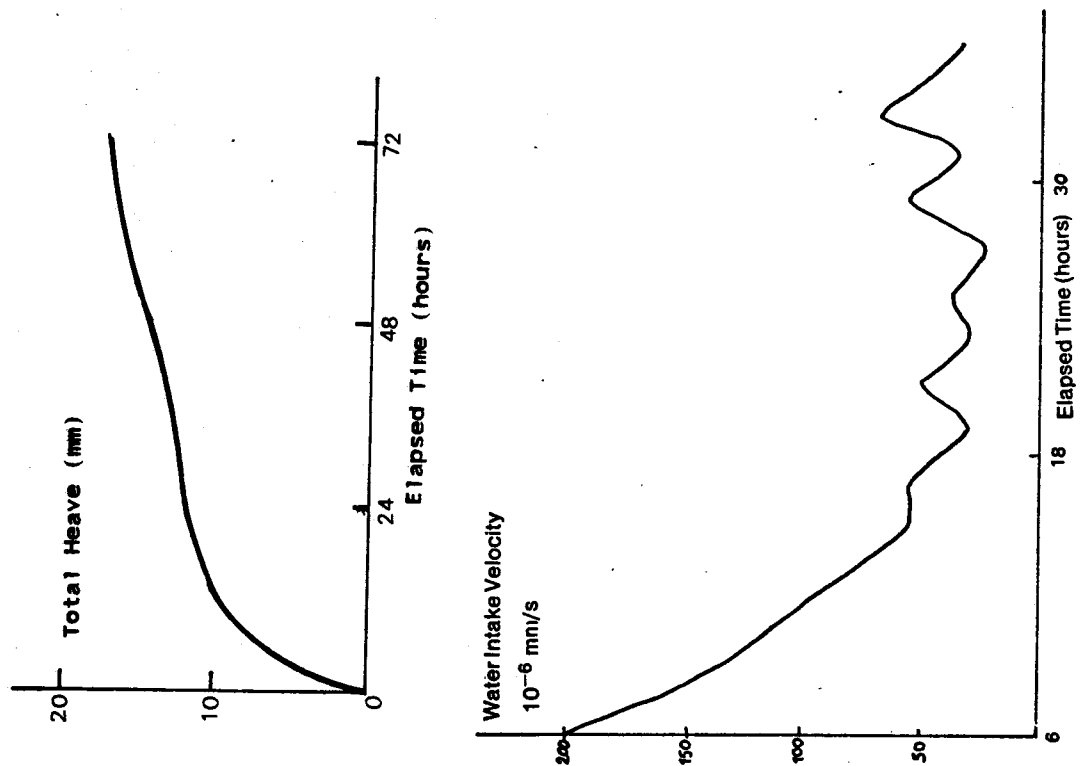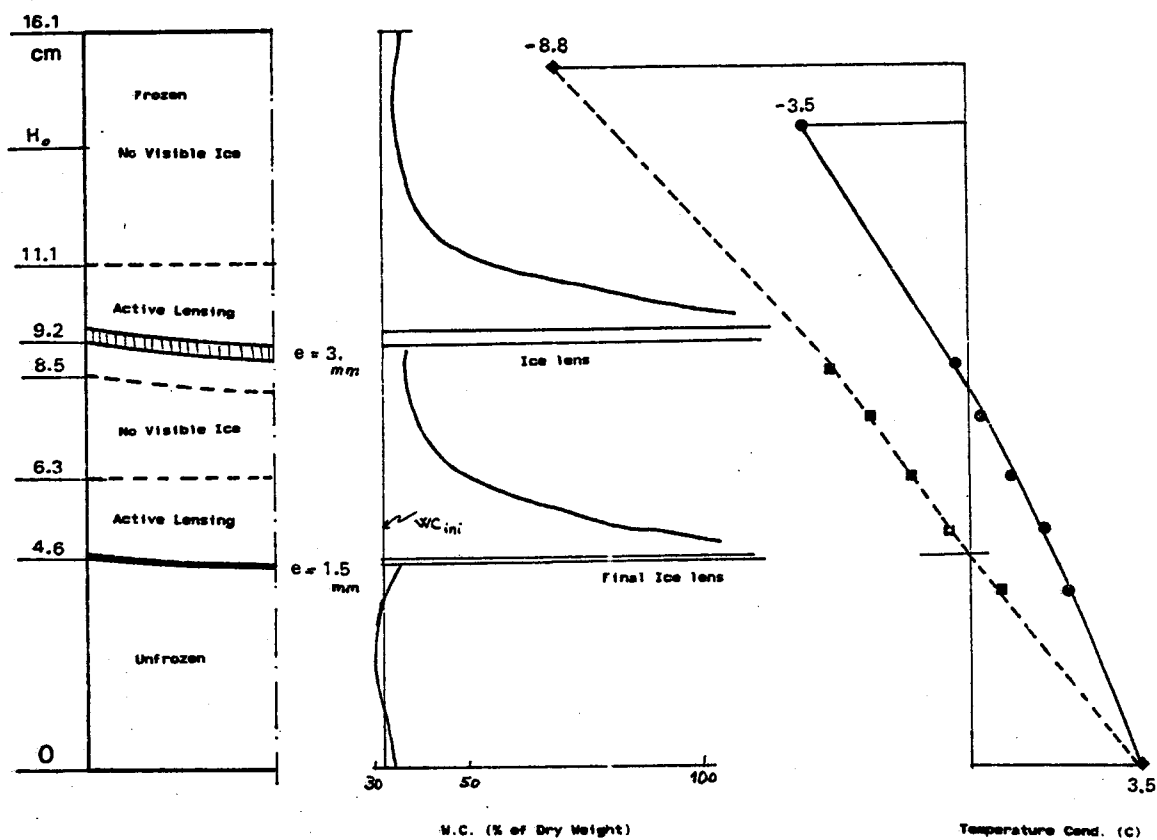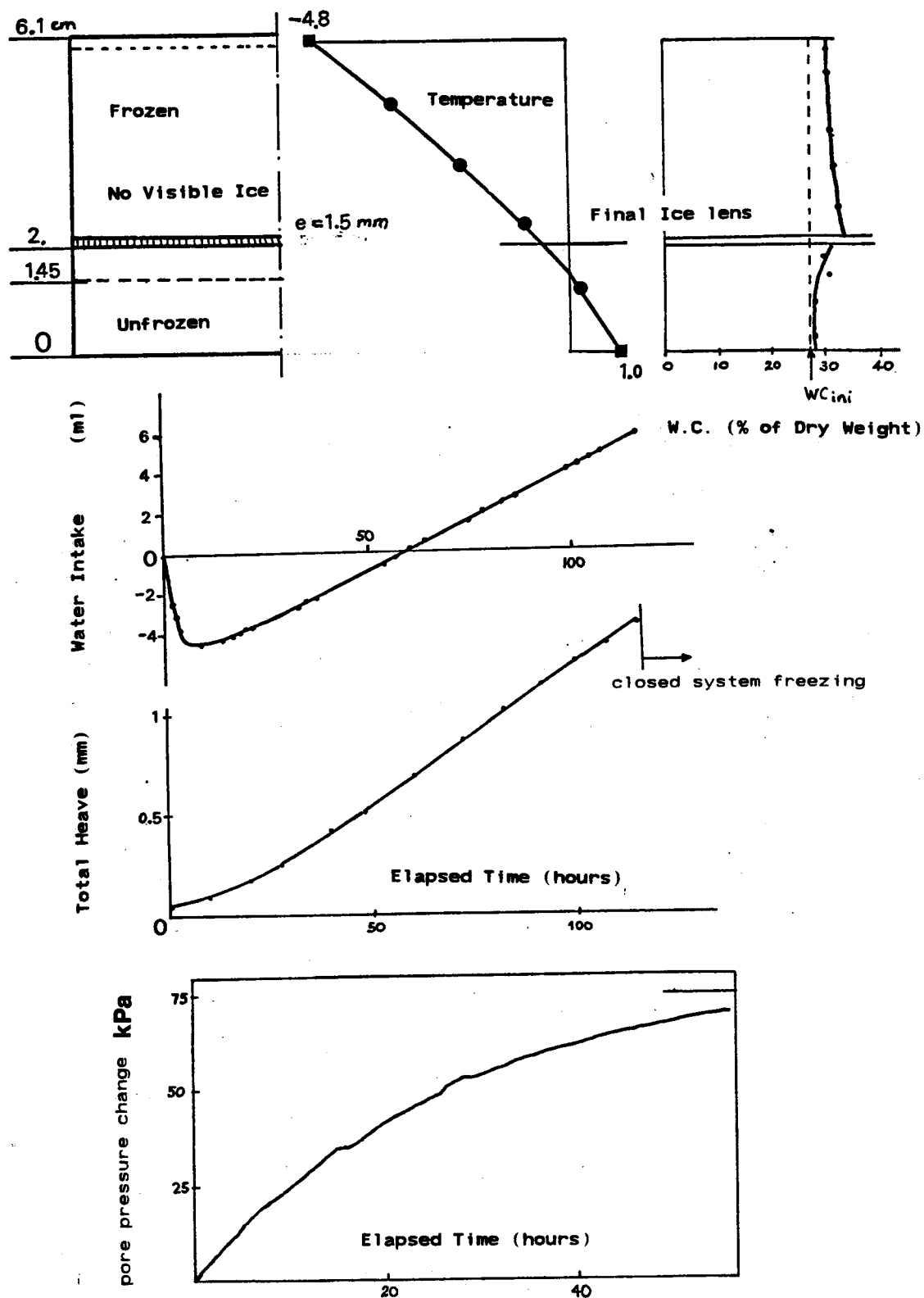Figure E.13 Experimental Results From Test C-14. Pe=400 kPa

APPENDIX F

Finite Difference Simulation of Frost Heave

      1. One Dimensional Heat Flow

      2. Radial Heat Flow

      3. Simple Frost Heave Calculation

```
      WRITE(6,55)ZU,POR,EPS,CF,CFR,CU,PERMU1,NI,TC,TW
   55 FORMAT('1',20X,'DATA INPUT',//,10X,'INITIAL UNFROZEN LENGTH IS:',
     +,F6.2,1X,'MM'
     +/,10X,'POROSITY IS :',3X,F6.2/,10X,'PHASE CHANGE FOR  :',F6.2,2X,
     +'INIWC'/,10X,'FROZEN THERMAL CONDUCTIVITY IS:',F6.2,'MCAL/C/MM/SEC'
     +//,10X,'FROZEN FRINGE THERMAL CONDUCTIVITY IS:',F6.2,'MCAL/C/MM/SEC'
     +//,10X,'UNFROZEN THERMAL CONDUCTIVITY IS:',F6.2,'MCAL/C/MM/SEC'
     +/,10X,'UNFROZEN PERMEABILITY IS:',2X,E10.3,'MM/SEC'
     +/,10X,'NUMBER OF NODES            ',2X,I4
     +/,10X,'COLD SIDE TEMPERATURE      ',2X,F5.2,'DEG.CELC.'
     +/,10X,'WARM SIDE TEMPERATURE      ',2X,F5.2,'DEG.CELC.')
      WRITE(6,51) DT
   51 FORMAT(//,10X,'THE TIME STEP IS :',F10.1,4X,'SEC')
      DZ=ZU/NI
      BE=DT*CU/(DZ*DZ*CAU)
C
C.....*INITIALIZE THE UNKNOWNS.
C
      HP=0.
      PU1=0.
      GRADT=0.
      W=0.
      H(1)=0.
      DF=0.
      CI=0.5
      RC=3.
      V=0.000
      HR=0.
      TIME=0.
      TVOL=0.
      DFM=0.
      HINT=0.
      HT=0.
      Z=ZU
      X=0.
      TPR1=0.5
      TPR2=10.
      TPR3=110.
      TPR4=2.
      TPR6=10.
      TPG=10.
      KO=1
      KOU=1
      JO=1
      TPR5=HLIM+0.1
      P=0.
      WRITE(6,150)
  150 FORMAT('1',//,4X,'TIME',2X,'TOTAL',2X,'UNFROZEN',
     +4X,'FROZEN',2X,'VELOCITY',3X,'TOTAL',2X,'HEAVE',
     +,3X,'RATE',2X,'GRAD T',3X,'HP',7X,'SUCTION',4X,'HEAT FLOW'
     +,'10X,'VOLUME',2X,'LENGTH',3X,'THICKNESS',2X,
     +'IN.FLOW',3X,'HEAVE',2X,'INTAKE',2X,'COOLING',2X,'C/MM',3X,'MM*MM'
     +,16X,'RATE  (MW)'
     +,3X,'(HRS)',3X,'(ML)',5X,'(MM)',6X,'(MM)',5X,'MM/S',5X,'(MM)'
     +,4X,'(MM)',4X,'(C/HR)',10X,'C*S',7X,'(M H2O)'//)
      CALL OUTPUT(HR,TVOL,Z,X,V,HT,HINT,RC,GRADT,HP,P,W)
      TIME=TIME+DT
C
```

```
C.....*********************************************
C.....**                                         **
C.....**    LE SOULEVEMENT UNIDIRECTIONEL DU AU GEL   **
C.....**                                         **
C.....*********************************************
C
C     PROGRAM TO SIMULATE THE ONE-DIMENSIONAL UNSTEADY HEAT FLOW
C     IN A FREEZING SOIL AND TO CALCULATE THE HEAVE WITH TIME AS
C     WELL AS THE ICE CONTENT PROFILE.
C   * THIS PROGRAM ALSO CALCULATES THE THICKNESS OF THE FINAL
C     ICE LENS DURING A RETREATING FROST FRONT FOR FIXED
C     TEMPERATURE BOUNDARY CONDITIONS.
C   * THE CRANK-NICHOLSON FINITE DIFFERENCE METHOD IS USED.
C     A FIXED GRID WITH A SUPPLEMENTARY NODE AT THE INTERFACE
C     PERMITS THE MOVING BOUNDARY SITUATION.
C   * BOTH FROZEN AND UNFROZEN SOIL THERMAL PROPERTIES ARE CONSI-
C     DERED AS INDEPENDENT WITH TEMPERATURE WATER REMAINING UNFRO-
C     ZEN BELOW ZERO DEGEE CELCIUS IS TAKEN INTO ACCOUNT BY THE
C     LUMP PARAMETER EPS.
C   * THE PHYSICS OF WATER MIGRATION TO THE SEGREGATION-FREEZING
C     FRONT HAS BEEN ADDED.THE SEGREGATION POTENTIAL DEFINED
C     AS THE RATIO OF THE WATER INTAKE RATE AND THE TEMPERATURE
C     GRADIENT IN THE FROZEN FRINGE IS DEPENDENT ON THE RATE OF
C     COOLING OF THE FRINGE AND THE SUCTION AT THE FROST FRONT.
C   * THE CHARACTERISTIC FREEZING SURFACE OF A GIVEN SOIL IS
C     OBTAINED FROM EXPERIMENTAL DATA.
C   * THE PROGRAM CAN INCORPORATE ANY SPECIFIED COLD AND WARM SIDE
C     TEMPERATURE VARIATION. NO LOAD IS APPLIED TO THE SAMPLE IN THE
C     FOLLOWING MODEL. HOWEVER, A DIFFERENT CHARACTERISTIC FREEZING
C     SURFACE CORRESPONDING TO THE DESIRED SURCHARGE IS SUFFICIENT
C     FOR PREDICTION OF FROST HEAVE UNDER EXTERNAL LOADS WITH THIS
C     MODEL.
C.....
C.....
C.....
      REAL A(2000),B(2000),C(2000),D(2000),AA(2000),BT(2000),DD(2000),
     +    DY(200),ZA(200),DWC(200),H(200),HS(200)
      REAL T(2000),U(2000),VO(2000),S(200),XP(200),FY(200)
C.....
C.....*ENTER THE PARAMETERS NECESSARY FOR SOLUTION.
C.....
      READ(5,1) KEY,NI,DT,EPSIL
      READ(5,2) TC,TW,CF,CFR,CU,CAF,CAU
      READ(5,3) ZU,AREA,POR,EPS,HRL
      READ(5,4) ZU2,PERMU1,PERMU2
      READ(5,5) HR1,HR2,TCI,TCF,TW1,TWF
      READ(5,6) HRF,HRL2,FA
      READ(5,7) FG,TS,RCC,CUE,CUI,TD
    7 FORMAT(6F8.4)
    6 FORMAT(2F10.2,F10.8)
    1 FORMAT(I2,I4,F8.1,F10.8)
    2 FORMAT(2F5.2,3F6.2,2F13.10)
    3 FORMAT(4F6.2,F10.2)
    4 FORMAT(F6.2,2E10.3)
    5 FORMAT(6F8.2)
```

```fortran
      ZM=ZU
      CK=CF-CU
      XO2=ABS((DT*CK**2.*TC)/(EPS*POR*79.6))
      XO=SQRT(XO2)
      DH=0.09*POR*EPS*XO
      Z=ZU+DH-XO

      HT=DH

C
      K=NI-1
      M=1
      MM=1
      DO 13 I=1,K
13    T(I)=TW
      U(1)=TC/2.
      U(2)=0.
1000  TIME=TIME+DT
      HR=TIME/3600.
C
C.....*SOLVE FOR TEMPERATURES IN THE UNFROZEN SOIL.
      NP=Z/DZ
      F=Z/DZ-NP
      N=NP
      T(N+1)=0.
      NB=N-1
      A(1)=2.+2.*BE
      B(1)=-BE
      C(1)=0.
      D(1)=2.*BE*TW+(2.-2.*BE)*T(1)+BE*T(2)
      DO 14 I=2,NB
      A(I)=2.+2.*BE
      B(I)=-BE
      C(I)=-BE
14    D(I)=BE*T(I-1)+(2.-2.*BE)*T(I)+BE*T(I+1)
      B(N)=0.
      A(N)=BE+F
      C(N)=-BE*F/(1.+F)
      D(N)=BE*F*T(N-1)/(1.+F)+(F-BE)*T(N)
      CALL GAUSEL(A,B,C,D,N)
      DO 16 I=1,N
16    T(I)=C(I)
610   IF(HR.GE.10.) GO TO 612
      IF(HR.GE.TP4) GO TO 610
      GO TO 600
613   WRITE(7,611) HR,(T(I),I=1,N)
611   FORMAT('ELAPSED TIME =',F10.2,3X,  'HOURS'/(10F10.2))
      GO TO 600
612   IF(HR.LT.TP6) GO TO 600
      TP6=TP6+10.
      GO TO 613
600   DERTU=(T(N-1))/((1.+F)*DZ)
      ST=K*ZU/NI
      IF(Z.LE.ST) GO TO 22
      IF(M.GT.2) GO TO 29
      IF(M.GT.1) GO TO 23
      H(1)=H(1)+DH
      DY(1)=DZ+H(1)-F*DZ
      DERTF=ABS(TC/DY(1))
      GRADT=CF*DERTF/CFR

      GO TO 50
22    IF(M.GT.1) GO TO 21
      DY(1)=DZ+H(1)
      GOTO 21
21    DWC(M)=91.74*H(M)/((1.-POR)*DZ*2.7)
      DY(M)=DZ+H(M)
C
      K=K-1
      M=M+1
      MM=M-1
29    HS(MM)=HS(MM-1)+H(MM)
C
23    HS(1)=H(1)
      H(M)=HT-HS(MM)
      DY(M)=DZ+H(M)-F*DZ
      G=DY(M)/DY(M-1)
      MP=NI-1-NP
      IF(MP.LE.1) GO TO 31
      N=MP
      NK=N-1
C.....*SOLVE FOR TEMPERATURES IN THE FROZEN SOIL.
C.....*POSSIBLE VARIATION OF COLD STEP TEMPERATURE.
C
      IF(KEY.GT.1) GO TO 510
      IF(HR.GE.HR1) GO TO 501
      TC=TCI
      TW=TWI
      GO TO 510
501   IF(HR.GE.HR2) GO TO 502
      TC=TCI-(TCI-TCF)*(HR-HR1)/(HR2-HR1)
      TW=TWI-(TWI-TWF)*(HR-HR1)/(HR2-HR1)
      GO TO 510
502   TC=TCF
      TW=TWF
510   U(N+1)=0.
      DO 26 I=1,NK
      DD(I)=DY(I)+DY(I+1)
      BT(I)=CF*DT/(CAF*DD(I))
      AA(I)=BT(I)*((1./DY(I+1))+(1./DY(I)))
      C(I)=-BT(I)/DY(I)
      B(I)=-BT(I)/DY(I+1)
26    A(I)=(AA(I)+1.)
      C(1)=0.
      D(1)=(2.*BT(1)/DY(1))*TC-(AA(1)-1.)*U(1)-B(1)*U(2)
      IF(NK.LE.1) GO TO 37
      DO 27 I=2,NK
27    D(I)=-C(I)*U(I-1)-(AA(I)-1.)*U(I)-B(I)*U(I+1)
37    B(N)=0.
      BF=(CF*DT)/(CAF*DY(N-1)*DY(N-1))
      A(N)=BF+G
      C(N)=-BF*G/(1.+G)
      D(N)=BF*G*U(N-1)/(1.+G)+(G-BF)*U(N)
      CALL GAUSEL(A,B,C,D,N)
      DO 28 I=1,N
28    U(I)=C(I)
      IF(HR.GE.10.) GO TO 712
      IF(HR.GE.TPR4) GO TO 710
      GO TO 700
```

```
710 TPR4=TPR4+2.
713 WRITE(7,711) (U(I),I=1,N)
711 FORMAT(10F10.2)
712 IF(HR.LT.TPR6) GO TO 700
    TPR6=TPR6+10.
    GO TO 713
700 DERTF=ABS(U(N-1)/(DY(N)+DY(N+1)))
    GRADT=CF*DERTF/CFR
    GO TO 50
 31 DERTF=ABS(TC/(DY(1)+DY(2)))
    GRADT=CF*DERTF/CFR
C
C.....*SOLVE FOR CONTINUITY AT THE INTERFACE AND CALCULATE HEAVE.
C
 50 HRC=DT/3600.
    IF(HR.GT.HRL2) GO TO 399
    IF(HR.GE.HRC) GO TO 399
    GO TO 453
399 RC=(1800./DT)*(DERTF*(2.*DX+DFM)-0.1)
    DFM=0.1/DERTF
301 IF(Z.LE.ZU2) GO TO 395
    PERMU=Z/(((Z-ZU2)/PERMU1)+(ZU2/PERMU2))
    GO TO 398
395 PERMU=PERMU2
398 S(1)=0.
    DO 470 JI=1,9
    P=S(JI)
    CALL SURF(POO,PO1,PO5,P1,P2,P5,P10,P,HP,RC)
    XP(JI)=HP
    IF(XP(1).LE.O.) GO TO 453
    FY(JI)=(XP(JI)*GRADT-(S(JI)*1000.*PERMU/Z))*1.E+05
    JIJ=JI+1
    S(JIJ)=S(JI)+1.
470 CONTINUE
    XP(9)=0.
    DO 471 JI=1,9
    IF(FY(JI).LT.O.) GO TO 472
471 CONTINUE
472 P=(FY(JI-1)*S(JI)-FY(JI)*S(JI-1))/(FY(JI-1)-FY(JI))
    CALL SURF(POO,PO1,PO5,P1,P2,P5,P10,P,HP,RC)
C
C.....*CALCULATE THE WATER FLUX AND FROST FRONT PENETRATION RATE.
C
451 V=HP*GRADT
    R=DERTF/DERTU
    RS=CU/(CF-(79.6*HP))
    W=(CF*DERTF-CU*DERTU)*4.1855
    IF(R.LE.RS) GO TO 1500
    GO TO 450
453 V=0.
    W=(CF*DERTF-CU*DERTU)*4.1855
    JO=1
450 DX=DT*(CF*DERTF-CU*DERTU-V*79.6)/(EPS*POR*79.6)
    IF(DX.LT.O.) GO TO 1500
C
    DHEX=0.09*EPS*POR*DX
    DHIN=1.09*V*DT
    DH=DHEX+DHIN
    HT=HT+DH

    HINI=HINI+DHIN
C
    DVOL=V*DT*AREA*0.1
    TVOL=TVOL+DVOL
C
C
    Z=Z-DX
    X=ZU+HT-Z
    IF(RC.LT.O.) GO TO 35
    IF(RC.LE.RCC) GO TO 341
    GO TO 35
341 KOU=KOU+1
    IF(KOU.GT.2) GO TO 35
    ZS=Z+(TS/DERTU)
    XS=X+Z-ZS
 35 IF(HR.GE.HRL) GO TO 1500
    IF(HR.GE.110.) GO TO 40
    IF(HR.GE.10.) GO TO 36
    IF(HR.GE.TPR1) GO TO 34
    GO TO 1000
 34 TPR1=TPR1+0.5
    CALL OUTPUT(HR,TVOL,Z,X,V,HT,HINT,RC,GRADT,HP,P,W)
    IF(RC.LE.EPSIL) GO TO 1500
    GO TO 1000
 36 IF(HR.GE.TPR2) GO TO 38
    GO TO 1000
 38 TPR2=TPR2+1.
    CALL OUTPUT(HR,TVOL,Z,X,V,HT,HINT,RC,GRADT,HP,P,W)
    IF(RC.LE.EPSIL) GO TO 1500
    GO TO 1000
 40 IF(HR.GE.TPR3) GO TO 42
    GO TO 1000
 42 TPR3=TPR3+10.
    CALL OUTPUT(HR,TVOL,Z,X,V,HT,HINT,RC,GRADT,HP,P,W)
    IF(RC.LE.EPSIL) GO TO 1500
C
C
    TIME INCREMENT
    GO TO 1000
1500 CALL OUTPUT(HR,TVOL,Z,X,V,HT,HINT,RC,GRADT,HP,P,W)
C
C
C....FROST HEAVE DURING THE RETREATING FROST FRONT PHASE
    IF(FG.GT.2.) GO TO 1505
    TIB=HR
    TIF=TIB+TD
    VO=V
    DH=0.
    DTIME=0.
    WRITE(7,72) DH,VO,DTIME
    FORMAT(10X,F10.2,10X,E10.4,10X,F10.1)
 72 HM=(CI*ABS(TC)*ZS/(CUE*TW))-(CI*XS/CF)
    HE=HM/40.
    DFF=(ZS-Z)/40.
 70 DH=DH+HE
    Z=Z+DFF
    IF(Z.GT.ZS) GO TO 32
    DERTU=ABS(TC)/(XS+DH)
    CFE=(XS+DH)/((XS/CF)+(DH/CI))
    IF(HR.GT.TIF) GO TO 73
    CU=CUI+((CUE-CUI)*(HR-TIB)/TD)
```

```
ZM=ZU
CK=CF-CU
XO2=ABS((DT*CK*2.*TC)/(EPS*POR*79.6))
XO=SQRT(XO2)
DH=0.09*POR*EPS*XO
Z=ZU+DH-XO

HT=DH

c
      K=NI-1
      M=1
      MM=1
      DO 13 I=1,K
   13 T(I)=TW
      U(1)=TC/2.
      U(2)=0.
 1000 TIME=TIME+DT
      HR=TIME/3600.
C
C......*SOLVE FOR TEMPERATURES IN THE UNFROZEN SOIL.
      NP=Z/DZ
      F=Z/DZ-NP
      N=NP
      T(N+1)=0.
      NB=N-1
      A(1)=2.+2.*BE
      B(1)=-BE
      C(1)=0.
      D(1)=2.*BE*TW+(2.-2.*BE)*T(1)+BE*T(2)
      DO 14 I=2,NB
      A(I)=2.+2.*BE
      B(I)=-BE
      C(I)=-BE
   14 D(I)=BE*T(I-1)+(2.-2.*BE)*T(I)+BE*T(I+1)
      B(N)=0.
      A(N)=BE+F
      C(N)=-BE*F/(1.+F)
      D(N)=BE*F*T(N-1)/(1.+F)+(F-BE)*T(N)
      CALL GAUSEL(A,B,C,D,N)
      DO 16 I=1,N
   16 T(I)=C(I)
      IF(HR.GE.10.) GO TO 612
      IF(HR.GE.TP4) GO TO 610
      GO TO 600
  610 TP4=TP4+2.
  613 WRITE(7,611) HR,(T(I),I=1,N)
  611 FORMAT('ELAPSED TIME =',F10.2,3X,  'HOURS'/(10F10.2))
      GO TO 600
  612 IF(HR.LT.TP6) GO TO 600
      TP6=TP6+10.
      GO TO 613
  600 DERTU=(T(N-1))/((1.+F)*DZ)
      ST=K*ZU/NI
      IF(Z.LE.ST) GO TO 22
      IF(M.GT.2) GO TO 29
      IF(M.GT.1) GO TO 23
      H(1)=H(1)+DH
      DY(1)=DZ+H(1)-F*DZ
      DERTF=ABS(TC/DY(1))
      GRADTF=CF*DERTF/CFR
```

```
      GO TO 50
   22 IF(M.GT.1) GO TO 21
      DY(1)=DZ*H(1)
      GOTO 21
   21 DWC(M)=91.74*H(M)/((1.-POR)*DZ*2.7)
      DY(M)=DZ*H(M)
c
      K=K-1
      M=M+1
      MM=M-1
   29 HS(MM)=HS(MM-1)+H(MM)
c
   23 HS(1)=H(1)
      H(M)=HT-HS(MM)
      DY(M)=DZ*H(M)-F*DZ
      G=DY(M)/DY(M-1)
      MP=NI-1-NP
      IF(MP.LE.1) GO TO 31
      N=MP
      NK=N-1
C......*SOLVE FOR TEMPERATURES IN THE FROZEN SOIL.
C......*POSSIBLE VARIATION OF COLD STEP TEMPERATURE.
C......
      IF(KEY.GT.1) GO TO 510
      IF(HR.GE.HR1) GO TO 501
      TC=TCI
      TW=TWI
      GO TO 510
  501 IF(HR.GE.HR2) GO TO 502
      TC=TCI-(TCI-TCF)*(HR-HR1)/(HR2-HR1)
      TW=TWI-(TWI-TWF)*(HR-HR1)/(HR2-HR1)
      GO TO 510
  502 TC=TCF
      TW=TWF
  510 U(N+1)=0.
      DO 26 I=1,NK
      DD(I)=DY(I)+DY(I+1)
      BT(I)=CF*DT/(CAF*DD(I))
      AA(I)=BT(I)*((1./DY(I+1))+(1./DY(I)))
      C(I)=-BT(I)/DY(I)
      B(I)=-BT(I)/DY(I+1)
   26 A(I)=+(AA(I)+1.)
      C(1)=0.
      D(1)=(+2.*BT(1)/DY(1))*TC-(AA(1)-1.)*U(1)-B(1)*U(2)
      IF(NK.LE.1) GO TO 37
      DO 27 I=2,NK
   27 D(I)=-C(I)*U(I-1)-(AA(I)-1.)*U(I)-B(I)*U(I+1)
   37 B(N)=0.
      BF=(CF*DT)/(CAF*DY(N-1)*DY(N-1))
      A(N)=BF+G
      C(N)=-BF*G/(1.+G)
      D(N)=BF*G*U(N-1)/(1.+G)+(G-BF)*U(N)
      CALL GAUSEL(A,B,C,D,N)
      DO 28 I=1,N
   28 U(I)=C(I)
      IF(HR.GE.10.) GO TO 712
      IF(HR.GE.TPR4) GO TO 710
      GO TO 700
```

```fortran
73    GO TO 75
      CU=CUE
75    V=(DERTF*CFE-(DERTU*CU))/79.6
      IF(V.GT.O.) GO TO 71
      V=0.
71    DTI=2.*HE/((1.09*3600.*(VO+V))
      DTIME=DTIME+DTI
      HR=HR+DTI
      HT=HT+HE
      HINT=HINT+HE
      X=X+HE
      DVOL=HE*AREA/10.9
      TVOL=TVOL+DVOL
      CALL OUTPUT(HR,TVOL,Z,X,V,HT,HINT,RC,GRADT,HP,P,W)
      WRITE(7,72) DH,V,DTIME
      VO=V
      GO TO 70
1505  WRITE(6,1501)
1501  FORMAT(//,10X,'STEADY TEMPERATURE STATE HAS BEEN REACHED')
      WRITE(7,599)
599   FORMAT(' 1'//,18X,'LENGTH OF',10X,'INCREASE IN'
     +/,15X,'UNFROZEN SOIL',10X,'WATER CONTENT'
     +/,20X,'(MM)',12X,'% DRY WEIGHT'//)
      DR=(1.-F)*DZ
      DWC(M)=91.74*H(M)/((1.-POR)*QR*2.7)
      ZA(1)=Z+X-DY(1)/2.
      DO 1502 I=2,M
1502  ZA(I)=ZA(I-1)-DY(I)
      WRITE(7,601) (ZA(I),DWC(I),I=1,M)
601   FORMAT(' ',15X,F10.2,10X,F10.2)
32    STOP
      END
C

      SUBROUTINE OUTPUT(HR,TVOL,Z,X,V,HT,HINT,RC,GRADT,HP,P,W)
      WRITE(6,151) HR,TVOL,Z,X,V,HT,HINT,RC,GRADT,HP,P,W
151   FORMAT(2F8.2,2X,F6.2,4X,F6.2,2X,E8.2,3X,F6.2,2X,F6.2,
     +2X,F6.4,2X,F6.4,2X,E8.2,2X,F6.2,6X,F6.4)
      RETURN
      END
      SUBROUTINE GAUSEL(A,B,C,D,N)
      REAL A(1),B(1),C(1),D(1)
      IF(N.GT.1) GO TO 3
      C(N)=D(N)/A(N)
      GO TO 2
3     DO 1 I=2,N
      A(I)=A(I)-B(I-1)*C(I-1)/A(I-1)
      D(I)=D(I)-D(I-1)*C(I-1)/A(I-1)
1     C(I)=0.
      C(N+1)=0.
      I=N
4     C(I)=(D(I)-B(I)*C(I+1))/A(I)
      IF(I.LE.1) GO TO 2
5     I=I-1
      GO TO 4
2     RETURN
      END

C     THIS SUBROUTINE GIVES THE FUNCTIONAL RELATIONSHIP
C     BETWEEN SP,PU,AND RATE OF COOLING OF THE FRINGE
C     FOR DEVON SILT WITH PE=O.

      SUBROUTINE SURF(POO,PO1,PO5,P1,P2,P5,P10,P,HP,RC)
      IF(P.LT.8.1) GO TO 302
      HP=0.
      GO TO 300
302   IF(P.LT.2.) GO TO 532
      POO=(8.-P)*2.2/6.
      PO1=(8.-P)*3./6.
      GO TO 534
532   POO=(8.-P)*2.2/6.+.75*(2.-P)*2.
      PO1=(8.-P)*3./6.+1.2*(2.-P)**1.735
534   P2=6.53-0.36*P+.1076*P**2.-0.0306*P**3.+0.00125*P**4.
      P5=3.76+.0784*P-.119*P**2.+.03105*P**3.-.003087*P**4.
      P10=2.19+.0722*P-.05966*P**2.+.015867*P**3.-.001241*P**4.
      IF(P.LT.6.) GO TO 520
      P1=(8.-P)*2.2/2.
      PO5=(8.-P)*1.7/2.
      GO TO 304
520   IF(P.LT.1.5) GO TO 521
      P1=2.2+(6.-P)*7.3/4.5
      PO5=1.7+(6.-P)*6.2/4.5
      GO TO 304
521   P1=(7.35-P)*10.9/7.35-(0.5*(1.5-P)**1.7)
      PO5=(7.35-P)*10./7.35-(0.4*(1.5-P)**1.4)
C
304   IF(RC.LT.2.5) GO TO 409
      HP=0.
      GO TO 300
409   IF(RC.LT.1.) GO TO 410
      HP=2.E-4*(2.5-RC)*P10/1.5
      GO TO 300
410   IF(RC.LT.0.5) GO TO 414
      HP=2.E-4*(P10+((1.-RC)*(P5-P10)/.5))
      GO TO 300
414   IF(RC.LT.0.2) GO TO 416
      HP=2.E-4*(P5+((.5-RC)*(P2-P5)/.3))
      GO TO 300
416   IF(RC.LT..1) GO TO 418
      HP=2.E-4*(P2+((.2-RC)*(P1-P2)/.1))
      GO TO 300
418   IF(RC.LT..05) GO TO 420
      HP=2.E-4*(PO5+((RC-0.05)*(P1-PO5)/0.05))
      GO TO 300
420   IF(RC.LT.0.01) GO TO 422
      HP=2.E-4*(PO1+((RC-0.01)*(PO5-PO1)/0.04))
      GO TO 300
422   HP=2.E-4*(POO+RC*(PO1-POO)/0.01))
300   RETURN
      END

LF.
```

469

```fortran
C ********************************************
C **                                        **
C **     FROST HEAVE BENEATH A CHILLED PIPE  **
C **                                        **
C ********************************************
C
C THIS PROGRAM SIMULATES RADIAL UNSTEADY HEAT FLOW
C IN A FREEZING SOIL BENEATH A CHILLED GAS PIPELINE.
C HEAVE WITH TIME IS OBTAINED FOR BOTH AN ADVANCING
C AND A RETREATING FROST FRONT. ICE CONTENT PROFILE
C IS ALSO OBTAINED AT ANY TIME.
C THE CHARACTERISTICS OF THE FREEZING SOIL ARE TAKEN
C AS THE SEGREGATION FREEZING TEMPERATURE (TSO , A)
C AND THE PERMEABILITY OF THE FROZEN FRINGE (KF0,B).
C THIS PROGRAM ALLOWS ALSO TO SIMULATE THE RESTRAINED
C TEST SECTION OF THE CALGARY FIELD TEST FACILITIES.
C (SLUCHARCHUK ET AL.1978).
      REAL A(2000),B(2000),C(2000),D(2000),AA(2000),BT(2000),DD(2000).
     +     DY(2000),H(2000),HI(2000),DWC(2000),HP(2000)
      REAL T(2000),R(1000),U(2000),VU(2000)
C     INPUT DATA
C
      READ(5,1) KIK,NI,DT,EPSIL
      READ(5,2) TC2,TW,CF,CU,CAF,CAU
      READ(5,3) ZU,AREA,PORS,EPS,ZL,ZC
      READ(5,4) PERMU,PERMU2,PERMFO,HR2,RC
      READ(5,5) RO,TCI,HLIM,HR1,KEY
      READ(5,6) P1,P2,TSO,PA,PD,HL,POV
    1 FORMAT(2I4,F6.1,F10.8)
    2 FORMAT(2F8.2,2F6.2,2F6.3)
    3 FORMAT(6F6.2)
    4 FORMAT(3E10.3,F8.2,F4.2)
    5 FORMAT(4F8.2,I2)
    6 FORMAT(5F8.4,F8.1,F6.2)
C
      WRITE(6,55)ZU,PORS,EPS,CF,CU,PERMU,PERMFO,TC2,TW,TSO,P1,P2,POV
   55 FORMAT('1',20X,'DATA INPUT:'/,10X,'INITIAL UNFROZEN LENGTH IS:'
     +,F8.2,1X,'CM'
     +/,10X,'POROSITY IS :',3X,F6.2/,10X,'PHASE CHANGE FOR  :',F6.2,2X,
     +'INIWC'/,10X,'FROZEN THERMAL CONDUCTIVITY IS:',F6.2,'CAL/C/CM/HR'
     +/,10X,'UNFROZEN THERMAL CONDUCTIVITY IS:',F6.2,'CAL/C/CM/HR'
     +/,10X,'UNFROZEN PERMEABILITY IS:',2X,E10.3,'CM/SEC'
     +/,10X,'FINAL FROZ. FRINGE PERMEAB.:',2X,E10.3,'CM/SEC'
     +/,10X,'COLD SIDE TEMPERATURE   :',2X,F8.2,'DEG.CELC.'
     +/,10X,'WARM SIDE TEMPERATURE    :',2X,F8.2,'DEG.CELC.'
     +/,10X,'SEGR. FREEZING TEMP. @ PE=O IS ...',F8.2,'DEG.CELC.'
     +/,10X,'SOIL PARAMETER FOR TS ......',2X,F6.4,'C/MPA'
     +/,10X,'SOIL PARAMETER FOR KF   .....',2X,F6.4,'CM/(S.MPA)'
     +/,10X,'OVERBURDEN ........',2X,F6.2,' KPA')
      WRITE(6,51) DT
   51 FORMAT(//,10X,'THE TIME STEP IS :',F5.1,'HRS')
      DZ=ZU/NI
      BE=DT*CU/(2.*DZ*DZ*CAU)
C     INITIALIZATION OF VARIABLES
C
      HM=0.
      PE=0.
      DFI=0.
      H(1)=0.
      DERTF=0.
      DERTU=0.
      V=0.000
      HR=0.
      TIME=0.
      TVOL=0.
      HINT=0.
      HT=0.
      Z=ZU
      X=0.
      TPR1=5.
      TPR2=50.
      TPR3=300.
      PERMF=PERMFO
C     OUTPUT FORMAT
C
      WRITE(6,150)
  150 FORMAT('1',//,10X,'TIME',2X,'TOTAL',2X,'UNFROZEN',
     +2X,'FROZEN',4X,'VELOCITY',3X,'TOTAL',2X,'HEAVE'
     +,2X,'GRAD(TF)',2X,'GRAD(TU)',2X,'KF(CM/S)',2X,'PRESSURE'
     +/,15X,'VOLUME',2X,'LENGTH',3X,'THICKNESS',2X,
     +'IN.FLOW',3X,'HEAVE',2X,'INTAKE'/,9X,'(DAYS)',
     +3X,'(ML)',5X,'(CM)',6X,'(CM)',5X,'CM/H',5X,'(CM)',
     +,4X,'(CM)',7X,'C/CM',5X,'C/CM',15X,'MPA'//)
      CALL OUTPUT(HR,TVOL,Z,X,V,HT,HINT,DERTF,DERTU,PERMF,PE)
      TIME=TIME+DT
C
C     START OF COMPUTATION
      CK=CF-CU
      XO2=ABS((DT*CK*2.*TC2)/(EPS*PORS*79.6))
      XO=SQRT(XO2)
      DH=0.09*PORS*EPS*XO
      Z=ZU+DH-XO
C
      HT=DH
      K=NI-1
      ST=K*DZ
      MK=K-1
      M=1
      MM=1
      DO 13 I=1,20
   13 T(I)=TW
      DO 133 I=21,K
  133 T(I)=TW
      U(1)=TCI/2.
      U(2)=0.
 1000 TIME=TIME+DT
C
C     TEMPERATURE DISTRIBUTION IN UNFROZEN SOIL
      HR=TIME/24.
      IF(HR.GT.HR1) GO TO 90
      TC=TCI+((TC2-TCI)*HR/HR1)
      GO TO 154
   90 TC=TC2
  154 IF(Z.GT.ST) GO TO 222
      K=K-1
      KK=K-1
      MK=K-1
      ST=K*DZ
      DO 305 I=2,KK
  305 T(I-1)=T(I)
```

```
      IF(M.GT.1) GO TO 20
      VOL(1)=TVOL
      GO TO 21
20    VOL(M)=TVOL-VO(MM)
21    DWC(M)=1000.*VO(M)/((1.-POR)*DZ*AREA*2.7)
      MM=M-1
222   NP=Z/DZ-NP
      F=Z/DZ-NP
      R(1)=X+RO+F*DZ
      R(1)=R(1)/DZ
      DO 9 J=1,MK
9     R(JJ+1)=R(J)+1.
      A(1)=F+2.*BE
      C(1)=0.0
      B(1)=-BE*F*((2.*R(1)+1.)/(2.*R(1)+2.*R(1)*F))
      D(1)=(F-2.*BE)*T(1)-B(1)*T(2)
      DO 14 I=2,MK
      R(I)=1./(2.*R(I))
      B(I)=-BE*(1.+R(I))
      C(I)=-BE*(1.-R(I))
      A(I)=1.+2.*BE
14    D(I)=-C(I)*T(I-1)+(1.-2.-BE)*T(I)-B(I)*T(I+1)
      B(K)=0.
      C(K)=-BE*(1.-1./(2.*R(K)))
      D(K)=-C(K)*T(K-1)+(1.-2.-BE)*T(K)+2.*BE*(1.+1./(2.*R(K)))*TW
      N=K
      CALL GAUSEL(A,B,C,D,N)
      DO 18 I=1,N
18    T(I)=C(I)
      DERTU=(2)/((1.+F)*DZ)
      IF(DERTU.LE.O.) GO TO 32
      IF(M.GT.2) GO TO 29
      IF(M.GT.1) GO TO 23
      H(1)=H(1)+DH
      DY(1)=DZ+H(1)-F*DZ
      DERTF=ABS(TC/DY(1))
      GO TO 50
29    HP(MM)=HP(MM-1)+H(MM)
23    HP(1)=H(1)
C     TEMPERATURE DISTRIBUTION IN FROZEN SOIL
      H(M)=HT-HP(MM)
      DY(M)=DZ+H(M)-F*DZ
      G=DY(M)/DY(M-1)
      MP=NI-1-NP
      IF(MP.LE.1) GO TO 31
      N=MP
      NK=N-1
      R(N)=X+RO-DY(M)
      DO 8 J=1,NK
      JJ=N-J
8     R(JJ)=R(JJ+1)-DY(JJ+1)
      U(N+1)=0.
      DO 26 I=1,NK
      DD(I)=DY(I)-DY(I+1)
      BT(I)=CF*DT/(CAF*DD(I))
      AA(I)=BT(I)*((1./DY(I+1))+(1./DY(I)))
      R(I)=1./(2.*R(I))
      C(I)=-BT(I)*((1./DY(I))-R(I))

      R(I)=-BT(I)*((1./DY(I))+R(I))
26    A(I)=+(AA(I)+1.)
      C(I)=0.
      D(1)=BT(1)*((2./DY(1))-R(1))*TC*(1.-AA(1)*U(1)-B(1)*U(2))
      IF(NK.LE.1) GO TO 37
      DO 27 I=2,NK
27    D(I)=-C(I)*U(I-1)-(AA(I)-1.)*U(I)-B(I)*U(I+1)
37    B(N)=0.
      BF=(CF*DT)/(CAF*DY(N)*DY(N))
      A(N)=2.*BF+G
      C(N)=-BF*((2.*R(N)-1.)/(2.*R(N)+2.*R(N)*G))
      D(N)=(G-2.*BF)*U(N)-C(N)*U(N-1)
      CALL GAUSEL(A,B,C,D,N)
      DO 28 I=1,N
28    U(I)=C(I)
      DERTF=-U(N-1)/(DY(N)+DY(N+1))
      GO TO 50
31    DERTF=ABS(TC/(DY(1)+DY(2)))
C     SOLVING MASS TRANSFER
C
50    TACC=TS0+(P1*PE)
      PERMFM=EXP(2.3*(ALOG10(PERMFO)-(P2*PE)))
      IF(HR.GT.HR2) GO TO 91
      PERMF=(RC+((1.-RC)*HR/HR2))*PERMFM
      GO TO 92
91    PERMF=PERMFM
92    DF=TACC/DERTF
      PW=12500.*TACC-(10000.*PE)
      IF(KEY.GT.2) GO TO 204
      DEP=ZU-Z
      IF(DEP.GT.ZC) GO TO 82
      PER=EXP(ALOG(PERMU2)-(ALOG(PERMU))*DEP/ZC)
      PERE=.2*PERMF+(.6*PERMF*DEP/ZC)
      PERM=(DEP+DF)/(DEP/PER+DF/PERE)
      V=PW*PERM*3600./(DF+DEP)
      GO TO 205
82    PERM=(ZL+DF)/(ZL/PERMU+DF/PERMF)
      V=PW*PERM*3600./(DF+ZL)
      GO TO 205
204   V=PW*PERMF*3600./DF
C
C     THERMAL BALANCE
205   DX=DT*(CF*DERTF-CU*DERTU-V*79.6)/(EPS*PORS*79.6)
      IF(DX.LT.O.) GO TO 1500
C
      DHEX=0.09*EPS*PORS*DX
      DHIN=1.09*V*DT
      DH=DHEX+DHIN
      HT=HT+DH
      HINT=HINT+DHIN
C
      DVOL=V*DT*AREA
      TVOL=TVOL+DVOL
C
C
      HR=TIME/24.
      Z=Z-DX
      X=ZU+HT-Z
C     EFFECT OF PRESSURE AT THE FROST FRONT
      PE1=PO*X/10000.+(POV/1000.)
```

```fortran
C     SIMULATION OF RESTRAINED SECTION (CALGARY TEST)
      IF(KIK.GT.2) GO TO 60
      PE=PE1
      GO TO 80
60    IF(HR.GT.90.) GO TO 70
      PE=PE1
      GO TO 44
70    IF(HR.GT.138.) GO TO 71
      PE=PE1+0.007
      GO TO 44
71    IF(HR.GT.216.) GO TO 72
      PE=PE1+.026
      GO TO 44
72    IF(HR.GT.238.) GO TO 73
      PE=PE1+.052
      GO TO 44
73    IF(HR.GT.248.) GO TO 74
      PE=PE1
      GO TO 44
74    IF(HR.GT.398.) GO TO 75
      PE=PE1+.052
      GO TO 44
75    IF(HR.GT.608.) GO TO 76
      PE=PE1+0.09
      GO TO 44
76    IF(HR.GT.630.) GO TO 77
      PE=PE1
      GO TO 44
77    PE=PE1+.090
      GO TO 44
C
80    IF(HR.GT.HL) GO TO 43
      GO TO 44
43    PE=PE+PA
44    IF(HR.GE.HLIM) GO TO 32
      IF(HR.GE.300.) GO TO 40
      IF(HR.GE.50.) GO TO 36
      IF(HR.GE.TPR1) GO TO 34
      GO TO 1000
34    TPR1=TPR1+5.
      CALL OUTPUT(HR,TVOL,Z,X,V,HT,HINT,DERTF,DERTU,PERMF,PE)
      IF(DX.LE.EPSIL) GO TO 1500
      GO TO 1000
36    IF(HR.GE.TPR2) GO TO 38
      IF(HR.GE.TPR1) GO TO 34
      GO TO 1000
38    TPR2=TPR2+10.
      CALL OUTPUT(HR,TVOL,Z,X,V,HT,HINT,DERTF,DERTU,PERMF,PE)
      IF(DX.LE.EPSIL) GO TO 1500
      GO TO 1000
40    IF(HR.GE.TPR3) GO TO 42
      GO TO 1000
42    TPR3=TPR3+30.
      CALL OUTPUT(HR,TVOL,Z,X,V,HT,HINT,DERTF,DERTU,PERMF,PE)
      IF(DX.LE.EPSIL) GO TO 1500
C     TIME INCREMENT
C
1500  DF=TACC/DERTF
      VO=V
      XS=X-DF
      ZS=Z
      TSF=.872*PE
      RS=RO+XS+ZS
      RF=RO+XS
      E=50.
1700  CALL SRM(RM,CU,CF,DF,XS,ZS,RS,RF,E,RO,TW,TC,TSF)
      EC=RM-RO-XS
      DE=ABS(EC-E)
      IF(DE.LT.1.) GO TO 1701
      E=EC
      GO TO 1700
1701  DFE=(TACC-TSF)*DF/TACC
      DFF=DFE/20.
      HMM=EC/20.
1740  HM=HM+HMM
      DFI=DFI+DFF
      IF(DFI.GT.DFE) GO TO 32
      R1U=RO+XS+HM
      R1=R1U+DF-DFI
      R2=R1+ZS+DFI
      DERTU=TW/((ALOG(R2/R1))*R1)
      DERTF=(-TC)/((ALOG(R1/RO))*R1)
      V=(DERTF*CF-(DERTU*CU))/79.6
      IF(V.GT.O.) GO TO 1710
      V=0.
1710  DTIME=2.*HM/(1.O9*24.*(V+VO))
      DTIME=DTIME+DTI
      HT=HT+HMM
      HINT=HINT+HMM
      HR=HR+DTIME
      Z=ZS+DFI
      X=XS+DF-DFI+HM
      CALL OUTPUT(HR,TVOL,Z,X,V,HT,HINT,DERTF,DERTU,PERMF,PE)
      VO=V
      GO TO 1740
C
C
32    STOP
      END
C
      SUBROUTINE OUTPUT(HR,TVOL,Z,X,V,HT,HINT,DERTF,DERTU,PERMF,PE)
      WRITE(6,151) HR,TVOL,Z,X,V,HT,HINT,DERTF,DERTU,PERMF,PE
151   FORMAT(F14.1,1X,F5.1,2X,F6.1,4X,F6.1,2X,E8.2,3X,F6.2,
     +2X,F6.2,2X,F6.4,2X,F6.4,2X,E10.3,2X,F6.4)
      RETURN
      END
      SUBROUTINE GAUSEL(A,B,C,D,N)
      REAL A(1),B(1),C(1),D(1)
      IF(N.GT.1) GO TO 3
      C(N)=D(N)/A(N)
      GO TO 2
3     DO 1 I=2,N
      A(I)=A(I)-B(I-1)*C(I)/A(I-1)
      D(I)=D(I)-D(I-1)*C(I)/A(I-1)
1     C(I)=O.
      C(N+1)=O.
      I=N
4     C(I)=(D(I)-B(I)*C(I+1))/A(I)
      IF(I.LE.1) GO TO 2
5     I=I-1
```

```
      GO TO 4
2     RETURN
      END
C
C     ****** THIS SUBROUTINE CALCULATES IN AN ITERATIVE MANNER
C     :::::: THE MAXIMUM THICKNESS OF THE FINAL ICE LENS
C     ****** FOR THE CASE OF FIXED TEMPERATURE BOUNDARY CONDITIONS.
C
      SUBROUTINE SRM(RM,CU,CF,DF,XS,ZS,RS,RF,E,RO,TW,TC,TSF)
      DERTU=(TW-TSF)/(ALOG((RS+E)/(RF+E))*(RF+E))
      DERTF=CU*DERTU/CF
      CC=-TC/DERTF
      RM=XS+RO+E
12    CA=RM*ALOG(RM/RO)
      DE=CA-CC
      DEE=ABS(DE)
      IF(DEE.LE.20.) GO TO 20
      IF(DE.GT.O.) GO TO 11
      RM=RM+100.
      GO TO 12
11    DEE=ABS(DE)
      IF(DEE.LE.20.) GO TO 20
      RM=RM-10.
14    CA=RM*ALOG(RM/RO)
      DE=CA-CC
      DEE=ABS(DE)
      IF(DE.LT.O.) GO TO 13
      IF(DEE.LE.20.) GO TO 20
      RM=RM-10.
      GO TO 14
13    DEE=ABS(DE)
      IF(DEE.LE.20.) GO TO 20
      RM=RM+1.
15    CA=RM*ALOG(RM/RO)
      DE=CA-CC
      DEE=ABS(DE)
      IF(DEE.LE.20.) GO TO 20
      RM=RM+1.
      IF(DE.GT.O.) GO TO 15
      GO TO 15
20    RETURN
      END

:ILE
```

```
C  ************************************
C  **                                **
C  **  SIMPLE FROST HEAVE COMPUTATION **
C  **  USING THE SEGREGATION POTENTIAL **
C  **                                **
C  ************************************
C
C  *     THIS PROGRAM CALCULATES IN A SIMPLE FORWARD
C        MANNER FROST HEAVE WITH A SINUSOIDAL VARIATION
C        OF THE COLD-STEP TEMPERATURE.
C  *     IT CAN EASILY BE ADAPTED FOR ANY DESIRED VARIATION
C        OF THE GROUND SURFACE FREEZING TEMPERATURE.
      READ(5,1) TMAX,TLIM,DT,CF,POR,EPS
      READ(5,2) SP,KEY,A,B,S,P
1     FORMAT(6F8.3)
2     FORMAT(E10.3,I2,4F8.3)
200   FORMAT(1OX,F8.1,4X,F8.2,4X,E10.3,3(2X,F8.2))
      HIN=O.
      HEX=O.
      HT=O.
      XO=O.
      TP=1O.
100   TIME=TIME+DT
      IF(KEY.GT.1) GO TO 10
      X=A*TIME**S
      TC=B*TIME**P
      GO TO 20
10    C=2.*CF*TMAX*TLIM*24./(3.1416*80.)
      CC=1.-(COS(3.1415*TIME/TLIM))
      CCC=C*CC
      X=SQRT(CCC)
      TC=TMAX*(SIN(3.1415*TIME/TLIM))
20    DX=X-XO
      GRADT=TC/(X+HT)
      V=GRADT*SP
      DHIN=1.09*V*DT*3600.*24.
      DHEX=O.09*POR*EPS*DX
      HIN=HIN+DHIN
      HEX=HEX+DHEX
      HT=HIN+HEX
      XO=X
      IF(TIME.LT.TP) GO TO 50
      WRITE(6,200) TIME,X,V,HIN,HEX,HT
      TP=TP+10.
50    TF=TLIM/2.
      IF(TIME.GT.TF)     GO TO 300
      GO TO 100
300   STOP
      END
```